Wolfgang Hauschild · Eberhard Lemke

High-Voltage Test and Measuring Techniques

Springer

High-Voltage Test and Measuring Techniques

Wolfgang Hauschild · Eberhard Lemke

High-Voltage Test and Measuring Techniques

Springer

Wolfgang Hauschild
Dresden
Germany

Eberhard Lemke
Radeburg
Germany

ISBN 978-3-642-45351-9 ISBN 978-3-642-45352-6 (eBook)
DOI 10.1007/978-3-642-45352-6
Springer Heidelberg New York Dordrecht London

Library of Congress Control Number: 2013956628

Printed on acid-free paper

Springer is part of Springer Science+Business Media (www.springer.com)

Foreword

Most textbooks on high-voltage (HV) engineering published in the recent years are focussed on general aspects of this field but not on the specifics of HV test and measuring techniques provided in this book. This topic is mainly experimentally based and essential for the wide range of present and future challenges, due to the increasing use of renewable power, the wider application of cable systems as well as the erection of long-distance ultra-high voltage (UHV) lines using not only alternating but also direct transmission voltages.

Therefore, researchers and engineers engaged in HV test and measuring techniques are developing new equipment, instruments and procedures. For a general basis, international organizations as CIGRE, IEC and IEEE summarise the results of research work and provide commonly accepted rules, guides and standards. Many researchers, designers and technicians engaged in the field of HV engineering are not well familiar with the approaches prepared and introduced by the above-mentioned organizations. In this situation, this book will close a gap and contribute to a better understanding of the advanced technique recently developed and adopted for quality assurance testing and diagnostics of HV insulation. Moreover, the book is a help for students to get well-understandable information on today's tools for insulation testing and diagnostics. Another main application will be the training, further education and individual learning of engineers.

In this context, it should be noted that great progress has been made in developing HV test systems including the associated measuring equipment which are the main topics of the book written by Hauschild and Lemke. In summary: The book gives a complete introduction and an overview of the state-of-the-art HV test and measuring techniques in close connection to practical aspects. For me, great work has been done by the authors, which I know since the beginning of the 1970s when I visited the HV Institute in Dresden for the first time. Thereafter we became good partners and close friends. I met the authors periodically, mainly when participating in various working groups of CIGRE and IEC where Wolfgang Hauschild was especially engaged in the field of HV test technique and Eberhard Lemke in the field of HV measuring

technique. Their outstanding work and fruitful cooperation with the HV Institute of the Graz University of Technology has been recognized by awarding both with the degree of a "Doctor honoris causa" in 2007 and 2009, respectively.

November 2013

Michael Muhr
Graz Technical University
Graz
Austria
Chairman of Cigre AG HV Test Techniques
Paris
France

Preface

A century after its beginning, high-voltage (HV) engineering still remains an empirical field. Experimental investigations are the backbone for the dimensioning of electrical insulations and indispensable for quality assurance by type, routine and commissioning tests as well as for insulation condition assessment by monitoring and diagnostic tests. There is no change in sight for such empiric procedures. The application of higher transmission voltages, improved insulation materials and new design principles require the further development of HV test and measuring techniques. The relevant bodies of experts in *CIGRE, IEC* and *IEEE* provide commonly accepted standards and guides of HV testing adapted to both, the needs and the level of knowledge.

Coming from the Dresden School of HV engineering of *Fritz Obenaus* and *Wolfgang Mosch*, the authors have been lucky to follow and to contribute to the development of HV test techniques for half of a century. This book is based on that experience and shall reflect the actual state-of-the-art of HV test and measuring techniques. According to our intention, the book shall close a gap in the international literature of HV engineering and lead to a better understanding of the relevant IEC and IEEE standards. It is hoped our text will fill the needs of designers, test field and utility engineers as well as those of senior undergraduate and graduate students and researchers. Today, many engineers who are confronted with or even engaged in HV testing did not have an in-depth education in HV engineering. Therefore, the book is intended to support the individual learning as it is useful for further training courses, too.

After an introduction related to the history and the position of HV test techniques within electric power engineering, the general basis of test systems and test procedures, the approval of measuring systems and the statistical treatment of test results are explained. In separate chapters for alternating, direct, impulse and combined test voltages, respectively, their generation, their requirements and their measurements are described in detail. Because partial discharge and dielectric measurements are mainly related to alternating voltage tests, separate chapters on these important tools are arranged after that of alternating test voltages. The book closes with chapters on HV test laboratories and on-site testing.

The cooperation with many experts from all over the world has been a precondition for writing this book. We are grateful to all of them, but we can mention only a few: We got our stamping at the HV Laboratory of Dresden Technical

University and acknowledge the cooperation of its staff, represented by *Eberhard Engelmann* and *Joachim Speck*. We consider our membership in the expert bodies of *CIGRE 33 (later D1), IEC TC 42* and *IEEE-TRC and ICC* as a school during our professional live. We have got numerous suggestions from this work on HV testing as well as from discussions with the members. We are grateful to *Dieter Kind, Gianguido Carrara, Kurt Feser, Arnold Rodewald, Ryszard Malewski, Klaus Schon, Michael Muhr* and all others who are not mentioned here. Of course, the daily work in our companies has been connected with many technical challenges of HV test techniques. As they have always been mastered in our reliable teams, we would like to express our sincere thanks to both, the management and the staff of *Highvolt Prüftechnik Dresden GmbH* and *Doble-Lemke GmbH*. Thanks to *Harald Schwarz*, Wolfgang Hauschild has been appointed to a lectureship at Cottbus Technical University on HV test techniques. This required a suitable structure for the subject which is also used in this book. For the careful proof-reading of the manuscript and the helpful advices we thank our friends *Jürgen Pilling* and *Wieland Bürger*. We would be grateful for further suggestions and critics of the readers of this book.

Dresden, October 2013

Wolfgang Hauschild
Eberhard Lemke

Acknowledgment

Due to the generous aid by Highvolt Prüftechnik Dresden GmbH, the book has got its coloured appearance. Furthermore, all photographic figures and three-dimensional drawings without reference are supplied by the Highvolt archives. Our sincere thanks are related to the management, especially to Bernd Kübler, Thomas Steiner and Ralf Bergmann, for their permanent support of our project.

Contents

Abbreviations

AC	Alternating current (in composite terms, e.g. AC voltage)
ACIT	HV units for feeding induced voltage tests
ACL	Accredited Calibration Laboratory
ACRF	HVAC series resonant circuit of variable frequency
ACRL	HVAC series resonant test circuit of variable inductance
ACTR	HVAC test circuit based on transformer
ADC	Analog–digital converter
AE	Acoustic emission
AMS	Approved measuring system
C	Capacitance
CD	Committee Draft (IEC)
CH	Channel
CRO	Cathode ray oscilloscope
DAC	Damped alternating current (in composite terms, e.g. DAC voltage)
DC	Direct current (in composite terms, e.g. DC voltage)
DCS	Directional coupler sensor
DNL	Differential non-linearity
DSP	Digital signal processing
EMC	Electromagnetic compatibility
GIL	Gas-insulated (transmission) line
GIS	(1) Gas-insulated substation (2) Gas-insulated switchgear
GST	Grounded specimen test
GUM	ISO/IEC Guide 98-3:2008
HF	High-frequency
HFCT	High-frequency current transformer
HV	High-voltage (in composite terms, e.g. HV tests)
HVAC	High alternating voltage
HVDC	High direct voltage
IEC	International Electrotechnical Commission
IEEE	Institute of Electrical and Electronic Engineers (USA)
IGBT	Power transistor

INL	Integral non-linearity
IVPD	Induced voltage partial discharge measurement
IVW	Induced voltage withstand test
L	Inductance
LI	Lightning impulse (in composite terms, e.g. LI test voltage)
LIC	Chopped lightning impulse
LIP	Liquid—impregnated paper (insulation)
LSB	Least significant bit
LTC	Life-time characteristic (or test)
LV	Low-voltage
M/G	Motor-generator (set)
ML	Maximum likelihood
MLM	Multiple level method
MS	Measuring system
MV	Medium voltage (do not mix-up with the dimension "Megavolt"!)
NMI	National Metrology Institute
OLI	Oscillating lightning impulse
OSI	Oscillating switching impulse
PD	Partial discharge (in composite terms, e.g. PD measurement)
PSM	Progressive stress method
R	Resistor
R&D	Research and development
RF	Radio frequency
RIV	Radio interference voltage
RMS	Reference measuring system
rms	Root of mean square
RoP	Record of performance
RVM	Return voltage measurement
SFC	Static frequency converter
SI	Switching impulse (in composite terms, e.g. SI test voltage)
TC	Technical Committee (of IEC)
TDG	Test data generator
TDR	Time domain reflectometry
THD	Total harmonic distortion
TRMS	Transfer reference measuring system
UDM	Up-and-down method
UHF	Ultra-high frequency
UHV	Ultra high voltage (in composite terms, e.g. UHV laboratory)
V	Voltage
VHF	Very-high frequency
X	Reactance
XLPE	Cross-linked polyethylene
Z	Impedance

Symbols

A	Area
a	Distance
α	Phase angel
ß	Overshoot magnitude
C	Capacitance
C_i	Impulse capacitance
C_l	Load capacitance
c	Velocity of light
D	Dielectric flux density
d	Diameter
dV	Voltage drop (DC)
Δf	Bandwidth
ΔT	Error of time measurement
ΔV	Voltage reduction (DC)
δ	(1) Air density (2) Weibull exponent (3) Ripple factor (4) Loss angel (tan δ)
δV	Ripple voltage (DC)
E	Electric field strength
e	(1) Elementary charge (e = $1.602 \cdot 10^{19}$ As) (2) Basis of natural logarithm (e = 2.71828…)
ε	Permittivity
ε_r	Relative permittivity
η	(1) 63 % quantile (Weibull and Gumbel distributions) (2) Utilization or efficiency factor
F	(1) Scale factor (2) Coulomb force
F_p	Polarization factor
F(f)	Transfer function
F(x)	Distribution function

f	Frequency
f_m	Rated frequency
f_t	Test frequency
f_0	(1) Natural frequency (2) Centre frequency (narrow band PD measurement)
f_1	Lower frequency limit
f_2	Upper frequency limit
Φ	Magnetic flux
φ	Phase angle
G	Current density
g	Parameter for atmospheric corrections
g(t)	Unit step response
H	(1) Magnetic field strength (2) Altitude
h	Humidity
I	Current
I_m	Rated current
I_{sc}	Short circuit current
i_L	Discharge current
K	Coverage factor for expanded uncertainty
K_t	Atmospheric correction factor
k	(1) Parameter for atmospheric corrections (2) Fixed factor
k_d	Constant in life-time characteristic
k_e	Field enhancement factor
k(f)	(1) Test voltage factor (2) Test voltage function for LI evaluation
k_1	Air density correction factor
k_2	Humidity correction factor
κ	Conductivity
L	(1) Inductance (2) Likelihood function
M	Pulse magnitude (PD measurement)
m	Estimated mean value
μ	Theoretical mean value
μ	Permeability
μ_r	Relative permeability
n	(1) Life time exponent (2) Number (e.g. of electrons)
ω	Angular frequency
P	Active test power

P_F	Feeding power
P_m	Dipole moment
P_N	Natural power of a transmission line
P_R	Loss power of a resonant circuit
p	(1) Probability (2) Pressure
p_0	Reference pressure
Q	(1) Charge (2) Quality factor (resonance circuit)
q	(1) Charge of a PD pulse (2) Charge of a leakage current pulse
R	(1) Resistance (2) Ratio between two results
R_d	Dampind resistance
R_f	Front resistor
R_t	Tail resistor
r	(1) Ratio (e.g. divider or transformer) (2) Radius
S	(1) Reactive test power (2) Steepness (LI/SI test voltage)
S_f	Scale factor
S_{50}	50 Hz equivalent test power
s_g	Mean square deviation (estimation of standard deviation)
σ	Standard deviation
T	Duration (AC period)
T_C	Time to chopping
T_N	Experimental response time
T_R	Residual response time
T_T	Duration of overshoot
T_1	Front time of LI voltage
T_2	Time to half-value of impulse voltages
t	(1) Temperature (2) Time
t_s	Settling time
t_t	Test time
t_0	Reference temperature
τ	Time constant
U	Expanded uncertainty
U_{cal}	Expanded uncertainty of calibration
U_M	Expanded uncertainty of measurement

u	Standard uncertainty
u_A	Type A standard uncertainty
u_B	Type B standard uncertainty
V	Voltage
V_B	Maximum of base curve (LI voltage)
V_E	Extreme value of recorded curve (LI voltage)
V_e	PD extinction voltage
V_F	Feeding voltage
V_i	(1) PD inception voltage (2) Impulse voltage
V_k	Short-circuit voltage (test transformer)
V_m	(1) Highest voltage of equipment, rated voltage (2) Arithmetic mean (DC)
V_{max}	Maximum of DC voltage
V_{min}	Minimum of DC voltage
V_n	Nominal voltage
V_{peak}	Peak voltage
V_r	Return or recovery voltage
V_{rms}	Root mean square value of voltage
V_T	Test voltage value
V(v)	Performance function
V_Σ	Cumulative charging voltage
V_0	(1) Line-to-ground voltage (2) Initial voltage for a test (3) Charging DC voltage
V_1	Primary voltage of a test transformer
V_2	Secondary voltage of a test transformer
V_{50}	50 % breakdown voltage
v	Variance
v(t)	Time-depending voltage
v_k	Short-circuit impedance of a test transformer
w	Number of turns of a winding
W	Energy
W_i	Impulse energy (impulse voltage generator)
X	Reactance
X_{res}	Short-circuit reactance of a transformer
Z	Impedance
Z_L	Surge impedance of a transmission line

Chapter 1
Introduction

Abstract High-voltage (HV) test and measuring techniques are considered in most general HV text books (e.g. Kuchler 2009; Kuffel et al. 2007; Beyer et al. 1986; Mosch et al. 1988; Schufft et al. 2007; Arora and Mosch 2011). There are teaching books on HV test techniques for students (Marx 1952; Kind and Feser 1999) as well as few text books on special fields, e.g. on HV measuring technique (Schwab 1981; Schon 2010). It is the aim of this book to supply a comprehensive survey on the state of the art of both, HV test and measuring techniques, for engineers in practice, graduates and students of master courses. A certain guideline for this is the relevant worldwide series of standards of the Technical Committee 42 (TC42: "HV Test and Measuring Techniques") of the *International Electrotechnical Commission (IEC),* largely identical with the corresponding standards of the Institute of *Electrical and Electronic Engineers (IEEE)*. This introduction contains also the relation between HV test and measuring techniques and the requirements of power systems with respect to the increasing transmission voltages and the principles of insulation coordination. Furthermore, HV testing for quality assurance and condition assessment in the life cycle of power equipment is investigated.

1.1 Development of Power Systems and Required High-Voltage Test Systems

Within the last 120 years, the development of transmission voltages of power systems from 10 to 1,200 kV has required a tremendous development of high-voltage (HV) engineering. This includes, e.g. the introduction of many new insulating materials and technologies, the precise calculation of electric fields, the knowledge about the phenomena in dielectrics under the influence of the electric field and the understanding of electric discharge processes. Nevertheless, as an empirical technical science, HV engineering remains closely related to experiments and verifications of calculations, dimensioning and manufacturing by HV

W. Hauschild and E. Lemke, *High-Voltage Test and Measuring Techniques*,
DOI: 10.1007/978-3-642-45352-6_1, © Springer-Verlag Berlin Heidelberg 2014

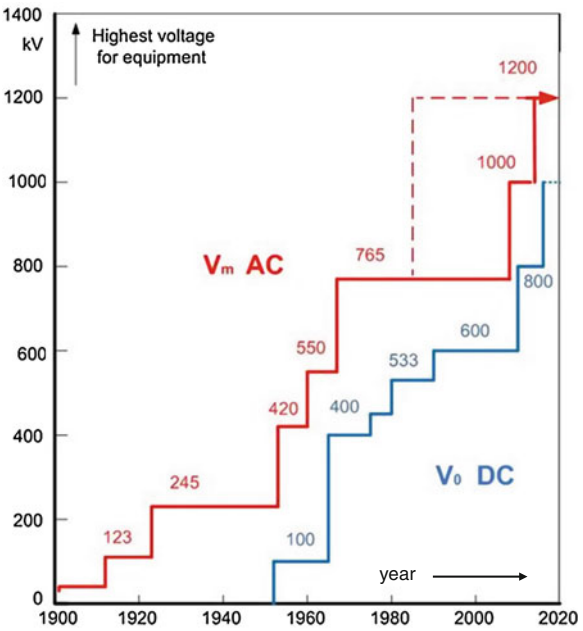

Fig. 1.1 History of HVAC and HVDC transmission systems

tests. The reasons for that are, e.g. unavoidable defects of the structure of technical insulating materials, imperfections of technical electrodes, but also failures of production and assembling. Therefore, in parallel to the development of HV engineering, national and international standards for HV testing have been developed, as well as equipment for the generation of test voltages and for measurements of (and at) these voltages.

Since the early beginning of the wider application of electrical energy, its transmission from the place of generation (power station) to that of consumption (e.g. industry, households, public users) influences the energy cost remarkably. The transportable power of a high-alternating voltage (HVAC) overhead line is limited by its surge impedance Z_L to a power transfer capability of approximately

$$P_L = V^2/Z_L. \tag{1.1}$$

Whereas the surge impedance ($Z_L \approx 250\ \Omega$) can only be influenced within certain limits by the geometry of the overhead line, the power transfer capability is mainly determined by the height of the transmission voltage, e.g. the power transfer capability of a 400 kV system is only a quarter of that of an 800 kV system. Consequently, increasing energy demand requires higher HVAC transmission voltages. Remarkable increases in the ratings *of HVAC transmissions are* to 123 kV in 1912 in Germany, to the 245 kV level in 1926 (USA), to 420 kV in 1952 (Sweden), to 800 kV in 1966 (Canada and Russia) and to UHV (1,000–1,200 kV in 2010, China) (Fig. 1.1).

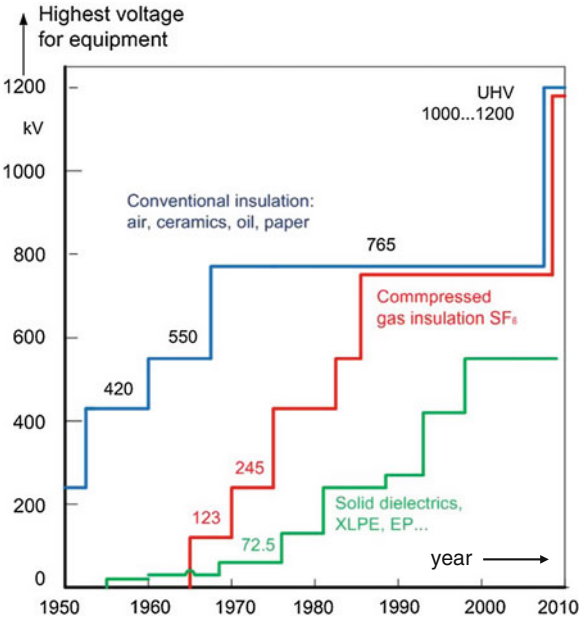

Fig. 1.2 History of the application of insulating materials

Because at direct voltage, no surge impedance becomes effective; the limitation of the power transfer capability is mainly caused by the current losses. For identical rated voltages, the HVDC power transfer capability is about three times higher than that at HVAC. This means that one 800-kV HVDC line with an efficiency of 94 % replaces three 800 kV HVAC overhead lines with an efficiency of only 88 % (Swedish Power Cycle 2009). But *HVDC transmission* requires expensive converter stations. Therefore, the application of HVDC transmission has been limited to very long transmission lines, where the cost reduction for the line compensates the higher station cost. The present cost reduction of power electronic elements, efficient HVDC cable production and other technical advantages of HVDC transmission has triggered worldwide activities in that field (Long and Nilsson 2007; Gockenbach et al. 2007; Yu et al. 2007). The historical development (Fig. 1.1) shows that the 1,000 kV level is reached in China now, but the next levels above 1,000 kV or more are under preparation (IEC TC115 2010).

The HV test and measuring techniques have to be able to test components which belong to both HVAC and HVDC power systems. But additionally, also the kind of insulation to be tested determines the kind of the test equipment. The "classical" insulating materials (air, ceramics, glass, oil, paper) are completed by insulating gases, e.g. SF_6 for gas-insulated substations and transmission lines (GIS, GIL), and synthetic solid materials, e.g. epoxy resin for instrument transformers and polyethylene for cables (Fig. 1.2).

The basic principle of HV testing expresses that test voltage stresses shall represent the characteristic stresses in service (IEC 60071-1). When electric power transmission started, not all these stresses were known. Furthermore, the kind and height of stresses depend on the system configuration, the used apparatus, the environmental conditions and other influences. The historical development of HV testing is closely related to the development of and the knowledge on power systems. It can be characterized by the following steps:

HV testing started in the first decade of the twentieth century with *alternating test voltages* of power frequency (50 or 60 Hz) (Spiegelberg 2003). The test voltages have been generated by test transformers, later also by transformer cascades (Fig. 1.3a, see also Sect. 3.1). It was assumed that suited *HVAC tests* would represent all possible HV stresses in service. Of course, HVDC equipment has been tested with DC voltages generated by DC generators (Fig. 1.3b, see also Sect. 4.1).

But independently on the performed HVAC tests, equipment has been destroyed in power systems, e.g. as a consequence of lightning strokes, which caused *external over-voltages*. These overvoltage impulses are characterized by front times of few microseconds and tail times of several ten microseconds. Based on that knowledge, tests with *lightning impulse (LI) test voltages* (front time $\approx$ 1…2 μs, time to half-value $\approx$ 40…60 μs) have been introduced in the 1930s. For LI voltage testing, suited generators have been developed (Fig. 1.3c, see also Sect. 7.1).

Another 30 years later, it has been found that *internal over-voltages* lead to lower breakdown voltages of long air gaps than LI or AC voltage stresses. They are caused by switching operations in the power system. Their durations lay between some hundreds of microseconds and few milliseconds. As a consequence, *switching impulse (SI) test voltages* have been introduced in the 1960s. *SI test voltages* can be generated by the same type of generators as *LI test voltages* (but with larger electrodes, Fig. 1.3d, see also Sect. 7.1) or by test transformers.

Again 30 years later, it has been found that disconnector switching of gas-insulated substations (GIS) causes oscillating *over-voltages of very fast front* (VFF, several ten nanoseconds) which may harm the GIS insulation itself, but also attached equipment. Whereas a test with *very fast front (VFF) test voltage* has been introduced for GIS, it is under discussion for other components of power systems (7.1.4).

1.2 The International Electrotechnical Commission and Its Standards

The International Electrotechnical Commission (IEC) is the worldwide organization for international standards on electrical engineering, electronics and information technology. It has been founded in 1906, and its first president was the famous physicist Lord Kelvin. Today, about 60 national committees are IEC

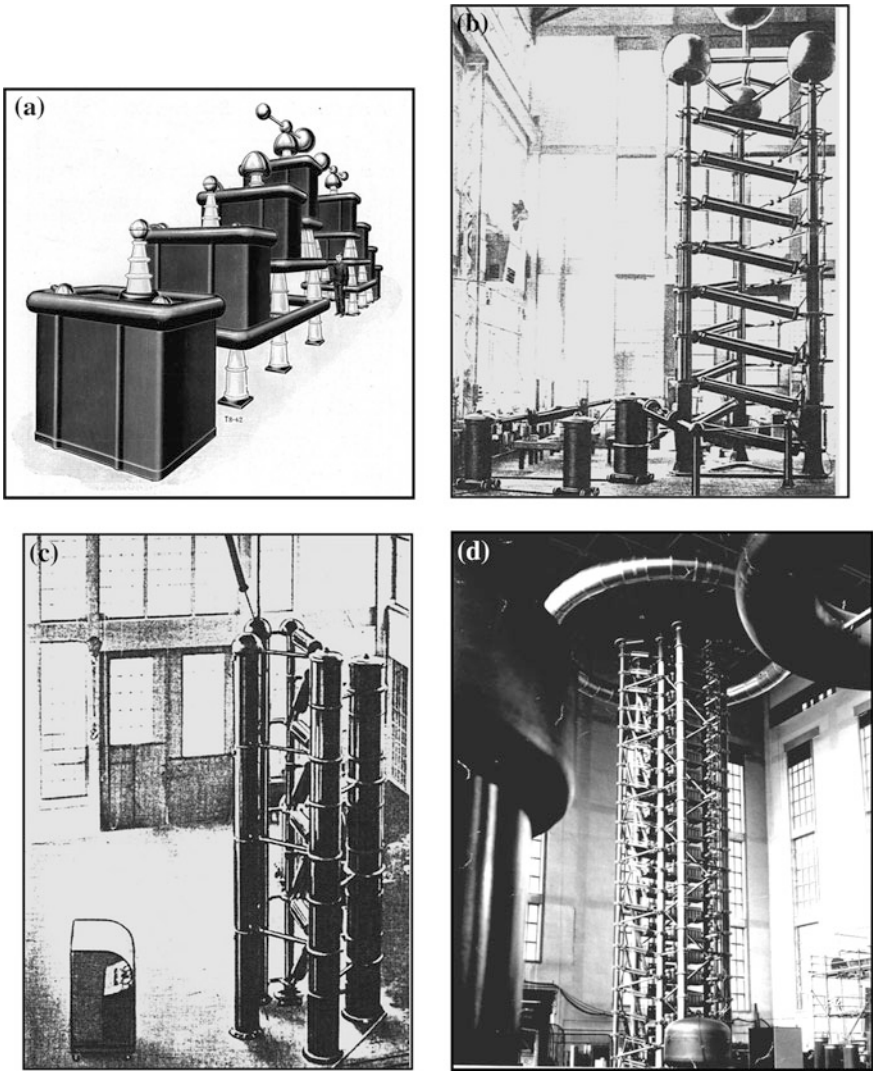

Fig. 1.3 Historical test voltage generators **a** world's first 1,000 kV cascade transformer (Koch and Sterzel Dresden 1923) **b** 1,000 kV DC test voltage generator (Koch and Sterzel Dresden 1936) **c** 2,000 kV LI test voltage generator (Koch and Sterzel Dresden 1929) **d** 7,000 kV LI/SI test voltage generator (TuR Dresden 1979)

members. During its first years, IEC tried to harmonize the different national standards. But now, more and more national committees contribute to maintaining existing or establishing new IEC standards which are later overtaken as national and regional standards (e.g. CENELEC Standards of the European Union). This book refers mainly to IEC Standards and mentions also relevant standards of the US organization "*Institute of Electrical and Electronic Engineers*" *(IEEE)* which play an important role in some parts of the world. IEEE publishes also "*IEEE Guides*" which may overtake the role of missing text books. The IEEE Guides supply only recommendations and no requirements as standards are doing. The actual trend shows a closer cooperation between IEC and IEEE for the harmonization of IEC and IEEE Standards.

The structure of IEC is given in Fig. 1.4: The national committees send delegates to the IEC Council which is the IEC parliament and controls the IEC activities performed by the IEC Executive Committee. The Executive Committee is supported by three management boards, one of them related to IEC Standards. For the different fields of the IEC activities, the Management Board is supported by special groups. The active standardization work is done by Technical Committees (TC) and Subcommittees (SC). Each TC or SC is responsible for a certain number of standards of a special field. Existing IEC Standards are observed by Maintenance Groups (MG); new IEC Standards are established by Working Groups (WG) based on proposals of national committees. Each National Committee can be a TC/SC member or observer (or not attend the activities of certain TCs and SCs) and sends members to the active WGs.

There are TCs which have to maintain IEC Standards important for power systems and all types of apparatus. These are so-called *horizontal standards*; the related TCs are shown in the first column of Table 1.1. IEC Standards related to apparatus or equipment are called "*vertical*" *(or apparatus) standards*. When a vertical standard is developed, all relevant horizontal standards shall be considered. Vice versa, during the development of a horizontal standard, the requirements of different apparatus should be known. This book is closely related to the tasks of the TC 42 "High-voltage and high-current test techniques". It explains the scientific and technical background of the TC 42 standards, but cannot replace any of them. Rather, it should be understood as an application guide to the relevant IEC Standards and stimulate their application.

1.3 Insulation Coordination and Its Verification by HV Testing

In service, an electrical insulation is stressed with the *operational voltage* (including its temporary increase, e.g. in case of a load drop) and with the overvoltages mentioned above. The reliability of a power system has to be guaranteed under all possible stresses of its insulations. This is realized by the *insulation coordination* and described in the relevant group of IEC Standards (IEC 60071).

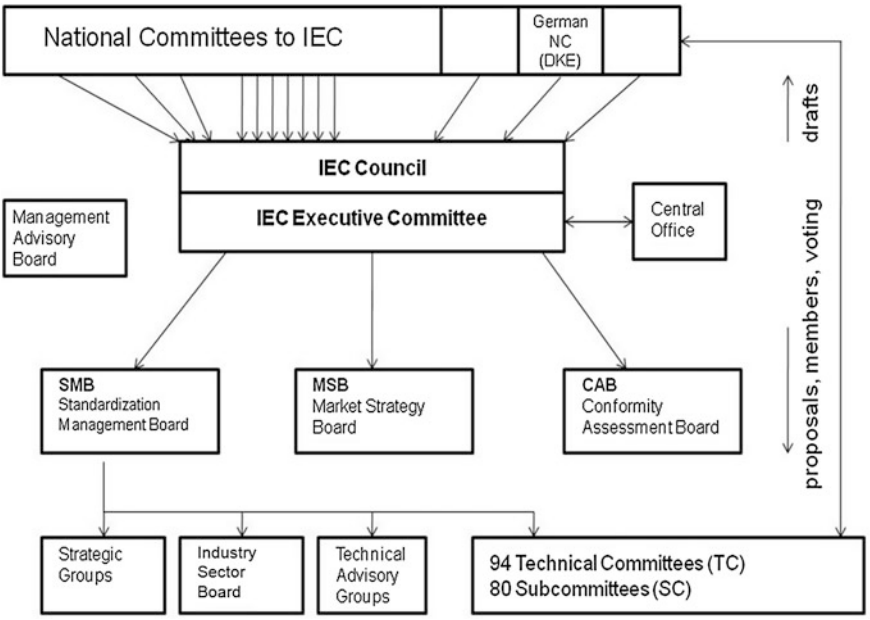

Fig. 1.4 Structure of the International Electrotechnical Commission (IEC)

Table 1.1 IEC technical committees for horizontal and vertical standards (examples)

Horizontal Technical Committees for systems and basic tasks	**Vertical Technical Committees** TC / SC for apparatus and equipment								
	Rotating Machines TC 2	Power Transformers TC 14	Switchgear TC 17	Cables TC 20	Power Electronics for T & D SC 22F	Capacitors TC 33	Insulators TC3 6	Arresters TC 37	Instrument Transformers TC38
TC 1 Terminology									
TC 8 System Aspects									
TC 28 Insulation Coordination									
TC 42 HV Test Techniques									
TC 77 Electrom. Compatibility									
TC 104 Environment. Conditions									
TC 115 HVDC Transmission									

Insulation coordination is the correlation of the *withstand voltages* of different apparatus in a power system among each other and with the characteristics of *protective devices*. Today, protective devices (IEC 60099-4 2009) are *mainly metal oxide arresters (MOA)*, and partly conventional silicon carbide arresters with internal gaps and protection air gaps are still in use. An ideal protective device conducts electric current for voltages above the *protection level* and is an insulator below that voltage (A MOA is near to that characteristic). In the design of a power system, protective devices are installed at sensitive points, guaranteeing the protection level and protecting the insulation from excessive over-voltages.

The *insulation level* of the apparatus is selected in such a way that it is—under consideration of economic viewpoints—by a safety margin below the protection level. The insulation levels are defined by values of the relevant test voltages. The insulation under test must withstand the test voltage in a certain procedure. Usually, the AC or DC test voltage procedure is a 1-min stress (see Sects. 3.6 and 6.5); an impulse voltage test consists of a number of impulses defined according to the kind of insulation (see Sect. 7.3.2). Tables 1.2 and 1.3 deliver the test voltages for apparatus of AC three-phase power systems, depending on its *highest voltage for equipment* V_m (rms value of the phase-to-phase voltage).

Note: Each apparatus has a nominal voltage (e.g. $V_n = 380$ or 400 kV), but the insulation is designed for insulation coordination according to the highest voltage of a group of nominal voltages. This voltage is also called rated voltage (IEC 60038-2009). For the mentioned nominal voltages, the insulation is designed and must be tested according to the rated voltage $V_m = 420$ kV.

For equipment of $V_m = 3.6$–245 kV, the AC voltage test covers also withstand against internal (switching) over-voltages and no SI impulse voltage withstand test is specified. For equipment of $V_m = 300$–1,200 kV, the switching impulse test covers for air insulations also the AC voltage test; for internal insulations, the AC test voltages are specified in the relevant apparatus standards.

For one and the same rated voltage, different protection levels can be applied depending on the required reliability, safety and/or economy. The example of Table 1.4 shows this for the rated voltage $V_m = 420$ kV: The three main lines represent three different protection levels, and each line is divided into two lines applicable for external (air) and internal insulation. The AC test voltages are related to internal insulation only and given in the relevant apparatus standard.

A diagram of the test voltage values versus the rated voltages (Fig. 1.5) shows that the SI test voltage (peak value) is identical with the AC test peak voltage (Tables 1.2, 1.3, 1.4 show AC rms values!). The chopped LI test voltages (LIC) are 10 % higher than the full LI test voltages. The diagram may help in the selection of the HV test systems required for a HV test field (See 9.1).

Table 1.2 Standard insulation levels for HVAC equipment $V_m = 3.6$–245 kV (IEC 60071-2: 2006)

Highest voltage for equipment V_m kV (rms, phase-to-phase)	Short-duration AC withstand voltage V_t kV (peak/$\sqrt{2}$, phase-to-earth)	LI withstand voltage V_t kV (peak value)
3.6	10	20
	10	40
7.2	20	40
	20	60
12	28	60
	28	75
	28	95
24	50	95
	50	125
	50	145
36	70	145
	70	170
72.5	140	325
123	(185)	(450)
	230	550
145	(185)	(450)
	230	550
	275	650
170	(230)	(550)
	275	650
	325	750
245	(275)	(650)
	(325)	(750)
	360	850
	395	950
	460	1,050

Explanation
Usually, the phase-to-earth withstand voltages are also applied to phase-to-phase insulation. If the values in brackets are considered too low, additional phase-to-phase withstand voltage tests are needed

Example: For a transformer test field, the selection of the rated voltage of an impulse voltage test system (equal to the cumulative charging voltage of the generator, see 7.1.1) shall be shown. Outgoing from the highest test voltage (LIC in Fig. 1.5), one has to consider that the utilization factor for large test objects may go down to $\eta = 0.85$. Furthermore, for internal development tests, a test voltage 20 % higher than the LIC withstand voltage might be necessary. This means the rated voltage of the impulse voltage test system should be by a factor $k = 1.2/0.85 \approx 1.4$ higher than the highest LIC test voltage. This means that for the rated voltage $V_m = 800$ kV, a 3,000 kV impulse test system is sufficient. If a later extension of the test capability to 1,200 kV equipment is planned, a 4,000 kV test system should be considered. The selection of impulse test systems according to Fig. 1.5 is recommended.

Table 1.3 Standard insulation levels for HVAC equipment V_m = 300–1,200 kV (IEC 60071-2: 2006), (IEC 60071-2-Amendment 2010)

Highest voltage for equipment V_m kV (rms, phase-to-phase)	SI withstand voltage kV (peak value)			LI withstand voltage[c] V_t kV (peak value)
	Longitudinal insulation[a]	Phase-to-earth insulation	Phase-to-phase insulation[b]	
300	750	750	1,125	850
	750	750	1,125	950
	750	850	1,275	950
	750	850	1,175	1,050
362	850	850	1,275	950
	850	850	1,275	1,050
	850	950	1,425	1,050
	850	950	1,425	1,175
420	850	850	1,360	1,050
	850	850	1,360	1,175
	950	950	1,425	1,175
	950	950	1,425	1,300
	950	1,050	1,575	1,300
	950	1,050	1,575	1,425
550	950	950	1,615	1,175
	950	950	1,615	1,300
	950	1,050	1,680	1,300
	950	1,050	1,680	1,425
	950	1,175	1,763	1,425
	1,050	1,175	1,763	1,550
800	1,175	1,300	2,210	1,675
	1,175	1,300	2,210	1,800
	1,175	1,425	2,423	1,800
	1,175	1,425	2,423	1,950
	1,175	1,550	2,480	1,950
	1,300	1,550	2,480	2,100
1,200	1,425	1,550	2,635	2,100
	1,425	1,550	2,635	2,250
	1,550	1,675	2,764	2,250
	1,550	1,675	2,764	2,400
	1,675	1,800	2,880	2,400
	1,675	1,800	2,880	2,550

Explanations

[a] Longitudinal insulation means the insulation between different parts of the grid, realized e.g. by disconnectors and tested with combined voltages (see Sect. 8.1) The column gives only the value of the SI voltage component of the relevant combined voltage test. The peak value of the AC component of opposite polarity is $(V_m \cdot \sqrt{2}/\sqrt{3})$

[b] This is the peak value of the combined voltage in the relevant combined SI/AC voltage test

[c] These values apply to both, phase-to-earth and phase-to-phase insulation. For longitudinal insulation, they apply as the standard rated LI component of the relevant combined voltage test, while the peak of the AC component of opposite polarity is $0.7 \cdot (V_m \cdot \sqrt{2}/\sqrt{3})$

Table 1.4 Simplified example for the selection of withstand test voltages

Highest voltage for equipment V_m	**AC test**	**SI test**	**LI test**	**LIC test** (transformers only)	**Application to insulation**
420 kV	(630kV)	850 kV	1050 kV	1175 kV	External insulation (atmospheric air)
			1175 kV	1300 kV	Internal insulation (SF_6, oil, solids)
	(680 kV)	950 kV	1175 kV	1300 kV	External insulation
			1300 kV	1425 kV	Internal insulation
	(680 kV)	1050 kV	1300 kV	1425 kV	External insulation
			1425 kV	1570 kV	Internal insulation

Note Consider that most test voltages are applied between phase and ground. The reference value for that is the *line-to-ground voltage* $V_0 = V_m/\sqrt{3}$, respectively, its peak voltage $V_p = \sqrt{2}\ V_0$.)

For HVDC connections, no rated voltages exist, because the nominal voltages and currents of the present point-to-point HVDC connections are optimized according to the available power electronic components (One can assume that rated voltages will be introduced, when HVDC grids (CENELEC 2010) are realized). The relevant standard on insulation coordination (IEC 60071-5: 2002) does not deliver test voltages but only formulas which allow the calculation of test voltage ranges from the nominal voltages of the HVDC connection (Fig. 1.6). For HVDC equipment, the difference between LI and SI test voltages is lower than for HVAC equipment. Considering the lower efficiency of the SI voltage generation $(\eta \leq 0.75)$, the selection of impulse voltage test systems should take the required SI test voltages into consideration.

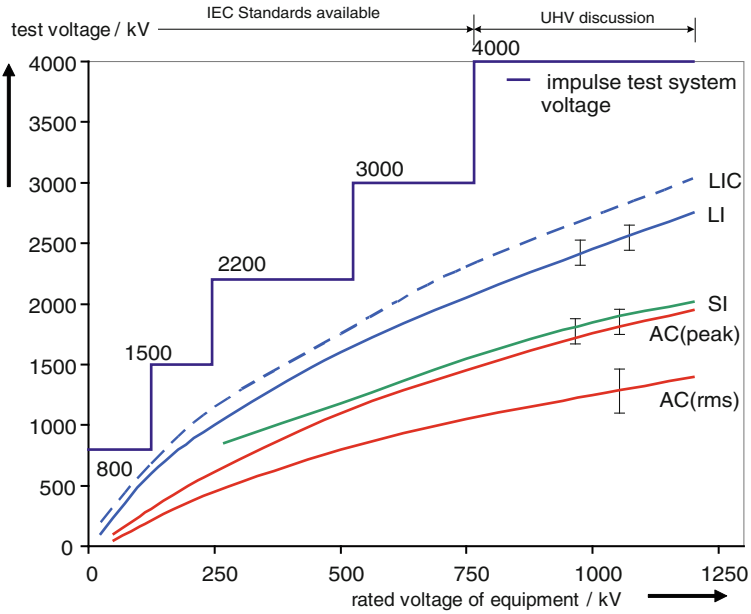

Fig. 1.5 Highest withstand test voltages for HVAC equipment and selection of impulse voltage test systems

1.4 Tests and Measurements in the Life Cycle of Power Equipment

The principles of insulation coordination are only applied to new equipment and verified in factory tests. These include *type tests* and *routine tests*. Both tests are *quality tests* of the insulation; a successful type test demonstrates the correct design according to the test voltages (Tables 1.2, 1.3), and a successful routine test verifies the correct production according to the confirmed design. The two tests are not the only tests in the *life cycle* of the insulations of power equipment (Fig. 1.7).

Development tests at model insulations are often performed before the insulation is finally designed. When type and routine tests are successfully performed, the power equipment is transported to the site and assembled there. It may happen that defects of the insulation are caused by transportation and assembling. Also some huge apparatus (e.g. power transformers) cannot be transported as complete units. The final assembling takes place not in the factory, but on site. Therefore, additional *quality acceptance tests* (*commissioning tests*) or even the routine test must be performed on site with mobile HV test systems. This test should always be performed in relation to factory tests (Fig. 1.7).

After the correct quality is confirmed in a successful on-site test, the equipment is overtaken to the user, can be commissioned and has to operate under electrical, thermal, mechanical and/or environmental influences. These influences cause an

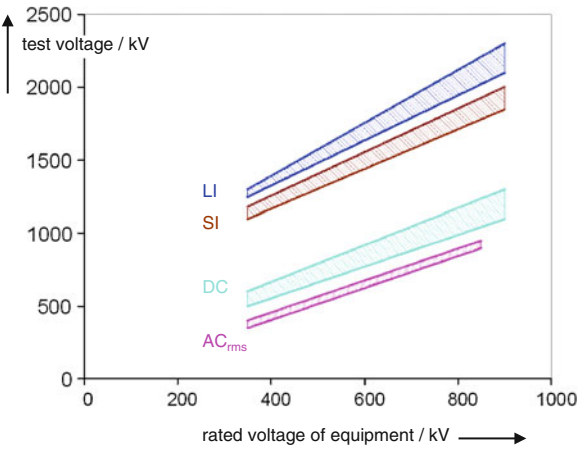

Fig. 1.6 Withstand test voltage ranges for HVDC equipment

ageing process of the insulation until—after tens of years—the end of the life cycle is reached. In the past, the duration of the life cycle has been estimated and the end of use has been defined by the user independently on the real condition of the equipment. To reduce the life cycle cost, tests and measurements have been introduced for *condition assessment* of the insulation and estimation of the remaining life time (Zhang et al. 2007; Olearczyk et al. 2010; Balzer et al. 2004). In opposite to the quality tests, these tests for condition assessment shall be called *diagnostic tests*.

Both quality and diagnostic tests require a test voltage application and measurements (in minimum a voltage measurement, but very often partial discharge or dielectric measurements). A withstand test is a *direct test*, which is directly related to the insulation capability of the test object. A healthy insulation which passes the test has a high withstand voltage. A defective insulation has a low withstand voltage and fails the test (This is much better than it fails in service!). It must be considered that a voltage stress may cause life-time consumption. An insulation shall be designed in such a way that the life-time consumption of the healthy insulation is negligible during a withstand test, whereas a defective insulation breaks down. When a withstand test is completed by a parallel partial discharge (PD) measurement (see Sect. 2.5), it can be excluded that such a successful "*PD-monitored*" *withstand test* has caused or enlarged insulation defects.

When a diagnostic test is decided according to measurements of a single parameter or a set of parameters (preferably of partial discharges), the test result must be compared with pre-given limits. These limits shall be related by experience or any physical model to the remaining life time. The sharpness of such an *indirect test* is lower than that of a monitored withstand test. Sometimes, it is published that withstand tests are "destructive" and diagnostic measurements are "non-destructive". Such qualifying terms are not suited to describe the quality and sharpness of a diagnostic HV test.

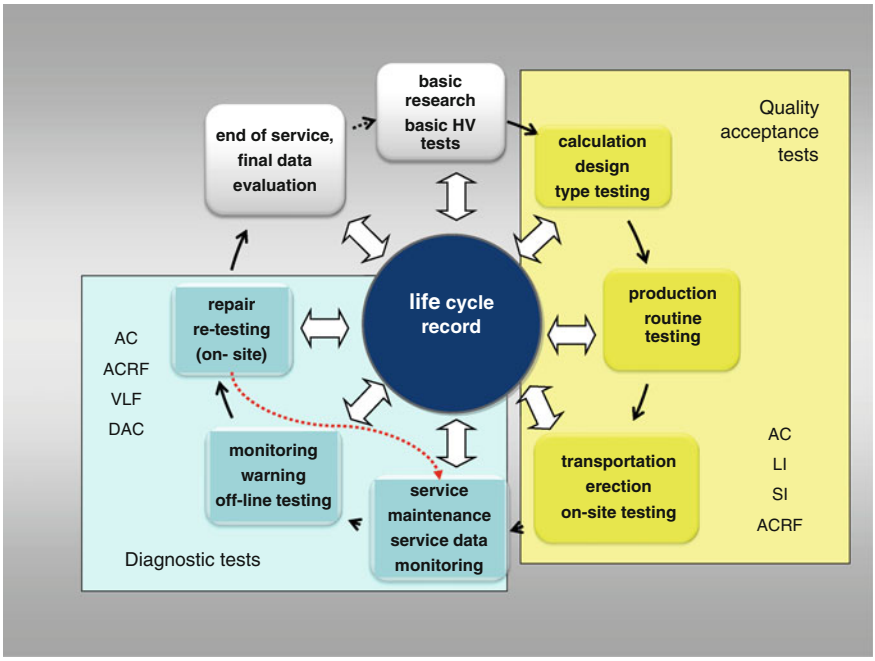

Fig. 1.7 Tests and measurements in the life cycle of HV insulation

Diagnostic measurements performed at operational voltage in service are called *on-line monitoring* (CIGRE TF D1.02.08 2005) (Monitoring is not only related to dielectric measurement; there is also monitoring of voltage, current, thermal or mechanic parameters). Automatic monitoring delivers a warning when the measured parameter exceeds a preset limit.

This brings one back to Fig. 1.7: In service, online monitored data deliver the data trend, describe the situation and may supply data for maintenance. In case of a warning by the monitoring system, the reason of the defect must be clarified. Often, the monitored data are not sufficient for a clarification. In that case, a more detailed investigation is necessary, e.g. by an (off-line) on-site test including appropriate measurements. This test with a separate test voltage source enables a withstand voltage test (with a test voltage value well adapted to the age of the insulation) and the measurement of the parameters depending on the applied voltage (instead of only one fixed voltage at monitoring). After the condition of the insulation has been clarified, it might be decided to repair the equipment in the factory or on site. Then, one or several loops in the scheme appear, and one has to go back to on-site testing and service again. At the end of the life cycle, the equipment is dismantled and also this may deliver some data for future development.

The data of all tests and measurements during the life cycle must be recorded in the—preferably electronic—life cycle record of the equipment. The life cycle

record is the most important document of the equipment, which delivers the trend of parameters and enables qualified decisions. As all stages of the life cycle are connected together, it must be stressed that quality and diagnostic testing have a common physical background. This is often forgotten, when quality testing and diagnostic testing/monitoring are considered separately. The only reference for all HV quality on-site tests of new equipment is the factory testing based on the test voltages of the insulation coordination. This may include that also the test voltages for diagnostic testing of service-aged equipment should be in close relation to stresses in service.

Chapter 2
Basics of High-Voltage Test Techniques

Abstract High-voltage (HV) testing utilizes the phenomena in electrical insulations under the influence of the electric field for the definition of test procedures and acceptance criteria. The phenomena—e.g., breakdown, conductivity, polarization and dielectric losses—depend on the insulating material, on the electric field generated by the test voltages and shaped by the electrodes as well as on environmental influences. Considering the phenomena, this chapter describes the common basics of HV test techniques, independent on the kind of the stressing test voltage. All details related to the different test voltages are considered in the relevant Chaps. 3–8.

2.1 External and Internal Insulations in the Electric Field

In this section definitions of phenomena in electrical insulations are introduced. The insulations are classified for the purpose of high-voltage (HV) testing. Furthermore environmental influences to external insulation and their treatment for HV testing are explained.

2.1.1 Principles and Definitions

When an electrical insulation is stressed in the electric field, ionization causes electrical discharges which may grow from one electrode of high potential to the one of low potential or vice versa. This may cause a high current rise, i.e., the dielectric looses its insulation property and thus its function to separate different potentials in an electric apparatus or equipment. For the purpose of this book, this phenomenon shall be called "*breakdown*" related to the stressing voltage:

W. Hauschild and E. Lemke, *High-Voltage Test and Measuring Techniques*,
DOI: 10.1007/978-3-642-45352-6_2, © Springer-Verlag Berlin Heidelberg 2014

Definition The breakdown is the failure of insulation under electric stress, in which the discharge completely bridges the insulation under test and reduces the voltage between electrodes to practically zero (collapse of voltage).

> **Note** In IEC 60060-1 (2010) this phenomenon is referred to as "*disruptive discharge*". There are also other terms, like "*flashover*" when the breakdown is related to a discharge over the surface of a dielectric in a gaseous or liquid dielectric, "*puncture*" when it occurs through a solid dielectric and "*sparkover*" when it occurs in gaseous or liquid dielectrics.

In homogenous and *slightly non-homogenous fields* a breakdown occurs when a critical strength of the stressing field is reached. *In strongly non-homogenous fields*, *a local stress concentration causes a localized electrical partial discharge (PD)* without bridging the whole insulation and without breakdown of the stressing voltage.

Definition A partial discharge is a localized electrical discharge that only partly bridges the insulation between electrodes, for details see Chap. 4.

Figure 1.2 shows the application of some important insulating materials. Till today atmospheric air is applied as the most important dielectric of the external insulation of transmission lines and the equipment of outdoor substations.

Definition External insulation means air insulation including the outer surfaces of solid insulation of equipment exposed to the electric field, atmospheric conditions (air pressure, temperature, humidity) and to other environmental influences (rain, snow, ice, pollution, fire, radiation, vermin).

External insulation recovers its insulation behaviour in most cases after a breakdown and is then called a *self-restoring insulation*. In opposite to that, the *internal insulation* of apparatus and equipment—such as transformers, gas-insulated switchgear (GIS), rotating machines or cables—is more affected by discharges, often even destroyed when a breakdown is caused by a HV stress.

Definition Internal insulation of solid, liquid or gaseous components is protected from direct influences of external conditions such as pollution, humidity and vermin.

Solid and liquid- or gas-impregnated laminated insulation elements are non-self-restoring insulations. Some insulation is partly self-restoring, particularly when it consists e.g., of gaseous and solid elements. An example is the insulation of a GIS which uses SF_6 gas and solid spacers. In case of a breakdown in an oil- or SF_6 gas-filled tank, the insulation behaviour is not completely lost and recovers partly. After a larger number of breakdowns, partly self-restoring elements have a remarkably reduced breakdown voltage and are not longer reliable.

The insulation characteristic has consequences for HV testing: Whereas for HV testing of external insulation, the atmospheric and environmental influences have to be taken into consideration, internal insulation does not require related special test conditions. In case of self-restoring insulation, breakdowns may occur during HV tests. For partly self-restoring insulation, a breakdown would only be

acceptable in the self-restoring part of the insulation. In case of non-self restoring insulation no breakdown can be accepted during a HV test. For the details see Sect. 2.4 and the relevant subsections in Chaps. 3 and 6–8.

The test procedures should guarantee the *accuracy* and the *reproducibility* of the test results under the actual conditions of the HV test. The different test procedures necessary for external and internal insulations should deliver comparable test results. This requires regard to various factors such as

- random nature of the breakdown process and the test results,
- polarity dependence of the tested or measured characteristics,
- acclimatisation of test object to the test conditions,
- simulation of service conditions during the test,
- correction of differences between standard, test and service conditions, and
- possible deterioration of the test object by repetitive voltage applications.

2.1.2 HV Dry Tests on External Insulation Including Atmospheric Correction Factors

HV dry tests have to be applied for all external insulations. The arrangement of the test object may affect the breakdown behaviour and consequently the test result. The electric field at the test object is influenced by *proximity effects* such as distances to ground, walls or ceiling of the test room as well as to other earthed or energized structures nearby. As a rule of thumb, the *clearance* to all external structures should be not less than 1.5 times the length of the possible discharge path along the test object. For maximum AC and SI test voltages above 750 kV (peak), recommendations for the minimum clearances to external earthed or energized structures are given in Fig. 2.1 (IEC 60060-1:2010). When the necessary clearances are considered, the test object will not be affected by the surrounding structures.

Atmospheric conditions may vary in wide ranges on the earth. Nevertheless, HV transmission lines and equipment with external insulations have to work nearly everywhere. This means on one hand that the atmospheric service conditions for HV equipment must be specified (and for these conditions it must be tested), and on the other hand the test voltage values for insulation coordination (IEC 60071: 2010) must be related to a *standard reference atmosphere* (IEC 60060-1:2010):

- temperature $T_0 = 20$ °C (293 K)
- absolute air pressure $p_0 = 1{,}013$ hPa (1,013 mbar)
- absolute humidity $h_0 = 11$ g/m^3

The temperature shall be measured with an expanded uncertainty $t \leq 1$ °C, the ambient pressure with $p \leq 2$ hPa. The absolute humidity$h$ can be directly measured with so-called ventilated dry-and wet-bulb thermometers or determined from the relative humidity$R$ and the temperature t by the formula (IEC 60060-1:2010):

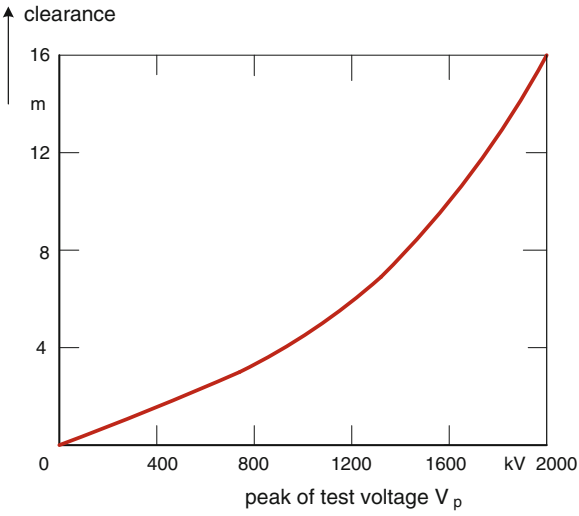

Fig. 2.1 Recommended clearances between test object and extraneous energized or earthed structures

$$h = \frac{6.11 \cdot R \cdot e^{\frac{17.6 \cdot t}{243+t}}}{0.4615 \cdot (273+t)}. \tag{2.1}$$

If HV equipment for a certain altitude shall be designed according to the pressure-corrected test voltages, the relationship between altitude H/m and pressure p/hPa is given by

$$p = 1,013 \cdot e^{\frac{H}{8150}}. \tag{2.2}$$

A test voltage correction for air pressure based on this formula can be recommended for altitudes up to 3,000 m. For more details see Pigini et al. (1985), Ramirez et al. (1987) and Sun et al. (2009). The temperature t and the pressure p determine the *air density*δ, which influences the breakdown process directly:

$$\delta = \frac{p}{p_0} \cdot \frac{273+t_0}{273+t}. \tag{2.3}$$

The air density delivers together with the air density correction exponent m (Table 2.1) the air density correction factor

$$k_1 = \delta^m. \tag{2.4}$$

The humidity affects the breakdown process especially when it is determined by partial discharges. These are influenced by the kind of test voltage. Therefore, for different test voltages different humidity correction factors k_2 have to be applied, which are calculated with the parameter k and the humidity correction exponent w

$$k_2 = k^w, \tag{2.5}$$

Table 2.1 Air density and humidity correction exponents m and w according to IEC 60060-1:2010

g	m	w
<0.2	0	0
0.2–1.0	$g(g - 0.2)/0.8$	$g(g - 0.2)/0.8$
1.0–1.2	1.0	1.0
1.2–2.0	1.0	$(2.2 - g)(2.0 - g)/0.8$
>2.0	1.0	0

with

$$\begin{aligned}
&\text{DC}: \quad k = 1 + 0.014(h/\delta - 11) - 0.00022(h/\delta - 11)^2 \quad \text{for } 1\,\text{g/m}^3 < h/\delta, < 15\ \text{g/m}^3,\\
&\text{AC}: \quad k = 1 + 0.012(h/\delta - 11) \quad \text{for } 1\,\text{g/m}^3 < h/\delta < 15\ \text{g/m}^3,\\
&\text{LI/SI}: \quad k = 1 + 0.010(h/\delta - 11) \quad \text{for } 1\,\text{g/m}^3 < h/\delta < 20\ \text{g/m}^3.
\end{aligned}$$

The correction exponents m and w describe the characteristic of possible partial discharges and are calculated utilizing a parameter

$$g = \frac{V_{50}}{500 \cdot L \cdot \delta \cdot k}, \tag{2.6}$$

with

V_{50} Measured or estimated 50 % breakdown voltage at the actual atmospheric conditions, in kV (peak),
L Minimum discharge path, in m,
δ Relative air density and
k Dimension-less parameter defined with formula (2.5).

Note For withstand tests it can be assumed $V_{50} \approx 1.1 \cdot V_t$ (test voltage). Depending on the parameter g (Eq. 2.6), Table 2.1 or Fig. 2.2 delivers the exponents m and w.

According to IEC 60060-1:2010 the atmospheric correction factor

$$K_t = k_1 \cdot k_2, \tag{2.7}$$

shall be used to correct a measured breakdown voltage V to a value under standard reference atmosphere

$$V_0 = V/K_t. \tag{2.8}$$

Vice versa when a test voltage V_0 is specified for standard reference atmosphere, the actual test voltage value can be calculated by the converse procedure:

$$V = K_t \cdot V_0. \tag{2.9}$$

Because the converse procedure uses the breakdown voltage V_{50} (Eq. 2.6), the applicability of Eq. (2.9) is limited to values of K_t close to unity, for $K_t < 0.95$ it is

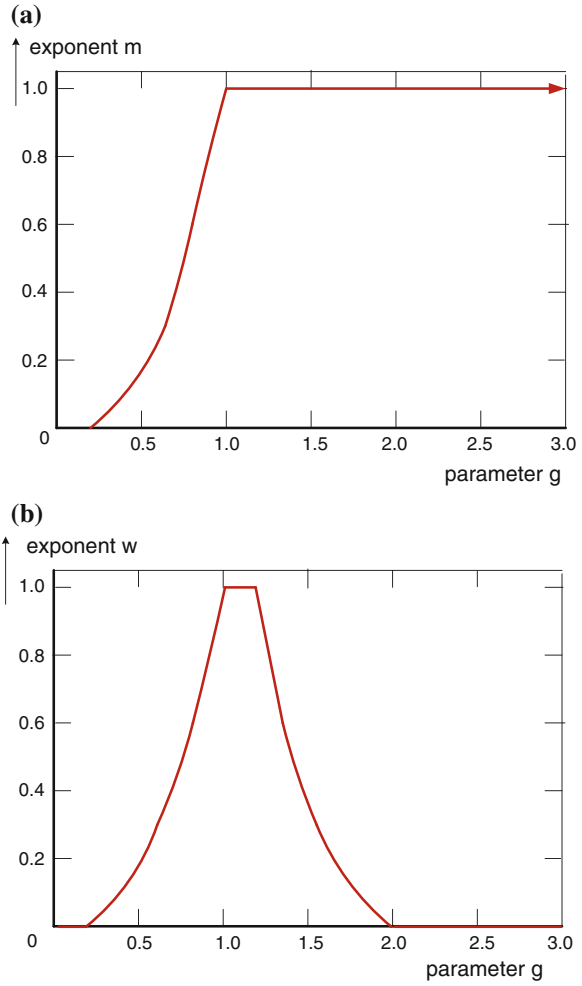

Fig. 2.2 Correction exponents according to IEC 60060-1:2010. **a***m* for air density. **b***w* for air humidity

recommended to apply an iterative procedure which is described in detail in Annex E of IEC 60060-1:2010.

It is necessary to mention that the present procedures for atmospheric corrections are not yet perfect (Wu et al. 2009). Especially the humidity correction is limited only to air gaps and not applicable to flashovers directly along insulating surfaces in air. The reason is the different absorption of water by different surface materials. Furthermore the attention is drawn to the limitations of the application of humidity correction to $h/\delta \leq 15$ g/m^3 (for AC and DC test voltages), respectively $h/\delta \leq 20$ g/m^3 (for LI and SI test voltages). The clarification of the humidity correction for surfaces as well as the extension of their ranges requires further research work (Mikropolulos et al. 2008; Lazarides and Mikropoulos 2010; 2011) as well as the atmospheric correction in general for altitudes above 2,500 m

(Ortega and Waters et al. 2007; Jiang et al. 2008; Jiang and Shu et al. 2008). Nevertheless, also the available correction to and from reference atmospheric conditions is important in HV testing of external insulation as it should be shown by two simple examples.

Example 1 In a development test, the 50 % LI breakdown voltage of an air insulated disconnector [breakdown (flashover) path L = 1 m, not at the insulator surface] was determined to $V_{50} = 580$ kV at a temperature of $t = 30$ °C, an air pressure of $p = 980$ hPa and a humidity of $h = 12$ g/m^3. The value under reference atmospheric conditions shall be calculated:

Air density	$\delta = (995/1{,}013) \cdot (293/303) = 0.95;$
Parameter	$k = 1 + 0.010 \cdot ((12/0.95) - 11) = 1.02;$
Parameter	$g = 580/(500 \cdot 1 \cdot 0.95 \cdot 1.02) = 1.20;$
Table 2.1: delivers the air density correction exponent	$m = 1.0;$
and the humidity correction exponent	$w = (2.2 - 1.2)\ (2.0 - 1.2)/0.8 = 1.0;$
With the density correction factor	$k_1 = 0.95;$
and the humidity correction factor	$k_2 = 1.02;$
one gets the atmospheric correction factor	$K_t = 0.95 \cdot 1.02 = 0.97.$
Under reference conditions the 50 % breakdown voltage would be	$\mathbf{V_{0-50} = 580/0.97 = 598\ kV.}$

Example 2 The same disconnector shall be type tested with a LI voltage of $V_0 = 550$ kV in a HV laboratory at higher altitude under the conditions $t = 15$ °C, $p = 950$ hPa and $h = 10$ g/m^3. Which test voltage must be applied?

Air density	$\delta = (950/1013)\ (293/288) = 0.954;$
parameter	$k = 1 + 0.010\ ((10/0.95) - 11) = 0.995;$
parameter	$g = 598/(500 \cdot 1 \cdot 0.95 \cdot 0.995) = 1.265;$
Table 2.1: delivers the air density correction exponent	$m = 1.0;$
and the humidity correction exponent	$w = (2.2 - 1.265)(2.0 - 1.265)/0.8 = 0.86;$
With the density correction factor	$k_1 = 0.954;$
and the humidity correction factor	$k_2 = 0.995^{0.86} = 0.996;$
one gets the atmospheric correction factor	$K_t = 0.954 \cdot 0.996 = 0.95.$
Under the actual laboratory conditions the test voltage is	$\mathbf{V = 550 \cdot 0.95 = 523\ kV}.$

The two examples show, that the differences between the starting and resulting values are significant. The application of atmospheric corrections is essential for HV testing of external insulation.

2.1.3 HV Artificial Rain Tests on External Insulation

External HV insulations (especially outdoor insulators) are exposed to natural rain. The effect of rain to the flashover characteristic is simulated in artificial rain (or *wet) tests* (Fig. 2.3). The artificial rain procedure described in the following is applicable for tests with AC, DC and SI voltages, whereas the arrangement of the test object is described in the relevant apparatus standards.

The test object is sprayed with droplets of water of given resistivity and temperature (Table 2.2). The rain shall fall on the test object under an angel of about 45°, this means that the horizontal and vertical components of the *precipitation rate* shall be identical. The precipitation rate is measured with a special collecting vessel with a horizontal and a vertical opening of identical areas between 100 and 700 cm^2. The rain is generated by an artificial rain equipment consisting of nozzles fixed on frames. Any type of nozzles which generates the appropriate rain conditions (Table 2.2) can be applied.

Note 1 Examples of applicable nozzles are given in the old version of IEC 60-1:1989-11 (Fig. 2, pp. 113–115) as well as in IEEE Std. 4–1995.

The precipitation rate is controlled by the water pressure and must be adjusted in such a way, that only droplets are generated and the generation of water jets or fog is avoided. This becomes more and more difficult with increasing size of the test objects which requires larger distances between test object and artificial rain equipment. Therefore, the requirements of IEC 60060-1:2010 are only related to equipment up to rated voltages of $V_m = 800$ kV, Table 2.2 contains an actual proposal for the UHV range.

The reproducibility of wet test results (*wet flashover voltages*) is less than that for dry HV breakdown or withstand tests. The following precautions enable acceptable wet test results:

- The water temperature and resistivity shall be measured on a sample collected immediately before the water reaches the test object.
- The test object shall be pre-wetted initially for at least 15 min under the conditions specified in Table 2.2 and these conditions shall remain within the specified tolerances throughout the test, which should be performed without interrupting the wetting.

Note 2 The pre-wetting time shall not include the time needed for adjusting the spray. It is also possible to perform an initial pre-wetting by unconditioned tap water for 15 min, followed without interruption of the spray by a second pre-wetting with the well conditioned test water for at least 2 min before the test begins.

- The test object shall be divided in several zones, where the precipitation rate is measured by a collecting vessel placed close to the test object and moved slowly over a sufficient area to average the measured precipitation rate.

Fig. 2.3 Artificial rain test on an 800 kV support insulator (Courtesy HSP Cologne)

Table 2.2 Conditions for artificial rain precipitation

Precipitation condition	Unit	IEC 60060-1:2010 range for equipment of $V_m \leq 800$ kV	Proposed range for UHV equipment $V_m > 800$ kV
Average precipitation rate of all measurements:			
• Vertical component	(mm/min)	1.0–2.0	1.0–3.0
• Horizontal component	(mm/min)	1.0–2.0	1.0–3.0
Limits for any individual measurement and for each component	(mm/min)	±0.5 from average	1.0–3.0
Temperature of water	(°C)	Ambient temperature ±15 K	Ambient temperature ±15 K
Conductivity of water	(μS/cm)	100 ± 15	100 ± 15

- Individual measurements shall be made at all measuring zones considering also one at the top and one near the bottom of the test object. A measuring zone shall have a width equal to that of the test object (respectively its wetted parts) and a

maximum height of 1–2 m. The number of measuring zones shall cover the full height of the test object.
- The spread of results may be reduced if the test object is cleaned with a surface-active detergent, which has to be removed before the beginning of wetting.
- The spread of results may also be affected by local anomalous (high or low) precipitation rates. It is recommended to detect these by localized measurements and to improve the uniformity of the spray, if necessary.

The test voltage cycle for an artificial rain test shall be identical to that for a dry test. For special applications different cycles are specified by the relevant apparatus committees. A density correction factor according to Sect. 2.1.2, but no humidity correction shall be applied.

Note 3 IEC 60060-1:2010 permits one flashover in AC and DC wet tests provided that in a repeated test no further flashover occurs.

Note 4 For the UHV test voltage range, it may be necessary to control the electric field (e.g., by toroid electrodes) to the artificial rain equipment and/or to surrounding grounded or energized objects including walls and ceiling to avoid a breakdown to them. Also artificial rain equipment on a potential different from ground might be taken into consideration.

2.1.4 HV Artificial Pollution Tests on External Insulation

Outdoor insulators are not only exposed to rain, but also to pollution caused by salt fog near the sea shore, by industry and traffic or simply by natural dust. Depending on the position of a transmission line or substation, the surrounding is classified in several different *pollution classes* between low (*surface conductivity* $\kappa_s \leq 10\ \mu$S) and extreme ($\kappa_s \geq 50\ \mu$S) (Mosch et al. 1988). The severity of the pollution class can also be characterized by the equivalent salinity (SES in kg/m^3), which is the salinity [content of salt (in kg) in tap water (in m^3)] applied in a salt-fog test according to IEC 60507 (1991) that would give comparable values of the leakage current on an insulator as produced at the same voltage by natural pollution on site (Pigini 2010).

Depending on the pollution class, the artificial pollution test is performed with different intensities of pollution, because the test conditions shall be representative of wet pollution in service. This does not necessarily mean that any real service condition has to be simulated. In the following the performance of typical pollution tests is described without considering the representation of the pollution zones. The pollution flashover is connected with quite high pre-arc currents supplied via the wet and polluted surface from the necessary powerful HV generator (HVG). In a pioneering work, Obenaus (1958) considered a flashover model of a series connection of the pre-arc discharge with a resistance for the polluted surface. Till today the *Obenaus model* is the basis for the selection of pollution test procedures and the understanding of the requirements on test generators (Slama et al. 2010; Zhang et al. 2010). These requirements to HV test circuits are

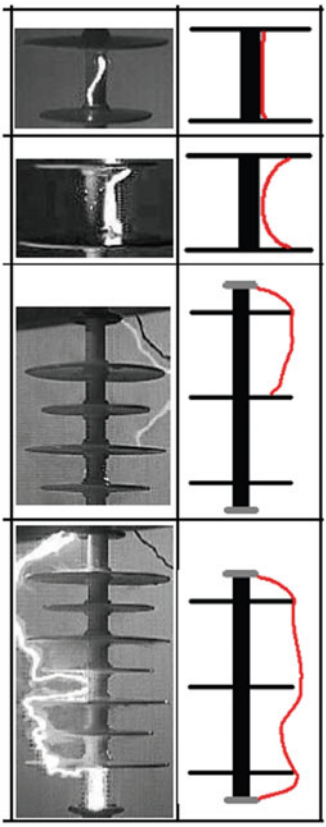

Fig. 2.4 Phases of a pollution flashover of an insulator (Courtesy of FH Zittau, Germany)

considered in the relevant Chaps. 3 and 6–8. Pollution tests of insulators for high altitudes have to take into consideration not only the pollution class, but also the atmospheric conditions (Jiang et al. 2009).

The test object (insulator) must be cleaned by washing with tap water and then the pollution process may start. Typically the pollution test is performed with subsequent applications of the test voltage which is held constant for a specified test time of at least several minutes. Within that time very heavy partial discharges, so-called pre-arcs, appear (Fig. 2.4). It may happen that the wet and polluted surface dries (which means electrically withstand of the tested insulator and passing the test) or that the pre-arcs are extended to a full flashover (which means failing the test). Because of the random process of the pollution flashover, remarkable dispersion of the test results can be expected. Consequently the test must be repeated several times to get average values of sufficient confidence or to estimate distribution functions (see Sect. 2.4). Two pollution procedures shall be described:

The *salt-fog method* uses a fog from a salt (NaCl) solution in tap water with defined concentrations between 2.5 and 20 kg/m^3 depending on the pollution zone. A spraying equipment generates a number of fog jets each generated by a pair of

nozzles. One nozzle supplies about 0.5 l/min of the salt solution, the other one the compressed air with a pressure of about 700 kPa which directs the fog jet to the test object. The spraying equipment contains usually two rows of the described double nozzles. The test object is wetted before the test. The test starts with the application of the fog and the test voltage value which should be reached—but not overtaken—as fast as possible. The whole test may last up to 1 h.

The *pre-deposit method* is based on coating the test object with a conductive suspension of Kieselgur or Kaolin or Tonoko in water (≈ 40 g/l). The conductivity of the suspension is adjusted by salt (NaCl). The coating of the test object is made by dipping, spraying or flow-coating. Then it is dried and should become in thermal equilibrium with the ambient conditions in the pollution chamber. Finally the test object is wetted by a steam-fog equipment (steam temperature ≤ 40 °C). The surface condition is described by the *surface conductivity* (μS) measured from the current at two probes on the surface (IEC 60-1:1989, Annex B.3) or by the equivalent amount of salt per square centimetre of the insulating surface [so-called salt deposit density (S.D.D.) in mg/cm^2]. The test can start with voltage application before the test object is wetted, or after wetting, when the conductivity has reached its maximum. Details depend on the aim of the test, see IEC 60507:1991.

Both described procedures can be performed with different aim of the pollution test:

- determination of the withstand voltage for a certain insulator of specified degree of pollution and a specified test time,
- determination of the maximum degree of pollution for a certain insulator at a specified test voltage and specified test time.

Pollution tests require separate *pollution chambers*, usually with bushings for the connection of the test voltage generator. Because of the salt fog and humidity, the HV test system itself is outside under clean conditions. Inside a salt-fog chamber, the clearances around the test object should be $\geq$0.5 m/100 kV but not less than 2 m. When no pollution chamber is available, also tents from plastic foil may be applied, to separate the pollution area from the other areas of a HV laboratory.

2.1.5 HV Tests on Internal Insulation

In a HV test field, the HV components of test systems are designed with an external indoor insulation usually. When internal insulation shall be tested, the test voltage must be connected to the internal part of the apparatus to be tested. This is usually done by bushings which have an external insulation. For reasons of the insulation co-ordination or of the atmospheric corrections, cases will arise that the HV withstand test level of the internal insulation exceeds that of the external insulation (bushing). Then the withstand level of the bushing must be enhanced to permit application of the required test voltages for the internal insulation. Usually

special "test bushings" of higher withstand level, which replace the "service bushings" during the test, are applied. A further possibility is the immersion of the external insulation in liquids or compressed gases (e.g., SF_6) during the test.

In rare cases, when the test voltage level of the external insulation exceeds that of the internal insulation a test at the complete apparatus can only be performed when the internal insulation is designed according to the withstand levels of the external insulation. If this cannot be done, then the apparatus should be tested at the internal test voltage level, and the external insulation should be tested separately using a dummy.

Internal insulation is influenced by the ambient temperature of the test field, but usually not by pressure or humidity of the ambient air. Therefore, the only requirement is the temperature equilibrium of the test object with its surrounding when the HV test starts.

2.1.6 Hints to Further Environmental Tests and HV Tests of Apparatus

There are also other environmental HV tests, e.g., under *ice* or *snow*. They are made with natural conditions in suitable open-air HV laboratories or in special climatic chambers (Sklenicka et al. 1999). Other environmental influences which are simulated in HV tests are UV light (Kindersberger 1997), sandstorms (Fan and Li 2008) and *fire* under transmission lines. The HV test procedures for apparatus and equipment are described in the relevant "vertical" standards, examples are given in the chapters of the different test voltages.

2.2 HV Test Systems and Their Components

This section supplies a general description of HV test systems and their components, which consist of the *HV generator*, the *power supply unit*, the *HVvoltage measuring system*, the *control system* and possibly additional measuring equipment, e.g., for PD or dielectric measurement. In all cases the test object cannot be neglected, because it is a part of the *HV test circuit*.

A *HV test system* means the complete set of apparatus and devices necessary for performing a HV test. It consists of the following devices (Fig. 2.5).

The *HV generator* (HVG) converts the supplied low or medium voltage into the high test voltage. The type of the generator determines the kind of the test voltage. For the generation of high alternating test voltages (HVAC), the HVG is a test transformer (Fig. 2.6a). It might be also a resonance reactor which requires a capacitive test object (TO) to establish an oscillating circuit for the HVAC generation (see Sect. 3.1). For the generation of high direct test voltages (HVDC) the HVG is a special circuit of rectifiers and capacitors (e.g., a Greinacher or Cockroft-Walton

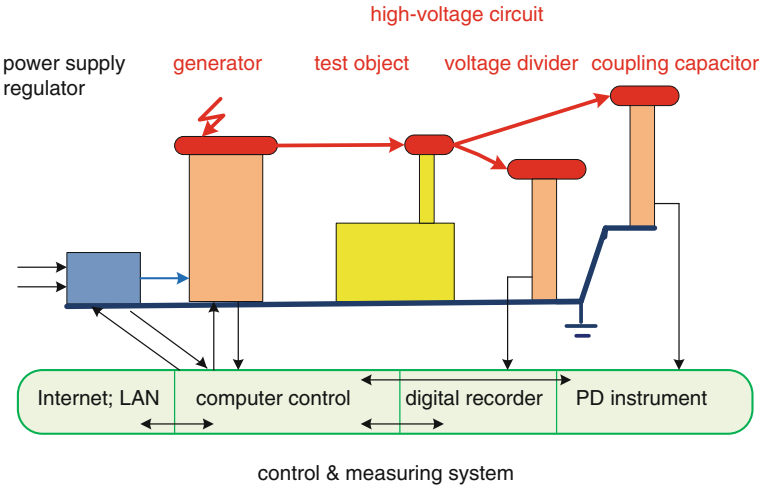

Fig. 2.5 Principle circuit of a HV test system

generator, Fig. 2.6b, see Sect. 6.1), and for the generation of high lightning or switching impulse (LI, SI) voltages, it is a special circuit of capacitors, resistors and switches (sphere gaps) (e.g., a Marx generator, Fig. 2.6c, see Sect. 7.1).

The test object does not only play a role for HVAC generation by resonant circuits, there is an interaction between the generator and the test object in all HV test circuits. The voltage at the test object may be different from that at the generator because of a voltage drop at the HV lead between generator and test object or even a voltage increase because of resonance effects. This means the voltage must be measured directly at the test object and not at the generator (Fig. 2.5). For this voltage measurement a sub-system—usually called *HV measuring system*—is connected to the test object (Fig. 2.7a, see Sect. 2.3). Further sub-systems, e.g., for dielectric measurement, can be added. Up to few 10 kV such systems can be designed as compact units including voltage source (Fig. 2.7b). Very often PD measurements are performed during a HVAC test. For that a *PD measuring system* is connected to the AC test system (Fig. 2.7c). All these systems consist of a HV component (e.g., voltage divider, coupling or standard capacitor), measuring cable for data transfer and a low-voltage instrument (e.g., digital recorder, peak voltmeter, PD measuring instrument, tan delta bridge).

All the components of a HV test system and the test object described above form the HV circuit. This circuit should be of lowest possible impedance. This means, it should be as compact as possible. All connections, the *HV leads* and the *ground connections* should be straight, short and of low inductance, e.g., by copper foil (width 10–25 cm, thickness depending of current). In HV circuits used also for PD measurement, the HV lead should be realized by PD-free tubes of a diameter appropriate to the maximum test voltage. Any loop in the ground connection has to be avoided.

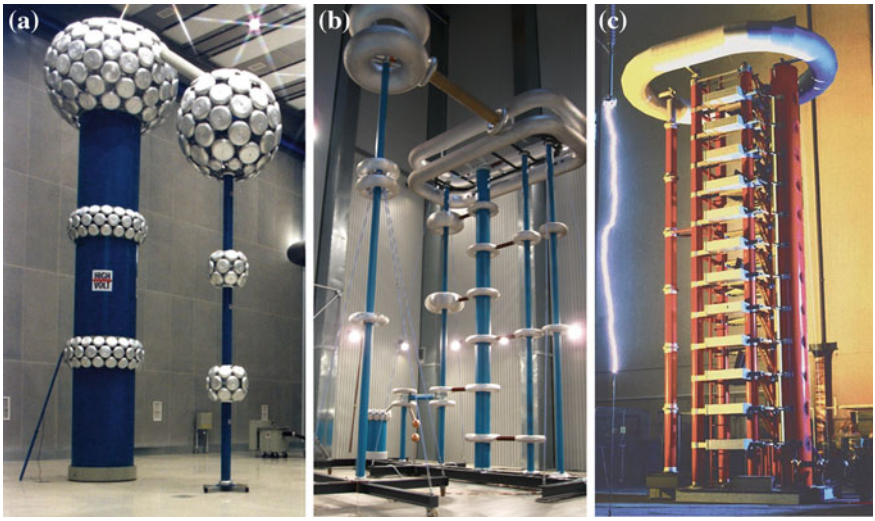

Fig. 2.6 HV generators. **a** For AC test voltage 1,000 kV at Cottbus Technical University. **b** For DC test voltage 1,500 kV at HSP Cologne. **c** For LI/SI test voltages 2,400 kV at Dresden Technical University

The necessary power for the HV tests is supplied from the power grid—in case of on-site testing also from a Diesel-generator set—via the *power supply unit* (Fig. 2.5). This unit consists of one or several *switching cubicles* and a *regulation unit* (regulator transformer or motor-generator set or thyristor controller or frequency converter). It controls the power according to the signals from the control system in such a way, that the test voltage at the test object is adjusted as required for the HV test. For safety reasons the switching cubicle shall have two circuit breakers in series; the first switches the connections between the grid and the power supply unit (power switch), the second one that between the power supply unit and the generator (operation switch). For the reduction of the required power from the grid in case of capacitive test objects, the power supply unit is often completed by a fixed or even adjustable *compensation reactor*.

When the generator is the heart of HV test system then the control and measuring sub-system—usually called *control and measuring system* (Fig. 2.8; Baronick 2003)—is its brain. Older controls were separated from the measuring systems and the adjustment of the test voltage was manually made by the operator (The brain was that of the operator). As a next step, programmable logic controllers have been introduced. Now a state-of-the-art control system is a *computer control* which enables the pre-selection of the test procedure with all test voltage values, gives the commands to the power supply unit, overtakes the data from the measuring systems, performs the test data evaluation and prints a test record. In that way one operator can supervise very complex test processes. The test data can be transferred to a local computer network (LAN) e.g., for combining with test data from other laboratories or even to the Internet. The latter can also be used in case of technical problems for *remote service*.

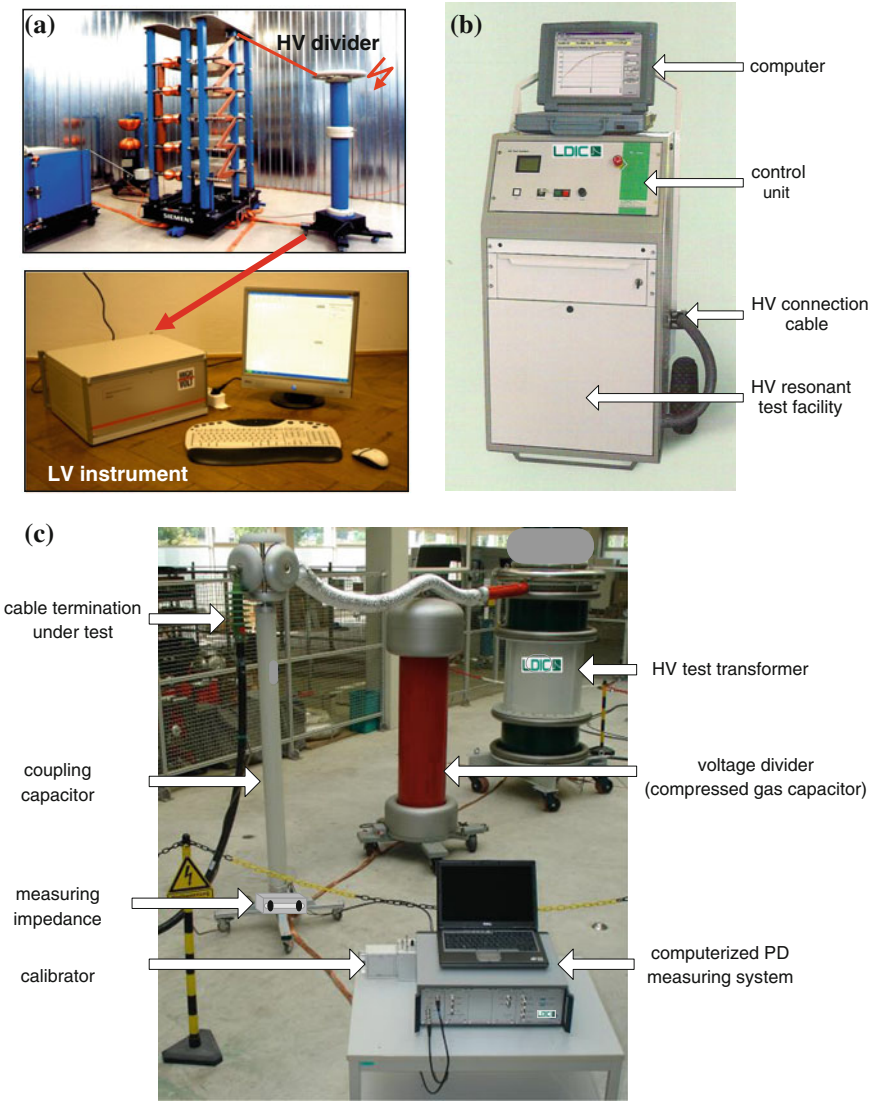

Fig. 2.7 Measuring systems. **a** Voltage measuring system with digital recorder including impulse generator. **b** Compact capacitance/loss factor measuring system with integrated AC voltage source (Courtesy of Doble-Lemke). **c** Partial discharge measuring system including AC voltage test circuit (Courtesy of Doble-Lemke)

A HV test system is only complete when it is connected to a *safety system* which protects the operators and the participants of a HV test. Among others, the safety system includes a fence around the test area which is combined with the electrical *safety loop*. The test can only be operated when the loop is closed, for details see Sect. 9.2.

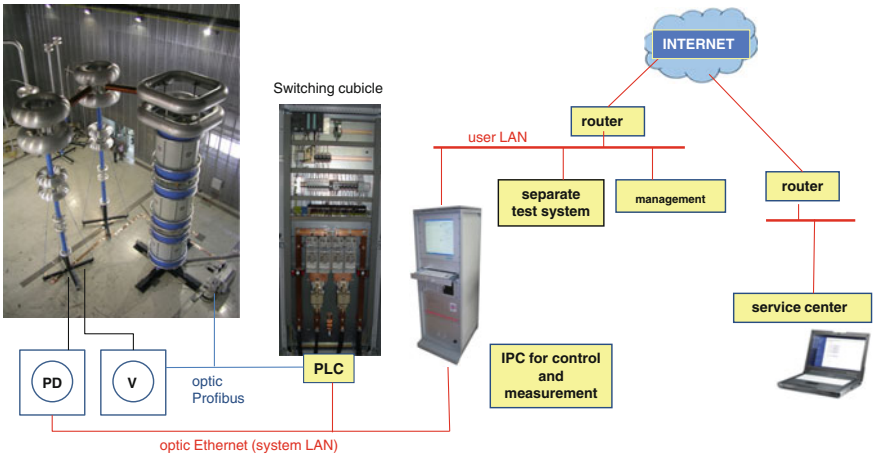

Fig. 2.8 Computerized control and measuring system

2.3 HV Measurement and Estimation of the Measuring Uncertainty

This section is related to voltage measurement and describes *HV measuring system*s, their *calibration* and the estimation of their *uncertainties of measurements*. Precise measurement of high test voltages is considered to be a difficult task for many years (Jouaire and Sabot et al. 1978; "Les Renardieres Group" 1974). This situation is also reflected by the older editions of the relevant standard IEC 60060-2. For good practice in HV test fields, this Sect. 2.3 on HV measurement and uncertainty estimation is closely related to the newest edition of the standard IEC 60060-2:2010.

The terms "*uncertainty*", "*error*" and "*tolerance*" are often mixed up. Therefore, the following clarification seems needed: The uncertainty is a parameter which is associated with the result of a measurement. It characterizes the dispersion of the results due to the characteristics of the measuring system. The *error* is the measured quantity minus a reference value for this quantity and the tolerance is the permitted difference between the measured and the specified value. Tolerances play a role for standard HV test procedures (Sects. 3.6, 6.5 and 7.6). Uncertainties are important for the decision, whether a measuring system is applicable or not for acceptance testing.

2.3.1 HV Measuring Systems and Their Components

Definition: A HV measuring system(MS) is a "complete set of devices suitable for performing a HV measurement". Software for the calculation of the result of the measurement is a part of the measuring system (IEC 60060-2:2010).

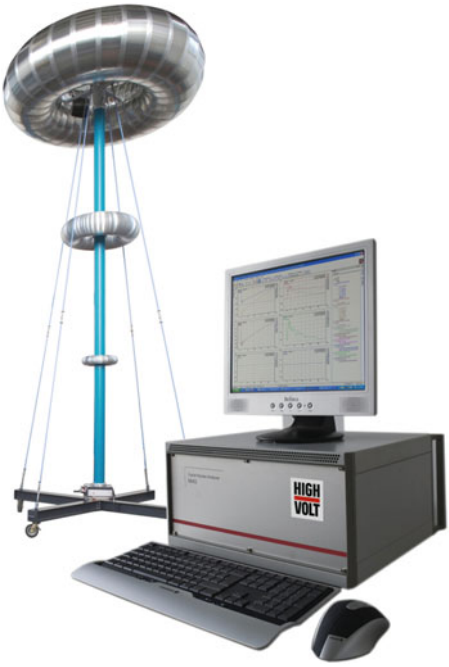

Fig. 2.9 HV measuring system consisting of voltage divider, coaxial cable and PC-based digital recorder

A HV measuring system (Fig. 2.9) which should be connected directly to the test object consists usually of the following components

- A *converting device* including its HV and earth connection to the test object which converts the quantity to be measured (*measurand*: test voltage with its voltage and/or time parameters) into a quantity compatible with the measuring instrument (low-voltage or current signal). It is very often a voltage divider of a type depending on the voltage to be measured (Fig. 2.10). For special application also a voltage transformer, a voltage converting impedance (carrying a measurable current) or an electric field probe (converting amplitude and time parameters of an electric field) may be used. The clearances between the converting device and nearby earthed or energized structures may influence the result of the measurement. Such *proximity effects* shall be considered by the uncertainty estimation (see Sect. 2.3.4). To keep the contribution of the proximity effect to the uncertainty of measurement small, the clearances of movable converting devices should be as those recommended for the test object (see Sect. 2.1.2 and Fig. 2.1). If the converting device is always in a fixed position and the measuring system is calibrated on site, the proximity effect can be neglected.
- A *transmission system* which connects the output terminals of the converting device with the input terminals of the measuring instrument. It is very often a coaxial cable with its terminating impedance, but may also be an optical link which includes a transmitter, an optical cable and a receiver with an amplifier. For special application also cable connections with amplifiers and/or attenuators are in use.

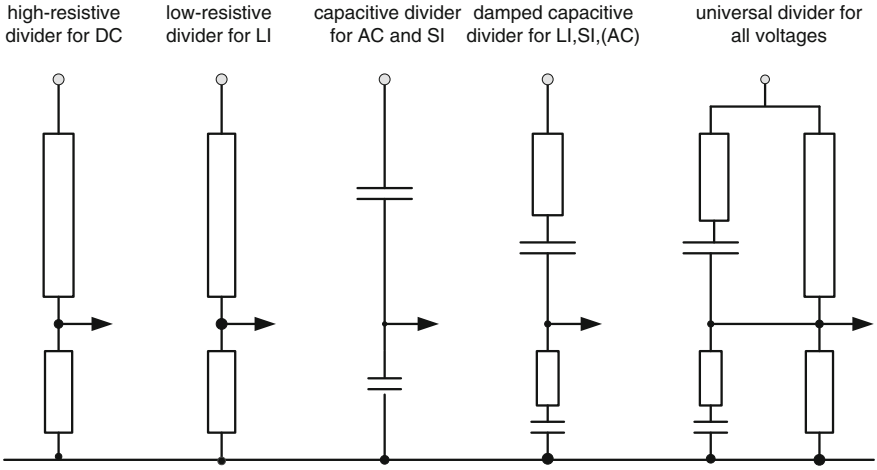

Fig. 2.10 Kinds and applications of voltage dividers

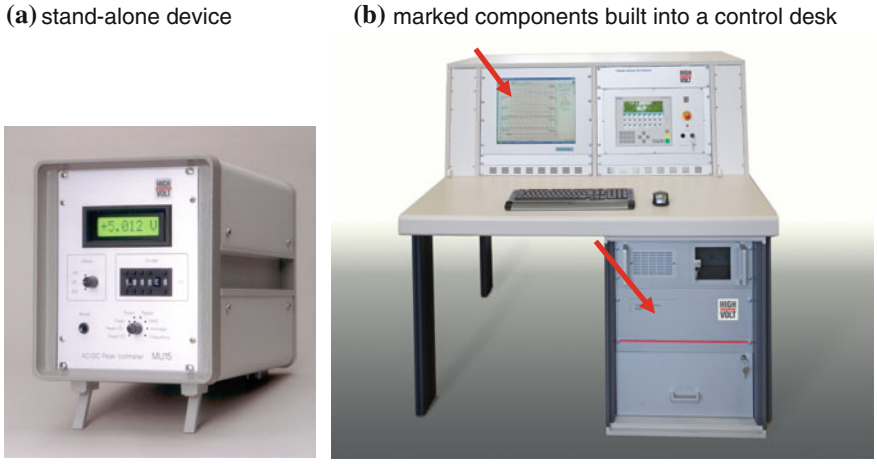

Fig. 2.11 Instruments for HV measurement. **a** Digital AC/DC peak voltmeter. **b** LI/SI digital recorder

- A *measuring instrument* suitable to measure the required test voltage parameters from the output signal of the transmission system. Measuring instruments for HV application are usually special devices which fulfil the requirements of the IEC Standards 61083 (part 1 and 2 for LI/SI test voltages has been published, part 3 and 4 for AC/DC voltages is under preparation). The conventional analogue peak voltmeters are replaced by digital peak voltmeters and more and more by digital recorders (Fig. 2.11). Digital recorders measure both test voltage and time parameters. This is mandatory for LI/SI test voltages, but more and more also for AC/DC test voltages with respect to changes in time by voltage

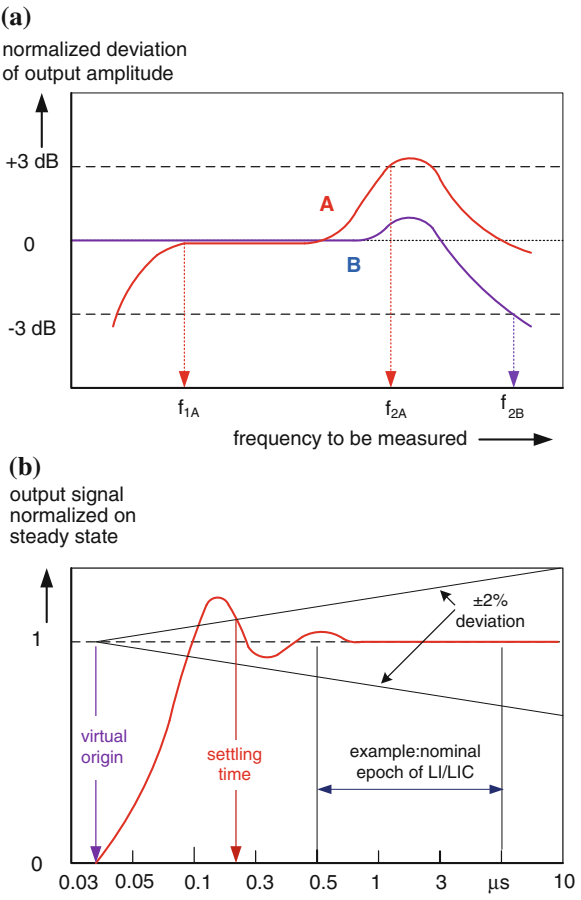

Fig. 2.12 Response of measuring systems (IEC 60060-2:2010). **a** Frequency response (*curve A* with lower and upper limit frequency, *curve B* with upper frequency limit, related to AC/DC measurement). **b** Unit step response after a step-voltage input (related to LI/SI voltage measurement, see Sect. 7.3)

drop (see Sects. 3.2.1 and 6.2.3.2), harmonics (AC, see Sect. 3.2.1) or ripple (DC, see Sect. 6.2.1).

Each HV measuring system is characterized by its *operating conditions*, as they are the rated operating voltage, the measurement ranges, the operating time (or kind and number of LI/SI voltage applications) and the environmental conditions. The dynamic behaviour of a measuring system can be described as an output signal depending on frequency (frequency response for AC and DC voltage measuring systems, Fig. 2.12a) or on a voltage step (*step response* for LI/SI voltage measuring systems, Fig. 2.12b) or by a sufficiently low uncertainty of LI/SI parameter measurement within the nominal epoch of the measuring system.

Note The nominal epoch of an impulse voltage, which will be explained more in detail in Sects. 7.2 and 7.3, is the range between the minimum and the maximum of the relevant LI/SI time parameter for which the measuring system is approved. The nominal epoch is

derived from the upper and lower tolerances of the front time parameter of the impulse voltage.

All these rated values have to be supplied by the manufacturer of the measuring system (respectively its components) after type and routine tests. They should fit to the requirements and the conditions of the HV test field where the measuring system shall be applied.

Furthermore each voltage measuring system is characterized by its *scale factor*, this means the value by which the reading of the instrument must be multiplied to obtain the input quantity of the HV measuring system (voltage and time parameters). For measuring systems that display the value of the input quantity directly, the scale factor is unity. In that case—and transmission by a coaxial cable—the scale factor of the instrument is the inverse of the scale factor of the converting device. A correctly terminated coaxial cable has the scale factor unity, other types of transmission systems may have one different from unity.

The scale factor must be calibrated to guarantee a voltage measurement traceable to the National Standard of measurement. The *calibration* consists of two main parts. On one hand the value of the scale factor shall be determined including the necessary dynamic behaviour. On the other hand, the uncertainty of the HV measurement shall be estimated. When the uncertainty and the dynamic behaviour are within the limits given by IEC 60060-2:2010, the *approved measuring system* (AMS) is applicable for measurement in an accredited HV test field (see the relevant Chaps. 3, 6 and 7).

2.3.2 Approval of a HV Measuring System for an Accredited HV Test Field

A HV measuring system is qualified for the use in an accredited HV test field by several successful tests and checks described in IEC 60060-2:2010. It becomes an "*AMS*" when it has passed the following tests and checks:

- The *type test* by the manufacturer on the system or its components on sample(s) from the production shall demonstrate the correct design and conformity with the requirements. These requirements include the determination of

– the scale factor value, its linearity and its dynamic behaviour,
– its short and long term stability,
– the ambient temperature effect, i.e., the influence of the ambient temperature,
– the proximity effect, i.e., the influence of nearby grounded or energized structures,
– the software effect i.e., the influence of software on the dispersion of measurements,
– the demonstration of withstand in a HV test.

- The *routine test* on each system or each of its components by the manufacturer shall demonstrate the correct production and the conformity with the requirements by

– the scale factor value, its linearity and its dynamic behaviour and also
– the demonstration of withstand in a HV test.

- The *performance test* on the "complete measuring system" shall characterize it at its place in the HV test field "under operation conditions" by determination of

– the scale factor value, its linearity and its dynamic behaviour;
– the long term stability (from repetitions of performance tests) and
– the proximity effects.

The user is responsible for the performance tests and should repeat them annually, but at least once in 5 years (IEC 60060-2:2010).

- The *performance check* is a "simple procedure"—usually the comparison with a second AMS or with a standard air gap (see Sect. 2.3.5)—"to ensure that the most recent performance test is still valid". The user is responsible for the performance checks and should repeat them according to the stability of the AMS, but at least annually (IEC 60060-2:2010).

The mentioned single tests are described together with the uncertainty estimation in Sect. 2.3.4. For the reliable operation of the measuring system a *HV withstand test* of the converting device is necessary as a type test and, if the clearances in the laboratory of use are limited, also in a first performance test. The usually required withstand test voltage level is 110 % of the rated operating voltage of the converting device. The test procedure shall follow those typical for the relevant test voltages (Sects. 3.6, 6.5 and 7.6). In case of a converting device for outdoor application, the type test should include an artificial rain test.

This first performance test shall also include an *interference test* of the transmission system (coaxial cable) and the instrument of LI/SI measuring systems disconnected from the generator, but in their position for operation. This test generates an interference condition at the short-circuited input of the transmission system by firing the related impulse voltage generator at a test voltage representative for the highest operating voltage of the measuring system. The interference test is successful, when the measured amplitude of the interference is less than 1 % of the test voltage to be measured.

The results of all tests and checks shall be reported in the "*record of performance*" of the measuring system, which shall be established and maintained by the user of the AMS (IEC 60060-2:2010). This record shall also contain a detailed technical description of the AMS. It is the right of an inspector of an acceptance test of any apparatus to see the record of performance for the used HV measuring system.

As required in performance tests, the scale factor, the linearity and the dynamic behaviour of a complete measuring system can be determined by different methods. The most important and preferred method is the comparison with a reference

measuring system (RMS), in the following called "*comparison method*" (IEC 60060-2:2010) and described in the following subsection.

Note An alternative is the "*component method*" which means the determination of the scale factor of the measuring system from the scale factors of its components (IEC 60060-2:2010). The scale factor of the components can be determined by the comparison with a reference component of lower uncertainty or by simultaneous measurements of input and output quantities or by calculation based on measured impedances. For each component, the uncertainty contributions must be estimated similar to those for the whole system qualified by the comparison method. Then these uncertainties of components must be combined to the uncertainty of measurement

2.3.3 Calibration by Comparison with a Reference Measuring System

The assigned scale factor of a measuring system shall be determined by calibration. Using the comparison method, the reading of the measuring system (AMS, index X) is compared for approval with the reading of the *reference measuring system* (RMS, index N) (Fig. 2.13). Both measuring systems indicate the same voltage V, which is the reading multiplied with the relevant scale factor F:

$$V = F_N \cdot V_N = F_X \cdot V_X \tag{2.10}$$

This simple equation delivers the scale factor of the measuring system under calibration:

$$F_X = (F_N \cdot V_N)/V_X \tag{2.11}$$

Note Because the usual symbol of the uncertainty is the letter "u" or "U" (ISO/IEC Guide 98-3:2008), for the voltage the symbol "V" is used.

For practical cases it is recommended to arrange the two dividers in the same distance from a support which is directly connected to the test voltage generator. This symmetric arrangement works well when the two voltage dividers have about the same size (Fig. 2.14). All HV and earth connections shall be without loops and as short and straight as possible.

When the rated voltage of the RMS is higher or equal to that of the system under calibration, one can assume ideal conditions, because the calibration can be performed in minimum at $g = 5$ voltage levels including the lowest and highest of the assigned operating range (Fig. 2.15). In this case the calibration includes also the linearity test.

However, as RMS are not available up to the highest test voltages, IEC 60060-2:2010 allows that the comparison may be made at voltages as low as 20 % of the assigned measurement range. An additional linearity test shows that the calibrated scale factor is applicable up to the upper limit of the measurement range which is often the rated operating voltage (see Sect. 2.3.4). In that case the symmetric

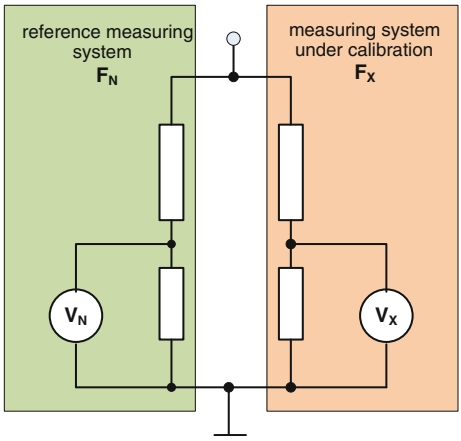

Fig. 2.13 Principle arrangement of the measuring systems for calibration using the comparison method

arrangement of the two measuring systems as in Fig. 2.14 is impossible, but one should use sufficient clearances (Fig. 2.1) that the RMS is not influenced by the often much larger system under calibration.

The used RMS shall have a calibration traceable to national and/or international standards of measurement maintained by a *National Metrology Institute* (NMI) (Hughes et al. 1994; Bergman et al. 2001). This means that RMS calibrated by a NMI or by an *accredited calibration laboratory* (ACL) with NMI accreditation are traceable to national and/or international standards. The requirements to RMS are given in Table 2.3. The calibration of RMS can be made with *transfer RMS* (TRMS) of lower uncertainty ($U_M \leq 0.5$ % for voltage and $U_M \leq 3$ % for impulse time parameter measurement). The *traceability* is maintained by inter-comparisons of RMS's of different calibration laboratories (Maucksch et al. 1996).

Calibrations can be performed by accredited HV test laboratories provided that a correctly maintained RMS and skilled personnel are available and traceability is guaranteed. This may be possible in larger test fields, the usual way is to order calibration by an ACL.

Table 2.3 Requirements to reference measuring systems (RMS)

Test voltage	DC (%)	AC (%)	LI, SI (%)	Front-chopped LIC (%)
Expanded uncertainty of **voltage** measurement U_M	1	1	1	3
Expanded uncertainty of **time parameter** measurement U_{MT}	–	–	5	5

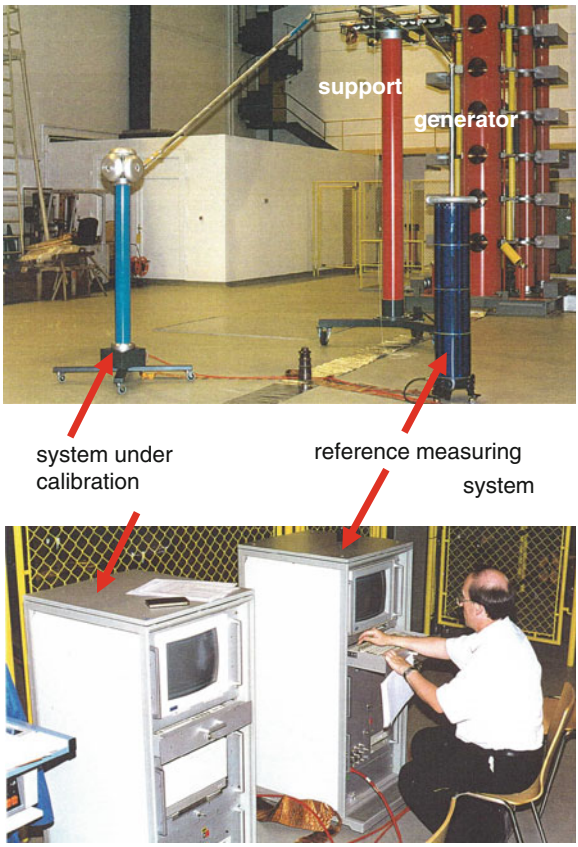

Fig. 2.14 Practical arrangement for LI voltage calibration using the comparison method (Courtesy of TU Dresden)

2.3.4 Estimation of Uncertainty of HV Measurements

The calibration process consists of the described comparisons with $n \geq 10$ applications on each of the $g = 1$ to $h \geq 5$ voltage levels provided the rated operating voltage of the RMS is not less than that of the AMS under calibration (Fig. 2.15). One application means for LI/SI voltage the synchronous readings of one impulse, for AC/DC voltage the synchronous readings at identical times. From each reading the scale factor according to Eq. (2.11) is calculated and for each voltage level V_g, its scale factor F_g is determined as the *mean value* of the n applications (usually $n = 10$ applications are sufficient):

$$F_g = \frac{1}{n}\sum_{i=1}^{n} F_{i,g}. \tag{2.12}$$

Under the assumption of a *Gauss normal distribution* the dispersion of the outcomes of the comparisons is described by the *relative standard deviation* (also called "variation coefficient") of the scale factors F_i:

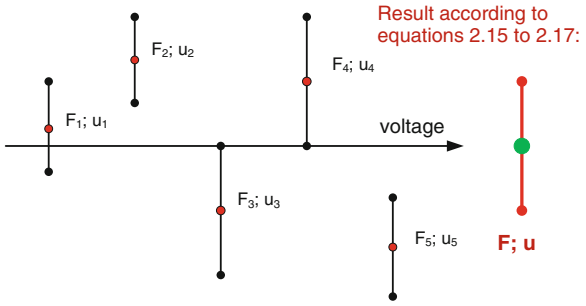

Fig. 2.15 Calibration over the full voltage range (IEC 60060-2:2010)

$$s_g = \frac{1}{F_g}\sqrt{\frac{1}{n-1}\sum_{i=1}^{n}\left(F_{i,g} - F_g\right)^2}. \tag{2.13}$$

The standard deviation of the mean value F_g is called the "*Type A standard uncertainty* u_g" and calculated for a Gauss normal distribution by

$$u_g = \frac{s_g}{\sqrt{n}}. \tag{2.14}$$

After the comparison at all $h \geq 5$ voltage levels V_g, the calibrated *AMS scale factorF* is calculated as the mean value of the F_g:

$$F = \frac{1}{h}\sum_{g=1}^{h} F_g, \tag{2.15}$$

with a Type A standard uncertainty as the largest of those of the different levels

$$u_A = \max_{g=1}^{h} u_g. \tag{2.16}$$

Additionally one has to consider the *non-linearity* of the scale factor by a Type B contribution

Note *Type A uncertainty* contributions to the standard uncertainty are related to the comparison itself and based on the assumption that the deviations from the mean are distributed according to a Gauss normal distribution with parameters according to (2.12) and (2.13) (Fig. 2.16a), whereas the *Type B uncertainty* contributions are based on the assumption of a *rectangular distribution* of a width $2a$ with the mean value $x_m = (a_+ + a_-)/2$ and the standard uncertainty $u = a/\sqrt{3}$ (Fig. 2.16b), details are described in IEC 60060-2:2010 and below in this subsection.

$$u_{B0} = \frac{1}{\sqrt{3}} \cdot \max_{g=1}^{h}\left|\frac{F_g}{F} - 1\right|. \tag{2.17}$$

When the RMS rated operating voltage is lower than that of the AMS under calibration, IEC 60060-2:2010 allows the comparison over a limited voltage range

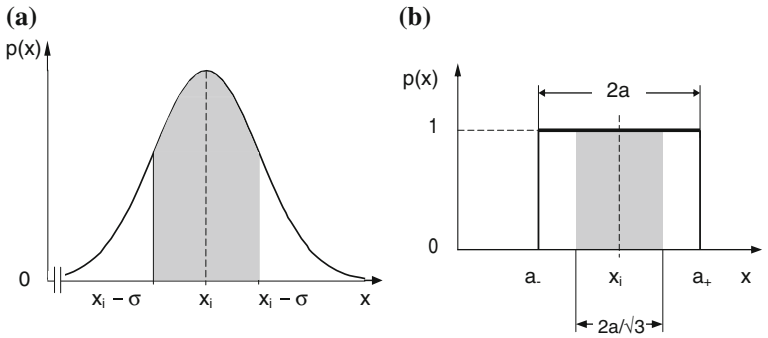

Fig. 2.16 Assumed density distribution functions for uncertainty estimation **a** Gauss normal density distribution for Type A uncertainty. **b** Rectangular density distribution for Type B uncertainty

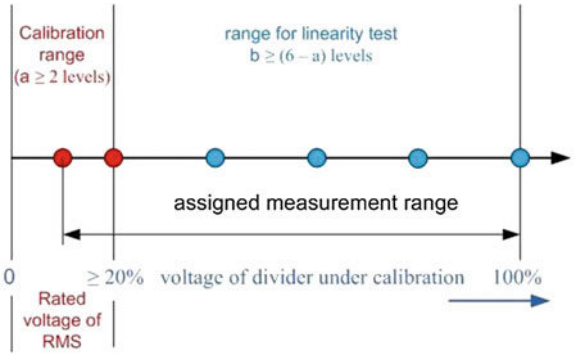

Fig. 2.17 Calibration over a limited voltage range and additional linearity test (IEC60060-2:2010)

($V_{RMS} \geq 0.2\ V_{AMS}$) using only $a \geq 2$ levels. The comparison shall be completed by a *linearity test* with $b \geq (6 - a)$ levels (Fig. 2.17). Then the scale factor F is estimated by

$$F = \frac{1}{a}\sum_{g=1}^{a} F_g, \tag{2.18}$$

the standard uncertainty by

$$u_A = \max_{g=1}^{a} u_g, \tag{2.19}$$

and the non-linearity contribution of the calibration by

$$u_{B0} = \frac{1}{\sqrt{3}} \cdot \max_{g=1}^{a} \left| \frac{F_g}{F} - 1 \right|. \tag{2.20}$$

Table 2.4 Comparison at the first level $V_1 \approx 0.2\ V_r$

No. of application	RMS measured voltage (V_N/kV)	AMS measured voltage (V_X/kV)	Scale factor F_i (Eq. 2.11)
$i = 1$	201.6	200.8	1.0291
2	200.7	200.9	1.0240
3	201.4	200.9	1.0276
4	199.9	199	1.0296
5	201.2	199.9	1.0317
6	201.3	200.3	1.0301
7	200.9	200.4	1.0276
8	201.3	200.4	1.0296
9	201.2	199.9	1.0317
$n = 10$	200.6	200.7	1.0245
Result by Eqs. (2.12)–(2.16)			**F_1 = 1.028** **s_1 = 2.73 %** **u_1 = 0.86**

Table 2.5 Scale factor and Type A uncertainty estimation (results of comparison at the five voltage levels)

No voltage level g	V_X/V_{Xr} (%)	Scale factor F_g	Standard deviation s_g(%)	Standard uncertainty u_g(%)
$g = 1$ (Example!)	20	1.0286	2.73	0.86
2	39	1.0296	1.94	0.61
3	63	1.0279	1.36	0.43
4	83	1.0304	2.15	0.68
$h = 5$	98	1.028	1.4	0.44
Result		**New scale factor F_X = 1.0289**		**Type A uncertainty u_A = 0.86 %**

An additional non-linearity contribution comes from the range of the linearity test and shall be calculated as described below under "*non-linearity effect*".

Example 1 A 1,000 kV LI voltage measuring system (AMS) with a scale factor of $F_{X0} = 1{,}000$ (calibrated 3 years ago) has shown peak voltage deviations of more than 3 % by comparison with a second AMS during a performance check. Therefore, it has to be calibrated by comparison with a RMS. A 1,200 kV LI reference measuring system (RMS) is available for that calibration. It has been decided to perform the comparison at $g = 5$ voltage levels with $n = 10$ applications each. The RMS is characterized by a scale factor $F_N = 1{,}025$ and an expanded uncertainty of measurement of $U_N = 0.80$ %. Table 2.4 shows the comparison at the first level. As a result, one gets the scale factor F_1 for that first voltage level ($g = 1$) and the related standard deviation s_1 and standard uncertainty u_1.

Table 2.5 summarizes the results of all five comparison levels and as a final result the new scale factor F_X and the Type A standard uncertainty u_A according to the Eqs. (2.15) and (2.16).

The uncertainty evaluation of Type B is related to all influences different from the statistical comparison. It includes the following contributions to the uncertainty.

2.3.4.1 Non-Linearity Effect (Linearity Test)

When the AMS is calibrated over a limited range, the linearity test is used to show the validity of the scale factor up to the rated operating voltage. It is made by comparison with an AMS of sufficient rated voltage or with the input (DC) voltage of a LI/SI test voltage generator (when the AMS is related to these voltages) or with a standard measuring gap according to IEC 60052:2002 or with a field probe (see Sect. 2.3.6). It does not matter when the linearity test shows a ratio R different from the scale factor, it is only important that it is stable over the range of the linearity test (Fig. 2.18). If this is guaranteed also other methods to investigate the linearity could be applied. The maximum deviation of the investigated $g = b$ ratios $R_g = V_x/V_{CD}$ (V_{CD} is the output of comparison device) from their mean value R_m delivers the Type B estimation of the standard uncertainty (Fig. 2.18) related to non-linearity effects:

$$u_{B1} = \frac{1}{\sqrt{3}} \cdot \max_{g=1}^{b} \left| \frac{R_g}{R_m} - 1 \right|. \tag{2.21}$$

2.3.4.2 Dynamic Behaviour Effect

For the investigation of the dynamic behaviour it is recommended to determine the scale factor of the AMS at $i = k$ different values within a frequency range or within a range of impulse shapes both representative for its use (e.g., for the rated frequency range or the nominal epoch). Then the related standard uncertainty contribution is evaluated from the maximum deviation of an individual scale factor F_i from the nominal scale factor F:

$$u_{B2} = \frac{1}{\sqrt{3}} \cdot \max_{i=1}^{k} \left| \frac{F_i}{F} - 1 \right|. \tag{2.22}$$

The dynamic behaviour can also be investigated by the unit step response method. For details see Sect. 7.4.1.

2.3.4.3 Short-Term Stability Effect

The short-term stability is often determined by the *self-heating* of the AMS, especially its converting device. The test shall be performed at rated operating voltage, it starts with the determination of the scale factor F_1 when the test voltage is reached and is terminated with a new determination of the scale factor F_2 when the pre-defined test time, usually the anticipated *time of use* or the assigned operating time, is over:

$$u_{B3} = \frac{1}{\sqrt{3}} \cdot \left| \frac{F_2}{F_1} - 1 \right|. \tag{2.23}$$

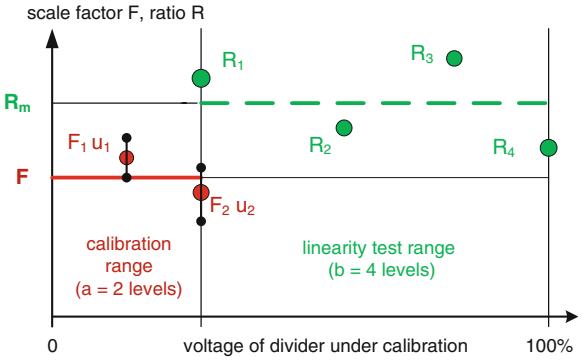

Fig. 2.18 Linearity test with a linear device in the extended voltage range (IEC 60060-2:2010)

The short time contribution to the measuring uncertainty should be given in the manufacturer's data of components.

2.3.4.4 Long-Term Stability Effect

A starting value for the contribution of the long-term stability may also be given by the manufacturer. Then it can also be determined for the time of use T_{use} from the change of the scale factor within the time of two *performance checks* (from F_1 to F_2 made at times T_1 respectively T_2, often the projected time of use is $T_{\text{use}} = T_2 - T_1$):

$$u_{B4} = \frac{1}{\sqrt{3}} \cdot \left| \frac{F_2}{F_1} - 1 \right| \cdot \frac{T_{\text{use}}}{T_2 - T_1}. \tag{2.24}$$

2.3.4.5 Ambient Temperature Effect

Usually the measuring system is specified for a certain temperature range. The scale factor is determined for the minimum and maximum temperature of that range. The larger deviation F_T from the nominal scale factor F is used to estimate the standard uncertainty contribution:

$$u_{B5} = \frac{1}{\sqrt{3}} \cdot \left| \frac{F_T}{F} - 1 \right|. \tag{2.25}$$

Often the uncertainty contribution related to the temperature effect within the specified temperature range may be taken from manufacturer's data.

2.3.4.6 Proximity Effect

The uncertainty contribution due to nearby earthed structures my be determined from the scale factors $F_{\min}$ and $F_{\max}$ at minimum and maximum distances from those structures:

$$u_{B6} = \frac{1}{\sqrt{3}} \cdot \left| \frac{F\max}{F\min} - 1 \right|. \tag{2.26}$$

The proximity effect for smaller HV measuring systems is often investigated by the manufacturer of the converting device and can be taken from the manual.

2.3.4.7 Software Effect

When digital measuring instruments, especially digital recorders, are used, a correct measurement is assumed when *artificial test data* (which are given in IEC 61083-2:2011) are within certain tolerance ranges, also given in IEC 61083-2:2011. It should not be neglected that there may be remarkable standard uncertainty contributions caused by that method. The assumed uncertainty contribution by the software is only related to the maximum width of these tolerance ranges T_{oi} given in IEC 61083-2:

$$u_{B7} = \frac{1}{\sqrt{3}} \cdot \max_{i=1}^{n}(T_{\mathrm{oi}}). \tag{2.27}$$

Note Only those tolerance ranges T_{oi} of artificial test data similar to the recorded impulse voltage must be taken into consideration.

Example 2 The AMS characterized in the first example is investigated with respect to the Type B standard uncertainty contributions. For the uncertainty estimation of the calibration also the standard uncertainties of the RMS which are not included in its measuring uncertainty must be considered. Table 2.6 summarizes both and mentions the source of the contribution.

Table 2.6 Type B uncertainty contributions

Uncertainty contribution	Symbol of contribution	Uncertainty contribution for RMS	Uncertainty contribution for AMS
Non-linearity effect Eq. (2.22)	u_{B1}	included in calibration: $u_N = U_N/2 = 0.4$ %	included in calibration u_A
Dynamic behaviour effect Eq. (2.23)	u_{B2}	included in calibration	0.43 % from deviation within nominal epoch
Short-term stability effect Eq. (2.24)	u_{B3}	included in calibration	0.24 % from deviation before and after a 3 h test
Long-term stability effect Eq. (2.25)	u_{B4}	included in calibration	0.34 % from consecutive performance tests
Ambient temperature effect Eq. (2.26)	u_{B5}	0.06 % because outside of specified temperature range	0.15 % from manufacturers data
Proximity effect Eq. (2.27)	u_{B6}	included in calibration	can be neglected because of very large clearances
Software effect Eq. (2.28)	u_{B7}	included in calibration	can be neglected because no digital recorder applied

2.3.4.8 Determination of *expanded uncertainties*

IEC 60060-2:2010 recommends a simplified procedure for the determination of the expanded uncertainty of the scale factor calibration and of the HV measurement. It is based on the following assumptions which meet the situation in HV testing:

- *Independence*: The single measured value is not influenced by the preceding measurements.
- *Rectangular distribution*: Type B contributions follow an rectangular distribution.
- *Comparability*: The largest three uncertainty contributions are of approximately equal magnitude.

> **Note** IEC 60060-2:2010 does not require the application of this simplified method, all procedures in line with the ISO/IEC Guide 98-3:2008 (GUM) are also applicable. In the Annexes A and B of IEC 60060-2:2010 a further method directly related to the GUM is described.

The relation between the standard uncertainty and the calibrated new scale factor can be expressed by the term ($F \pm u$) which characterizes a range of possible scale factors (Not to forget, F is a mean value and u is the standard deviation of this mean value!). Under the assumption of a Gauss normal density distribution (Fig. 2.17a) this range covers 68 % of all possible scale factors. For a higher confidence, the calculated standard uncertainty can be multiplied by a "covering factor" $k > 1$. The range ($F_X \pm k \cdot u$) means the scale factor plus/minus its "expanded uncertainty" $U = k \cdot u$. Usually a coverage factor $k = 2$ is applied which covers a confidence range of 95 %.

To determine first the *expanded uncertainty of the calibration* U_{cal}, the standard uncertainty u_N of measurement of the RMS from its calibration, the Type A standard uncertainty from the comparison and the Type B standard uncertainties related to the reference measuring system are combined according to the geometric superposition:

$$U_{\mathrm{cal}} = k \cdot u_{\mathrm{cal}} = 2 \cdot \sqrt{u_N^2 + u_A^2 + \sum_{i=0}^{N} u_{\mathrm{BiRMS}}2.} \tag{2.28}$$

The *expanded uncertainty of calibration* appears on the calibration certificate together with the new scale factor. But in case of a HV acceptance test, the *expanded uncertainty of a HV measurement* is required. When the AMS is calibrated and all possible ambient conditions are considered (ambient temperature range, range of clearances, etc.), then the expanded uncertainty of HV measurement can be pre-calculated by the standard uncertainty of the calibration u_{cal} and the Type B contributions of the AMS u_{BiAMS}

$$U_M = k \cdot u_M = 2 \cdot \sqrt{u_{\text{cal}}^2 + \sum_{i=0}^{N} u_{\text{BiAMS}}^2} \cdot \tag{2.29}$$

The pre-calculated expanded uncertainty of measurement should also be mentioned on the calibration certificate together with the pre-defined conditions of use. The user of the HV measuring system has only to estimate additional uncertainty contributions when the HV measuring system has to operate outside the conditions mentioned in the calibration certificate.

Example 3 For the calibrated AMS the expanded uncertainties of calibration and HV measurement shall be calculated under the assumption of certain ambient conditions mentioned in the calibration certificate. The calculation uses the results of the two examples above:

Calibration results:		
Reference measuring system (RMS):		
RMS: measuring uncertainty	$U_N = 0.80$ %	$u_N = 0.4$ %
RMS: temperature effect		$u_{B5} = 0.06$ %
Calibration by comparison		$u_A = 0.86$ %
Expanded calibration uncertainty (95 % confidence, $k = 2$)		$U_{\text{cal}} = 1.90$ %
Standard uncertainty of calibration		$u_{\text{cal}} = 0.95$ %
HV measurement:		
AMS: non-statistical influences		$u_{B2} = 0.43$ %
		$u_{B3} = 0.24$ %
		$u_{B4} = 0.\ 4$ %
		$u_{B5} = 0.15$ %
Expanded uncertainty of measurement (95 % confidence)		$U_M = 2.26$ %
Precise measurement result:		$V = V_x\ (1 \pm 0.0226)$

The HV measuring system shall be adjusted according to its new scale factor of $F = 1.0289$ (Table 2.5), possibly with a change of the instrument scale factor to maintain the direct reading of the measured HV value on the monitor. IEC 60060-2:2010 requires an uncertainty of HV measurement of $U_M \leq 3$ %. Because of $U_M = 2.26\ \% < 3\ \%$ (Example 3), the system can be used for further HV measurement. But it is recommended to investigate the reasons for the relatively high expanded uncertainty U_M for improvement of the measuring system.

2.3.4.9 Uncertainty of Time Parameter Calibration

IEC 60060-2:2010 (Sect. 5.11.2) describes a comparison method for the estimation of the expanded uncertainty of time parameter measurement. Furthermore in its

Annex B.3, it delivers an additional example for the evaluation according to the ISO/IEC Guide 98-3:2008. Instead of the consideration of the dimensionless scale factor for voltage measurement, the method applies to the time parameter (e.g., the LI front time T_{1X}) itself, considers the error of the time measurement T_{1N} by the reference measuring system as negligible and gets from the comparison directly the mean error ΔT_1,

$$\Delta T_1 = \frac{1}{n}\sum_{i=1}^{n}\left(T_{1X,i} - T_{1N,i}\right), \tag{2.30}$$

the standard deviation

$$s(\Delta T_1) = \sqrt{\frac{1}{n-1}\sum_{i=1}^{n}\left(\Delta T_{1,i} - \Delta T_1\right)^2}, \tag{2.31}$$

and the Type A standard uncertainty

$$u_A = \frac{s(\Delta T_1)}{\sqrt{n}}. \tag{2.32}$$

The Type B contributions to the measuring uncertainty of time parameters are determined as maximum differences between the errors of individual measurements and the mean error of the time parameter T_1 for different LI front times, e.g., the two limit values of the nominal epoch of the measuring system.

For external influences, the procedure of the Type B uncertainty estimation follows the principles described above for voltage measurement Eqs. (2.22–2.27). For the expanded uncertainty of time calibration and time parameter measurement an analogous application of Eqs. (2.28) and (2.29) is recommended.

A performance test includes the calibration of the scale factor, for impulse voltages also of the time parameters, and the described full set of tests of the influences on the uncertainty of measurement. The data records of all tests shall be included to the record of performance. The comparison itself and its evaluation can be aided by computer programs (Hauschild et al. 1993).

2.3.5 HV Measurement by Standard Air Gaps According to IEC 60052:2002

The breakdown voltages of uniform and slightly non-uniform electric fields, as e.g., those between sphere electrodes in atmospheric air, show high stability and low dispersion. Schumann (1923) proposed an empirical criterion to estimate the critical field strength at which self-sustaining electron avalanches are ignited. If

modified, this criterion can also be used to calculate the breakdown voltage V_b of uniform fields versus the gap spacing S. For a uniform electric field in air at standard conditions the breakdown voltage can be approximated by the empirical equation

$$V_b/\mathrm{kV} = 24.4\left[S + \left(\frac{S}{13.1\,\mathrm{cm}}\right)^{0.5}\right]. \tag{2.33}$$

This equation is applicable for sphere gaps if the spacing is less than one-third of the sphere diameter Fig. (2.19).

Based on such experimental and theoretical results, *sphere-to-sphere gaps* are used for peak voltage measurement since the early decades of the twentieth century (Peek 1913; Edwards and Smee 1938; Weicker and Hörcher 1938; Hagenguth et al. 1952) and led to the first standard of HV testing, the present IEC 60052:2002. Meanwhile it is fully understood that this applicability is based on the so-called streamer breakdown mechanism, e.g., Meek (1940), Pedersen (1967), and breakdown voltage-gap distance characteristics of sphere gaps can also be calculated with sufficient accuracy (Petcharales 1986).

For a long time *measuring sphere gaps* with gap diameters up to 3 m formed the impression of HV laboratories. But the voltage measurement by sphere gaps is connected with the breakdown of the test voltage therefore their application is not simple. Furthermore they need a lot of clearances (see below), well maintained clean surfaces of the spheres and atmospheric corrections (see Sect. 2.1.2) for measurement according to the standard.

Today they are not used for daily HV measurement and do not play the same important role in HV laboratories as in the past. Their main application is for *performance checks* of AMSs (see Sect. 2.3.2) or linearity checks (see Sect. 2.3.4). For acceptance tests on HV apparatus the inspector may require a check of the applied AMS by a sphere gap to show that it is not manipulated. For these applications mobile measuring gaps with sphere diameters $D \leq 50$ cm are sufficient.

The IEC Standard on voltage measurement by means of sphere gaps has been the oldest IEC standard related to HV testing. Its latest edition IEC 60052 Ed.3:2002 describes the measurement of AC, DC, LI and SI test voltage with horizontal and vertical sphere-to-sphere gaps with sphere diameters $D = (2 \ldots 200$ cm) and one of the spheres earthed. The spacing S for voltage measurement is required $S \leq 0.5\,D$, for rough estimations it can be extended up to $S = 0.75\,D$. The surfaces shall be smooth with maximum roughness below 10 μm and free of irregularities in the region of the sparking point. The curvature has to be as uniform as possible, characterized by the difference of the diameter of no more than 2 %. Minor damages on that part of the hemispherical surface, which is not involved in the breakdown process, do not deteriorate the performance of the measuring gap. To avoid erosion of the surface of the sphere after AC and DC breakdowns, pre-resistors may be applied of 0.1–1 MΩ.

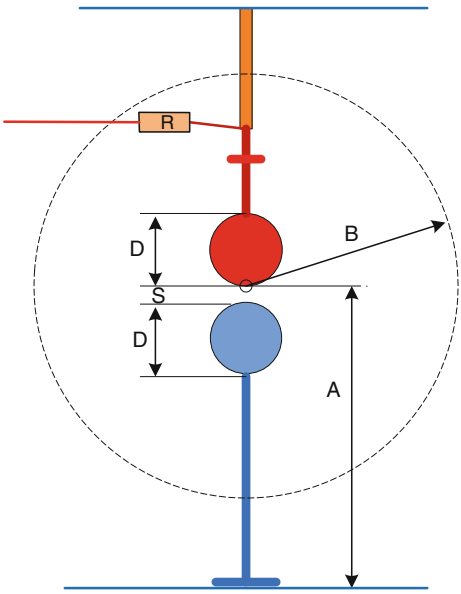

Fig. 2.19 Vertical measuring sphere gap (explanations in the text)

Surrounding objects may influence the results of sphere gap measurements. Consequently the dimensions and *clearances* for standard air gaps are prescribed in IEC 60052 and shown in Figs. 2.19 and 2.20. The required range of the height A above ground depends on the sphere diameter, and is for small spheres $A = (7 \ldots 9)\ D$ and for large spheres $A = (3 \ldots 4) \cdot D$. The clearance to earthed external structures depends on the gap distance S, and shall be between $B = 14\ S$ for small and $B = 6\ S$ for large spheres.

The dispersion of the breakdown voltage of a measuring gap depends strongly from the availability of a free starting electron, especially for gaps with $D \leq 12.5$ cm and/or measurement of peak voltages $U_p \leq 50$ kV. Starting electrons can be generated by photo ionization (Kuffel 1959; Kachler 1975). The necessary high energy radiation may come from the far ultra-violet (UVC) content of nearby corona discharges at AC voltage, or from the breakdown spark of the open switching gaps of the used impulse generator, or a special mercury-vapour UVC lamp with a quartz tube.

Note In the past, even a radioactive source inside the measuring sphere has been applied. For safety reasons this is forbidden now.

Table 2.7 gives the relationship of the measured breakdown voltage U_b depending on the distance S between electrodes for some selected sphere diameters $D \leq 1$ m which are mainly used for the mentioned checks, for other sphere diameters see IEC 60052:2002. A voltage measurement with a sphere gap means to establish a relation between an instrument at the power supply input of the HVG (e.g., a primary voltage measurement at the input of a test transformer) and the known breakdown voltage of the standard measuring gap in the HV circuit

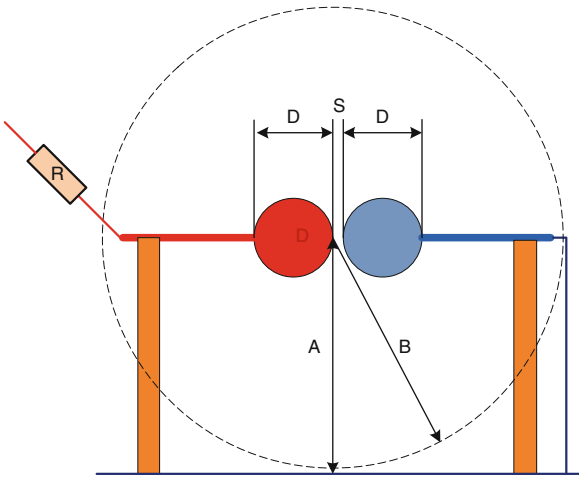

Fig. 2.20 Horizontal measuring sphere gap

depending on its gap distance D (Table 2.7). This is similar to the calibration by comparison (Sect. 2.3.3).

For *AC voltage measurement* a progressive stress test (see Sect. 2.4) delivers 10 successive breakdown voltage readings by the instrument. Their mean value (Eq. 2.12) and the relative standard deviation (Eq. 2.13) are determined. The voltage shall be raised sufficiently slowly to allow accurate readings. The mean value characterizes the breakdown voltage according to the gap parameters (D, S). When the standard deviation is $\leq$1 %, one can assume that the measuring gap was correctly maintained and the relative expanded uncertainty of measurement is $\leq$3 %.

> **Note** With $n = 10$ measurements and a standard deviation of 1 % one gets a standard uncertainty of $u = 0.32$ % (Eq. 2.14). This means there are about 1.2 % for the other contributions to the standard uncertainty when the expanded uncertainty ($k = 2$) shall be $\leq$3 % (Eq. 2.29).

For *LI/SI voltage measurement*, the pre-selected breakdown voltages (D, S in Table 2.7) are compared e.g., with charging voltage of the impulse voltage generator. The 50 % breakdown voltages U_{50} are determined in a multi-level test of $m = 5$ voltage levels with $n = 10$ impulse voltages each (see Sect. 2.4), and the corresponding reading is taken as the pre-selected reading. When the evaluated standard deviation is within 1 % for LI and 1.5 % for SI voltages it is assumed that the measuring gap works correctly.

For *DC voltage measurement*, sphere gaps are not recommended because external influences as dust or small fibres are charged in a DC field and cause a high dispersion. Therefore, a *rod–rod measuring gap* shall be applied if the humidity is not higher than 13 g/m^3 (Feser and Hughes 1988; IEC 60052:2002). The rod electrodes of steel or brass should have a square cross section of 10–25 mm for each side and sharp edges. When the gap distance S is between 25 and 250 cm the breakdown is caused by the development of a streamer discharge

Table 2.7 Peak value of breakdown voltages of selected standard sphere gaps

Gap distance S/mm	50 % breakdown voltage V_{b50}/kV at sphere diameter D/mm[b]							
	100		250		500		1,000	
	AC, DC[a], −LI, −SI	+LI, +SI	AC, DC[a], −LI, −SI	+LI, +SI	AC, DC[a], −LI, −SI	+LI, +SI	AC, DC[a], −LI, −SI	+LI, +SI
5	16.8	16.8						
10	31.7	31.7	31.7	31.7				
15	45.5	45.5	45.5	45.5				
20	59	59.0	59.0	59.0	59.0	59.0		
30	84	85.5	86.0	86.0	86.0	86.0	86.0	86.0
50	123	130	137	138	138	138	138	138
75	(155)[c]	(170)	195	199	202	202	203	203
100			244	254	263	263	266	266
150			(314)	(337)	373	380	390	390
200			(366)	(395)	460	480	510	510
300					(585)	(620)	710	725
400					(670)	(715)	875	900
500							1,010	1,040
600							(1,110)	(1,150)
750							(1,230)	(1,280)

Explanations:

[a] For measurement of DC test voltages >130 kV standard sphere gaps are not recommended, apply rod–rod gaps and see Eq. (2.34)

[b] For correctly maintained standard sphere gaps, the expanded uncertainty of measurement of AC, LI and SI test voltages is assumed to be $U_M \approx 3$ % for a confidence level of 95 %. There is no reliable value for DC test voltages

[c] The values in brackets are for information, no level of confidence is assigned to them

of a required average voltage gradient $e = 5.34$ kV/cm. Then the breakdown voltage can be calculated by

$$V_b/\text{kV} = 2 + 5.34 \cdot \text{S/cm}. \tag{2.34}$$

The length of the rods in a vertical arrangement shall be 200 cm, in a horizontal gap 100 cm. The rod–rod arrangement should be free of PD at the connection of the rods to the HV lead, respectively to earth. This is realized by toroid electrodes for field control. For a horizontal gap the height above ground should be ≥400 cm. The test procedure is as that for AC voltages described above.

2.3.6 *Field Probes for Measurement of High Voltages and Electric Field Gradients*

The ageing of the insulation and thus the reliability of HV apparatus is mainly governed by the maximum electrical field strength. Even if the field distribution in

dielectric materials can well be calculated based on the Maxwell equations using advanced computer software, the validity of the theoretical results should be validated experimentally. For this purpose *capacitive sensors*, commonly referred to as field probes, can be used. The field distribution, however, may substantially be affected by the presence of such field probes which should thus be designed as small as possible to minimize the field distortion und thus the inevitable measuring uncertainty (Les Renardieres Group 1974; Malewski et al. 1982). In specific cases, however, field probes can be designed such that the field is not disturbed, as in the case of coaxial electrode configurations representative for bushings, power cables and SF_6 switchgears. Moreover, field probes can be integrated in the earth electrode of a plane-to-plane electrode arrangement of Rogowski profile, as sketched in Fig. 2.21. Under this condition the voltage applied to the HV electrode can simply be deduced from the field strength at the sensing electrode.

The fundamental measuring principle is based on the first Maxwell equation which reads:

$$\mathrm{rot}\,\vec{H} = \partial\vec{D}/\partial t + \vec{G}, \tag{2.35}$$

with $\vec{H}$—vector of the magnetic field strength, $\vec{D}$—vector of the electric displacement flux density, $\vec{G}$—vector of the current density at the sensor electrode.

For gaseous dielectrics the conductivity is extremely low so that the second term in Eq. (2.35) can be neglected:

$$\mathrm{rot}\,\vec{H} = \partial\vec{D}/\partial t, \tag{2.36a}$$

In contrast to this the conductivity of the sensing electrode is extremely high so that for this case the first term in Eq. (2.35) can be neglected:

$$\mathrm{rot}\,\vec{H} = \vec{G}, \tag{2.36b}$$

Combining the Eqs. (2.36a and 2.36b) and substituting the density of the displacement flux by the electrical field strength, i.e., $\vec{D} = \varepsilon \cdot \vec{E}$, one gets

$$\vec{G} = \partial\vec{D}/\partial t \;=\; \varepsilon \cdot \partial\vec{E}/\partial t, \tag{2.37}$$

with ε—permittivity of the dielectric between both electrodes.

For the here considered homogenous field configuration the field gradient occurs perpendicular to the surface of the sensing electrode. Thus, instead of the vector presentation the simple scalar presentation valid for one dimensional configurations is applicable. Consequently the current $I(t)$ captured by the sensor can simply be expressed by the current density G multiplied with the area A of the sensing electrode:

$$I(t) = A \cdot G = A \cdot \varepsilon \cdot \mathrm{d}E(t)/\mathrm{d}t. \tag{2.38}$$

To convert the current induced at the sensor surface into an equivalent voltage signal $V_m(t)$ it is a common practice to connect the sensor via a measuring

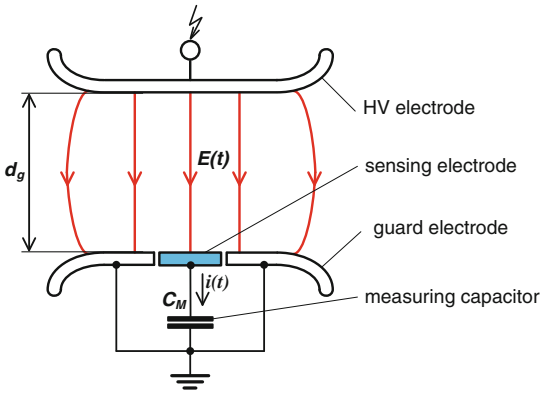

Fig. 2.21 Principle of a field probe for measurements of high alternating voltages

capacitance C_m to earth potential, see Fig. 2.21. As this provides a capacitive voltage divider, the time-dependent voltage $V_h(t)$ applied to the HV electrode can simply be determined from the voltage $V_m(t)$ measurable across C_m using the following equation:

$$V_h(t) = \frac{d_{g \cdot C_m}}{A \cdot \varepsilon} \cdot V_m(t) = S_f \cdot V_m(t), \tag{2.39}$$

with S_f—scale factor, d_g—gap distance.

In principle the measuring capacitance C_m shown in Fig. 2.21 could also be replaced by a resistor, in the following denoted as R_m. Under this condition one gets from Eq. (2.38):

$$V_m(t) = R_m \cdot A \cdot \varepsilon \cdot \mathrm{d}E(t)/\mathrm{d}t. \tag{2.40}$$

Based on this, the peak voltage V_{hp} applied to the top electrode can be determined by

$$V_{\mathrm{hp}} = \frac{d_g}{R_m \cdot A \cdot \varepsilon} \cdot \int_0^t V_m(t)\mathrm{d}t = \frac{d_g}{R_m \cdot A \cdot \varepsilon \cdot 2\pi f} \cdot V_{\mathrm{mp}} = S_f \cdot V_{\mathrm{mp}} \tag{2.41}$$

From this equation follows that the scale factor S_f is inversely proportional to the test frequency f, so that not only R_m but also the test frequency f must be exactly known, to determine the peak value of the applied high voltage from the measured low voltage, where harmonics should not appear because they may cause severe measuring errors.

Example Consider an arrangement according to Fig. 2.21 in ambient air with $\varepsilon_0 = 8.86$ pF/V m. Assuming a gap distance $d_g = 10$ cm and an area of the sensing electrode $A_s = 10\ \mathrm{cm}^2$ as well as a capacitance $C_m = 2$ nF, one gets the following scale factor:

$$S_f = \frac{d_g \cdot C_m}{A \cdot \varepsilon_0} = \frac{(10\,\mathrm{cm}) \cdot (2\,\mathrm{nF})}{(10\,\mathrm{cm}^2) \cdot (8.86\,\mathrm{pF/m})} = 22.6 \times 10^3.$$

If, for instance, a low voltage of $V_m = 5$ V across C_m is measured, the applied high voltage becomes $V_m = 113$ kV. Substituting the capacitor C_m by a measuring resistor of $R_m = 500$ kΩ and assuming a test frequency $f = 50$ Hz, one gets the following scale factor:

$$S_f = \frac{d_g}{R_m \cdot A_s \cdot \varepsilon_0 \cdot 2\pi f} = 18 \times 10^3.$$

The curves plotted in the graph according to Fig. 2.22, which are based on the above calculations, enable a simple determination of the applied high voltage V_h from the measured low voltage V_m. In this context it has to be taken into account that the scale factor is dependent on the test frequency, if a measuring resistor is used.

The main disadvantage of the arrangement shown in Fig. 2.21 is that it is only capable for measuring the field gradients occurring adjacent to earth potential. To measure also arbitrarily oriented field vectors in the space between HV and LV electrodes, *spherical sensors* are employed (Feser and Pfaff 1984). As illustrated in Fig. 2.23a, the surface of such a sphere is subdivided into six partial sensors to receive the three cartesian components of the electromagnetic field. To minimize the inevitable field disturbance caused by the metallic probe, it is battery powered and the whole components required for signal processing are integrated in the hollow sphere. The evaluated data are transmitted to earth potential via a fiber optic link. An essential benefit of the spherically shaped probe is that the admissible radius depending on the field strength to be measured can be calculated without large expenditure.

Practical realized spherical field probes are capable for measuring field strengths up to about 1 kV/cm where the measuring frequency ranges between approx. 20 Hz and 100 MHz. The application is not only restricted to field strength measurements. If calibrated with a reference measuring system it can also be employed for high voltage measurements if the field is free of space charges which could be caused by corona discharges.

As the field probe provides a capacitive sensor it has to be taken into account that the induced charge and thus the measurable current $i(t)$ is a consequence of the displacement flux which is correlated with the time dependent field strength $E(t)$. Thus, only time dependent voltages, such as LI, SI, AC and other transients, induce a measurable displacement current. To measure also DC voltages, the desired alternating displacement current could be generated if the sensing electrode is periodically shielded by a rotating electrode connected to earth potential. This approach, schematically shown in Fig. 2.23b, is applied by the so-called f*ield mill* (Herb et al. 1937; Kleinwächter 1970). Here the sensing electrode is established by two half-sectioned discs providing the measuring electrodes, which must be well isolated from each other. The vane electrode is connected to the guard electrode on earth potential. If the vane electrode is rotating in front of the measuring electrodes, an alternating displacement flux exposes these both electrodes

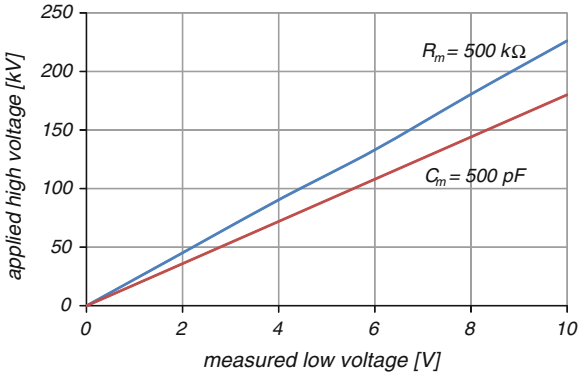

Fig. 2.22 Applied high voltage versus low voltage measurable across a capacitive respectively a resistive measuring impedance using parameters given in the text

and induces thus an alternating current. This is correlated with the electrostatic field strength on the electrode surface which is usually indicated by means of a high sensitive amplifier, where the input impedance must be extremely high.

Another option for the measurement of high DC voltages by means of a field probe is the replacement of the electrical method by a mechanical one. That means the measuring impedance C_m shown in Fig. 2.21 is replaced by a sensitive force measurement system, as first applied by Kelvin in 1884 for absolute measurement of DC voltages. The principle applied is based on the Coulomb law discovered in 1785. For a homogeneous field the force attracting the sensing electrode of an area A if subjected to a field gradient E can be expressed by:

$$F_e = \frac{1}{2} \cdot \varepsilon \cdot A \cdot E^2. \tag{2.42}$$

Example If, for instance, a voltage of $V_h = 100$ kV is applied to the top electrode and the gap distance is $d_g = 10$ cm, then the field strength at the sensing electrode achieves 10 kV/cm. Inserting these values in Eq. (2.42), the force attracting the sensing electrode becomes $F_e \approx 3.5 \times 10^{-2}$ N ≈ 3.6 p.

The torsion due to the attracted sensing electrode is usually amplified and indicated by a spot light and mirror system. As the electric force is proportional to the quadratic value of the field gradient and thus also proportional to the quadratic value of the applied test voltage, the indication is independent from the polarity. Thus, *electrostatic voltmeters* are capable not only for DC voltage measurements but also for measuring the r.m.s. value of HVAC test voltages, as treated in Sect. 3.4.

2.4 Breakdown and Withstand Voltage Tests and Their Statistical Treatment

Electrical discharges and breakdown of insulations are stochastic processes which must be described by statistical methods. This subsection gives an introduction to

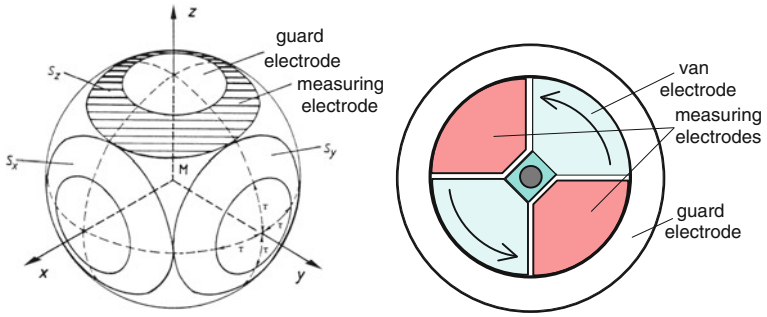

Fig. 2.23 Field probes using fixed and rotating electrodes

the planning, performing and evaluation of HV tests on a statistical basis. It describes tests with voltages increasing up to the breakdown ("progressive stress method") and with multiple application of pre-given voltages and estimation of breakdown probabilities ("multiple level method", "up-and-down method"). Lifetime tests of insulation are performed with pre-given voltages, but progressive test durations and can be evaluated accordingly. Also standardized HV withstand tests are described and valuated from the viewpoint of statistics. The subsection submits first tools for the application of statistical methods and supplies hints to the special literature, e.g., (Hauschild and Mosch 1992).

2.4.1 Random Variables and the Consequences

The phenomena of *electrical discharges*—as most others in nature, society and technology—are based on stochastic processes and characterized by their randomness (Van Brunt 1981; Hauschild et al. 1982). This is often ignored and only an average trend is considered in order to interpret a relationship being investigated. Quite often, however, it is not the mean value, but an extreme value that determines the performance of a system. In technology this is often taken into account by applying a "safety factor". A rather better approach is the statistical description of stochastic phenomena. Therefore, *HV tests* shall be selected, performed and evaluated on a statistical basis: They are *random experiments (trials)* and described by *random variables* (sometimes also called "random variates").

When a pre-given *constant voltage stress*—e.g., a certain LI test voltage—is applied to an insulation—e.g., an air gap—one can observe the random event "breakdown" (A) or the complimentary event "withstand"(A^*). The relative breakdown frequency$h_n(A)$ is the relation between the number of breakdowns k and the number of applications n

$$h_n(A) = k/n. \tag{2.43}$$

The relative *withstand frequency* follows to

$$h_n(A*) = (n-k)/n = 1 - h_n(A). \tag{2.44}$$

The relative frequency depends on the number of performed tests (often called *sample size*) and the respective test series as shown for the breakdown frequency in Fig. 2.24. The relative frequencies vary around a fixed value and reach it as the limiting value "*breakdown probability*" p:

$$\lim_{n\to\infty} h_n(A) = p. \tag{2.45}$$

The *probability of a withstandq* follows accordingly

$$\lim_{n\to\infty} h_n(A*) = q. \tag{2.46}$$

Because a characteristic value of withstand cannot be measured ("Nothing happens!"), the withstand probability is determined from the complementary breakdown probability $q = 1 - p$. Consequently the statistical definition of a withstand voltage is a voltage which causes a breakdown with low probability, usually $p \leq 0.10$. The relative breakdown frequency is a *point estimation* of the breakdown probability.

The larger the number of applications for the estimation of the frequency, the better is the adaptation of the estimate to the true, but unknown probability (Fig. 2.24). A confidence estimation delivers a feeling for the accuracy of the estimation by the width of the calculated confidence region. This region covers the true but unknown value of p with a certain *confidence level*, e.g., $\varepsilon = 95$ %. From the sample the upper and the lower limit of the confidence region are determined on the basis of the assumption of a theoretical distribution function, in this case based on the *binomial distribution function* and the Fisher (F) distribution as test distribution.

Explanation: The binomial distribution is based on two complementary events A and $A*$ (as breakdown and withstand) occurring with the known probabilities p and q (Bernoulli trial). The binomial distribution indicates the probability $P(X = k)$ with which the event A will occur k-times in n independent trials.

$$P(X = k) = \binom{n}{k} p^k (1-p)^{n-k} \tag{2.47}$$

where $k = 0, 1, 2, \ldots, n$ and

$$\binom{n}{k} = \frac{n!}{k! \cdot (n-k)!} = \frac{n \cdot (n-1) \cdot \ldots (n-k+1)}{1 \cdot 2 \cdot 3 \cdot \ldots \cdot k}$$

Figure 2.25 shows the 95 % *confidence limits* depending on the relative breakdown frequency and the number of applications (sample size).

Example For $h_n(A) = 0.7$ and $n = 10$ applications, Fig. 2.25 delivers the lower limit $p_l = 0.37$ and the upper limit $p_u = 0.91$. With a statistical confidence $\varepsilon = 95$ %, the real probability is within a range of $0.37 \leq p \leq 0.91$. For $n = 100$ applications one would get

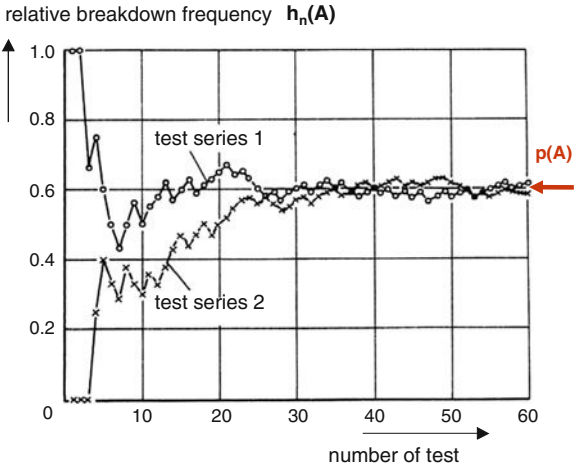

Fig. 2.24 Relative breakdown frequencies of two test series depending on the number of tests performed

the much smaller range $0.60 \leq p \leq 0.78$. Again, with increasing sample size the estimation becomes better, this means the confidence region becomes smaller.

When a constant voltage test has been performed for the estimation of the breakdown probability, it must be checked whether the test is "independent" or not. *Independence* means that the previous voltage applications have no influence on the result of the application under consideration. This can be shown by the investigation of the trend (Table 2.8). A sample of $n = 100$ is subdivided into five samples of $n^* = 20$ each. If the relative frequencies of the sub-samples scatter around that of the whole sample, it could be considered as independent (case a). If there is a clear trend (case b) it would be dependent and any statistical evaluation is forbidden. Independence can only be ensured due to an improvement of the test procedure, e.g., breaks of sufficient duration between single stresses. Further details of constant voltage tests are described in (Hauschild and Mosch 1992).

There is a second group of HV breakdown tests with increasing stress, e.g., continuously raising AC or DC test voltages or LI or SI voltages raising in steps until breakdown (Fig. 2.26). Now the breakdown is sure, but the height of the breakdown voltage is random. This group of tests is called "progressive stress tests". The random variable is the breakdown voltage V_b. But in life-time tests at constant voltage, the time-to-breakdown T_b becomes the random variable. In both cases we have a continuous variable.

Note In case of stepwise increasing voltages, the starting value may be varied to get continuous outputs (realizations) of the random variable.

The evaluation of progressive stress tests follows the typical treatment of *random variables* in mathematical statistics as described in many text books as e.g., by Mann et al. (1974), Müller et al. (1975), Storm (1976) or Vardeman (1994). Descriptions especially related to HV tests are given by Lalot (1983), Hauschild and Mosch (1984) (in German) and (1992) (in English), Carrara and

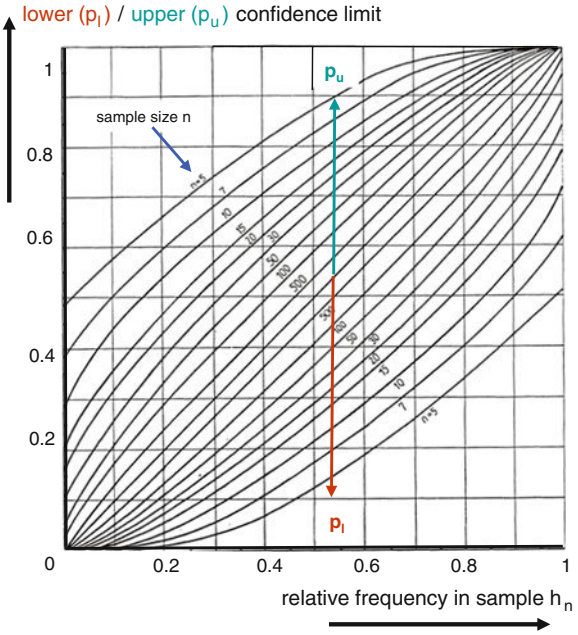

Fig. 2.25 Confidence limits of the breakdown probability for a confidence level $\varepsilon = 95$ %. Depending on sample size

Table 2.8 Check of independence of two tests with sample size $n = 100$

(a) Independent sample: Sphere-plane gap in atmospheric air (withstand: -; breakdown: **x**)	breakdown frequency	
	h_{20}	h_{100}
- x x x - - - x - x x x x x x x - x - x	0.65	
x - x- - x x x x x - x x- x x x x x x	0.75	
- x x x x - x x x x x x - x - x x x –	0.70	
x x x - x x - x - x - - - x - x x x - x	0.6	0.68
x x - x x x x - - x - x - x x x x x x -	0.7	
(b) Dependent sample: As above, but enclosed air in a tank (withstand: -; breakdown: x)	h_{20}	h_{100}
x x x x x x x x x x x x x x x x x x x - x	0.95	
x - x- x x - x x - - x x x - x - - x x -	0.55	
- - - x x x - x - - - x - x x - x- x x	0.5	
- x x - - - - - - x - - - x - x - - x x	0.35	0.48
- - - - - - x - - - - - - - - - - - - -	0.05	

Hauschild (1990) and Yakov (1991) as well as in Appendix A of (IEC 60060-1:2010).

The distribution of a random variable X with realizations x_i found in a progressive stress test is described by a *distribution function*. It is defined by

$$F(x_i) = P(X < x_i), \tag{2.48}$$

and it indicates the probability P with which the random variable X will assume a value below the considered value x_i. A distribution function (Fig. 2.27) is any mathematical function with the following properties:

$0 \leq F(x_i) \leq 1$ (realizations between impossible and sure events),
$F(x_i) \leq F(x_{i+1})$ (monotonously increasing),
$\lim_{x \to -\infty} F(x) = 0$ and $\lim_{x \to +\infty} F(x) = 1$ (boundary conditions).

Note Instead of the distribution function also the density function delivers a complete mathematical description, but it is not meaningful for HV test evaluation.

A distribution function is characterized by parameters describing the mean value and the dispersion, sometimes in addition to the position of the function. The evaluation of a progressive stress test means the selection of a well adapted type of distribution function and the estimation of its parameters. The parameter estimation can be made as a point or confidence estimation based on formulas of functional parameters (e.g., the mean value), quantiles (realization of the random variable related to a pre-given probability) or intervals (difference between two quantiles) (Fig. 2.27).

2.4.2 HV Tests Using the Progressive Stress Method

The *progressive stress method* (PSM) with continuous increasing voltage shall be considered for an electrode arrangement in SF_6 gas (Fig. 2.26a). The initial voltage v_0 must be low enough to avoid any influence on the result, the rate of rise of the voltage shall be so that a reliable voltage measurement can be performed, and the interval between two individual tests shall guarantee the *independence* of the realizations v_b. The independence may be checked by a graphic plot of the measurements. Other independence tests are described in the above mentioned literature.

Example Figure 2.28 shows the sequence of four test series at four different pressures of the SF_6 gas. A series is considered to be independent if the realizations fluctuate in a random manner around a mean value. A dependence must be assumed, if there is a falling, raising or periodically fluctuating tendency. According to this simple rule, the series at gas pressures of 0.40, 0.25, and 0.15 MPa can be considered as independent and are well suited for a statistical evaluation. That at 0.10 MPa is dependent and shall not be statistically evaluated. The reason for the dependence should be clarified and the series repeated under improved conditions.

Each independent series shall be evaluated statistically, this means graphically represented and approximated by a theoretical distribution function. Both tasks can be connected when a so-called *probability grid* is used for the representation. A probability grid uses the inverse function of the considered theoretical distribution function on the ordinate. For each type of theoretical distributions, a probability

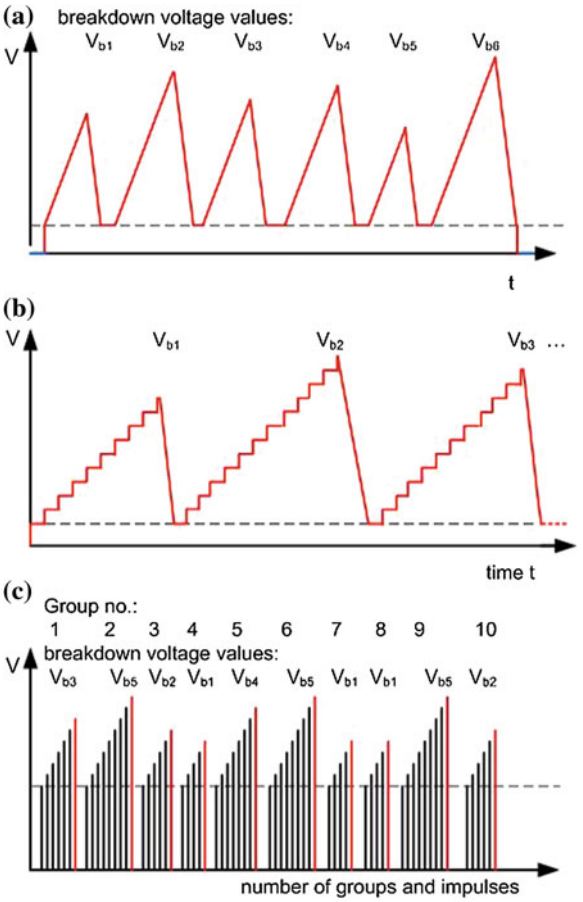

Fig. 2.26 Procedures of progressive stress tests. **a** Continuous increasing AC or DC voltage. **b** Stepwise increasing AC or DC voltage. **c** Stepwise increasing LI or SI voltage

grid can be constructed. Any empirical distribution of the same type as the grid appears as a straight line.

The following theoretical distribution functions are recommended for HV applications:

The *Gauss or normal distribution* is characterized by the parameters μ (estimated by the arithmetic mean value or the 50 % quantile u_{50}) and the standard deviation σ [estimated by the mean square root of $(x_i - \mu)$ or the difference of quantiles $(x_{84} - x_{50}) = (x_{50} - x_{16})$]:

$$F(x;\mu;\sigma^2) = \frac{1}{\sqrt{2\pi}\sigma} \int_{-\infty}^{x} \mathrm{e}^{-\frac{(z-\sigma^2)}{2\sigma^2}} \mathrm{d}z. \tag{2.49}$$

The application of a certain distribution function should be based on its stochastic model: A normal-distributed random variable is the result of a large

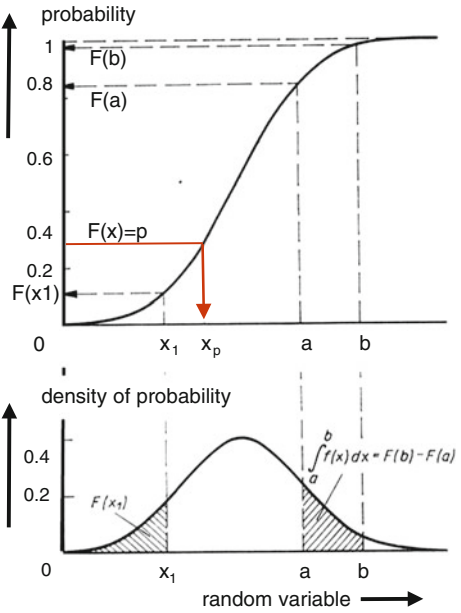

Fig. 2.27 Distribution (**a**) and density (**b**) function with the definitions of quantile x_1 and probability interval $(F(b) - F(a))$

number of independent, randomly distributed influences when each of these makes only an insignificant contribution to the sum. This model is very well applicable to many random events, also to breakdown processes with partial discharges.

The *Gumbel or double exponential distribution* is—as the normal distribution—an unlimited function $(-\infty < x < +\infty)$ characterized by two parameters, its 63 % quantile η and the dispersion measure γ [estimated by $\gamma = (x_{63} - x_{05})/3$]:

$$F(x;\eta;\gamma) = 1 - \mathrm{e}^{-\mathrm{e}^{\frac{x-\eta}{\gamma}}}. \tag{2.50}$$

Stochastic model: The double exponential distribution describes the distribution of realisations according to an extreme value, in case of HV tests it is the minimum of the electric strength. It is a mathematical description of the simple fact that "the breakdown of a slightly uniform electric field takes place at the weakest point". It can be well applied if there are slightly uniform insulations which show a quite high dispersion (Mosch and Hauschild 1979).

The *Weibull distribution* is also a distribution describing extreme values, but it is limited and characterized by three parameters, its 63 % quantile $\eta = x_{63}$, the Weibull exponent δ as a measure of dispersion and the initial value x_0

$$F(x;\eta;\delta;x_0) = 1 - \mathrm{e}^{-\left(\frac{x-x_0}{\eta}\right)^{\delta}} \quad x > x_0, \tag{2.51a}$$

$$F(x;\eta;\delta;x_0) = 0 \quad x \leq x_0, \tag{2.51b}$$

$$\delta = 1.2898/\log(x_{63}/x_{05}). \tag{2.51c}$$

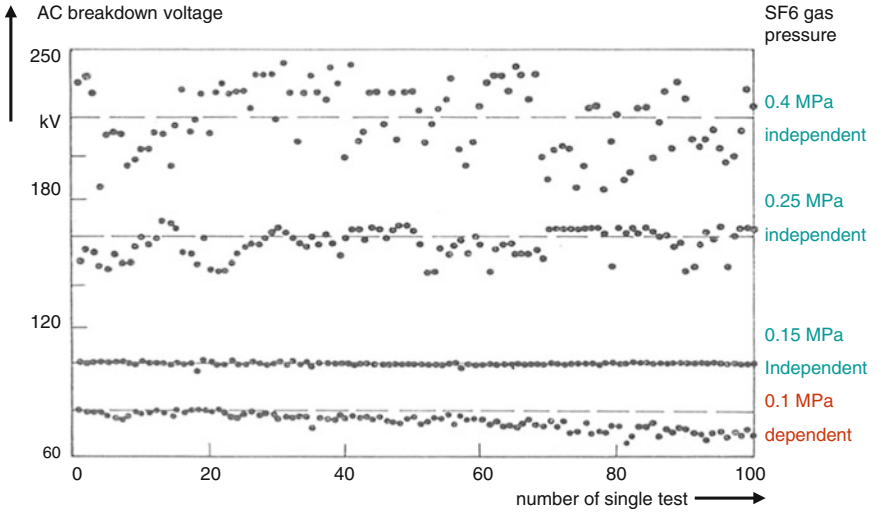

Fig. 2.28 Graphical check of independence of four test series in SF_6 gas

The Weibull distribution is highly adaptable in its structure and therefore applicable for many problems (Cousineau 2009). For the case $x_0 = 0$ it is the ideal function for breakdown time investigation (two-parameter Weibull distribution), see e.g., Bernard (1989) and Tsuboi et al. (2010). In the case $x_0 > 0$, the initial value becomes an absolute meaning, e.g., as an ideal withstand voltage of the breakdown probability $p = 0$! Therefore consequences must be carefully considered when it is applied to breakdown voltage problems.

For all three theoretical distribution functions a *probability grid* can be constructed. Figure 2.29 shows the comparison of the different ordinates of these grids. It can be seen that in the region x_{15}–x_{85} the grids are very similar, but for very low and very high probabilities remarkable differences exist. This means that for estimation of withstand voltages the correct selection of a theoretical distribution function for the adaptation of empirical data (test results) is very important.

In HV tests the *empirical distribution function* is usually determined from a quite limited number of realizations, e.g., $10 \leq n \leq 100$. In that case it is recommended to arrange the realisations x_i according to increasing magnitude between x_{min} and x_{max} and to complete them by their relative, *cumulative frequencies*

$$h_{\Sigma i} = \sum_{m=1}^{i} \frac{h_m}{(n+1)} \tag{2.52}$$

where n is the total number of realizations and h_m is the absolute frequency of the mth voltage value (Eq. 2.43). Then the data are plotted as a "stair" in a suited probability grid. If the empirical (stair) function can be approximated by a straight line, the adaptation with the theoretical function of the grid is acceptable.

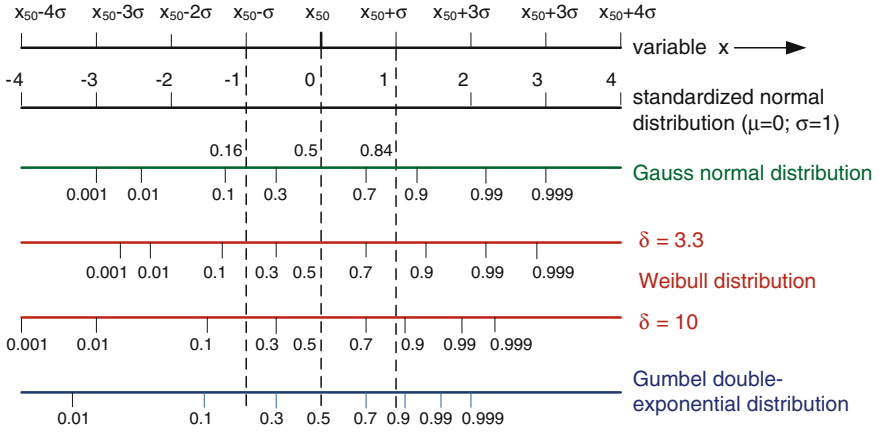

Fig. 2.29 Comparison of ordinates of probability grids with identical 50 % quantiles (logarithmic abscissa for Weibull distribution)

Example Figure 2.30 shows, the stair function can be well adapted by a straight line in the Gauss grid of a normal distribution. This means a normal distribution describes the randomness of the performed test sufficiently. Its parameters can be estimated by quantiles: The mean value by $u_{50} = 953$ kV and the standard deviation by $s = u_{50} - u_{16} = 18.2$ kV.

A *confidence estimation* of the parameters can be performed using so-called test distributions, the *t*-distribution for confidence estimates of the mean value and the χ^2-distribution for the standard deviation. For details see e.g., Hauschild and Mosch (1992).

The *maximum likelihood method* delivers the most efficient estimation of parameters including their confidence limits. As the term "likelihood" is a synonym for "probability", the method delivers estimates of parameters of the selected distribution function, which are those of maximum probability for the given sample. The method has been introduced many years ago, but got its broad application with numerical calculations by personal computers (PC). It can be applied for all classes of HV breakdown tests and any type of theoretical distribution function (Carrara and Hauschild 1990; Yakov 1991; Vardeman 1994).

The mathematical calculations are based on the so-called "*likelihood function* L". It is proportional to the probability p_R to obtain a description of the investigated sample (realizations x_i with $i = 1 \ldots n$) using a distribution function, e.g., with the parameters δ_1 and δ_2. The n realizations of the sample are distributed to m levels of the random variable x_i (breakdown voltage or time). The likelihood function L is based on the probability p_R which is proportional to the product of the probabilities f_{Ri}:

$$L = Ap_R = A\prod_{i=1}^{m} f_{Ri}(x_i/\delta_1, \delta_2) = L(x_i/\delta_1, \delta_2). \tag{2.53}$$

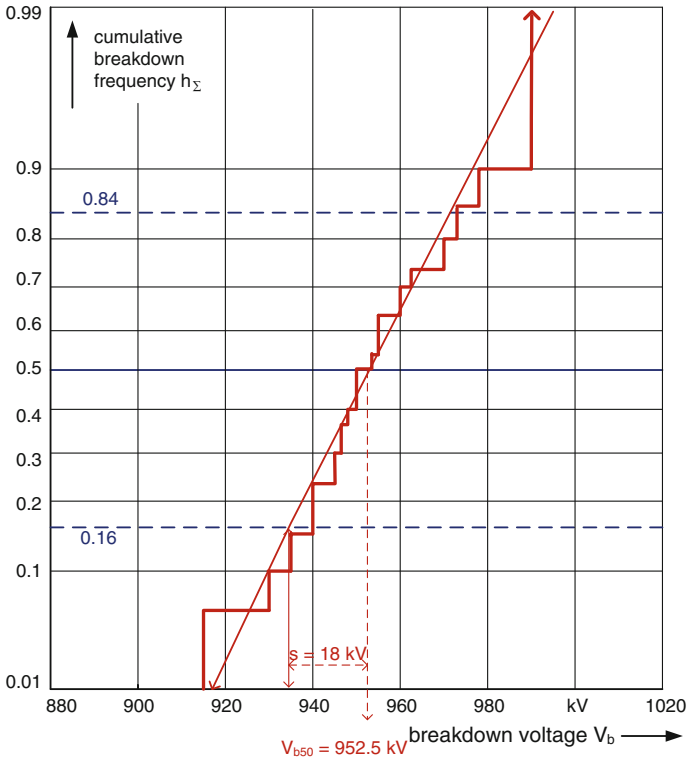

Fig. 2.30 Cumulative frequency distribution function on a Gauss grid

The factor "A" is for normalization only. The most likely *point estimates* of the parameters δ_1 and δ_2 are those which maximize L as shown in Fig. 2.31 (δ^*_1 and δ^*_2). They are calculated from the maximum conditions $dL/d\delta_1 = 0$ and $dL/d\delta_2 = 0$, usually performed with the logarithms where the same parameters indicate the maximum

$$d(\ln L)/d\delta_1 = 0 \quad \text{and} \quad d(\ln L)/d\delta_2 = 0. \tag{2.54}$$

The three-dimensional diagram shows the likelihood function (L normalized to its maximum) on the area of the two parameters. By help of a cross section through the "likelihood mountain" one can define the confidence limits of the parameters (δ_{1min}, δ_{1max}, δ_{2min}, δ_{2max}). Each parameter combination of the *confidence region* (Fig. 2.31) delivers one straight line on the probability grid (Fig. 2.32). The upper and lower border lines of the bundle of straight lines are considered as confidence limit for the whole distribution function. Figure 2.32 shows this schematically in the relevant probability grid used for the approximation. The maximum-likelihood method can also be applied to "*censored*" *test results*, e.g., when a life-time test is terminated after a certain time and only k of the n test objects have broken down. Then the likelihood function gets the form

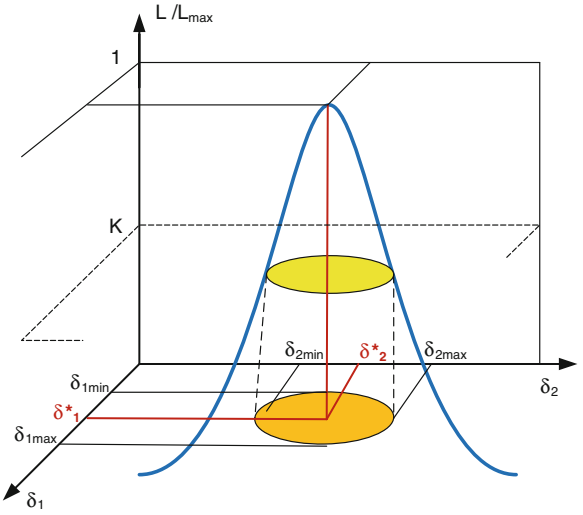

Fig. 2.31 Point and confidence estimation by the maximum likelihood function (schematically)

$$L = A \cdot p_R = A \cdot \prod_{i=1}^{k} f_{Ri}(x_i/\delta_1, \delta_2) \cdot \prod_{i=k+1}^{n-k} (1 - f_{Ri}(x_i/\delta_1, \delta_2)). \tag{2.55}$$

The same sample as shown in Fig. 2.30 is evaluated by a commercially available PC program of the ML method (Speck et al. 2009) under the assumption of a Weibull distribution (Fig. 2.33). The program delivers after *independence tests* a plot of the *cumulative frequency distribution* on a Weibull grid with logarithmic abscissa. The parameters are estimated as follows: initial value $v_0 = 750$ kV, 63 % quantile $V_{b63} = (v_0 + x_{63}) = (750 + 211)$ kV and dispersion parameter $\delta = 8.4$. The evaluated lower 95 % confidence limit of the cumulative frequency function should be taken for technical conclusions.

2.4.3 HV Tests Using the Multiple-Level Method

The *multiple-level method* (MLM) means the application of constant voltage tests (see Sect. 2.4.1) at several voltage levels (Fig. 2.34). For each level the test delivers an estimation of the breakdown probability including its confidence limits (Fig. 2.25). The relationship between stressing voltage and breakdown probability is not a distribution function in the statistical sense and therefore called "*performance function*" (sometimes also called "*reaction function*"). The performance function is not necessarily monotonically increasing, it can decrease (Fig. 2.35), e.g., in case of a change of the discharge mechanism depending on the height of the voltage. But it delivers exactly the information necessary for the reliability estimation and insulation coordination of a power system: The performance function supplies the probability of a breakdown in case of a certain overvoltage stress.

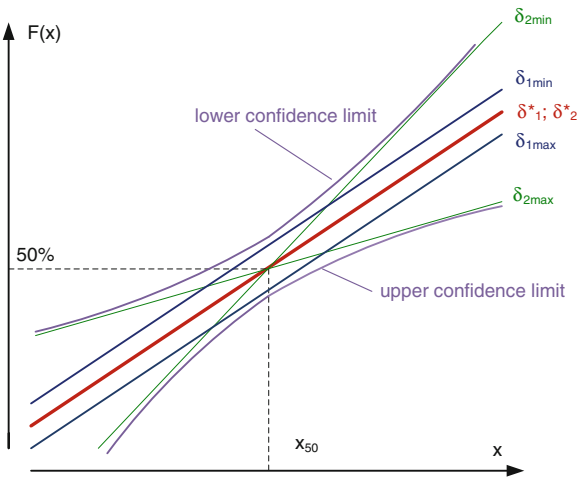

Fig. 2.32 Confidence limits of the distribution function derived from Fig. 2.31 (schematically)

In most cases also the performance function shows a monotonic increase and can be mathematically described by a theoretical distribution function. Figure 2.36 shows the difference between the performance function $V(x)$ (simulated by a standardized normal distribution with $\mu = 0$ and $\sigma = 1$) and derived cumulative frequency functions $S_{\Delta x}(x)$ of different heights Δx of the voltage steps in the test. For statistical reasons, the principle relation is $S_{\Delta x}(x) > V(x)$. Both functions have a different meaning: *cumulative frequency functions* consider the probability of breakdown *at all stresses up to a certain stress* value, performance functions do it *at a certain stress.* Cumulative frequency functions from stepwise increased voltages should be converted into *performance functions* (Hauschild and Mosch 1992).

A MLM test shall be performed at $m \geq 5$ voltage levels and $n \geq 10$ stresses per level. The number of stresses is not necessarily identical at all levels. If withstand voltages are considered, the number of stresses at low breakdown frequency might be higher. Then the *independence* of the outcomes of each level must be checked (see Table 2.8) and confidence estimations for the breakdown probability are determined (Fig. 2.25) and plotted in a probability grid.

Example From earlier experiments it can be expected that the performance function is monotonic increasing and can be approximated by a double exponential distribution function. Therefore, the point and confidence estimations are plotted in a Gumbel grid (Fig. 2.37). Because a straight line can be drawn through all confidence regions, the assumption of a double exponential or Gumbel distribution is confirmed. The small reduction of the relative breakdown frequency between 1,083 and 1,089 kV is not significant as it can be seen from the confidence limits. The parameters can be estimated from quantiles, $v_{63} = 1{,}112$ kV and $\gamma = (v_{63} - v_{31}) = 12$ kV.

Also the maximum likelihood estimation can be applied when the performance function is approximated by a certain distribution function (parameters δ_1, δ_2). According to Fig. 2.34 there are $j = 1 \ldots m$ voltage levels and apply at each level n_j

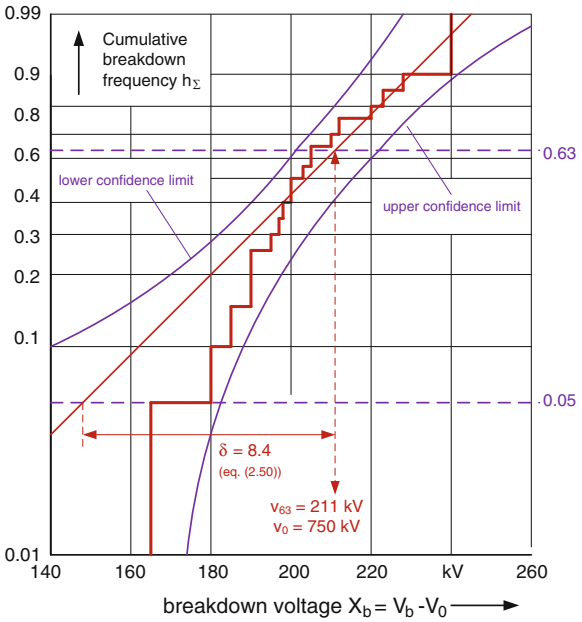

Fig. 2.33 Cumulative frequency function with confidence limits on Weibull grid

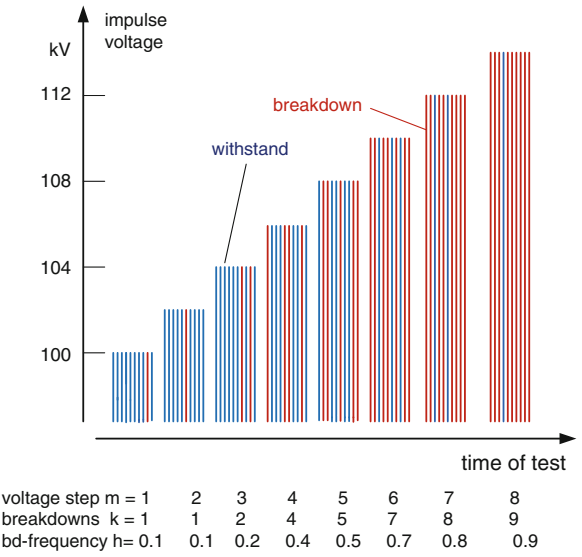

Fig. 2.34 Test procedure according to the multi-level method with $m = 8$ voltage steps and $n = 10$ impulses per step

stresses. The probability of obtaining k_j breakdowns and $w_j = (n_j - k_j)$ withstands at the voltage u_j is expressed by the *binomial distribution* (Eq. 2.47) on the basis of the breakdown probabilities given by the performance function $V(v_j) = V(v_j/\delta_1, \delta_2)$. The corresponding *likelihood function* for all m voltage levels with n_j stresses is given by

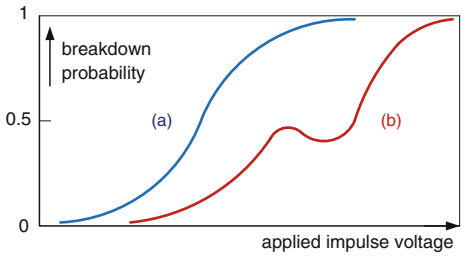

Fig. 2.35 Performance functions with monotonic (**a**) and non-monotonic (**b**) increase

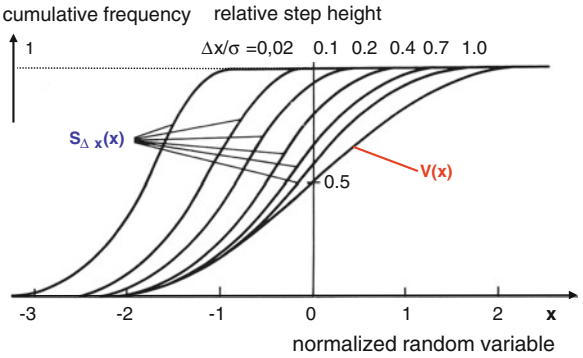

Fig. 2.36 Calculated cumulative frequency functions $S_{\Delta x}(x)$ determined at different step heights $\Delta x/\sigma$ based on an identical performance function $V(x)$

$$L = \prod_{j=1}^{m} V\left(v_j/\delta_1, \delta_2\right)^{kj} \left(1 - V\left(v_j/\delta_1, \delta_2\right)\right)^{wj}. \tag{2.56}$$

Varying the parameters δ_1 and δ_2 the maximum of Eq. (2.56) is found as described above. One gets point and confidence estimates as well as a confidence region for the whole performance function which is also shown in Fig. 2.33.

For practical applications of the maximum likelihood method the application of suitable software is necessary. An optimum software package (Speck et al. 2009) contains all necessary steps of the HV test data evaluation, from several independence tests, tests for best fitting with a theoretical distribution function, representation of the empirical performance function (or the cumulative frequency distribution) on probability grid up to point and confidence estimations for the parameters and the whole performance (or distribution) function.

2.4.4 HV Tests for Selected Quantiles Using the Up-and-Down Method

A whole *performance function* is not always required, e.g., the withstand voltage of an insulation can be confirmed, when the test voltage value u_t is lower than the 10 % quantile v_{10}. In that case it is sufficient to determine the value v_{10}, in other

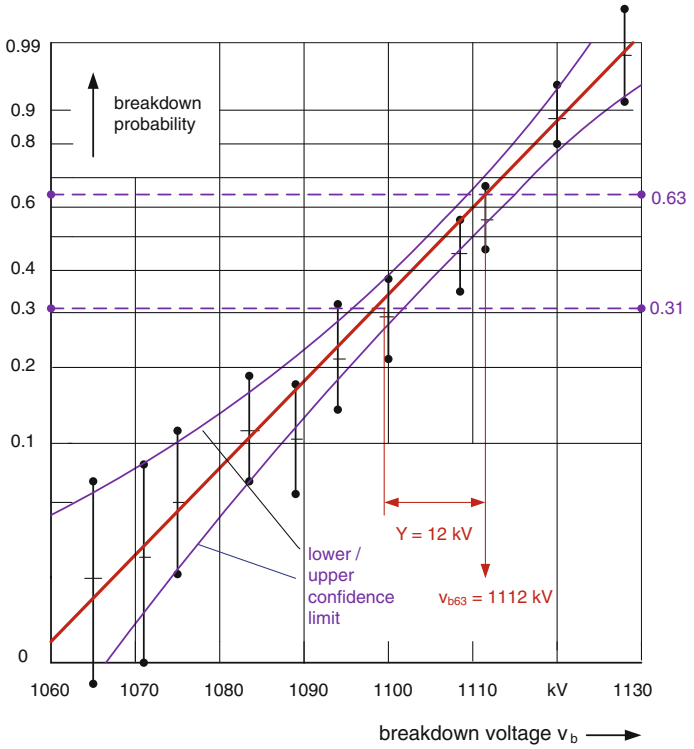

Fig. 2.37 Performance function with its confidence region according to a ML estimation and confidence limits of the single breakdown probabilities and *a*

cases it might be sufficient to look for the quantiles v_{50} or v_{90}. The related up-and-down test method (UDM) which is based on the constant voltage tests (Sect. 3.4.1) has been introduced by Dixon and Mood (1948).

The method requires that the voltage is initially raised in fixed voltage steps Δv, from an initial value v_{00} at which certainly no breakdown occurs, until a breakdown occurs at a certain voltage (Fig. 2.38: v_1 is the first counted value). Now the voltage is reduced by Δv, if no breakdown occurs the voltage is increased in steps again until the next breakdown, otherwise in case of breakdown it is reduced by Δv. The procedure is repeated until a predetermined number $n \geq 20$ of voltage values $v_1, v_2, \ldots v_n$ have been obtained. The mean value of these applied voltages is a first estimate for the *50 % breakdown voltage* v_{50}:

$$v_{50}* = \frac{1}{n}\sum_{l=1}^{n} v_l. \tag{2.57}$$

A more detailed evaluation considers the influence of the step height Δv and uses the number of breakdowns k and the number of withstands q. The sum of the

two complimentary events is identical with the number of voltage applications $n = k + q$ starting with the first breakdown. Additionally, the number of voltage levels or steps v_i (with $i = 0 \ldots r$) is taken into account. It is counted $i = 0$ from the step of the lowest breakdown. On a certain voltage level v_i, there are k_i breakdowns. Then the 50 % breakdown voltage can be estimated by

$$v_{50} = v_0 + \Delta v \left(\frac{\sum_{i=1}^{r} i \cdot k_i}{k} \pm \frac{1}{2} \right). \tag{2.58}$$

Example The test in Fig. 2.38 starts at $v_{00} = 120$ kV and has voltage steps of $\Delta v = 5$ kV. Including the first breakdown there are $l = 20$ voltage applications. The first estimate of v_{50}* by Eq. (2.57) delivers v_{50}* = 145.5 kV.

The lowest voltage level at which a breakdown occurs is $v_0 = 140$ kV. The number of breakdowns is $k = 9$, that of withstands is $q = 11$ and there are $i = 3$ voltage steps above the lowest breakdown voltage. With these data Eq. (2.58) delivers $v_{50} = 145.3$ kV. The difference between the two methods is very small, for most practical conclusions it can be neglected.

The UDM test is independent when the single voltage applications do not show a decreasing or increasing mean tendency. A UDM test according to the breakdown procedure starts at an initial voltage at which the breakdown is sure and goes down until the first withstand. It also delivers v_{50}, if the withstands are counted as the breakdowns above. Furthermore it should be mentioned that there are methods for the estimation of the standard deviation of the performance function, but the method cannot be recommended (see e.g., Hauschild and Mosch 1992). Confidence limits shall be calculated by the maximum likelihood function (see below) and not by the only roughly estimated dispersions.

Carrara and Dellera (1972) proposed an "*extended up-and-down-method*" which applies series of stresses (Fig. 2.39) for the determination of pre-selected quantiles instead of single stresses (Fig. 2.38). For the determination of a certain quantile, a certain number of impulses in one series is necessary. Table 2.9 gives the relation between the order p of the quantile and the required number of impulses in one series. The "*withstand procedure*" starting with a withstand voltage v_{00} and raising the voltage delivers the quantiles v_p of the order $p \leq 0.50$, the "*breakdown procedure*" starting with a breakdown voltage and decreasing voltage to withstands delivers the quantiles of the order $p \geq 0.50$.

Figure 2.39b shows the estimation of the statistical withstand voltage determined as the 10 % breakdown voltage (quantile u_{10}) using the *withstand procedure* with $n = 7$ stresses per series. As soon as only withstands occur in a series, the voltage is increased by Δv to the next higher level. As soon as a breakdown occurs the voltage is decreased to the next lower level.

When the *breakdown procedure* is applied, the voltage is decreased when in a series only breakdowns occur and only increased when the first withstand appears. The expected *quantile* for this breakdown procedure is v_{90}. The evaluation of the point estimation of the quantile can be performed according to the simplified evaluation by Eq. (2.57).

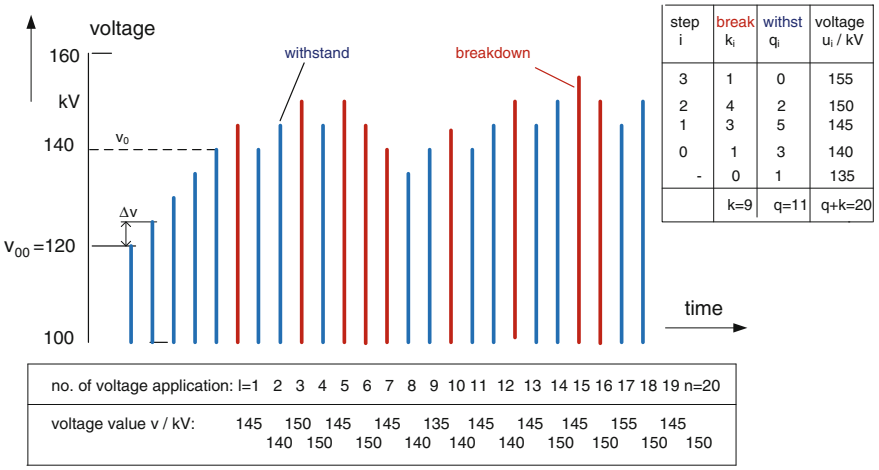

Fig. 2.38 Up-and-down method (*UDM*) for the estimation of the 50 % quantile v_{50}

Table 2.9 Number of stresses n per UDM group for the estimation of the order p of quantiles

n	70	34	14	7	4	3	2	1	
p	0.01	0.02	0.05	0.10	0.15	0.20	0.30	0.50	(withstand procedure)
p	0.99	0.98	0.95	0.90	0.85	0.80	0.70	0.50	(breakdown procedure)

Also the computer-aided maximum-likelihood method can be applied for the UDM tests provided related software is available (Speck 1987; Bachmann et al. 1991): The principle corresponds to the MLM (see Sect. 2.4.3). For each of the applied voltage levels the relative breakdown frequency including its confidence region is estimated (Fig. 2.40 for estimation of v_{10} with $n = 7$ stresses per series) and plotted in a suited probability grid (Fig. 2.40: Gauss grid). The maximum of the likelihood function delivers the expected quantile v_{10} including its confidence limits. The confidence region ($\varepsilon = 95$ %) of all quantiles is calculated and plotted as a violet line.

2.4.5 Statistical Treatment of Life-Time Tests

A *life-time test* is the stress of the insulation at a certain constant AC or DC voltage (or a series of impulses). The random variable is the breakdown time (or the number of impulses) which can be evaluated according to the PSM (see Sect. 2.4.2). When this test is performed at several voltage levels, the relationship between breakdown voltage and breakdown time—usually known as the *life-time characteristic* (LTC)—can be evaluated (Speck et al. 2009). It is described for a p-order quantile of the breakdown voltage v_p by

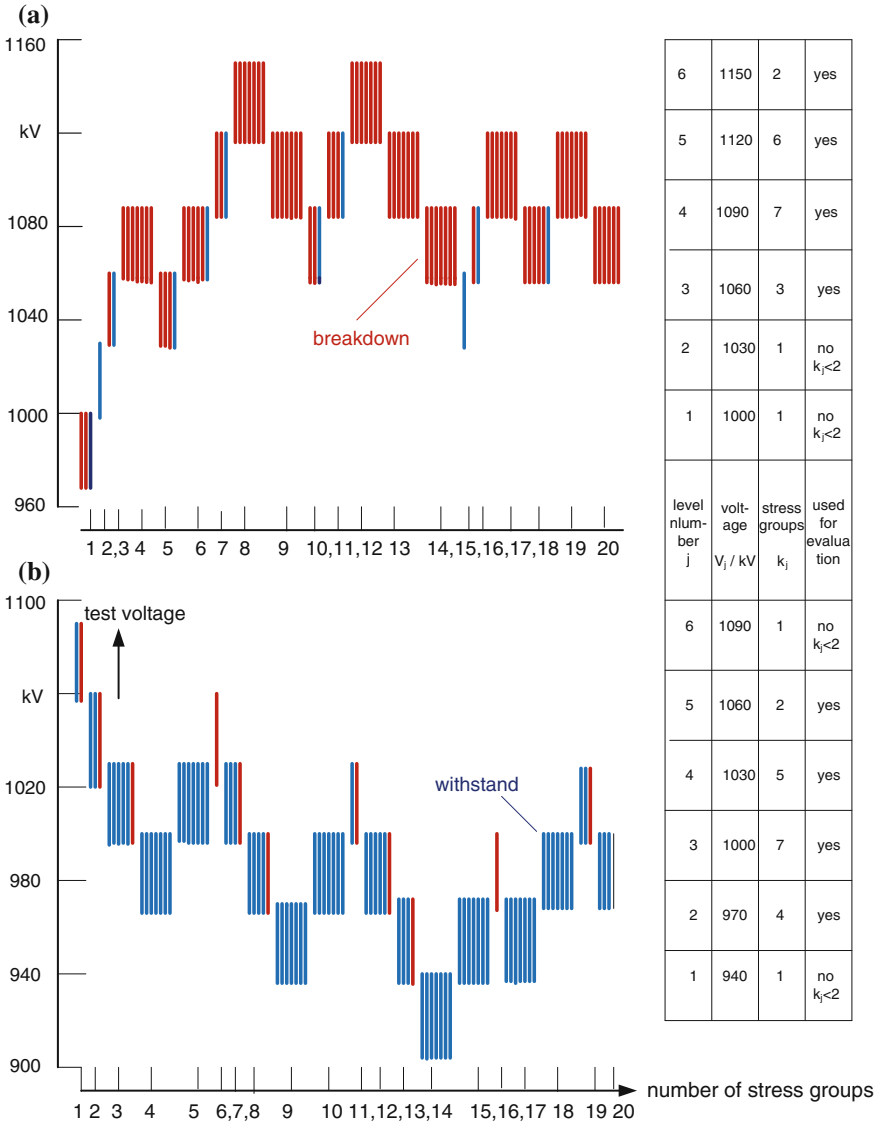

level number j	voltage V_j / kV	stress groups k_j	used for evaluation
6	1150	2	yes
5	1120	6	yes
4	1090	7	yes
3	1060	3	yes
2	1030	1	no $k_j<2$
1	1000	1	no $k_j<2$
6	1090	1	no $k_j<2$
5	1060	2	yes
4	1030	5	yes
3	1000	7	yes
2	970	4	yes
1	940	1	no $k_j<2$

Fig. 2.39 Up-and-down test for the determination of the 90 % quantile v_{90} (**a**), and respectively the 10 % quantile v_{10} (**b**)

$$v_p = k_d t_p^{-1/n} \quad \text{or} \quad t_p = \left(\frac{k_d}{v_p}\right)^n, \tag{2.59}$$

where t_p—p-order quantile of breakdown time, n—life time exponent mainly characterizing the insulating material and k_d—a constant mainly characterising the

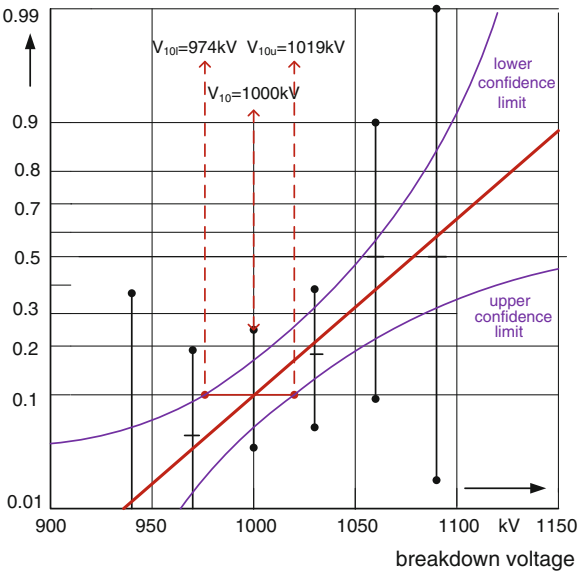

Fig. 2.40 ML evaluation of an extended UDM test for the determination of the performance function in the vicinity of the 10 % quantile

field geometry. In a logarithmic grid the formula delivers a falling straight line which allows the estimation of the parameters n and k_d.

The breakdown time can be described by a Weibull distribution under the consideration of Eq. (2.59) and the relation that v_q is the applied voltage of the constant voltage test $v_q = v_t$:

$$F(t, v_t) = 1 - \exp\left(-\left(t\left(\frac{v_t}{k_d}\right)^n\right)^\delta\right). \tag{2.60}$$

Now the computer-aided maximum likelihood method (Speck 1987; Speck et al. 2009) is applied for the unknown triplet of the parameters k_d, n and δ. The maximum of the likelihood function delivers the best estimation for the triplet. In the usual way also confidence limits can be estimated. The life time-characteristic (Fig. 2.41) includes confidence limits now.

The method enables also the evaluation of censored life-time data, this means test objects are also considered, which have not yet broken down when the test has been terminated.

2.4.6 Standardized Withstand Voltage Tests

At a *standardized withstand voltage test*, the test object has to withstand a test voltage according to the insulation coordination (IEC 60071-1:2006) during an agreed *test procedure*. In the following the procedures for type and routine tests

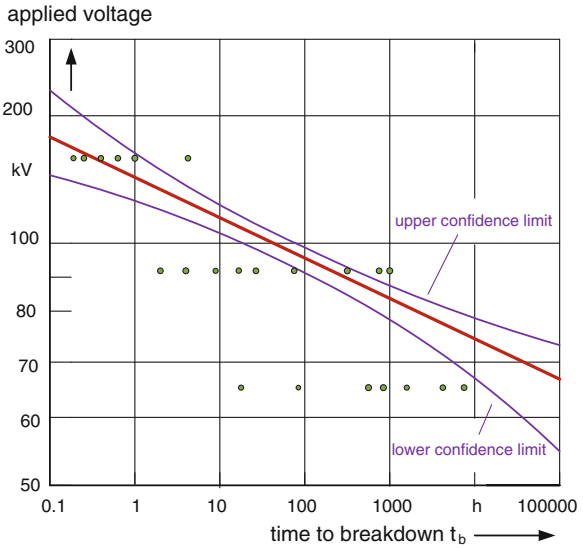

Fig. 2.41 Life-time characteristic including confidence intervals

are considered statistically in brief. The procedures have a long tradition, had been introduced without detailed statistical considerations but are connected with the remarkable experience of test field engineers. A simple change of the procedures would not be accepted and cannot be recommended. But it seems to be necessary that the statistical consequences of these procedures are understood.

The stochastic nature of electrical discharges causes, that a defective test object is not always rejected in a test. With a certain low probability it may pass the test and fail during the operation. This is called the risk of the user. But it may also happen that a test object without defects is rejected in the test. This is the risk of the manufacturer. Which risk is higher depends on the design and the quality of production of the object. If there is only a very small distance between real breakdown voltage and test voltage the risk of the user might be higher than that of the manufacturer. But with a sufficient safety margin the risk of both sides is acceptable.

For AC and DC test voltages (Fig. 2.42a, IEC 60060-1:2010) the voltage shall be rapidly increased up to 75 % of the test voltage value. Then it shall be raised with about 2 % of the test voltage value per second. When the test voltage value is reached it has to be maintained within ±1 % for the test duration T_t, which is very often 1 min. Then the voltage shall be decreased to 50 % and switched off. Such a test is a kind of constant voltage test, the test voltage is a single stress and without knowing any details from the development, a statistical judgement of the single test is impossible. But if many test objects of the same type are tested, one should have a statistical evaluation of failure statistics for improvement of design and/or production.

AC and DC withstand tests are more and more completed by PD measurement ("*PD monitored withstand tests*"). Then a step test procedure has to be applied

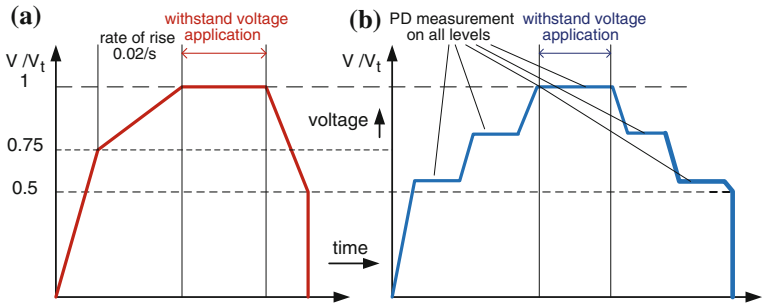

Fig. 2.42 Conventional (**a**), and PD monitored (**b**) withstand test procedure for AC and DC test voltages

Fig. 2.43 Probability of passing a LI/SI voltage test depending on the breakdown probability of the test object for different test procedures

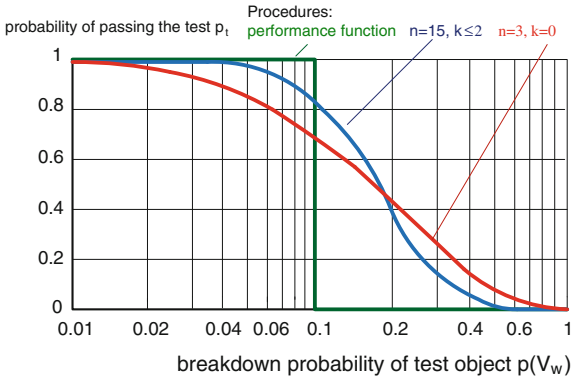

(Fig. 2.42b). The upwards and downwards steps should be at identical voltages to enable a comparison of the PD characteristics before and after the withstand test. The PD measurement should also be performed at the withstand test voltage for the specified test duration. Also the duration of the steps for PD measurement must be specified. For all steps, a duration $T \geq 1$ min is necessary. Which step voltage is considered for the withstand test is also a matter of specification. The combination of withstand and PD testing is the most efficient method for AC/DC testing today.

For *LI and SI withstand tests* several methods are recommended (IEC 60060-1:2010):

(A1) A withstand test of external insulations is passed, when it can be shown that the 10 % quantile of the performance function is higher than the specified withstand voltage. The 10 % quantile may be taken from a measured performance function or from an up-and-down test (see Sect. 2.4.4).

(A2) For external insulations $n = 15$ test voltage impulses shall be applied and $k \leq 2$ breakdowns are allowed

(B) For internal insulations $n = 3$ test voltage impulses may be applied and no breakdown is allowed.

By help of the *binomial distribution* (Eq. 2.47) the methods can be compared: Fig. 2.43 shows a diagram of the probability of passing the test depending on the *breakdown probabilityp* of the test object at the test voltage. The method A1 has a sharp criterion: When the breakdown probability reaches $p = 0.10$, the test object fails the test. The procedure A2 is not sharp, because at $p = 0.08$, 10 % of the test objects fail, although according to procedure A1 they are considered as acceptable. But when $p = 0.30$—a too high breakdown probability—there is 15 % probability of passing the test in case of method A1. The procedure B is still worse: A test object of the high breakdown probability $p = 0.30$ will pass the test with even 30 % probability.

The example shows, no manufacturer shall design its products with a breakdown probability of 0.10 at the test voltage value. The breakdown probability for design should be $p < 0.01$!

Chapter 3
Tests with High Alternating Voltages

Abstract *HVAC test voltages* represent the stress of insulations by operational alternating voltages (50 or 60 Hz) and temporary over-voltages. For that reason they are the most important test voltages and applied for all kinds of withstand tests, lifetime tests and dielectric or partial discharges (PD) measurements. After the detailed description of *HVAC voltage generation,* the requirements of HVAC test voltages and the interaction between test system and test object are investigated. Measuring systems for HVAC test voltages are mainly based on capacitive voltage dividers and peak voltmeters, but for measurements during HVAC tests with an expected voltage drop, with harmonics or fast voltage changes, digital recorders become more and more necessary. The chapter is closed with a section on procedures for HVAC breakdown and withstand tests, dry, wet as well as pollution tests, long duration or lifetime testing. Examples for HVAC tests on cables, gas-insulated switchgear, power and instrument transformers are given.

3.1 Generation of HVAC Test Voltages

This section investigates the different possibilities for the HVAC test voltage generation. HVAC test voltages can be generated by test transformers or transformer cascades as well as by resonant circuits with reactors of tuneable inductance or of fixed inductance and by a power supply of variable frequency (frequency converters). The principles of voltage generation are described and recommendations for application are given. Also the special application of HVAC test voltage generation by power or voltage transformers under test (induced voltage tests) is considered.

W. Hauschild and E. Lemke, *High-Voltage Test and Measuring Techniques*,
DOI: 10.1007/978-3-642-45352-6_3, © Springer-Verlag Berlin Heidelberg 2014

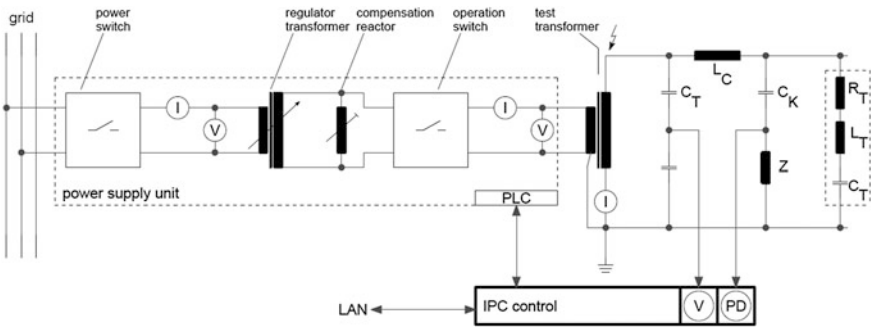

Fig. 3.1 Circuit diagram of an HVAC test system based on a test transformer (ACT)

3.1.1 HVAC Test Systems Based on Test Transformers (ACT)

3.1.1.1 General Principle

The components of an HVAC test system based on *test transformers* (ACT, Fig. 3.1) are described as introduced for a general HV test circuit (Sect. 2.2; Fig. 2.5). The test transformer is the HV generator, the power supply is usually realized by one (for higher power several) switching cubicle(s), a regulating transformer and a compensation reactor and the voltage measuring system by a capacitive voltage divider with a peak voltmeter connected via a measuring cable. The control-and-measuring system (4) completes the HVAC test system.

A *test transformer*—characterized by its

rated primary voltage (LV) V_{1m},
rated secondary voltage (HV) V_{2m},
rated current I_m and/or
rated test power S_m, both with a
rated duty cycle

—is a usual single-phase transformer with layer windings. The *transformer ratio* is the number of turns of the high-voltage winding w_2 over those of the low-voltage winding w_1. For the generation of a high voltage, a certain magnetic flux is necessary that requires a certain number of HV turns w_2. The number of the LV turns w_1 is then depending on the available (or selected) feeding voltage V_{1m}.

For basic considerations, the HV circuit can be simplified as given in Fig. 3.2a. The introduction of the *transformer ratio* w_2/w_1 for the feeding voltage V_1* (Fig. 3.2b) delivers a simple R–L–C circuit where L_T represents the transformer stray inductance, R_T the active transformer losses and C the acting capacitance from test object, voltage divider and transformer.

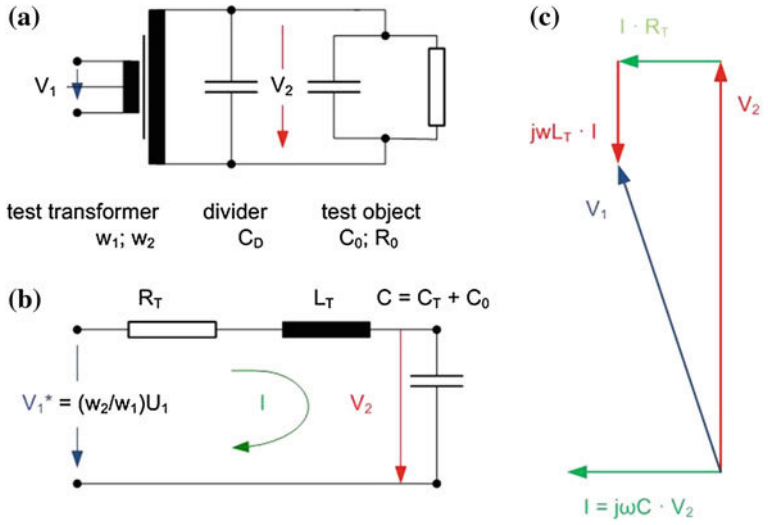

Fig. 3.2 HVAC test circuit. **a** Simplified HV test circuit. **b** Equivalent circuit. **c** Phasor diagram

The voltage at the test object V_2 is shown in the phasor diagram (Fig. 3.2c). With the pre-given current I in the test circuit, the test voltage becomes

$$V_\mathrm{T} = V_2 = \frac{I}{\mathrm{j}\omega C}.$$

There is a resistive *voltage drop* on the transformer

$$V_\mathrm{R} = I \cdot R_\mathrm{T}.$$

The inductance of the transformer causes a reactive voltage drop

$$V_\mathrm{L} = I \cdot \mathrm{j}\omega L_\mathrm{T},$$

which partly compensates the capacitive test voltage $V_2 = V_\mathrm{T}$. It can easily be seen that the transformed feeding voltage $V_1{}^*$ is for a capacitive test object lower than expected from the test voltage V_2.

> **Note** Correspondingly a feeding voltage $V_1{}^*$ higher than expected from the test voltage V_2 would be required if the test object is inductive. In case of a resistive test object and low losses in the test transformer, $V_2 \approx V_1{}^*$ applies.

One can conclude that *the relation between the feeding primary voltage of a test transformer and the generated secondary test voltage depends on the parameters of the test object*. Therefore, the primary voltage cannot be used for the measurement of the test voltage (see Sect. 3.4).

If also the resistive losses in the test object are neglected ($V_\mathrm{R} = 0$), the feeding and the test voltage would be almost in phase, one gets

$$V_2 = V_1^* + V_L \quad \text{and}$$
$$V_2 = \frac{V_1^*}{1 - \omega^2 C L_T}. \tag{3.1}$$

This delivers a second important conclusion: For $(1 - \omega^2 L_T C) \to 0$ one gets oscillations with the *natural frequency* of the test circuit

$$\omega_0 = \frac{1}{\sqrt{C \cdot L_T}} = 2\pi f_0 \tag{3.2}$$

and *resonance when the natural frequency f_0 is equal to the frequency f of the feeding voltage V_1** (e.g. $f_0 = 50$ Hz). For the considered theoretical case without active losses ($R_T \to 0$), at resonance the test voltage would go ad infinitum ($V_2 \to \infty$). In practical test circuits with losses, it can reach quite high values and the circuit is out of control. *Consequently, resonance must be avoided and the test circuit protected against over-voltages.*

Note Such an *over-voltage protection* can be realized by an order from the control to reduce the test voltage and switch it off, e.g. for the case that the measured test voltage has reached 105 % of its preselected value.

The *short-circuit voltage* V_{kT} of a transformer is the necessary primary voltage V_1 to drive the rated current I_m through the transformer when the secondary side is short-circuited ($V_2 = 0$). For the simplified equivalent circuit (Fig. 3.2b) without resistive losses ($R_T = 0$), one gets the short-circuit voltage

$$V_{kT}^* = \omega L_T I_m, \tag{3.3}$$

the relation of this short-circuit voltage to the rated secondary voltage $V_{2m} = I_m/\omega C$ of the transformer defines the *short-circuit impedance* (sometimes also "impedance voltage")

$$v_{kT} = \frac{V_{kT}^*}{V_{2m}} = \omega^2 C L_T. \tag{3.4}$$

For test transformers, the short-circuit impedance is an important parameter with values between 5 and 25 %. A high short-circuit impedance causes voltage enhancements at capacitive load and—in case of heavy discharges or breakdown—current limitations that may impede the breakdown process. With the short-circuit impedance, one can estimate the capacitive enhancement of the test voltage based on Eqs. (3.1) and (3.4).

Example An HVAC test transformer is loaded with a capacitive test object (Fig. 3.2b) that requires its rated current at rated frequency. The enhanced voltage can be calculated by $V_2 = V_1^*/(1 - v_{kT})$. For an impedance voltage of $v_{kT} = 18$ %, one gets $V_2 = V_1^*/0.82 = 1.22\ V_1^*$. This means, the test voltage is enhanced by 22 % compared with the transformer ratio. Vice versa the primary voltage for a certain secondary test voltage is lower.

A further increase in the total impedance voltage for complete HVAC test circuits is caused by the impedance voltage of the regulating transformer v_{kR} and impedances in the HVAC circuit (e.g. a feeding transformer v_{kF} between the mains and the regulator, limiting reactances or resistors on the LV or HV side). The short-circuit current can be calculated from the resulting impedance voltage which means the weighted sum of all impedance voltages. The weight is the power of the considered components. When only the test transformer (reactive test power S_T and impedance voltage v_{kT}), the regulator transformer (S_R, v_{kR}) and a feeding transformer (S_F, v_{kF}) are considered, the resulting impedance voltage at the test transformer is

$$v_k = v_{kT} + \frac{S_R}{S_T} \cdot v_{kR} + \frac{S_F}{S_T} \cdot v_{kF}. \tag{3.5}$$

The continuous *short-circuit current* I_k, which is important, e.g., for HVAC pollution testing (Sect. 3.2), follows from the rated current I_m with the resulting impedance voltage v_k

$$I_k = \frac{I_m}{v_k}. \tag{3.6}$$

Note This estimation of the short-circuit current describes the steady state conditions and neglects the transient currents after the instant of the breakdown. Furthermore, the impedance voltage is given as a dimension-less figure. When it is given in percent (%), Eq. 3.6 has to be modified accordingly.

In case of a breakdown of the test object, the short-circuit current causes a high mechanic stress to the windings of the test transformer. Due to this, some turns can be displaced and cause the damage of the transformer. Therefore, a stable mechanic design of the windings is important when a high short-circuit current is required, e.g. for wet and pollution tests.

A stable mechanic design is difficult because of the necessary high number of turns (sometimes several thousands) consisting of quite thin wires (diameter often in the order of 1 mm). This has to be realized under the strong HV insulation requirements. Therefore, the stable design is necessary, for example as follows: In a larger oil–paper-insulated test transformer, the whole winding is subdivided into winding elements (or "coils"), each based on a pressboard cylinder of different diameter, manufactured separately and—later on—coaxially arranged around a leg of the magnetic core. Such a coil consists of several layers of wires wrapped in insulating paper of some centimetres thickness (Fig. 3.3). The layers are connected together, and the coil is connected to the neighbouring coils. The mechanic stability depends strongly on a reliable design considering the shrinking of the paper, on the quality of making the windings and on a careful drying process.

Some test transformers and regulators are not resistant enough against short-circuit currents and require an impedance, often an inductance, in the HV circuit between test transformer and test object. This indicates certain problems of the

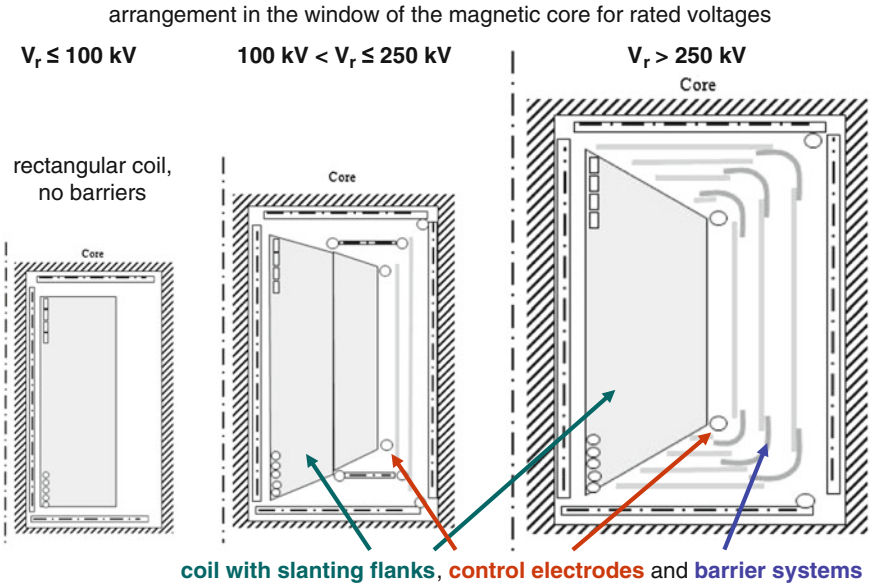

Fig. 3.3 Principle arrangement of layers, coils and windings of an oil–paper-insulated test transformer

mechanic stability of the windings that should not happen at a modern test transformer under normal test procedures in a test field.

In addition to the dielectric and the mechanic design, the thermal design is of great importance. Due to the thick layers of paper, the heat transfer from the windings to the oil is hampered. Therefore, cooling channels between the single layers are arranged to enable the heat convection to the streaming oil. Usually test transformers operate with natural cooling by oil streaming because of temperature differences inside the tank. In rare case also forced cooling is applied for further improvement of the heat transfer. The heated oil is cooled at the walls of the transformer by the surrounding air. Sometimes the walls are made from corrugated sheet or equipped with radiators or special heat exchangers.

Two types of oil–paper-insulated test transformers, with metal tank and with insulating cylinders, are in wide application. Each type has characteristic parameters and correspondingly its preferred application, both summarized in Table 3.1. In addition to these transformers with oil–paper-insulated windings, test transformer with SF_6-impregnated foil insulation (for some mobile HVAC test systems) and epoxy resin cast (for small test systems of low power up to 100 kV) insulation are in use.

Table 3.1 Parameters and application of different types of test transformers (single units)

Type and insulation characteristics	Tank type with oil–paper insulation	Cylinder type with oil–paper insulation	Metal-enclosed SF_6-impregnated foil insulation	Epoxy-resin insulation
Max. rated voltage (kV)	1,000	500	1,000	100
Max. rated current (A)	10	<2	<0.5	0.2
Max. test power (kVA)	10,000	<1,000	<500	<20
Max. duty cycle	Continuous	Short time 10 h	Short time <1 h	Short time <2 h
Impedance voltage (%)	5–10	10–15	20	20
HV taps	Yes	No	No	Not important
Specific weight (kg/kVA)	10–15	8–12	8–10	15–20
Lab height demand	Low	High	Not important	Not important
Ground area demand	Average	Average	Small	Not important
For parallel connection provided	Yes	Conditioned	Yes	Not important
For cascades provided	Yes	Yes	No	Not important
Applicable for metal-enclosed circuits	Yes	No	Yes (preferred)	Conditioned
Outdoor application	Yes	No	No	No

3.1.1.2 Tank-type Test Transformers

Tank-type test transformers guarantee best cooling conditions because its active part is arranged in a metal (steel) tank that can additionally be equipped with "radiators" to increase the cooling surface of the tank (Fig. 3.4). Therefore, these transformers can be designed for the highest test currents, respectively, test powers, and enable continuous operation (Table 3.1). The magnetic core of the transformer has often three legs, and the inner LV and the outer HV winding are arranged around the central leg (Fig. 3.5). The core is on the same ground potential as the tank is, the lower end of the HV winding is usually also grounded via a bushing. At this bushing, the current in the HV test circuit can be measured. For an HVAC testing in ambient air, the transformer must be equipped with an oil-to-air bushing (Fig. 3.4), but metal tank transformers can also be connected by oil-to-SF_6 bushings to metal-enclosed test circuits that are mainly applied for testing of gas-insulated systems (GIS) and their components (Fig. 3.6; see also Sects. 3.2.3 and 10.4.1).

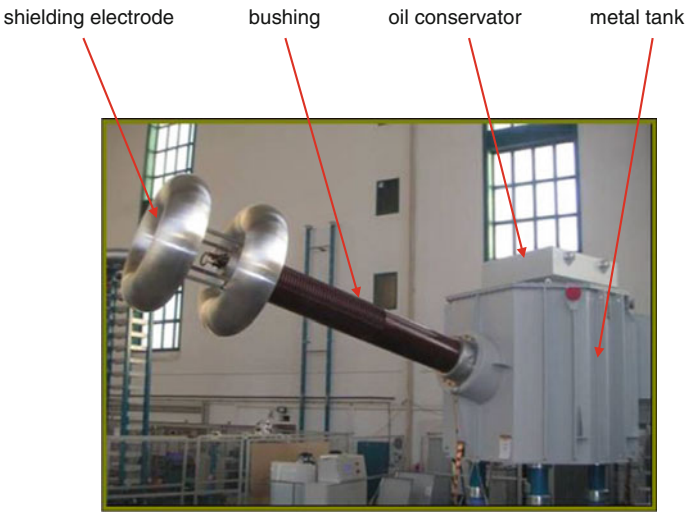

Fig. 3.4 Metal-tank test transformer 600, 2,000 kVA

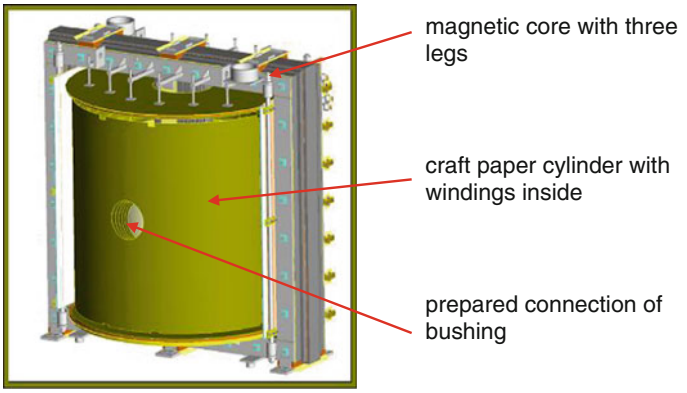

Fig. 3.5 Principle design of the active part of a metal tank test transformer (winding and magnetic core)

Because of the grounded tank, the tank-type test transformer does not require any clearance to neighbouring walls from the electrical point of view. In case of horizontal or diagonal bushings, other components (voltage divider and coupling capacitor) can be placed below or very near to the end electrode of the bushing. This enables a very compact and space-saving arrangement in a test laboratory, often the ground space is lower than that for a cylinder-type transformer (Fig. 3.7).

Metal tank transformers are well suited for outdoor operation. Therefore, this design should be applied for all open-air HV test fields. Furthermore, there is the

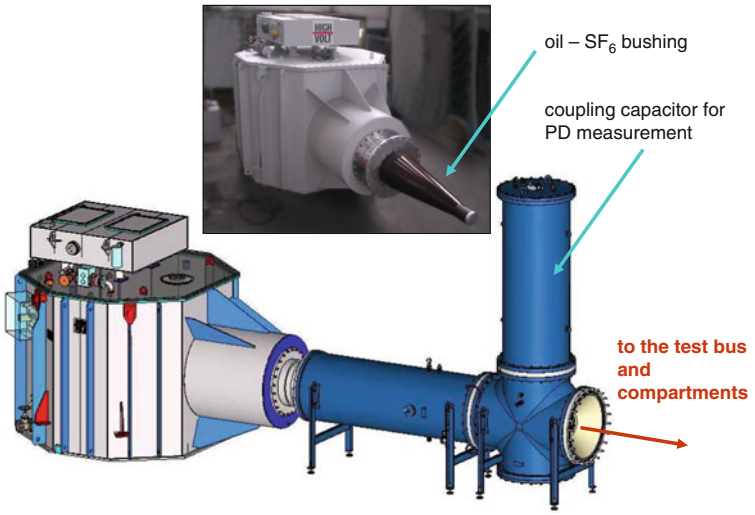

Fig. 3.6 Metal tank transformer 800, 1,000 kVA, for connection to a metal-enclosed test circuit

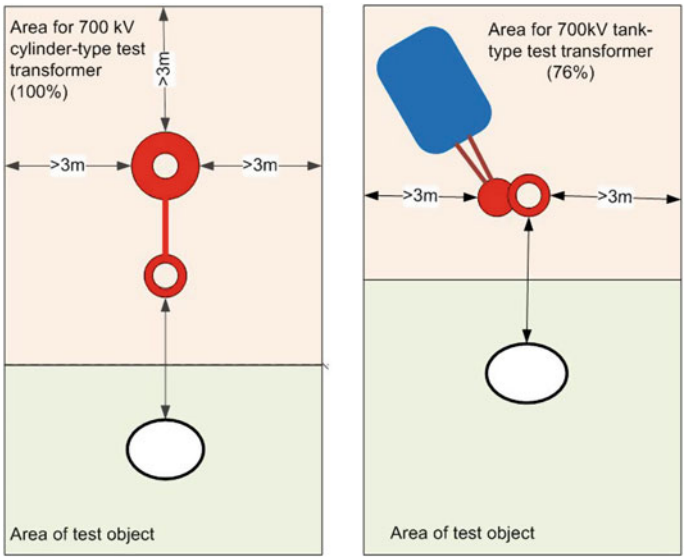

Fig. 3.7 Ground area demand of a cylinder-type test transformer compared with that of a tank-type test transformer (both 700 kV)

opportunity to arrange the test transformer outside of a HV test hall and to have only its bushing inside of that hall. This is a further possibility to save the expensive space in the test laboratory.

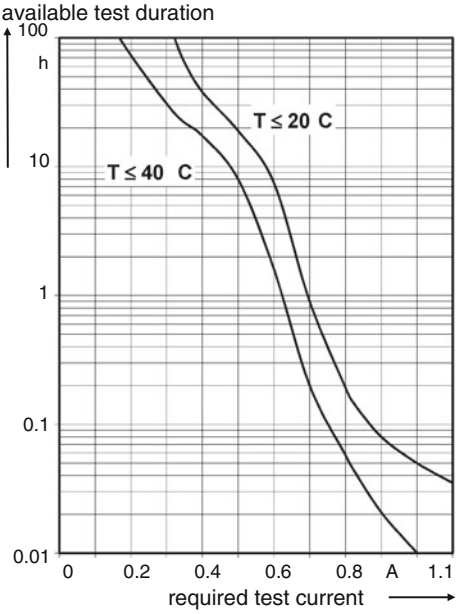

Fig. 3.8 Available test duration of a cylinder-type test transformer depending on the required test current (*T* ambient temperature)

Considering the possibility of AC test voltage generation by resonant circuits, tank-type transformers are mainly applied for wet and pollution testing (Sect. 3.2.4), for outdoor application and for metal-enclosed test circuits.

3.1.1.3 Cylinder-type Test Transformers

Cylinder-type test transformers do not require a bushing because their case is an insulating cylinder. Consequently, the thermal behaviour is limited, which limits also generation of higher reactive test power (Table 3.1). Usually they are provided for short-term operation up to 10 h (Fig. 3.8), long-term operation would require a forced cooling of the oil, e.g. with external coolers connected by houses. In any case, the duty cycle of this type of test transformers should be carefully considered.

The insulating cylinder has on both sides metallic covers. The lower cover carries the active part. There are two principles of the design of the active part, one is with one common coaxial LV and HV winding (Fig. 3.9a) and the core on ground potential, the other one is with divided windings and the core on half potential (Fig. 3.9b). The latter requires an insulating support for the core, but it is better adapted to the geometry of the cylinder. The lower windings have the LV potential on its outer side and the HV "half" potential on its inner side. The core is connected to this "half" potential as well as a transfer winding for the upper windings. There, the exciter winding is next to the core, whereas the second HV "half"-potential winding is on the outer side. This means, between the two HV

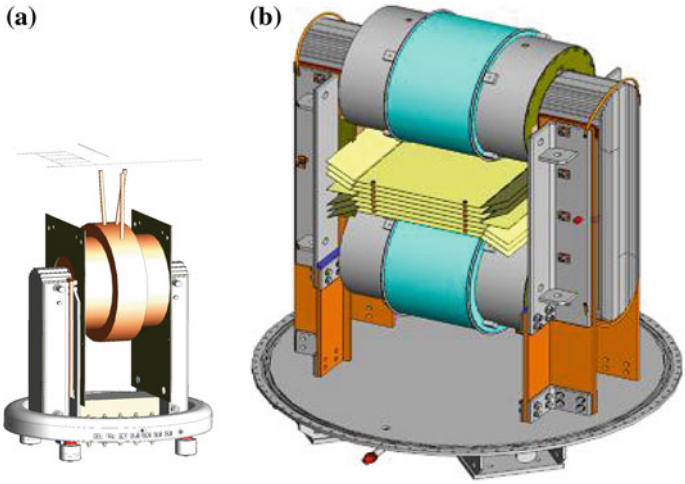

Fig. 3.9 Principle design of cylinder-type test transformers. **a** Single winding and core on ground potential. **b** Divided windings and core on half potential

windings, one has the full high voltage, therefore, the oil gap in between is divided by insulating barriers to improve the insulation for a higher withstand voltage (Fig. 3.10).

Cylinder-type transformers are well suited for transformer cascades up to 1,500 kV (Fig. 3.11), but only recommended for indoor laboratories. They are well suited for multi-purpose test laboratories without special requirements, e.g. at universities or at test service suppliers.

3.1.1.4 Test Transformers with SF6-impregnated Foil or Solid Insulation

Test transformers with SF_6-impregnated foil insulation (Fig. 3.12) are derived from instrument transformers of the same insulation type (Moeller 1975) and mainly used for GIS testing. In that case, they can be directly flanged to the GIS under test to establish a metal-enclosed, and therefore well-shielded HV test and partial discharges (PD) measuring circuit, also under on-site conditions.

The thermal behaviour of the SF_6-insulated foil insulation is poor compared with oil–paper insulation. Therefore, this type of test transformer has limited rated current and a very short duty cycle. Also the weight is relatively high due to the necessary magnetic core. For GIS testing, SF_6-insulated test transformers are more and more replaced by resonant circuits with SF_6-insulated reactors of much better weight-to-test power relation (Hauschild et al. 1997).

Test transformers with epoxy-resin insulation are only realized up to rated voltages of about 100 kV because of the necessary PD-free design. Because of the necessary thermal design, only quite low-rated currents for short-time operation

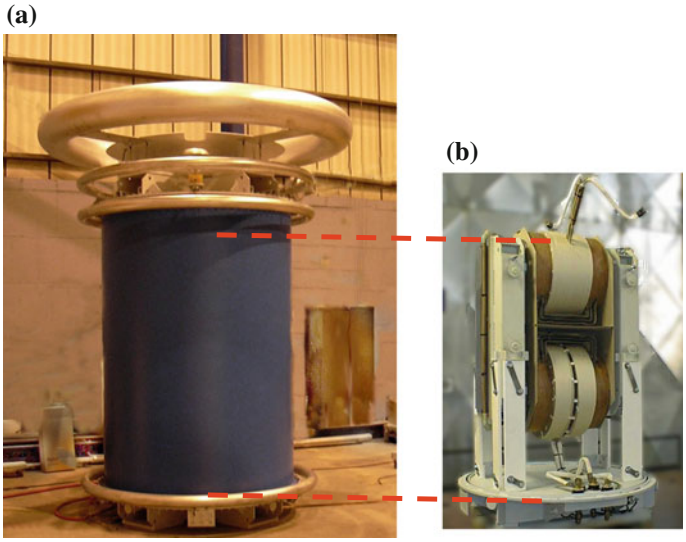

Fig. 3.10 Cylinder-type test transformer 500 kV/500 kVA. **a** Complete transformer. **b** Active part with divided windings

Fig. 3.11 Transformer cascade 1,000 kV/350 kVA of three cylinder-type transformers (Courtesy of TU Cottbus, Germany)

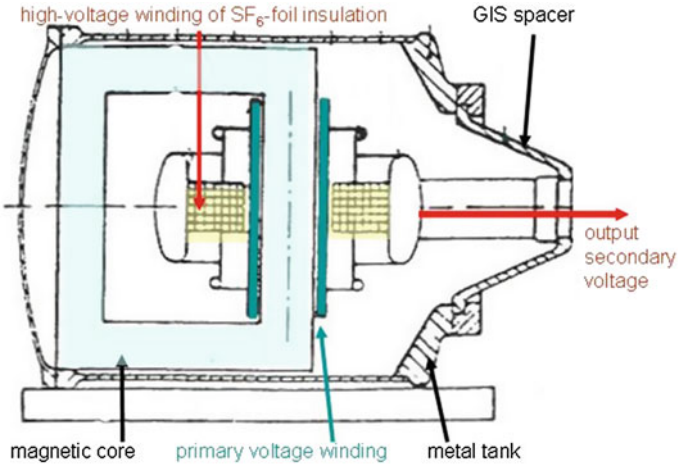

Fig. 3.12 Test transformer with SF_6-impregnated foil insulation

are allowed (Table 3.1). Therefore, epoxy-resin-insulated test transformers can be used for limited HV test applications of low- and medium-voltage equipment, voltage generation in "testers" (e.g. for insulating oil), student's training and demonstrations.

3.1.1.5 Test Transformer Cascades

Test transformer cascades are applied for the generation of test voltages that cannot be generated by single-test transformers. The principle of transformer cascades is an early design of the HV test technique with contributions of W. Petersen with co-workers and A.-J. Fischer in 1915 (Fig. 3.13). It is useful only for oil–paper-insulated transformers that are considered in the following.

The application of a transformer cascade can be taken into consideration for voltages above 600 kV (Fig. 3.11). A test transformer used for transformer cascades has in addition to the primary and secondary winding a *transfer winding* (w_3 turns) on the HV potential with a transformer ratio to the primary winding of w_3:w_1 = 1:1 (Fig. 3.14). This winding feeds the primary (exciter) winding of the following stage of the cascade. Usually, the transformers of a cascade have identical design with three windings each. This enables its application on all stages in the cascade, although not used in the highest stage. Figure 3.15 shows the largest cascade transformer manufactured till now (TuR Dresden). This cascade is equipped with three test transformers of divided HV winding, magnetic core and tank on half potential and two bushings each of half-rated voltage (Fig. 3.16). This transformer type is well suited for outdoor cascades without limitations of the ground area demand.

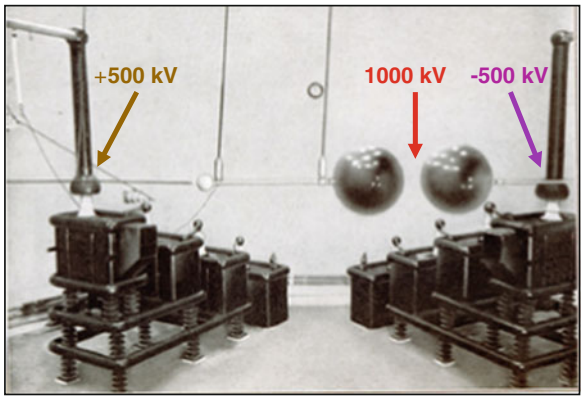

Fig. 3.13 World's first transformer cascade for 1 MV, consisting of two cascades 4 × 125 kV in phase opposition (made by Koch & Sterzel GmbH, Dresden 1921)

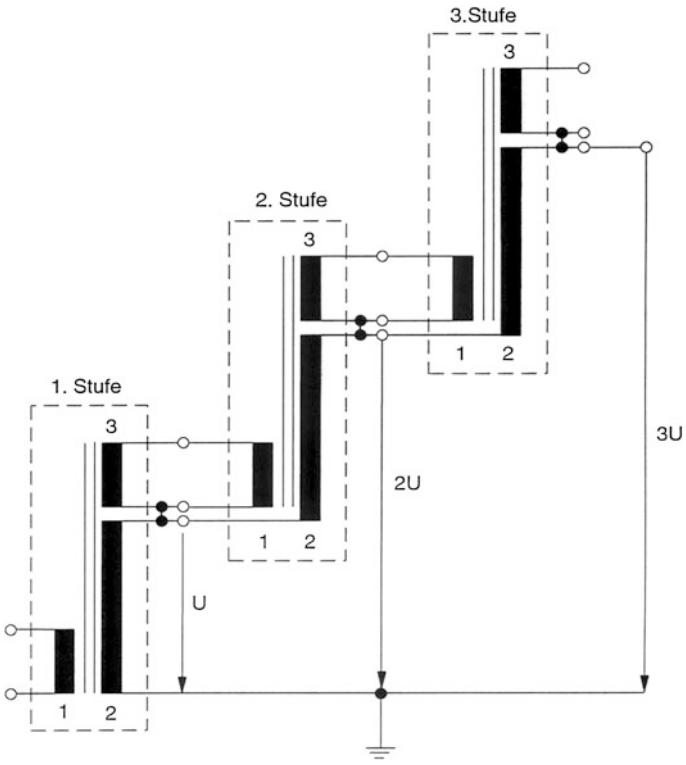

Fig. 3.14 Principle circuit of a three-stage transformer cascade

The *transformer cascade* is helpful for the generation of high voltages but one has to consider that all the test power must be supplied via the lower stages. This means the rated power of the cascade cannot be higher than the rated power of its

Fig. 3.15 World's largest transformer cascade for 3,000 kV/4.2 A with capacitor banks for SI voltage generation

lowest stage. Sometimes also the rated voltage of the cascade is a bit lower than the voltage of its components multiplied by the number of stages to meet non-linear voltage distributions in the cascade. For instance, the rated parameters of the single transformers of Fig. 3.15 are 1.2 MV and 14 MVA compared with 1 MV and 12.6 MVA when used in the cascade. To generate higher currents in transformer cascades, two transformers can be switched in parallel for the lowest stage.

Not only the available test current is reduced, the *short-circuit impedance* of the cascade transformer is increased according to the number of stages of the transformer cascade drastically. There are simplified calculations of the *short-circuit reactance* (Hylten-Cavallius 1988; Kind and Feser 1999). Kuffel et al. (2006) calculated the short-circuit reactance of the cascade X_{res} from the reactances of the single units (X_{HV} of the HV winding, X_{LV} for the LV exciter winding and X_{TV} for the transfer winding) and the number of stages n by

$$X_{\mathrm{res}} = \sum_{i=1}^{n} \left(X_{\mathrm{HV}i} + (n-i)^2 X L_{\mathrm{LV}i} + (n+1-i)^2 + X_{\mathrm{TV}i} \right), \tag{3.7}$$

where it is presumed that all reactances are related to the same voltage, e.g. the HV output of the lowest transformer, and active losses, e.g. in the windings or in the core, are neglected. When three identical transformers ($n = 3$) are used for the cascade, one gets the resulting short-circuit reactance:

$$X_{\mathrm{res}} = 3 \cdot X_{\mathrm{HV}} + 5 \cdot X_{\mathrm{LV}} + 14 \cdot X_{\mathrm{TV}}. \tag{3.8}$$

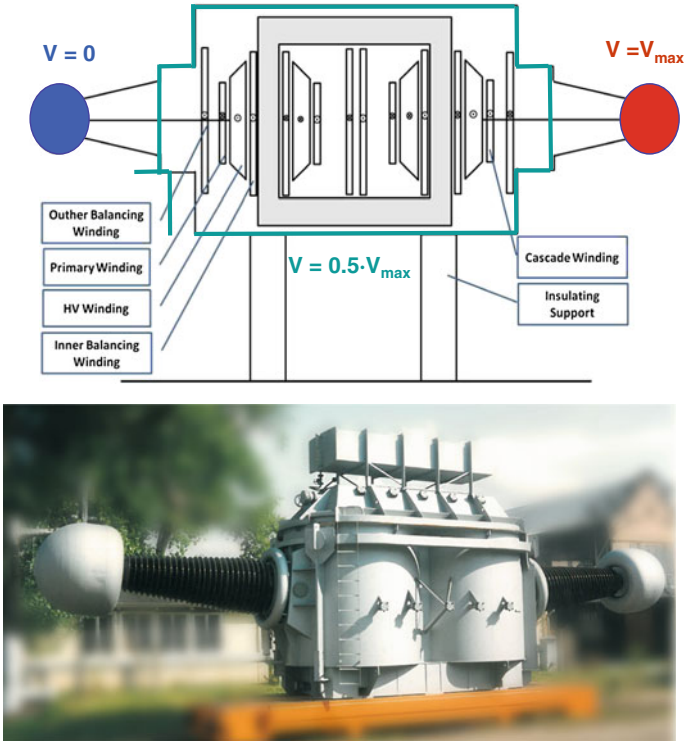

Fig. 3.16 Test transformer used for cascades with divided HV winding and tank on half potential

The formula indicates different voltage changes in the different stages and consequently non-linearities of the voltage distribution. The voltage distribution can be improved by compensation reactors on the stages. This remains without considerable influence on the short-circuit impedance. Test current reduction and increasing short-circuit impedance are the main reasons that cascades consist of no more than three stages usually.

To avoid the overload of the lower stages, the capacitive currents are compensated by reactors in parallel to the primary windings of the transformer and placed on the stages of the cascade. The *compensation reactors* are equipped with taps or even tuneable for the adaptation to the test object capacitance. In most cases, the reactors are separately arranged on the level of the stage. In some cases, fixed reactors inside of the tank of the test transformer are used, if only the capacitances of the test transformer itself shall be compensated. This can also be reached with a suited gap in the core of the transformer.

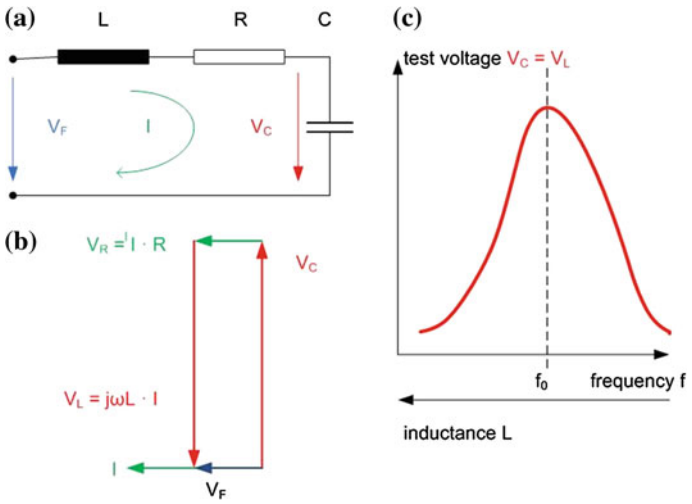

Fig. 3.17 HVAC resonant test circuit. **a** Equivalent circuit. **b** Phasor diagram. **c** Resonant curve

3.1.2 HVAC Test Systems Based on Resonant Circuits (ACR)

3.1.2.1 Principles of Resonant Circuits

If in the simplified test circuit based on a transformer (Fig. 3.2b), the inductance is modified to full compensation of the capacitive current of the capacitive load, one gets the phasor diagram *of a series resonant circuit* given in Fig. 3.17. This "*oscillating circuit*" is characterized by its *natural frequency* (Eq. 3.2)

$$f_0 = \frac{1}{2\pi\sqrt{L \cdot C}}. \tag{3.9}$$

When the resistive losses $P_R = V_R \cdot I$ are replaced by feeding a voltage of the natural frequency f_0, into this circuit, the system operates in series resonance. Then, the voltage is increased according to the so-called *quality factor Q,* which is the relation of the capacitive test power $S_C = V_C \cdot I$ to the resistive loss power P_R, and this is also identical with the relation between the test voltage V_C and the feeding voltage V_F:

$$Q = \frac{S_C}{P_R} = \frac{V_C}{V_F} = \frac{\frac{I}{\omega_0 C}}{I \cdot R} = \frac{1}{\omega_0 C \cdot R} = \sqrt{\frac{L}{C \cdot R^2}} \approx \frac{V_T}{V_F}. \tag{3.10}$$

There are two possibilities to reach resonance (Fig. 3.17c): One can adjust the inductance of the HV reactor until the natural frequency f_0 becomes identical to the feeding frequency f_F (inductance-*tuned resonant circuit*: ACRL, see Sect. 3.1.2.2) or one can feed the circuit via a frequency converter with the natural frequency

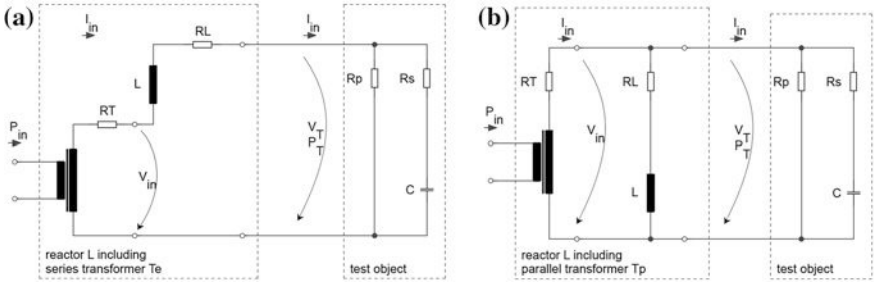

Fig. 3.18 Equivalent circuit of resonant circuits including exciter circuit. **a** Series resonant circuit. **b** Parallel resonant circuit

determined before (*frequency-tuned resonant circuit*: ACRF, see Sect. 3.1.2.3). For both cases, one has to consider that the tuning ranges are limited, because the resonance condition $f_F = f_0$ cannot be fulfilled for very low or very high capacitive load (there is no oscillation without a capacitive load). In case of a breakdown of the test object, the load capacitance changes drastically, the system goes out of resonance and the following "short-circuit current" is negligible. This means, in case of breakdown, the test object does not burn out.

The feeding into the resonant circuit is realized by an "*exciter transformer*" which adapts the voltage from the mains to the required output voltage $V_C = Q \cdot V_F$. The exciter transformer is designed according to the maximum necessary feeding power $P_F = P_R$ and voltage V_F, both following for the minimum assumed quality factor Q. In a series resonance circuit, the HV reactor is connected in series with the HV winding of the exciter transformer (Fig. 3.18a). Series resonant circuits are the most important application of the resonance principle.

The so-called *parallel resonant circuits* are applied for special tests at very huge capacitive test objects of relatively low voltage, e.g. capacitors for capacitor banks. In this case, the exciter transformer is switched in parallel to the HV reactor (Fig. 3.18b). This means that the voltage is fully controlled by the transformer. In case of resonance, the whole capacitive current is compensated by the reactor. Consequently, the *quality factor* becomes

$$Q_p = \frac{S_c}{P_R} = \frac{I_C}{I_F} \approx \frac{I_T}{I_F}. \tag{3.11}$$

A parallel resonant circuit is a HV test transformer circuit that is fully compensated on the HV side. It is usual to combine the test transformer with a resonant reactor to one unit in one tank. In that case, the magnetic core is designed with gaps. Because of the HV transformer, the test voltage may be remarkably disturbed by harmonics whereas series resonant circuits supply a fine sine wave. In the following, only the more important *series resonant circuits* will be considered.

The complete test system may be understood as the parallel connection of the feeding circuit (with the quality factor Q_F) and the test object (with Q_T). The

combination of the two quality factors delivers the total quality factor of the test circuit:

$$Q = 1 \Big/ \left(\frac{1}{Q_F} + \frac{1}{Q_T} \right) = \frac{Q_F \cdot Q_T}{Q_F + Q_T}. \tag{3.12}$$

The quality factor is a related parameter, and therefore depending on the test condition. The value of Q_F may be considered as a fixed value for a fixed frequency (depending on the design between $Q_F = 50$ and 200). When, e.g., a long XLPE cable system is tested on site, the capacitive test power and Q_T are high, then the resulting quality factor is determined by Q_F. Vice versa in case of a type test on a short-cable sample using a water termination (see Sect. 3.6), the test object capacitance is low and the parallel resistance of the water termination causes additional resistive losses, then the resulting quality factor is determined by Q_T. Therefore, for the correct design of a resonant test system, the conditions of the later application should be well known.

Example A series resonant test system shall be selected for HVAC routine tests on XLPE cables with a length of 400 m at $V_T = 280$ kV/50 Hz. The total load capacitance is that of the cable (400 m · 260 pF/m = 104 nF) plus that of the capacitive divider, coupling capacitor and basic load (4 nF) $C_T = 108$ nF. The parallel water resistance of the termination has active losses of 22 kW (cooling power demand), which corresponds to a resistance R_p of 3.6 MΩ. Both parameters deliver the following parameters:

• Quality factor of the test object	$Q_T = 2\pi f \cdot C \cdot R_p = 121$ (for parallel capacitance and resistance: $Q = I_c/I_r$!!)
• Quality factor of the power supply	$Q_F = 70$ (assumption)
• Total quality factor	$Q = 44.3$ (Eq. 3.12)
• Required test power	$S_T = 2\pi f \cdot C \cdot V_T^2 = 2,650$ kVA
• Necessary exciter voltage	$V_F = V_T/Q \approx 6.3$ kV
• Necessary exciter power	$P_F = P_T = S_T/Q = 60$ kW

The *exciter transformer* should deliver an "*exciting*" *voltage*, which is well adapted to the required output test voltage and test power. The exciter transformer must be designed to deliver the active feeding power P_F that follows from the capacitive test power S_T and the quality factor Q by the equation $P_F = S_T/Q$.

If the exciter transformer would have only one voltage output and a test voltage should be generated, which is only 50 % of the rated voltage, then only a quarter of the test power is available. The full test power can be used at the 50 % test voltage level, when the exciter transformer has a tap for 50 % output voltage. An optimum adaptation to both, output voltage and power, requires an exciter transformer with a well selected number of taps. Its rated voltage has to be selected

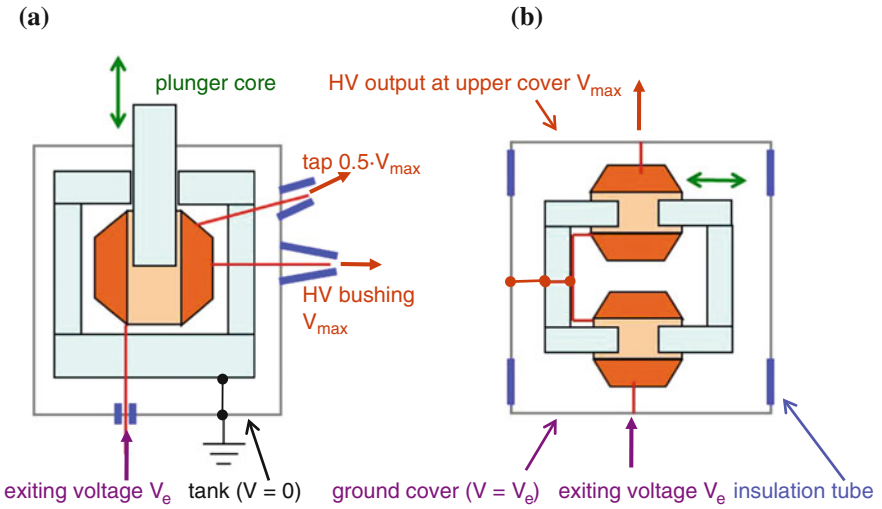

Fig. 3.19 Active part of a tuneable reactor **a** Shell-type core with one gap of width a. **b** Two half-cores with two half gaps, each a/2

according to the maximum voltage necessary for the HVAC test, and the test is controlled via a regulator transformer. As the above example shows the voltages and powers necessary for exciting, the oscillation circuit are low compared with those of the test object.

First ideas of HV resonant circuits came up by (Charlton et al. 1939), a certain technical perfection has been reached for ACRL test systems after 1960 (Reid 1974). ACRF test systems have been proposed by Zaengl and co-workers (Bernasconi et al. 1979; Zaengl et al. 1982; Schufft et al. 1995). In the following, the two basic types of series resonant circuits are described and compared.

3.1.2.2 Inductance-tuned Resonant Circuits of Fixed Frequency (ACRL)

The inductance of a reactor can be changed when its magnetic core has a gap of an adjustable width (Fig. 3.19). The inductance of the reactor is proportional to the square of the number of the turns w^2 of the winding, the permeability μ_0 of the air in the gap, the area A of the cross section of the magnetic core at the gap as well as inversely proportional to the width a of the gap (k is a factor of proportionality)

$$L = \frac{k \cdot \mu_0 \cdot w^2 \cdot A}{a}. \tag{3.13}$$

The maximum inductance L_{max} is connected with the minimum gap a_{min} and enables resonance (Eq. 3.9) with the minimum load capacitance C_{min}. Vice versa the maximum load C_{max} is related to the minimum inductance L_{min} and the

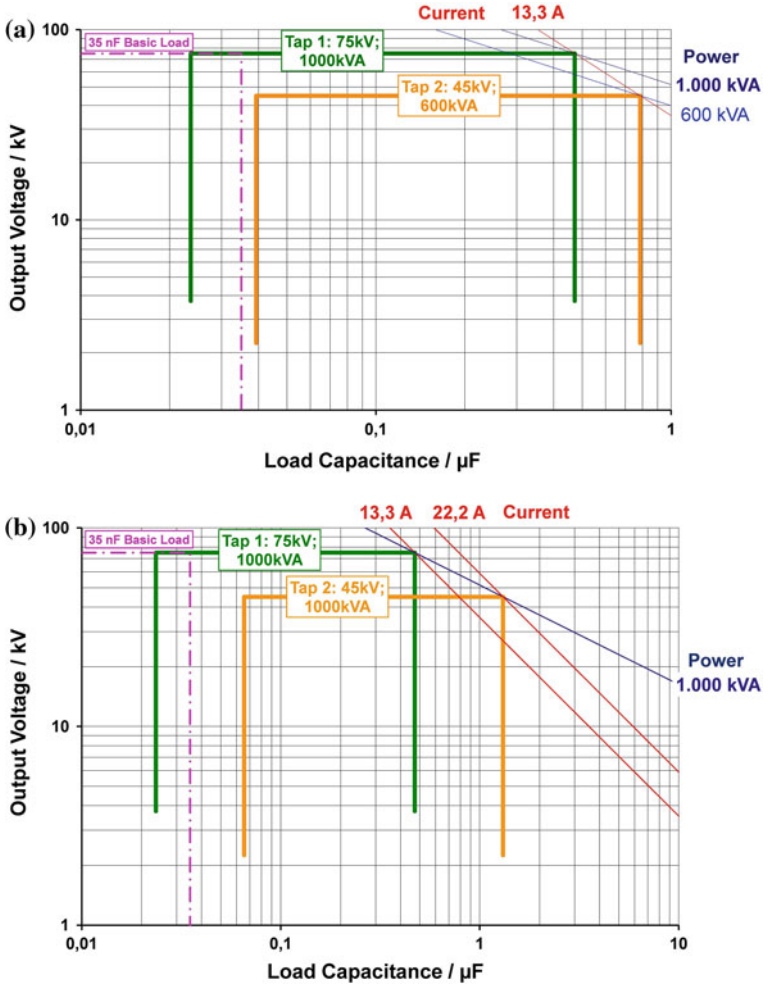

Fig. 3.20 Load diagram of an inductance-tuned resonant circuit. **a** Design for a tap of identical (constant) current. **b** Design for a tap of identical (constant) power

maximum gap a_{max}. With increasing gap width, the magnetic stray flux and also the losses increase, too, and lead to a certain non-linearity of the inductance and a decrease of the quality factor. These—and also some technological limitations—cause the technical useable change of the gap up to $a_{max}/a_{min} \approx 20$. Based on Eqs. 3.9 and 3.12, the limits in a load-output voltage diagram (Fig. 3.20) are also $C_{max}/C_{min} \approx 20$:

$$\frac{C_{max}}{C_{min}} = \frac{L_{min}}{L_{max}} \approx \frac{a_{max}}{a_{min}}. \tag{3.14}$$

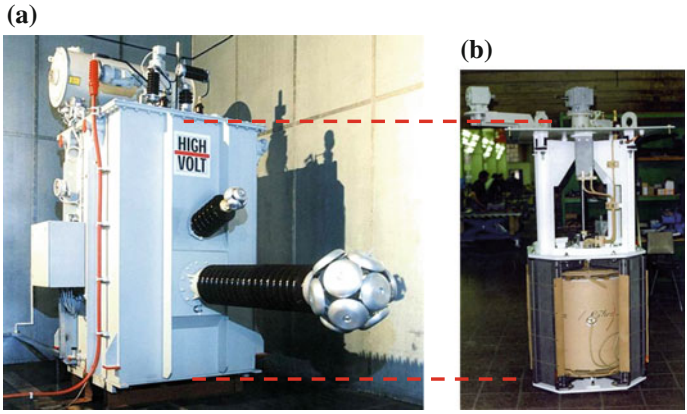

Fig. 3.21 Tank-type reactor (250–100 kV, 2,000 kVA). **a** Reactor with two bushings. **b** Active part with drive for core adjustment

The precise adjustment of the gap is controlled on the basis of the phase angle between test voltage and test current. When this angle is maximized, also the maximum of the resonant curve is reached. The higher the quality factor, the steeper is the resonant curve and the higher are the requirements to the accuracy of the gap control.

Usually a resonant circuit is equipped with a *basic load capacitor* $C_b \geq C_{\min}$, which enables resonance and operation without a capacitive test object. This is important when the resonant test system itself is to be checked. The basic load capacitor is used as a voltage divider and/or a coupling capacitor for PD measurement or as for a HV filter.

Tank-type reactors: The design of a reactor depends also on the insulation and the thermal conditions. Often tank-type reactors are designed with taps for voltages V_i lower than their rated voltage V_m. Then, the winding can be designed for constant current I, which means it is made with one type of wire and the power at lower voltage is according to the ratio of the voltage V_i/V_m lower (Fig. 3.20a), the winding is made of identical sub-windings. It can also be designed for constant power. Then, the current ratio I_i/I_m must increase inversely to the voltage ratio V_i/V_m. Higher currents require thicker wires for the winding, the winding is made of different sub-windings.

For the tank-type design (Fig. 3.21), a *shell-type core* (Fig. 3.19a) is useful, because the very stable magnet core of one tuneable central leg and three-fixed outer legs can overtake the high mechanic forces (Spiegelberg et al. 1993). The mechanic stability means less vibrations that results in a stable output voltage and less noise. The layer winding is designed similar to that described above for oil-insulated test transformers. As shown in Fig. 3.20, the winding of tank-type reactors is often designed with taps. If there is only one additional tap, a second bushing may be an economic solution. In case of three or more taps, the reactor is equipped with a no-load tap-changer. The advantages of tank-type reactors can be

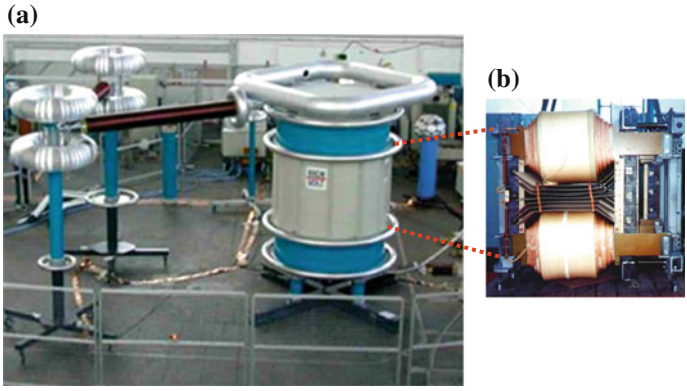

Fig. 3.22 Cylinder-type reactor (400 kV, 14 MVA). **a** Complete test reactor. **b** Active part with two coils and one adjustable half-core

compared with those of tank-type test transformers (Table 3.1), but they are not used for cascading for higher voltages. Their main application is for *cable testing* up to 400 kV including PD measurement. For that application with a Faraday cage, they can be arranged outside the cage, the tank is flanged to the grounded, metallic wall of the cage and only their bushing is arranged inside the test area.

Cylinder-type reactors: For the cylinder design of reactors (Fig. 3.22), a magnetic core of two half-cores (Fig. 3.19b) is applied. Depending on the design, both or only one half-core are adjusted by gears for the gap. The gap is designed for a certain distance—corresponding to the required inductance—which gives resonance with the capacitive object under test (Reid 1974). The winding is divided into two parts. The beginning of the lower part of the winding is connected with the grounded lower cover of the cylinder. The end of the upper part is connected with the upper cover on HV potential. The active part is behind the metallic middle part of the cylinder (grey on Fig. 3.22a) that is on half potential as the magnetic core itself. The metal cylinder controls the electric field inside for the active part in oil and outside for the surface of the reactor in air. The (blue) insulating cylinders overtake the role of the bushings of the reactor. The outer field strength distribution is controlled by the toroid electrodes. For a good utilization of the limited space inside the cylinder, the windings have a rectangular cross section (Fig. 3.23). Care is taken for the high mechanic stability of the wire layers by a special compact insulation.

Reactor cascades: Cylinder-type reactors can easily be connected in series for higher voltages by stacking one above the other. In opposite to a transformer cascade such a reactor cascade (Fig. 3.24) increases the test power by each additional reactor. Reactor cascades are applied when higher test voltages are required, with not too high test currents for *GIS testing* and for *applied voltage tests* on transformers. Very powerful types of cylinder-type reactors with external cooling are also used when cable tests require voltages higher than the mentioned 400 kV.

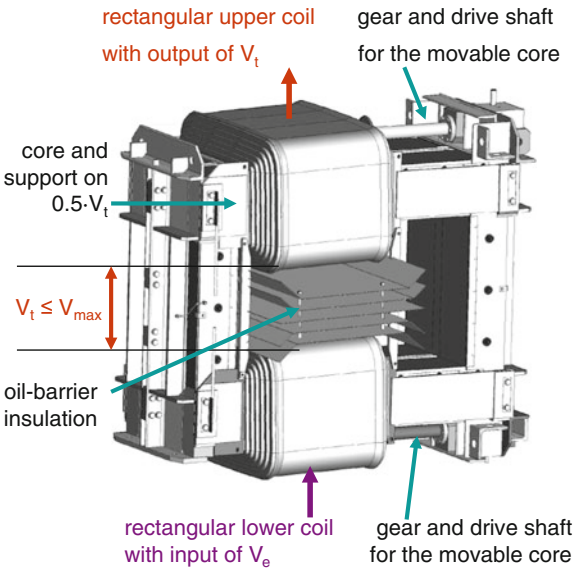

Fig. 3.23 Rectangular layer winding for a cylinder-type reactor

Higher test currents can be generated by the parallel connection of reactors. This is simple when each reactor is placed separately. But the parallel connection of the single reactors—arranged in a cascade of one column—requires special bars and workmanship. The effort with up to three modules remains reasonable.

3.1.2.3 Frequency-tuned Resonant Circuits of Variable Frequency (ACRF)

An oscillating circuit with a fixed reactor of inductance L and of fixed capacitive test object C_0 has a fixed *natural frequency* f_0 according to Eq. 3.9:

$$f_0 = \frac{1}{2\pi\sqrt{L \cdot C_0}}.$$

It must be excited with that frequency for resonance. For a different test object, a different natural frequency appears. The tuning range of this resonant circuit depends on the acceptable frequency range. The maximum load capacitance C_{max} determines the minimum test frequency f_{min} for a pre-given inductance L of the reactor and vice versa. Usually, the standards for HVAC testing allow a certain frequency range and this determines the load range:

$$C_{max} = \frac{1}{(2\pi f_{min})^2 \cdot L} \quad \text{and} \quad C_{min} = \frac{1}{(2\pi f_{max})^2 \cdot L}. \tag{3.15}$$

Fig. 3.24 Reactor cascade 1,200 kV of three identical modules 400 kV each

The tuning range follows to

$$\frac{C_{\max}}{C_{\min}} = \left(\frac{f_{\max}}{f_{\min}}\right)^2, \tag{3.16}$$

and the maximum current to

$$I_{\max} = 2\pi f_{\min} \cdot C_{\max} \cdot V_{\mathrm{T}} = V_{\mathrm{T}} \cdot \sqrt{\frac{C_{\max}}{L}}. \tag{3.17}$$

From Eqs. 3.9, 3.15 and 3.16, the operation characteristic of an ACRF test circuit (Fig. 3.25) can be calculated. With increasing load from $C_{\min}$ to $C_{\max}$, the frequency is decreasing from $f_{\max}$ to $f_{\min}$ (Fig. 3.25a). At the same time, the current is increasing with the capacitive load. It may happen that the required current $I_{\max}$ is higher than the current that results from the thermal design $I^*_{\max}$. Then, the current must be limited to the technically acceptable value $I^*_{\max}$ by reduction of the test voltage in the relevant load range (Fig. 3.25b). The voltage can be generated in the range between minimum and maximum load, possibly with certain reductions for a necessary current limitation.

The maximum *capacitive test power* at $f_{\min}$ follows to $S_{\mathrm{T}} = V_{\mathrm{T}} \cdot I_{\max}$, but this is not a typical parameter because it depends on the test frequency. Therefore, it is usual for comparisons to use the 50 Hz (*or* 60 Hz) *equivalent power*

$$S_{50} = \frac{50}{f_{\min}} \cdot S_{\mathrm{T}}. \tag{3.18}$$

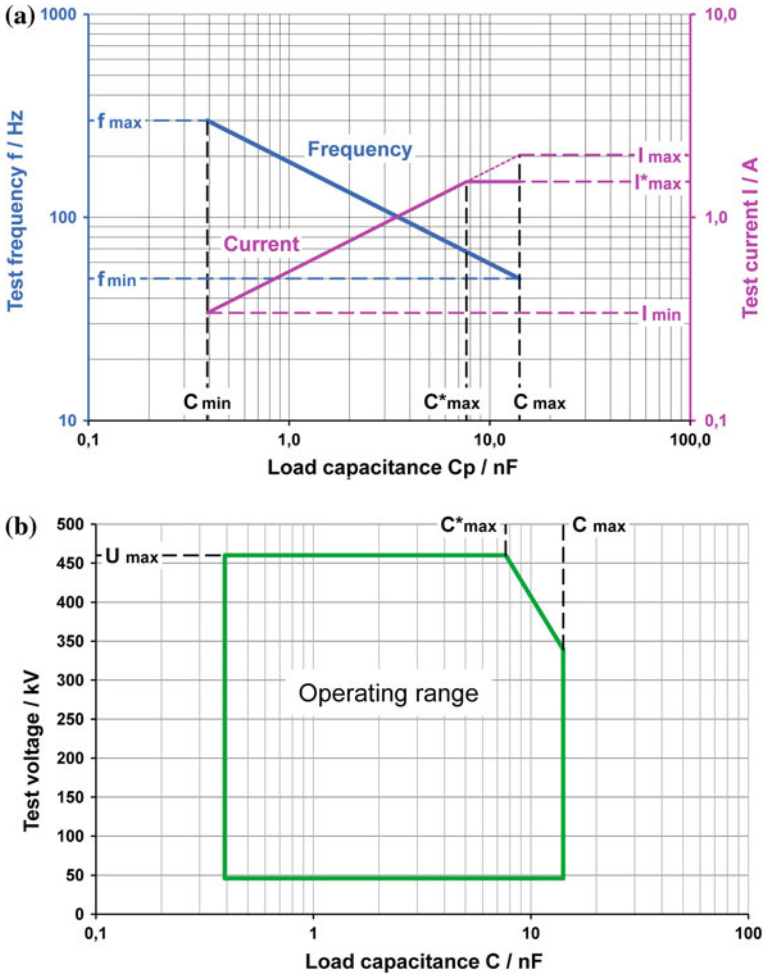

Fig. 3.25 Operation characteristic of a frequency-tuned resonant system. **a** Frequency and current versus load capacitance. **b** Voltage operating range versus load capacitance

The necessary *feeding power* that is equal to the loss power of the circuit can be calculated by the help of the quality factor from the test power S_T:

$$P_F = S_T/Q. \tag{3.19}$$

The *quality factor* of a frequency-tuned resonant test system is higher than that of an inductance-tuned system, because the design of a fixed reactor enables reduced stray fluxes, and consequently lower losses compared with a tuneable one. It can be assumed with values in the order $Q = 50$–150 (for ACRL systems it is about $Q = 20$–60).

It should be noted that the above mentioned feeding power is related to mains of a stiff network. If, for instance, on site a *Diesel motor-generator set* is used for the power supply, it is recommended to apply one with a rated power about three times higher than the calculated P_F.

Example For on-site tests at cable systems, a test frequency range of 20–300 Hz is accepted. An HVAC resonant test system based on a reactor 160 kV/80 A is available for that frequency range. Which maximum capacitance can be tested with this system at its rated voltage? Which basic load is necessary to check the test system without test object? Which length of cable can be tested when the specific capacitance of the cable is 200 nF/km? Which feeding power is required when a quality factor $Q = 100$ is assumed?

Maximum load by Eq. 3.15

$$C_{max} = \frac{1}{(2\pi \cdot 20\,s^{-1})^2 16\ V\ s\ A^{-1}} = 3{,}962\ nF$$

Basic load by Eq. 3.16

$$C_{min} = C_{max}\left(\frac{f_{min}}{f_{max}}\right)^2 = 3{,}962 \cdot \frac{1}{225} = 18\ nF$$

At 160 kV, a capacitance of 18 nF is quite large and expensive. One can think about to use, e.g., a capacitance of that value, but only for 50 kV and check the performance of the test system at that reduced voltage.

Maximum current by Eq. 3.17

$$I_{max} = 160 \cdot 10^3\ V \cdot \sqrt{\frac{3.962\ A\ s\ V^{-1}}{10^6 \cdot 16\ V\ s\ A^{-1}}} = 79.6\ A$$

This current is below the rated value, and there is no limitation due to the current. The testable length of the cable results C_{Cable}/200 nF/km = (3,962 nF – 18 nF)/200 nF/km = 19.7 km.

Required feeding power by Eq. 3.19

$$P_F = \frac{I_{max} \cdot V_T}{Q} = \frac{79.6\ A \cdot 160 \cdot 10^3\ V}{100} \approx 130\ kVA$$

This power must be supplied from a stiff network. In case of the application of a mobile power supply, a 400 kVA motor-generator set should be used.

The necessary feeding power of variable frequency is generated by static *frequency converters* (Fig. 3.26). The three-phase power from the mains is first rectified to a direct voltage, and then a circuit of power transistors (IGBT's) or of SKIIP modules converts the DC voltage to a rectangular AC voltage (Figs. 3.26a, 3.27). The oscillation circuit acts as a HV filter and generates a fine sine wave. There is a phase shift of 90° between the rectangular voltage, which replaces the active power losses of the circuit and the test voltage at the capacitive test object.

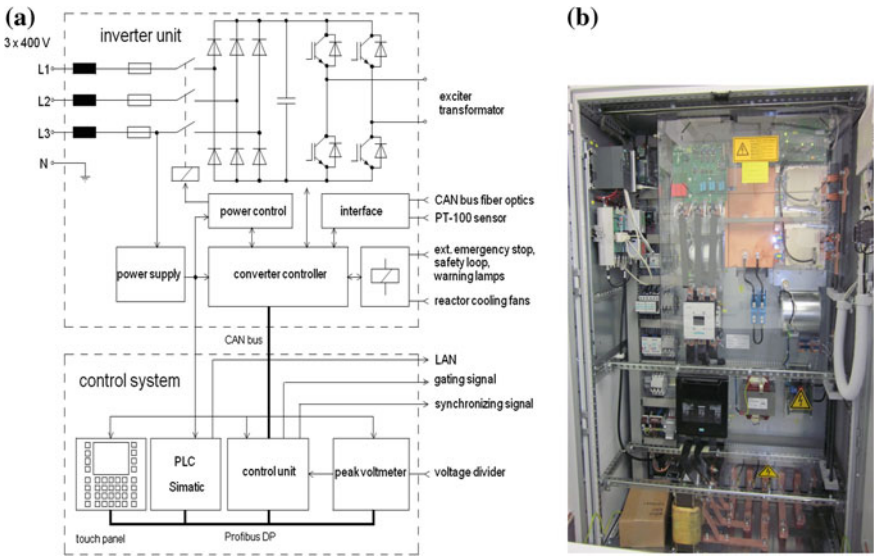

Fig. 3.26 Frequency converter for a frequency-tuned resonant test system. **a** Principle circuit diagram. **b** Cubicle of the frequency converter

With respect to the high quality factors of ACRF test systems, the adjustment of the frequency must be guaranteed with high precision (better than ±0.1 Hz). The height of the voltage is determined by pulse-width modulation. The frequency converter—together with the control-and-measuring system—can be arranged in one cubicle (Fig. 3.26b) or—for lower power—in a movable desk (Fig. 3.28b).

Tank-type fixed reactors: As tank-type test transformers (Fig. 3.5), tank-type fixed reactors (Fig. 3.29) are related to high test power (50 Hz equivalent power up to the order of 50 MVA). Their design with oil–paper insulation is derived from that of test transformers. In the central leg, the magnetic core has several small gaps of very low stray flux. Therefore, the fixed reactors have a higher quality factor than tuneable reactors. The tank of a single reactor is grounded, but they can be arranged in cascades when the higher stages are arranged on insulating support (Fig. 3.29b). The main application of these reactors is *on-site testing* of cable systems after laying or repair. But more and more they are also used for *routine testing* of the long submarine cables and for *pre-qualification tests* of newly developed cables (see Sects. 3.6 and 7.3; Hauschild et al. 1997, 2002; Schufft et al. 1999; Gockenbach and Hauschild 2000).

Cylinder-type fixed reactors: The design of these cylinder-type reactors (Fig. 3.30) is similar to that of the cylinder-type transformers (Fig. 3.10). They are for lower test power, but well-suited for reactor cascades by simple stacking one above the other. Their application is therefore for objects of higher required test voltages at lower required test power: Therefore, they are used for on-site testing of gas-insulated systems (GIS and GIL) and for *applied voltage tests* of power

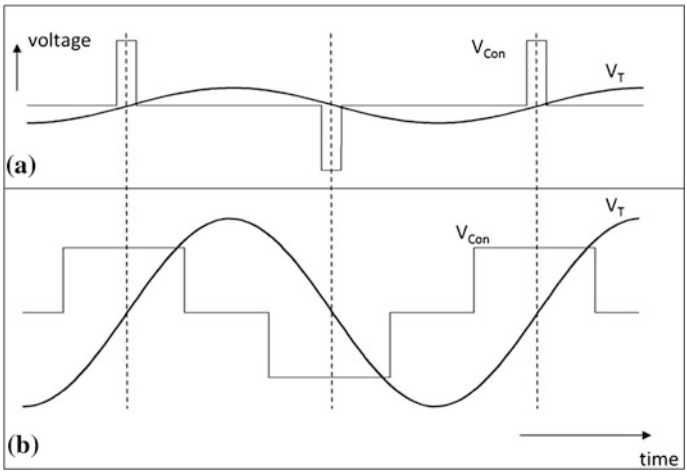

Fig. 3.27 Rectangular output voltage of the frequency converter for low (*above*) and high (*below*) sinusoidal test voltage on the capacitive test object

transformers, both in factories and on site (see Sects. 3.2.3, 3.2.5, 10.4). Additionally small, lightweight reactors are realized with a bar core and a relatively small oil volume. The combinations of several reactors in series and/or in parallel (Fig. 3.30c) enable a good adaptation to different test objects (Kuffel and Zaengl 2006; Hauschild et al. 1997). Their low thermal capacity limits both, the rated current and the duty cycle remarkably.

Fixed reactors with SF_6-impregnated foil insulation: This type of reactor is arranged in a metal enclosure that can be flanged directly to a gas-insulated test object (Fig. 3.28). It is designed without iron core but with a divided winding of a very high number of turns. The single layers of each half winding are arranged on a conducting cylinder each. The SF_6 insulation of the gas gap between the two cylinders must be designed for the rated voltage of the reactor, whereas the voltage between the outer layers and the enclosure corresponds to the half of the full voltage. The thermal design is difficult because of the large number of turns and the control of the magnetic flux. This type of reactors is for rated voltages up to 750 kV per unit, test currents of few Amps and short-time operation. It can be recommended to clarify the necessary load-time characteristic of these reactors carefully. Their application is for testing GIS and their components (see Sects. 3.6 and 7.3).

3.1.2.4 Comparison of ACRL and ACRF Test Systems

The comparison of the most important component in a resonant circuit, the *HVAC reactor*, shows that a *fixed reactor* is much simpler, more compact, more robust and consequently cheaper than one with tuneable inductance. The principle circuit

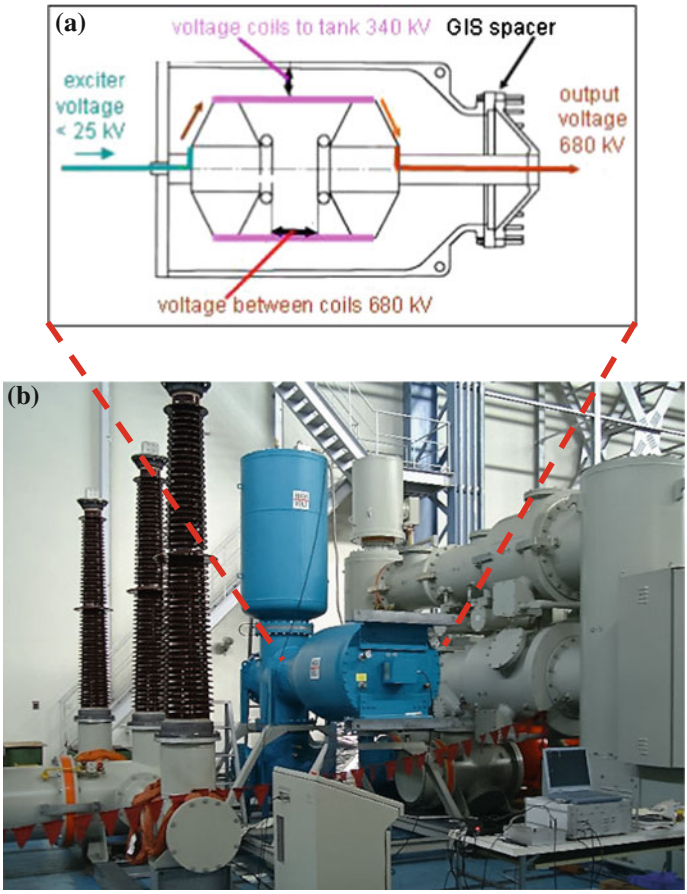

Fig. 3.28 ACRF test system for GIS routine tests. **a** Principle design of the SF_6-impregnated, foil-insulated reactor. **b** Reactor (*blue*, *horizontally*) and coupling capacitor (*blue*, *vertically*)

diagram of both solutions (Fig. 3.31) shows that the *ACRF test system* has less components, also because of the cubicle that includes the switches, the frequency converter and the control.

But for most tests in factory, there is the disadvantage of the variable frequency. The frequency tolerance for HVAC test voltages between 45 and 65 Hz, accepted by IEC 60060-1: 2010, is too small for a sufficient tuning range for the load. It corresponds only to a factor $(f_{max}/f_{min})^2 = 2$ between highest and lowest load.

Table 3.2 summarizes a comparison between the two principles for the application of on-site testing of HV and EHV cables. There is a *frequency range* of 20–300 Hz accepted (IEC 62067; IEC 60840) and used by the ACRF system, but not helpful for a system of fixed frequency of 50 or 60 Hz. The extended frequency range with the lower limit 20 Hz enables a 2.5 times higher test power (or a 2.5 times higher capacitance of the test object) of the ACRF system than the ACRL

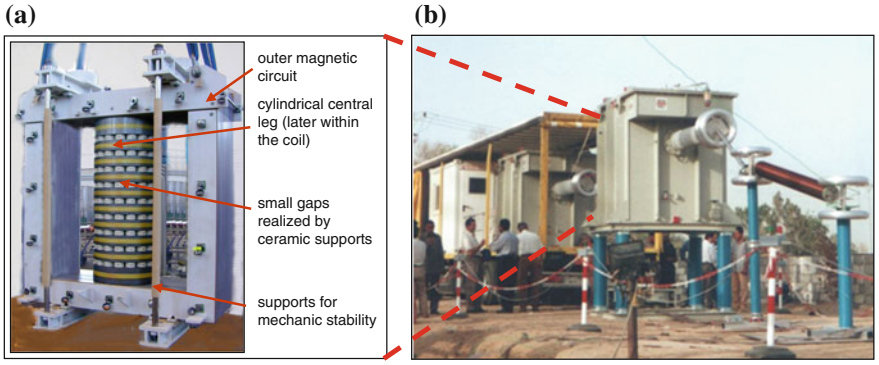

Fig. 3.29 Tank-type fixed reactor with oil–paper insulation. **a** Principle design of the magnetic core. **b** Two reactors in series for test voltages up to 520 kV

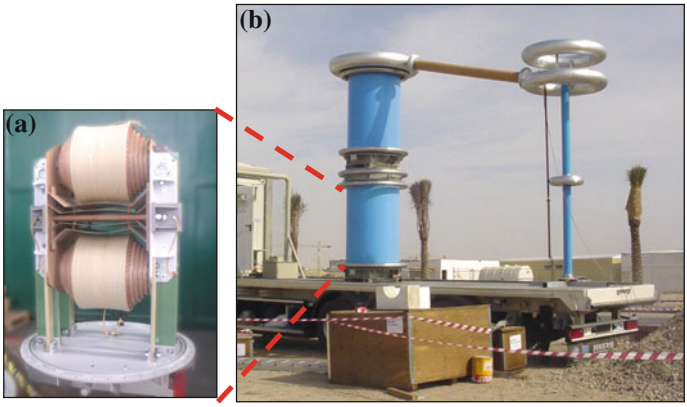

Fig. 3.30 Cylinder-type fixed reactor with oil–paper insulation. **a** Principle design of the active part. **b** Two reactors 250/10 kV in series for a test voltage of 500 kV

system at identical voltage. Because of the lower losses of the reactor, the *quality factor* of the ACRF system is about twice of that of the ACRL system. The frequency range enables an ACRF *load range* about ten times wider than that of an ACRL system. Both, wider frequency range and higher quality factor result in a feeding power that is about five times lower for ACRF than for ACRL test systems. The power supply of an ACRL system requires single- or two-phase operation. The *frequency converter* of an ACRF system uses a three-phase power supply that is a symmetric and lower load and simpler to handle on site. For rough transportation and operation conditions on site, the absence of moving parts is an advantage of ACRF systems, whereas the ACRL systems use regulator transformers and tuneable reactors. As also seen from Table 3.2 and Fig. 3.31, the number of components of an ACRF system is lower.

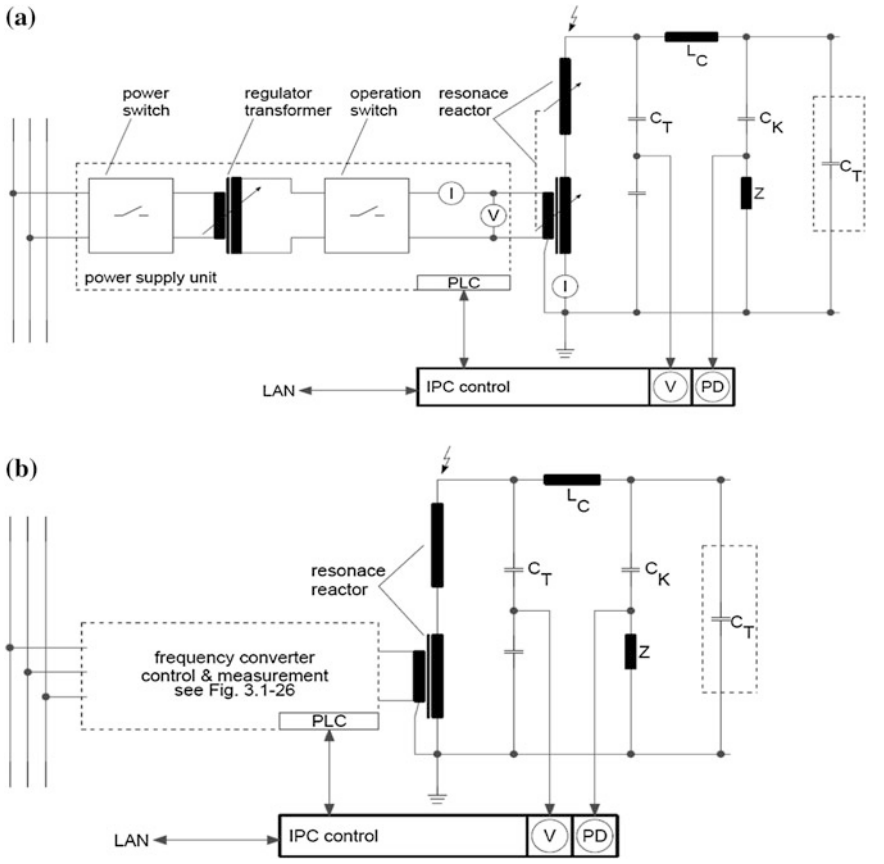

Fig. 3.31 HVAC test systems based on series resonant circuits. **a** Equivalent circuit of a complete ACRL test system. **b** Equivalent circuit of a complete ACRF test system

The comparison shows clearly that an ACRF test system is always the better economic solution if the frequency range is sufficient for an acceptable tuning range. This is the case for most on-site tests (see Chap. 7), but it can be applied also for some factory tests: The applied AC voltage test of power transformers (IEC 60076-3: 2012) shall be performed at a frequency of > 40 Hz, when an upper limit of 200 Hz is assumed, a sufficient load range of 1 to 25 can be reached. For super-long *submarine cables* (some 10 km long), no other solution than ACRF testing can be performed with acceptable economic effort. There are discussions for using the full frequency range 10–500 Hz given in IEC 60060-3 for on-site testing also for the factory tests (Karlstrand et al. 2005). A wider application of ACRF systems in factory tests requires the definition of acceptable frequency ranges. This can only be based on new research work on the influence of the frequency—e.g. in the range 20–100 Hz—on the discharge processes in the relevant insulations.

Table 3.2 Comparison between ACRL and ACRF test systems for cable-testing on site

Resonant circuit	ACRL (inductance-tuned)	ACRF (frequency-tuned)
Frequency	$f_L = 50$ Hz (60 Hz)	$f_F = 20$–300 Hz (Cables)
Max. test power	$S_{L\max} = 2\pi f \cdot CU^2$	$S_{F\max} = 2.5\ S_{L\max}$
Quality factor	$Q_L = 40$–60	$Q_F = 80$ to >120
Load range	$C_{\max}/C_{\min} = L_{\min}/L_{\max} \approx 20$	$C_{\max}/C_{\min} = (f_{\max}/f_{\min})^2 \approx 225$
Feeding power	$P_{eL} = (2\pi f\ C\mathrm{U}^2)q_L$	$P_{eF} = P_{eL} \cdot (f_F/f_L) \cdot (Q_L/Q_F)$
Power supply	Single or two phase	Three phase
Weight-to-power ratio (kg/kVA)	3–8	0.8–1.5
Components with moving parts	Tuneable reactor, regulator transformator	None
Number of main components	Six components: Tuneable reactor, HV divider/PD coupler, exciter transformer, switching cubicle, control-and-measuring rack	Four components: Fixed reactor, HV divider/PD coupler, exciter transformer, control-and-feeding unit

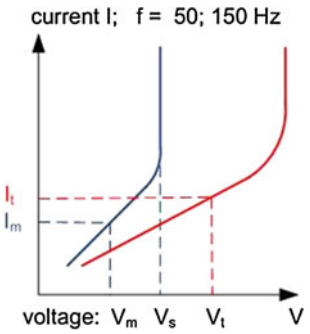

Fig. 3.32 Schematic voltage-current characteristic of a transformer under induced voltage test

3.1.3 HVAC Test Systems for Induced Voltage Tests of Transformers (ACIT)

Above it has been shown that in a resonant test system, the capacitive test object, e.g. a HV cable, becomes a part of the HV generation circuit. Also in testing power or instrument transformers, the test object may become a part of the generation circuit. When it is energized on its low-voltage side, the test voltage on the HV side can be generated by this test object. This so-called *induced voltage test* (IEC 60076-3, Draft 2011) requires a feeding circuit that matches the low voltage to both, the required test voltage and the ratio of the transformer under test. This has to consider the non-linear magnetic behaviour of the transformer as a part of the test circuit.

Saturation effects of the iron core mean under test conditions that an increase of the test voltage causes an over-proportional increase in the test current (Fig. 3.32). Finally, a test voltage remarkably higher than the operational voltage cannot be generated at operational frequency $f_m = 50$ or 60 Hz (Fig. 3.32). Because of the limitation of the magnetic flux Φ, the voltage can only be increased up to a certain value V_s when saturation becomes considerable. There is a frequency-depending relationship between voltage and magnetic flux:

$$V_S \sim f \cdot \Phi_S,$$

which shows that the "saturation" voltage V_s can only be increased for a certain "saturation" flux Φ_s when a higher test frequency is applied. Therefore, the induced voltage tests has to be performed at higher test frequencies f_t, usually higher than twice the operational frequency ($f_t \geq 2\, f_m$).

The transformer under test is not a simple load, its characteristic changes with the frequency (Fig. 3.33). The upper curve is the total test power demand S_t and the lower one the active power demand P_t. The difference between the two curves is the reactive power demand. At lower frequencies, the test object is an inductive load, at higher frequencies, it is a capacitive load for the feeding circuit. In between, there is the frequency of *self-compensation*, in Fig. 3.33 at $f \approx 160$ Hz. If this frequency is selected for a test, the required test power becomes a minimum.

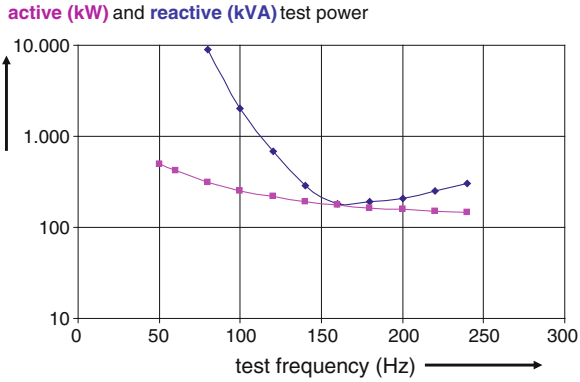

Fig. 3.33 Example for the frequency–load characteristic of a power transformer under induced voltage test

In transformer testing not only the insulation of the windings must be tested at induced voltage, also the no-load and the short-circuit losses shall be measured with induced voltage of operational frequency. Therefore, the feeding system has to supply in minimum test voltages of two frequencies, operational frequency and test frequency $f_t \geq 2\, f_m$. For that reason, a frequency converter for single-phase and three-phase operation is the basic element of the feeding circuit:

For a very long time *rotating frequency converters*, so-called *motor-generator (M/G) sets*, are applied and most transformer test fields are equipped with such sets (Fig. 3.34a). They consist of a motor of variable revolutions (traditionally a DC motor, nowadays a thyristor-controlled AC motor) that is mechanically coupled with a synchronous generator. The frequency is changed according to the revolutions of the motor, at the same time, the output voltage can be adjusted. In case of induced voltage tests (usually $f_t > 100$ Hz), the test object represents often a capacitive load that may cause dangerous over-voltages. To avoid such *self-excitations* ("*runaways*") exceeding the limits of the M/G set, sufficient inductive compensation must be applied. The output voltage of the M/G set is adapted to the necessary input voltage of the transformer under test by a matching (also called step up) transformer.

A modern alternative is the application of *static frequency converters* (SFC) based on power electronic modules (Fig. 3.34b; Kübler and Hauschild 2004; Hauschild et al. 2006; Martin and Leibfried 2006; Werle et al. 2006; Thiede and Martin 2007; Winter et al. 2007; Thiede et al. 2010). The converter itself (Fig. 3.35) uses a three-phase power supply. The voltage is rectified and then transferred into a single-phase or three-phase sine voltage by a unit of power transistors (IGBT) operating with pulse-width modulation. A sine-wave filter is very important for the suppression of the noise signals caused by the switching of the IGBT's. The SFC has a control for frequency and voltage height, which automatically adjusts the converter to the above mentioned self-compensation. The *self-excitation* cannot happen. A SFC requires a matching transformer.

In opposite to a M/G set, a SFC is able to compensate also the capacitive power demand that may play a role in induced voltage tests at higher frequency

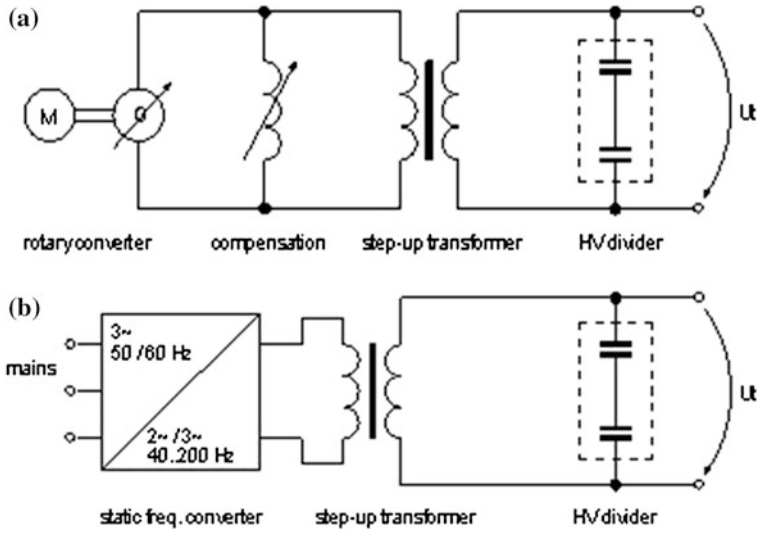

Fig. 3.34 Principles of frequency converters in circuits for induced voltage tests. **a** Rotating converter by M/G set. **b** Static frequency converter (*SFC*)

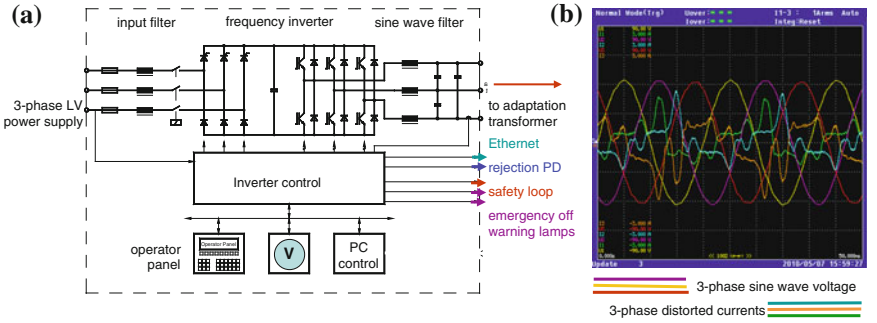

Fig. 3.35 Static frequency converter (*SFC*) for induced voltage tests (Thiede et al. 2010). **a** Principle circuit diagram. **b** Sinusoidal voltages and disturbed currents

(Fig. 3.33). In case of loss measurements at operational frequency of 50 or 60 Hz, for both principles an adjustable *capacitor bank* for compensation of the high inductive power demand is necessary. It is arranged after the matching transformer in the circuit for the induced voltage test (Fig. 3.36). Furthermore, *a medium-voltage filter (MVHF)* for the reduction of conducted noise signals is arranged between compensation unit and test object. Except for the two different frequency converters, the elements of the circuit may be identical (Fig. 3.37). Table 3.3 compares therefore only the two converters.

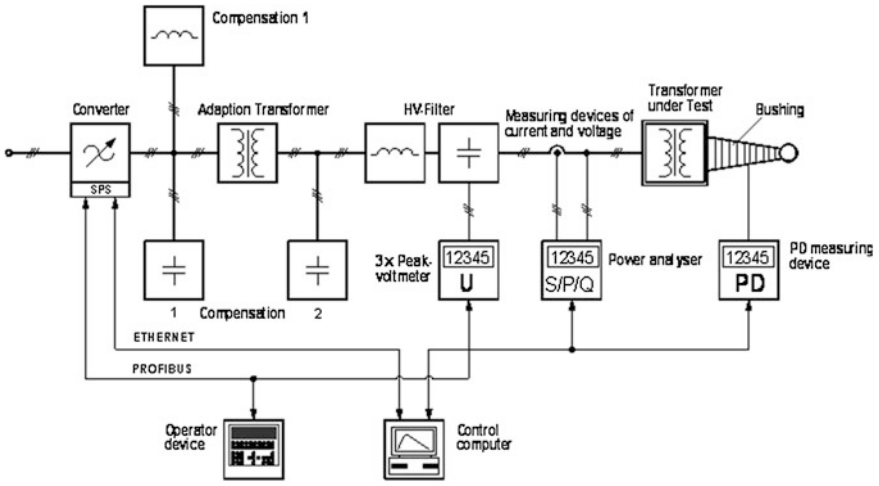

Fig. 3.36 Complete circuit for tests and measurements at induced voltage

3.2 Requirements to AC Test Voltages and Selection of HVAC Test Systems

3.2.1 Requirements for AC Test Voltages

The requirements for AC test voltages for *laboratory testing* are fixed in IEC 60060-1: 2010 and described here, those for *testing on site* are described in Chap. 10 according to IEC 60060-3: 2006. For research purposes, each interesting type of alternating voltages may be used.

The AC test voltage shall be of approximately sinusoidal *wave shape* and its value is determined by the peak value because the highest stress determines usually the breakdown process (Fig. 3.38). To have the direct comparison with the usually applied rms value, the test voltage value is defined by

$$V_{\mathrm{T}} = \frac{V_{\mathrm{peak}}}{\sqrt{2}} = \frac{V_{\mathrm{peak+}} + \left|V_{\mathrm{peak-}}\right|}{2\sqrt{2}}. \tag{3.20}$$

If the peak values at the two polarities are different, the average value of both is applied as peak value. For some special test application, e.g. when heating processes influence the development of the breakdown, the *rms value* might be applied:

$$V_{\mathrm{rms}} = \sqrt{\frac{1}{T}\int_0^T V(t)^2 \mathrm{d}t}, \tag{3.21}$$

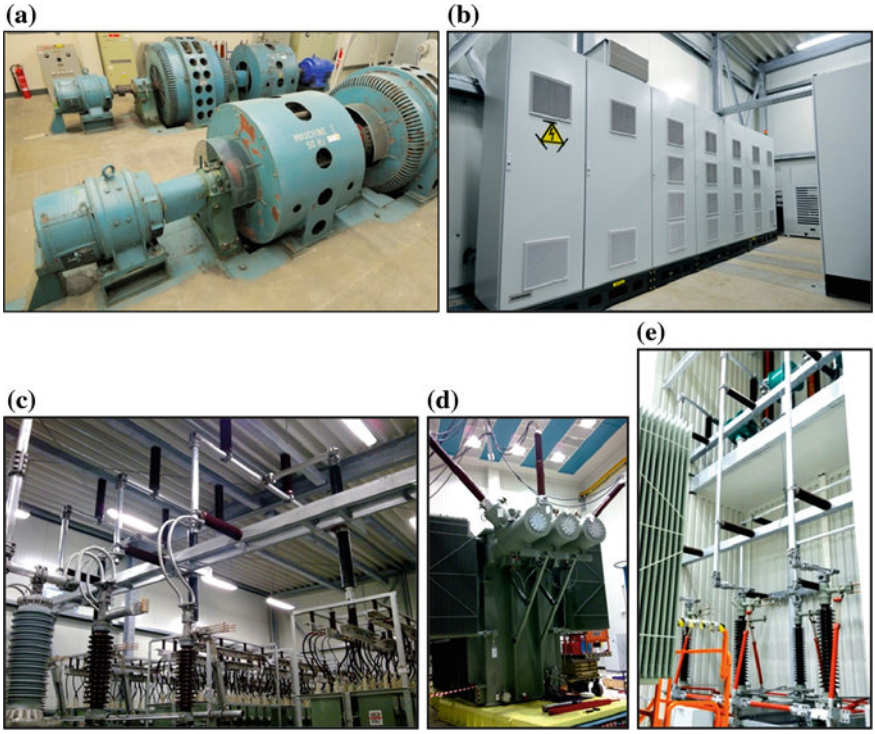

Fig. 3.37 Components of a circuit for induced voltage testing (Courtesy of Siemens Transformers Dresden). **a** Motor-generator (*M/G*) set. **b** Static frequency converter (*SCF*). **c** Top of matching transformer and capacitor bank. **d** and **e** Transformer under test and medium-voltage (*MV*) filter

where T is the duration of a period. The two half waves should be symmetric within 2 %

$$|\Delta V| = \left| \frac{V_{\text{peak}+} - |V_{\text{peak}-}|}{V_{\text{peak}+}} \right| < 0.02 \tag{3.22}$$

The tolerance of the *test voltage frequency* is 45–65 Hz according to IEC 60060-1: 2010.

Note This range is simply related to the "European" frequency of 50 − 5 Hz and the "American" frequency of 60 + 5 Hz. It is assumed that within the range 45–65 Hz, the influence of frequency on the breakdown process can be neglected for all types of insulations. Some IEC apparatus standards define tolerance ranges of frequency different from the previous. There are no physical investigations known which would deliver physical reasons for the selection of the frequency ranges.

Table 3.3 Comparison of motor-generator sets (M/G) and static frequency converters (SFC) without additional compensation elements

Characteristic	M/G	SFC
General characteristic	Set of electric machines with special parameters	Power electronic modules that can be combined, replaced or added
Max. available active power (MW)	5	6
Max. available inductive power (MVA)	30[a]	12[a]
Max. available capacitive power	This load has to be avoided by additional reactors	10 MVA
Frequency values or range	Usually only two fixed frequencies, e.g. 50 and 150 Hz	Continuously adjustable, e.g. 40–200 Hz
Power electronic application	For control of the driving motor	For the whole converter
PD noise suppression necessary	Yes	Yes
PD characteristics described by basic noise level with optimum circuit harmonics (THD)	<30 pC is usually reached Standard value <5 % fulfilled	<10 pC can be reached Standard value <5 % fulfilled
Dynamic behaviour	Limited, because determined by the rotating machines	Excellent, because determined by short reaction of power electronics
Self-excitation	May happen, to avoid it adjustment of reactors at lower voltage necessary	Cannot happen
Weight and size	Large and heavy, M/G set requires foundations	Relatively lightweight and compact
Principle design, upgrade, repair	Conventional structure, Upgrade of power is impossible	Modular design, upgrade of power or repair by additional or exchange of modules
Application	Traditionally for stationary application in factory testing	Application for both, factory and on-site testing
Availability	Difficult to get these special machines on the market	With further development of power electronics more and more easy to get it.
Conclusion	Traditional product with limited future for HV test application.	With future development of power electronics unlimited application for HV tests can be assumed.

[a] The range of inductive power can be extended by a capacitor bank

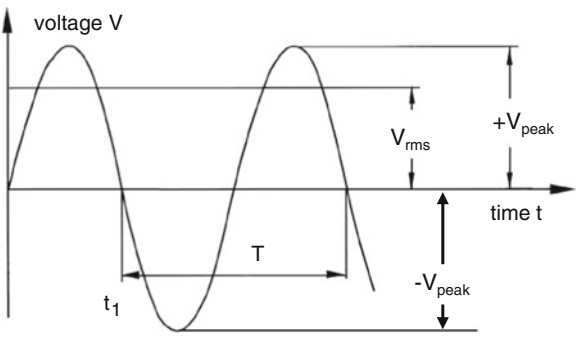

Fig. 3.38 Parameters of AC test voltages

For the deviation of the test voltage wave shape, IEC 60060-1: 2010 defines the *peak factor* as the relation between the peak and the rms value, which should be equal to $\sqrt{2}$ within ±5 %, this means

$$1.344 \leq \left| \frac{V_{\text{peak}}}{V_{\text{rms}}} \right| \leq 1.485.$$

This definition is only related to the peak voltage value, it does not consider the wave shape of the test voltage as a whole. This might be sufficient to withstand or breakdown tests, but PD are influenced by other instants of the test voltage, too. For such applications, the *total harmonic distortion (THD)* considers the peak values $V_{n\text{peak}}$ of the superimposed *harmonics* on the basic frequency (peak value $V_{1\text{peak}}$):

$$\text{THD} = \frac{1}{V_{1\text{peak}}} \sqrt{\sum_{n=2}^{m} V_{n\text{peak}}^2}. \tag{3.23}$$

The IEC Technical Committee 42 had discussed to introduce an acceptable limit of 5 % of the THD, but did not decide for its binding introduction with the last revision of IEC 60060-1 in 2010. One reason for that decision is that peak factor and THD are not proportional to each other. Table 3.4 (Engelmann 2007) shows an example: The voltage of a cascade transformer of a rated voltage $V_m = 1{,}200$ kV was evaluated at very low output voltages and compared with a 5 % limit of deviation of the peak factor, respectively, the THD. Whereas the output voltage of 2.8 % related to V_m shows strong harmonics and both, peak factor and THD are too high to be accepted as an AC test voltage. The little voltage increase by 3 % causes an improvement in the wave shape and acceptance by the peak factor, but none by the THD. The 24.1 % output voltage shows a better sine wave and acceptance by both criteria.

Note The content of harmonics depends on all elements of the HVAC test circuit and consequently also from the position of the regulator. Some harmonics that come from the power supply might be amplified by resonances of certain parts of the test circuit. For very low positions of the regulator, a high content of harmonics is typical. Therefore, a peak

Table 3.4 Deviations from sinusoidal wave shape (Measurement on a 1,200 kV cascade transformer by Engelmann 2008)

Voltage shape Output voltage $V_{peak}/V_T \cdot 100$ % Parameter	2.8% 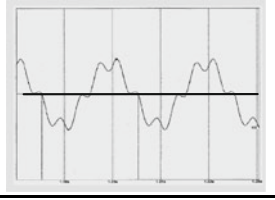	3.0% 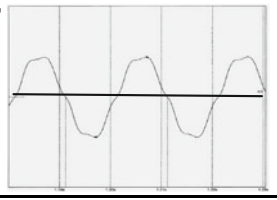	24% 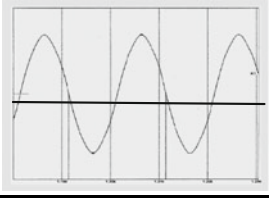
V_{peak}/kV	48.4	51.6	410
$V_t = V_{peak}/\sqrt{2}$/kV	32.2	36.5	290
V_{rms}/kV	30.8	37.4	287
$F = V_{peak}/V_{rms}$	1.571	1.380	1.413
Comparison: Peak factor			
$1.344 \leq F \leq 1.485$	Rejected	Accepted	Accepted
THD (%)	25	7	2.5
Comparison THD $\leq$ 5 %	Rejected	Rejected	Accepted

factor (or a THD) within the mentioned limits of 5 % is usually only specified for output voltages $V_t > 10$ % of the rated voltage of an HVAC test system. When the HVAC test system shall be applied at lower test voltages, the wave shape has to be checked. Usually, it is sufficient to consider in Eq. 3.23 the harmonics of the numbers $n = 3, 5, 7$ and 9.

A partial discharge that causes a heavy current pulse may cause a drop ΔV of the test voltage for few periods. IEC 60060-1: 2010 allows $\Delta V/V_t < 20$ %. The standard did not specify the duration of that *voltage drop*. There is also no physical background for the value 20 % [Compare the voltage drop for DC voltage $\Delta V < 10$ % (Sect. 6.2)!]. The specified voltage drop should be understood as step in the right direction. A more detailed consideration of that is expected with the next revision of IEC 60060-1.

Last but not least, the *tolerance* of the test voltage value must be mentioned. For a test duration T_t up to one minute (1 min), the tolerance is ±1 %. For $T_t > 1$ min, it is ±3 %. The wider range for longer test durations is necessary because larger changes of the supply voltage are expected at longer test durations.

Note The tolerances mean if a withstand test is performed, e.g. at $V_t = 500$ kV for $T_t = 1$ min, the measured and displayed voltage should remain within 495–505 kV. If the test duration is 1 h, the test voltage should be within 485–515 kV. When one considers an accepted *uncertainty of the voltage measurement* (Sect. 2.3.4) of 3 % additionally, the true, but unknown real stress during the 1 h test may lay approximately between 470 and 530 kV.

3.2.2 Test Systems for Multi-purpose Application

The selection of test systems is strongly dependent upon their use. HVAC test systems for multi-purpose application are for HV research work, for training in HV engineering, for calibration of measuring systems or for development of HV insulations testing model insulations. Whereas, e.g., the HVAC test systems for routine testing of a certain group of products are selected according to the test parameters, for this special-purpose application, systems for multi-purpose application require detailed analyses of the later application. Usually, they are applied for dry tests on air insulations, tests on model insulation of gaseous, liquid or solid dielectrics. The objects have to be stressed up to few hundred kilovolts, in rare cases up to 1,000 kV. Often a test current below 0.5 A is sufficient, but a quite sensitive PD measurement is mandatory today.

Under the mentioned conditions, HV test transformers (or transformer cascades) of rated voltage $V_m = 30$–1,000 kV and rated current $I_m = 0.2$–0.5 A (in rare cases up to $I_m = 1$ A) are the ideal HV generators for multi-purpose test systems. Especially, cylinder-type test transformers are well suited. Their duty cycle should be some hours, only for long-term tests continuous operation is required. The control system should enable both, manual and computer-aided testing.

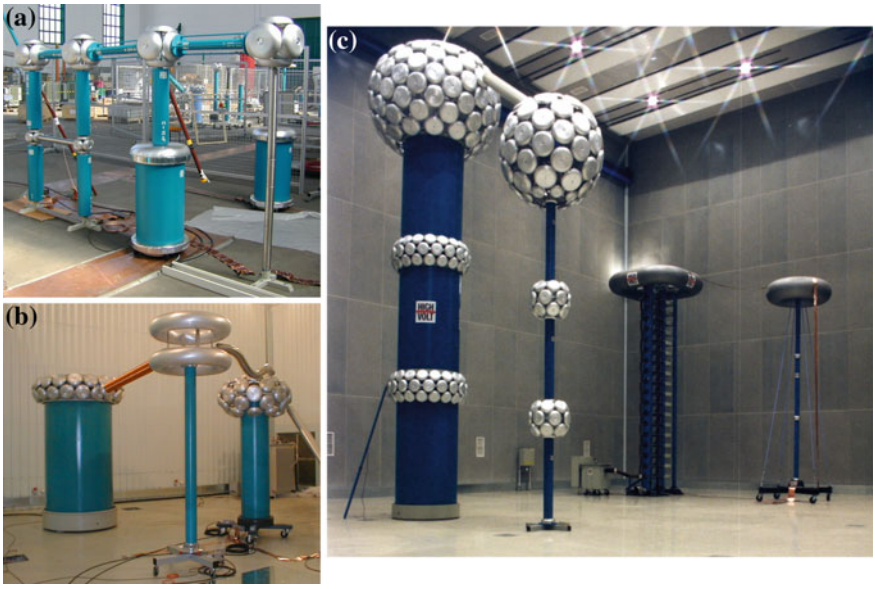

Fig. 3.39 Test transformers for multi-purpose application. **a** AC test circuit of a modular system. **b** Test system with a 350 kV cylinder-type transformer. **c** 1,000 kV test system with cylinder-type transformers (Courtesy of BTU Cottbus)

The HV circuit should be completed by a voltage measuring system based on a capacitive voltage divider with a peak voltmeter or—even better—with a transient recorder (IEC 61083-3 and -4, Draft 2011) for the measurement of all parameters mentioned above (Sect. 3.2.1). Furthermore, a PD measuring system, often also measuring systems for dielectric parameters should be available.

For rated voltages up to 200 kV and low currents, modular HV test systems can be recommended, for voltages up to 500 kV, single cylinder-type transformers and for higher voltages, cascade transformers should be applied (Fig. 3.39).

3.2.3 AC Resonant Test Systems (ACRL; ACRF) for Capacitive Test Objects

The capacitive load of an HVAC test system can cover a very wide range, from few 100 pF for the voltage divider and no-load conditions up to some 10 μF for submarine cables or capacitors. The limit of application between multi-purpose test systems based on test transformers and resonant test systems is not sharp, but should be characterized by the available current. Using the relation between total load capacitance C, test voltage V_t and test current I_t

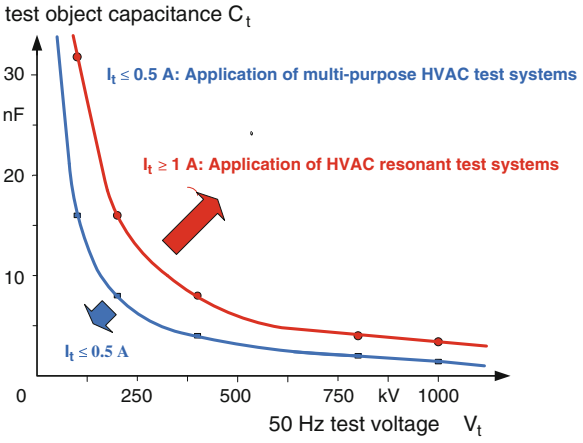

Fig. 3.40 Testable capacitive load depending on test voltage and rated current of the HVAC test system (lower limit for resonant test systems application)

$$I_t = \omega C \cdot V_t \leq 1 \text{ A} \tag{3.24}$$

of a multi-purpose HVAC test system, one gets a limiting curve for the testable capacitance

$$C = \frac{I_t}{\omega V_t}. \tag{3.25}$$

Figure 3.40 shows this relationship. For total load capacitances C above the curve of 1 A (depending on the situation possibly 0.5 A), the application of HVAC resonant test systems is better suited than that of a transformer-based system. One has to consider that the total capacitance includes in addition to the test object also the voltage divider, a coupling capacitor and—for resonant circuits—a capacitive basic load.

Typical test objects in the range up to few 10 nF are components or complete bays of gas-insulated substations (GIS), power and instrument transformers, bushings and cable samples. In an HVAC routine test, a complete cable drum may have a capacitance of some 100 nF.

In case of *GIS testing*, the load of the test object can easily be estimated from the length of the GIS tubes and the specific capacitance $C_t \approx 60$ pF/m for a single-phase bus bar. Often, the HVAC test system is connected to a test bus, which can be arranged in the production hall (Fig. 3.41). The bus has several connection points for the GIS to be tested. Only one of the connection points is connected to the HVAC test system for a test. The others are separated and grounded, e.g. at a second, a GIS tested before is disassembled and at a third, a GIS is prepared for the next test. This solution does not require any separate test field, because the test bus and the test object have metal enclosures and are grounded. But the test bus increases the total load capacitance and the required test current.

When the *applied voltage test of a power transformer* is performed, the transformer acts as a capacitance in an approximate range of $C_t \approx$ 4–30 nF, in

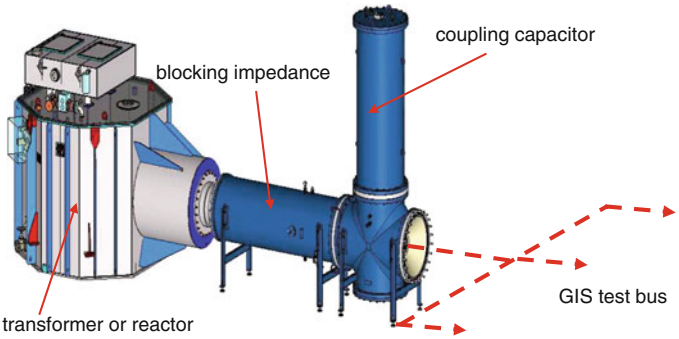

Fig. 3.41 AC test system for GIS testing with test bus

Fig. 3.42 ACRL test system during applied voltage test of a power transformer

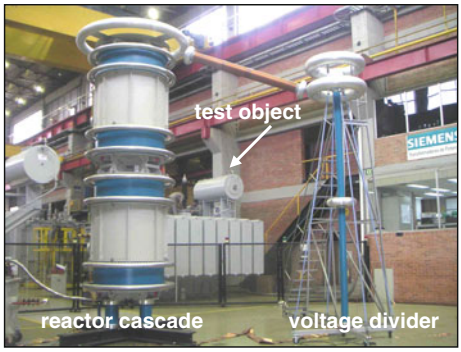

very rare cases higher. Usually, cylinder-type resonant reactors are applied (Fig. 3.42). According to IEC 60076-3, the application of a fixed frequency of 50 or 60 Hz is not mandatory, moreover only a test frequency $f_t > 40$ Hz is required for the applied voltage test. This enables not only the application of ACRL test systems, but also of frequency-tuned ACRF systems. *ACRF test systems* are very economic solutions for that application.

The testing of power cables is the traditional case for the application of resonant circuits (Fig. 3.43). The relevant standards for liquid impregnated and extruded cables require a fixed test frequency of 50 or 60 Hz for the AC voltage withstand test and the PD measurement. Therefore, ACRL test systems are applied for land cables that are manufactured with lengths up to 1000 m per drum, for medium-voltage cables even longer. The specific capacitance—depending on the cable design (relation between conductor and cable shield) and the insulating material—is usually within 0.15 and 0.4 nF/m. The connection between the cable to be tested and the test system must be realized by a test *termination*. If a *water termination* is used for that application (Fig. 3.43), one gets a resistive load component causing a reduction in the quality factor (Eq. 3.11). It has to be checked that the test system can sufficiently operate for short-cable samples connected with water terminations.

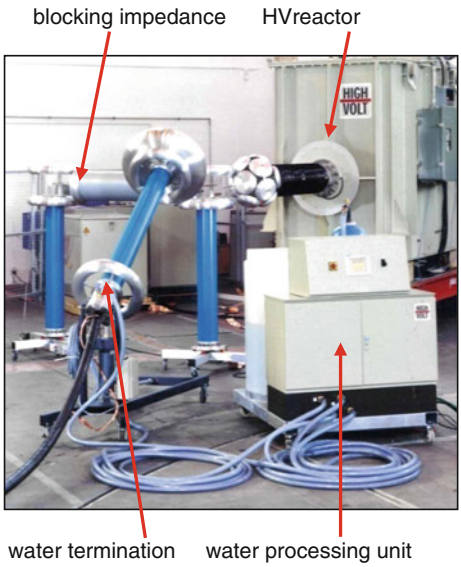

Fig. 3.43 ACRL test system for cable testing with controlled water termination

Cables require different HVAC tests, Table 3.5 mentions, e.g., those for EHV cables of 220–500 kV: HVAC test voltage is required for the voltage withstand tests, the partial discharge tests, the heating cycle test in combination with the high-current heating (Naderian et al. 2011), the LI and the SI voltage test with an HVAC repetition after the impulse voltage test. Especially, for heat cycle and pre-qualification tests (Bolza et al. 2002), HVAC test systems of high reliability are required. Therefore, test transformers have been applied, but now also resonant test systems with tuneable inductance and even more with variable frequency are applied for these tests.

Nowadays, *submarine cables* up to many ten kilometres length must be tested in factory. The capacitive load may reach more than 10 μF, and an ACRL test system becomes very huge and expensive. The way out is an ACRF test system (Fig. 3.44). Up to a required test current of the order of few 10 A, ACRL test systems can be realized, but for higher currents, only ACRF test systems are recommended, also by the latest IEC draft on HVAC submarine cables (Karlstrand 2011). Figure 3.45 shows the rotating table for submarine cables and the ACRF test systems in a factory as well as the laying ship with its cable drums.

Capacitors with very high capacitances are also tested with resonant circuits. In case of the so-called cold duty test on series capacitors (IEC 60143-1: 2004), an additional over-voltage period (Fig. 3.46) requires a dynamic change of the test voltage within less than 10 cycles. For the better control of the test voltage, this test is performed with a parallel resonant circuit. This test voltage must be recorded using an adapted digital recorder (Draft IEC 61083-3: 2012).

ACRF test systems may also be optimum for special applications as shown in Fig. 3.47. Each spacer insulator for GIS is carefully PD tested after its production.

Table 3.5 Test voltages for extruded cables 220–500 kV (IEC 62067: 2001)

Rated voltage, V_r	Highest voltage for equipment, V_m	Conductor to ground voltage, V_0	AC withstand voltage test		AC PD test voltage,	AC Heat cycle test,	LI voltage test	AC voltage after LI	SI voltage test
			Voltage, V_t	Duration, T_t	1.5 V_0	2 V_0		2 V_0	
(kV)	(kV)	(kV)	(kV)	(min)	(kV)	(kV)	(kV)	(kV)	(kV)
220–230	245	127	318	30	190	254	1,050	254	–
275–287	300	160	400	30	240	320	1,050	320	850
330–345	362	190	420	60	285	380	1,175	380	950
380–400	420	220	440	60	330	440	1,425	440	1,050
500	550	290	580	60	435	580	1,550	580	1,175

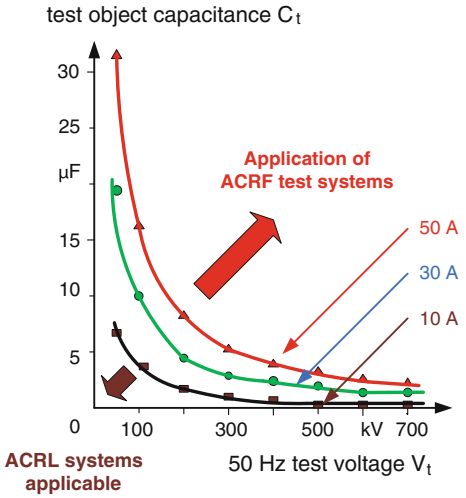

Fig. 3.44 Testable capacitive load on test voltage and rated current of the HVAC test system (limit between ACRL and ACRF test system application)

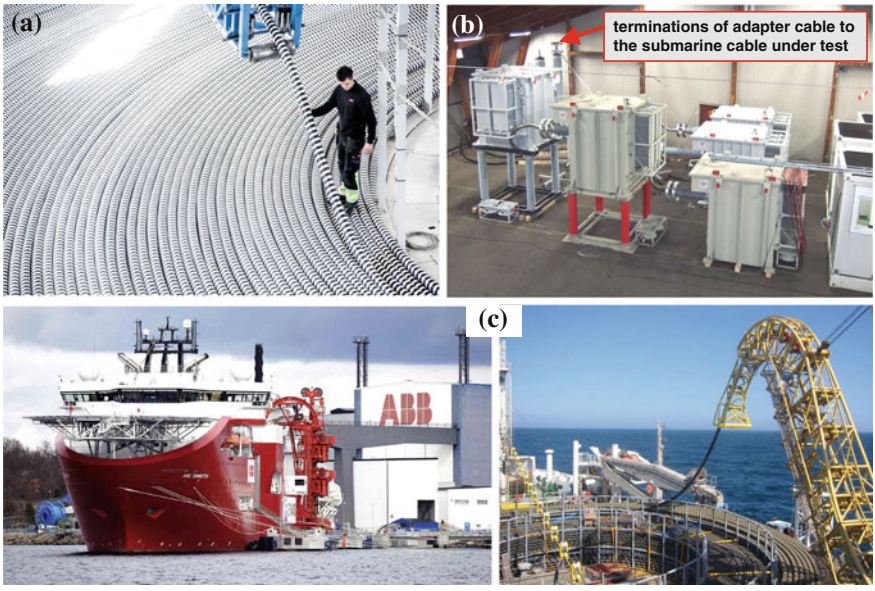

Fig. 3.45 ACRF test system for submarine cables (courtesy of ABB Karlskrona). **a** Rotating cable table. **b** ACRF test system of two reactors and cable terminations. **c** Laying ship with cable aboard

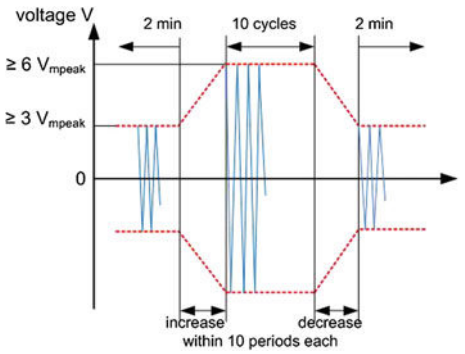

Fig. 3.46 Dynamic overload test for series capacitors (IEC 60143: 2004)

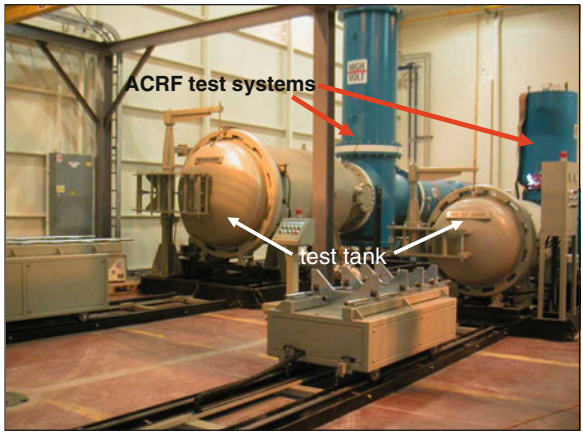

Fig. 3.47 Two ACRF test systems of 1,000 and 600 kV for routine testing of GIS spacers (courtesy of HYOSUNG Industries, Changwon)

This test is done at voltages up to 1,000 kV and requires a metal-enclosed test system in the production hall. Because all test objects are identical, the inductance can be designed to guarantee a frequency range within 45–65 Hz. For that application, the ACRF test system is by far the most economic one.

3.2.4 HVAC Test Systems for Resistive Test Objects

A resistive or active load of an HVAC test system requires an *active test power* which can only be supplied by a *test transformer*. In this sense, also the above mentioned, so-called parallel resonant circuit is a transformer circuit. A mainly active characteristic of a test object is caused by one or by a combination of the following influences:

- a volume resistance of the tested insulation that is lower than the value of the capacitive impedance, e.g. a strongly aged oil–paper insulation;

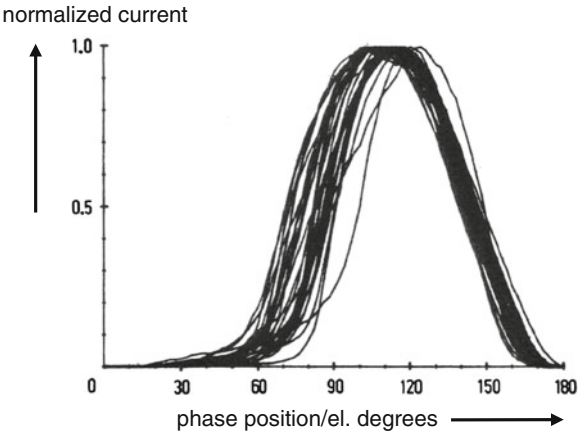

Fig. 3.48 Normalized current pulses in pollution tests depending on the phase position

- a high surface conductivity of the insulator under test, e.g. by wet and/or polluted surfaces due to *rain*, *pollution* and *humidity*;
- heavy pre-discharges at test objects in air, e.g. caused by leader discharges at very high AC voltages or by pre-arcs in pollution tests;
- continuous, quasi-stationary *corona discharges* on conductors, e.g. on overhead test lines or corona tests. The active power demand of the test object may be a quasi-stationary *leakage current*—e.g. for high volume resistance or for corona discharges. But for many other cases, the current impulse connected with a strong discharge requires a very fast active power supply by the test transformer. If the voltage source cannot supply the current fast enough, the voltage would drop down. This *voltage drop* can delay or even interrupt the development of pre-discharges to a breakdown, and this may lead to wrong, source-dependent test results. Up to a certain degree, a too weak HVAC voltage source can be "supported" by a capacitor in parallel to the test object (Reichel 1977).

3.2.4.1 HVAC Test Systems for Artificial Pollution Tests

On a polluted insulator surface, the leakage current pulses have a typical shape as shown in Fig. 3.48 (Verma and Petrusch 1981). Many measured impulses are normalized to their peak currents and displayed versus their phase position. The currents start to increase at about 50° (el.), reach their peak at about 110° (el.) and extinguish at about 170° (el.). The current peak may reach values up to few Amperes (Rizk and Bourdage 1985). It causes a *voltage drop* over the internal impedances of the HV test system. Figure 3.49 shows a voltage drop of 20 % at a peak current of 1.8 A. Such a voltage drop influences the measuring result remarkably, but in the relevant IEC Standard 60507 (1991), no measurement of the current or of the voltage drop is required. Several publications consider a voltage drop up to 10 % as acceptable.

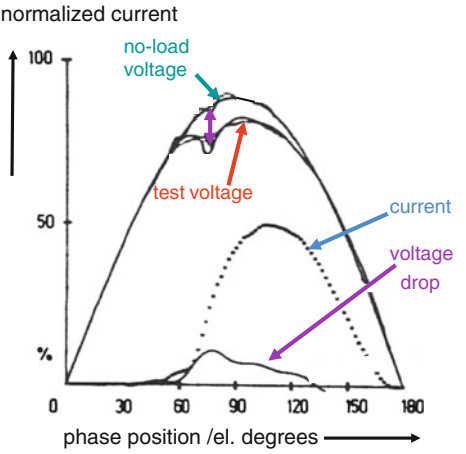

Fig. 3.49 Measured no-load voltage, leakage current, test voltage and voltage drop

In pollution testing (see Sect. 2.1.4), instead of direct measurement of the voltage drop, the rather old IEC Standards 60507 (1991) and the old IEC 60-1 (1989) define a set of requirements to the HVAC test system.

Note The actual IEC 60060-1 (2010) does not contain any requirement for pollution testing and contains only a hint to the latest edition of IEC 60507 that is at the moment the version of 1991. But consider that the voltage drop of 10 % does not coincide with a voltage drop of 20 % mentioned in IEC 60060-1 (2010). Pollution tests require a remarkably lower value.

These requirements are based on the voltage drop via the internal impedance of the HVAC voltage source that can be expressed by the short-circuit current. A high internal impedance means a low short-circuit current (see Sect. 3.1.1.1). To avoid a critical voltage drop, the *short-circuit current* must have a minimum value that varies with the test conditions. The test conditions can be expressed by the *specific creepage distance* (in mm/kV) of the insulator, which characterizes the type and shape of the insulator. An insulator with a certain specific creepage distance is selected according to the *pollution class*. Depending on the specific creeping distance, Fig. 3.50 shows the short-circuit current $I_{sc\min}$ in minimum required by IEC60507 (1991), to avoid the influence of the test system as the result of a pollution test.

A short-circuit current higher than $I_{sc\min}$ is necessary, but not sufficient requirement for the HVAC test system that shall comply also with

$$\text{a resistance/reactance ratio:} \quad \frac{R}{X} \geq 0.1 \tag{3.26}$$

and, according to Fig. 3.2 with

$$X = \left(\frac{1 - \omega^2 LC}{\omega C}\right),$$

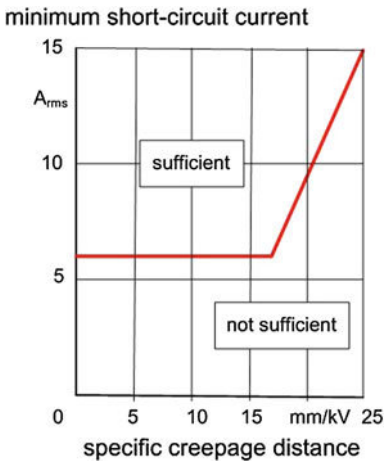

Fig. 3.50 Required short-circuit current of the HVAC test system depending on the specific creeping distance (IEC 60507: 1991)

a capacitive current/short circuit current ratio: $0.001 < (I_c/I_{sc}) < 0.1$. (3.27)

The value of $I_{sc} = 6$ A is considered as an absolute minimum value for the short-circuit current of an HVAC test system for pollution testing. But for higher specific creeping distances, higher values are necessary according to Fig. 3.50. When the test system does not reach the necessary short-circuit current I_{sc}, IEC 60507 allows to measure the highest leakage current pulse $I_{h\max}$. If the ratio between I_{sc} (as a rms value) and $I_{h\max}$ (as a peak value) becomes

$$\frac{I_{sc}}{I_{h\max}} \geq 11, \tag{3.28}$$

the test result can be considered as independent from the test system.

Under the assumption of a uniform pollution of an insulator chain, the flashover characteristic can be determined on one insulator of the chain. This is based on the assumption that the voltage distribution along the chain is a resistive one. The withstand characteristic of the *insulator chain* is determined by multiplying the parameters (voltage values) by the number of insulators in the chain. In case of parallel insulators and known distribution function, the statistical enlargement rule (Hauschild and Mosch 1992) delivers the withstand parameters. The described principle of testing of only single insulators enables that the used powerful HVAC test systems (recommended rated current $I_m = 3$–10 A, recommended short-circuit current $I_{sc} > 20$ A) remain limited to rated voltages below 500 kV. Therefore, also the *pollution test chambers* and the other equipment for pollution testing are usually limited in size.

Salt fog test: In the withstand test procedure (IEC 60507: 1991) for the salt fog test (see Sect. 2.1.4), the insulator is subjected to a preconditioning process with a series of progressive voltage tests at the reference salinity of the water sprayed as a fog. Then, for the withstand test itself, the insulator is cleaned, pollution conditions are adjusted (specified salinity) and the test at the specified withstand voltage level

is performed for the duration of 1 h. Repetitions of the test might be specified. Before each repetition, the insulator must be carefully cleaned. The insulator has passed the test, if no flashover occurs during all withstand procedures.

Solid layer test: In case of the solid layer method (IEC 600507: 1991), the withstand test procedure can be performed when the test voltage is applied after the wetting of the insulator under test has started (procedure A), or the test voltage is applied before the wetting starts (procedure B). For procedure A and specified pollution layer conditions, the voltage is applied for 15 min (or until a flashover occurs). For procedure B, the test voltage is maintained for 100 min (or until a flashover occurs). Both procedures must be repeated three times. The insulator complies with the specification if no flashover occurs during three repetitions. If only one flashover occurs and a fourth repetition remains without flashover, the insulator has also passed the test.

The IEC 60507: 1991 is related to ceramic insulators. At present, there is no standardized method for pollution testing of *composite and other polymeric insulators*. Therefore, the methods described above are often applied also for polymeric insulators. Gutman and Dernfalk (2010) present a modified solid layer method for composite and polymeric insulators. Dong et al. (2012) found relationships between the shape of composite insulators and the pollution method. These tests might be completed by tests related to the *hydrophobicity* (Bärsch et al. 1999; Schmuck et al. 2010). It can be assumed that HVAC test systems suited for pollution testing of ceramic insulators fulfil the requirements for pollution tests on polymeric insulators, too.

It can be expected for the future that during pollution tests both, the test voltage and the leakage current, will be measured and that a certain voltage drop, e.g. <10 %, becomes a criterion for an acceptable test. Even now, it is recommended that these most important parameters are recorded during a pollution test using suited digital recorders.

3.2.4.2 HVAC Test Systems for Artificial Rain Tests

In artificial rain (or wet) tests (see Sect. 2.1.3), heavy streamer and even leader discharges connected with remarkable current pulses may occur. The peak currents do not reach a magnitude as the leakage current pulses of pollution tests, but multi-purpose test systems cannot guarantee that the related voltage drop remains within acceptable limits (<10 %) and cannot influence the discharge processes. Therefore, more powerful HVAC test systems are applied for wet tests. Usually, an HVAC test system based on a transformer with a rated current of $I_m = 1$ A and a short-circuit current $I_{sc} > 10$ A (short-circuit impedance $v_k < 15$ %) is sufficient. A capacitor of about $C_p \approx$ 1–3 nF in parallel to the test object is recommended additionally (e.g. related voltage divider).

When series resonant test systems shall be applied for wet tests, a parallel capacitor has to be applied with a capacitance even higher than mentioned above. In any case, the voltage should be recorded by a digital recorder to ensure that any

voltage drop does not exceed 10 %. The supervision of the voltage seems to be helpful in wet tests, too, and one can hope that for wet tests an upper limit of the voltage drop should be agreed in a future standard.

3.2.5 HVAC Test Systems for Inductive Test Objects: Transformer Testing

Power and distribution transformers, instrument transformers and compensation reactors have quite complicated insulation systems and are for certain frequencies of the AC test voltage an inductive load for the voltage source.

As an example, power transformers shall be considered: Table 3.6 gives an overlook on the main HV tests on power transformers in the sequence of their application. The tests with AC voltage follow the tests with impulse voltage. This means, the AC tests, considered in the following, shall supply the final statement about the condition of the insulation.

In the AC "*applied voltage test*", the good condition of the insulation between the short-circuited HV line terminals and the grounded low-voltage side (winding, magnetic core, tank, etc.) shall be verified with an external HVAC source. The transformer is a capacitive test object and can be tested with a resonant circuit (see Sect. 3.2.3; Fig. 3.42). Because the relevant standard IEC 60076-3 does not require a fixed frequency, but allows a frequency range $f > 40$ Hz, frequency-tuned resonant test systems are very economic for applied voltage tests.

For AC induced voltage tests on the insulation of the line terminals and the connected windings, the transformer under test generates the HVAC test voltage by itself and must be excited with an appropriate voltage on its low-voltage side as described in detail in Sect. 3.1.3. This exciting voltage should be a three-phase voltage for three-phase transformers. Because of the saturation of the magnetic core, the AC test voltage requires a frequency of more than twice of the operational frequency ($f_t \geq 2 \cdot f_m$). The voltage is traditionally generated by a *motor-generator set*, but nowadays more and more by *static frequency converters*. It is stepped up to the necessary excitation voltage by a *step-up transformer*. The test system for exciting the power transformer is also used for the *heat run tests* and for the measurement of *no-load and short-circuit losses* at their operational frequency of 50 or 60 Hz. In those tests, the transformer is always an inductive load that needs always a well-adapted compensation. This is realized by a switchable capacitor bank on the low-voltage side of the transformer under test, for fine tuning sometimes additionally on the primary side of the step-up transformer (Figs. 3.36, 3.37c).

According to IEC 60076-3, power transformers shall be applied to an "*induced voltage withstand test (IVW)*" and after that to an "*induced voltage partial discharge measurement (IVPD)*" in both cases, at the same test frequency f_t. The duration of the IVW test depends on the relation between the rated frequency f_r of the transformer under test and the test frequency f_t:

Table 3.6 Main tests on power transformers for different rated voltages according to IEC 60076-3

Rated voltage, U_m	≤72.5 kV	72.5 kV ≤ U_m ≤ 170 kV	≥170 kV
Full lightning impulse voltage (LI)	Type test	Routine test	Included in LIC test
Chopped lightning impulse (LIC)	Special test	Special test	Routine test
Switching impulse test (SI)	Not applicable	Special test	Routine test
Applied voltage test (AC-AV)	Routine test	Routine test	Routine test
Induced voltage withstand test [AC-(IVW)]	Routine test	Routine test	Replaced by SI and AC-IVPD tests
Induced voltage test with PD measurement (IVPD)	Special test	Special or routine test	Routine test

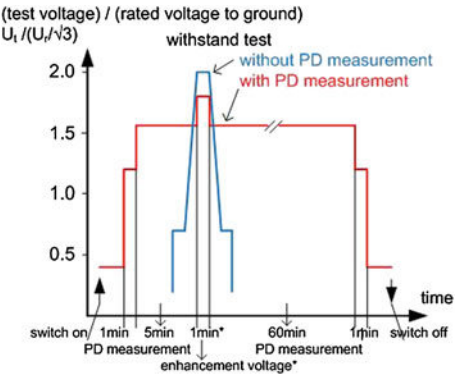

Fig. 3.51 Test cycles of an induced voltage test without (*blue*) and with PD measurement (*red*) on power transformers (Draft IEC 60076-3: 2011)

$$t_t/s = 120 \cdot \frac{f_r}{f_t} \geq 15. \tag{3.29}$$

The IVW test shall commence at a voltage ≤0.33U_t, and the voltage shall be raised to the test voltage U_t and there maintained for the frequency-dependent test duration t_t. After that time, the voltage shall be reduced to ≤0.33 U_t before switching off (Fig. 3.51, blue).

The IVPD test shall verify that the transformer is free of harmful PD. In the IVPD test, the voltage follows a step procedure (Fig. 3.51, red) with the highest (enhancement) level. The duration of the enhancement level is identical to the IVW test, only for power transformers with $U_m > 800$ kV, this duration is five times longer. At the three voltage levels before the enhancement level, a PD measurement is performed for a time long enough to have a stable result. At the enhancement level, no PD measurement is required in the standard, but should also be performed. Immediately after that, the PD level shall be recorded for 60 min on the specified PD measurement level. Then, the voltage is reduced to the same level

as in the voltage increase and a PD measurement is made as before. The PD inception and extinction levels shall be determined. The IVPD test is passed, if no breakdown occurs during the cycle, none of the PD level recorded during the 60 min test exceeds 250 pC, raises by not more than 50 pC or does not show any rising trend and at the next lower level not more than 100 pC. The specified Picocoulombs may be modified according to contracts. For more details, see IEC 60076-3.

3.3 Procedures and Evaluation of HVAC Tests

The general statistical basis of this Sect. 3.3 has been described in Sect. 2.4 and more details are given by Hauschild and Mosch (1992), see also Yakov (1991), Carrara and Hauschild (1990) and Annex A of IEC 60060-1 (2010). In the following, procedures are considered that are relevant for tests with high alternating voltages.

3.3.1 HVAC Tests for Research and Development

Before a test starts, its clear statistical aim must be defined and transferred into an appropriate test procedure with well-defined parameters. This can be done based on similar earlier experiments, literature or own pretests and includes the clarification whether a complete *cumulative frequency function* (as an estimation of the *distribution function*) or only a certain *quantile* (for the estimation of a withstand voltage or an *assured breakdown voltage*) should be evaluated.

Sample size: The width of the *confidence region* of the estimate (quantile, distribution function) depends on the dispersion of the discharge process (expressed by its standard deviation) and the sample size (number of single tests). The higher the confidence requirements, the larger is the necessary sample size. Figure 3.52 shows the width of the confidence region (or interval) of the mean value $(V_{50\text{upper}} - V_{50\text{lower}})/V_{50}$ depending on the variance $v = s/V_{50}$ and of the number of single tests. With a variance of $v = 6$ % and $n = 10$ single tests, the confidence interval becomes 7 %. To reduce that to 3 %, one would require $n = 50$. The finally selected sample size should consider also the effort necessary for the test.

HVAC Test Procedures: The usual test procedure in an HVAC test is a *progressive stress test* (Fig. 2.26; Sect. 2.4.2). The voltage starts at an initial voltage V_0 and is continuously increased with a rate of rise $\mathrm{d}V_{\text{peak}}/\mathrm{d}t$ until a breakdown occurs. The value of the breakdown voltage is a first realization V_{b1}. Then, the voltage is rapidly reduced to V_0, after a break Δt_{p}, the next single test follows. In total, n single tests are performed. The rate of rise may influence the results (e.g. by surface or space charges), therefore it is recommended to clarify the

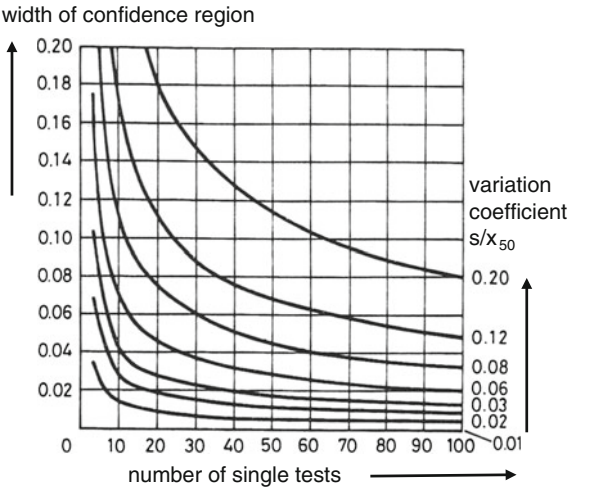

Fig. 3.52 Relative width of the confidence region depending on the variance of the measuring result and the sample size of the test (confidence level 95 %)

influence of the rate of rise on the measured breakdown voltages and to select a rate that enables independent results.

More efficient than a continuous voltage might be a stepwise rise (Fig. 2.26b). The initial voltage should be varied within limits lower than the step height to generate continuous breakdown voltages. Instead of the rate of voltage rise, the step height ΔV_s and the step duration Δt_s must be defined. This is better related to the procedures of withstand testing (see Sects. 2.4.6, 3.3.2), especially when the step duration is equal to the duration of a withstand test (see Sect. 3.3.2). Under the assumption of independence—that the previous steps do not influence the following steps—one can calculate from the result of this test [cumulative frequency function) the *performance function* of single stresses that is directly related to withstand testing (Hauschild and Mosch 1992)]. There are actual applications of this principle, e.g. described by Tsuboi et al. (2010a, b, c).

Check of independence: When the test has been performed with the preselected parameters and n random breakdown voltages are available, their statistical independence must be checked. By means of a simple graphical method, the breakdown voltages (V_{b1} to V_{bn}) are graphically presented in the order of their occurrence. A visual assessment delivers an impression of the independence: If the realizations fluctuate in a random manner about the mean value, then there is no objection against the assumption of independence (Fig. 2.28: Upper three SF_6 pressures). When there is a falling or raising tendency, dependence must be assumed (Fig. 2.28: Lower SF_6 pressure). Numerical *independence tests* are available and applied in related computer programs.

Approximation by a theoretical distribution function: Then the adaptation of the empirical cumulative frequency function by a theoretical distribution function is performed considering the correspondence between the physical model of the investigated breakdown process and the mathematical model of the applied distribution function, the good matching and the convenience of application

Table 3.7 Theoretical distribution functions recommended for the approximation of breakdown voltage data

Insulation and field	Air and gases		Liquids		Solids	
Distribution function	With PD	Without PD	With PD	Without PD	With PD	Without PD
Gauss (Eq. 2.48)	X		X		X	
Gumbel (Eq. 2.49)		X		X		
Weibull (Eq. 2.50)				X	X	X

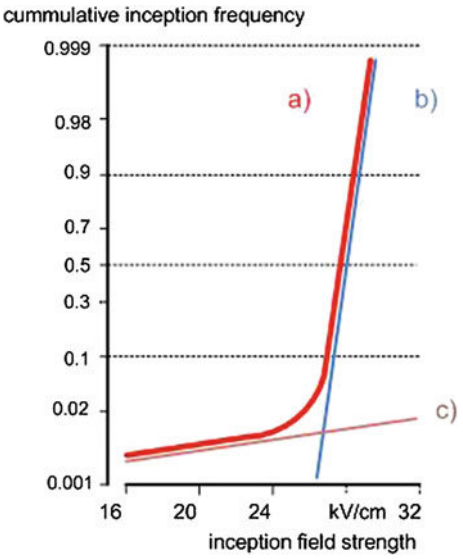

Fig. 3.53 Mixed distribution function of the breakdown voltage of a sphere-to-plane gap with a rough sphere surface (radius $r = 75$ cm; gap $d = 50$ cm)

(Hauschild and Mosch 1992). Table 3.7 gives an overview that theoretical distribution functions could be recommended for the approximation of breakdown test data: "Without PD" means that the insulation is slightly non-uniform, has no defects and the breakdown occurs immediately without stable PD. "With PD" means the insulation is strongly non-uniform or slightly non-uniform with defects and stable PD grow to the breakdown.

Note Not all experimental results can be approximated by one theoretical distribution function. Quite often so-called *mixed distributions* appear, e.g. in a slightly non-uniform field with defects (Fig. 3.53): When the breakdown process finds a starting electron at a defect, the breakdown voltage is quite low and shows a large dispersion (flat curve c). If the breakdown voltage is higher, the dispersion is low (steep curve b). For a mixed distribution, it is often sufficient to look for an approximation of the lower part of the mixed distribution. For more details, see Hauschild and Mosch (1992).

The application of a computer program of the *maximum-likelihood method* (MLM) delivers the best estimations and is expressly recommended. The MLM software is commercially available, and the evaluation can perform

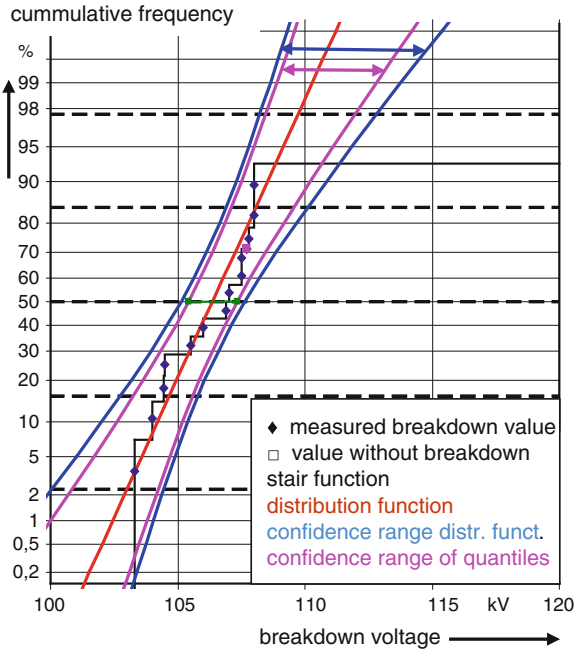

Fig. 3.54 Presentation of the results of a progressive stress test evaluated by the maximum-likelihood method and Gauss normal distribution function

approximations by different distribution functions. In addition to the parameter of the selected distribution function, it delivers also the confidence limits of the distribution itself and those of their quantiles (Fig. 3.54). Especially the lower confidence limits are important for the determination of design criteria of insulation, because they deliver "data on the save side".

Multi-level method: When an AC voltage of a certain height V and a certain duration Δt (e.g. 1 min) is defined as single stress, the multi-level method can be applied in a similar way as for impulse voltages. For details, see Sects. 2.4.3 and 7.3.1.1.

Lifetime tests: A certain number of samples of mainly solid insulation can be stressed at a constant voltage until the breakdown occurs. The random variable is the stressing time and the statistical evaluation is related to the breakdown time that can be well described by a *Weibull distribution* (Eq. 2.50a). If such tests are performed at different voltages, one can derive the lifetime characteristic (see Sect. 2.4.5) including its confidence limits using the MLM (Fig. 2.41). For each value of the breakdown time, one requires one single-test object (sample). Usually, a certain test time (e.g. 1,000 h) is pre-given in such lifetime tests. The statistical evaluation allows also the consideration of *censored data*, this means samples that did not break down within the pre-given test time (Speck et al. 2009). Their information is, e.g., that they withstood the test time without breakdown.

3.3.2 HVAC Quality Acceptance Tests and Diagnostic Tests

Usually acceptance tests shall verify the product quality—which consists of proper design, exact production of components and careful final assembling of the insulation of apparatus or systems—by withstand tests alone or withstand tests that include PD or dielectric measurement (*monitored withstand test*). In withstand tests, the products have to pass a certain procedure with the relevant test voltage values [(IEC 60071-1: 2006) and/or relevant apparatus standards] as, e.g., described in Sect. 2.4.6. If this is successfully done in type, routine and commissioning tests, the product can be handed over to the user for operation.

The classical withstand test procedure with continuously increasing voltages up to the test voltage value has been described in Sect. 2.4.6 and Fig. 2.42a. The test voltage value should be maintained on the test voltage level for a certain duration, usually of 1 min, quite often also of 1 h.

A monitored withstand test according to the step test procedure (Fig. 2.42b) delivers more information on the quality of the insulation than a simple withstand test. During the single steps and—for information—also during the withstand duration, PD—in special cases also the dissipation factor—shall be measured. Usually, the acceptable PD level is not specified for the withstand voltage level, but for a certain specified PD measuring level after the withstand test. This level might have a longer duration (up to 1 h) than the steps before the withstand test. In a quality acceptance test, the PD level must be lower than a specified value, but also the comparison of the PD magnitude on identical voltage levels before and after the withstand test shall be taken into consideration. Consequently, the acceptance test is successful if

- there is no breakdown during the whole test procedure, and
- the PD level at the PD measuring voltage does not exceed the specified limit and
- PD levels should not be significantly higher on voltage levels after the withstand test than on identical voltages before the withstand test.

The first two requirements are given in the relevant apparatus standards. The last one is usually not mentioned in apparatus standards. It is additionally recommended to demonstrate that preceding test voltage stresses have not amplified PD phenomena at defects neither indicating a remaining deterioration, nor exceeding the specified PD level. It should be mentioned that in some cases, the withstand test procedure and the PD measurement procedure are performed separately and not in one common cycle.

For *condition assessment* of aged insulation also withstand tests are performed offline with suited mobile HVAC test systems. The aim of a diagnostic test is to estimate the remaining lifetime by suited stresses and measurements for detecting defects. The test voltage values can be lower than for a quality assurance test, they are often in the order of 80 %. The selected measurements depend on the apparatus under test, the kind of its insulation and the experience of the test engineer. Very

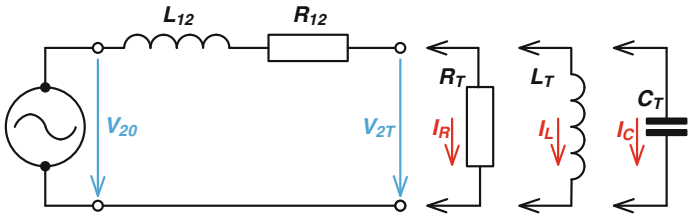

Fig. 3.55 Simplified equivalent circuit of a HV test transformer

often, any kind of PD measurement is most suited, because PD—as the breakdown—are weak point phenomena.

For a *diagnostic test*, the PD- or a tanδ-monitored step procedure is advisable, but it should be adapted to the expected condition of the insulation (age, load, over-voltage stresses, climatic conditions, etc., Pietsch et al. 2012) Therefore, the performed procedure (e.g. selection and duration of steps, selection of measurands) should be left to the experience of the test engineer. Especially, the duration of PD measurements must often be related to the actual observations. For the evaluation, not only one PD parameter—e.g. the measured PD charge—should be used, but the full set of available PD characteristics (see Chap. 4).

3.4 HVAC Test Voltage Measurement

To measure high alternating test voltages, originally sphere gaps have been utilized, see Sect. 2.3.5. Even if these enable a direct measurement of high voltages, the procedure is extremely time-consuming. Another drawback is that the actual breakdown voltage of a test object cannot be determined by such a discontinuous method due to the fact that a simultaneous breakdown of both the test object and the sphere gap is impossible. To overcome these crucial problems, one option would be to deduce a measurand from the primary voltage V_1 of the test transformer if multiplied with the turn ratio. This was a common practice at the beginning of the 1900s when HVAC voltages became increasingly of importance for technical application. Such a simple approach, however, may cause severe measuring errors due to the inevitable voltage reduction across the internal impedances of the test transformer, as can readily be shown based on the simplified equivalent circuit illustrated in Fig. 3.55.

Here, a virtual voltage source V_{20} is connected in series with the inductance L_{12} and the resistance R_{12} representing the effective series impedance transformed to the HV side. Under this condition, the secondary voltage without burden equals V_{20} that can thus be deduced from the primary voltage V_1 if multiplied by the turn ratio:

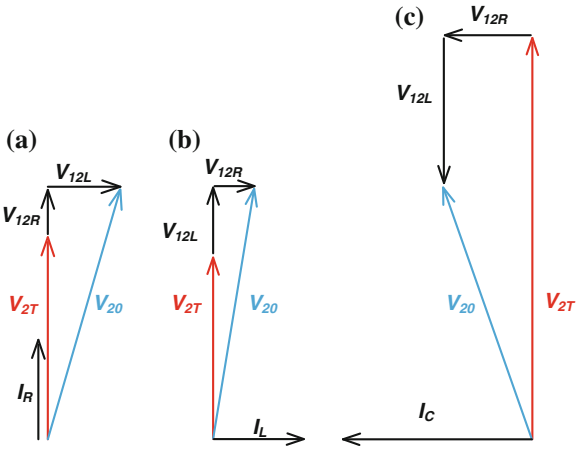

Fig. 3.56 Typical cursor diagrams deduced from the simplified equivalent circuit of a test transformer at various loads according to Fig. 3.55

$$V_{20} = V_1 \cdot \frac{w_2}{w_1}, \tag{3.30}$$

with w_1 and w_2—the turn numbers of the primary and secondary transformer coils, respectively, (see also Sect. 3.1.1.1). The cursor diagrams illustrated in Fig. 3.56 reveal that the actual test voltage V_{2T} appearing across the test object is strongly different from the source voltage V_{20} without burden and depends strongly on the kind of load, even at equal current magnitude.

Example Consider a test transformer having a turn ratio of $w_2/w_1 = 1{,}000/1$ excited at frequency $f_e = 50$ Hz, so that without burden an assumed primary voltage of $V_1 = 100$ V causes a secondary voltage of $V_{20} = 100$ kV. The internal inductance and resistance shall be assumed as $L_{12} = 1{,}000$ H and $R_{12} = 40$ kΩ, respectively. Moreover, each kind of test object connected to the transformer shall cause an equal current magnitude given by $I_R = I_L = I_C = 50$ mA. The voltages determined under this condition appearing across the terminals of the test object are listed in Table 3.8 which reveal, that at constant primary voltage $V_1 = 100$ V the output voltage V_{2T} decreases for both a resistive and an inductive load, but increases for a capacitive burden.

In this context, it should be emphasized that the ratio between secondary and primary voltage is not only affected by the magnitude and phase angle of the current but also by the higher harmonics due to non-linear hysteresis and core saturation effects. Therefore, it is not recommended to deduce the HVAC test voltage from the primary voltage, particularly if a low measuring uncertainty is desired as in the case of quality assurance tests.

Electrostatic voltmeters provide another option for continuous measurement of high alternating voltages, see Sect. 2.3.6. Such devices, however, can only be manufactured at reasonable expenditure for rated voltages up to approx. 100 kV. Thus, nowadays indirect methods are mostly applied where the high voltage is reduced to a magnitude conveniently measurable with classical low-voltage instruments. This procedure is a common practice since the 1930s (Raske 1937).

Table 3.8 Variation in the secondary voltage at different load and constant source voltage according to Fig. 3.55 ($V_{20} = 100$ kV)

Load	Resistive	Inductive	Capacitive
Test object	Polluted insulator	Instrument transformer	Power cable (length 10 m)
Value of circuit element	$R_T = 2$ MΩ	$L_T = 5350$ H	$C_T = 1.6$ nF
Test voltage generated	$V_{2T} \approx 97$ kV	$V_{2T} \approx 84$ kV	$V_{2T} = 110$ kV
Relative deviation (%)	−3	−16	+10

As illustrated in Fig. 3.57, systems applied for indirect high-voltage measurements comprise the following components:

- converting device (voltage divider and instrument transformer),
- transmission system (coaxial measuring cable and fibre optic link),
- measuring instrument (peak voltmeter and digital recorder).

3.4.1 Voltage Dividers

To reduce high alternating voltages down to an adequate magnitude, basically resistive, capacitive or even inductive elements could be utilized. However, inductive converting devices, such as instrument transformers, are only recommended for calibration purposes. This is because they are very expensive, particularly if intended for HVAC measurements above 500 kV. Thus, in HV test fields commonly only capacitive, resistive or even mixed voltage dividers are used, see Fig. 2.10. To avoid erroneous measurements, the top electrode and grading electrodes of the divider must be PD-free. Moreover, it has to be taken care that PD's are not ignited due to dust and pollution on the surface of the divider column, which could especially happen in case of high air humidity. To keep the load of the HV test equipment as low as possible, the current through the divider should be less than 10 mA that is equivalent to an impedance/voltage ratio of 1 MΩ/10 kV. This requirement can hardly be accomplished for resistive voltage dividers rated 100 kV and above due to the impact of earth capacitances on the divider ratio, as treated more in detail in Sect. 7.4. Thus, *capacitive dividers* provide the most convenient solution for measuring high alternating voltages. As individual HV capacitors cannot be designed at appropriate expenditure for voltages above 300 kV, the HV arm is commonly composed of stacked capacitors, as obvious from Fig. 3.58.

Considering the capacitive divider shown in Fig. 3.57, the high voltage V_1 could be deduced from the measurable low voltage V_2 by

$$V_1 = V_2 \cdot (1 + C_2/C_1) \approx V_2 \cdot C_2/C_1. \tag{3.31}$$

This simple relation, however, is not applicable in practice due to the impact of the inevitable *stray capacitances* between divider column and earth.

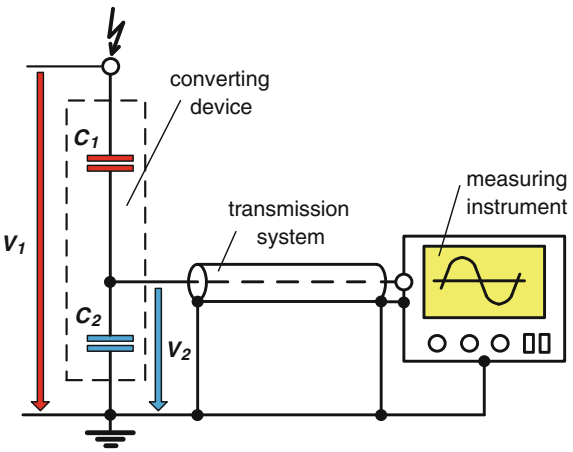

Fig. 3.57 Components of a system for indirect measurement of HVAC test voltages

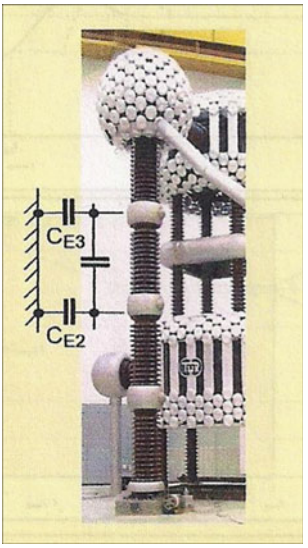

Fig. 3.58 Stacked capacitive voltage divider of a 1.2 MV test transformer composed of four units, 300 kV each (Courtesy of TU Dresden)

Example Consider Fig. 3.59 where the HV arm is composed of two HV capacitors denoted C_{11} and C_{12}. For a simple estimation, it shall be assumed that each HV capacitor is screened by a metallic cylinder of length l and diameter d where each screen is connected to the bottom of the capacitor. Under this condition, the current distribution is affected only by the earth capacitance C_e of the upper screen shielding the capacitor C_{11} arranged at a high h above ground. Using the so-called antenna formula (Küpfmüller 1932), the following approximation applies for vertical cylinders with $l \gg d$:

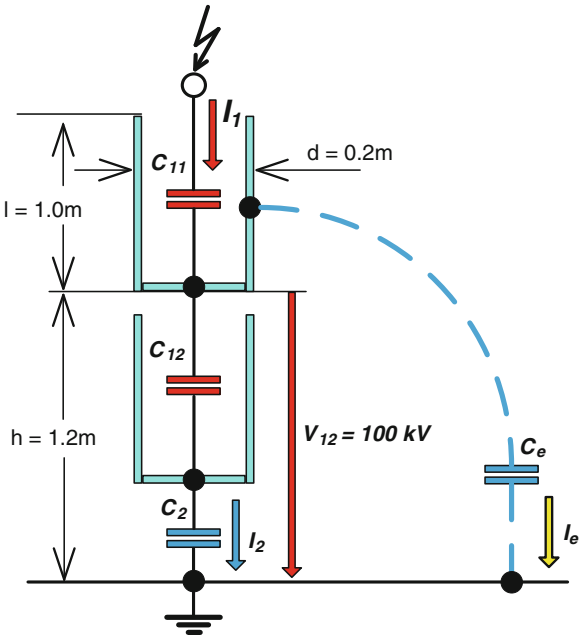

Fig. 3.59 Significant parameters utilized for the estimation of the earth capacitance C_e of a double-stage capacitive divider

$$C_e = \frac{2\pi\varepsilon l}{\ln\left\{\frac{2l}{d}\sqrt{\frac{4h+l}{4h+3l}}\right\}}, \tag{3.32}$$

with $\varepsilon = 8.86$ pF/m—the dielectric permittivity of the ambient air. For a quantitative estimation, the following practical values shall be introduced: $C_{11} = C_{12} = 200$ pF, $d = 0.2$ m, $l = 1$ m, $h = 1.2$ m. Inserting these parameters in Eq. (3.32), the earth capacitance of the upper HV capacitor C_{11} becomes $C_e \approx 26$ pF that is about 13 % of C_{11}. Considering a power frequency voltage with $f = 50$ Hz, a voltage of $V_{12} = 100$ kV would cause the following current I_{12} through C_{12} and thus also through C_2:

$$I_{12} = I_2 = 2 \cdot \pi \cdot f \cdot V_{12} \cdot C_{12} = 6.28 \text{ mA}.$$

For the current through the stray capacitance C_e between the shielding electrode of the upper capacitor C_{11} and earth one gets for $V_{12} = 100$ kV

$$I_e = 2 \cdot \pi \cdot f \cdot V_{12} \cdot C_e = 0.81 \text{ mA}.$$

Adding these both values, the total current through the upper HV capacitor C_{12} becomes

$$I_{11} = I_{12} + I_e = 7.09 \text{ mA}.$$

Due to this, the voltage drop across the upper HV capacitor C_{12} amounts

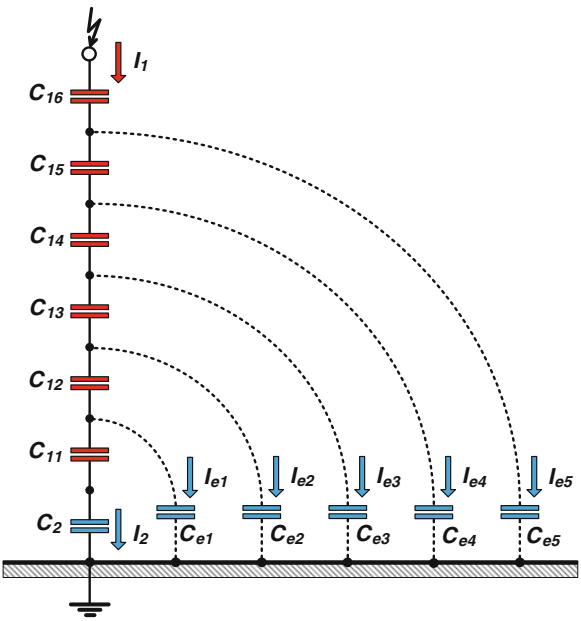

Fig. 3.60 Simplified equivalent circuit of a capacitive divider composed of six stacked HV capacitors, where the proximity effect due to surrounding walls and metallic structures is neglected

$$V_{11} = \frac{I_{11}}{2 \cdot \pi \cdot f \cdot C_{11}} = 113\ \text{kV}.$$

Thus, the total voltage appearing across the HV arm is given by $V_1 = V_{11} + V_{12} = 113\ \text{kV} + 100\ \text{kV} = 213\ \text{kV}$, which is 6.5 % above the theoretical value $2 \cdot 100\ \text{kV} = 200\ \text{kV}$

Consequently, the earth capacitance causes a fictive reduction in the capacitance of the HV arm. This becomes more pronounced as greater the number n of stacked capacitors is and thus as lower the capacitance C_u of each unit is. To estimate the voltage distribution along the complete HV divider column and thus to determine the effective capacitance of the HV arm, the equivalent circuit according to Fig. 3.60 is commonly utilized (Raske 1937; Hagenguth 1937; Elsner 1939).

Based on this, the effective capacitance C_1 of the HV arm composed of n stacked capacitors, each of capacitance C_{1n}, can roughly be approximated by

$$C_1 \approx \frac{C_{1n}}{n} - \frac{n \cdot C_e}{6}. \tag{3.33}$$

Theoretical and experimental studies revealed that the *earth capacitance* C_e of each capacitor depends only slightly on the high h above earth. Thus, Eq. 3.32 can further be simplified:

Fig. 3.61 800 kV HVAC-RMS during calibration of an AC voltage divider of 1,000 kV

$$C_e = \frac{2 \cdot \pi \cdot \varepsilon \cdot l}{\ln\left(\frac{2 \cdot l}{d}\right)} \approx \left(56 \frac{pF}{m}\right) \cdot \frac{l}{\ln\left(\frac{2 \cdot l}{d}\right)}. \tag{3.34}$$

Inserting this in Eq. (3.33) one gets

$$C_1 \approx \frac{C_{1n}}{n} - \left(9.3 \frac{pF}{m}\right) \cdot \frac{n \cdot l}{\ln\left(\frac{2 \cdot l}{d}\right)}. \tag{3.35}$$

Example Consider a 2 MV divider consisting of $n = 10$ stacked capacitors, each of nominal capacitance $C_{1n} = 2{,}000$ pF. The length of each unit shall be $l = 1$ m and the diameter $d = 0.2$ m. Inserting these values in the Eqs. (3.34) and (3.35), one gets $C_e \approx 40$ pF and $C_1 \approx 160$ pF. Consequently, the effective capacitance of the HV arm is approx. 20 % lower than the theoretical one given by $C_u/n = 2{,}000$ pF/10 = 200 pF.

Even if the *effective divider capacitance* C_1 is only slightly affected by the stray capacitances between divider column and top electrode, it must be emphasized that C_1 cannot be calculated at sufficient accuracy. The only way is to determine the actual divider ratio and thus the scale factor experimentally, as described in numerous publications and text books (Zaengl 1965; Kuffel and Zaengl 1984; Schon 2010) and specified in IEC 60060-2:2010. Basically, the Schering bridge or even a transformer ratio arm bridge could be utilized for this purpose. More convenient are comparative measurements using a *reference measuring system (RMS)*, see Sect. 2.3.3. A typical arrangement for reference voltage measurements is shown in Fig. 3.61. Here, the standard capacitor providing the reference divider is located at the left (red), and the divider under calibration in the middle (blue). The 1,000 kV test transformer cascade is located at the right-hand side.

Standard capacitors are generally composed of coaxial cylinder electrodes with guard rings at the LV side, as originally suggested by Schering and Vieweg in 1928. To achieve a high breakdown voltage at low gap distance, standard capacitors are filled with compressed gas, such as SF_6, which ensures an excellent stability against temperature changing. The construction principle is obvious from

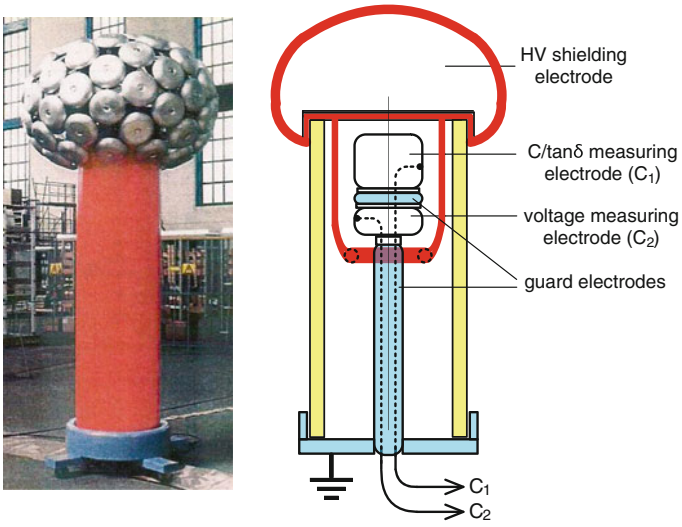

Fig. 3.62 SF_6-filled standard capacitor (rated voltage 800 kV, nominal capacitance 100 pF)

Fig. 3.62 which reveals that the capacitance between the coaxial electrodes may not be affected by earth capacitances, so that a proximity effect typical for stacked capacitors must not be taken into account.

As the capacitance of "long" coaxial cylinder electrodes is proportional to the cylinder length l and inversely proportional to the logarithm of the ratio between outer and inner conductor radius r_a/r_i, the following simple equation can be used to estimate the geometrical parameters:

$$C_1 = \frac{2 \cdot \pi \cdot \varepsilon \cdot l}{\mathrm{In}\left(\frac{r_a}{r_i}\right)} \approx \left(55.7 \frac{\mathrm{pF}}{m}\right) \cdot \frac{l}{\mathrm{In}\left(\frac{r_a}{r_i}\right)}, \tag{3.36}$$

Example For compressed gas capacitors rated ≥500 kV, the ratio of radii is chosen such that the breakdown voltage becomes a maximum. This is accomplished for $r_a/r_i = e = 2.718$ and thus for $\ln(r_a/r_i) = 1$. From Eq. 3.36, it follows that the length of the coaxial cylinder electrode arrangement must be 1.8 m to achieve a capacitance of $C_1 = 100$ pF.

For rated voltages below 500 kV, the expenditure can substantially be reduced if a ratio $r_a/r_i < e$ is used. If, for instance, the ratio $r_a/r_i = \sqrt{e}$ is chosen then follows with $\ln(\sqrt{e}) = 0.5$ that a capacitance of $C_1 = 100$ pF is already achieved for a $l = 0.9$ m.

To determine the dynamic behaviour of HV dividers, it is a common practice to subject the top electrode to a sinusoidal voltage of tuneable frequency and known magnitude, where the output voltage across the LV arm is recorded versus the frequency using a calibrated digital oscilloscope or a spectrum analyser. A simplified block diagram of such a circuit is depicted in Fig. 3.63.

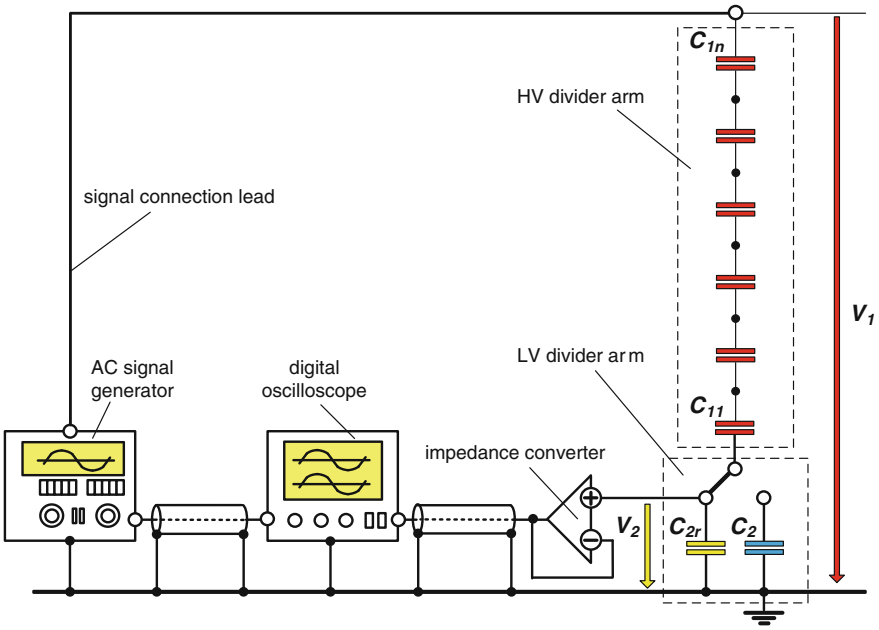

Fig. 3.63 Set-up for measuring the effective capacitance C_1 of a voltage divider

To minimize the impact of ambient noises and thus to enhance the measuring sensitivity at extremely high divider ratios, it seems reasonable to replace the original LV capacitance C_2 by a reference capacitor C_r substantially lower than C_2 to achieve a divider ratio of 1:1,000. This will not change the dynamic behaviour because this is governed only by the performance of the HV arm but not by the LV arm. Under this condition, a signal magnitude of several 100 V applied to the top electrode causes a voltage of several 100 mV across the LV arm that can accurately be measured by means of digital oscilloscopes if equipped with a peak detector and averaging tool. To avoid an enhancement of the upper limit frequency due to the input impedance of the oscilloscope, which is commonly in the order of 1 MΩ, the voltage across C_r should be captured via an impedance converter having a minimum input impedance of 10 MΩ.

Example Consider a 2 MV capacitive voltage divider where the HV arm constitutes of $n = 5$ stacked capacitors, each of nominal capacitance $C_{11} = C_{12} = \cdots C_{15} = 1$ nF. If the impact of the stray capacitance between divider column and earth is neglected, the theoretical capacitance of the HV arm would be $C_{1t} = 200$ pF. As mentioned above, for calibration purpose, it seems reasonable to replace the capacitor of the LV arm, having a capacitance of $C_2 = 877$ nF, by a reference capacitor of $C_r = 200$ nF which enhances the output voltage by almost 5 times. Applying a signal voltage of $V_1 = 500$ V peak to the top electrode, an output voltage across C_r of $V_1 \approx 0.5$ V could be expected, which can accurately be measured by classical digital oscilloscopes. As the input impedance of the impedance converter applied was 10 MΩ, the time constant of the LV arm becomes 2 s which is equivalent to a lower limit frequency of 0.8 Hz. This seems sufficient for the

lowest nominal frequency of $f_{1n} = 20$ Hz applied. Tuning the frequency of the AC signal generator between $f_{1n} = 20$ Hz and $f_{2n} = 300$ Hz, across C_r a mean peak value $V_1 = 0.438$ V was indicated by the built-in peak detector of the digital oscilloscope using the averaging mode. Thus, the "true" capacitance of the HV arm can be calculated as

$$C_1 = \frac{C_2}{\frac{V_1}{V_2} - 1} = \frac{200\text{ nF}}{\frac{500}{0.438} - 1} = 172\text{ pF}.$$

This is 14 % below the theoretical value given by $C_{1t} = 2{,}000$ pF/10 = 200 pF, as presented above. Replacing the reference capacitor $C_r = 200$ nF by the original capacitor of value $C_2 = 877$ nF, the true divider ratio becomes

$$1/(1 + C_2/C_1) = 1/(1 + 877/0.172) = 1/5{,}099$$

Neglecting the earth capacitance the divider ratio would deliver the wrong value of

$$1/(1 + C_2/C_1) = 1/(1 + 877/0.200) = 1/4{,}386.$$

In this context, it seems noticeable that C_1 is strongly affected by the clearance between divider column and the surrounding walls as well as other conducting structures. Thus, the geometrical configuration should not be changed after C_1 has been determined. Moreover, it has to be taken into account that C_1 may also be affected by the temperature of the dielectric material used for HV capacitors, which is often oil-impregnated paper. Due to dielectric losses, the temperature may rise after longer testing time so that the expanded uncertainty of the measuring system could also increase, particularly at higher voltage and longer test duration. Thus, a measuring uncertainty below 3 % specified in the relevant IEC publications can hardly be achieved if voltage dividers are composed of stacked capacitors using oil-impregnated paper.

3.4.2 Measuring Instruments

The first approach for indicating the output signal of a converting device if subjected to HVAC voltages was proposed by Chubb and Fortescu in 1913. The basic circuit comprises a standard capacitor, connected in series with two anti-parallel diodes. One of these diodes is directly connected to earth whereas the other is connected to earth via an ammeter. Under this condition, the instrument reads the integrated current through the capacitor during either the positive or the negative half-cycle that is correlated with the mean value of the test voltage.

As the occurrence of PD as well as the breakdown is mainly governed by the peak value of alternating voltages, the measurement of this quantity is more of interest. The first circuit for this purpose was proposed by Davis et al. in 1930

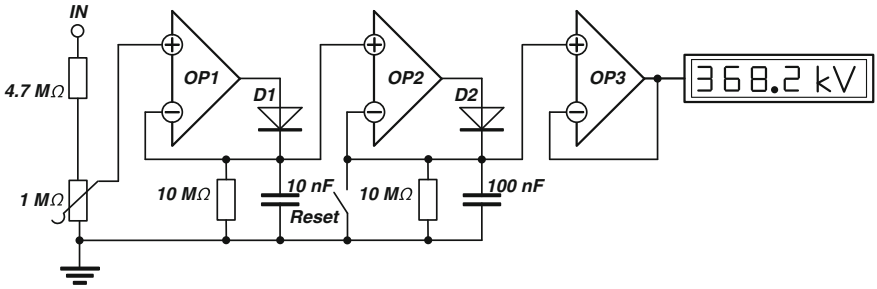

Fig. 3.64 Simplified circuit for measurement of AC peak voltages using a compensation of the forward conduction voltage of the diodes

which comprises a capacitive voltage divider where the LV arm is connected to a storage capacitor via a vacuum tube diode. To minimize the leakage current, the peak voltage across the storage capacitor was measured by an electrostatic voltmeter. In the 1950s, when the first fast semiconducting diodes of high reverse resistance were available, so-called sample and hold circuits have been used, as exemplarily shown in Fig. 3.64. The main benefit of such circuits is that the inevitable voltage drop across the rectifying diodes can completely be compensated.

Due to further achievements in microelectronics, the first *digital peak voltage* meters have been introduced in the 1970s. A typical block diagram and photograph of such a device are shown in Fig. 3.65. Here, an integrated microprocessor serves for an adjustment of the divider ratio and for controlling the measuring procedure. The A/D converter of high resolution ensures a measuring uncertainty as low as 0.5 % for input voltages between 10 and 1,000 V and test frequencies ranging between 0 Hz (DC) and 1,000 Hz.

Nowadays, digital recorders are more and more employed. Using the advanced digital signal processing and special software tools, all HVAC test voltage quantities presented in Sect. 3.2 are measurable. For more information, see also Sect. 7.4. In principle, also conventional digital oscilloscopes equipped with a peak detector are applicable for accurate measurement of HVAC test voltages, particularly if an averaging feature is available. To ensure the requirements according to IEC 60060-2:2010, however, only calibrated measuring instruments should be applied. Moreover, it has to be taken into account that the capacitance of the measuring cable between divider and measuring instrument, which is in the order of 200 pF/m, may contribute to the capacitance C_2 of the LV arm and should thus not be replaced after the complete measuring system has been calibrated.

Another problem encountered with HVAC voltage measurements is related to the input resistance R_i of the measuring instrument. A rule of thumb is that the characteristic time constant $\tau_m = R_i \cdot C_2$ multiplied with the minimum test frequency $f_{1\min}$ should be equal or greater than 100. This condition is accomplished for

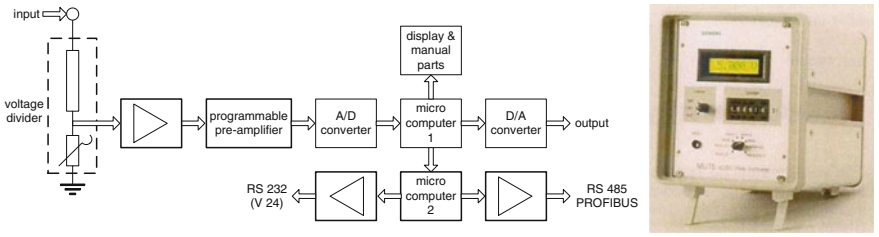

Fig. 3.65 Block diagram and photograph of a digital peak voltmeter

$$R_i \geq \frac{100}{C_2 \cdot f_{1\min}}. \tag{3.37}$$

Example Consider a capacitance $C_2 = 1$ μF and a minimum test frequency of $f_{1\min} = 20$ Hz. From Eq. (3.37), it follows $R_i \geq 5$ MΩ. As the input impedance of the digital recorder amounts commonly 1 MΩ, it seems reasonable to apply a resistive divider at the input of the recorder, as obvious from Fig. 3.64.

The *electromagnetic compatibility (EMC)* has also to be taken into account because fast transient over-voltages may appear in case of breakdowns of the test object. Due to this, the voltage across the LV arm of the voltage divider might substantially be enhanced and thus damage the measuring instrument. To prevent this, a proper over-voltage protection is required, using gas discharge tubes combined with spark gaps and special designed surge arresters of extremely high input impedance. Moreover, the impedance of the ground return should be as low as possible to reduce the impact of hazardous over-voltages, as treated more in detail in Sect. 9.2.

3.4.3 Requirements for Approved Measuring Systems

As specified in IEC 60060-2:2010, HVAC measuring systems applied for quality assurance tests of HV equipment should have an expanded uncertainty $U_M \leq 3$ %, where U_M shall be evaluated with a coverage probability of 95 %. For more details in this respect, see also Sect. 2.3.4. Traditionally, the peak voltage V_p is measured where the test voltage is defined in IEC 60060-1:2010 as $V_p/\sqrt{2}$. For sinusoidal test voltages, this quantity is equivalent to the rms value. In practice, however, superimposed harmonics may appear (see Sect. 3.2.1) so that the term $V_p/\sqrt{2}$ may substantially deviate from the rms value. In such cases, particularly when thermal processes play a rule as in the case of pollution tests, not only $V_p/\sqrt{2}$ but also the true rms value should be measured.

As HVAC test systems operate not only at the nominal frequency, such as 50 or 60 Hz, but also at variable frequencies, desired for induced voltage tests of power

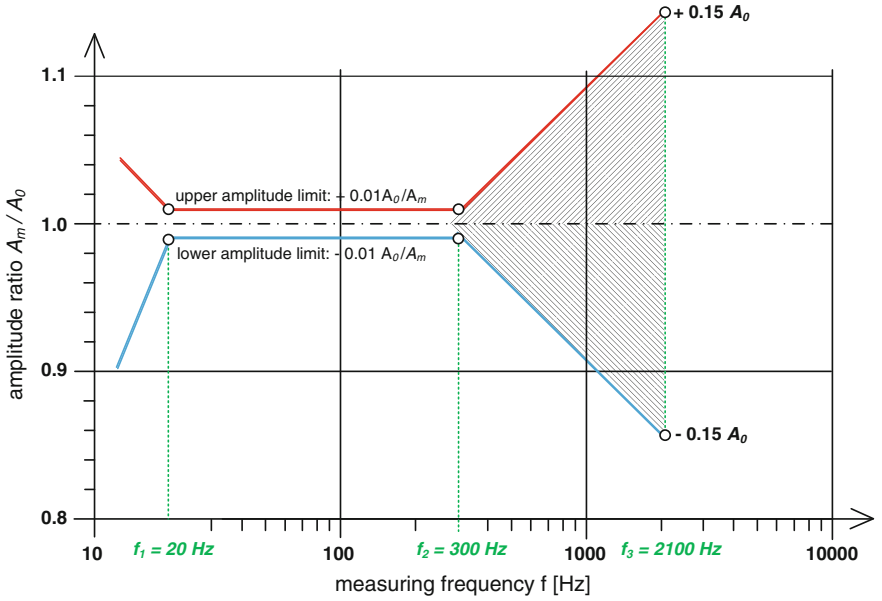

Fig. 3.66 Normalized limits for the amplitude–frequency response of an AC voltage measuring system to ensure a measuring uncertainty $\leq$3 % for the nominal frequency range 20 Hz $\leq f_{1n} \leq$ 300 Hz

transformers and instrument transformers as well as for on-site testing of long-power cable lines (Hauschild et al. 2002), the experimental investigations have to be extended also for a larger frequency range. So, the normalized amplitude A_m/A_0 representing the scale factor shall be constant within 1 % between the lowest nominal frequency f_{1n} and the highest nominal frequency f_{2n}. An example for this is shown in Fig. 3.66 that refers to $f_{n1} = 20$ Hz and $f_{n2} = 300$ Hz, respectively. For this specific case, the normalized amplitude limit shall be within the red and blue curve plotted in Fig. 3.66. To ensure an acceptable measuring uncertainty in case of harmonic distortions of the test voltage in the higher frequency range, the amplitude–frequency response between $f_{n2} \leq f \leq 7f_{n2}$ should also be investigated, as indicated by the shaded area in Fig. 3.66. This is also of relevance for measuring composite test voltages, i.e. if transient voltages are superimposed on the HVAC test voltage, as treated in Chap. 8.

It seems important to note that *type tests* and *routine tests* of the components of measuring systems, such as the voltage divider and the measuring instrument as well as the transmission system if other than cable (for instance, fibre optic link) have to be performed by the manufacturer, see Table 3.9, whereas *performance tests* (see Sect. 2.3.3) for the qualification of complete HVAC measuring systems must be performed under the responsibility of the user, see Table 3.10.

Additionally to the performance tests, *performance checks* are required using the comparison method with a second approved measuring system or even with a

Table 3.9 Survey on tests recommended in IEC 60060-2:2010 for approved HVAC measuring systems to be performed on each component by the manufacturer

	Type test	Routine test
Linearity		X
Dynamic behaviour	X	
Short-term stability		X
Long-term stability	X	
Ambient temperature effect	X	
Proximity effect	X (if applicable)	
Software effect	X (if applicable)	
Dry withstand test on converting device	X	X (if applicable)
Wet or polluted withstand test on converting device	X (if applicable)	
Scale factor of converting device	X	X
Scale factor of transmission system other than cable	X	X
Scale factor of measuring instrument	X	X
Repetition rate (recommended)		

Table 3.10 Survey on tests recommended in IEC 60060-2 for approved HVAC measuring systems to be performed by the user

	Performance test	Performance check
Scale factor calibration	X	
Scale factor check		X
Linearity	X (if applicable)	
Dynamic behaviour	X	
Long-term stability	X (if applicable)	
Proximity effect	X (if applicable)	
Repetition rate (recommended)	Annually, at least every five years	According to the stability, at least annually

sphere gap according to IEC 60052. The assigned scale factor can be accepted if the deviation between the comparative measurements is less than 3 %. Otherwise, the scale factor has to be determined repeating the *calibration procedure* as described above and in Sect. 2.3, as well. For the clarification of too large deviations, it is highly recommended to check the scale factor for the components

separately, i.e. the voltage divider and the measuring device including the signal transmission link if other than cable. For this, a calibrated AC voltage source of expanded uncertainty less than 1 % should be employed. The deviation between the comparative measurements should not exceed 1 %. Otherwise, it seems necessary to determine the actual value of the assigned scale factor.

Chapter 4
Partial Discharge Measurement

Abstract This chapter is devoted to the measurement of partial discharges (PD) localized in weak spots of dielectrics if subjected to high test voltages. As standards for *PD measurements* have been introduced only for quality assurance tests of HV apparatus energized by power frequency AC voltages (50/60 Hz), the following treatment refers mainly to this test voltage. Specific aspects to be taken into account for DC test voltages and also impulse voltages will only briefly be treated in the relevant chapters. Nowadays, PD measurements are performed not only in electromagnetically well-shielded laboratories but also under noisy on-site conditions, as discussed in this chapter.

For a better understanding, the principles and procedures employed for measuring the fundamental PD quantities in compliance with the standard IEC 60270:2000; first, some fundamentals of the PD occurrence will be presented. In the following section, the PD charge transfer in test samples is analysed where the existing PD models are critically reviewed. Based on this, the major components required for PD measuring circuits as well as the fundamentals for the calibration of PD measuring circuits are treated. Then, the visualization and evaluation of PD test results are described. The last section deals with the fundamentals of non-conventional PD detection based on the measurement of electromagnetic and acoustic signals.

4.1 PD Occurrence

Partial discharges in technical insulation are the consequence of dielectric imperfections, such as sharp edges in ambient air and gaseous inclusions in liquid and solid dielectrics. These cause a local field enhancement, which might exceed the intrinsic field strength, so that self-sustaining electron avalanches can be ignited. The movement of the charge carriers inside gaseous inclusions is associated with fast transient current pulses detectable at the electrodes of the test

W. Hauschild and E. Lemke, *High-Voltage Test and Measuring Techniques*,
DOI: 10.1007/978-3-642-45352-6_4, © Springer-Verlag Berlin Heidelberg 2014

object, which can advantageously be used for the recognition of partial discharges. According to IEC 60270:2000, partial discharges are defined as

> localized electrical discharges that only partially bridge the insulation between conductors and which can or cannot occur adjacent to a conductor. Partial discharges are in general a consequence of local electrical stress concentrations in the insulation or on the surface of the insulation. Generally such discharges appear as pulses having durations of much less than 1 μs.

The first experimental method applied for recognition of electrical discharges dates back to the year 1777 when Lichtenberg discovered dust figures like stars and circles on the surface of an amber cake after it has been hidden by sparks of about 40 cm in length (Lichtenberg 1777, 1978). In the middle of the nineteenth century, the Lichtenberg figure technique became a valuable tool to study electrical discharge phenomena using not only dust but also photographs for recording typical discharge patterns (Blake 1870; Toepler 1898; Müller 1927). Since the beginning of the last century, when high voltages were increasingly used for the long-distance transmission of electrical power, it became known that discharges in gas-filled inclusions of solid dielectrics can be considered as a precursor for an ultimate breakdown. Therefore, the *PD detection* became increasingly of interest where various tools have been adopted, such as optical, chemical, acoustical and electrical methods. Since the 1960s, the electrical PD measurement is a widely accepted tool for quality assurance tests of HV apparatus after manufacturing, which shall thus be discussed in more detail in the following sections.

As partial discharges are associated with the ionization of gas molecules, such events occur not only in ambient air but also in gas-filled cavities of solid dielectrics or in bubbles and water vapour of liquid dielectrics. Thus, the fundamental discharge mechanism known from ambient air, such as Townsend, streamer and leader discharges, extensively investigated since the beginning of the last century (Townsend 1915, 1925; Schuman 1923; Meek and Craggs 1953; Loeb 1956; Raether 1964; Park and Cones 1963) might also occur in gaseous inclusions. Typical photographs of discharge channels developing in ambient air and insulating oil as well as in PMMA are exemplarily shown in Fig. 4.1 (Lemke 1967; Hauschild 1970; Pilling 1976).

Due to the formation of electron avalanches within the nanosecond range, each individual PD event is associated with a very fast current pulse caused by the moving charge carriers. In 1966, Bailey estimated theoretically that the shortest rise time of original *PD pulses* could be in the nanosecond range. This has been manifested experimentally by Fujimoto and Boggs (1981) as well as by Boggs and Stone (1982) using the first available high-speed oscilloscope having a bandwidth of 1 GHz, as shown in Fig. 4.2. As for technical insulation the PD defect is not accessible, the true shape of PD current pulses cannot be measured. The only way is to decouple the PD transients from the terminals of the test object. Under this condition, however, the frequency content of the PD signal is dramatically reduced due to the inevitable attenuation and dispersion of the PD pulses when propagating from the *PD source* to the terminals of the test object.

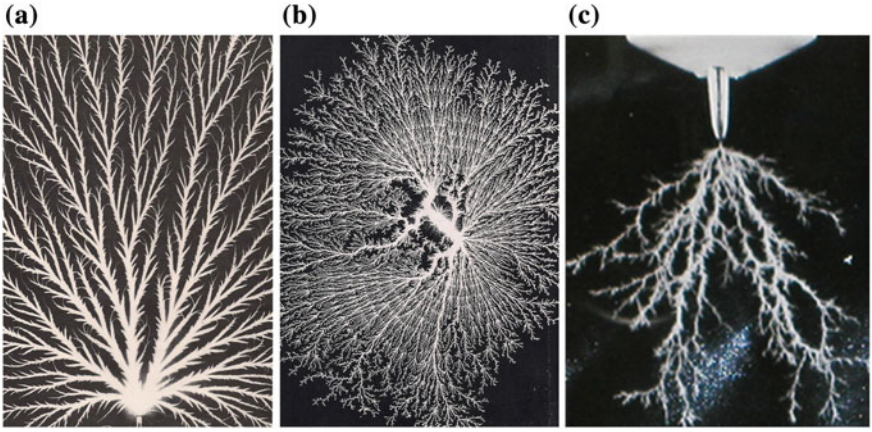

Fig. 4.1 Photographs of discharge channels. **a** Streamer discharge in air (Lemke 1967). **b** Leader discharge in oil (Hauschild 1970). **c** Trees in PMMA (Pilling 1976)

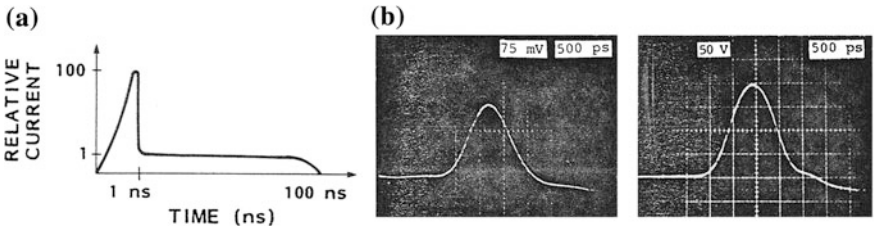

Fig. 4.2 Time parameters of PD current pulses. **a** Theoretical pulse shape calculated by Bailey for small voids in solid dielectrics. **b** Pulse shapes measured by Boggs and Stone for a sharp point (*left*) and a floating particle in SF6 (*right*)

For a better understanding, the PD pulse attenuation in power cables is considered (Fig. 4.3). Here, artificial PD pulses were injected in a 16-m-long polyethylene-insulated MV cable using a PD calibrator. To record the pulses at the *near* cable end, a digital oscilloscope has been used changing the overall bandwidth between 200 and 20 MHz, respectively. The records shown in Fig. 4.3 refer to an injection point located 4 m far from the *near* end where the oscilloscope was connected. Thus, the second pulse is reflected at the remote end and travelled in total $(2 \cdot 12 + 4) = 28$ m before arriving the near end. Comparing Fig. 4.3b with c, it can be shown that the magnitude ratio between the direct and the reflected pulse is reduced from originally 2.5:1, obtained for 200-MHz bandwidth, down to approx. 1.4:1 for a bandwidth of 20 MHz. Decreasing the bandwidth down to 1 MHz or below the magnitudes of both the direct and the reflected pulse would become equal. With other words: if the *measuring frequency* is chosen as low as possible, the recorded pulse magnitudes are invariant, i.e. independent on the travelling distance. This behaviour is comparable to that of a low-pass filter that

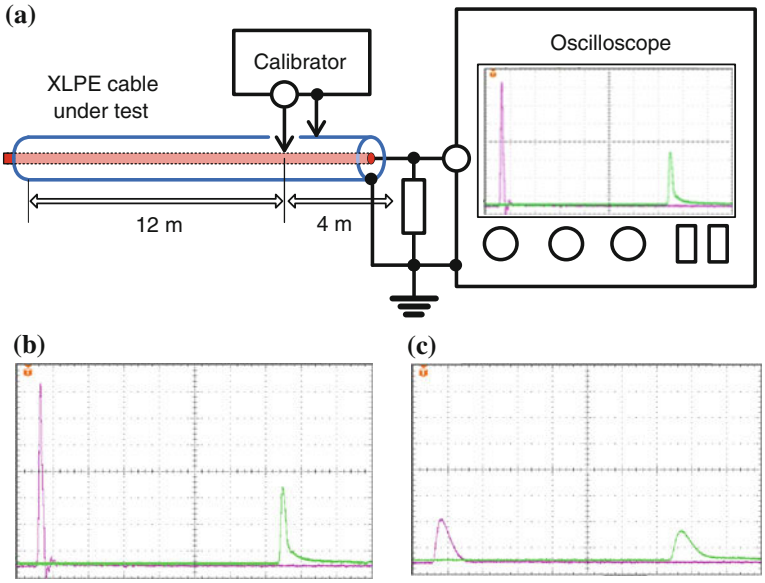

Fig. 4.3 Influence of the measuring frequency on the attenuation of a PD pulse travelling in a XLPE power. **a** Experimental set-up. **b** Bandwidth and upper limit frequency 200 MHz. **c** Bandwidth and upper limit frequency 20 MHz

causes a so-called quasi-integration. That means, if the measuring frequency is much lower than the frequency content of the input pulses, the magnitudes of the output pulses become equal to the time integral and thus to the charge of the input pulses (Kind 1963; Schon 1986; Zaengl and Osvath 1986). This behaviour can thus be considered as the background that IEC 60270 recommends the measurement of the PD quantity "*apparent charge*" to ensure comparative and reproducible PD measurements. The following treatment refers mainly to specific aspects of pulse charge measurements.

4.2 PD Models

As known, the electromagnetic transients due to PD events are only detectable at the terminals of HV apparatus. Therefore, it seems of interest if this *external pulse charge* is correlated with the *internal pulse charge* flowing through the PD defect. To analyse the PD charge transfer, instead of realistic imperfections shown in Fig. 4.4 (Kreuger 1989), simple cavity shapes are commonly investigated, such as spherical, elliptical and cylindrical cavities. Generally, it can be distinguished between the (network-based) *capacitive model* and the *dipole PD model*, as discussed in the following.

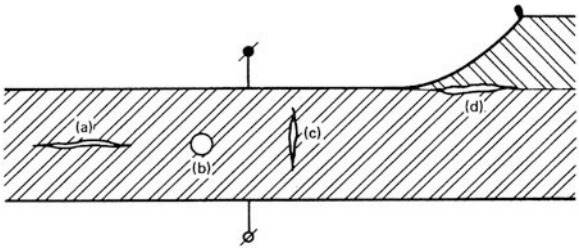

Fig. 4.4 Typical sizes of gaseous inclusions in solid dielectrics according to Kreuger (1989). Flat cavity perpendicular to the electric field spherical flat cavity aligned with the electric field interfacial cavity

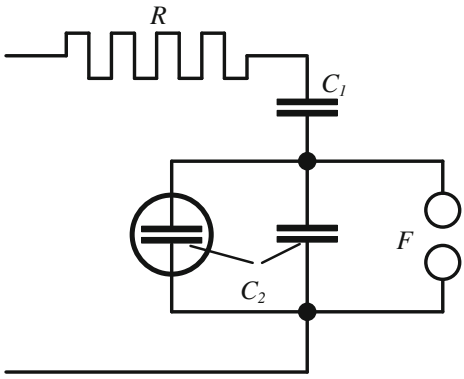

Fig. 4.5 Experimental set-up used by Gemant and Philippoff (1932) to explain the characteristic recurrence of PD pulses at power frequency AC test voltage

4.2.1 Capacitive PD Model

To assess the losses due to discharges in laminated solid dielectrics subjected to AC voltages, Byrstlyn investigated in 1928 the breakdown sequences of a spark gap connected in series with a capacitance. This simple approach has systematically been investigated by Gemant and Philippoff (1932) to estimate the power losses in mass-impregnated power cables caused by heavy cavity discharges. For this purpose, the discharges per half-cycle of the applied power frequency test voltage have been recorded by means of an oscilloscope using the equivalent circuit shown in Fig. 4.5. The spark gap F was directly connected with the horizontal deflection plates of a high-voltage oscilloscope. Moreover, the effective capacitance C_2 of the spark gap was varied by additional parallel capacitors. The series capacitance C_1 and resistance R served for the limitation of the transient current through the spark gap F. Typical oscilloscopic records gained for two different test voltage levels are shown in Fig. 4.6 where the number of voltage collapses depending on the test voltage level showed a surprisingly well agreement with theoretical calculations.

To calculate not only the pulse count versus the test voltage level but also the ratio between the detectable *external PD charge* and the *internal PD charge* flowing through the cavity, the equivalent circuit shown in Fig. 4.5 has been modified by Whitehead as well as by Kreuger in the 1950s (Fig. 4.7). In this

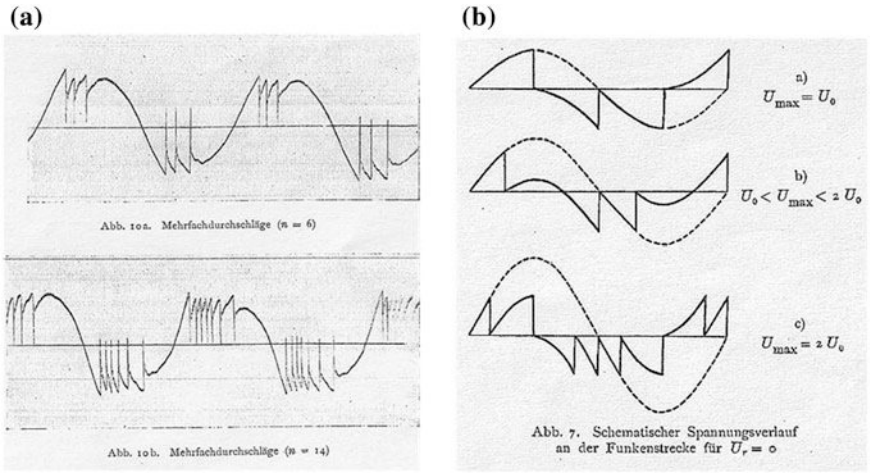

Fig. 4.6 Oscilloscopic records made by Gemant and Philippoff (**a**) and approach for the calculation of the pulse count versus the test voltage level (**b**)

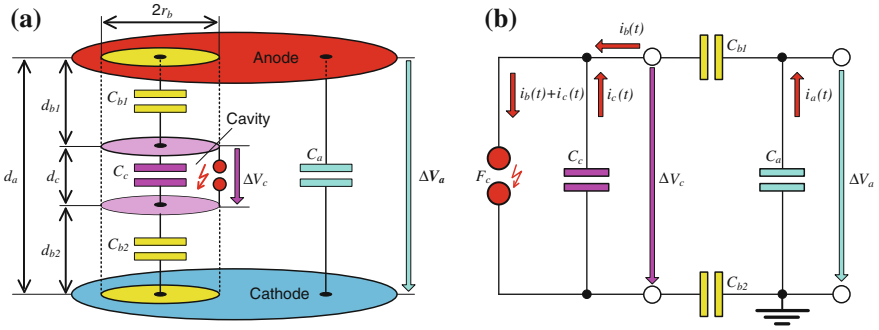

Fig. 4.7 Network-based capacitive PD model. **a** Parallel-plane electrodes with circuit elements. **b** Capacitive equivalent circuit (abc-model)

circuit, C_a is the capacitance of the bulk dielectric between the electrodes of the test object, C_b is the stray capacitance of the healthy dielectric column between cavity and electrodes, and C_c is the cavity capacitance that is bridged by the spark gap F_c, originally introduced by Gemant and Philippoff. Due to these three characteristic capacitances, the equivalent circuit according to Fig. 4.7 is traditionally referred to as *abc-model*.

To analyse the PD charge transfer from the cavity to the terminals of the test sample, commonly a cylindrical dielectric column of constant diameter $2r_b$ is considered, as shown in Fig. 4.7a. For technical insulation, the condition $d_c \ll d_{b1} + d_{b2} \approx d_a$ is generally satisfied. Thus, the resulting capacitance of the solid dielectric column can simply be expressed by $C_b = \varepsilon_0 \cdot \varepsilon_r \cdot \pi \cdot r_b^2 / d_c$. To simplify

the calculation equal radii are assumed for both the solid dielectric column and the cylindrical cavity (r_c), i.e. $r_c = r_b$. Thus, the cavity capacitance is estimated by $C_c = \varepsilon_0 \cdot \pi \cdot r_b^2/d_c$. Assuming that the spark gap shown in Fig. 4.7a breaks down at inception field strength E_i, the voltage collapse across the cavity capacitance can be approximated by $\Delta V_c \approx E_i \cdot d_c$. Based on this, the internal PD charge q_c flowing through the gas-filled cavity ($\varepsilon_r = 1$) can be expressed by

$$q_c \approx \Delta V_c \cdot C_c \approx E_i \cdot \varepsilon_o \cdot \pi \cdot r_b^2. \tag{4.1}$$

As obvious from Fig. 4.7b, the transient current $i_b(t)$ and thus the charge q_b flowing through the capacitances C_{b1} and C_{b2} are also flowing through the capacitance C_a, representing the bulk dielectric of the test sample, i.e. $q_a = q_b$. Therefore, the following approach can be used to estimate the *external* charge q_a detectable at the terminals of the test sample:

$$\mathrm{dq}_a = \mathrm{q}_b \approx \Delta V_c \cdot C_b \approx E_i \cdot \varepsilon_o \cdot \varepsilon_r \cdot \pi \cdot r_b^2 \cdot \frac{d_c}{d_a} \tag{4.2}$$

For technical insulation, the inequality $d_c \ll d_{b1} + d_{b2} \approx d_a$ is always satisfied and the relative permittivity ε_r of the applied solid dielectrics is commonly below 5. Under this condition, the ratio between *external* detectable charge and *internal* charge flowing through the cavity becomes

$$\frac{q_a}{q_c} \approx \varepsilon_r \frac{d_c}{d_a} \ll 1. \tag{4.3}$$

Due to this relation, the *external* detectable charge is commonly referred to as *apparent* charge and it is noted in IEC 60270 that "*the apparent charge is not equal to the amount of that charge involved at the site of the discharge, which cannot be measured directly*".

When the apparent charge concept has been introduced (Kreuger 1964), however, it has unfortunately been overlooked that the capacitance of the solid dielectric column shown in Fig. 4.7a, and thus, the effective radius r_b increases drastically if a discharge channel (radius r_d) is formed, as extensively investigated by Boggs (2004). Moreover, the effective capacitance C_c is not any longer governed by the effective radius r_b of the solid dielectric column shown in Fig. 4.7a but by the radius r_d of the discharge channel developing inside the cavity, where the condition $r_d \ll r_b$ is always satisfied. Thus, instead of Eq. (4.3), the following approach applies

$$\frac{q_a}{q_c} \approx \varepsilon_r \frac{d_c}{d_a} \cdot \left(\frac{\mathrm{r}_b}{\mathrm{r}_d}\right)^2. \tag{4.4}$$

Due to the inequalities $d_c \ll d_b$ and $r_b \gg r_d$, it cannot simply be claimed that the *external PD charge* is only a small fraction of the *internal PD charge*. As will be investigated more in detail in the next section, the apparent charge concept deduced from the capacitive equivalent circuit according to Fig. 4.7 is not true.

Another mistake is the assumption that the applied test voltage induces charge carriers at the anode-side and cathode-side cavity boundary. That means the *internal* charge has already been produced just before PD event is ignited, which is in contrast to the physics of gas discharges as will also be discussed more in detail in the following section.

4.2.2 Dipole Model

The apparent charge concept presented above has been criticized by Pedersen and his co-workers since the middle of the 1980s because this is deduced from the network-based *capacitive model*, which is not capable to reflect the physics of gas discharges. So the cavity is not discharged via a spark gap but charged due to the creation of charge carriers as consequence of ionization processes in the gas-filled cavity. As the charge carriers of both polarities are deposited at the anode-side and cathode-side cavity boundary, a dipole moment is established, as illustrated in Fig. 4.8a. The space charge field, commonly referred to as Poisson field, opposes the electrostatic field caused by the applied test voltage, commonly referred to as Laplacian field. As a consequence, the ionization of gas molecules is quenched immediately after the PD event has been ignited, where the time interval is usually in the nanosecond range.

As can readily be deduced from Fig. 4.8, the continuity equation applies for the transient PD current. That means that the current $i_c(t)$ caused by the charge carriers moving inside the cavity continues like a displacement current $i_b(t)$ through the solid dielectric column which is replaced in Fig. 4.8b by the capacitances C_{b1} and C_{b2}. From this follows that the *external* PD charge q_a detectable at the terminals of the test sample must be equal to the *internal* PD charge q_c flowing through the cavity, which is in contrast to the apparent charge concept presented previously.

To estimate the PD charge transfer quantitatively, Pedersen proposed a field theoretical approach. However, this concept has been ignored in the past, whereas the *abc*-model is widely promoted also nowadays (Achillides et al. 2008, 2013). The reason for that is, apparently, that a PD charge transfer can easily be explained based on the capacitive PD model according to Fig. 4.7, which is not the case if the electromagnetic field theory based on the Maxwell equations (Maxwell 1873) is adopted. As described in the following, however, the analysis can substantially be simplified if instead of spherical, ellipsoidal or even cylindrical cavities, as commonly investigated in the relevant literature, the establishment of a dipole moment under quasi-uniform field conditions is considered (Lemke 2012). Moreover, it shall be assumed that the Laplace field between the electrodes remains constant during the time duration of a PD event which is usually in the order of nanoseconds (Raether 1939; Loeb 1940; Baily 1966). Thus, only the Poisson field caused by the separation of the charge carriers of opposite polarity has to be considered to estimate the PD charge transfer.

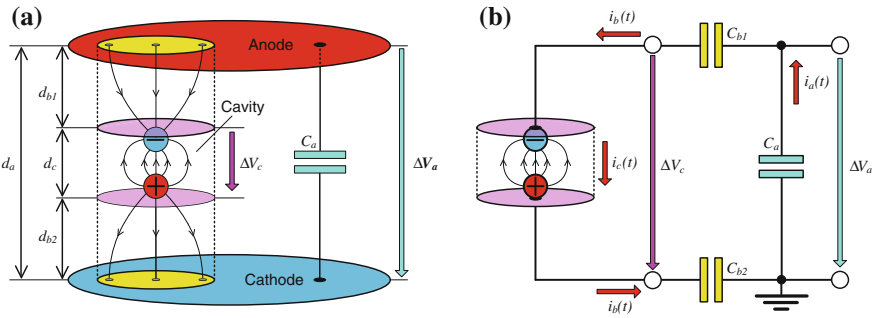

Fig. 4.8 Dipole model of a cavity discharge. **a** Space charge field due to bipolar point charges deposited at the cavity wall. **b** Circuit elements

For a better understanding, one considers first the movement of a single electron and the associated positive ion, where the propagation to the electrodes is hampered by two dielectric layers of spacing d_c, as illustrated in Fig. 4.9. Assuming that at inception field strength E_i, only a single electron carrying the elementary charge $-e$ is liberated from a neutral molecule at position $x = x_i$, the electron is attracted by the anode due to the Coulomb force $F = -e \cdot E_i \cdot x_i$. Thus, after travelling the maximum possible distance x_i, the field energy transferred to the electron becomes

$$W_e = F \int_{x_i}^{o} \mathrm{d}x = -e \cdot E_i(0 - x_i) = e \cdot E_i \cdot x_i. \tag{4.5}$$

In an analogue manner, one gets for the energy transferred from the field to the associated positive ion carrying the elementary charge e

$$W_p = F \int_{x_i}^{o} \mathrm{d}x = e \cdot E_i \cdot (d_c - x_i). \tag{4.6}$$

Combining Eqs. (4.5) and (4.6), the total field energy transferred to both the electron and the associated positive ion after approaching the dielectric layers becomes

$$W_t = W_e + W_p = e \cdot E_i \cdot d_c. \tag{4.7}$$

It is obvious that this equation is independent from the actual site x_i where the electron is liberated from a neutral molecule. Thus, also the field energy transferred to an electron avalanche created by the ionization of n_i molecules is given by

$$W_a = e \cdot n_i \cdot E_i \cdot d_c. \tag{4.8}$$

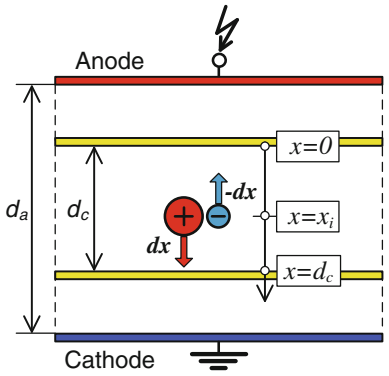

Fig. 4.9 Parameters used for the estimation of the field energy transferred to an electron and the associated positive ion

If one imagines the test sample is disconnected from the HV test supply just before a PD event is ignited at the inception voltage V_i, the energy desired for the movement of the charge carriers is delivered from the test sample capacitance C_a, as shown in Fig. 4.8b. If the movement of the charge carriers occurs within a time interval t_d, the energy balance theorem can be expressed as follows:

$$W_a = V_i \int_o^{t_d} i_a(t) \cdot \mathrm{d}t = V_i \cdot q_a = e \cdot n_i \cdot d_c \cdot E_i = P_m \cdot E_i, \tag{4.9}$$

where the term $P_m = e \cdot n_i \cdot d_c$ represents the dipole moment and E_i the inception field strength. Separating the charge q_a delivered from the electrodes of the test sample, one gets

$$q_a = e \cdot n_i \cdot d_c \cdot \frac{E_i}{V_i} = P_m \cdot \frac{E_i}{V_i}. \tag{4.10}$$

It seems to be noticeable that a similar approach can also be deduced from the concept of image charges (Shockley 1938; Kapcov 1955; Frommhold 1956), which has also been employed by Meek and Craggs (1953) as well as by Reather (1964) and many other researchers accounting the charge carrier currents between plane electrodes.

Generally, it can be postulated that the insulation deterioration due to PD events is mainly governed by the field energy transferred to the charge carriers. Comparing the Eqs. (4.9) and (4.10), it can thus be concluded that the *external charge* q_a detectable at the terminals of the test sample seems to be a reasonable quantity to assess the *PD severity*, which is in contrast to the traditional apparent charge concept. In this context, it seems to be noticeable that the detectable external PD charge q_a increases with the cavity length d_c and thus with the danger for an insulation breakdown, even if the number n_i of molecules ionized in case of a single PD event remains constant. This is because the dielectric flux density at the anode and cathode increases with increasing cavity length, as exemplarily illustrated in Fig. 4.10.

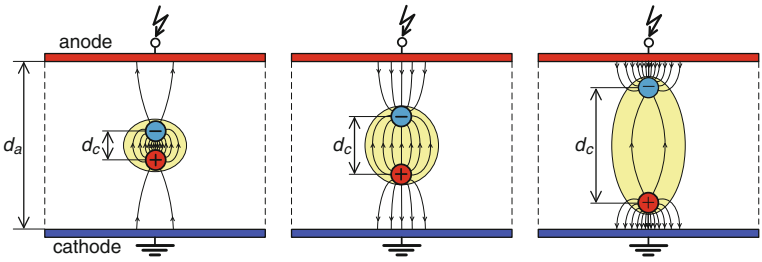

Fig. 4.10 Dielectric flux density at the anode and cathode depending on the cavity length

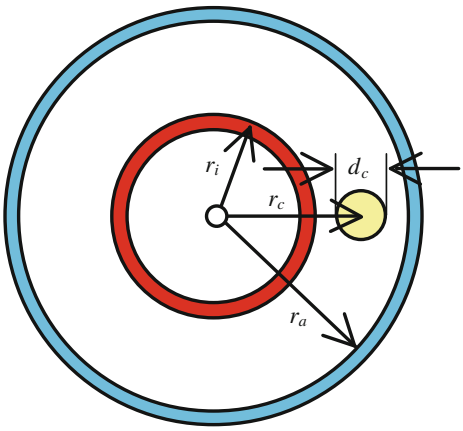

Fig. 4.11 Parameters used for the analysis of the PD charge transfer in extruded power cables

Even if Eq. (4.10) has been deduced for quasi-homogenous field conditions, it is also applicable for technical electrode configurations provided the cavity length d_c in field direction is substantially lower than the electrode spacing (Lemke 2013). As an example, consider Fig. 4.11, which refers to a spherical cavity embedded in the bulk dielectric between coaxial cylinder electrodes representative for power cables.

To simplify the following treatment, a virgin (space-charge-free) cavity shall be considered, which seems reasonable because the charge carriers affecting the field distribution are created just after the instant when the inception field strength E_i is exceeded. Under this condition, the field enhancement factor k_ε inside the cavity can be approximated as follows (Schwaiger 1925):

$$k_\varepsilon = \frac{3\varepsilon_r}{1 + 2\varepsilon_r}. \tag{4.11}$$

For a polyethylene-insulated cable having the relative dielectric permittivity $\varepsilon_r = 2.3$, one gets $k_\varepsilon \approx 1.2$. Inserting this in Eq. (4.10), the detectable pulse charge can be expressed by

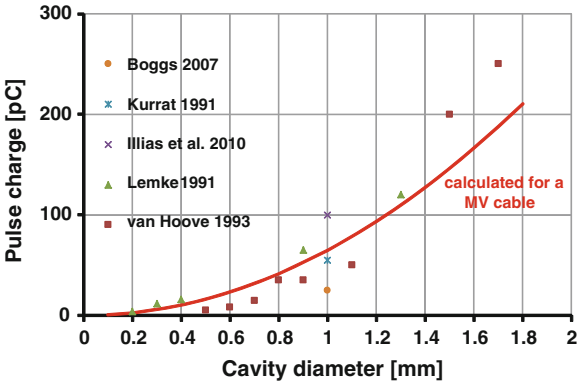

Fig. 4.12 PD charge versus cavity diameter calculated for a MV cable and experimental data

$$q_a \approx P_m \cdot \frac{1.2}{r_c \left[\ln\left(\frac{r_a}{r_i}\right)\right]}. \tag{4.12}$$

To determine the dipole moment P_m quantitatively, however, it is a challenge because the number n_i of ionized molecules may vary over an extremely wide range. Thus, it seems reasonable to investigate the worst case, which arises if a streamer-like discharge is ignited. Under this condition, the dipole moment can be expressed by the following semiempirical approach (Lemke 2013):

$$P_m \approx (270\ \text{pC/mm}) \cdot d_c^2 \quad \text{for } 0.1\ \text{mm} < d_c < 2\ \text{mm}. \tag{4.13}$$

Introducing this in Eq. (4.12) and inserting the following assumed geometrical parameters $r_i = 8.5$ mm, $r_a = 14$ mm and $r_c = 10$ mm, which are representative for a 20-kV polyethylene-insulated power cable, one gets

$$q_a \approx (67\ \text{pC}) \cdot \left(\frac{d_c}{d_o}\right)^2. \tag{4.14}$$

With a reference diameter of the cavity of $d_o = 1$ mm, the curve q_a versus d_c is plotted in Fig. 4.12. For comparison purposes, also experimental data are plotted in this figure. In this context, it should be noted that the experimental data refer also to configurations other than the coaxial cylinder electrodes investigated here. The calculated curve meets the measured data quite well, where a better agreement cannot be expected due to the large scattering of the PD magnitudes under practical condition.

With respect to quality assurance tests of extruded power cables, the pulse charge q_a versus the *PD inception voltage* V_i is the most interesting function. To solve Eq. 4.10, the ratio E_1/V_i must be known. An appropriate approach can be deduced from the Schumann curves (Schumann 1923). Based on this, the dependence of the inception field strength E_i on the cavity diameter d_c becomes

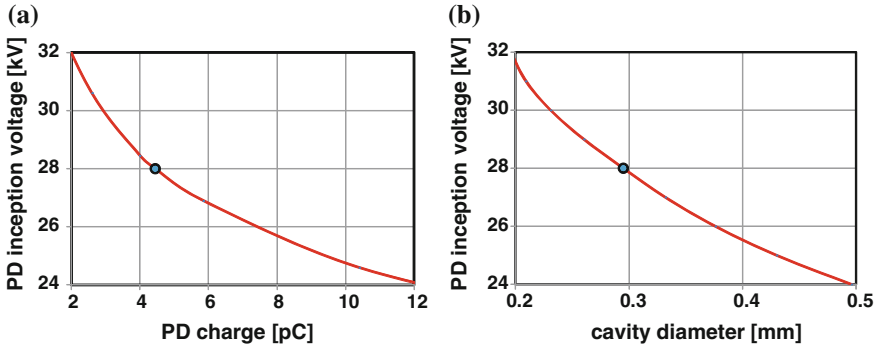

Fig. 4.13 PD inception voltage versus PD charge (**a**) and cavity diameter (**b**) calculated for an extruded MV cable

$$E_i \approx E_0\left(1+\sqrt{\frac{d_r}{d_c}}\right) \quad \text{for } 0.1\text{ mm} < d_c < 2\text{ mm}, \tag{4.15}$$

with the reference values $E_0 = 2.47$ kV/mm and $d_r = 0.82$ mm. Inserting these values in Eq. 4.10, the inception voltage of a virgin spherical cavity embedded in the bulk dielectric between coaxial cylinder electrodes can be calculated by the following approach:

$$V_i = \frac{E_0}{k_\varepsilon}\cdot r_c \cdot \left[\ln\left(\frac{r_a}{r_i}\right)\right]\cdot\left(1+\sqrt{\frac{d_r}{d_c}}\right) \approx V_i \approx (10.5\text{ kV})\cdot\left(1+\sqrt{\frac{0.82\text{ mm}}{d_c}}\right). \tag{4.16}$$

Combining Eqs. (4.14) and (4.16), the detectable pulse charge q_a versus the inception voltage V_i has been calculated and displayed in Fig. 4.13. In this context, it seems noticeable that in IEC 60502: 1997 a maximum test voltage level of 1.73 V_0 is recommended for medium voltage cables with extruded insulation, where V_0 is the *rms* value of the conductor to ground voltage, which is equivalent to a peak voltage of 28 kV. This value is indicated in Fig. 4.13 by a circle, which yields that the cable would pass the test only if the *PD level* is below 5 pC. This result is in good agreement with IEC 60502: 1997, which recommends that *the magnitude of the discharge at* 1.73 V_0 *shall not exceed* 10 *pC*. Moreover, it can be deduced from Eq. (4.16) that the cavity diameter d_c should be less than 0.3 mm to guarantee a PD inception voltage above 28 kV.

Even if the calculated curves plotted in the Figs. 4.12 and 4.13 are in satisfying with practical experience, it must be emphasized that the quantitative values are only approximations. This is because Eq. (4.10) refers to a virgin cavity filled with air under atmospheric normal condition. However, for technical insulation, neither the cavity size nor the gas pressure is known. Moreover, the dipole moment established by subsequent PD events may strongly be affected by the space charge

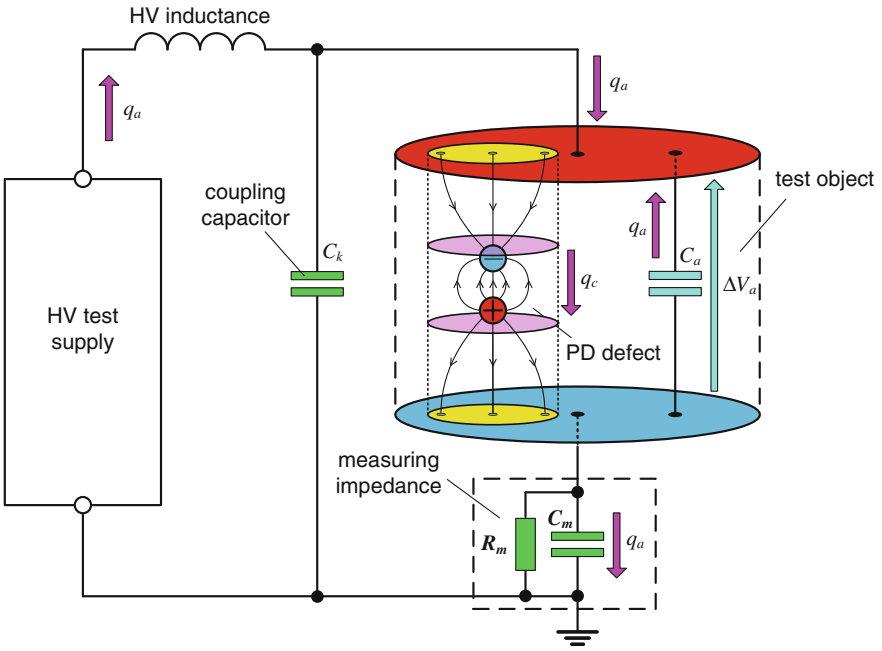

Fig. 4.14 Principle of pulse charge measurement

created by previous PD events. This might be the reason for the large scattering of the pulse charge magnitudes encountered in practice.

4.3 PD Pulse Charge Measurement

4.3.1 Decoupling of PD Signals

As already discussed in Sect. 4.1, the high-frequency *PD current pulses* are strongly be distorted when travelling from the origin to the electrodes of the test object, as shown in Fig. 4.3. Different to this, the time integral of the transient PD current and thus the pulse charge is more or less invariant. For a better understanding, consider Fig. 4.14, which refers to a cavity embedded in the bulk dielectric between plane electrodes, as investigated more in detail in Sect. 4.2.

As the PD transients are characterized by time parameters in the nanosecond range, the leads between test object and HV test supply can be considered as disconnected due to its extremely high inductive impedance. Consequently, the charge q_c flowing through the PD defect is almost completely delivered from the test object capacitance C_a, which is associated with a voltage collapse ΔV_a across the electrodes of the test object. Consequently, the *pulse charge* q_c flowing through

the PD defect, which is delivered from the electrodes of the test object, can be expressed as follows:

$$q_c = q_a = \Delta V_a \cdot C_a. \tag{4.17}$$

After the fast PD process is quenched, the transient PD current approaches zero so that the impedance of the connection leads is drastically reduced. Thus, the test object capacitance C_a will be recharged by the HV test supply, i.e. the former voltage step ΔV_a is inverted. That means the time integral of the charging current can also be approximated by Eq. (4.17), even if the shape of this charging current is very different from that of the original PD current. This fact offers the possibility to measure the pulse charge flowing through the PD defect by means of a *measuring impedance*, if connected between the LV electrode of the test object and the ground, as illustrated in Fig. 4.14. Additionally, the measuring circuit should be bridged by a coupling capacitor C_k to ensure a short duration of the recharging process, and thus, well-reproducible PD measurements as will be discussed below. Moreover, an appropriately designed HV inductor should be connected between HV test supply and test object to reject electromagnetic noises coming from the HV test voltage supply, as obvious from Fig. 4.14.

For a direct measurement of the pulse charge, the measuring impedance could be equipped with a measuring capacitance C_m. Under this condition, the magnitude of voltage jump appearing across C_m is direct proportional to the pulse charge to be measured. At alternating test voltages, however, the capacitive load current through the test object might become substantially higher than the signal of the charge pulses as obvious from the oscilloscopic record shown in Fig. 4.15a. To overcome this crucial problem, the measuring capacitance C_m can be shunted by a measuring resistor R_m, as can be seen from the records shown in Fig. 4.15b, c. Practical experience revealed, however, that a measuring impedance equipped with a RC network according to Fig. 4.14 is only applicable for fundamental PD studies on point-to-plane samples, where the capacitance between the electrodes is extremely low, but not for technical HV equipment and their components.

To suppress the disturbing signal due to the capacitive load current through the test object, a measuring resistor R_m equal to the characteristic impedance of the measuring cable, which is commonly 50 Ω, is employed and shunted by an appropriately designed inductance. Under this condition, however, the transient voltage appearing across the measuring impedance is proportional to the transient current flowing through the leads of the test object. Consequently, this signal must be integrated to measure the charge of the PD pulses, which is performed by the PD instrument, as described in Sects. 4.3.3 and 4.3.4, respectively.

Even if the highest measuring sensitivity is achieved if the measuring impedance is connected between LV side of the test object and ground, this approach is not applicable in general. On one hand, the ground connection lead of the test object cannot be interrupted in many cases, and on the other hand, the measuring impedance must carry the complete load current through the test object and additionally the fast transient current that occurs in case of an unexpected

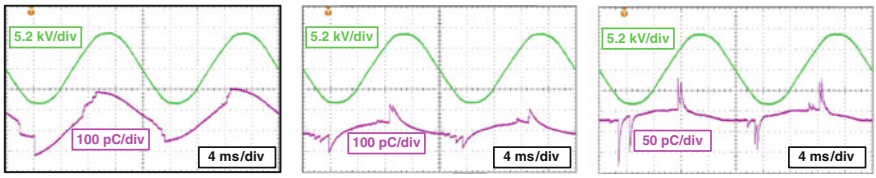

Fig. 4.15 Records of the voltage signal captured from a RC measuring impedance connected in series with a point-to-plane electrode arrangement (*violet trace*) and associated AC test voltage (*green trace*)

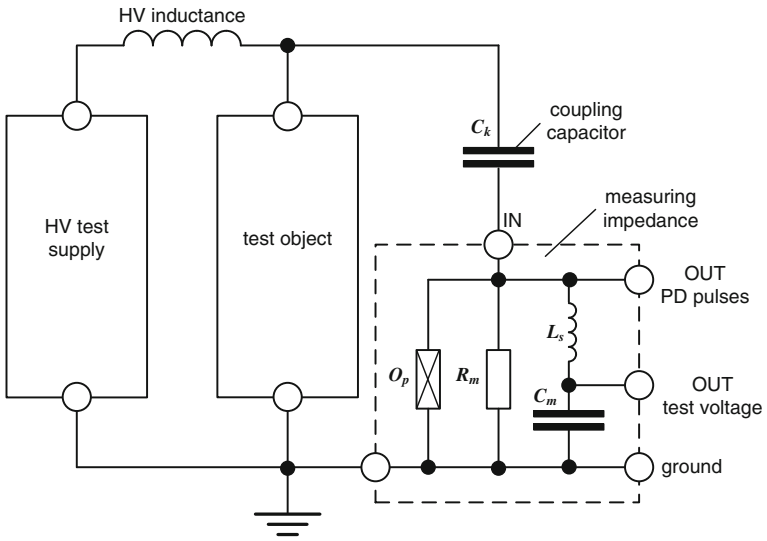

Fig. 4.16 PD measuring circuit using a coupling capacitor in series with a measuring impedance

breakdown and might exceed the kA range. Thus, the measuring impedance is commonly connected in series with the coupling capacitor C_k, as illustrated in Fig. 4.16. Here, the measuring resistor R_m must be shunted by an inductance L_m to carry the alternating load current trough the coupling capacitor. The over-voltage protection unit O_p is required to suppress fast over-voltages due to an insulation breakdown, which could damage not only the measuring impedance but also the measuring instrument. As the PD coupling unit shown in Fig. 4.16 provides a high-pass filter, the lower limit frequency f_1 should be chosen preferably below 100 kHz to capture the complete frequency spectrum of the transient PD current recharging the test object capacitance after each PD event, as discussed previously.

Example To design a coupling device according to Fig. 4.16, which is intended for induced voltage tests of power transformers, the following parameters shall be assumed:

Lower limit frequency:	$f_l = 50$ kHz
Effective measuring impedance:	$R_m = 1$ kΩ
Maximum applied test voltage level:	$V_a = 200$ kV
Maximum test frequency:	$f_{ac} = 400$ Hz

From the lower limit frequency,

$$f_l = \frac{1}{2\pi \cdot C_k \cdot R_m} = 50 \text{ kHz}$$

follows for the minimum capacitance required for the coupling capacitor

$$C_k = \frac{1}{2\pi \cdot f_l \cdot R_m} \approx 3.2 \text{ nF}.$$

Applying the maximum exciting frequency $f_{ac} = 400$ Hz to the transformer under test, the load current through the coupling capacitor becomes

$$I_c = 2\pi \cdot f_{ac} \cdot C_k \cdot V_{ac} = 1.6 \text{ A}.$$

If flowing through the measuring resistor $R_m = 1$ kΩ, this current would cause a voltage drop of 1,600 V, which would be extremely harmful for the operator as also for the connected PD measuring instrument. Thus, the voltage drop across R_m must substantially be reduced. This can effectively be achieved if R_m is shunted by an inductance L_s, as obvious from Fig. 4.16. Applying this option, it has to be taken care, however, that the lower limit frequency is not significantly decreased, which is accomplished for

$$2\pi \cdot f_m \cdot L_s \geq 5R_m; \quad L_s \geq 16 \text{ mH}$$

For the considered maximum test frequency $f_{ac} = 400$ Hz, the inductive impedance of L_s becomes

$$Z_l = 2\pi \cdot f_{ac} \cdot L_s \approx 40\ \Omega.$$

Under this condition, the load current $I_c = 1.6$ A flowing through the coupling capacitance $C_k = 3.2$ nF causes a voltage drop across L_s of only 64 V. This value can further be reduced using a high-pass filter of higher order, which shall not be investigated here.

To display the phase-resolved PD pulses by means of an oscilloscope or a computer-based PD measuring system, the PD coupling unit can be configured inserting a measuring capacitor, designated in Fig. 4.16 as C_m. Due to the very different frequency spectra of both the PD pulses and the AC test voltage, the associated signals appear completely separated at the outputs "PD pulses" and "test voltage". If, for instance, the above-introduced maximum test voltage level of $V_{ac} = 200$ kV is applied, which should be attenuated down to 50 V, a divider ratio of 1:4,000 is required. For a coupling capacitor $C_k = 3.2$ nF, a low-voltage measuring capacitance of $C_m = 12.8$ μF is required.

4.3.2 PD Measuring Circuits According to IEC 60270

A survey on the basic *PD measuring circuits* recommended in IEC 60270: 2000 is shown in Fig. 4.17. To avoid any danger for the operator, the measuring impedance should always be placed inside the HV test area. Moreover, it has to be taken care that the HV leads are PD-free up to the highest test voltage level. The grounding leads for current return should be kept as short as possible and made of

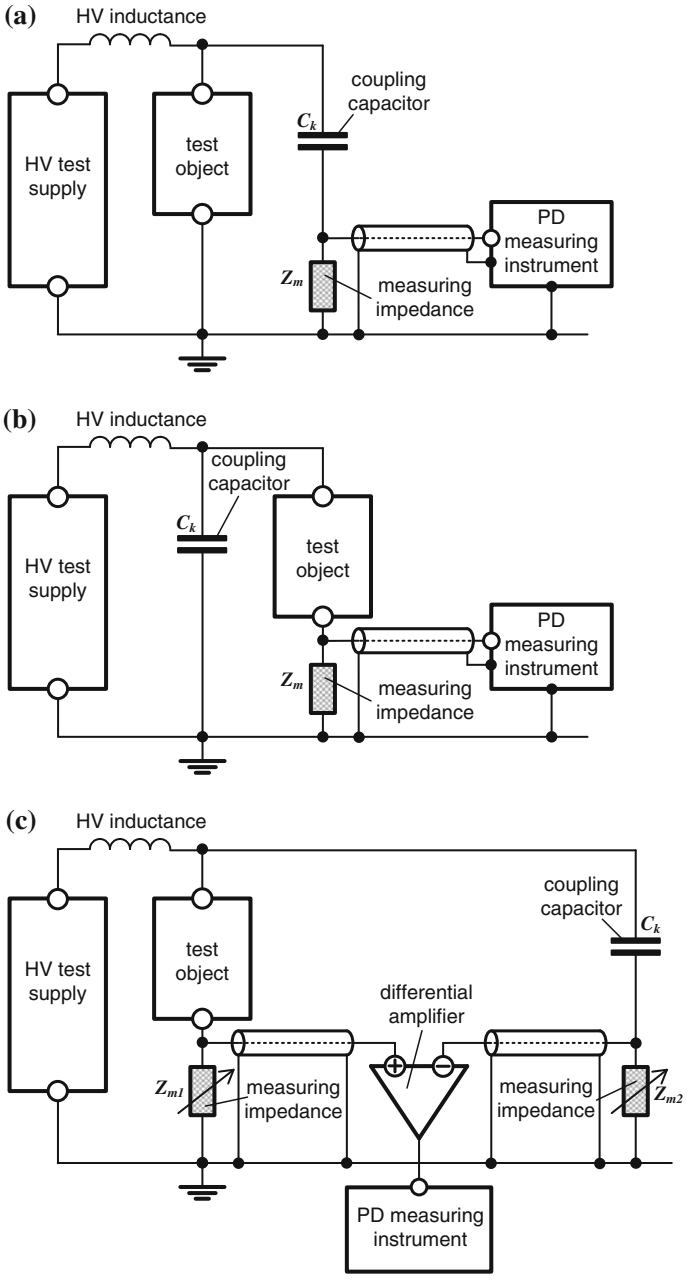

Fig. 4.17 Basic PD measuring circuits according to IEC 60270: 2000. **a** Measuring impedance in series with coupling capacitor for grounded test objects **b** test object grounded via the measuring impedance **c** bridge circuit for noise reduction

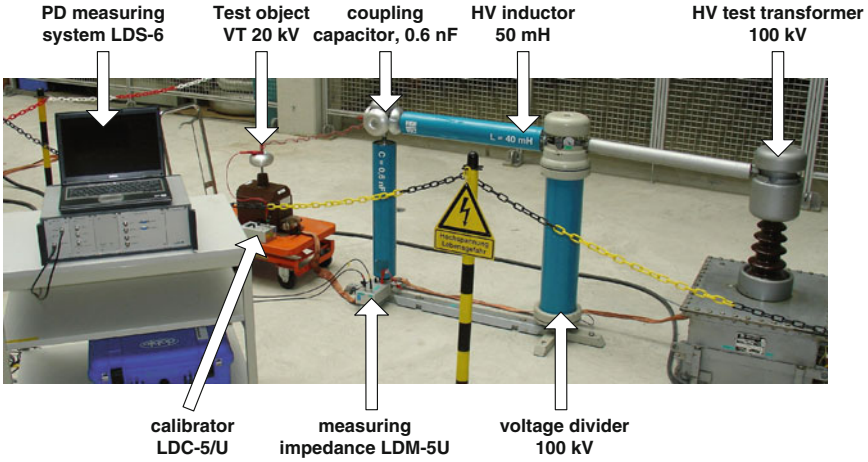

Fig. 4.18 PD measuring circuit designed according to IEC 60270 (Courtesy of Doble Lemke)

Cu or AL foil (approx. 100 mm in width) to minimize the inductance in the higher-frequency range and thus the impact of electromagnetic interferences on PD test results. For more information in this respect see Sect. 9.2.2. The most commonly employed coupling mode is the use of a coupling capacitor in series with a measuring impedance, as shown in Fig. 4.18 and presented more in detail previously based on Fig. 4.16.

Electromagnetic noises disturbing sensitive PD measurements can be eliminated at certain extend if the so-called balanced PD bridge shown in Fig. 4.17c is adopted. Here, the adjustable measuring impedances Z_{m1} and Z_{m2} are installed in the ground connection leads of the test object, providing the measuring branch, and the coupling capacitor, providing the reference branch. Adjusting Z_{m1} and Z_{m2} accordingly, the bridge can be balanced. That means the common mode noises appearing at the high-voltage terminals are more or less suppressed by the differential amplifier so that only the PD signal originating in the test object appears at the output and is thus measured by the PD instrument. To ensure a high common mode rejection, the bridge should be designed as symmetrical as possible. Thus, it is advisable to use instead of the coupling capacitor a complementary PD-free test object as reference. Despite of the benefits of the balanced bridge for noise suppression, this is not generally employed in practice because the design is a challenge due to the fact that both branches must have an equivalent frequency response over the full bandwidth used for the PD signal processing.

An option is the so-called *bushing tap coupling* mode shown in Fig. 4.19. This circuit is commonly employed for capacitive-graded bushings equipped with a bushing tap originally intended for C/tan δ measurements, where the HV bushing capacitance C_1 provides in principle the coupling capacitor C_k shown in Fig. 4.17a.

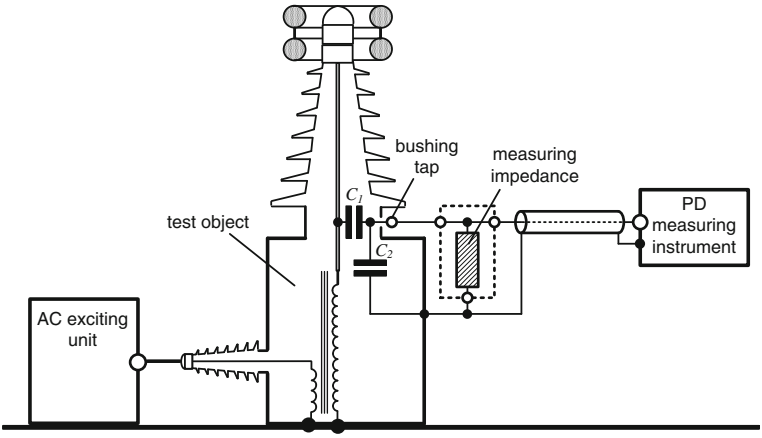

Fig. 4.19 Set-up for an induced voltage test of a power transformer using the bushing tap coupling mode

4.3.3 PD Signal Processing

As discussed in Sect. 4.2.2, the time integral of the transient PD current flowing through the connection leads of the test object is more or less correlated with that charge amount flowing through the PD defect. That means the pulse charge is invariant even if the transient current is substantially distorted due to attenuation, dispersion and reflection phenomena when travelling through large test objects. Thus, the transient voltage appearing across a resistive measuring impedance must be integrated to measure the pulse charge. This can conveniently be achieved by a so-called quasi-integration using a *band-pass filter*, i.e. if the signal processing is performed in a frequency range where the amplitude–frequency spectrum of the captured PD pulses is nearly constant, as shown in Fig. 4.20 (Kind 1963; Kuffel et al. 2006; Schon 1986; Zaengl and Osvath 1986; König and Narayana 1993; Lemke 1997). Practical experience revealed that this requirement is accomplished for most test objects using an upper limit frequency not higher than 1 MHz.

Depending on the bandwidth $\Delta f = f_2 - f_1$ used for PD signal processing, it is generally distinguished between *wide-band instruments* and narrow-band instruments. For wide-band PD measurements on technical test objects, the following frequency parameters are recommended in the Amendment to IEC 60270: 2000:

$$\begin{aligned} \text{Lower limit frequency:} &\quad 30\ \text{kHz} \leq f_1 \leq 100\ \text{kHz} \\ \text{Upper limit frequency:} &\quad 130\ \text{kHz} \leq f_2 \leq 1{,}000\ \text{kHz} \\ \text{Bandwidth:} &\quad 100\ \text{kHz} \leq \Delta f \leq 970\ \text{kHz} \end{aligned}$$

Note According to IEC 60270: 2000, the term "wide-band" is deduced from the band-pass filter characteristics of the PD processing unit having a bandwidth $\Delta f = f_2 - f_1$, which is substantially greater than the lower limit frequency f_1. In this context, it must be

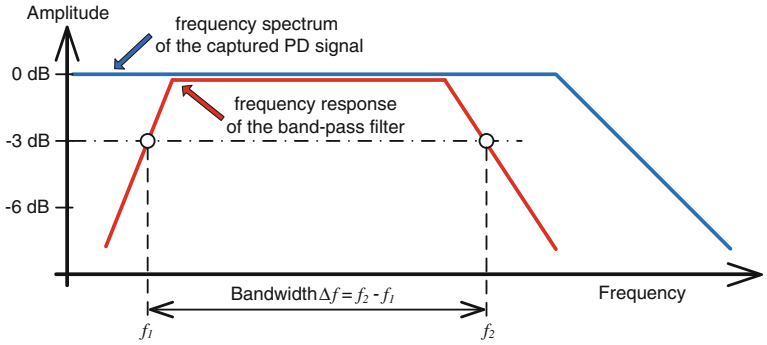

Fig. 4.20 Comparison between frequency spectrum of PD pulses and bandwidth recommended for PD pulse charge measurements

emphasized that this term is not correlated with the frequency spectrum of real PD current pulses, which might cover a frequency range up to the GHz range, as shown in Sect. 4.1.

The pulse response of a band-pass filter having an upper and a *lower limit frequency* of $f_2 = 320$ kHz and $f_1 = 40$ kHz, respectively, is shown in Fig. 4.21a. Based on the network theory, it can be concluded that the magnitude of the output pulse is proportional to the time integral of the input current pulse where the output signal is significantly stretched if compared with the input pulse.

It seems noticeable that the integration performance is governed only from the *upper limit frequency* f_2, but not from the lower limit frequency f_1. Thus, also narrow-band filter circuits could be used in principle, which are characterised by a bandwidth Δf much below the centre frequency $f_0 = (f_2 - f_1)/2$ required for the quasi-integration of the captured PD signal. Under this condition, the maximum value of the envelope of the oscillating response is direct proportional to the pulse charge, as can be deduced from the network theory (Schon 1986). A typical measuring example is shown in Fig. 4.21b, which refers to the PD pulse response of a narrow-band amplifier characterized by a centre frequency of $f_0 = 720$ kHz and a bandwidth of $\Delta f = 9$ kHz, respectively.

Using the narrow-band PD signal processing (Fig. 4.21b), the following frequency parameters are recommended in IEC 60270: 2000:

$$\begin{aligned} &\text{centre frequency:} && 50\ \text{kHz} \leq f_o \leq 1,000\ \text{kHz} \\ &\text{bandwidth:} && 9\ \text{kHz} \leq \Delta f \leq 30\ \text{kHz} \end{aligned}$$

The main advantage of the *narrow-band amplifiers* is the noise immunity because continuous high-frequency noises received from radio broadcasting stations can effectively be rejected, tuning the centre frequency f_0 accordingly, as discussed in Sect. 4.5. In this context, it should be emphasized that fatal superposition errors might appear due to the comparatively long duration of the oscillating response, which might exceed several 100 µs. As an example, Fig. 4.22 shows the response of a narrow-band amplifier against double pulses, which may

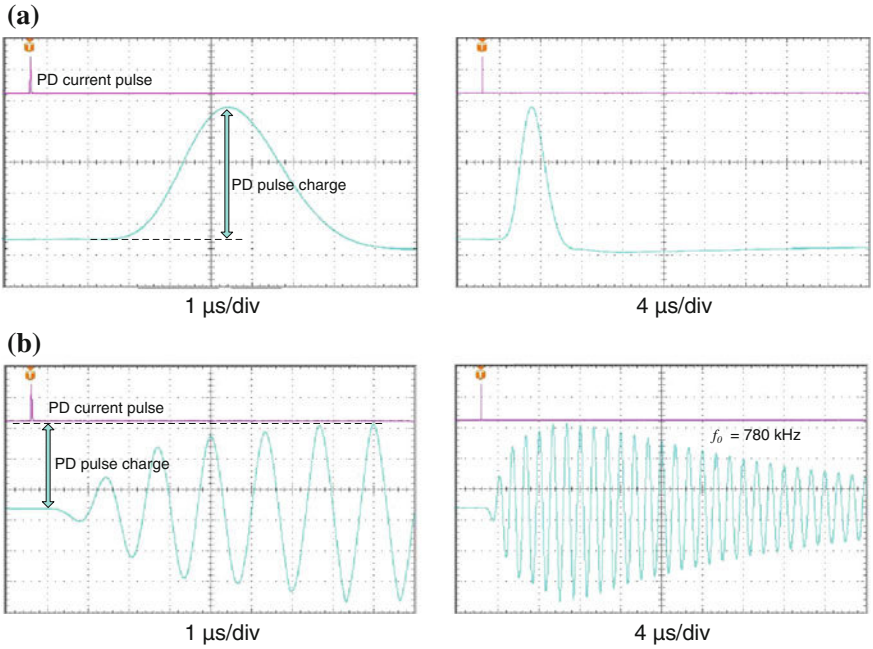

Fig. 4.21 PD pulse responses of a wide-band (**a**) and a narrow-band (**b**) processing unit. **a** Lower limit frequency $f_1 = 40$ kHz and upper limit frequency $f_2 = 320$ kHz. **b** Mid-band frequency $f_0 = 780$ kHz and bandwidth $\Delta f = 9$ kHz

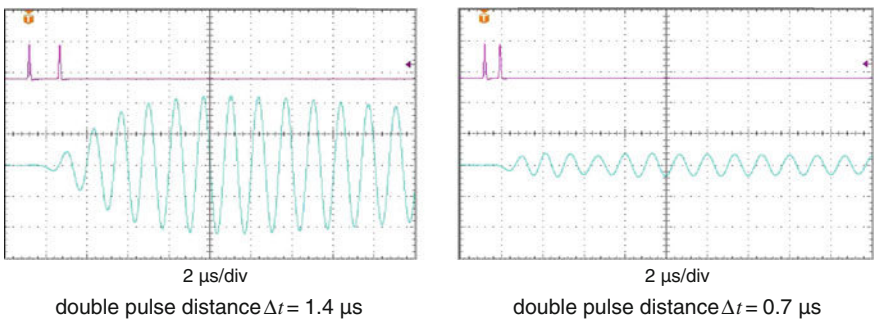

Fig. 4.22 Impact of the double-pulse distance on the oscillation magnitude of a narrow-band PD processing unit

occur if PD tests of power cables are performed, as discussed in Sect. 4.4. The magnitude of the excited oscillations decreases substantially if the time interval between both pulses is reduced from originally 1.4 µs down to 0.7 µs. A similar behaviour is encountered for inductive test objects, such as power transformers and rotating machines, where oscillations are excited in the windings due to the fast PD

transients. Similar phenomena may also occur at comparatively high repetition rate of the PD pulses. Thus, narrow-band amplifiers are not recommended in general for measuring the PD pulse charge in terms of pC under practical condition.

4.3.4 PD Measuring Instruments

4.3.4.1 General

To evaluate the PD severity of HV apparatus, chemical, optical, acoustical and electrical measuring methods have been introduced in the past. In the following, only instruments intended for electrical PD measurement in compliance with IEC 60270: 2000 will be considered.

The first facilities used for the recognition of harmful PD defects were Schering bridges in combination with oscilloscopes, where the detection sensitivity was comparatively low. A substantial progress was made in the 1920s when the first superheterodyne receivers equipped with narrow-band amplifiers were available (Armann and Starr 1936; Dennhardt 1935; Koske 1938; Lloyd and Starr 1928; Müller 1934; Schering 1919). The requirements for such instruments intended for PD detection were first specified in the USA and North America in 1940, when the "*National Electrical Manufactures Association NEMA*" published the standard "*Methods for Measuring Radio Noise*", which was later revised by the *NEMA Publication 107* "*Methods of Measurement of Influence Voltage (RIV) of High-Voltage Apparatus*", issued in 1964. An equivalent standard for RIV measurements of HV apparatus was also edited in Europe by the "*Comité International Spécial des Perturbation Radioélectrique (CISPR)*", which appeared in 1961.

As *radio interference voltages* (*RIV*) are commonly weighted based on the acoustical noise impression of the human ear, these are not correlated with the charge of PD pulses expressed in terms of pC, as confirmed by experimental studies (Harrold and Dakin 1973; Vaillancourt et al. 1981). Moreover, fatal superposition errors might appear in case of high PD pulse repetition rates or in case of reflections and oscillations excited by the fast PD transients, as discussed previously. As a consequence, the *"International Technical Commission (IEC), Technical Committee No. 42: High-Voltage Testing and Measuring Technique"* decided the edition of a separate standard on PD measurements. The first edition of "*IEC Publication 270*" appeared in 1968, where besides the definition of the *PD quantity "apparent charge*" as well as the inception and extinction voltages, several other PD quantities were introduced, such as the repetition rate as well as the energy and power of consecutive PD pulses. Additionally, rules for calibrating PD measuring circuits were specified and guidelines were attached which refer to the identification of typical PD sources based on oscilloscopic records using either the elliptical or the linear time base for displaying phase-resolved PD pulse sequences along each cycle of the applied AC test voltage.

The second edition of IEC Publication 270 appeared in 1981, which contained more details on the calibration procedure. Additionally, the PD quantity "*largest repeatedly occurring PD charge*" was specified. Based on this standard, the electrical PD measurement has been proven as an indispensable tool for tracing dielectric imperfections in HV apparatus, which might be caused not only by design failures and dielectric impurities but also by a poor assembling work. Therefore, the increased quality requirements as well as the enhancement of the electric field strength and last but not least the demands on an enlargement of the lifetime of HV equipment required not only an early detection of severe PD events but also reproducible and well comparable test results.

The following treatment is based on the third edition IEC 60270, which appeared in 2000 and can be considered as an extensive revision of the second edition. The specification covers not only the traditional analogue PD signal processing but also the digital acquisition and processing of the captured PD pulses. Moreover, a section has been added which refers to maintaining the characteristics of PD measuring systems and the associated calibrators, as will be considered in Sect. 4.3.7.

4.3.4.2 Analogue PD Instruments

A simplified block diagram representative for analogue PD instruments is shown in Fig. 4.23. The desired measuring sensitivity is adjusted by means of an attenuator at the input of the device. This is commonly equipped with a fast overvoltage protection unit to avoid a damage of the instrument in case of an unexpected breakdown of the test object. The desired integration of the PD signal is performed by an amplifier providing a band-pass filter, as treated previously. As alternative, also a wide-band amplifier in combination with an electronic integrator can be used (Lemke 1969), as illustrated in Fig. 4.23. This offers the possibility to record the true shape of the captured PD signal, which can advantageously be used for the localization of the PD site, as described in Sect. 4.4. Another benefit of this concept is that pulse-shaped noises can effectively be rejected using an automatic gating, as described also in Sect. 4.5.

The quasi-peak detector in combination with the reading instrument is intended to measure the "*largest repeatedly occurring PD magnitude*" according to IEC 60270: 2000. This concept has been introduced to get a more or less constant reading even if the pulse magnitudes are scattering over an extremely large range, as exemplarily shown in Fig. 4.24. Another benefit of this concept is that stochastically appearing noise pulses of low repetition rate can effectively be rejected. As specified in IEC 60270: 2000, the charging and discharging time constant of the quasi-peak detector should be $\tau_1 \leq 1$ ms and $\tau_2 \approx 440$ ms, respectively, to accomplish the pulse train response according to Fig. 4.25. It should be emphasized that this approach ensures only reproducible test results for power frequency (50/60 Hz) test voltages, but not if the test frequency is varied, as usual for PD tests of power transformers and instrument transformers, where the test frequency

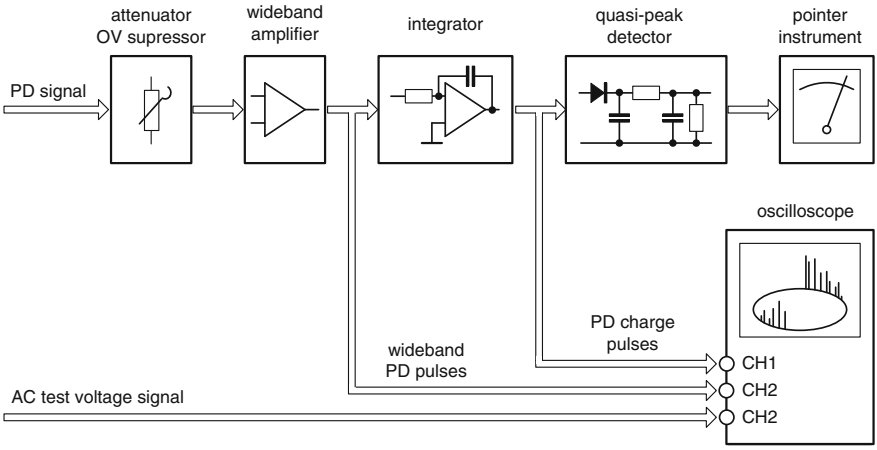

Fig. 4.23 Simplified block diagram of an analogue PD instrument

is occasionally increased up to 200 Hz, as well as for on-site PD tests of power cables, where the test frequency may vary between 20 Hz and 400 Hz (Rethmeier et al. 2012).

Measuring partial discharges, it is highly recommended to display the *phase-resolved charge pulses*, which enables often the identification of potential PD defects as well as the recognition of disturbing noises. For this purpose, either the built-in oscilloscope can be used or even an external connected multichannel oscilloscope.

As discussed previously, narrow-band instruments are not recommended for pulse charge measurements in terms of pC. Nevertheless, such devices, which are commonly designed for measuring the electromagnetic capability (EMC) of communication systems and other electronic units, are even nowadays employed for PD diagnostics of HV apparatus, particularly under on-site condition due to their noise immunity. Even if the PD signal is measured in terms of μV and not in terms of pC, there is no doubt that the PD inception and extinction voltage can well be determined. Moreover, information on the PD trending is obtained which is valuable for an insulation condition assessment.

4.3.4.3 Digital PD Instruments

Due to the achievements in digital signal processing (DSP), the traditional analogue PD measurement is increasingly replaced by the advanced digital technique. The first computerized PD measuring instrument has been employed by Tanaka and Okamoto (1978). After that, numerous concepts for digital PD signal processing have been proposed as, for instance, by Kranz (1982), Haller and Gulski (1984), Okamoto and Tanaka (1986), van Brunt (1991), Gulski (1991), Kranz and

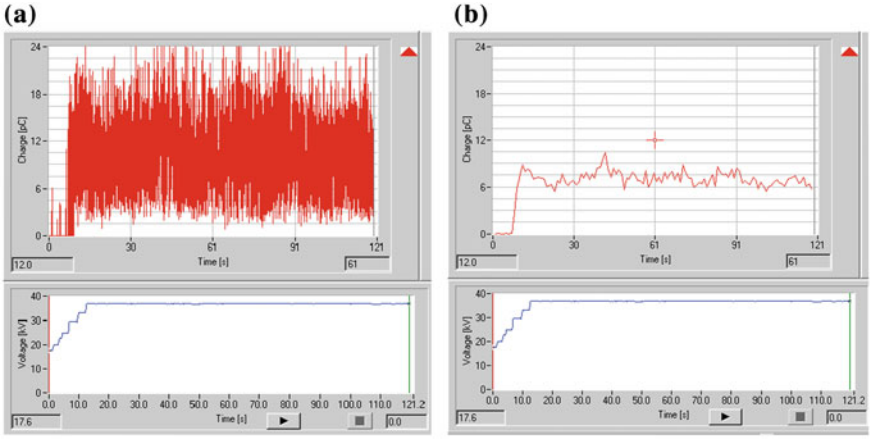

Fig. 4.24 Screenshots of a computerized PD measuring system showing PD level of a MV power cable termination subjected to a 50-Hz test voltage level of 38 kV, recording time 120 s. **a** Peak values of each individual charge pulse. **b** Largest repeatedly occurring PD magnitude according to IEC 60270: 2000

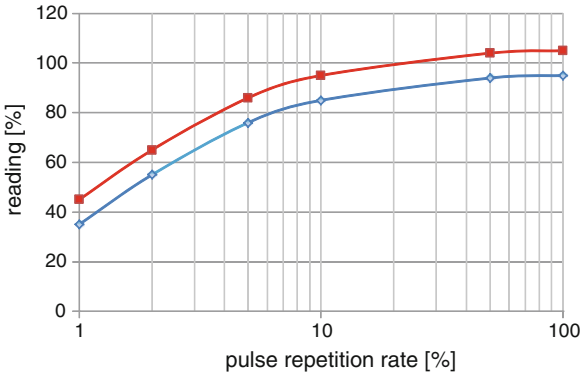

Fig. 4.25 Pulse train response specified in IEC 60270: 2000 for measuring the largest repeatedly occurring PD magnitude

Krump (1992), Fruth and Gross (1994), Shim (2000), Lemke et al. (2002), Plath et al. (2002).

Currently, two basic measuring principles are in use. The first one is illustrated in Fig. 4.26a, which utilizes an *analogue pre-processing unit* to establish the charge signal of the PD pulses, as treated previously. After that, a *digital signal processing* is performed, where a comparatively low sampling rate is required for the A/D conversion. Another option is the use of a very fast A/D converter to digitize the PD signal captured from the test object. The band-pass filtering required for the quasi-integration of the PD pulses is commonly performed by an adjustable digital filter and a numerical integrator. The main advantage of digital

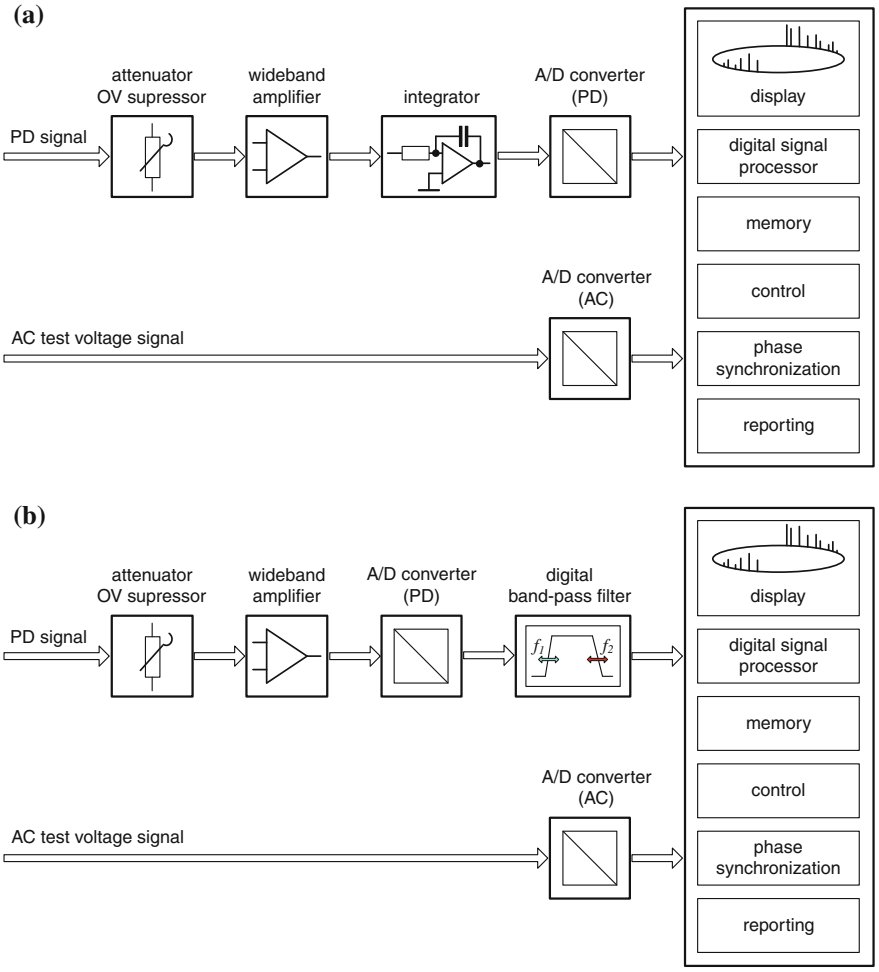

Fig. 4.26 Block diagram of digital PD instruments. **a** Analogue pre-processing of the PD signal. **b** Direct conversion of the wide-band amplified PD signal

PD measuring instruments is the ability to acquire and store the following characteristic PD parameters:

t_i instant of PD occurrence
q_i pulse charge at t_i
u_i test voltage value at t_i
ϕ_i phase angle at t_i

These parameters ensure not only an evaluation of all PD quantities recommended in IEC 60270: 2000 but also an in-depth analysis of the very complex PD occurrence using the following basic features:

- Statistical analysis using phase-resolved 2D and 3D pattern and pulse sequence pattern capable for classification and identification of PD sources as well as for noise rejection.
- Clustering the PD pulses in homogenous families, based on waveform analysis and spectral amplitude diagrams in order to separate the PD pattern of different PD sources.
- Localization the PD sites using either time-domain reflectometry for power cables or multichannel techniques for electrical machines and power transformers.

More details on the capabilities of digital PD measuring systems (Fig. 4.27) are presented in Sects. 4.4–4.8.

4.3.5 Calibration of PD Measuring Circuits

The aim behind the *PD calibration procedure* is to determine the scale factor S_f required for the calculation of the pulse charge q_a from the magnitudes of the PD pulses denoted M_p indicated by the reading instrument in terms of scales, or even in terms of divisions if recorded by an oscilloscope. For this purpose, a calibrating charge of known magnitude q_0 is injected in the terminals of the test object, which causes the pulse magnitude M_0. Based on this, it can be written:

$$q_a = \frac{q_0}{M_0} \cdot M_p = S_f \cdot M_p. \tag{4.18}$$

This procedure is based on the fact that each PD event is associated with a pulse charge transfer from the capacitance C_a to the PD site which causes a fast voltage step ΔV_a across the electrodes of the test object, as described in Sect. 4.2. An equivalent response is obtained by means of the calibrating circuit illustrated in Fig. 4.28 (Lemke et al. 1996; Lukas et al. 1997).

Example Assuming that a calibrating charge of $q_0 = 200$ pc is injected in the terminals of the test object. This shall cause a pulse magnitude of 5.4 divisions on the display of an oscilloscope connected to the PD instrument. Thus, the scale factor becomes $S_f = 200$ pC/5.4 div $= 3.7$ pC/div. Performing an actual PD measurement, a reading of 8.6 div is obtained. Consequently, the PD pulse magnitude can be accounted for as $q_a = (3.7 \text{ pC/div}) \times 8.6 \text{ div} \approx 32$ pC.

In practice, it seems reasonable to substitute the two capacitances C_{01} and C_{02} shown in Fig. 4.28 by only a single calibrating capacitor C_0 to be connected between pulse generator and the HV termination of the test object, whereas the other output of the pulse generator is connected directly to the housing of the device and thus also connected to the LV termination of the test object, as obvious from Fig. 4.29.

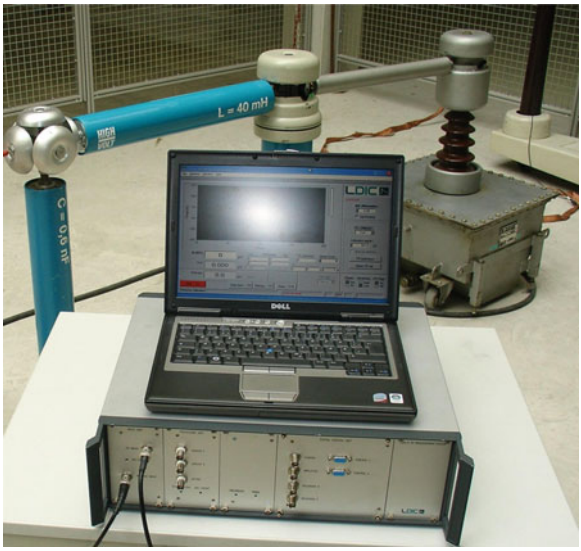

Fig. 4.27 View of a digital PD measuring system (Courtesy of Doble Lemke)

Typical oscilloscopic records (Fig. 4.30) are gained by the injection of a calibrating pulse (CH 1) at the HV site of a 110-kV transformer bushing using the bushing tap coupling mode. The calibrating signal appearing across the measuring impedance is differentiated (CH 2). This is due to the high-pass response of the series connection of the HV bushing capacitance, which was close to 200 pF, and the resistive measuring impedance having a value of 50 Ω so that the characteristic time constant is about 10 ns. Thus, this signal has been integrated (CH 3) using an electronic integrator to get the charge signal which is proportional to the step voltage, as expected based on the network theory.

To ensure reproducible test results, the step voltage shape of the calibrator is specified in the Amendment to IEC 60270: 2000 by the following time and voltage parameters obvious from Fig. 4.31:

rise time:	$t_r \leq 60$ ns
time to steady state:	$t_s \leq 200$ ns
step voltage duration:	$t_d \geq 5$ µs
absolute voltage deviation:	$\Delta V \leq 0.03\ V_o$

To minimize distortions of the step voltage, which might occur at comparatively high capacitive load, the calibrating capacitor C_0 should be as low as possible, preferably below 200 pF. Additionally, the condition $C_0 \leq 0.1\ C_a$ should be satisfied, to accomplish the complete charge transfer from the calibrator to the test object capacitance C_a.

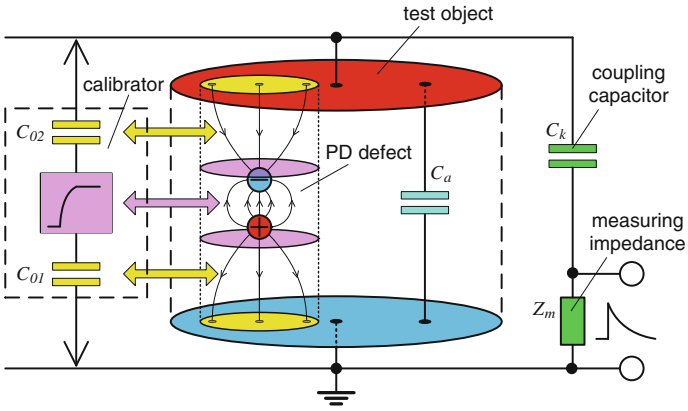

Fig. 4.28 Set-up for calibrating of PD measuring circuits

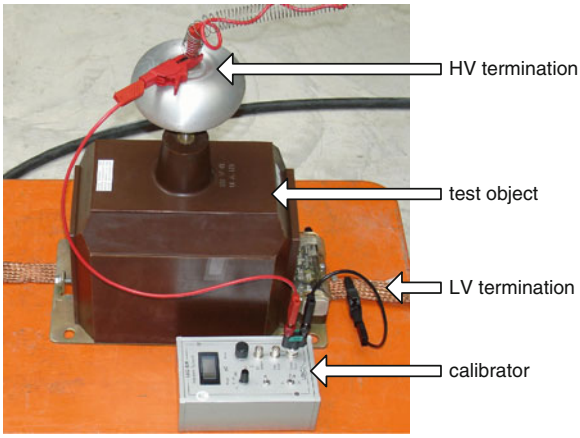

Fig. 4.29 Calibrator connected to a 20 kV instrument transformer

4.3.6 Performance Tests of PD Calibrators

To verify the characteristic time and voltage parameters of PD calibrators specified in the Amendment to IEC 60270: 2000, a performance test is required. The simplest approach would be the injection of the charge q_0 created by the calibrator into a measuring capacitor C_m, as shown in Fig. 4.32a. To apply the equation $q_0 = C_m \cdot \Delta V_m$, the condition $C_m \geq 100\ C_0$ is necessary for the complete charge transfer. If, for instance, the calibrator is equipped with a capacitor of $C_0 = 100$ pF, the measuring capacitor should be $C_m \geq 10$ nF. Applying a conventional foil capacitor to guarantee a high-temperature stability, however, the front of the step pulse is drastically distorted due to the inherent inductive component, as obvious from Fig. 4.32b which refers to a calibrating charge of

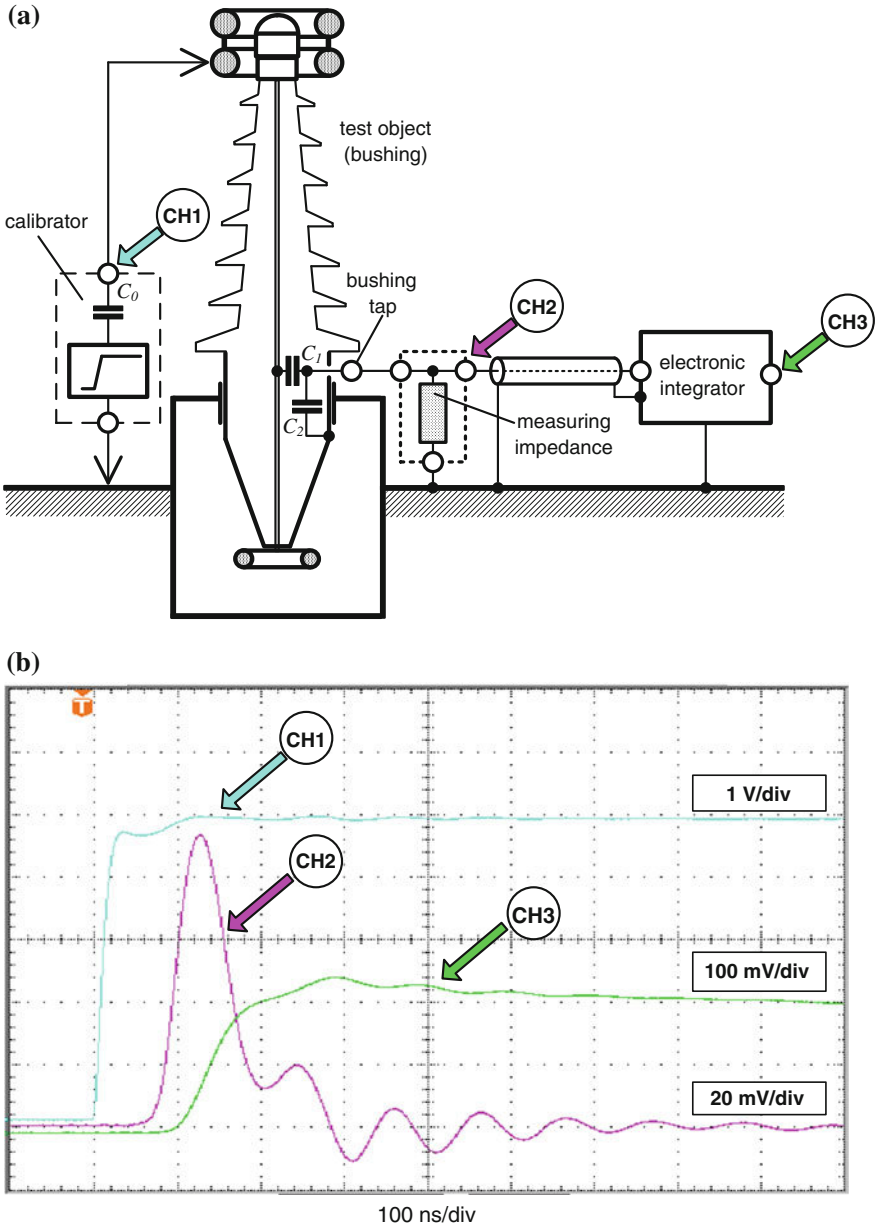

Fig. 4.30 Set-up for calibration a 110-kV transformer bushing (**a**) and characteristic signals appearing at the output of the calibrator (CH1) and at the bushing tap (CH2) as well as at the output of the electronic integrator (CH3) (**b**)

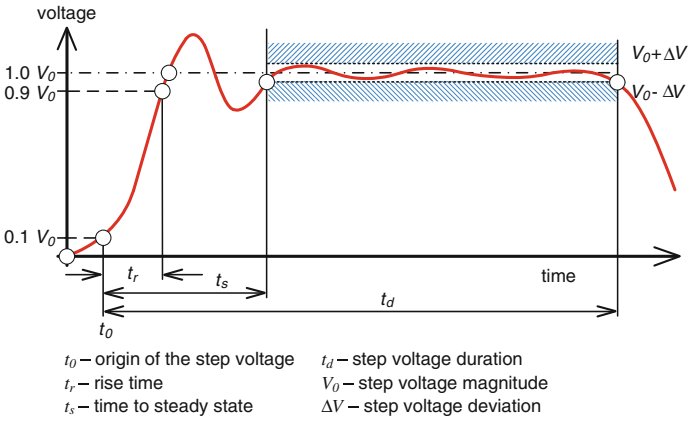

Fig. 4.31 Step voltage parameters of PD calibrators (Draft of amendment 2013 to IEC 60270: 2000)

$q_0 = 120$ pC. To overcome this crucial problem, an appropriate damping resistor R_d should be connected in series between calibrator and measuring capacitor, as shown in Fig. 4.32c. Another option is the use of numerous parallel connected capacitors of lower capacitance to reduce the effective inductance.

The main drawback of the circuit shown in Fig. 4.32a is, however, that calibrating charges below 50 pC can hardly be measured at desired uncertainty by means of conventional digital oscilloscopes, even if the averaging mode for minimizing the background noise is applied: For $C_m = 10$ nF, the voltage jump for $q_0 = 50$ pC amounts to only $\Delta V_m = 5$ mV, which requires the measurement of a voltage deviation below 0.2 mV. To overcome this crucial problem, an electronic integrator can be employed to enhance the measuring sensitivity accordingly (Lemke 1996). The schematic diagram of the circuit shown in Fig. 4.33 ensures the complete charge transfer from the calibrator to the integrating capacitor C_m, even if the capacitance is reduced from originally 10 nF down to approx. 100 pF. As obvious from the oscilloscopic records shown in Fig. 4.33, which refers to a calibrating charge of approx. 6 pC, a sufficient high-voltage magnitude of approx. 60 mV is achieved, which can accurately be measured. It seems noticeable that despite the comparatively low integrating capacitance of only 100 pF, the decay time constant is sufficiently high (Fig. 4.33c). The voltage magnitude of CH 2 decreases only slightly within the time interval of 5 μs, which corresponds to the step voltage duration t_d specified in the Amendment to IEC 60270: 2000.

Another option recommended in IEC 60270 is the injection of the calibrating charge into a known measuring resistor R_m, as illustrated in Fig. 4.34a. Because the series connection of C_0 with R_m represents a high-pass filter, the time-dependent voltage $v_m(t)$ appearing across R_m must be integrated to determine the charge q_0 created by the calibrator under test. For this purpose, usually the numerical integration is adopted using a digital oscilloscope equipped with such a

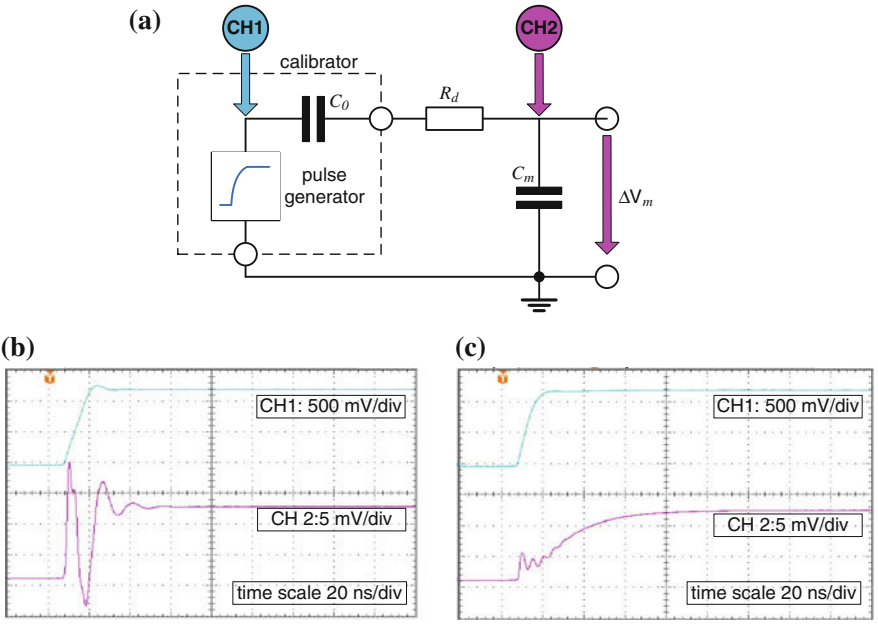

Fig. 4.32 Set-up for measuring the calibrating charge (**a**) and typical oscilloscopic records using a damping resistor of $R_d = 0\ \Omega$(b) and $R_d = 390\ \Omega$(c), respectively

feature. The A/D converter applied should have a vertical resolution of 10 bits at 50 MS/s sampling rate to achieve an adequate resolution of the digitized input signal. Additionally, the analogue bandwidth should be above 50 MHz, where the oscilloscopes should be calibrated according to IEC 61083-1: 2002.

4.3.7 Maintaining the Characteristics of PD Measuring Systems

The third edition of IEC 60270: 2000 introduced the following three levels for maintaining the characteristics of PD measuring devices consisting of the coupling device, the PD instrument and the PD calibrator as well as the associated measuring connection leads:

1. The routine calibration of the complete PD measuring system connected to the HV test circuit that is performed prior to a PD test. This calibration provides the scale factor S_f of the system to be used in the actual PD test. Nowadays, it is mainly used to adjust the reading of the instrument to obtain a direct reading of the PD magnitude, i.e. S_f should satisfy preferable values (e.g. 1, 2, 5, 10,

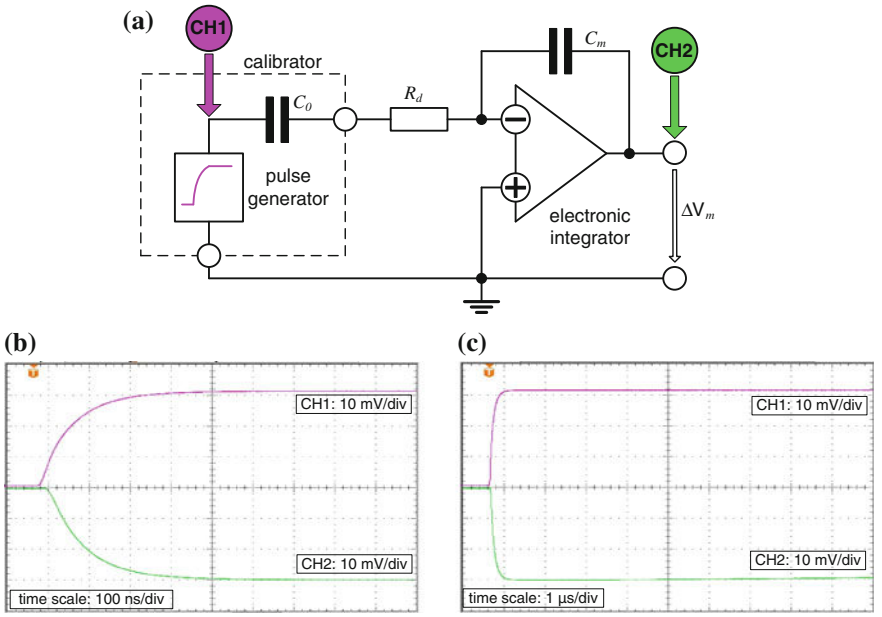

Fig. 4.33 Principle of an electronic integrator for measuring the charge of calibrators (**a**) and typical oscilloscopic records at time scale of 100 ns/div (**b**) and 1 µs (**c**), respectively

20….). For this routine calibration, there are no major changes as compared to the IEC edition of 1981.
2. The determination of the specified characteristics of the complete PD measuring system should be performed at least once a year or after major repair.
3. The calibration of the PD calibrator.

In general, manufacturers of PD measuring devices provide the necessary guidelines for the verification of the specified technical parameters. Independent from such guidelines the third edition of IEC 60270: 2000 recommends additional test procedures, where the results are recorded in a "Record of Performance (RoP)" established and maintained by the user. The RoP should include the following information:

- Nominal characteristics (identification; operation conditions, measuring range, supply voltage)
- Type test results
- Routine test results
- Performance test results (date and time)
- Performance check results (date and time; result: passed/failed: if failed: action taken)

Verifications of PD measuring systems and PD calibrators shall be performed once as acceptance tests. Performance tests should be performed annually or after

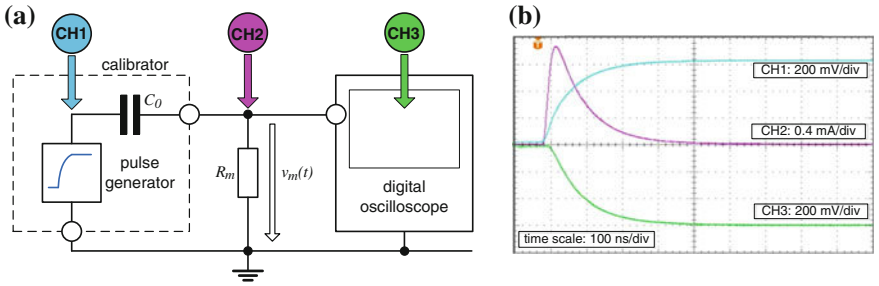

Fig. 4.34 Set-up for numerical integration of the calibrating charge q_0 injected in a measuring resistor of $R_m = 50\ \Omega$(a) and a typical oscilloscopic record (**b**) which refers to $q_0 = 150$ pC

any major repair, but at least every 5 years. Performance checks have to be performed at least once a year. To maintain the characteristics of *PD measuring instruments*, the following tests should be performed:

(a) *Type tests* are to be done by the manufacturer and shall be performed for one PD measuring system of a series and shall at least include the determination of the following parameters:

- The frequency-dependent *transfer impedance Z(f)* and the lower and upper frequencies f_1 and f_2 over a frequency range in which it has dropped to 20 dB from the peak pass-band value;
- The *scale factor k* to calibrating pulses of at least three different pulse charge magnitudes ranging between 10 and 100 % of the full reading at a pulse repetition rate n around 100 s^{-1}. In order to prove the linearity of the PD measuring instrument, the variation of k shall be less than 5 %;
- The *pulse resolution time* T_r by applying calibration pulses of constant magnitude but decreasing time interval between consecutive pulses;
- *The pulse train response* for pulse repetition rates N ranging between 1 s^{-1} and >100 s^{-1}.

(b) *Routine tests* are to be done by the manufacturer and shall include all tests required in a performance test as listed below. Routine tests shall be performed for each measuring system of a series. If the test results are not available from the manufacturer, the required tests shall be arranged by the user.

(c) *Performance tests* shall include the determination of the following parameters:

- The frequency-dependent transfer impedance $Z(f)$ and the lower and upper frequencies f_1 and f_2 over a frequency range in which it has dropped to 20 dB from the peak pass-band value.
- The linearity of the scale factor k to be verified between 50 % of the lowest and 200 % of the highest specified PD magnitude. Using calibrating pulses of adjustable magnitude having a repetition rate of approximately $n = 100\ s^{-1}$, the scale factor k shall vary not more than 5 %.

(d) *Performance checks* shall include the determination of the transfer impedance $Z(f)$ at one frequency selected in the band-pass range in order to verify that the value deviates not more than 10 % from that one recorded in the performance test.

To maintain the characteristics of *PD calibrators*, the following tests should be performed:

(a) *Type tests* are to be done by the manufacturer and shall be performed for one PD calibrator of a series. Type tests shall include at least all tests required in a performance test. If results of type tests are not available from the manufacturer, the required tests for verification the technical parameters of PD calibrators shall be arranged by the user.
(b) *Routine tests* are to be done by the manufacturer and shall include all tests required in a performance test. Routine tests are to be performed by the manufacturer for each measuring system of a series. If the test results are not available from the manufacturer, the required tests shall be arranged by the user.
(c) *Performance tests* shall include the determination of the following parameters:
    - The actual magnitude of the pulse charge q_0 for all nominal settings, where a measuring uncertainty within 5 % or 1 pC, whichever is greater, is recommended.
    - Rise time t_r of the voltage step U_0, where a measuring uncertainty within 10 % is recommended.
    - Pulse repetition frequency N, where a measuring uncertainty within 1 % is recommended.
(d) *Performance checks* include the determination of the actual magnitude of the calibrating charge q_0 for all nominal settings, where a measuring uncertainty within 5 % or 1 pC, whichever is greater, is recommended.

4.3.8 PD Test Procedure

The main aim behind PD tests according to IEC 60270:2000 is to prove the integrity of insulation systems applied for HV apparatus and their components. The test procedures applied for quality assurance tests after manufacturing and repair as well as the test voltage levels and the limits of tolerated pulse charge magnitudes are deduced from long-term experience. They are specified for each kind of HV apparatus by the relevant Technical Committee. As the test procedures vary for the different HV equipment, only one typical application shall be presented in the following. This refers to an *induced voltage test* of a single-phase power transformer based on the test circuit sketched in Fig. 4.35. The PD test procedure applied can generally be divided into the following steps:

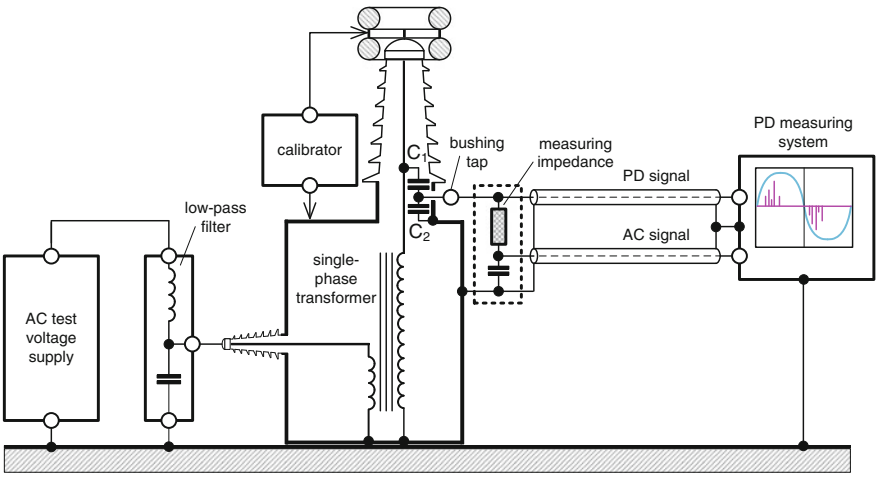

Fig. 4.35 Set-up applied for an induced voltage test of a power transformer using the bushing tap coupling mode for PD measurement

(a) Configuration of the HV test circuit:

To minimize the impact of noises the transformer under test should be well grounded. Moreover, the use of a *low-pass filter* at the LV site is highly recommended. Using the bushing tap coupling mode, the measuring impedance should be located as close to the test object and connected to the PD measuring instrument not only via the measuring cable but also via a ground connection lead made of Cu or Al foil. Occasionally shielding electrodes should be arranged on the top electrodes of the bushings, as obvious from Figs. 4.35 and 4.36 which refers to a 500 kV single-phase transformer. Moreover, it has to be taken care that the surface of the bushings is clean and dry to avoid any disturbing surface discharges. To record the phase-resolved PD patterns, additionally to the PD signal, a reference AC voltage should be taken from the measuring impedance connected to the bushing tap, as shown in Sect. 4.3.1 and Fig. 4.16.

(b) Adjustment of the *measuring frequency range*:

For tall and inductive test objects, such as power transformers, the frequency content of the detectable PD signal is drastically reduced. Thus, the upper limit frequency f_2 should be selected preferably below 300 kHz. To ensure a wide-band PD signal processing for measuring the PD pulse charge, the lower limit frequency f_1 should be adjusted below 100 kHz. Reducing f_1 substantially below this value, however, serious disturbances might appear due the possible iron core saturation of the transformer under test as well as other core-related noises and even harmonics of the exciting AC voltage.

Fig. 4.36 Shielding electrodes assembled at the *top* of the bushings of a 500 kV single-phase transformer to avoid corona discharges disturbing the PD test

(c) *PD calibration*:

The main objective of the calibration procedure is to determine the ratio between calibrating charge q_0 injected in the top electrode of the bushing and reading M_0 of the PD instrument, which provides the scale factor S_f of the PD measuring system, as presented in Sect. 4.3.5. The ground connection lead between calibrator and transformer tank should be of low inductance and thus kept as short as possible to minimize the impact of the inevitable stray capacitances. To prove the linearity of the PD measuring system, calibrating charges of different magnitudes should be injected into the top electrode of the transformer bushing. If, for instance, the full reading of the PD instrument is adjusted for a calibrating charge of 200 pC, it is recommended to reduce the charge magnitudes thereafter down to 100 pC and finally down to 50 pC, where the deviation of the reading should be limited below ± 10 % of the reading expected for a linear operating instrument. It has to be taken care that after finishing the calibration procedure, the calibrator is removed from the test object to avoid any damage when the HV test voltage is applied.

(d) Actual PD test under HVAC voltage:

The test voltage profile to be applied for quality assurance tests is specified in the relevant apparatus standards, as exemplarily shown in Fig. 4.37, which refers to the IEEE standard C57.113: 2010. First, the AC test voltage is raised up to approx. 50 % of the rated voltage, denoted as V_1 to determine the "energized background noise level" in terms of pC, which should not exceed the 50 % value of the specified pulse charge. Thereafter, the test voltage is raised up to the

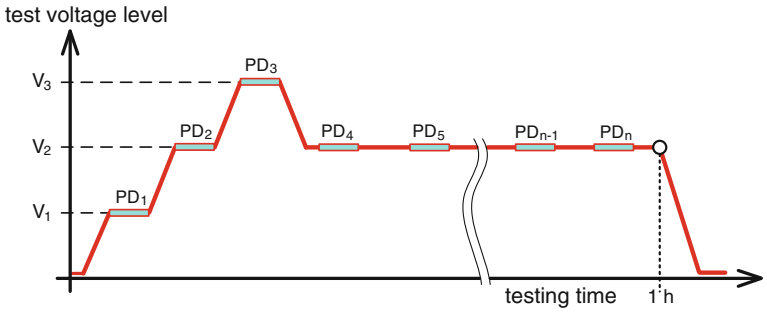

Fig. 4.37 HVAC test voltage profile recommended in the IEEE Standard C57.113 for PD testing of power transformers

specified 1 h test value V_2 and held constant for few minutes to verify whether there are any PD problems. If not, the test voltage is then raised up to the enhancement (withstand) level V_3 and held constant for 7,200 cycles to observe the PD trending.

> **Note** As the HVAC test voltage exceeds substantially the rated voltage, the exciting frequency has to be enhanced accordingly using a HVAC test set of variable test frequency. For this reason, the duration of the test period at enhancement voltage level is expressed in terms of cycles. If, for instance, a test frequency of 120 Hz is applied, 7,200 cycles are equivalent to a test period of 60 s. For more details, see Sect. 3.2.5.

Finally, the applied HVAC test voltage is reduced down to the 1 h test voltage level V_2. Under this condition, the PD level is recorded at subsequent five-minute intervals, where the recording time can be limited to approx. 1 min at each interval.

(e) Evaluation of the test results

The transformer has passed the PD test if the mean value of the maximum pulse magnitudes recorded during the 1 h test interval

- are below a specified value,
- are within a specified tolerance band,
- do not exhibit any steadily rising trend and
- do not suddenly increase during the last 20 min of the 1 h test.

In this context, it has to be taken into account that during the above-mentioned 5-min test intervals sporadic noise might appear caused, for instance, by switching of cranes. If the test results do not comply with the specified limits, the PD-tested transformer should not warrant immediate rejection but lead to consultation between purchaser and manufacturer to decide on further actions.

4.4 PD Fault Localization

For assessing the PD severity besides the charge and repetition rate, also the origin of the PD events must be known. This is particularly of importance for high-polymeric insulation, which is irreversibly deteriorated by partial discharges of only few pC. Therefore, the localization of PD failures became an established method for quality assurance tests since the 1970s, when extruded dielectrics where applied for the insulation of power cables (Eager and Bahder 1967, 1969; Lemke 1975, 1979; Beinert 1977; Kadry et al. 1977; Beyer and Borsi 1977). The main benefit of the *PD fault localization* in power cables using time-domain reflectometry (TDR) is, on one hand, the technology for manufacturing such cables can be improved because the reason for typical PD defects becomes known. On the other hand, the total cable length must not be replaced but only a very short section containing the PD defect. In this context, it seems noticeable that in case of routine tests of polymeric power cable systems, most of the recognized PD sources are caused by poor assembling of the stress cones required for grading the electric field. Thus, the total cable length passes commonly the PD test when PD events have been recognized at the joints or terminations.

The first step required for PD fault localization is the determination of the *travelling wave velocity* v_c using the set-up shown in Fig. 4.38a. Here, the calibrating pulses are injected in that cable end where the coupling unit is connected, usually referred to as *near* end. As electrically long power cables behave like an electromagnetic waveguide, the injected pulse travels first at wave velocity v_c towards the *far* or *remote* end where the signal is reflected and thereafter travelling towards the near *end*. Consequently, the reflected pulse also measurable at the near end must travel twice the cable length l_c, which requires the travelling time t_c. Thus, the travelling wave velocity can simply be accounted for by

$$v_c = \frac{2l_c}{t_c} \tag{4.19}$$

If a PD test is performed under high-voltage condition where a PD shall occur at distance x_r from the remote end, the PD signal travels from the site of origin into both directions, i.e. directly towards the near end and also to the remote cable end where it is reflected, as shown in Fig. 4.38b. Thus, the reflected pulse must travel additionally twice the distance x_r between PD site and remote end, if compared with the distance travelled by the direct PD pulse. Based on this, the distance between PD source and remote cable end is calculated from the additional travelling time t_r:

$$x_r = 0.5 \cdot v_c \cdot t_r. \tag{4.20}$$

From this follows for the distance of the PD site from the near cable end

$$l_c - x_r = 0.5 \cdot v_c(t_c - t_r). \tag{4.21}$$

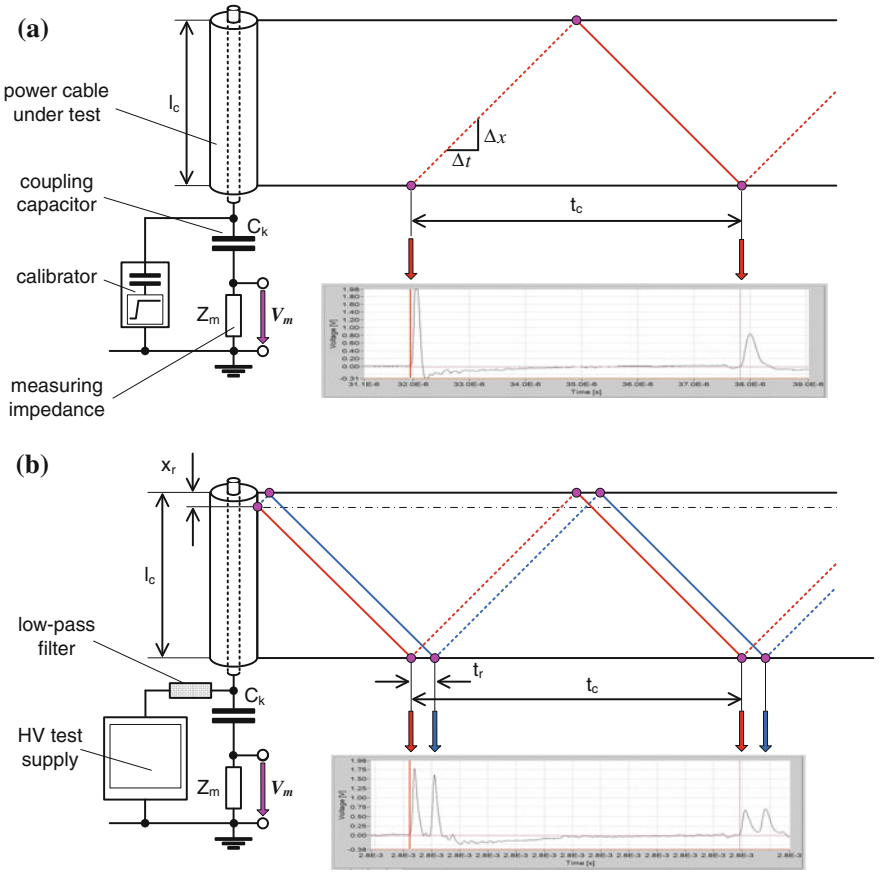

Fig. 4.38 Principle of PD fault localization in electrically long power cables. **a** Determination of the travelling wave velocity. **b** Determination of the PD site using the time-domain reflectometry (*TDR*)

Nowadays, mostly computerized PD measuring systems are used for the localization of PD failures in power cables (Lemke et al. 1996, 2001). The main challenge is, however, to measure the time difference t_r between the direct and the reflected PD pulse as accurately as possible. The minimum requirements for the A/D converter applied are a sampling rate of 100 MS/s and a resolution of 10 bit. To record the complete PD data stream occurring during a single half-cycle of a 50-Hz test voltage, the memory depth should be at least in the GByte range. The overall bandwidth of the PD localization system should cover a frequency range between approx. 50 kHz and 20 MHz.

For a better understanding of the fundamentals of the *time-domain reflectometry* (TDR), a typical practical example will be presented in the following. This refers to a periodical energizing of the cable under test by a so-called DAC test voltage

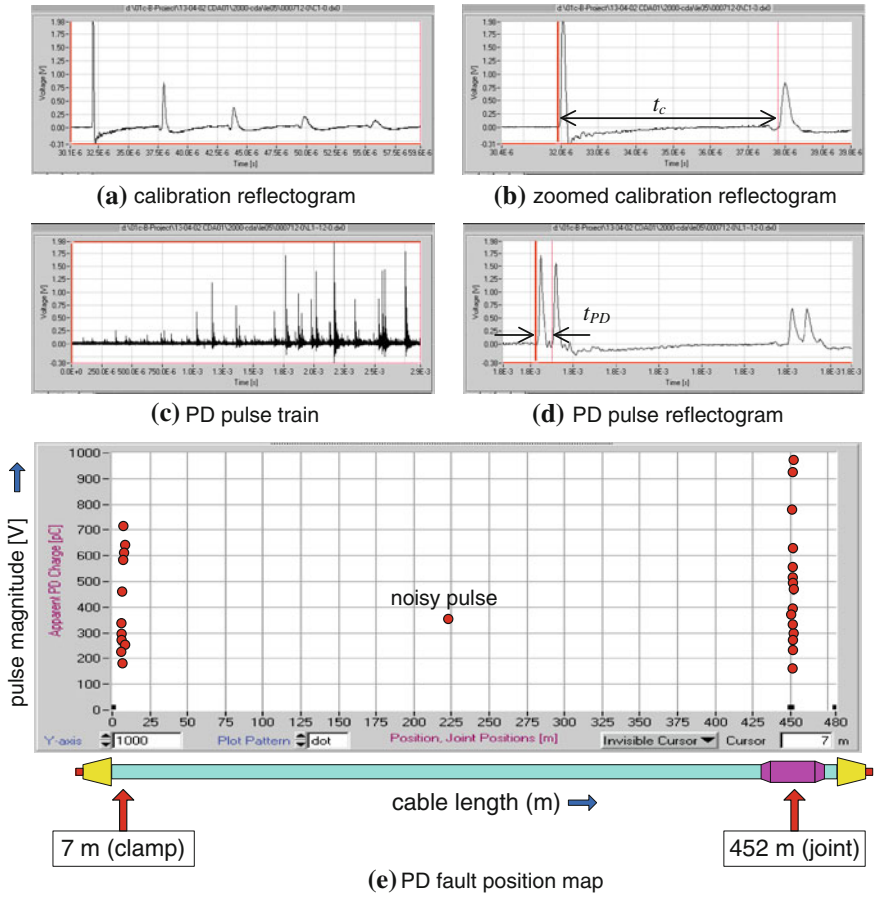

Fig. 4.39 Screenshots of a computer-based PD fault localization system (explanation in the text)

(see Sects. 7.1.3 and 10.2.2.2), which is based on the following steps, see Fig. 4.39 (Lemke et al. 2001):

(a) Inserting the *cable data* which include besides the cable parameters (manufacturer, type and insulation of the cable, rated voltage, operation voltage, recently performed tests, etc.) and the test voltage parameters to be applied (test voltage levels, number of shots at each test voltage level), first of all, the cable length and the positions of the accessories (joints and terminations) which are of interest to localize the PD defects as accurately as possible.

(b) *Calibration* which includes the determination of both the measuring sensitivity and the travelling wave velocity of the PD pulses. As shown in Fig. 4.39a, besides the calibrating pulse injected at the near cable end, several pulse reflections might occur, where only the first one is of interest. Therefore, this

signal is zoomed, as obvious from Fig. 4.39b, and the cursors are adjusted accordingly by the computer software to determine the time interval t_c and thus the travelling wave velocity v_c based on Eq. 4.19 as precisely as possible.

(c) *PD measurement* (Fig. 4.39c) to evaluate consecutive PD pulses occurring within a pre-selected time interval. Based on this, the magnitude of each PD pulse is indicated in terms of Volts, and the charge of the pulses captured for each voltage application is calculated by the computer software and stored in the memory to perform a statistical analysis of the data stream.

(d) *PD fault localization* based on the evaluation of PD pulses showing typical reflections with the time interval t_r shorter than twice the travelling time t_c along the whole cable length. Thereafter, the extracted pulses are zoomed. Setting the cursors accordingly, the characteristic time interval between each direct and reflected pulse is measured, as shown in Fig. 4.39d. Based on this, the distance between PD source and remote cable end is determined. This procedure is repeated many times. Occasionally, a digital filtering of the captured signal is performed to minimize the disturbing impact of radio noises.

(e) *PD mapping* to provide a map of all evaluated PD fault positions along the cable system length. A typical example is shown in Fig. 4.39e, which refers to a 20 kV XLPE cable of 480 m length. There are two potential PD defects, where the first one is located at 3 m and the second one 452 m from the near end. Usually, the PD fault localization is performed automatically. Only if it is decided to repair an identified joint or termination, it seems feasible to apply the manual feature to prove the validity of the automatically located PD site.

For some equipment, the time of arrival measurement can also be applied to identify the defective component of a three-phase system. An example for this is shown in Fig. 4.40, which refers to a power transformer where the wide-band PD signal was decoupled simultaneously from the bushing taps of all three phases using measuring impedances of 20-MHz upper limit frequency. The oscilloscopic records reveal that a potential PD source is located in the phase "T", because the transient signal appeared first and showed also a substantial higher magnitude if compared with the signals decoupled from the other phases "R" and "S", respectively. This was later confirmed by a visual inspection.

The synchronous three-phase PD measurement seems also feasible for in-service diagnostics of power cable terminations, as shown in Fig. 4.41. Recording only the time-dependent PD level, it could be supposed that PDs appear in all three terminations. Displaying the phase-resolved PD pulses versus the recording time, however, the defective termination could clearly be identified in the phase "red". This is not only that the highest pulse magnitudes were obtained for this phase but also because the PD pulses appeared at equal phase angles for all three phases which means that the signal is radiated from only one single PD source. This conclusion was also confirmed by a visual inspection after the supposed defective termination has been de-assembled. Replacing this termination, no any PD event could be recognized thereafter.

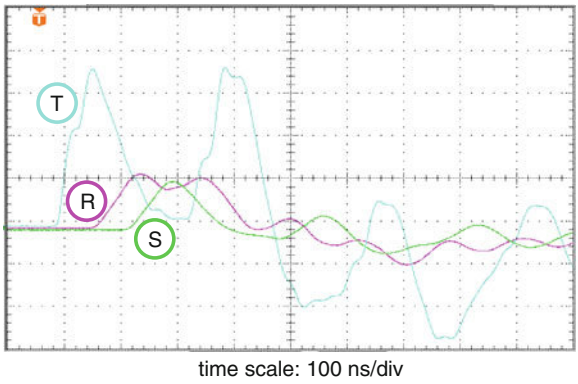

Fig. 4.40 PD signals decoupled simultaneously from the three phases (*R*, *S*, *T*) of a power transformer using the bushing tap coupling mode

Another approach to distinguish between different PD sources is the presentation of typical clusters in a 3-phase amplitude relation diagram, which is based on a synchronous multichannel PD measurement (Emanuel et al. 2002). An enhancement of this method is the presentation of the so-called three-centre-frequency relation diagrams where three different frequencies selected from the spectrum of a single PD pulse are evaluated and displayed on the computer screen. This provides not only information on the discharge nature itself but can also be used to localizate the origin of PD defects (Rethmeier 2009). For more details in this respect, see Sect. 4.6. Another promising tool for the localization of potential PD sources is the pulse waveform analysis. This is based on the extraction of a set of pulse parameters, such as the rise and decay time and the pulse width (Montenari 2009). Displaying the characteristic clusters like star diagrams, also multiple PD failures can be recognized, as discussed also in Sect. 4.6.

In this context, it should be noted that besides the above-described electrical methods, also the acoustic emission (AE) technique is widely used, particularly to localize PD defects in metal-encapsulated HV apparatus, such as gas-insulated switchgears (GIS) and power transformers, as discussed in Sect. 4.8. The combination of both the electrical and the acoustic method can also be very effective to enhance the signal-to-noise ratio.

Even if advanced computerized measuring systems are widely employed for PD fault localization, it should not be overlooked that in many cases, potential PD sources can also be recognized and localized by means of commercially available oscilloscopes. Finally, it should be emphasized that a great deal of practical experience is required for the decision if HV equipment affected to potential PDs should be taken out of order or should be kept in service for a certain time and PD monitored.

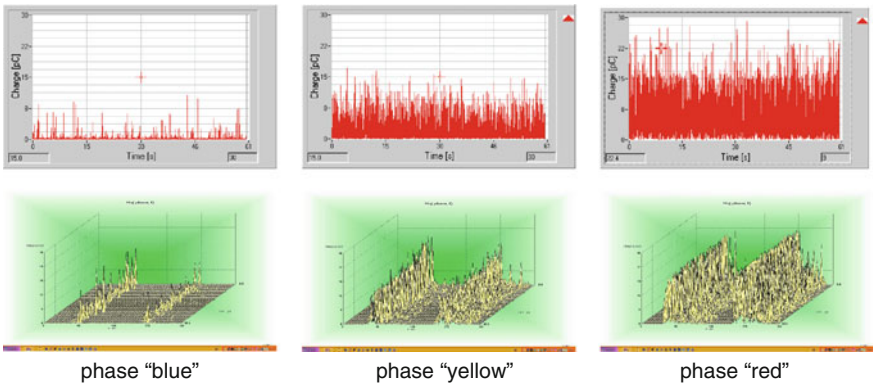

Fig. 4.41 Characteristic PD signatures of the cable terminations connected to a three-phase gas-insulated switchgear

4.5 Noise Reduction

4.5.1 Sources and Signatures of Noises

Electromagnetic interferences encountered in PD test fields may exceed substantially the PD signal level to be detected, which is commonly in the order of mV or even μV. To discriminate disturbing interferences from PD pulses, the sources and signatures of typically noises must be known. Depending on the mode of propagation, it is generally distinguished between *radiated noises* and *conducted noises*.

Noises radiated from radio broadcast stations, which are modulated and appear permanently, are entering into the test area via the electromagnetic field, where the HV electrodes and measuring loops of the PD test arrangement act like antennas. Also high-frequency corona discharges, igniting at protrusions of HV electrodes in the vicinity of the test area, can be classified as radiated noises.

Electromagnetic noises originating in the mains or even in the HV test voltage supply, which might appear stochastically or periodically, are transmitted via the conductors to the PD test and measuring system. PD events igniting at sharp edges of metallic structures adjacent to the HV test supply as well as sparks between metallic parts on floating potential due to a poor grounding are also classified as conductive noises. Screenshots of typical conductive noises, encountered often in PD test laboratories, are presented in Figs. 4.42 and 4.43.

4.5.2 Noise Reduction Tools

To minimize the impact of radiated noises, it is a common practice to erect electromagnetically well-*shielded test laboratories*, as described in Sect. 9.2.2.

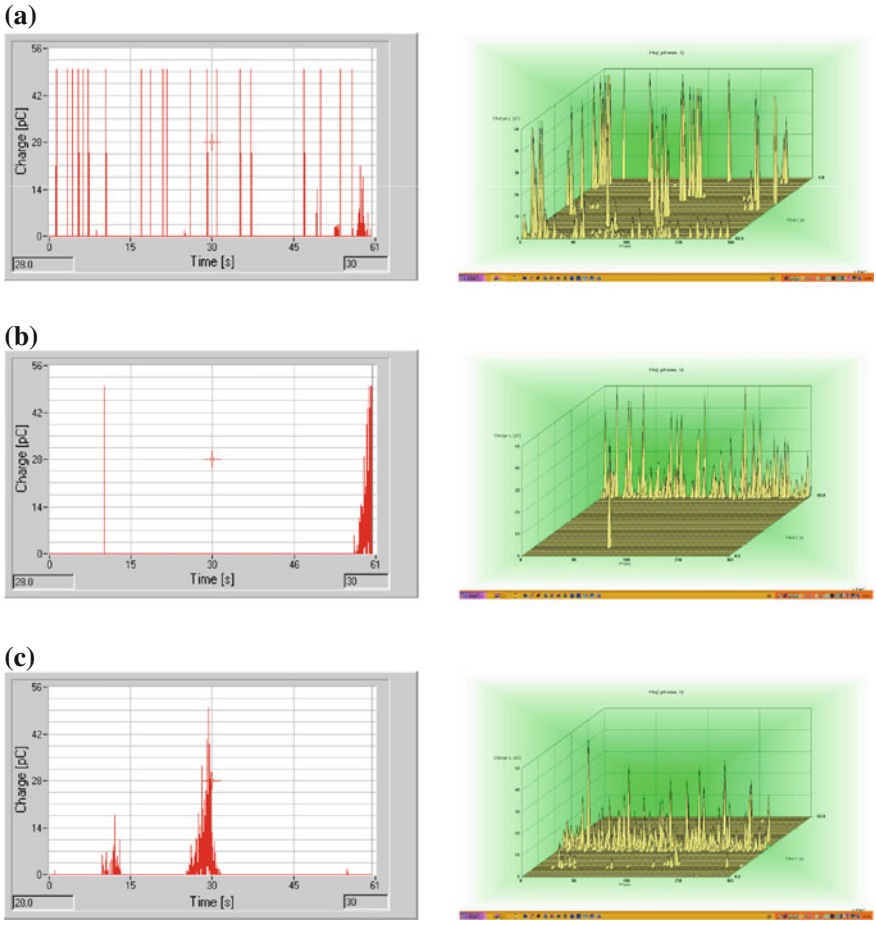

Fig. 4.42 Signatures of stochastically appearing pulse-shaped noises **a** Maintenance work (drill), **b** Car starting nearby, **c** Switching of a crane

Moreover, the fundamental laws of HF technology have to be taken into consideration for designing the PD test and measuring circuit. Particularly the area of the inevitable wire loops—acting as antennas for radiated noise—should be kept as low as possible to minimize the induction of interference voltages, and the ground connection leads should be of low inductance which is best accomplished by using copper foil.

If PD test laboratories are not carefully shielded against radiated electromagnetic noises, it could be helpful to use the *balanced bridge circuit* according to Fig. 4.17c. Practical experiences yield that for comparatively small test objects, such as instrument transformers and bushings, the signal-to-noise ratio can be

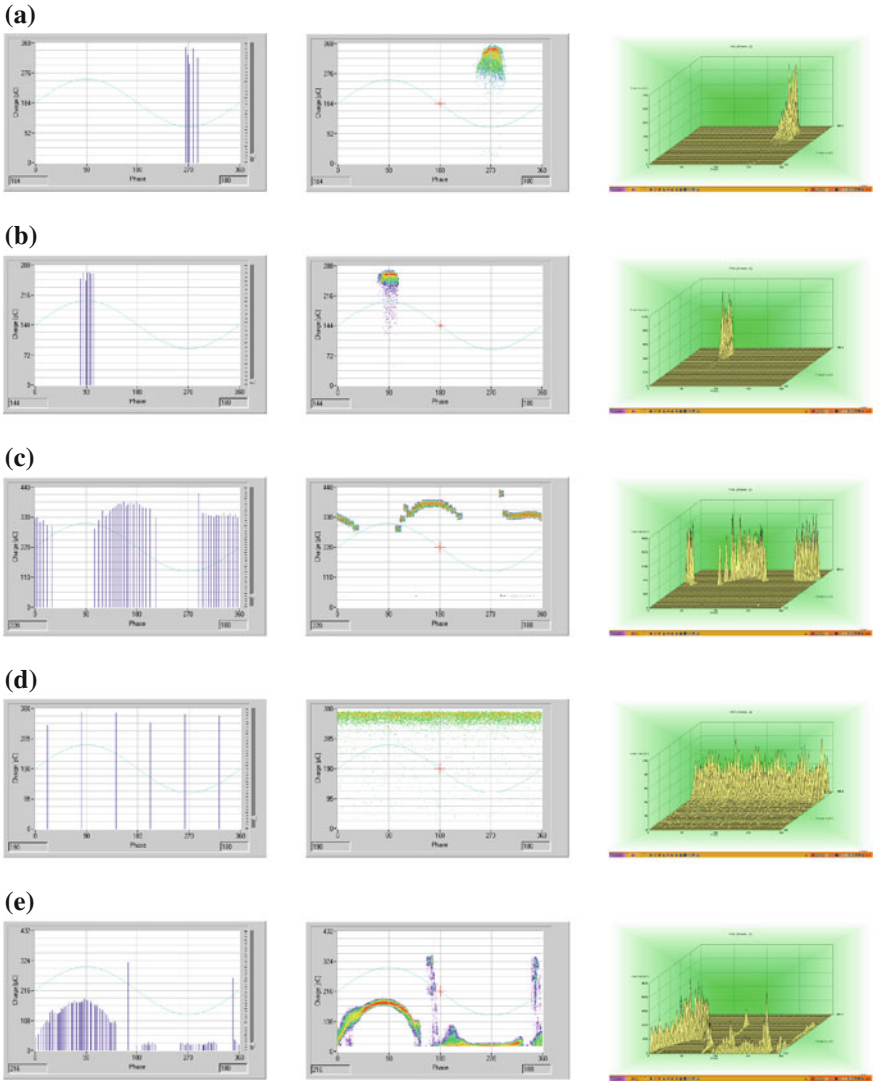

Fig. 4.43 Signatures of periodically appearing pulse-shaped noises **a** Protrusion on the surface of a HV shielding electrode, **b** Sharp edge of a metallic structure on ground potential,**c** Sparks between metallic parts on floating potential, **d** Frequency converter feeding a transformer of variable frequency, **e** Defective xenon lamp in the control room

enhanced by a factor up to 10. For tall test objects, such as power transformers, this method is commonly not effective.

An option of the bridge method is the *pulse polarity discrimination* proposed by Black (1975), where a balancing is not required. As the PD pulses decoupled from both bridge branches appear at opposite polarity, a discrimination seems possible

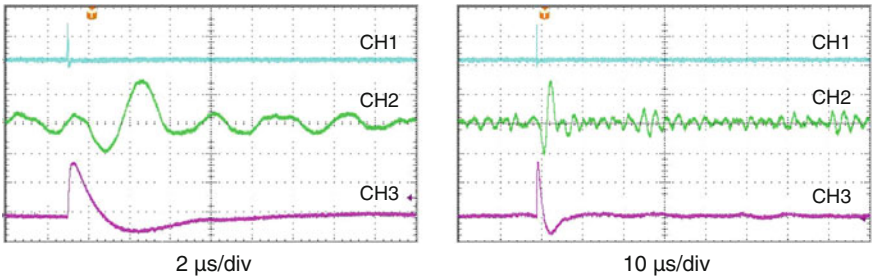

Fig. 4.44 Screenshots gained for a 20-pC calibrating pulse injected in a XLPE MV power cable: CH 1: Input signal captured from a wide-band measuring impedance ($f_2 = 20$ MHz) CH 2: Signal after band-pass filtering ($f_2 = 600$ kHz) CH 3: Signal after wide-band amplification ($f_2 = 20$ MHz) and electronic integration

because noisy pulses originating outside the bridge appear at equal polarity. For tall test objects, however, this method is commonly not applicable because the PD pulses transmitted via both branches are drastically distorted and may also excite oscillations, so that the true polarity is lost.

From a theoretical point of view, the *signal-to-noise ratio* can also be enhanced if a broader frequency spectrum of the PD signal is processed, i.e. if the measuring frequency is increased to much higher frequencies than the 1 MHz limit specified in the Amendment to IEC 60270:2000. This concept has first been adopted by Lemke (1968), where the PD pulses were first amplified using a frequency range up to approx. 10 MHz followed by an electronic integration. A comparison of this concept with the classical method, where the measuring frequency was limited to 600 kHz, is shown in Fig. 4.44. The oscilloscopic records refer to 20 pC calibrating pulses injected in a 20 kV XLPE cable. The charge pulse gained by a limitation of the bandwidth below 600 kHz shows much higher superimposed interferences if compared with the charge pulse gained by an electronic integration.

Based on this benefit, a new concept for PD measurements of extruded power cables has proposed (Lemke 1979), introduced in practice in the 1980s (Hauschild et al. 1981; Lemke 1981). The operation principle of the developed PD measuring system covers the following major stages for signal processing, as shown in Fig. 4.45:

- Wide-band amplification of the signal captured from the measuring impedance, where a bandwidth in the order of 10 MHz seems reasonable.
- *Automatic gating* of stochastically or periodically appearing pulse-shaped noises. To receive the noisy signals for triggering the gating unit, rod or loop antennas are installed as close as possible to the supposed noise sources.
- Reduction in the impact of radio interference voltages. This is achieved by adjusting the threshold level for passing the RIV rejection unit slightly above the noise level which is performed automatically.

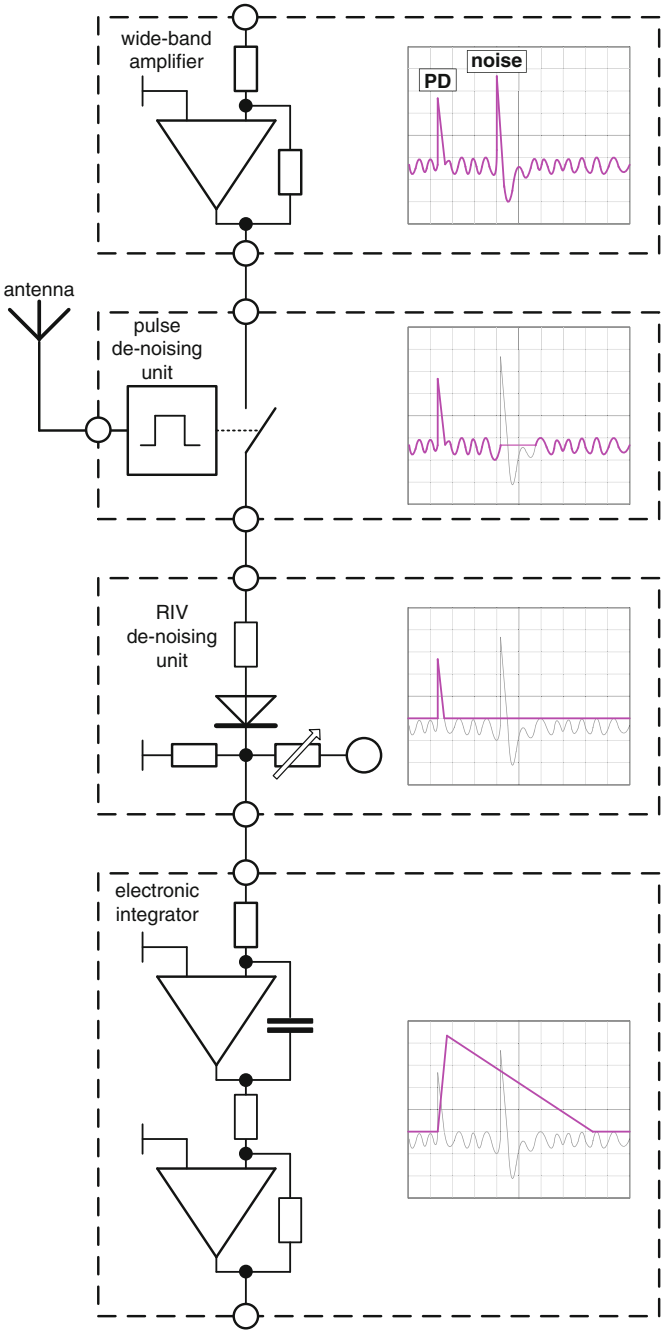

Fig. 4.45 Block diagram of a wide-band PD measuring system equipped with various de-noising tools described in the text

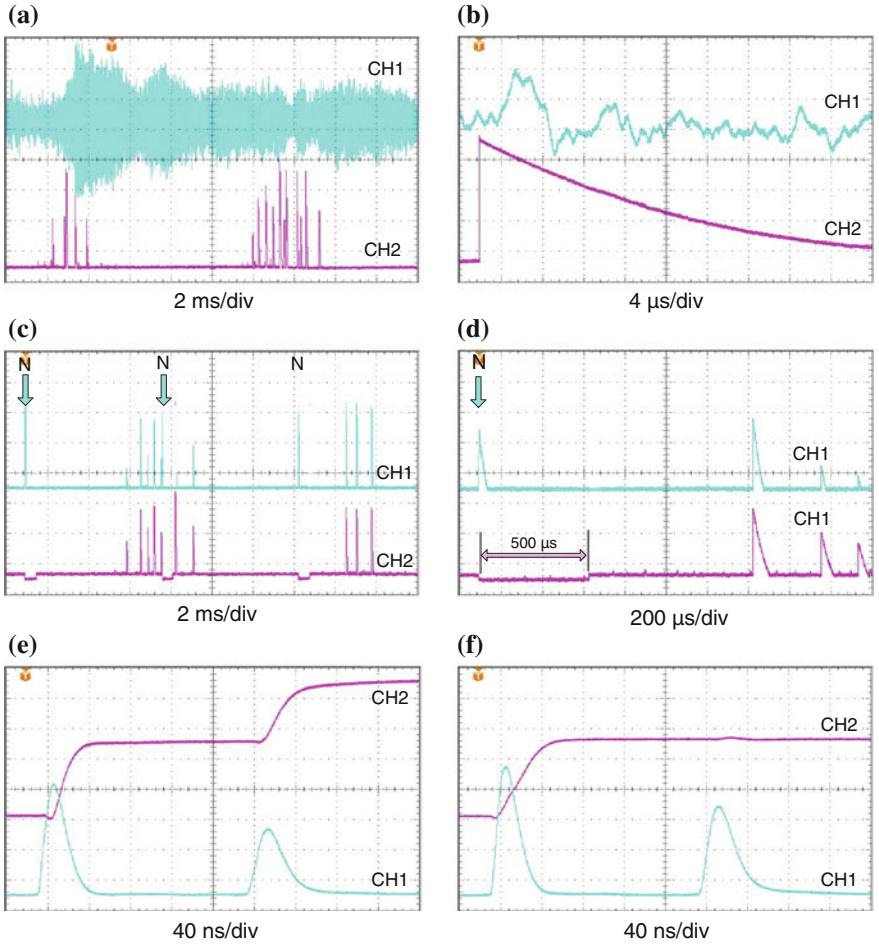

Fig. 4.46 Oscilloscopic records gained for a wide-band PD measuring system equipped with an electronic integrator and various tools for de-noising interfered PD signals (description in the text.)

- Electronic integration of the de-noised PD signal to measure the charge of the captured PD pulses.

Typical oscilloscopic records gained in an industrial PD test field are shown in Fig. 4.46. The screenshot displayed in Fig. 4.46 a, b reveal that under practical condition the signal-to-noise ratio can substantially be enhanced if the above-described non-conventional concept is adopted. In this context, it should be mentioned that the above-described concept was also beneficial employed for a hand-held, battery-powered PD probe to enhance the signal-to-noise ratio required for PD diagnostics of HV apparatus under on-site condition (Lemke 1985, 1988,

1991). Powerful tools for rejection of pulse-shaped noises, which might appear either periodically or even stochastically, can also effectively be realized based on the above-presented concept, as obvious from the Fig. 4.46c, d.

In this context, it seems noticeable that erroneous measurements due to the superposition of reflected pulses, which are typical for power cables, can also be avoided. An example for this is shown in Fig. 4.46f, where the reflected pulse recorded in Fig. 4.46e is eliminated by an electronic reflection suppressor recommended in IEC 60885-3:2003. This tool operates similar to the gating unit mentioned above. As this unit is triggered by the first (direct) PD pulse, the reflected pulses arriving the measuring system approx. 200 ns later than the direct pulse are suppressed (Lemke 1979, 1981).

Today's digital PD measuring systems are commonly equipped with various *de-noising software* tools, which are more or less capable to reject electromagnetic interferences. In this context, it should not be overlooked that the above-described "gating" of the PD signal developed for analogue PD signal processing can also be adopted for digital PD measuring systems if the de-noising is performed just prior the analogue/digital conversion (Lemke 1996; Lemke and Strehl 1999). A practical example for this is shown in Fig. 4.47 which refers to PD tests of a defective instrument transformer, rated voltage 110 kV. Applying an AC test voltage of variable frequency, the phase-resolved PD patterns showed the superposition of two characteristic noise signatures, as shown in Fig. 4.47a. The randomly distributed dots, showing a large scattering in magnitude and phase angle, are due to pulse-shaped noises not correlated with the applied 92-Hz test frequency, but apparently with the 60-Hz frequency of the mains. Thus, an inductive sensor has been attached close to power supply of the HV test facility to trigger the gating unit implemented in the digital PD measuring system applied. Under this condition, the randomly distributed noisy pulses appearing not correlated with the 92-Hz test frequency could completely be eliminated, as obvious from Fig. 4.47b. To reject also the remaining noise pulses originating in the frequency converter, an additional inductive sensor has been installed close to the IGBT switches inside the converter to capture the signal for triggering a second channel of the gating unit to reject also the converter noises, as shown in Fig. 4.4c.

> **Note** In practical tests using ACRF test systems (see Sect. 3.2.3), the noise impulses caused by the frequency converter have a stable phase position and can be simply identified as noise signals. There is no absolute need to gate them, because the gate is always wider than the noise signal and reduces the information from the PD pattern a bit.

Different to the above procedure, the pulse-shaped noises shown in Fig. 4.47b could also be eliminated after the actual PD measurement has been finished using a "*windowing*" tool. This is because the phase angle of the noisy pulses received from the converter is very different from those of the PD events. An example for this is shown in Fig. 4.48 using both the 2D and the 3D display modes. In this context, it should be noted that most of digital PD measuring systems are not equipped with the hardware required for an automatic gating of the PD signal but

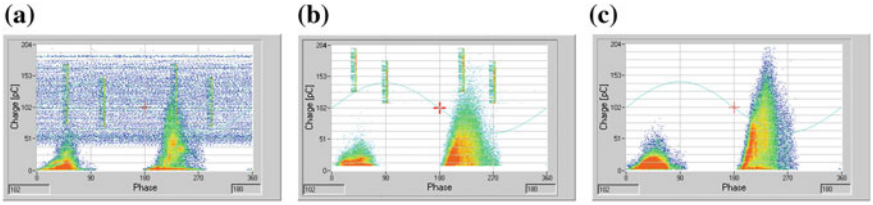

Fig. 4.47 Phase-resolved PD pattern of a defective 110-kV instrument transformer interfered by pulse-shaped noises originating in the mains (60 Hz) and in the frequency converter (92 Hz), as well. **a** PD signatures obtained at the very beginning of the test series. **b** Gating of noise pulses originating in the mains. **c** Additional gating of the noise pulses originating in the frequency converter

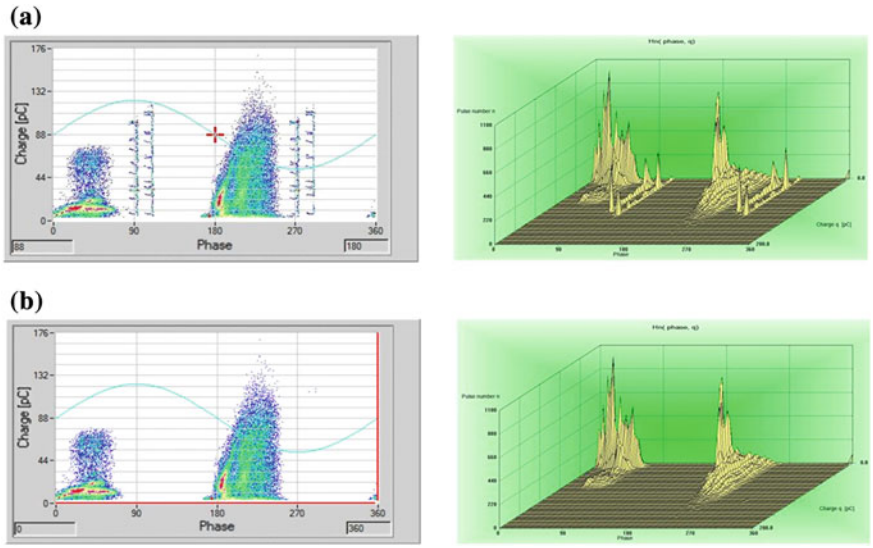

Fig. 4.48 Screenshots of phase-resolved PD patterns and synchronously appearing pulse noises originating in the frequency converter (**a**) and de-noising the PD patterns by gating (**b**)

usually with software packages to discriminate pulse-shaped noises from real PD events.

Due to the achievements in digital signal processing, very promising *de-noising* tools have been introduced during the last decade, mainly based on the *cluster separation* approach. An example for this is the establishment of *star diagrams* using synchronous three-phase PD measurements (Plath 2002; Kaufhold et al. 2006). A practical example is shown in Fig. 4.49, which refers to a PD test of a power transformer. Here, external noises due to corona discharges showing almost equal magnitude were detectable in all three phases, which is indicated by the three blue clusters in Fig. 4.49. PD pulses originating in the "Yellow" phase,

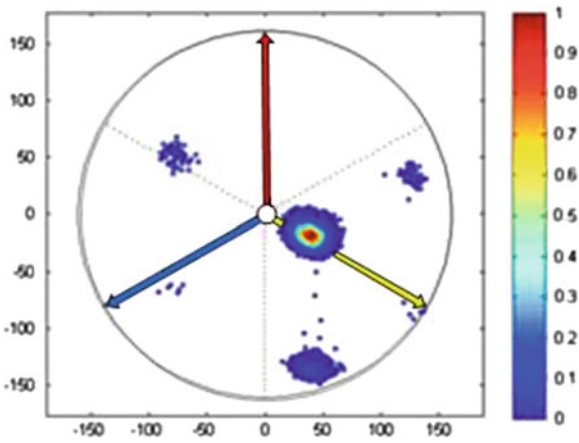

Fig. 4.49 Three-phase star diagram showing three typical clusters (*blue*) for each phase due to external noises as well as a single cluster (*coloured*), indicating that a potential PD defect is located in phase "Yellow" of the investigated power transformer (Plath 2002)

however, created a coloured cluster. Facilitating phase-resolved PD pattern recognition, a harmful PD source could indeed be identified in phase "Yellow". In principle, the vectors obtained by the three-phase PD measurement could also be added to establish a three-phase amplitude relation diagram. Under this condition, only one single *noise cluster* is established, which is located close to the centre point, whereas PDs in the single phase appear outside the centre point, providing that the impact of crosstalking phenomena can be neglected.

Another approach using cluster separation is the decomposition of the acquired PD pulse waveforms using pulse parameters in either the frequency or time domain, such as the pulse rise and decay time and the pulse width (Cavallini et al. 2002; Rethmeier et al. 2008). A typical measuring example is illustrated in Fig. 4.50 which refers to fundamental PD studies in a poor-screened test field investigating a defective power cable termination. After acquiring the complete data stream captured from the test object, the phase-resolved PD pattern shown in Fig. 4.50a is heavily interfered by noises. Analysing the captured pulse shapes in the time domain, as shown in Fig. 4.50b, the PD pattern could clearly be separated from the noise signatures, as obvious from Fig. 4.50c. In principle, this approach can also be applied for multi-source PD separation (Plath 2005).

In this context, it should be emphasized, however, that advanced de-noising tools can successfully be applied only by experienced test engineers, appropriately familiar not only with the fundamentals of PD measurements but also with the operation principle and the capabilities and limits of the software features adopted. Even if nowadays sophisticated de-noising software is implemented in many digital PD measuring systems, it should not be overlooked that electromagnetic interferences can often conveniently be recognized by the use of multichannel digital oscilloscopes and thus suppressed based on conventional analogue procedures, such as windowing and automatic gating, as presented above.

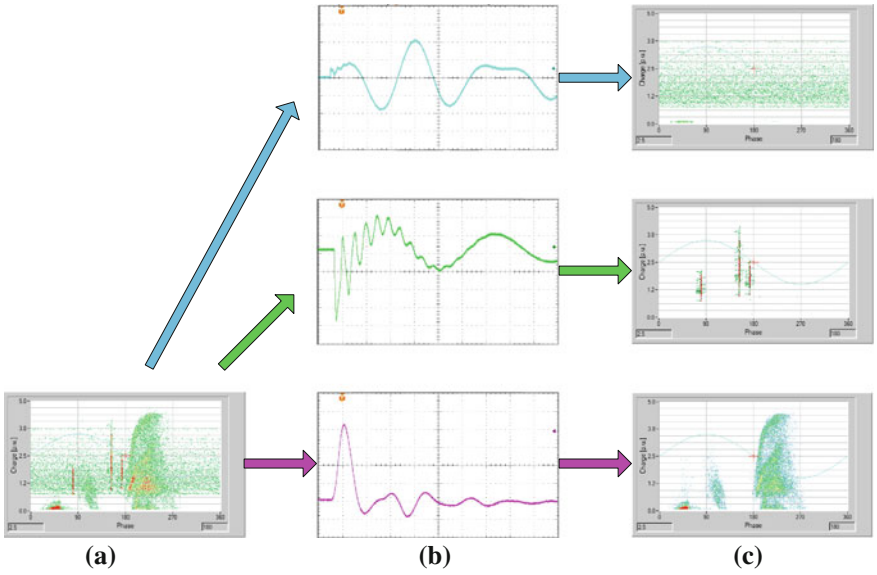

Fig. 4.50 Principle of PD signal de-noising using cluster separation (Cavallini and Montenari 2007). **a** Acquired data stream captured for a testing time of 10 min. **b** Waveform analysis. **c** Cluster separation

4.6 Visualization of PD Events

The main aim behind the visualization of phase-resolved PD pattern by means of oscilloscopes or computerized PD measuring system is the recognition and identification of typical PD sources. The first tool applied for this purpose was the Braun tube. In 1928, Lloyd and Starr used the perpendicular deflection plates of an electron beam oscilloscope to record the charge of PD events versus the instantaneous AC test voltage. Subjecting the horizontal deflection plates to the test voltage and bridging the vertical deflection plates by a measuring capacitance using for grounding the test object, typical Lissajous figures were obtained, as exemplarily shown in Fig. 4.51a. In this context, it seems noticeable that this circuit can be regarded as the precursor for the integrating bridge used by Dakin and Malinaric (1960) to measure the power losses of discharges per cycle by means of the so-called parallelogram method.

When the first PD detectors were available (Arman and Starr 1936; Mole 1954), the classical Lissajous figure technique has also been employed for oscilloscopic records of *pulse charge trains*, as shown in Fig. 4.51b. Later the recording of the pulse charge trains versus the phase angle of the applied AC test voltage became also a common practice. Typical oscilloscopic screenshots for this are shown in Fig. 4.52 which refers to needle-plane test samples, often used for the investigation of the discharge physics as well as for the classification of PD defects. As shown in

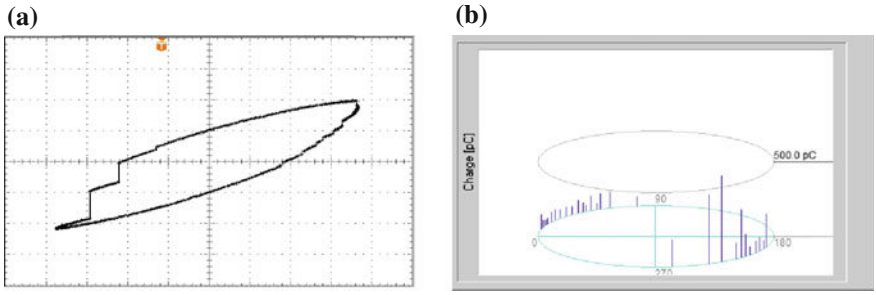

Fig. 4.51 Display of PD events occurring within a single AC voltage cycle using the traditional Lissajous figure technique. **a** Voltage across the measuring capacitance of an integrating bridge. **b** Charge pulses occurring at the output of an analogue PD signal processing unit displayed by means of a digital PD instrument

Fig. 4.52a, which is representative for corona in ambient air igniting at sharp edges of electrodes on HV potential, PD events occur at onset voltage only at the negative electrode. Such discharges, which have comprehensively been investigated by Trichel (1938), are characterized by a nearly constant magnitude almost independent on the test voltage level. Thus, the well-reproducible Trichel discharges are feasible for performance checks of PD test circuits and can also be used to determine the polarity of PD pulses captured from more complex test arrangements. As shown in Fig. 4.52b, corona discharges appear at positive electrode polarity if the test voltage level is significantly increased above the inception level. This behaviour is in contrast to that of cavity and surface discharges, which occur at inception voltage simultaneously in both half-cycles, even if the PD magnitudes are scattering in magnitude and repetition rate over an extremely wide range. Moreover, discharges on surfaces or in cavities of dielectrics appear typically in the vicinity of the zero-crossing of the AC test voltage and disappear commonly in the crest region.

Essential steps in statistical PD data acquisition where achieved in 1969, when Bartnikas and Levi presented a *pulse-height analyser* for PD rate measurement, and in 1978, when Tanaka and Okamoto presented the first minicomputer-based PD measurement system. At the very beginning of computerized PD measurements, single screenshots of consecutive PD pulse trains appearing within individual AC cycle have been recorded like waterfall diagrams, as shown in Fig. 4.53.

Today's digital PD measuring systems are capable to store the vector $[q_i; u_i; t_i; \varphi_i]$ for each captured PD pulse. Here are

q_i the pulse charge of the individual PD current pulse
u_i the instantaneous value of the applied test voltage
t_i the instant of occurrence
φ_i the phase angle at instant of occurrence

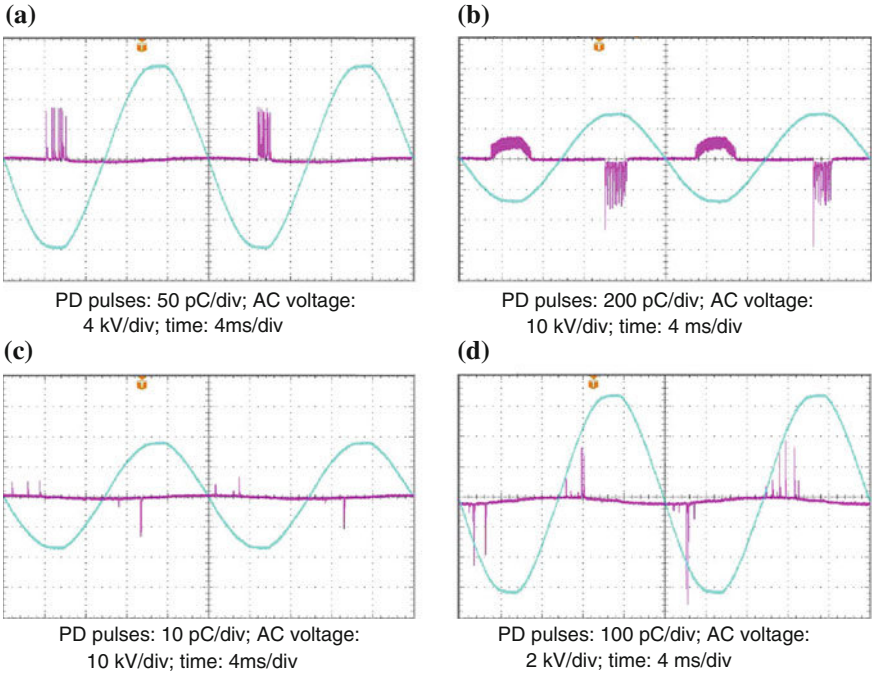

Fig. 4.52 Oscilloscopic screenshots of phase-resolved PD patterns gained for point-to-plane test samples subjected to power frequency (50 Hz) AC test voltage. **a** Discharges in air near-onset voltage (peak value 12 kV_{peak}). **b** Discharges in air significantly above onset voltage (14.5 kV_{peak}). **c** Cavity discharges in XLPE near onset (18 kV_{peak}). **d** Surface discharges near onset (6.2 kV_{peak})

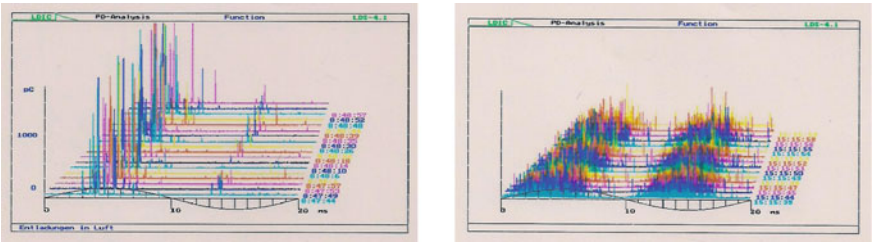

Fig. 4.53 PD signatures of defective cable accessories displayed like waterfall diagrams

Based on this, the cumulative (integral) *phase-resolved PD pattern* is commonly displayed on the computer screen, as shown in Figs. 4.54 and 4.55. Since the 1980s, this feature is widely used for PD pattern recognition (Kranz and Krump

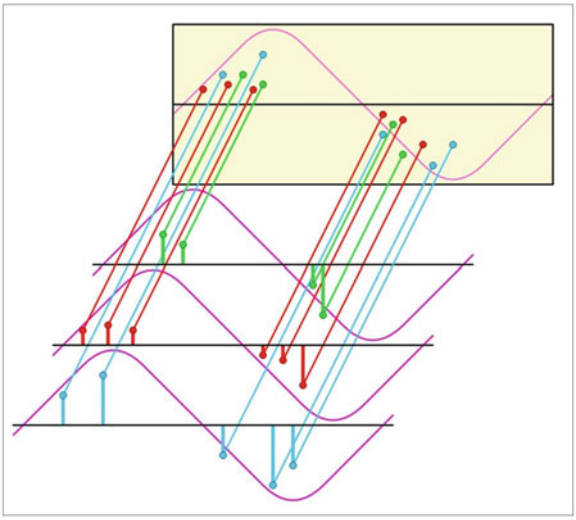

Fig. 4.54 Principle for displaying cumulative phase-resolved PD patterns

1988; Ward 1992; Fruth and Gross 1994). As the PD data stream acquired in the real-time mode and stored in the computer memory, these can be recalled again after the actual PD measurement has been finished. Thus, the phase-resolved PD patterns can also be replayed comparable with real-time measurements (Lemke et al. 1996; Lemke and Strehl 1999) (Fig. 4.54).

Besides the traditional two-dimensional graphs shown in Fig. 4.55, also the 3D presentation might provide valuable information not only on the PD activity but also on disturbing electromagnetic interferences, as already presented in the Figs. 4.42 and 4.43. Moreover, the phase-resolved PD patterns can be displayed in a traditional manner using the elliptical or linear time base, as shown in Fig. 4.56.

Another approach sometimes adopted for *PD pattern recognition* is the analysing of PD pulse sequences, as proposed by Hoof and Patsch (1994). The algorithm is based on the evaluation of the voltage differences measured between three subsequent PD pulses, as illustrated in Fig. 4.57a. That means, the voltage difference ΔV_{n-1} between the reference pulse "n" and the previous occurring pulse "$n-1$", as well as the voltage difference ΔV_n between the reference pulse "n" and the thereafter following pulse "$n+1$", is plotted in a graph displaying the value pairs ΔV_n versus ΔV_{n-1}. A measuring example for this is shown in Fig. 4.57b which refers to potential slot discharges detected for a rotating machine.

To classify typical discharge sources, Tanaka and Okamoto proposed (1986) the establishment of PD fingerprints based on the following statistical operators:

- standard deviation,
- skewness,
- kurtosis and
- cross correlation.

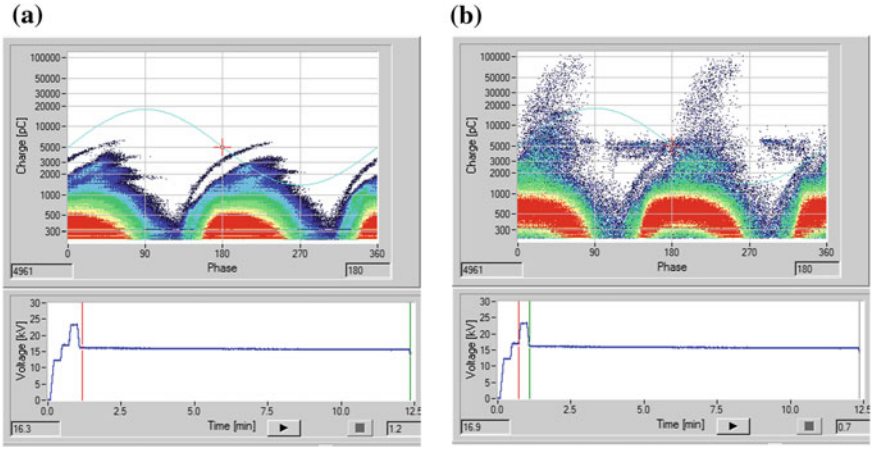

Fig. 4.55 Screenshots of phase-resolved PD patterns gained in the course of development tests of stator bars for hydro-generators. **a** Recorded at long-term test voltage level (18 kV, 10 min, 30,000 cycles). **b** Recorded at enhanced test voltage level (24 kV, 2 min, 6,000 cycles)

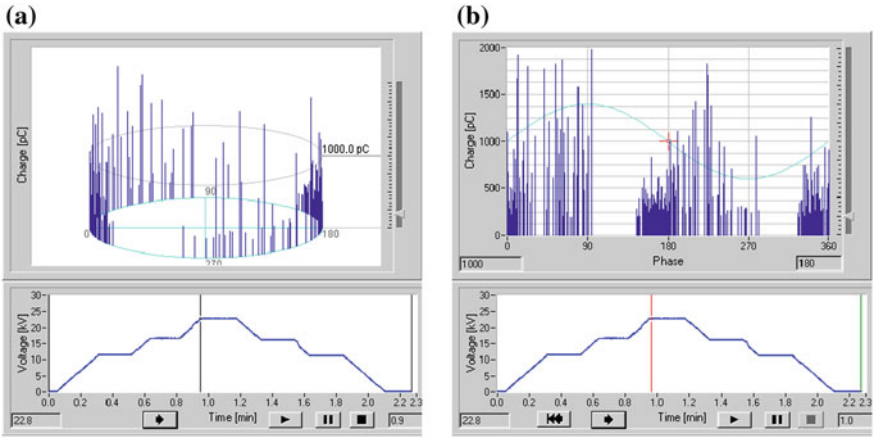

Fig. 4.56 Screenshots of phase-resolved PD pulses of a stator bar occurring within a single cycle at 24 kV of the applied 50-Hz AC test voltage (see cursor position obvious from the test voltage profile). **a** Elliptical time base. **b** Linear time base

Later the feasibility of such statistical operators used for the establishment of PD fingerprints as well as for the identification and classification of PD sources has comprehensively been investigated by Gulski and his co-workers (Gulski 1991). To create characteristic PD fingerprints, the following statistical parameters shown in Fig. 4.58 are commonly measured and displayed:

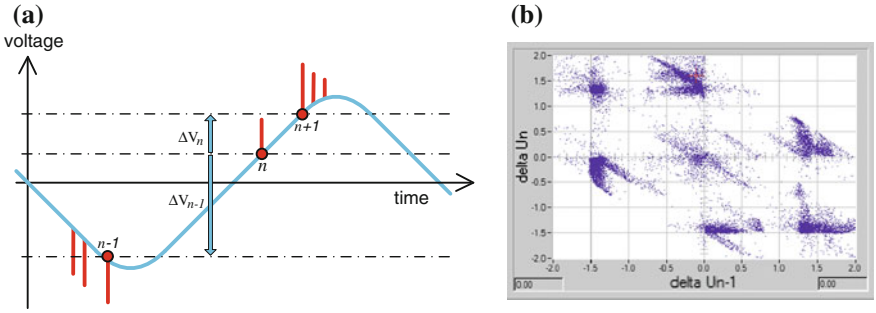

Fig. 4.57 Principle of PD pulse sequence analysis (**a**) and measuring example (**b**) gained for cavity discharges in a power cable termination

$H_n(phi)$: PD pulse count representing the number of pulses occurring within each phase window versus the phase angle,
$H_q(phi)peak$: Peak values of PD pulses occurring within each phase window versus the phase angle,
$H_q(phi)mean$: Mean values of PD pulses occurring within each phase window versus the phase angle. This quantity is deduced from the total charge amount within each phase window divided by the pulse number occurring in this phase window.

Based on PD fingerprints established for various types of failures and stored in the computer memory, these can be compared with each other, where the test conditions have also to be taken into consideration. Thus, graphs according to Fig. 4.59 provide a valuable tool not only for the recognition of potential PD defects in HV apparatus recognized after manufacturing and thus to improve the design accordingly, but also for maintenance decisions.

4.7 PD Detection in the VHF/UHF Range

4.7.1 General

PD events in the pico-Coulomb (pC) range might deteriorate extruded and moulded insulations. Performing PD measurements in compliance with IEC 60270:2000, where a measuring frequency below 1 MHz is recommended, PD magnitudes in the pC range can only be detected in electromagnetically well-shielded test areas. Under on-site conditions, however, the required measuring sensitivity is only achievable for measuring frequencies much above 1 MHz, as discussed in Sect. 4.5. The PD detection in the much higher frequency range has first been proposed for quality assurance tests of gas-insulated substations by

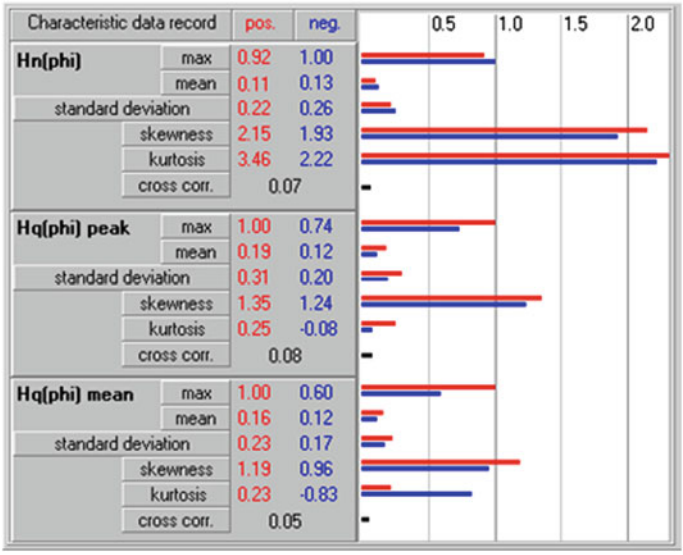

Fig. 4.58 PD fingerprint of a discharge source recognized in a HV cable termination in service

Fujimoto and Boggs (1981). This non-conventional technique has also been proven for PD diagnostics of HV/EHV cable accessories since the middle of the 1990s (Pommerenke et al. 1995) and at the beginning of the 2000s also for power transformers (Judd et al. 2002). The capability of the PD detection in the VHF/UHF range has also extensively been investigated in the past by various CIGRE Working Groups, as summarized in the CIGRE Technical Brochures No. 444 (2010) and 502 (2012), to provide recommendations and specifications for the application of the electromagnetic PD detection technique particularly for on-site application (Draft IEC 62478:2013).

Due to the extremely wide frequency spectrum of PD pulses, which covers the ranges of radio frequency (RF 3–30 MHz), very high frequency (VHF 30–300 MHz) and ultra-high frequency (UHF 300–3,000 MHz), various kinds of PD couplers have been developed in the past, which are commonly classified as capacitive, inductive and electromagnetic sensors, as discussed in the following.

4.7.2 Design of PD Couplers

4.7.2.1 Capacitive PD Couplers

To capture the PD signal from the test object, in IEC 60270:2000 a coupling device is recommended providing a series connection of a coupling capacitor with a measuring impedance. The upper limit of classical coupling devices (Fig. 4.60a)

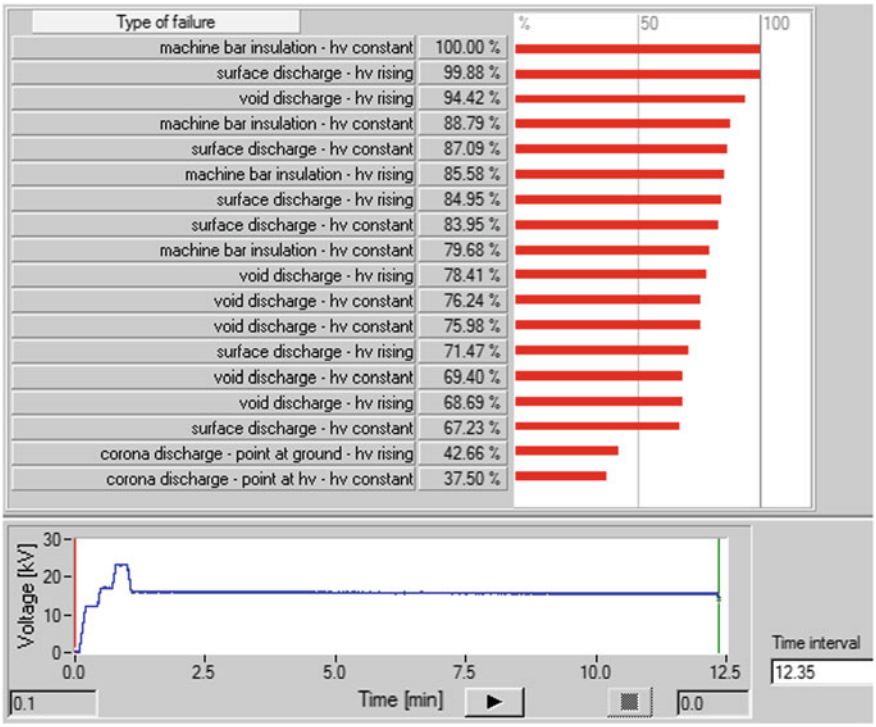

Fig. 4.59 Comparison of the PD fingerprint of a PD-tested machine bar insulation with earlier established ones gained for various test samples

is commonly limited below 10 MHz, which is equivalent to a rise time slightly above 30 ns. To increase the upper limit frequency, it seems convenient to decrease the value of the coupling capacitor, which is associated with a reduction in the internal inductance responsible for the limitation of the upper cut-off frequency (Fig. 4.60b). Consequently, the highest measuring frequency is achievable for capacitive sensors providing simple metallic discs, as initially used for pinpointing of PD sources by means of a hand-held PD probe shown in Fig. 4.60c, as described also in Sect. 10.4.4 and Fig. 10.43. Such kinds of capacitive sensors, often referred to as C-sensors, receive the electric field component of electromagnetic PD transients. A sketch of a coaxial C-sensor intended for detection of PD defects in power cables is shown in Fig. 4.61, where a section of the outer semiconductive layer covering the cable insulation has to be removed to receive the electric field component from the inner cable conductor in case of travelling waves due to PD events. The achievable measuring sensitivity lies in the pC range and is governed by the capacitance C_s between sensor electrode and inner cable conductor.

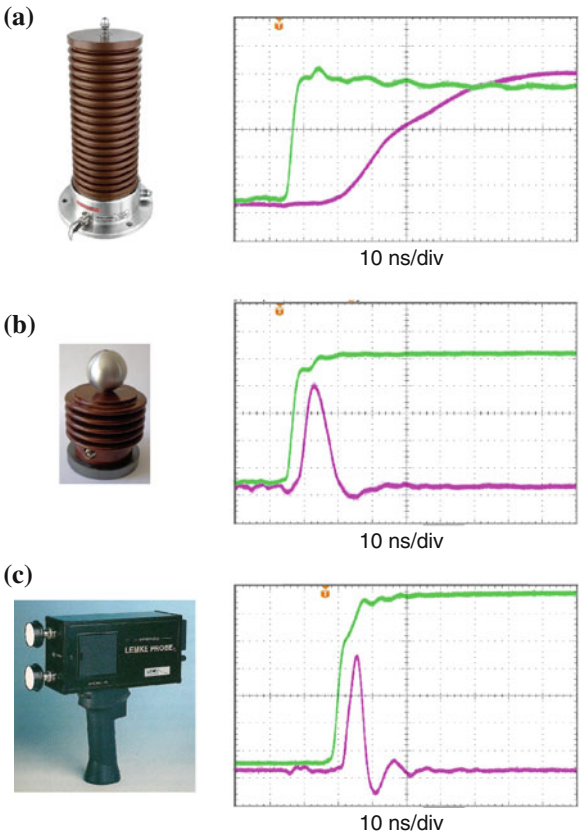

Fig. 4.60 Step voltage response measured for capacitive PD couplers. **a** High capacitive coupling capacitor designed according to IEC 60270:2000 (2,000 pF, rated 24 kV). **b** Low capacitive coupling device (50 pF, rated 12 kV). **c** Disc-shaped C-sensors used for PD probing

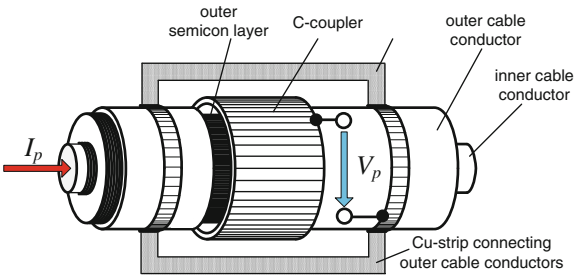

Fig. 4.61 Sketch of a capacitive coupler attached to a power cable

Example Consider a polyethylene-insulated power cable of dielectric permittivity of $\varepsilon_r = 2.2$. Assuming a ratio between outer and inner cable conductor of $r_a/r_i = e = 2.718$, one gets for a coaxial C-sensor of the length $l_a = 100$ mm the following approximation:

$$C_s \approx 2 \cdot \pi \cdot \varepsilon_0 \cdot \varepsilon_r \cdot l_a \approx 12 \text{ pF}$$

If the received PD signal is transmitted via a measuring cable matched by its characteristic impedance Z_m, the peak voltage V_p appearing across Z_m and thus at the input of the peak detector can roughly be accounted for by

$$V_p \approx C_s \cdot Z_c \cdot Z_m \cdot \frac{I_p}{t_r}.$$

I_p and t_r are the peak value and the rise time of the PD pulse current, respectively, and Z_c is the characteristic impedance of the power cable. Assuming a cavity discharge of a current pulse with a rise time of $t_r = 1$ ns and a peak value of $I_p = 1$ mA, one gets for the above-introduced circuit parameters ($C_s = 12$ pF, $Z_c = 30\ \Omega$, $Z_m = 50\ \Omega$) a detectable peak voltage of $V_p = 18$ mV, which is well measurable by digital oscilloscopes.

4.7.2.2 Inductive PD Couplers

Inductive PD couplers, commonly referred to as L-sensors, are in principle pulse transformers where the primary coil is formed by a single conductive lead, i.e. the turn number is $n = 1$. To capture the complete magnetic flux surrounding the primary conductor, the windings of the secondary coil are wounded around a high permeable ferrite core. Under this condition, the transient PD current $i_p(t)$ through the primary conductor induces a voltage $v_p(t)$ in the secondary coil (Fig. 4.62). Therefore, L-sensors are also referred to as high-frequency current transformers (HFCT) or sometimes as "yoke coils". In this context, similarities to the Rogowski coils designed without ferrite core (see Sect. 7.5.2) should be mentioned.

A simple PD coupling unit, which is formed by a L-sensor attached to the ground connection lead of a power cable terminal, is shown in Fig. 4.62. To characterize the dynamic behaviour, it seems convenient to determine the step current response in the time domain according to Fig. 4.63. Comparing the oscilloscopic records shown in the Fig. 4.63c and d, it can be concluded that the transmitted pulse length is drastically reduced if the turn number of the secondary coil is decreased from originally $n = 10$ down to $n = 1$, as expected. From this follows also that a pulse length shorter than 1 μs is hardly achievable if classical L-sensors are employed. Consequently, only PD signals in the RF range (3–30 MHz) but not in the VHF/UHF range can be decoupled.

4.7.2.3 Electromagnetic PD Couplers

The operation principle of electromagnetic (EM) PD couplers is comparable with that of antennas operating in the near-field region. That means the output signal is determined by both vectors referring to the electric field component $\vec{E}$ and the magnetic field component $\vec{H}$, respectively, given by the Maxwell equations:

$$\mathrm{rot}\vec{H} = \varepsilon \cdot \frac{\delta \vec{E}}{\delta t}, \quad \mathrm{rot}\vec{E} = -\mu \cdot \frac{\delta \vec{H}}{\mathrm{d}t}. \tag{4.22}$$

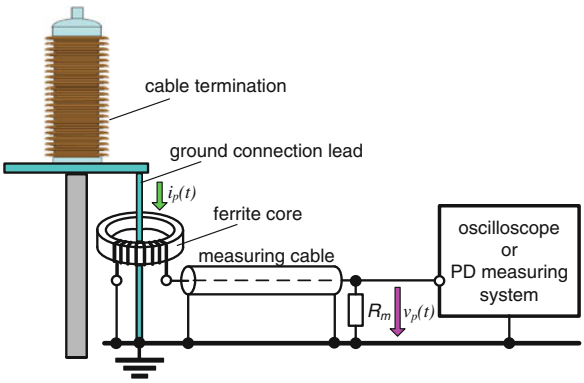

Fig. 4.62 PD measuring circuit using signal decoupling via L-sensor commonly used for power cable terminations

Depending on the geometrical configuration of the test object, various kinds of EM sensors are applied for the PD detection in the VHF/UHF range, such as rod, disc or conical antennas. The latter are commonly used for PD diagnostics of gas-insulated substations (Pearson et al. 1991) to avoid the ignition of disturbing PDs at the sharp edges of rod and disc electrodes. A sketch of a conical UHF PD sensor installed in a flange of a GIS compartment is shown in Fig. 4.64. Such antennas are capable for PD detection up to a frequency range of approx. 1.5 GHz. The upper cut-off frequency is governed by the reciprocal value of the time constant given by the inevitable stray capacitance between sensor electrode and ground flange and the characteristic impedance of the measuring cable matched by its characteristic impedance (Meinke and Gundlach 1968; King 1983; Küpfmüller 1984).

For PD detection in power cable joints, so-called directional coupler sensors (DCS) have well been proven for both off-line and on-line PD detection using measuring frequencies between 2 and 500 MHz (Pommerenke et al. 1995). The design is similar to that of capacitive sensors where the signal is captured from both sensor ends. Installing a pair of DCS at both joint sides, the PD signals originating inside the joint can be discriminated between noise and PD signals originating in the connected power cables. This is because a PD event inside the joint causes signals at the ports "B" and "C" which are significantly higher than those occurring at the ports "A" and "D" (Fig. 4.65). Another benefit of this arrangement is that one sensor can be used to calibrate the other one. Practical experience revealed that under noisy on-site condition, a measuring sensitivity in the range of few pC is achievable.

To capture the PD signal from grounding leads of the test object high-frequency current transformers (HFCTs) can advantageously be used, as discussed previously. The drawback of such PD couplers is, however, that the measuring frequency is limited to the RF range (3–30 MHz). A well-promising alternative is the employment of pulse transformers using the concept of transmission line inverters shown in Fig. 4.66 (Lemke et al. 2003). Here, a coaxial cable of few cm length is used its inner conductor is terminated with its characteristic impedance at the

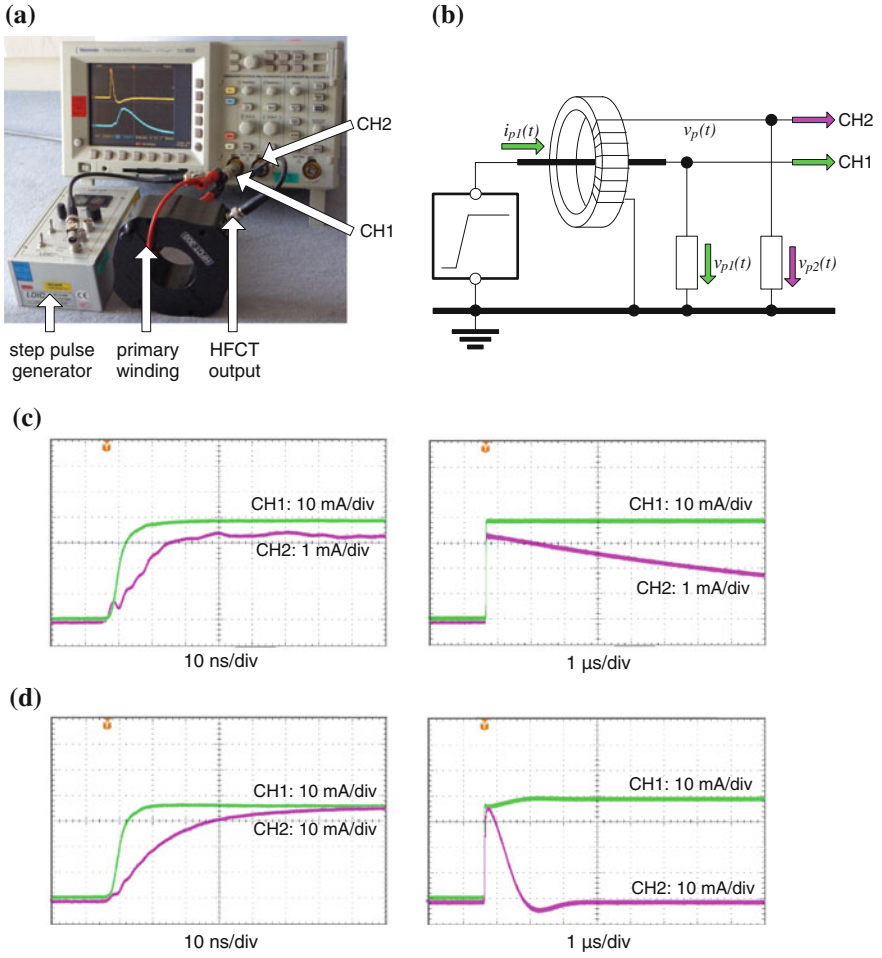

Fig. 4.63 Determination of the step current response of an inductive sensor (HFCT). **a** Photograph of the experimental set-up. **b** Equivalent circuit. **c** Step current response for $n = 10$. **d** Step current response for $n = 1$

output, respectively, its outer conductor is terminated at the input. The inner conductor is grounded at the input and the outer sheath at the output. Under this condition, both the magnetic and electric field components are transmitted in the UHF range where the pulse polarity is inverted (Lewis 1959). PD couplers based on this concept have well been proven in practice for both periodical and continuous PD monitoring of cable joints and terminations (Fig. 4.67).

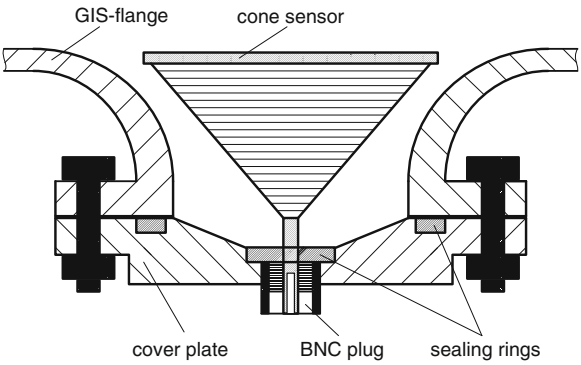

Fig. 4.64 Sketch of an UHF sensor installed in a GIS flange

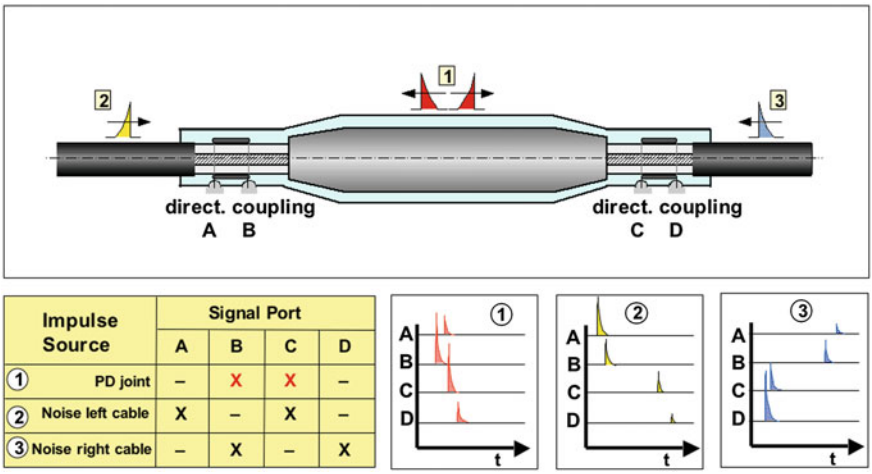

Fig. 4.65 Operation principle of directional coupler sensors (*DCS*) installed at both sides of a power cable joint

4.7.3 Basic Principles of PD Detection in the VHF/UHF Range

As discussed already in Sect. 4.1, the main benefit of the PD detection in the VHF/UHF range is the comparatively high signal-to-noise ratio. In compliance with the IEC method, it can be distinguished between wide-band and narrow-band PD signal processing. Instruments using the first approach are equipped with a high-sensitive wide-band amplifier in combination with a very fast peak detector to capture the crest value of the appearing voltage signal, as obvious from Fig. 4.68a. Using the narrow-band method, slowly damped oscillations are excited by the PD pulses. In this case, the maximum magnitude of the envelope is evaluated using also a fast peak detector, as shown in Fig. 4.68b.

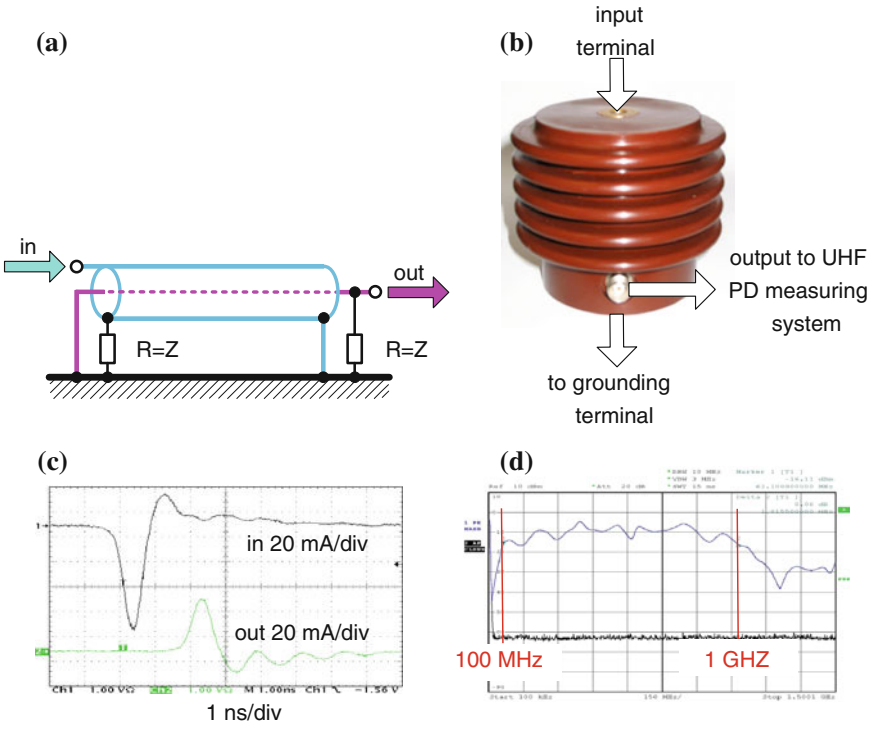

Fig. 4.66 PD coupler based on the principle of a nanosecond pulse inverter. **a** Equivalent circuit. **b** Technical design. **c** PD pulse response in the time domain, time base: 1 ns/div. **d** Transfer function in the frequency domain

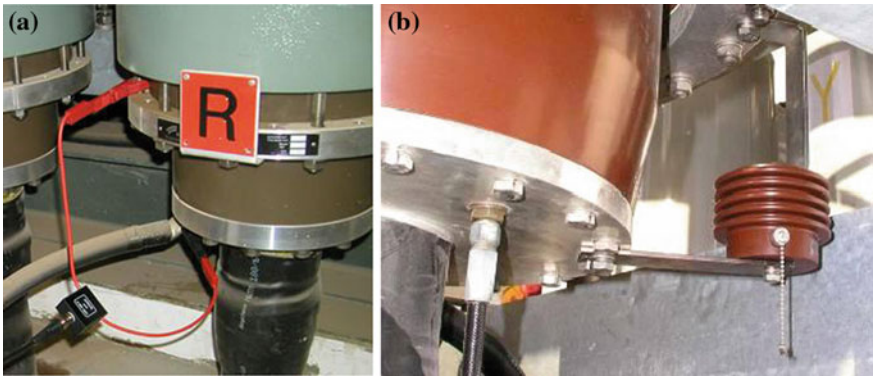

Fig. 4.67 PD couplers based on the pulse inverter technique. **a** Flexible PD sensor used for periodical PD monitoring of GIS cable terminations. **b** Installed PD sensor used for continuous PD monitoring of outdoor cable terminations

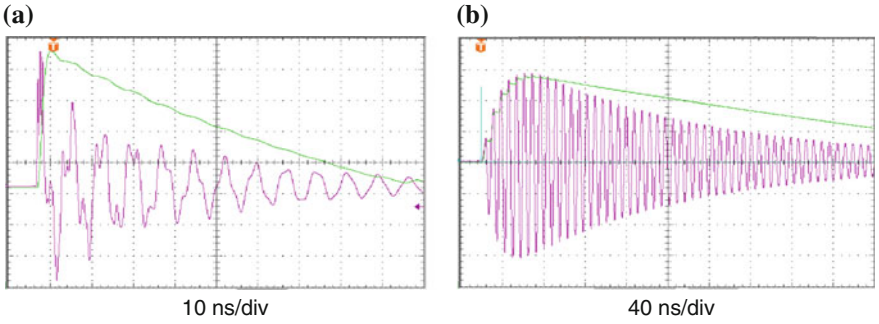

Fig. 4.68 PD pulse response of UHF measuring circuits showing the output signal of the amplifier (*violet trace*) and the peak detector (*green trace*). **a** Wide-band measuring instrument. **b** Narrow-band measuring instrument

The peak detectors used for both the wide-band and narrow-band PD signal processing are commonly designed such that the duration of the output signal is stretched from the ns up to the μs range. Under this condition, the further signal processing can be performed by means of classical PD measuring systems to display the phase-resolved PD patterns. A survey on the basic measuring principles commonly used for the PD detection in the VHF/UHF range is shown in Fig. 4.69.

For wide-band PD detection in the VHF/UHF range, also digital oscilloscopes, nowadays available for measuring frequencies above 1 GHz, can conveniently be applied. The design of narrow-band measuring instruments is similar to that of conventional spectrum analysers, where either the full-span or zero-span mode can be used, as shown in Fig. 4.70.

Using the full-span mode, the frequency spectrum of the captured PD signal as well as the superimposed noise is recorded for the pre-selected start and stop frequencies. Noises can be distinguished from actual PD signals if the background noise level is recorded prior the actual PD test, as shown in Fig. 4.70. The main drawback of the full-span mode is that phase-resolved PD patterns cannot be created because the measurement is performed in the frequency domain. Thus, frequently the zero-span mode is preferred, which is in principle comparable with the technique used for radio interference voltage (RIV) measurements (Sect. 4.3.3). That means the centre frequency is adjusted such that the noise level becomes a minimum. This can conveniently be determined using the full-span mode.

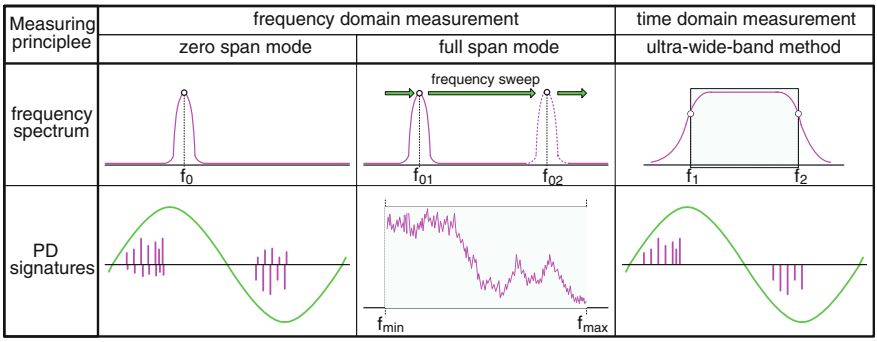

Fig. 4.69 Survey on UHF/VHF PD detection principles

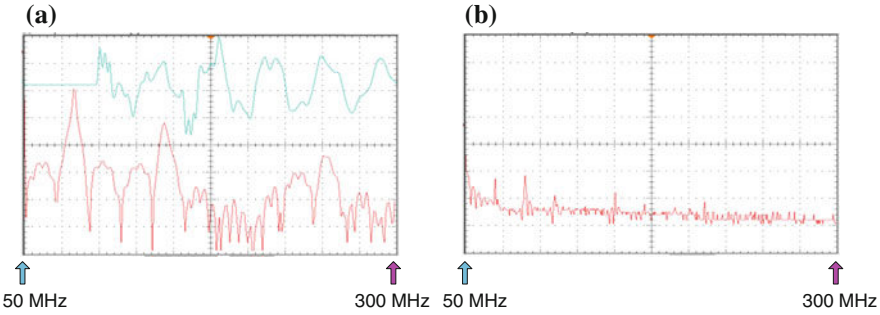

Fig. 4.70 Screenshots of a spectrum analyser using the full-scan mode (50–300 MHz). **a** Background noise level of the measuring surroundings. **b** Frequency response against a calibrating pulse

4.7.4 Comparability and Reproducibility of UHF/VHF PD Detection Methods

As discussed previously, the main benefit of the UHF/VHF PD detection method is the substantial enhancement of the signal-to-noise ratio if compared with the classical IEC method. This offers the chance to perform sensitive PD diagnosis test of HV apparatus under noisy on-site condition, which is commonly impossible if the IEC method is applied. In this context, it must be emphasized, however, that the PD quantities measured by both methods are not sufficiently correlated with each other which can simply be proven if the phase-resolved PD patterns are recorded simultaneously, as exemplarily shown in Fig. 4.71 for a power cable termination. Analysing the individual PD pulses for each instant of occurrence gained for multiple screenshots, a large scattering of the magnitudes can be observed, as exemplarily shown in Fig. 4.72.

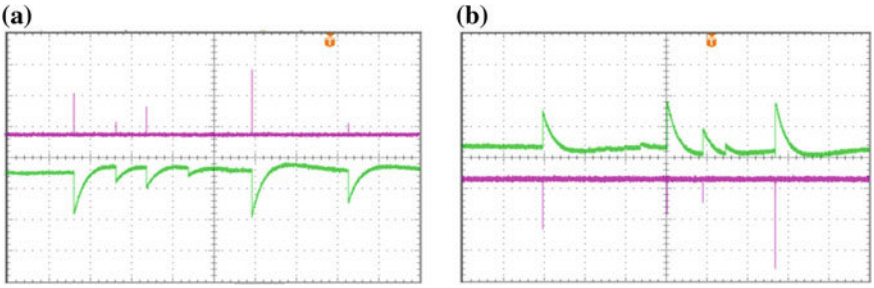

Fig. 4.71 Screenshots of phase-resolved PD pulses recorded simultaneously for a VHF measuring circuit (*violet trace*) and the classical IEC circuit (*green trace*) investigating a defective power cable termination subjected to power frequency AC test voltage. **a** Positive half-cycle. **b** Negative half-cycle

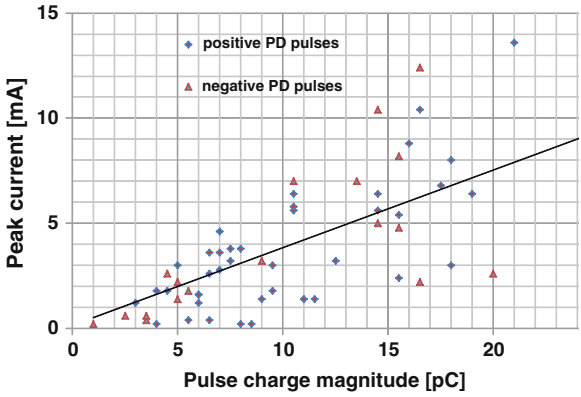

Fig. 4.72 Results of comparative PD tests showing the peak values of PD current pulse measured the VHF method versus the pulse charge measured by the IEC method

This behaviour is expected due to the fact that the duration of the individual PD pulses and thus the frequency content varies over a wide range. Consequently, at constant peak value of the PD current, which is evaluated by the here applied VHF method, the pulse charge magnitudes increases with the width of the captured PD pulses. Thus, the pulse magnitude measured in terms of mA will never correlate with the pulse charge measured according to IEC 60270:2000. Thus, instead of a calibration, a sensitivity check is recommended in the draft of IEC 62478) for estimating the PD threshold level in terms of pC based on comparative PD studies.

In this context, it must also be emphasized that the test results gained by various UHF/VHF PD instruments might also not be comparable. This is due to the fact that the signal magnitude is strongly affected by the distance between PD site and sensor position due to attenuation and dispersion phenomena. The reproducibility of PD test results can thus only be improved if the sensors are permanently installed at fixed positions in the HV apparatus to be inspected and the measuring frequency range is not changed for repetitive PD diagnosis tests.

Despite the drawback that the UHF/VHF PD detection method cannot be calibrated in terms of pC, there are various benefits. So the signal-to-noise ratio is essentially higher if compared to the IEC method, as mentioned previously. This offers the possibility to determine the PD inception voltage also under noisy on-site conditions. Moreover, the PD severity can be estimated under service voltage using continuous PD monitoring where the long-term PD trending is judged. Another advantage is that for geometrically extended HV apparatus, such as GIS/GIL and large power transformers, potential PD defects can precisely be located using time-of-flight measurements (Pearson 1991), as described in Sect. 10.4.1.3.

4.8 Acoustic PD Detection

PD events radiate not only electromagnetic transients but also pressure waves covering a frequency range between some kHz up to several 100 kHz. The main benefit of the acoustic emission (AE) detection is the immunity against electromagnetic interferences. To ensure also a high immunity against mechanical noises not associated with PD events, usually the ultrasonic frequency range is selected, preferably between 40 kHz and few 100 kHz. In the field of high-voltage engineering, the AE technique has first been employed for the detection and localization of airborne noises due to corona discharges, such as the identification of discharges igniting on shielding electrodes of HV test facilities as well as for the detection of corona discharges occurring on the surface of HV insulators and HV transmission lines. A photograph of a hand-held battery-powered ultrasonic PD detector intended for the localization of air-borne noises is shown in Fig. 4.73. As the acoustic signal will be very close to the PD sources, these can be localized by moving the ultrasonic transducer around until the maximum signal is received.

In the late 1950s, the AE technique was also employed for detection of structure-borne noises due to PD defects in HV apparatus (Anderson 1956) and became thereafter a widely established tool for preventive PD diagnostics of gas-insulated substations (Graybill 1974; Lundgaard et al. 1990; Albiez and Leijon 1991) as well as for large power transformers (Harrold 1975; Nieschwitz and Stein 1976; Howels and Norton 1978; Lundgard et al. 1989; Fuhr et al. 1993). Besides the magnitude, also the shape of the detected AE signal could be very informative due to the fact that the frequency content of the AE signal is reduced as larger the distance between sensor and PD source is.

Using only a single AE transducer, however, the localization procedure becomes extremely time-consuming, particularly in case of intermitting PD events. As an alternative, the so-called *triangulation* has been introduced using three or even more transducers to measure the *flight time* of the AE signal, as illustrated in Fig. 4.74. For a homogenous medium, the distances x_1, x_2 and x_3 between the PD source and the AE transducers are proportional to the flight time t_1, t_2 and t_3 determined from the records gained for each transducer in connection with a

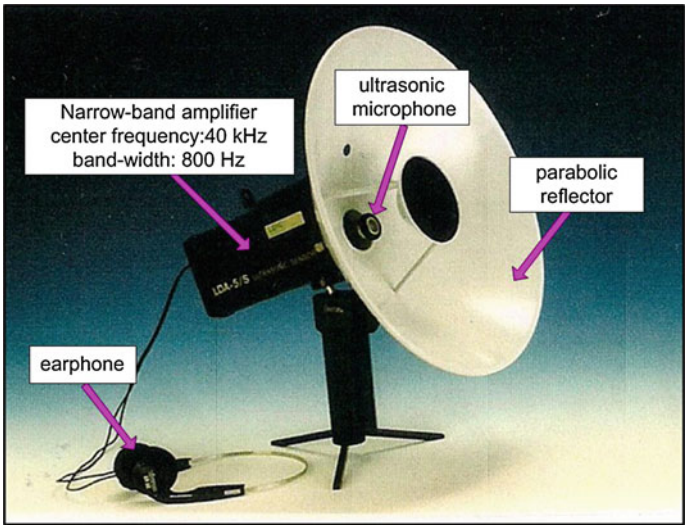

Fig. 4.73 View of an AE probe intended for ultrasonic PD detection of airborne noises (Courtesy of Doble Lemke)

multichannel digital oscilloscope. Thus, the trajectories shown in Fig. 4.74 are crossing the location of the PD source.

To minimize the localization uncertainty, it is a common practice to use of the AE technique in conjunction with the electrical PD measurement. This offers the possibility to trigger the oscilloscope by an electrical signal appearing at instant of the PD event, as obvious from Fig. 4.75a. As the time lag of the electrical signal is significantly below 1 μs, this can be neglected if compared with flight time of the AE signal because this travels only 1.2 mm in oil within this time interval. Under noisy condition, the signal-to-noise ratio can substantially be enhanced if the averaging mode is used, i.e. if the scope is triggered by numerous consecutive electrical PD pulses, as obvious from Fig. 4.75. The combined acoustic-electrical method provides also confirmation that indeed a PD defect has been detected and not a disturbing acoustic noise.

Under laboratory condition, the electric signal required for triggering the oscilloscope is commonly captured from the test object via a coupling capacitor or even from the bushing tap, if available. Under noisy on-site condition, however, it is more beneficial to use the VHF/UHF technique to enhance the signal-to-noise ratio, as discussed more in detail in Sect. 4.7. In this context, it must be emphasized that the triangulation according to Fig. 4.74 provides only correct results for acoustic waves travelling in a continuum where the sound velocity is constant. For HV equipment of complex design, such as power transformers, the wave velocity is strongly affected by the very different construction materials, such as copper, steel, wood, pressboard and insulating oil. Thus, instead of the direct sound wave, propagating the shortest distance between PD source and AE transducer, two wave

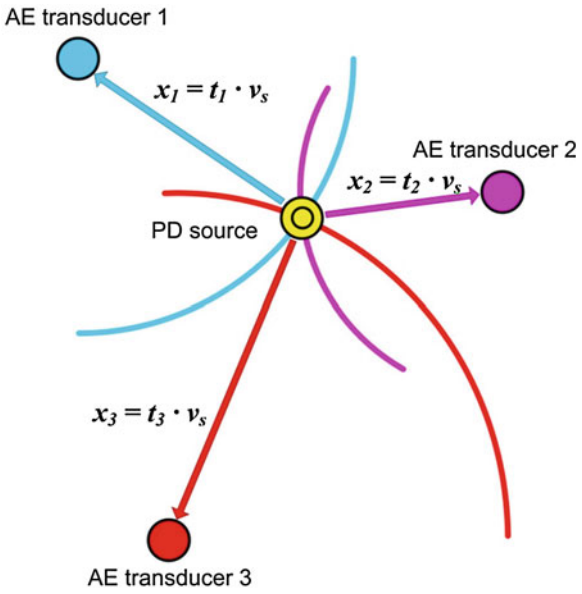

Fig. 4.74 Principle of triangulation for localization of PD sources

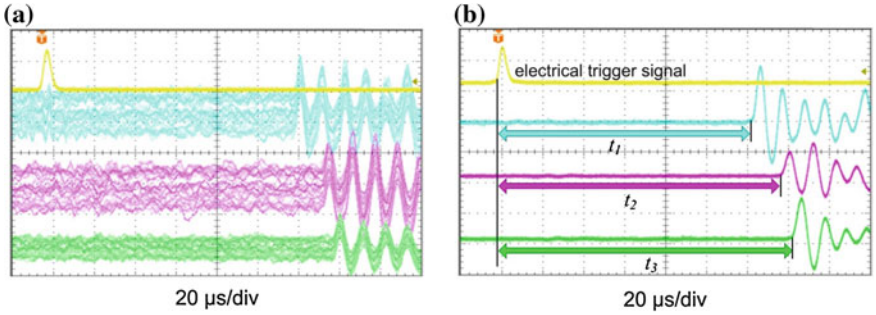

Fig. 4.75 Flight time measurement of AE signals received by three ultrasonic transduces attached to the tank of a 110-kV instrument transformer triggering the oscilloscope by an electrical signal due to the PD event. **a** single-pulse triggering. **b** multi-pulse triggering (averaging)

fronts of very different velocity have to be considered. These are commonly referred to as longitudinal (pressure) and transversal (shear) wave. Without going into further details, it should be mentioned that the shortest path is not the fastest one for the AE wave, as shown in Fig. 4.76. This is due to the different velocities which are, for instance, approx. 1.25 mm/µs in oil and 5.1 mm/µs in steel. To solve the very complex equations gained for the wave velocity in real HV

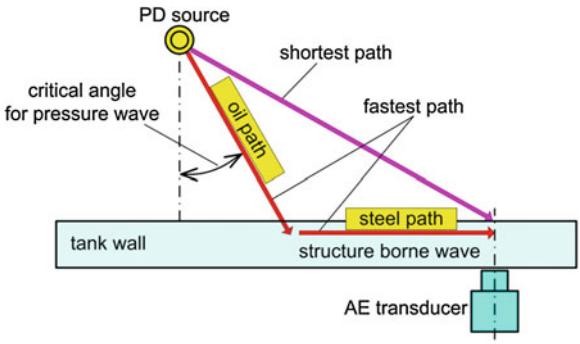

Fig. 4.76 Shortest and fastest path between a PD source in oil and an acoustic sensor placed on a power transformer tank

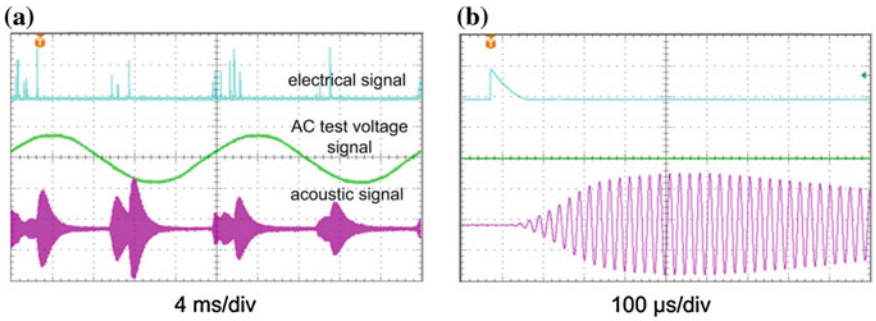

Fig. 4.77 PD pulse response of a narrow-band AE measuring system having a centre frequency of 42 kHz and a bandwidth of 800 Hz. **a** Superposition of PD pulse trains. **b** Response against a single PD pulse

equipment, nowadays advanced computer systems equipped with sophisticated software packages are available.

The facility required for acoustic detection and location of PD sources in HV equipment comprises usually an array of AE transducers, a signal transmission unit (cabling or fibre optic link) and an acquisition system (digital oscilloscope or computer-based measuring system) to perform the processing, visualization and storage the captured ultrasonic data. The following types of AE transducers are commonly applied for capture the mechanical pressure waves associated with of PD events:

- Piezo-electric transducers,
- Structure-borne sound resonance transducers,
- Accelerometers,
- Condenser microphones and
- Electro-optic transducers.

As the acoustic impedance of the transducers differs substantially from that of the metallic enclosure of the HV apparatus to be investigated, the transducer surface is usually covered with hard epoxy resin for efficient signal transmission, which provides also the required electrical insulation. Moreover, special attention should be paid to the coupling method due to the fact that the transmitted acoustic signal might be reflected at the interface between transducer and enclosure of the HV equipment. Thus, acoustic couplant gel or grease should be used to minimize the impact of reflections.

Generally, it seems beneficial to integrate a pre-amplifier in the AE transducer to attain high sensitivity due to the enhancement of the signal-to-noise ratio. Using narrow-band amplifier operating at centre frequencies around 40 kHz might also contribute to reliable test results because AE noises are not associated with PD events, such as mechanical vibrations due to pumps and fans as well as noises emanated from the iron core due to magnetostriction and Barkhausen effect, can effectively be rejected. In case of narrow-band measurements, the pulse response is characterized by an oscillation where the envelope covers often a time span substantially above several 100 μs. Thus, a superposition of subsequent PD pulse trains might appear, as shown in Fig. 4.77. Among others, this is the reason that the AE method is not capable to measure the PD activity in terms of pC. Another reason for this is the strong attenuation and dispersion of AE signals if travelling through various insulation structures of HV equipment. That means insulation materials feature a low-pass character for the AE waves where the attenuation of AE waves increases nearly proportional with the square of the characteristic frequency (Beyer 1987). Nevertheless, the AE method has been proven as a valuable tool for reliability centred maintenance.

Chapter 5
Measurement of Dielectric Properties

Abstract The ageing of the insulation of HV apparatus is not only caused by the high electric field strength but also by thermal and mechanical stresses that evolve during normal operation condition. This may lead to chemical processes associated with a gradual deterioration of the integral insulation properties. Finally, weak spots and, in extreme case, a breakdown might occur, which causes not only an unexpected outage of HV equipment but also physical, environmental and financial damage. To ensure a reliable operation of the HV assets encourages high standards of quality assurance tests after manufacturing as well as advanced tools for preventive diagnostics in service. As treated already in Chap. 4, PD measurements have become an indispensable tool to trace local dielectric imperfections since the 1960s. In contrast to this, the measurement of the integral dielectric properties became already of interest for insulation condition assessment of HV equipment used for the first HV transmission systems at the beginning of the twentieth century. In this context, it seems noticeable that the dielectric properties are not only determined at test frequencies close to the service frequency, as in the case of loss factor measurements, but also at very low frequencies not representative for service conditions. Valuable results are also obtained if the dielectric response against DC exciting voltages is measured, as will be treated in the following.

5.1 Dielectric Response Measurements

Subjecting a solid dielectric between plane electrodes to a high DC field strength, the capacitance will rapidly be charged. After that, a comparatively low current is detectable which is not only caused by the DC conductivity of the dielectric material but also by polarization phenomena. This is due to the Coulomb force (Coulomb 1785) which causes a small displacement of the positive and negative charge carriers, originally neutralizing each other. Thus, after a certain time lag, a dipole moment is established. Vice versa, a depolarization occurs after the DC source is disconnected and the electrodes of the test sample are short-circuited.

W. Hauschild and E. Lemke, *High-Voltage Test and Measuring Techniques*,
DOI: 10.1007/978-3-642-45352-6_5,

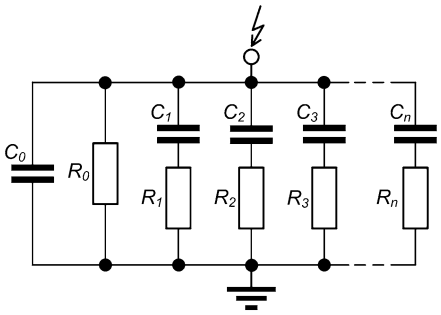

Fig. 5.1 Equivalent circuit of solid dielectrics

As the return of the charge carriers to its origin follows also after a certain time lag, a so-called *return voltage* (sometimes also referred to as "recovery voltage") is measurable between the electrodes of the test sample after removing the short circuit. Such a dielectric *relaxation* has first been discovered by Maxwell in 1888 and explained more in detail by Wagner in 1914 based on an equivalent circuit according to Fig. 5.1. This network is composed of the basic capacitor C_0 and the resistor R_0 representing the DC resistance as well as various R–C elements reflecting various relaxation time constants $\tau_1 = R_1 \cdot C_1$, $\tau_2 = R_2 \cdot C_2$, … $\tau_n = R_n \cdot C_n$. These characterize transition frequencies associated with typical polarization phenomena, such as trapping of charge carriers, interfacial and orientation polarization and ion and electron polarization.

Nowadays, the return voltage measurement (RVM) is one of the most established diagnostic tools for insulation condition assessment. This method has first been introduced by Boening in 1938 and is widely utilized for preventive diagnostics of HV equipment since the 1960s (Nemeth 1966, 1972; Reynolds 1985; Csepes et al. 1994; Lemke and Schmiegel 1995; Gubanski et al. 2002). The basic circuit applied as well as typical voltage signals gained by the RVM method is shown in Fig. 5.2. First, the test sample is excited by a constant DC voltage of magnitude V_e. For this, the switch S_1 is closed, whereas the switch S_2 remains still open. As a result of the continuous DC stress, the basic capacitance C_0 is rapidly charged, whereas a certain time lag appears for charging the other capacitances C_1, C_2, C_3, … C_n. This is due to the characteristic *relaxation time constants* τ_1, τ_2, … τ_n, as mentioned above. After a DC stressing time t_1, which lasts usually several tens of minutes or even more, the switch S_1 is opened and the test sample is short-circuited by closing the switch S_2 at instant t_1 for several minutes or even more. Under this condition, the basic capacitance C_0 is completely discharged, whereas the capacitances C_1, C_2, C_3, … C_n are only partially discharged due to the characteristic relaxation time constants τ_1, τ_2, τ_3, … τ_n.

If at instant t_2 the switch S_2 is opened, the residual charges stored in the capacitances C_2, C_3, … C_n cause a charging of the basic capacitance C_0. Thus, across the terminals of the test object, a return voltage $v_r(t)$ is measurable. As C_0 is not only charged but also discharged due to the volume resistance R_0 of the investigated dielectric material, after an initial rise characterized by the slope

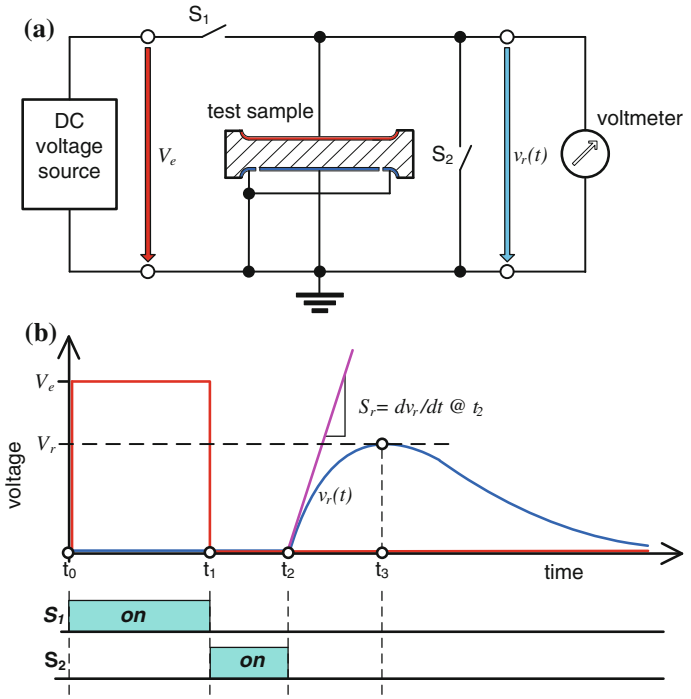

Fig. 5.2 Principle of return voltage measurement (*RVM*). **a** Basic circuit. **b** Characteristic signals

$dv_r(t)/dt$, the return voltage reaches a maximum value V_r at time instant t_3 and decays thereafter more or less exponentially to zero, as obvious from Fig. 5.2b.

Additional information on the insulation condition is gained by establishing so-called polarization spectra performing a series of recovery voltage measurements. For this, a constant DC stress is applied, where the duration of both the charging time t_1 and the short-circuit duration $(t_2–t_1)$ is stepwise increased. With respect to reproducible measurements, it seems reasonable to keep the ratio $(t_2–t_1)/t_1$ constant where often a value of 0.5 is used. Commonly for each test sequence both the initial slope $dv_r(t)/dt$ at time instant t_2 and the peak value V_r of the return voltage is plotted versus the charging time t_1. A practical example is shown in Fig. 5.3 which refers to an oil-impregnated insulation where the moisture content has been changed. Generally, it can be stated that each maximum of the return voltage belongs to a dominant relaxation time constant, which is often in unambiguous relation with a typical ageing phenomenon. Based on practical experience, it seems thus possible to assess the insulation condition of HV apparatus, in particular the moisture content and the depolymerization of oil-impregnated paper insulation used for power transformers and power cables.

Another approach is the analysis of the *polarization current* and *depolarization current*, as illustrated in Fig. 5.4. Comparable to the return voltage measurement,

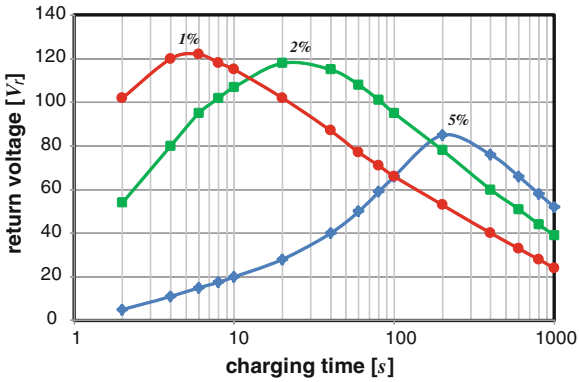

Fig. 5.3 Depolarization spectra measured for oil-impregnated paper at moisture content of 1, 2 and 5 %

the test sample is first subjected to a DC voltage V_c where the switch S_1 remains closed up to the instant t_2. Thus, the main capacitance C_0 is almost completely charged, which lasts usually few seconds.

To avoid an overload and thus a possible damage of the sensitive ammeter due to the high charging current at the fast rising DC test voltage, this instrument is initially short-circuited by the switch S_2 and opened delayed at instant t_1 to measure the time-dependent polarization current i_p (t) due to charging the additional capacitances C_1, C_2, C_3, … C_n, see Fig. 5.1. This current decays more or less exponentially up to a steady-state value I_{DC}, which is governed by the DC resistance R_0.

The next step starts at instant time t_2 when the switch S_2 is short-circuited again and the test sample is disconnected from the DC source. Just thereafter the switch S_3 is short-circuited so that the main capacitance C_0 is almost completely discharged. Few seconds thereafter the switch S_2 is opened at instant t_3, whereas S_3 remains closed. Under this condition, the time-dependent depolarization current $i_d(t)$ is measurable. Even if the polarity of this current is opposite to the polarization current, the time function fits more or less the polarization current. The only difference is that different to the first stage a resistive current component is not detectable due to the short-circuited terminals of the test object.

In this context, it should be noted that also other tools than the above are utilized for insulation condition assessment, such as the measurement of isothermal relaxation currents (Simmons et al. 1973; Beigert et al. 1991). In principle, all circuits adopted are more or less modifications of those treated above. An example is presented in the following which refers to the analysis of the *recovery charge* which is based on an electronic integration of the depolarization current (Lemke and Schmiegel 1995). A schematic diagram of the circuit adopted for this method as well as typical signals are shown in Fig. 5.5.

As usual for return voltage measurements as well as polarization/depolarization measurements, the test object capacitance is first excited by a constant DC voltage V_e, usually in the order of few kV. According to practical experience, the prestressing time is preferably chosen between 2 and 10 min. During this time

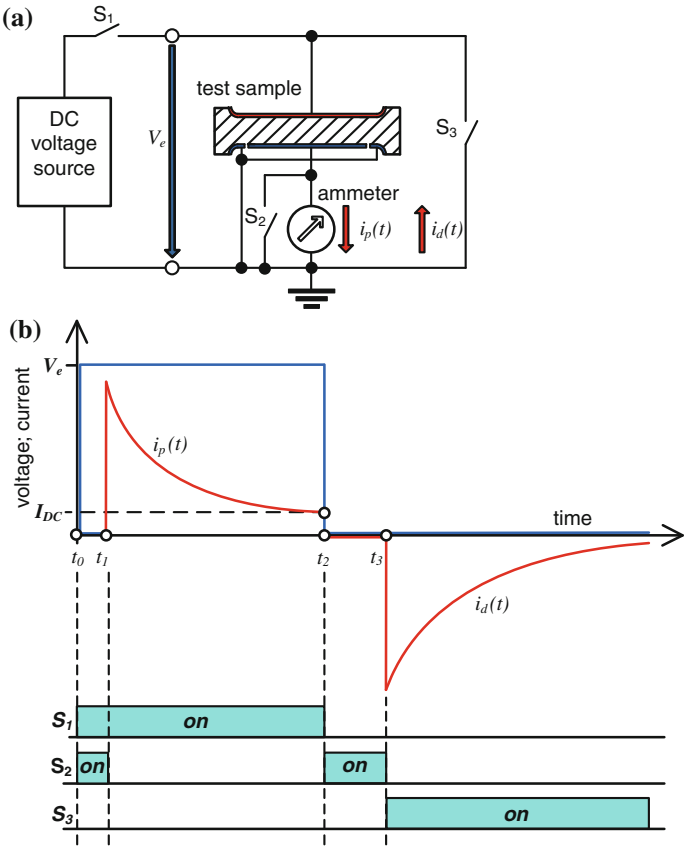

Fig. 5.4 Principle of polarization and depolarization measurement. **a** Basic circuit. **b** Characteristic signals

interval, the switch S_1 is closed, whereas all other switches remain still open. The second step starts at instant t_1 when the switch S_1 is opened and immediately thereafter the switch S_2 is closed. As the condition $C_m \gg C_0$ is always satisfied for power cables, the charge, originally stored in the main capacitance C_0 of the test object, is almost completely transferred to the measuring capacitor C_m of known capacitance. Thus, the test object capacitance C_0 can simply be deduced from the exciting voltage V_e and the voltage magnitude V_m appearing across C_m within the time interval t_1–t_2:

$$C_0 \approx C_m \cdot \frac{V_m}{V_e}. \tag{5.1}$$

The next step starts at instant t_2 when the measuring capacitor C_m is disconnected from the test object, opening the switch S_2. Few seconds thereafter the switch S_3 is closed up to the instant t_3 in order to discharge the residual

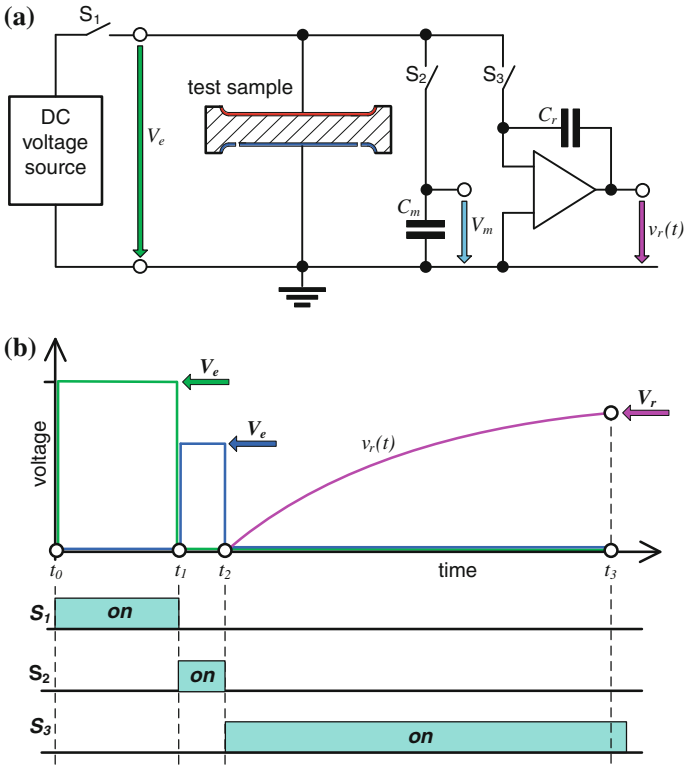

Fig. 5.5 Principle of the recovery charge measurement. **a** Basic circuit. **b** Characteristic signals

capacitances of the test object. According to practical experience, both time intervals t_1–t_0 and t_2–t_1 should be in the order of 10 s. For a known capacitance C_r of the active integrator, the recovery charge q_r (t) can simply be determined from the output voltage v_r (t):

$$q_r(t) = C_r \cdot v_r(t). \tag{5.2}$$

The measurement is commonly finished when steady-state conditions appear where the output voltage v_r (t) of the electronic integrator attains a maximum value V_r. This is usually the case after approx. 10 min. An appropriate quantity to assess the insulation condition is the polarization factor F_p, which is provided by the ratio between the magnitude Q_r of the recovery charge and the total charge Q_m stored during the DC pre-stressing in the main capacitance of the test object. Combining Eqs. (5.1) and (5.2), the *polarization factor* becomes

$$F_P = \frac{Q_r}{Q_m} = \frac{C_r}{C_m} \cdot \frac{V_r}{V_m}. \tag{5.3}$$

Here, the ratio C_r/C_m can be considered as a scale factor so that the polarization factor F_P can simply be determined from the ratio between the voltage magnitudes appearing across C_r and C_m, respectively. Based on practical experiences gained for XLPE-insulated power cables, the insulation condition can be assessed as "good" for $F_p < 10^{-4}$.

Example Figure 5.6 shows typical voltage signals recorded for a service aged 20 kV XLPE cable. To get appropriate readings, the following settings of the polarization factor measuring instruments have been chosen:

Divider ratio	$R_2/R_1 = 1{:}400$
Measuring capacitance	$C_m = 100\ \mu F$
Integrating capacitance	$C_r = 1\ \mu F$

Using the Eqs. (5.1) and (5.3), the following values can be drawn from the record shown in Fig. 5.6:

Test voltage	$V_e = (5\ V) \cdot 400 = 2{,}000\ V$
Main capacitance	$C_0 = (100\ \mu F) \cdot (2.3\ V)/2{,}000\ V = 145\ nF$
Polarization factor	$F_p = [(1\ \mu F)/(100\ \mu F)] \cdot [(0.64\ V)/(2.3\ V)] = 28 \times 10^{-4}$

As this value exceeds the above-mentioned limit $Fp < 10^{-4}$ substantially, the presence of water trees has been supposed. This could be confirmed by deeper investigation of samples of the exposed cable under laboratory conditions.

5.2 Loss Factor and Capacitance Measurement

As the insulation of HV apparatus is mainly stressed by power frequency voltages, the knowledge of the dielectric properties at this test frequency is primarily of interest. For this comparatively low frequency, the equivalent circuit according to Fig. 5.1 can substantially be simplified, as shown in Fig. 5.7, which constitutes of a series connection of the test object capacitance C_s with a hypothetical resistance R_s, reflecting the losses dissipating in technical HV insulation.

As the resistivity R_s of semiconducting materials and thus of technical insulations decreases at rising temperature, the current density may increase in regions where the convection of the dissipated power is comparatively limited. Finally so-called hot spots appear, accelerating the deterioration to weak points in the insulation and thus causing an ultimate puncture. Thus, the measurement of *dielectric losses* became an indispensable tool for completing withstand tests of HV apparatus since the beginning of the last century, when high alternating voltages were introduced for power supply.

As known from the classical network theory, the series connection of C_S an R_S causes a phase shifting φ between the applied test voltage $V_S = V_C + V_R$ and the current I_S feeding the test object. From a technical point of view, it seems

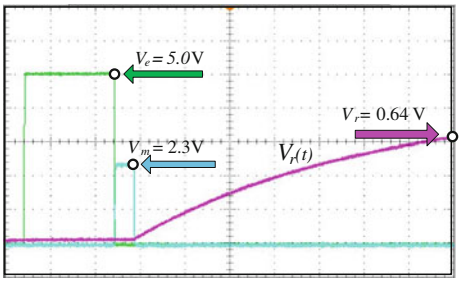

Fig. 5.6 Record of a recovery charge measurement performed on an aged MV XLPE power cable

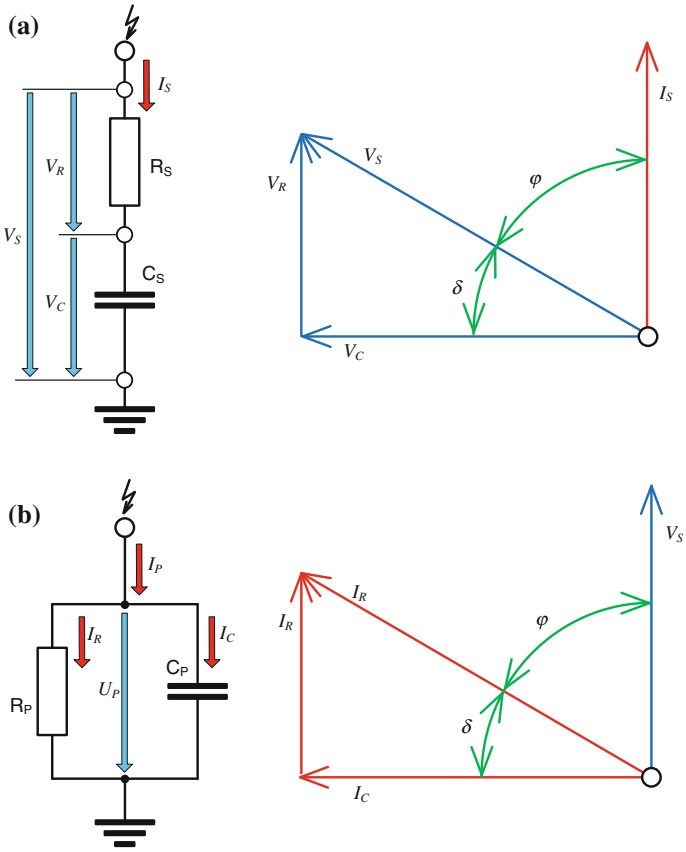

Fig. 5.7 Equivalent circuits and associated vector diagrams commonly used for the definition of the loss factor tanδ of the insulation of HV apparatus. **a** Series circuit. **b** Parallel circuit

convenient to evaluate the tangent δ between the voltages V_S and V_R appearing across C_S and R_S, respectively (Fig. 5.7a). Multiplying both voltages with the current I_S through the test sample, the *loss factor* $\tan\delta$ can also be expressed by the ratio between the resistive power P_R dissipating in the test object and the capacitive (reactive) power P_C:

$$\tan\delta = \frac{V_R}{V_C} = \frac{V_R \cdot I_S}{V_C \cdot I_S} = \frac{P_R}{P_C} = \omega \cdot C_S \cdot R_S. \tag{5.4}$$

Based on the classical network theory, a series circuit can also be converted into parallel circuit as shown in Fig. 5.7b. For this, the following relation applies:

$$\tan\delta = \frac{I_R}{I_C} = \frac{I_R \cdot V_S}{I_C \cdot V_S} = \frac{P_R}{P_C} = \frac{1}{\omega \cdot C_P \cdot R_P}. \tag{5.5}$$

Comparing both equations, it can readily be shown that the loss factor becomes equal for both equivalent circuits illustrated in Fig. 5.7 if expressed by the ratio between active (resistive) and reactive (capacitive) power. Therefore, the following equation can be considered as the general definition of the loss factor:

$$\tan\delta = \frac{P_R}{P_c}. \tag{5.6}$$

5.2.1 Schering Bridge

To measure the loss factor of dielectrics as well as the insulation of complete HV equipment, the classical Schering bridge is commonly applied (Schering 1919). In principle, this is composed of a measuring and a reference branch, as illustrated in Fig. 5.8. The HV arm of the measuring branch, being formed of the capacitance C_X in series with the hypothetical resistance Rx of the test object, is grounded via the tunable resistor R_3 providing the LV arm. The HV arm of the reference divider being formed by the loss-free standard capacitor C_N is grounded via a parallel connection of the resistor R_4 and the tunable capacitor C_4, both forming the LV arm.

To balance this bridge circuit, the elements R_3 and C_4 are adjusted accordingly to minimize the voltage across the LV arms of both branches. The remaining voltage difference is indicated by a so-called zero detector Z_I. Applying a HVAC test voltage, the criterion of the balanced bridge can be expressed by the following impedance ratio:

$$\begin{aligned} &\frac{Z_X}{Z_3} = \frac{Z_N}{Z_4}, \quad \text{with } Z_X = R_X + \frac{1}{j\omega \cdot C_X}, \quad Z_N = \frac{1}{j\omega \cdot C_N}, \quad Z_3 = R_3, \\ &Z_4 = \left(R_4 + \frac{1}{j\omega \cdot C_4}\right) \Big/ \left(\frac{R_4}{j\omega \cdot C_4}\right). \end{aligned} \tag{5.8}$$

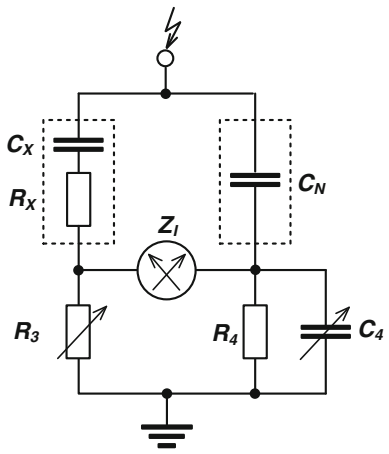

Fig. 5.8 Circuit elements of a Schering bridge

Inserting these relations into Eq. (5.8), the loss factor becomes

$$\tan\delta = \omega \cdot C_4 \cdot R_4. \tag{5.9}$$

Commercially available Schering bridges are often equipped with a fixed resistor of $R_4 = 318.3\ \Omega$ and a tunable capacitor C_4. Applying a test frequency of 50 Hz, the loss factor is simply given by

$$\tan\delta = C_4/10\,\mu\text{F} \tag{5.10}$$

If, for instance, the bridge is balanced for $C_4 = 0.02\ \mu$F, the loss factor becomes $\tan\delta = 2 \times 10^{-3}$.

Due to ageing processes after longer service time, not only the loss factor $\tan\delta$ but also the capacitance C_X of HV equipment may change. Based on Eq. (5.8), this can be determined by

$$C_X = C_N \cdot \frac{R_4}{R_3}. \tag{5.11}$$

For high capacitive test objects, such as power cables, power transformers and rotating machines, it has to be taken into account that the current through the test could heat up the measuring resistor R_3 which might thus be damaged. Due to this, it seems reasonable to shunt R_3 by a well-defined parallel resistor much lower than R_3 to carry almost the complete current through the test object.

As the loss factor of technical insulation, such as polyethylene-insulated cables, is as low as 10^{-4}, the impedances of the LV elements may be affected by stray capacitances. Therefore, it seems reasonable to screen the low-voltage parts of the bridge accordingly. Connecting the screening electrodes to the ground potential, however, acts like a bypass and causes thus a non-controlled phase shifting of the voltages across the LV arms. To overcome this crucial problem, the low-voltage parts are commonly screened by an *auxiliary branch* with adjustable potential

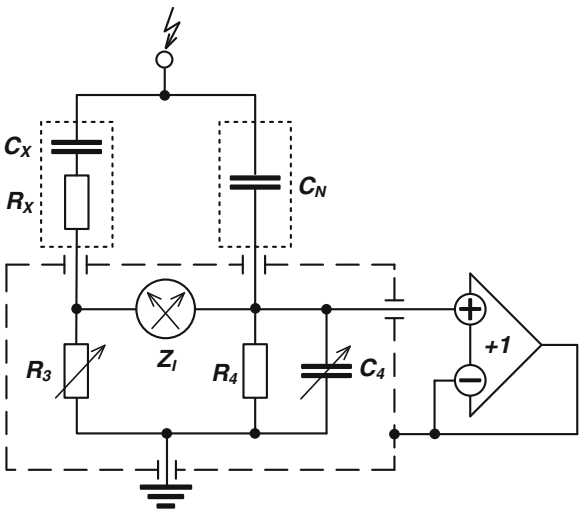

Fig. 5.9 Schering bridge with an auxiliary branch for automatic potential control of the screening electrodes

(Wagner 1912). This can advantageously be done by shifting the potential of the screening electrode automatically using an impedance converter of extremely high input impedance and low output impedance, as illustrated in Fig. 5.9.

Another challenge is the loss factor measurement of grounded HV apparatus, such as power transformers, rotating machines and power cables. This method, commonly referred to as *grounded specimen test* (GST), requires a disconnection of the HVAC test voltage supply from the earth potential (Poleck 1939). Under this condition, however, the test results may also strongly be affected by non-controlled stray capacitances between the HV test supply and the bridge circuit. To overcome this crucial problem, the Schering bridge is modified as illustrated in Fig. 5.10. Before starting the actual loss factor measurement, first a pre-balancing of the circuit is required where the test specimen is disconnected via the switch S_X from the HV terminal to adjust the auxiliary elements R_5 and C_5 accordingly, where the switch S_4 is closed. After that S_4 is opened and S_X is closed to start the actual HV test where the bridge is balanced as usual, i.e. adjusting R_3 and C_4.

For GST of three-phase arrangements, such as power transformers, various modifications of the bridge circuit have been proposed, such as GST-ground-guard, GST-ground-ground and GST-guard-guard. The basic configurations recommended for loss factor and capacitance measurements of HV apparatus are specified in the standards IEC 60250: 1969 and IEC 60505: 2011.

5.2.2 *Automatic* C-*tanδ Bridges*

Classical Schering bridges are capable for measurement of tanδ variations down to 10^{-5} as well as capacitance values below 1 pF. The measuring uncertainty is in the

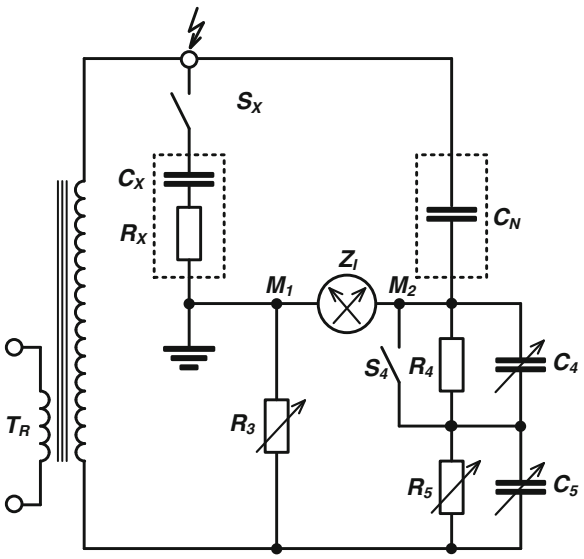

Fig. 5.10 Schering bridge modified for C-tanδ measurement of grounded specimen test (*GST*)

order of 1 % for loss factor measurements and approx. 0.1 % for capacitance measurements. However, the main drawback is the time-consuming balancing procedure so that classical Schering bridges are not qualified for measuring rapidly changing dielectric properties. To overcome this disadvantage, fully automatic computer-based loss factor and capacitance measuring bridges have been introduced in the 1970s when the first microcomputers were available (Seitz and Osvath 1979).

The concept shown in Fig. 5.11 is based on the compensation of the current I_X through the test specimen by the current I_N through the standard capacitor C_N utilizing a high precision differential current transformer which is controlled by a microcomputer. The primary coils with windings W_1 and W_2 provide the low-voltage arms of the bridge and induce inverse magnetic fluxes in the core.

The residual flux is detected by the secondary coil with W_3 windings. The output signal controls the further data signal processing by means of a microcomputer. So the flux in the core of the differential transformer is fully compensated by the currents through the auxiliary coils with windings W_4 and W_5, respectively. If the bridge is balanced, the computer calculates the actual values of C_X and tanδ as well as of the applied AC test voltage.

Due to the progress in digital signal processing (DSP), nowadays more sophisticated computer-based solutions are available (Kaul et al. 1993; Strehl and Engelmann 2003). A simplified block diagram of a DSP-based C-tanδ measuring system is shown in Fig. 5.12. Basically, the HV circuit is composed of two capacitive voltage dividers. The measuring branch constitutes of the test object, being formed by the series connection of $C_X + R_X$, and the measuring capacitor C_M. The reference branch contains the series connection of the HV standard capacitor C_N and the LV capacitor C_R.

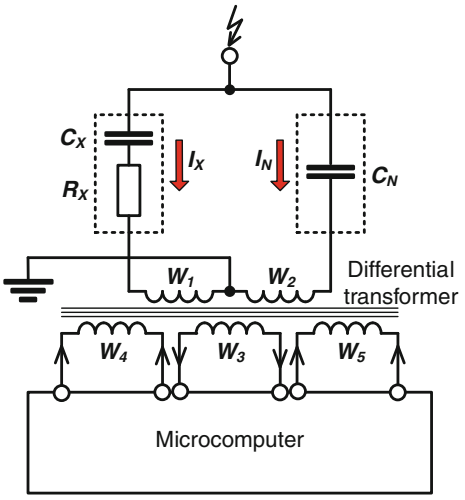

Fig. 5.11 Concept of an automatic C-tanδ bridge circuit

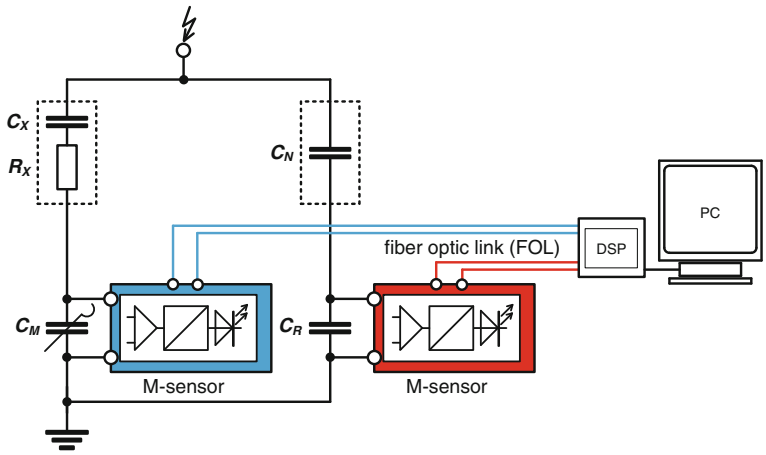

Fig. 5.12 Concept of a computerized DSP-based C-tanδ measuring system

Different to the automatic C-tanδ bridge, where the current I_X through the test object is compensated by the reference current I_N, an exact balance is not required. This is because the loss factor is independent from the actual voltage magnitudes, so that the dielectric properties can also be determined by measuring the voltage vectors captured from C_R and C_M, as illustrated in Fig. 5.13. Thus, it seems sufficient to adjust the voltage across C_M only such that the magnitude approaches almost the voltage across C_R where a deviation in the order of several tens of percentage is acceptable.

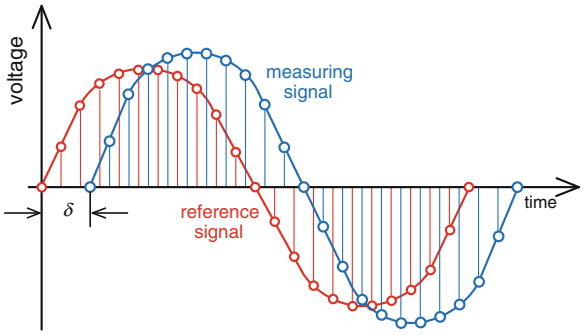

Fig. 5.13 Digitalization of the reference and measuring signal used by *DSP-based C*-tanδ measuring system

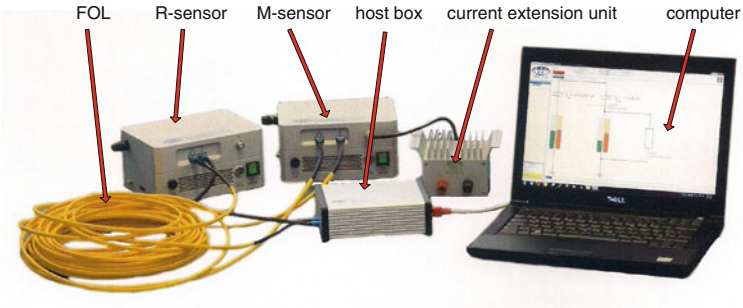

Fig. 5.14 Components of a DSP-based computerized *C*-tanδ measuring system (Courtesy Doble-Lemke GmbH)

The major components of a computerized DSP-based *C*-tanδ measuring system are obvious from Fig. 5.14. The LV signals across C_M and C_R are captured by battery powered, potential-free operating sensors. Both are equipped with a low noise differential amplifier of high input impedance (>1 GΩ), a fast A/D converter (resolution 16 bit at 10 kHz sample), and an electro-optical interface. The digitized signals are transmitted via fibre optic links (FOL) to the measuring system, which also transmits the control signals from the computer to both sensors. After a fast discrete Fourier transformation performed by a DSP, the data are calculated, stored and displayed.

Real-time multitasking software ensures a calculation of the dielectric quantities for each cycle of the applied HVAC test voltage. This ensures a substantial improvement of the measuring accuracy using the averaging mode. As the measuring principle is based on the determination of the phase angle of a non-balanced bridge in a frequency-independent but frequency-selective mode, the actual test frequency can be varied over a wide range, typically between 0.01 and 500 Hz.

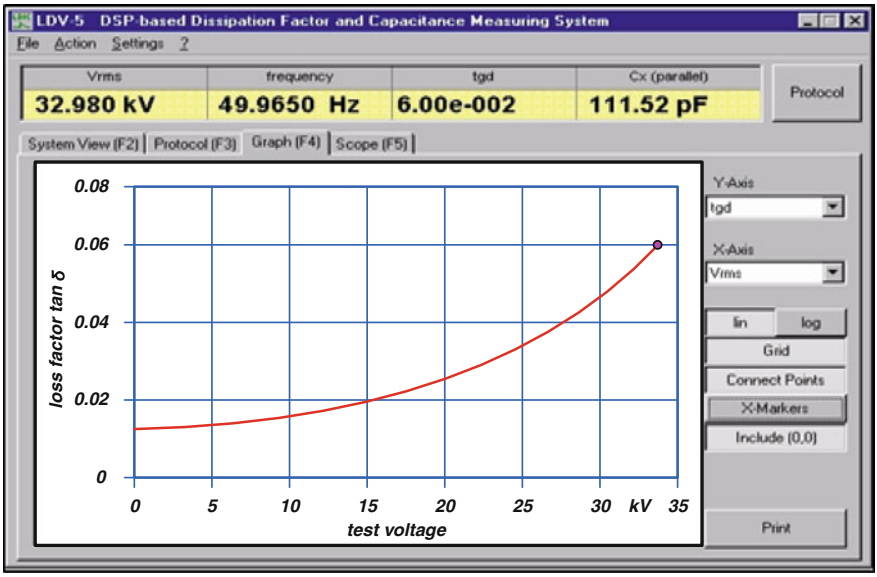

Fig. 5.15 Screenshot showing the loss factor versus the test voltage gained for an aged machine bar

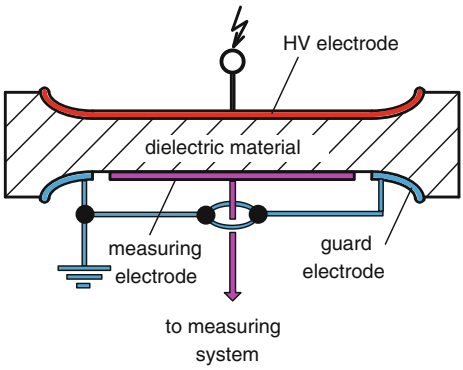

Fig. 5.16 Electrode configuration of a test sample for C-tanδ measurement using a guard electrode

All measured quantities can be displayed numerically in the real-time mode. Moreover, the data, such as the loss factor, the capacitance, the current through the test object, the frequency and the test voltage level in terms of rms. or the peak value can be exported using an Excel-compatible data-format. Another benefit is that the dielectric quantities can be plotted on the PC screen depending on various parameters, such as the test voltage, exemplarily shown in Fig. 5.15, and the recording time for trending purposes. At power frequency (50/60 Hz), an "internal" measuring uncertainty below 10^{-5} could be achieved for the loss factor.

The "extended" measuring uncertainty, however, is mainly governed by the behaviour of the standard capacitor C_N (Schering and Vieweg 1928; Keller 1959).

It has to be taken care that the measuring uncertainty is also affected by the design of the test sample. The impact of stray capacitances and parasite surface currents can be minimized if so-called guard electrodes are employed, as illustrated in Fig. 5.16.

Chapter 6
Tests with High Direct Voltages

Abstract HVDC test voltages represent the stress of insulations in HVDC transmission systems. Today, HVDC transmission systems are long point-to-point connections for the transmission of high power. These links are realized by HVDC overhead lines and HVDC cables, especially submarine cables. In the near future, it is expected that the application of the HVDC technology will increase and also HVDC networks will be established (Shu 2010). Therefore, also HVDC test voltage is becoming more important. This chapter starts with the different circuits for HVDC test voltage generation. Then, the requirements for HVDC test voltages according to IEC 60060-1: 2010 and the consequences for the components of test systems are considered. The interactions between test generator and test object are investigated for capacitive load—e.g. of submarine cables—and for resistive load in case of wet, pollution and corona tests. A short description of test procedures with HVDC test voltages follows. Finally, it is described how direct voltages can be measured by suitable measuring systems of resistive dividers and suited measuring instruments, and how measurements—e.g. PD measurements—at DC voltage are performed.

6.1 Circuits for the Generation of HVDC Test Voltages

Today, HVDC test voltages are generated by rectification of HVAC voltages of transformers (see Sect. 3.1.1). Modern solid state rectifier elements, in the following "*diodes*" (silicium diodes), enable the generation of all necessary test voltages and currents, but the limitations in the reverse voltage to few 1,000 V require the series connection of these diodes for HV rectifiers with reverse voltages up to several 100 kV's or even MV's. When the circuits for HVDC test voltage generation are considered, all mentioned rectifiers are HV rectifiers assembled from many diodes (see Sect. 6.2.2).

W. Hauschild and E. Lemke, *High-Voltage Test and Measuring Techniques*,
DOI: 10.1007/978-3-642-45352-6_6,

6.1.1 Half-Wave Rectification (One-Phase, One-Pulse Circuit)

When a HV rectifier, a load capacitor C (e.g. capacitive test object or smoothing capacitor) and a resistive load R (e.g. resistive voltage divider or resistive test object) are connected to the output of a simple HVAC transformer circuit (Fig. 6.1a), a HVDC voltage is generated. The rectifier opens for half-waves of one polarity and closes for the opposite polarity. It opens only as long as the HVAC voltage at the "stiff" transformer output is higher than the voltage of the charged capacitor. As soon as the capacitor carries any charge, its discharging starts and becomes significant when the rectifier closes after the voltage has reached its maximum $V_{\max}$ (Fig. 6.1b). The capacitor is discharged to a minimum voltage $V_{\min}$, until the rectifier opens again for a short time ΔT (also expressed by a phase angel α). This means the output voltage is not constant, and it shows a so-called "*ripple*" *voltage* δV which is defined by

$$\partial V = \frac{V_{\max} - V_{\min}}{2}. \tag{6.1}$$

The discharging current $i_L(t)$ is connected with a charge Q which must be replaced within the short time ΔT by a current pulse $i(t)$ from the transformer

$$Q = \int_T i_L(t)\mathrm{d}t = I \cdot T = 2 \cdot \partial V \cdot C = \int_{\Delta T} i(t)\mathrm{d}t. \tag{6.2}$$

The term "*one-phase, one-pulse circuit*" reflects that the feeding voltage is a single-phase one and the DC charging is performed by one current pulse per period. With the mean direct current

$$I = \frac{V_{\max} + V_{\min}}{2 \cdot R}$$

and the relation between the duration of period T and frequency f of the feeding AC voltage, one gets an important relation for the ripple

$$\partial V = \frac{I \cdot T}{2 \cdot C} = \frac{I}{2 \cdot f \cdot C}. \tag{6.3}$$

The lower the ripple, the smoother is the HVDC test voltage. The ripple decreases with increasing load resistance (This means with decreasing load!), increasing load capacitance and increasing frequency of the charging AC voltage. But, in case of half-wave rectification, the ripple remains quite large. Equation 6.2 shows additionally that the feeding HVAC transformer circuit must be able to supply a sufficient current $i(t)$.

If the test object shows heavy predischarges of relatively high pulse currents which may happen during wet and pollution tests, the voltage drops down as the

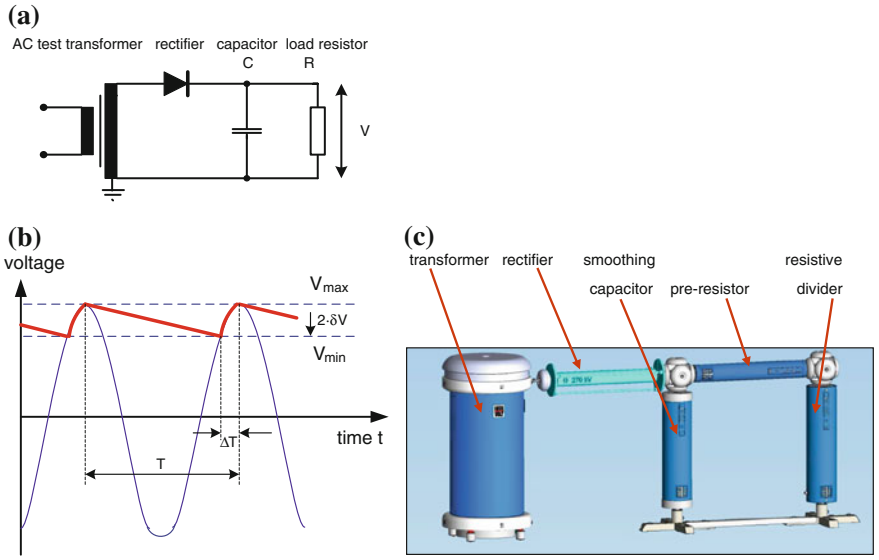

Fig. 6.1 One-phase, one-pulse half-wave rectification. **a** Equivalent circuit diagram. **b** Feeding AC voltage and DC voltage with ripple. **c** Modular test system for HVDC 135 kV/10 mA and HVAC 100 kV/11 kVA

transient energy demand cannot be supplied via the transformer, it must be taken from the smoothing capacitor C. To limit this *voltage drop* d_V, the smoothing capacitance should be large enough.

> **Note** According to IEC 60060-1:2010, the voltage drop is the "instantaneous reduction of the test voltage for a short duration of up to few seconds". Here, it will be used according to this definition. In literature, e.g. Kuffel et al. (2006) or Kind and Feser (1999), the term voltage drop is used for the continuous voltage reduction between the no-load case and the load case, especially of multi-stage cascades. The term "*voltage reduction*" will be used for this phenomenon in the following. The voltage reduction is caused due to the "forward voltage drop" and the internal resistance of the rectifiers.

HVDC sources with half-wave rectification are usually not powerful enough. They are used as HVDC attachments to HVAC test systems especially for demonstration circuits and for student's training (Fig. 6.1c). The half-wave rectification causes a non-symmetric load of the HVAC power supply. This can even lead to saturation effects in the transformer. If a transformer with symmetric output—this means grounded midpoint—of the winding is available (Fig. 6.2), the opposite polarity of the AC voltage contributes to the charging of the smoothing capacitor C and avoids saturation effects, since each of the rectifiers opens for one half-wave. Consequently, two charging current pulses appear, and this *one-phase, two-pulse circuit* halves the ripple. The two-way half-wave rectifier circuits are also basic stages for HVDC cascade generators.

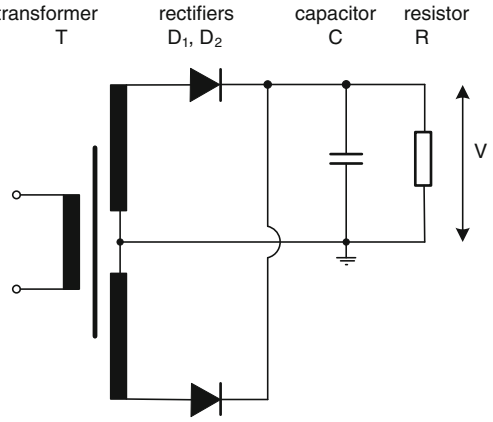

Fig. 6.2 One-phase two-pulse rectifier circuit

6.1.2 *Doubler and Multiplier Circuits (Greinacher/ Cockcroft-Walton Cascades)*

With the circuit of Fig. 6.3a, the output voltage can be doubled: The so-called doubler capacitor C_1 is charged to the voltage V_{C1}, and then, the voltage over the rectifier D_1 is oscillating around this value V_{C1}. Consequently, the smoothing capacitor is charged to a voltage which doubles the peak of the feeding AC voltage (Fig. 6.3b) if the losses in the circuit are neglected ($R \rightarrow \infty$). With losses—this means with a load resistor R— the output voltage is reduced below the theoretical no-load value. For the usual design of a HVDC attachment with doubler circuit connected to a HVAC generator (Fig. 6.3c) of a rated direct current of few 10 mA and a ripple factor $\delta V/V = \delta \leq 3$ %, this reduction might be in the order of 10 %. Therefore, the smoothing capacitance should be selected large enough.

The *doubler circuit* shall be understood as the basic stage of a multiplier circuit first proposed by Greinacher (1920) for HVDC power supply for nuclear physics and improved by Cockcroft and Walton later on in 1932. The principle shall be discussed for a cascade of three stages (Fig. 6.4): The left column of the capacitors contains the doubler capacitors [sometimes also called "blocking capacitors" (Kind and Feser 1999)], and the right column contains the smoothing capacitors (Fig. 6.4a). When voltage reduction and load resistance are neglected, the AC voltage $V_{AC}(t)$ with a peak value of V_{max} is oscillating around a DC offset of $1 \cdot V_{max}$ at the first doubler capacitor and delivers a DC value of $V_1 = 2 \cdot V_{max}$ at the output of the first stage of the smoothing column (Fig. 6.4b). At the second stage, the DC offset is $V_{12} = 3 \cdot V_{max}$ and the voltage at the smoothing column is $V_2 = 4 \cdot V_{max}$. Consequently, the DC offset at input of the third stage is $V_{13} = 5 \cdot V_{max}$, and the output of the generator is a DC voltage of $V_3 = 6 \cdot V_{max}$.

The direct voltage per stage is twice the peak voltage V_{max} of the feeding alternating voltage. In stationary operation and rated voltage, the necessary *reverse voltage* of the rectifiers is $2 \cdot V_{max}$. Doubler capacitors (except that of the lowest

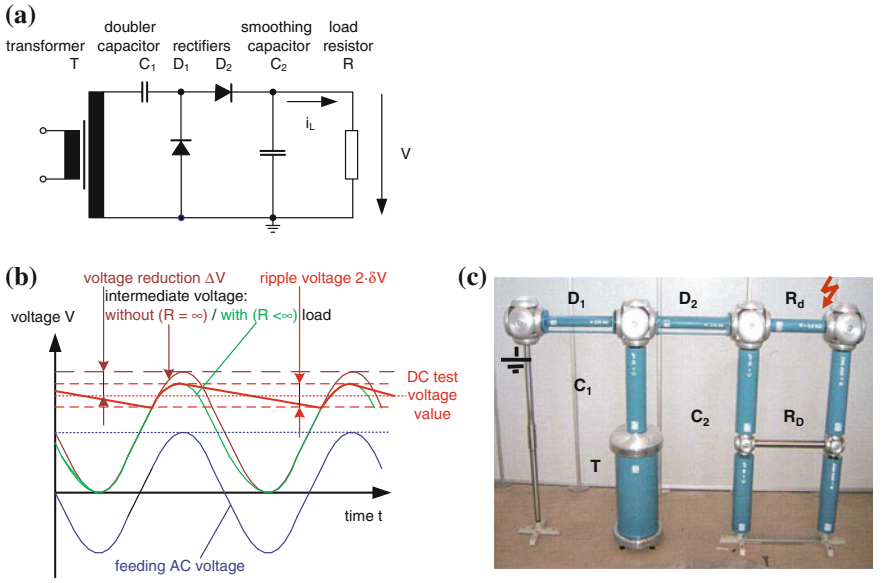

Fig. 6.3 One-phase, one-pulse doubler circuit with half-wave rectification. **a** Equivalent circuit diagram. **b** AC feeding, oscillating intermediate and DC voltages ($R \rightarrow \infty$). **c** Modular test system with doubler circuit 270 kV/10 mA

stage) must be able to withstand a DC stress of $2 \cdot V_{\max}$ plus the AC stress of the feeding voltage. Smoothing capacitors have to withstand a direct voltage of $2 \cdot V_{\max}$. The lowest doubler capacitor is only stressed with half of that voltage but causes the largest contribution to the ripple. Therefore, it should have the double value of the capacitance, this fits to the voltage distribution and reduces the ripple. The 1,500 kV cascade with a stage voltage of 500 kv—shown in Fig. 6.4c—is fed for its rated voltage with an AC voltage of $250\ \text{kV}/\sqrt{2} = 177\ \text{kV}$ (rms).

The ripple depends for this *one-phase, one-pulse multiplier circuit* also from the number of stages. The continuous current I through the test object is supplied from the smoothing capacitors. Usually, all capacitors in the smoothing column have the same capacitance, which is necessary for a linear voltage distribution in case of transient stresses, e.g. at breakdown of the test object. The ripple caused by the discharging of each smoothing capacitor could be calculated with Eq. (6.3) if no charge is transferred through the rectifiers to the oscillating doubler capacitors. But, in reality, the charge transfer causes a higher ripple δV and a *voltage reduction* ΔV for cascades with n stages which can be estimated (Elstner et al. 1983) by:

$$\partial V = \frac{I}{f \cdot C} \cdot \frac{n + n^2}{4}, \tag{6.4}$$

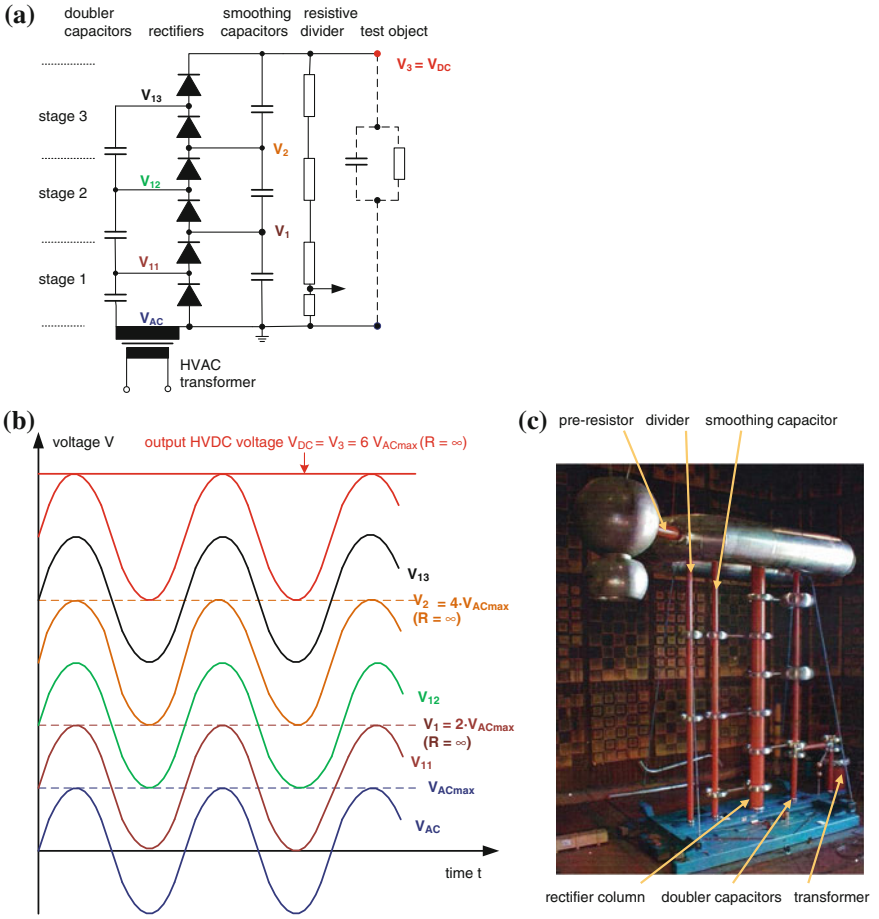

Fig. 6.4 Greinacher cascade (one-phase, one-pulse multiplier circuit). **a** Equivalent circuit diagram. **b** Potential at the three stages. **c** Generator with 500 kV per stage for 1,500 kV/30 mA

$$\Delta V = \frac{I}{f \cdot C} \cdot \frac{2 \cdot n^3 + n}{3}. \tag{6.5}$$

The relation between the real output voltage ($V_\Sigma - \Delta V$) and the cumulative no-load charging voltage $V_\Sigma = nV_1$ of a HVDC multi-stage generator can be understood as an efficiency factor (as usual for impulse voltage generators)

$$\eta_{DC} = \frac{V_\Sigma - \Delta V}{V_\Sigma}. \tag{6.6}$$

For practical cases, the voltage reduction can be remarkably higher than expressed by Eq. (6.5) which considers only the parameters of the generator.

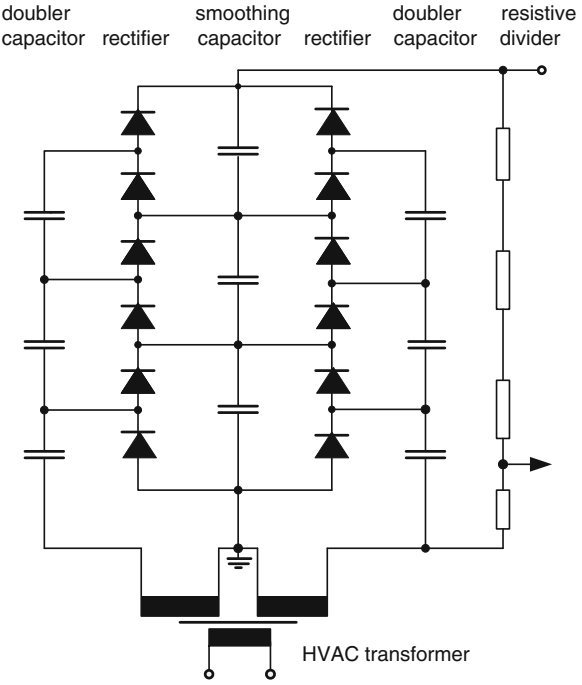

Fig. 6.5 Symmetric Greinacher cascade (one-phase, two-pulse multiplier circuit)

Mainly, stray capacitances in the feeding circuit cause an additional voltage reduction (Spiegelberg 1984).

Greinacher cascades are the most applied generators in HVDC testing. The polarity can be reversed by turning the rectifiers inside the generator by hand or motor. They are well suited for capacitive test objects, but have limits in case of a resistive load. The ripple can be reduced and the efficiency factor improved when the smoothing capacitances C and the frequency f of the feeding voltage are increased. Furthermore, the number of stages should be limited and the stage voltage increased as much as possible. For rated currents above 100 mA, more efficient circuits should be applied.

6.1.3 Multiplier Circuits for Higher Currents

Similar to the one-phase two-pulse circuit (Fig. 6.2), also doubler circuits can be designed. They are base stages of the so-called symmetric Greinacher cascade, a one-phase two-pulse multiplier circuit for currents of some 100 mA (Fig. 6.5). This principle can also be applied with three phases. Figure 6.6 shows a three-phase, six-pulse multiplier circuit with six charging pulses within one period of the feeding three-phase voltage. Therefore, this circuit is suited for high test currents in the order up to few amperes.

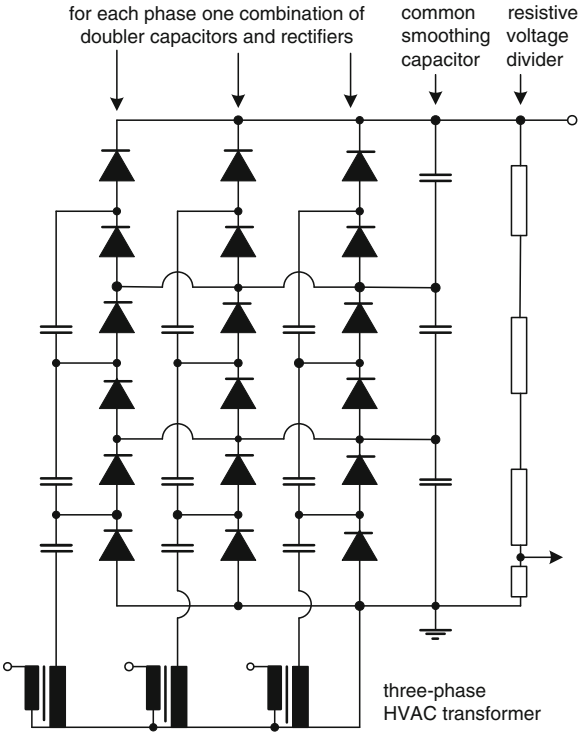

Fig. 6.6 Three-phase, six-pulse multiplier circuit

Table 6.1 compares the ripple values and the voltage reductions for the conventional and the symmetric Greinacher cascades as well as for the three-phase, six-pulse multiplier circuit. They are related to the influence of the number of stages n on the voltage reduction and on the ripple. They are valid under the assumptions that all capacitors have the identical capacitance C, only the lowest doubling capacitor has $2C$. Furthermore, in all cases, the current I required by a load R and the test frequency f are identical.

The conclusions are drawn from the comparison of multiplier circuits of $n = 5$ stages. They show that both, voltage reduction and ripple, are about five times lower when a symmetric Greinacher cascade is used instead of a conventional one. When the three-phase cascade is used, a further improvement by a factor of three appears. As mentioned before, the investigated circuits should be applied as follows:

- for rated currents below 100 mA, the conventional Greinacher cascade (Fig. 6.4),
- for rated currents of some 100 mA, the symmetric Greinacher cascade (Fig. 6.5),
- for rated currents higher than 500 mA, the three-phase multiplier circuit (Fig. 6.6).

Table 6.1 Comparison of voltage reduction and ripple for multiplier circuits of n stages (the term "y" is the factor according to lines 2 and 3 depending on the number of stages "n")

Type of circuit parameter	Greinacher cascade (one-phase, one-pulse multiplier circuit) (Fig. 6.4)	Symmetric Greinacher cascade (one-phase, two-pulse multiplier circuit) (Fig. 6.5)	Three-phase, six-pulse multiplier circuit (Fig. 6.6)
Voltage reduction ΔV	$\frac{I}{f \cdot C} \cdot \frac{2n^3+n}{3}$	$\frac{I}{f \cdot C} \cdot \frac{2n^3-3n^2+4n}{12}$	$\frac{I}{f \cdot C} \cdot \frac{2n^3-3n^2+4n}{36}$
Ripple voltage δV	$\frac{I}{f \cdot C} \cdot \frac{(n^2+n)}{4}$	$\frac{I}{f \cdot C} \cdot \frac{n}{4}$	$\frac{I}{f \cdot C} \cdot \frac{n}{12}$
Example $n = 5$: $\Delta V = \frac{I}{f \cdot C} \cdot y$	$y = 85$ (assumed 100 %)	$y = 16.25$ (19 %)	$y = 5.4$ (6.3 %)
Example $n = 5$: $\delta = \frac{I}{f \cdot C} \cdot y$	$y = 0.5$ (assumed 100 %)	$y = 1.25$ (16.7 %)	$y = 0.42$ (5.6 %)

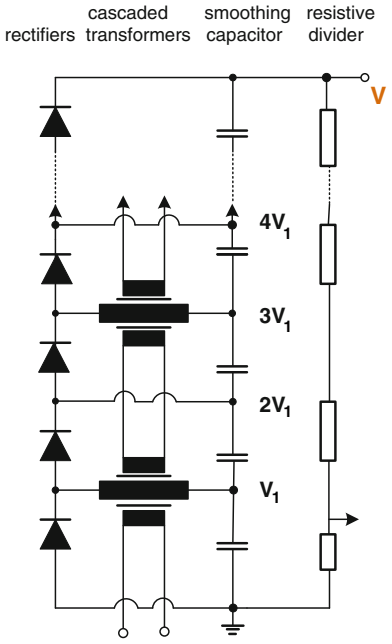

Fig. 6.7 Multiplier circuit with cascaded transformers

6.1.4 Multiplier Circuits with Cascaded Transformers

When a suited transformer cascade supplies the AC feeding voltage into each stage of a HVDC multiplier circuit, the influence of the stages is compensated, and ripple and voltage reduction are reduced to the case $n = 1$ according to Table 6.1. Figure 6.7 shows the simplest circuit with $n = 2$ stages. All of them are based on a one-phase, two-pulse rectifier circuit (Fig. 6.2). The transformers of the cascade are not grounded and have to be isolated against the HVDC stress. The secondary winding of the lowest transformer (Fig. 6.7) is connected to the lowest smoothing capacitor and must be isolated in minimum for its DC potential V_1. The transformer winding (also on V_1) is connected to the primary winding of the next transformer which is on the DC potential $3 \cdot V_1$. Therefore, the second and all further transformers have to be isolated for a DC potential of $2 \cdot V_1$. Usually, all transformers are of the same design with a DC isolation of $2 \cdot V_1$ each. The DC insulation might be subdivided into the primary and the transfer (tertiary) winding.

The multiplier circuits with cascaded transformers enable the design of HVDC sources of medium rated currents with relatively low-ripple and low-voltage reduction. This can also be modified by feeding, e.g. a Greinacher cascade not only into the lowest stage, but also in one of the higher stages. Even the single charging into upper stages improves ripple and voltage reduction. As an example, Fig. 6.8 shows a cascade for 2,000 kV with seven stages and feeding into the third stage.

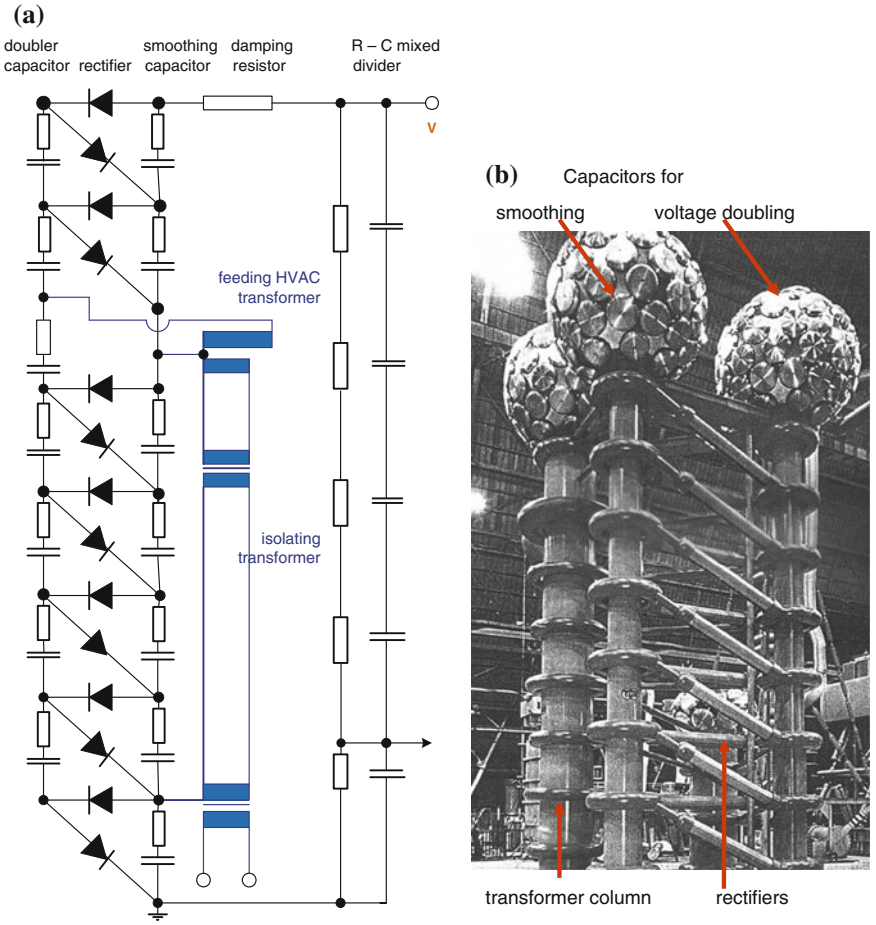

Fig. 6.8 Greinacher cascade with feeding into the sixth stage. **a** Simplified circuit diagram. **b** Generator for 2,000 kV and for very fast polarity reversal up to 700 kV

A second application of HVDC sources with cascaded transformers is that for modular DC test systems. One 400-kV oil-filled module may contain two 200-kV stages of a one-phase, one-pulse doubler circuit (Fig. 6.9), each equipped with its own transformer, the elements of the rectifying circuit including smoothing capacitor. Also a voltage divider is arranged inside the module. Then, several modules can be arranged one above the next to a very space-saving HVDC test system. The polarity reversal is motor-driven. Figure 6.10 shows such a system including a circuit for PD measurement. After connection of the power supply and the control unit, the system is ready for voltage testing. Such HVDC test systems for currents up to few 10 mA can easily be assembled and used for on-site testing, too.

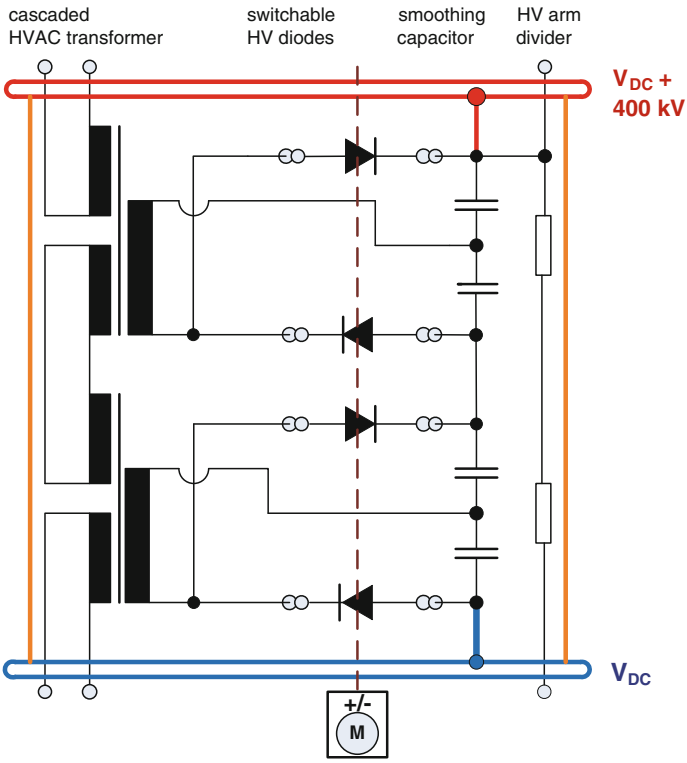

Fig. 6.9 Simplified circuit diagram of a HVDC module with two internal stages

6.2 Requirements to HVDC Test Voltages and Selection of HVDC Test Systems

After the description of the requirements to HVDC test voltages according to IEC 60060-1 (2010) (Fig. 6.11), some necessary features of the design of HVDC test systems are discussed. There is a strong interaction between the test system and the test object (load). Therefore, the role of capacitive and resistive test objects is described for the selection of the generation circuit and its parameters.

6.2.1 Requirements of IEC 60060-1 to HVDC Test Voltages

The *HVDC test voltage value* is not—as for the other test voltages—the peak value (V_{max}), but the *arithmetic mean value* during one period T of the charging process:

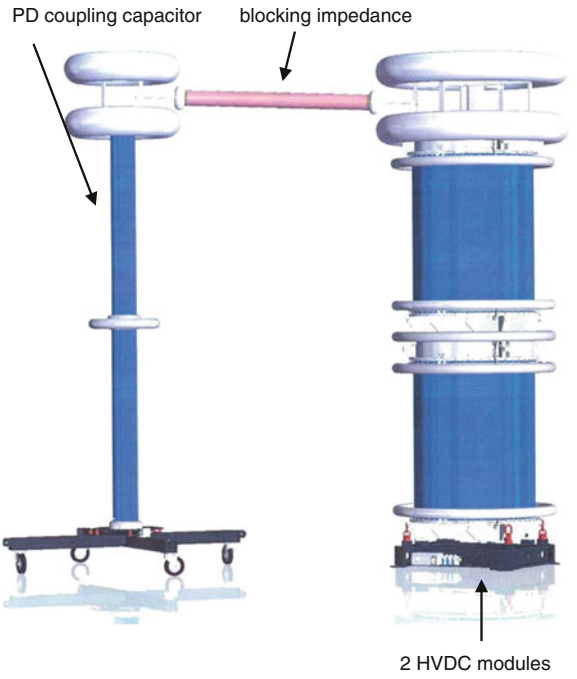

Fig. 6.10 Modular HVDC generator 800 kV/30 mA of two modules with external circuit for PD measurement

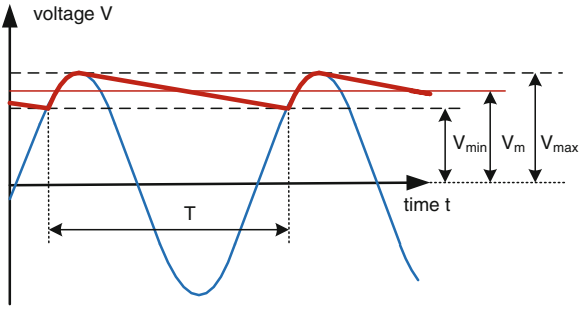

Fig. 6.11 Definitions to direct test voltages

$$V_m = \frac{1}{T} \cdot \int_{t_1}^{t_1+T} v(t) \cdot dt. \tag{6.7}$$

The *tolerance* of the test voltage value is 1 % for test durations up to 1 min, but for longer durations, 3 % are acceptable. The definition of the mean value results mainly from the voltage measurement with conventional voltmeters (moving-coil meters) which measure the mean value. One has to consider that the peak voltage determines breakdown processes and must be applied for research work.

With the *ripple voltage* δV (Eq. 6.1), one gets the dimensionless *ripple factor* δ as a relation to the test voltage value

$$\delta = \frac{V_{\max} - V_{\min}}{2 \cdot V_m} \cdot 100 \leq 3\%. \tag{6.8}$$

The requirement $\delta \leq 3$ % accepts that a remarkable difference appears between the peak voltage—which determines discharge phenomena in the insulation—and the test voltage value. A high ripple reduces also the inception voltage of partial discharges. Therefore, for both sides of an acceptance test, it is useful to have a ripple factor as low as possible.

Heavy predischarges, especially during wet and pollution tests cause remarkable current pulses which may reduce the test voltage value V_m to a lower value $V_{m\,\min}$. The HVDC test system should be able to supply these transient discharge current pulses up to few seconds without an instantaneous *voltage drop* given by:

$$d_{\mathrm{v}} = \frac{V_m - V_{m\,\min}}{V_m} \leq 10\%. \tag{6.9}$$

Unfortunately, IEC 60060-1: 2010 does not specify the current value and its duration, e.g. for an assumed rectangular pulse or any indication of the required charge. For more details, see Sect. 6.2.3.2. Some publications consider $d_{\mathrm{V}} \leq 10$ % as a too high value, (e.g. Hylten-Cavallius 1988; Köhler and Feser 1987). See also Sect. 6.2.3.2 below.

The reference value of the parameters δ and d_{V} is always the measured test voltage value $V_{m.}$ Therefore, the *voltage reduction* ΔV (Eq. 6.5) is not a parameter of the test voltage, but of the HVDC test system. It characterizes the utilization factor of the used test system and has to be considered when a new test system is required.

6.2.2 General Requirements to Components of HVDC Test Systems

The circuit diagrams discussed above are simplified because they consider ideal elements and stationary conditions. Additionally, a HVDC generator has to withstand also transient stresses, e.g. in cases of a breakdown of the test object or a fast polarity reversal. If no countermeasures are taken, the stray inductances and capacitances would influence the distribution of the stressing voltages inside the generator. Furthermore, high breakdown currents have to be taken into consideration.

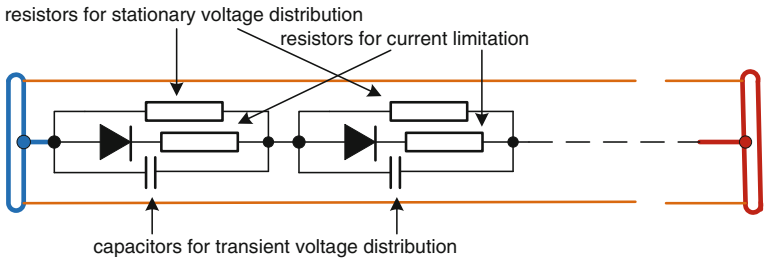

Fig. 6.12 Example of a protection circuitry of the diodes in a rectifier

6.2.2.1 Protection Against Transient Stresses

The fast breakdown of the test object may excite oscillations of the HV test circuit consisting of the generator capacitances and/or the unavoidable stray capacitances and inductances. Also the diodes and the feeding transformer are not ideal elements and have certain impedances. All this forms a quite complicate equivalent network which should not be considered here, only the most important practical consequences of related calculations are summarized. The oscillations may cause non-linear voltage distributions in the generator and over-stresses of the components. The only way to avoid damages of components is a protection scheme of the generator. This starts with an *external damping resistor* between the generator and the voltage divider or the test object (Fig. 6.8a). Furthermore, there should be an internal damping resistor in all capacitances. Also the rectifiers should be equipped with grading capacitors for a linear voltage distribution at transient stresses and with internal damping resistors for both, over-current and voltage limitation. A rectifier consists of many diodes in series. Figure 6.12 shows an example of the *protection circuitry* of diodes for both cases, stationary and transient stress of the rectifier (Kind and Feser 1999). The protection scheme should be completed by *protection gaps* or surge *arresters* on especially endangered parts of the generator, e.g. the uppermost rectifiers or the output of the feeding HVAC transformer.

> **Note** The protection scheme operates only if a breakdown occurs at the test object connected via the external damping resistor. A breakdown between any point of the generator and any grounded or energized object, e.g. due to wrong arrangements in the HV test hall, may change the relation between the single components of the protection scheme in such a way that rectifiers and/or capacitors of the generator are endangered.

6.2.2.2 Polarity Reversal and Switch-off

A reversal of the voltage is a very hard stress for HVDC insulation. Therefore, several standards require it in type tests. The used HVDC test system must have a motor-driven polarity reversal as, e.g. indicated in Fig. 6.9. The principle of the polarity reversal for a column of three rectifiers is shown in Fig. 6.13a: It is

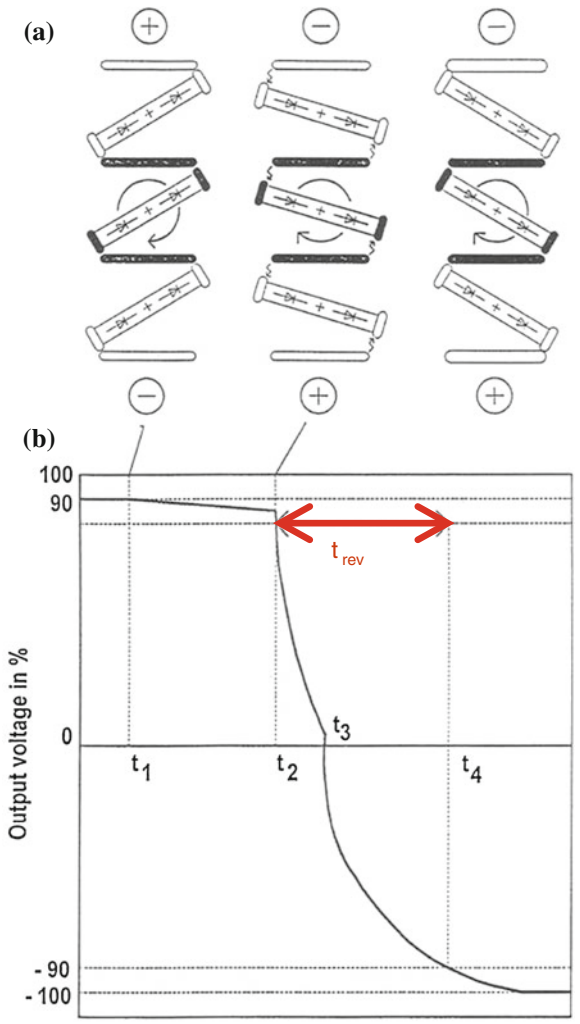

Fig. 6.13 Polarity reversal. **a** Switching process of the rectifiers. **b** Definition of the reversal time

presumed that the rectifiers are connected to a column of smoothing capacitors and a capacitive test object (Frank et al. 1983; Schufft and Gotanda 1997). The reversal cycle starts at t_1 with switching-off the feeding AC voltage and a turn of the rectifiers. The capacitors are slowly discharged via the resistive part of the voltage divider (compare Fig. 6.8a). When the rectifiers approach the opposite electrodes at t_2, sparkovers between their electrodes and the related opposite fixed electrodes occur. Within a very short time of some milliseconds, the capacitances are rapidly discharged to zero via the rectifier column. Now, the AC voltage is switched on again, and the capacitances are charged into the opposite polarity (t_3). The charging time depends on the time constant determined by the capacitances to be

Fig. 6.14 Grounding of smaller HVDC generators

charged (generator plus test object), the impedances of the charging circuit and the available power of the HVAC feeding circuit. It may range from few seconds to few 10 s which is sufficient for most test applications.

Under certain conditions a much faster polarity reversal is required, e.g. within 200 ms. For that, the reversal time is defined as the interval between 90 % of the outgoing voltage and the same 90 % value of the opposite polarity (Fig. 6.13); whereas, the discharge phase is fast enough, the charging phase must be accelerated. This is realized by selecting a rated value for the charging much higher than necessary and interrupting the charging when 90 % of the required voltage is reached (t_4). To avoid an overshoot of the opposite polarity, the feeding must be pulse-controlled to the exact voltage value.

A HVDC voltage cannot be simply switched off; the charged capacitance must be discharged via a resistor when the voltage shall be reduced. It is reduced when the feeding stops because the resistive divider and other resistances to ground cause a discharge process. The time constants are in a range of several seconds (see Sect. 6.2.3.1). The slow discharge can be accelerated by a *discharging bar*, consisting of a damping resistor, a hook (connected to the test field earth by a metal cord) and an isolating bar (Fig. 6.14). After the discharging, the same earthing bar is used for earthing by its grounding hook instead of its discharge contact (Fig. 6.14b).

When the HVDC test system is designed for polarity reversals as described above, then the capacitors might be discharged via the turning rectifiers. After the feeding AC voltage is switched off, the grounding procedure starts with the discharge via the divider resistor down to about one-third of the rated voltage before the rectifiers are applied. They should not be applied for higher voltages to avoid an over-stress of the rectifiers. The permanent grounding of the capacitor columns shall only be used, after the generator is discharged. This can be done by earthing ropes or—for smaller generators by earthing switches. (see Sect. 9.26 and Fig. 9.28.)

A new HVDC generator should be equipped with a well-established protection scheme and with a reliable discharge and grounding system. When the generator is not used, it shall be carefully grounded. For safety reasons, all capacitors of each stage of multi-stage generators must be directly grounded by a metal rope which can be moved through the generator by motor preferably. If protection scheme and grounding system of an older generator do not correspond to these requirements, an upgrade is urgently recommended.

6.2.2.3 Voltage Control, Selection of Smoothing Capacitances and Frequency

The output of the HVDC generator is controlled via the feeding AC voltage. This means that the control is one of the AC generation circuit. Traditionally, this is a regulating transformer and nowadays mainly a *thyrister controller* operating in a pulse-width mode. The wider the voltage pulse the higher is the output voltage. The shape of the AC voltage is not important for the output DC voltage because the HVDC generator can be understood as a filter which connects harmonics of the alternating voltage to ground. The DC output voltage is hardly influenced by conducted noise signals. The thyristor controller can be switched within less than a millisecond, what is necessary for the mentioned fast polarity reversals. When a very sensitive PD measurement shall be performed at direct voltage, the switching pulses of the thyristor controller could disturb. In such cases, the application of a regulating transformer can be recommended instead of or in addition to the thyristor controller.

With respect to voltage reduction and ripple, capacitance and frequency are interchangeable (Table 6.1). This means the system can be improved either by increasing the capacitances or by increasing the frequency of the feeding voltage. Of course, also both can be applied for improving a design. It must be taken into consideration that the frequency range of capacitors is limited. Capacitors for frequencies >300 Hz are remarkably more expensive than those for power frequency. Therefore, the selection of capacitances and frequencies of the feeding voltage should take the economic situation into account. There is no general rule for an optimum now. Each design and parameter combination has to be considered separately for a reasonable economic solution.

In the past, motor-generator sets have been applied for the generation of AC voltages of higher frequencies than 50/60 Hz for HVDC test systems. Today, static frequency converters are available (Figs. 3.26 and 3.35) and connect the selectable higher frequencies with the advantages of a thyristor controller. It can be assumed that in the next future, the power supply and control of HVDC test systems will be based on static frequency converters.

6.2.3 Interaction Between HVDC Test System and Test Object

6.2.3.1 Capacitive Test Objects

In some respect, HVDC testing of *liquid-impregnated paper-insulated* (*LIP*) *cables* is the classic example for direct voltage application to AC insulation, especially for testing on site (see Sect. 10.4.2). Mobile HVAC test systems were not available in the past, and therefore, HVDC test systems have been used. Quite small HVDC test systems are able to charge the high capacitance of a cable system. Also a certain relationship between the lifetime under AC operational stress and the results of suited HVDC tests has been found. HVDC testing of oil-paper cables is applied till today. But, when HVAC cables with extruded insulation of much higher resistance have been introduced, it was found that a HVDC test is not only without benefit, it is even dangerous.

When the test object is an ideal capacitance C_c, this means there is no leakage current, the charging time up to a certain voltage increases with the capacitance of the test object. It decreases with the available charging current. Figure 6.15 shows the controlled charging for cables of different lengths for the case of a test voltage of 250 kV and an available direct current of 10 mA. The charging time is directly proportional to the length of the cable. If the available current would be 5 mA, the charging time would be twice of that shown in Fig. 6.15. The voltage increase can only be controlled from the AC regulator when the charging process is fast enough, e.g. as shown in Fig. 6.15. In any case, the fastest voltage increase is determined by the charging process. A slower voltage increase is controlled via the HVAC control.

At a test object of very low leakage current, the highest voltage value can remain for hours after switching-off the feeding voltage. To avoid serious safety problems, all capacitances must be discharged and grounded immediately (see Sect. 6.2.2.2). The necessary *discharge and grounding switch* must be equipped with a carefully designed damping resistor R_d which can be adapted to different capacitances of the test object and transfers the discharge energy into heat. At a test voltage V_t, the time-dependent discharge current i_e, the maximum discharge current $I_{e\ \max}$ and the discharge time constant are given by:

$$i_e(t) = I_{e\max} \cdot e^{\frac{-t}{\tau_e}} \quad \text{with} \quad I_{e\max} = \frac{V_t}{R_d} \quad \text{and} \quad \tau_e = R_d \cdot C_c. \tag{6.10}$$

In the mentioned example of the 10-km cable (corresponding to $C_c \approx 2\mu F$) and $V_t = 250$ kV (Fig. 6.15), the stored energy is 125 kJ which may be discharged within few seconds ($\tau_e \approx 1$ s). The damping resistance must be able to absorb this energy. Therefore, the resistor needs a careful thermal design. With respect to the *recovery voltage* (see Chap. 5), it is necessary to guarantee a permanent grounding of the generator and the capacitive test object when not in use.

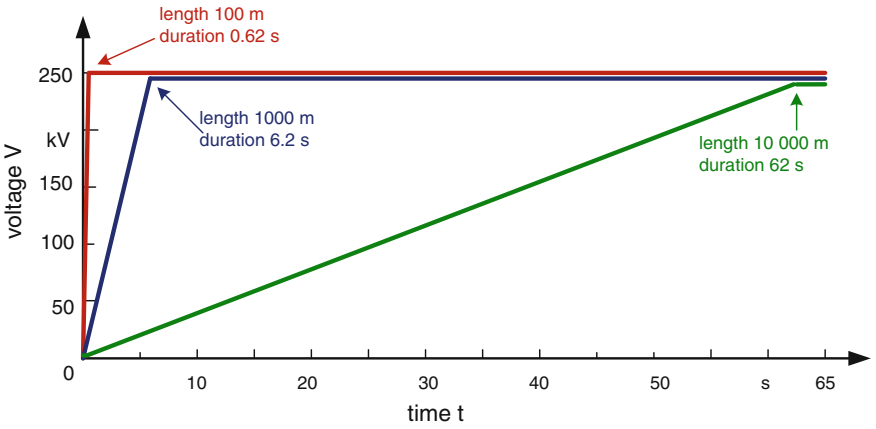

Fig. 6.15 Controlled charging of cables with 10 mA to 250 kV test voltage

6.2.3.2 Resistive Test Objects (Wet and Pollution Tests)

Wet and pollution tests require an active current due to a low surface resistance and/or to heavy predischarges. The limitation of the required current by the HVDC test system leads to a limitation of the test voltage (*voltage reduction* ΔV) in case of a permanent stress in stationary operation and to an instantaneous *voltage drop* (d_V) in case of transient stress. In both cases, the test cannot be performed correctly. Therefore, a lot of research work has been related to amplitude and shape of the required current (e.g. Reichel 1977; Rizk 1981; Matsumoto et al. 1983; Kawamura and Nagai 1984; Merkhalev and Vladimirsky 1985; Rizk and Nguyen 1987; Cigre TF 33.04.01 2000). As a result, the IEC Technical Report 61245: 2013 gives hints for HVDC pollution testing, and the necessary specification of HVDC test systems is described in several publications.

Whereas the voltage reduction becomes only acceptable, when a HVDC test system of sufficient rated current is applied, the voltage drop d_V can be reduced to an acceptable value by a very large smoothing capacitor, possibly by an additional capacitor (Reichel 1977; Spiegelberg 1984) or by a feedback control with a higher feeding voltage (Köhler and Feser 1987).

According to the above references, the *leakage current impulse* (Fig. 6.16) increases with the surface conductivity from some 10 mA up to the order of 1–2 A, but its duration decreases from some 10 s with the increasing current amplitude down to the range of few 100 ms. The maximum charge of one-pulse might be in the order of 200–300 mC. The real pulse is replaced for calculations by triangular or rectangular current pulses (Fig. 6.16). The acceptable voltage drop at such an impulse is between 5 % (Hylten-Cavallius 1988) and 8 % (IEC 61245:1993; Köhler and Feser 1987). Merkhalev and Vladimirski (1985) estimated the relation of the measured flashover voltage (V_{FL}) of a polluted insulator when a current pulse with the charge q_p appears and an unregulated Greinacher

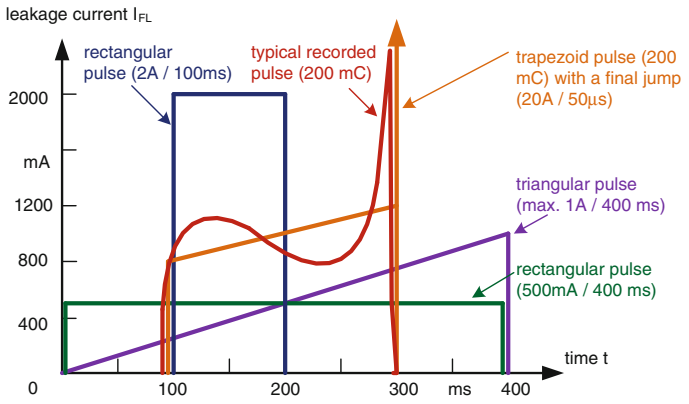

Fig. 6.16 Leakage current impulse (*red*) and its simplified replacements for calculations

generator with a limited smoothing capacitance $C_{sl,}$ (charge Q_{sL}) has been used in comparison to a generator with values C_{s0} (of a charge Q_{s0}) which do not influence the flashover voltage (V_{F0}):

$$\frac{V_{FL}}{V_{F0}} = 1 + 0.5\left(1 - \exp\left(\frac{-q_p}{Q_{sL}}\right)\right). \tag{6.11}$$

The deviation between the measured, too high flashover voltage V_{FL} (caused by an insufficient generator) and the correct value V_{F0} depends on the relation between the charge of the current pulse ($q_p \approx 200$ mC) and that of the smoothing capacitor Q_{sL}. If the charge stored in the smoothing capacitor exceeds the charge of the current pulse by a factor of 10 (this means $Q_{sL} \approx 10 \cdot q_{p,} = 2{,}000$ mC), then one gets the terms "$\exp(-q_p/Q_{sL}) \approx 0.9$" and "$V_{FL}/V_{F0} \approx 1.05$". The influence of the generator on the flashover voltage is below 5 %. That means, for the above-considered generator of $V_r = 300$ kV, a smoothing capacitor of

$$C_s = \frac{Q_{sL}}{V_r} = \frac{2\text{ As}}{0.3\text{ MV}} \approx 6\ \mu\text{F}$$

would be necessary. This very high capacitance is too pessimistic (Hauschild et al. 1987; Mosch et al. 1988) when a powerful feeding and an optimized multiplier circuit (e.g. three-phase, six-pulse) are used. This shows that only the consideration of the required charge is too much simplified. A more detailed calculation shows that for $q_p = 200$ mC, a rectangular leakage current pulse of high peak and short duration causes a higher voltage drop than a lower current of longer duration (Fig. 6.17). This is related to the internal impedances of the test system. Consequently, the voltage drop—as also the above-mentioned voltage reduction—increases with the number of stages. The shape, maximum value and duration of leakage current pulses depend also from the height of the test voltage, the applied pollution test method and the parameters of the tested insulator.

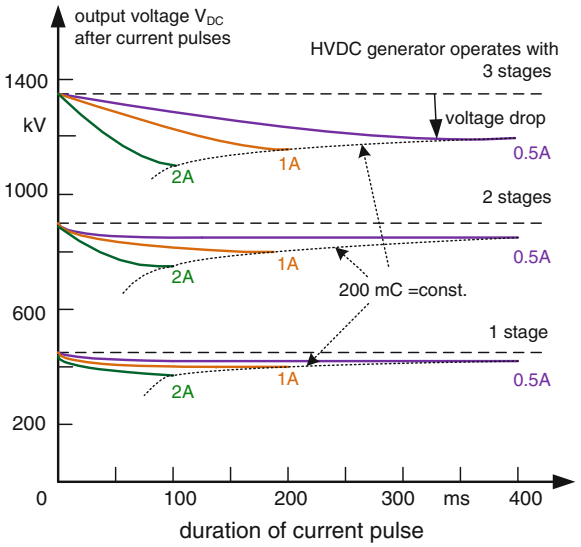

Fig. 6.17 Output voltage of a HVDC generator (Fig. 6.19) on amplitude and duration of a rectangular leakage current impulse

For checking the suitability of a HVDC test system for pollution testing, a computer simulation of the behaviour of the whole test circuit under a leakage current pulse of, e.g. 200 mC, is recommended. Additionally, the assumed shape of that pulse must be selected (compare Fig. 6.16). This can be done using the results of earlier circuit simulations shown in Fig. 6.18 (Mosch et al. 1988): It compares the voltage drop caused by a trapezoid—recorded currents well describing—pulse of 200 mC including a very fast final jump—simulating the fast heating of the residual pollution layer and the immediate final leader discharge—with that of a short rectangular pulse (2 A, 100 ms). It has been shown, a rectangular pulse delivers an even larger voltage drop. The charge demand of the final jump is only few millicoloumbs. Therefore, it is sufficient for the estimation of the voltage drop, to simulate the performance of a HVDC generator assuming short rectangular current pulses.

When the HVDC generator is fed by a thyristor controller with feedback control, the voltage drop can be limited to a preselected value by a suited regulator interval, e.g. to the required $d_V \leq 5$ % (Draft IEC 61245: 2013). Feedback control means that the test voltage and the leakage current are measured (Fig. 6.19) and used for the control of the feeding HVAC voltage. When a certain voltage drop is recorded, higher feeding AC pulses are applied for the duration of the leakage current pulse. Figure 6.20 shows that with increasing leakage current, the required frequency of the feeding pulses and, consequently, the ripple frequency of the output voltage increases. The regulating interval has to be selected in such a way that too high voltage drops and also overshoots (Draft IEC 61245: 2013 requires $\leq$10 %) are avoided. Today, most HVDC pollution tests are often performed with *feedback-controlled HVDC test systems* (Seifert et al. 2007; Jiang et al. 2010, 2011; Zhang et al. 2010a, b).

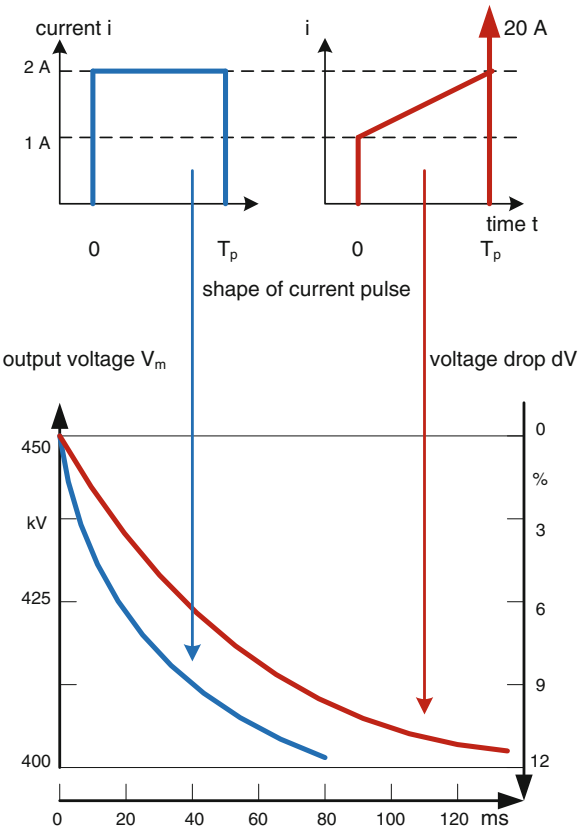

Fig. 6.18 Voltage drop for current pulses of rectangular and trapezoid shape

HVDC pollution tests must not be performed at complete insulator chains; it is sufficient to test one insulator of a chain because a linear voltage distribution can be assumed within one chain of uniform pollution. Therefore, powerful HVDC test systems for pollution tests are usually limited to test voltages up to 600 kV.

In opposite to that, for insulators under *artificial rain* conditions, no uniform voltage distribution can be assumed, therefore wet tests must be performed up to the highest DC test voltages. This means HVDC test systems for rated voltages of 2,000 kV are able to test open air insulations for 1,000 kV HVDC transmission systems. Current pulses due to heavy streamer discharges in transition to leader discharges are characterized by charges up to 10 mC. These charges can be supplied by generators without feedback control and rated currents of few 100 mA. If it shall also be used for wet testing of contaminated insulators higher rated currents and feedback control might be useful (Su Z et al. 2005).

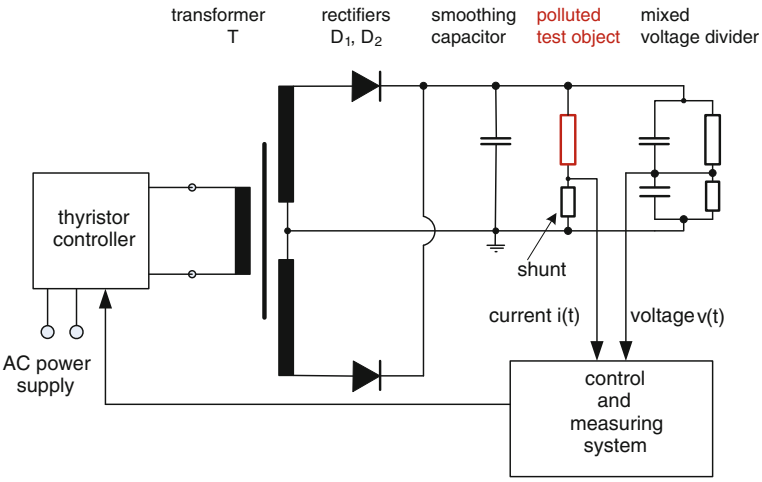

Fig. 6.19 HVDC test system with feedback control

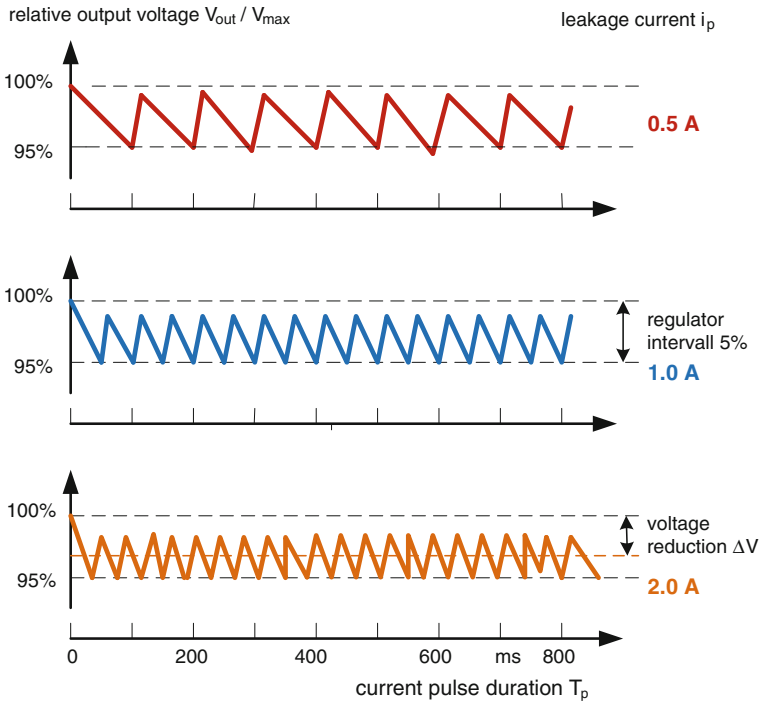

Fig. 6.20 Calculated output voltage of a feedback-controlled generator at different leakage currents, but identical pulse charge $Q_p = 200$ mC

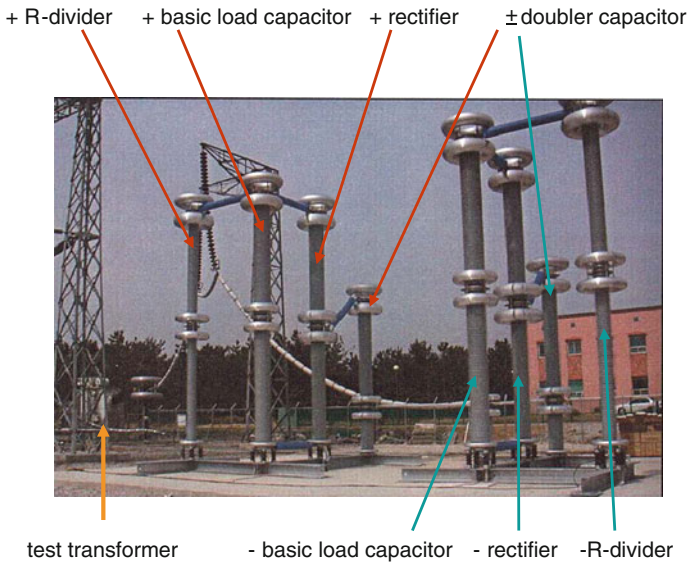

Fig. 6.21 Bipolar HVDC attachment of ±1,000 kV/500 mA to a 600 kV/3.3 A HVAC test system (Courtesy of KEPRI Korea)

6.2.3.3 Corona Cages and HVDC Test Lines

A remarkable part of the active losses of an air insulated HVDC transmission system is caused by partial discharges which are usually designated "*corona" discharges*. The design of the bundle conductors of a HVDC transmission line is usually verified by tests in a corona cage and/or on a test line. A corona *cage* is a coaxial electrode system with an outer electrode up to few metres diameter, realized by metal rods, and the bundle conductor to be investigated forms the inner electrode on HVDC potential. The outer electrode is grounded via an impedance for measurement of corona current pulses or the average corona current. A *HVDC test line* is a one-to-one model of a future HVDC overhead line. It shall demonstrate the performance of all components under operational conditions. Both, corona cages and test lines are outdoor arrangements and require outdoor HVDC test systems (Elstner et al. 1983; Spiegelberg 1984).

Such test systems have to supply continuous currents of several 100 mA for avoiding a voltage reduction due to continuous corona discharges and short-term currents up to few amperes for avoiding voltage drops due to leakage current pulses. For a test line, both polarities must be supplied. This can be made by two separate HVDC test systems or by one system with bipolar output (Fig. 6.21). The shown system is a *bipolar HVDC attachment* to a 600 kV/3.3 A HVAC test system. It consists of two one-phase one-pulse doubler circuits, one for each polarity.

The test system itself must withstand its output voltage at all environmental conditions under which tests shall be performed. The details of those conditions (temperature range, atmospheric pressure range, humidity up to 100 %, rain, natural contamination) must be carefully specified as well as a possible reduction of the rated voltage for certain test conditions. The external surface of all components shall be equipped with silicon rubber sheds (Fig. 6.21).

6.3 Procedures and Evaluation of HVDC Tests

Developed for all continuous voltages, the procedures and evaluations of HVAC tests (see Sect. 3.3 based on Sect. 2.4) can be applied for HVDC tests, too. Therefore, the described methods will not be repeated in this section, only few differences shall be mentioned.

The *progressive stress test* with continuously or step by step increasing direct voltage (Fig. 2.26) is used to determine a *cumulative frequency distribution* which can be approximated by a *theoretical distribution function*. The approximation can be performed according to the recommendations of Table 3.7. Also for *life-time tests* the remarks of Sect. 3.3.1 are applicable.

Compared with HVAC tests, it is more difficult to guarantee *independence* in HVDC tests. The reason is based on the phenomenon that partial discharges (and the trace of flashovers) at direct voltage cause surface and space charges of a long lifetime. Therefore, preceding stresses may influence the result of following stresses. It is absolutely necessary to check the independence of a test result before a further statistical evaluation will be made. The graphical check (Fig. 2.28) should be performed during the tests, and the test procedure should be modified if independence appears. Modifications are, e.g. the change of the rate of voltage rise, the careful cleaning of test objects after flashovers, the application of a new test object for each stress cycle or the application of a low alternating voltage between two stress cycles ("cleaning" by an alternating electric field). When a solid insulation is investigated, usually each test cycle requires a new sample.

In quality-acceptance testing, the procedure described in Sect. 2.4.6 and Fig. 2.39a is recommended also for direct voltages (IEC 60060-1:2010). The test should be performed at the polarity which delivers the lower breakdown voltages. If this is not clear testing at both polarities is necessary. Also PD-monitored withstand tests (Sect. 3.3.2) are applicable, but the randomness of partial discharges at direct voltage shall be considered (see Sect. 6.5). This may require longer durations on the different voltage levels (Fig. 2.39b). Other measurands than partial discharges, e.g. the leakage current or the insulation resistance, might be taken into consideration for diagnostic withstand testing.

6.4 HVDC Test Voltage Measurement

For measurement of high DC voltages *sphere gaps* have been used originally. As described in Sect. 2.3.5, these are also capable of measuring the peak value of other kinds of HV test voltages, such as AC, LI and SI. Based on experimentally determined breakdown curves under clean laboratory conditions (Schumann 1923), a measuring uncertainty of about 3 % seemed to be achievable for test voltage levels ranging between 20 and 2,000 kV (Weicker 1927; Weicker and Hoercher 1938; IEC Publication 52: 1960). As the DC breakdown voltage of sphere gaps depends not only on nearby earthed objects (Kuffel 1961), it is also strongly affected by the roughness and cleanness of the electrode surface as well as by the humidity and density of ambient air. Therefore, sphere gaps cannot be recommended for DC voltage measurement above 200 kV (see Table 2.7). The revised version of the standard IEC 60052:2002 uses the finding that high DC test voltages can also be measured at sufficient measuring uncertainty by means of *rod–rod gaps* (Peschke 1968; Feser and Hughes 1988). Taking into account the correction factors for the humidity and density of air, a measuring uncertainty of 2 % seems to be achievable for voltages ranging between approx. 20 and 1,300 kV. The main disadvantage of air gaps, however, is not only the proximity effect, but also the discontinuous measuring procedure which is extremely time-consuming. Thus, spark gaps have been increasingly replaced by continuously measuring *electrostatic voltmeters* since the 1920s (Starke and Schröder 1928). Measuring systems using high-resistive converting devices have been introduced in the 1930s (Kuhlman and Mecklenburg 1935), where the high voltage was indicated by either current or voltage meters, as illustrated in Fig. 6.22. Nowadays, the converting device is commonly a resistive voltage divider, sometimes in parallel with a capacitive divider. This is because this circuit is capable for recording the time-dependent voltage, which is particularly of interest for measurement of changing voltages, such as the ripple of DC voltages as well as the voltage shapes at polarity reversal.

An important design parameter of *resistive voltage dividers* for DC application is the current which should not below 0.5 mA, as recommended in IEC 60060-2:2010. This is to minimize the measuring uncertainty due to parasitic leakage currents which might be caused by dust or pollution deposited on the surface of the divider column, which may affect the divider ratio, particularly at high air humidity. In this context, it should be noted that charged dust particles are always attracted in direction of the increasing electric field strength which forces the deposition of dust on the surface of the divider column. To reduce the impact of dust and pollution, the resistance of the HV arm should thus be as low as possible. However, this is limited not only by the additional load acceptable for the HVDC test supply, but also by the permitted operation temperature which increases with the power dissipated in the divider column.

Example Consider a 100 kV voltage divider having a total resistivity of 10 MΩ, which shall be composed of 100 low-voltage resistors, each of 100 kΩ and designed for a

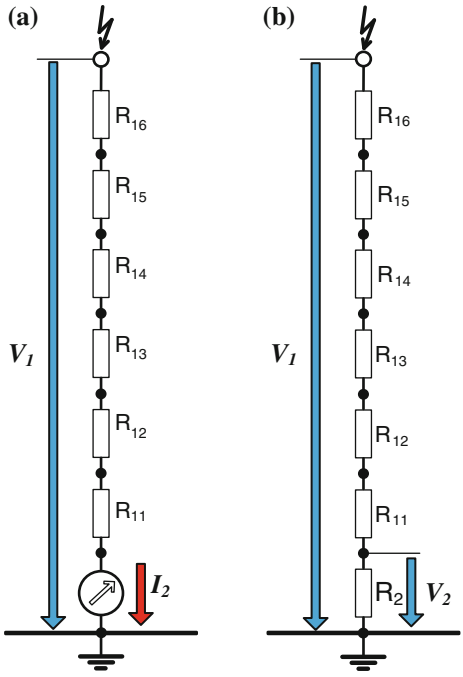

Fig. 6.22 Basic principles of resistive HVDC measurements. **a** Ammeter in series with a HV preresistor. **b** Voltmeter across the LV arm (principle of a voltage divider)

maximum voltage of 1 kV. Applying the rated voltage of 100 kV, the current through the divider becomes 10 mA. Under this condition, the power dissipated in each resistor amounts 10 W, so that the power dissipated in the whole divider column becomes 1,000 W. This would cause a very high operation temperature which can never be accepted. Thus, the current through the HV arm is commonly limited below 1 mA, where the voltage drop across each LV resistor should not exceed 1 kV which is equivalent to 1 MΩ/kV.

To prevent too high radial and tangential field gradients, the HV resistor is commonly wounded around an insulated cylinder forming a helix, as obvious from Fig. 6.23 which refers to a 300 kV DC divider designed by Peier and Greatsch in (1979). The HV arm constitutes of 2 MΩ LV resistors, where 300 pieces of them are connected in series. The bottom 2 MΩ resistor provides the LV arm, so that the divider ratio amounts 1:300. The pitch of the helix varies, so that the potential distribution along the resistor helix becomes comparable with the electrostatic field distribution caused by the top electrode without divider column, as originally proposed by Goosens and Provoost for impulse voltage dividers already in 1946. The resistor is arranged in an oil-filled PMMA cylinder to improve the convection of the dissipated power, which is only 150 W at rated voltage. Moreover, this design reduces the impact of dust and pollution on the divider current. Using wire-wounded resistors, which have been artificially aged by a temperature treatment, a measuring uncertainty of around 3×10^{-5} was achieved.

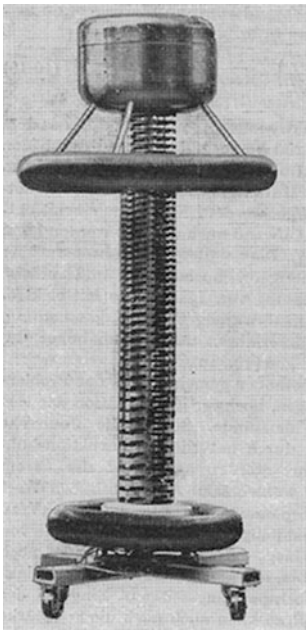

Fig. 6.23 DC divider, rated voltage 300 kV, HV resistance 600 MΩ, total high 2.1 m

Even if excellent parameters are achieved for this divider of the German National Institute of Metrology (PTB Braunschweig), it is not applicable for DC voltage measurements in industrial test fields but for *reference measurements* in calibration laboratories. This is because in case of a breakdown of the test object, fast transient voltages may cause an overload of the wire-wounded resistors due to its comparatively high self-inductance. To enhance the energy capability, metal-oxide film or carbon composition resistors could be applied as an alternative. The main drawback of such resistors is the comparatively high temperature coefficient. Thus, the measuring uncertainty may increase during the test duration at rising temperature. Even if this effect can be minimized by preageing using a long-term temperature treatment, such a conditioning is extremely time-consuming and thus applied only in very specific cases.

The best solution to avoid a possible damage of resistive dividers in case of breakdowns is the use of mixed or resistive–capacitive or capacitive-graded dividers. An optimum performance is achieved by means of staked capacitors connected to specific points of the resistive divider column, as obvious from Fig. 6.24. As a rule of thumb, the capacitance of such a mixed divider should be in the order of 200 pF. Moreover, shielding electrodes of comparatively large surface should be applied to avoid the ignition of partial discharges which could also affect the divider ratio.

For measuring DC test voltages in principle *analogue instruments* capable for indicating the arithmetic mean value could be used. The better approach, however, is the use of an oscilloscope or nowadays a digital recorder. This is because under

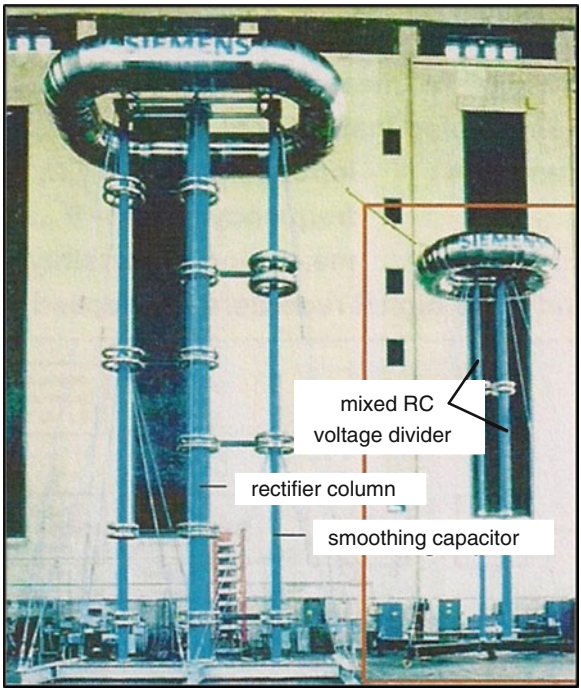

Fig. 6.24 DC generator and a resistive–capacitive divider (2 MV, 1 mA) designed for the measurement of static and dynamic voltages

real test condition not only the static DC voltage but also typical dynamic voltages have to be measured, such as the *ripple*, the *voltage drop* as well as the parameters characterizing the *polarity reversal*. The requirements for approved DC voltage measuring systems are specified in IEC 60060-2: 2010. So, the arithmetic mean value shall be measured with an expanded uncertainty $U_M \leq 3$ %, which corresponds to a coverage probability of 95 %. To determine the dynamic behaviour of the measuring system, it is subjected to a sinusoidal voltage at the input. Changing the frequency between 0.5 and 7 times of the fundamental ripple frequency f_r the difference of the measured output voltage magnitude shall be within 3 dB.

The above-given uncertainty limits shall not be exceeded in the presence of the maximum ripple specified in IEC 60060-1. The ripple magnitude shall be measured with an expanded uncertainty ≤ 1 % of the arithmetic mean value of the DC test voltage or ≤ 10 % of the ripple magnitude, whichever is greater. To measure the mean value of the DC voltage and the ripple magnitude, either separate measuring systems or the same converting device may be used in connection with two separate measuring modes for DC and AC voltages.

The scale factor of the ripple measuring system shall be determined at the fundamental ripple frequency f_r with an expanded uncertainty ≤ 3 %. This scale factor may also be determined as the product of the scale factors of the components. Measuring the amplitude/frequency response of the ripple measuring system in a frequency range between 0.5 and 5 f_r; the amplitude shall not be lower than 85 % of that value occurring at the fundamental ripple frequency f_r.

To measure rising and falling DC test voltages as well as the ripple and the voltage shape at polarity reversal, the characteristic time constant of the DC measuring system shall be ≤0.25 s. In case of pollution tests, the time constant shall be ≤1/3 of the rise time typical for the appearing transients (voltage drop).

The results of the type and routine tests of HVDC measuring systems can be taken from the test protocol of the manufacturer, where routine test shall be performed on each component of the measuring system. *Performance tests* of the complete measuring system as well as performance checks must be performed under the responsibility of the user himself or by a calibration service. The performance test shall include the determination of the scale factor at the calibration as well as the dynamic behaviour for the ripple and shall be performed annually but at least every 5 years. *Performance checks* cover scale factor checks and should be performed at least annually or according to the stability of the measuring system; for more information, see Sects. 2.3.3 and 2.3.4, respectively.

6.5 PD Measurement at DC Test Voltages

The physics of gas discharges occurring under DC stress has extensively been studied in the 1930 (Trichel 1938; Loeb 1939; Raether 1939) when DC was increasingly used as operation voltage for X-ray equipment, cathode-ray tubes, electron-accelerators, image intensifiers and radar facilities. In the 1960s, DC voltages became of interest not only for physical, medical and military application but also for energy supply. Since that time, the measurement of partial discharges became an indispensable tool for quality assurance tests of HVDC equipment, such as power cables and power capacitors (Rogers and Skipper 1960; Salvage 1962; Renne et al. 1963; Melville et al. 1965; Salvage and Sam 1967; Kutschinski 1968; Kind and Shihab 1969; Müller 1976; Densley 1979; Meek and Craggs 1978; Devins 1984).

Subjecting air gaps to high DC voltage, the PD phenomena are comparable with those occurring under power frequency AC voltages, particularly if discharges ignite at negative electrodes (Fig. 6.25). Due to the regular appearance of negative discharges in air, first discovered by Trichel (1938) and thus commonly referred to as *Trichel pulses*, these are often used for performance checks of PD measuring circuits.

For technical insulation, internal discharges, such as surface, interfacial and cavity discharges, are more of interest than corona discharges in air. To describe the typical PD occurrence of internal discharges at DC stress, the classical capacitive PD model originally developed for AC stress (see Fig. 4.7 in Sect. 4.2) has been modified accordingly. So, all capacitances are bridged by resistive elements, and the recovery time between consecutive discharges is deduced from a characteristic time constant (Fromm 1995; Beyer 2002; Morshuis and Smit 2005). Replacing the cavity by an equivalent capacitance, however, contradicts the

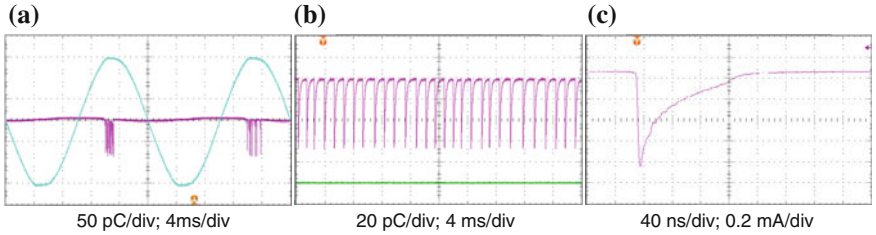

Fig. 6.25 Trichel pulses recorded for a grounded point electrode close to the PD onset level 12 kV. **a** Charge pulse train at AC voltage. **b** Charge pulse train at DC voltage. **c** Single current pulse at DC voltage

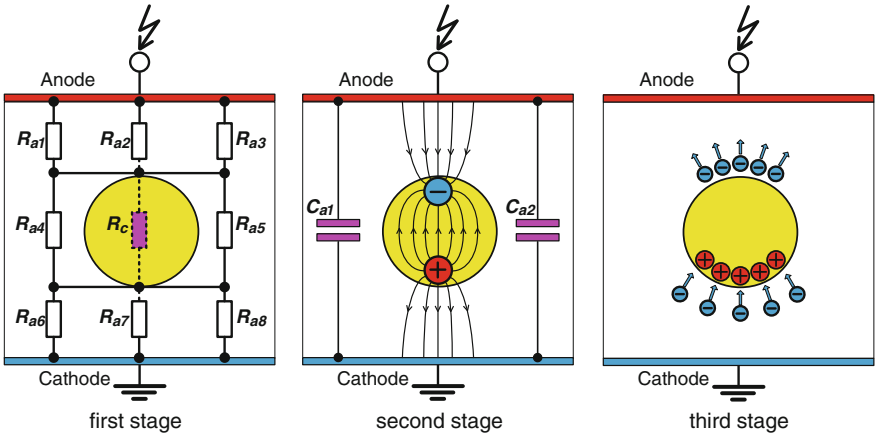

Fig. 6.26 Stages determining the recovery time between subsequent cavity discharges at DC stress

physics of gas discharges and leads to fatal misinterpretations, as argued by Pedersen (1986) and discussed more in detail in Sect. 4.2. The following treatment is thus based on the alternative *dipole model*, also presented in Sect. 4.2. Considering a gaseous cavity embedded in the bulk dielectric between plane-parallel electrodes, one can distinguish between three basic stages (Fig. 6.26):

Stage I: Initializing of ionization processes

At constant DC voltage, the field distribution between the electrodes is governed by the resistive potential distribution. To calculate the inception voltage analytically, it has to be taken into account that the conductivity of dielectrics used for HV application is strongly affected not only by the field strength but also by the temperature.

Stage II: Establishment of the dipole moment
As charge carriers of opposite polarity are created by the ionization of neutral molecules, these are separated due to the electrostatic field where the movement is hampered by the cavity boundary. Consequently, a dipole moment is established, see Sect. 4.2. As the dipole field opposes the electrostatic field, the resulting field strength occurring in the cavity is drastically reduced which is associated with a comparatively high-voltage collapse across the cavity, so that the residual voltage approaches zero. Due to this, the further ionization of gas molecules is suddenly quenched.

Stage III: Dissipation of the dipole moment
As also presented in Sect. 4.2, at AC stress consecutive PD pulses might appear in each half cycle. These occur at rising and falling voltage at an instant, when the voltage difference is high enough to compensate the field reduction caused by the dipole moment. At DC stress, however, subsequent PD's can only be ignited if the dipole moment disappears. It can be supposed that the positive point charge is neutralized due to attachment of electrons which are attracted if drifting adjacent to the cavity. Simultaneously, the electrons, originally deposited at the cavity boundary, are attracted by the anode and enter thus the dielectric boundary. As the conductivity of solid dielectrics used for technical insulations is very low, the *electron current* is also extremely low. Therefore, *recovery times* in the order of several seconds or even minutes are often encountered if PD tests at DC voltages are performed.

Example Consider a cavity discharge in a polyethylene insulated cable, where 10^7 electrons are deposited at the anode-directed dielectric boundary, so that the negative point charge of the dipole being 1.6 pC. The field strength in the bulk dielectric adjacent to the cavity shall be $E_p = 50$ kV/mm, and the conductivity $\kappa_d = 10^{-17}$ $(\Omega \cdot \text{mm})^{-1}$. After the discharge is quenched, the electrons originally deposited on the cavity boundary, are entering into the bulk dielectric. Assuming an effective area of $A_e = 0.1$ mm^2 crossed by the electrons, the total electron current can be approximated as follows:

$$I_e \approx \kappa_d \cdot E_p \cdot A_e \approx 5 \cdot 10^{-14} \text{ A} = 0.05\text{pA}$$

Assuming a constant mean electron current, the recovery time becomes 32 s, i.e. the PD pulse repetition rate is in the order of 0.03 Hz which is in accordance to practical experience.

Performing PD tests at DC test voltages, it has to be taken into account that only two basic PD quantities are available: The magnitude of the *pulse charge* q_i appearing at instant t_i and the *recovery time* Δt_i between consecutive PD pulses. Generally, the measuring systems intended for PD tests under power frequency voltages are also applicable for PD tests of HV apparatus subjected to DC voltages, where some particularities have to be taken into account. So, PD events can be encountered only from time-to-time, as discussed previously and shown in Figs. 6.27 and 6.28. Thus, appropriately long recording times have to be chosen. Under this condition, however, the charge pulses received from the output of conventional PD detectors, having commonly a width in the order of 0.1 ms, can hardly be recognized. To overcome this crucial problem, the charge pulses should

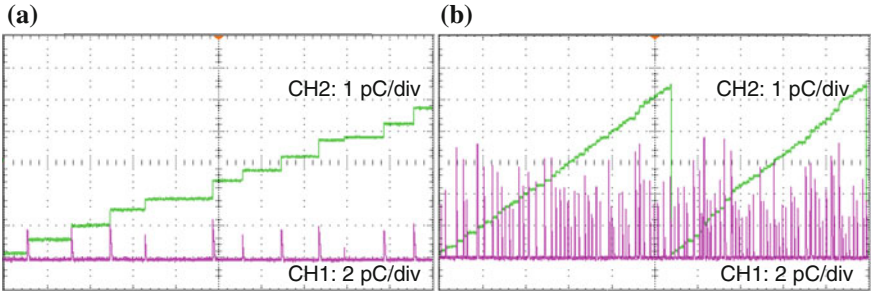

Fig. 6.27 Charge pulse trains (CH1) and accumulated charge pulses (CH2) recorded for a cavity in an extruded power cable sample subjected to DC test voltage. **a** Recording time 20 s, test voltage close to PD onset level. **b** Recording time 100 s, test voltage approx. 20 % above PD onset level

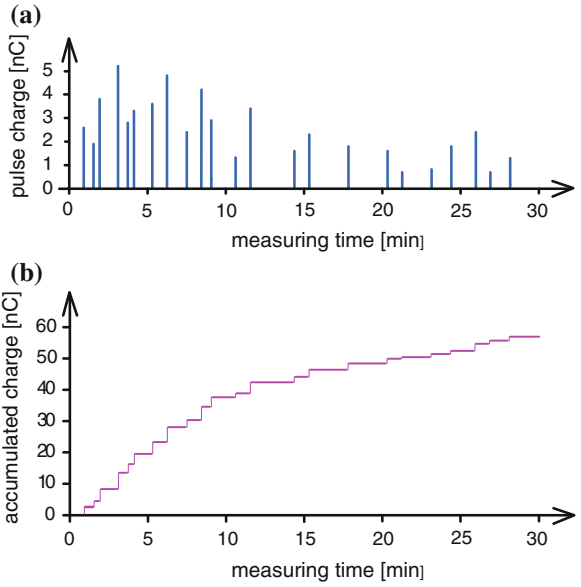

Fig. 6.28 Graphs recommended in the Amendment to IEC 60270 for the evaluation of PD tests results. **a** Consecutive charge pulses recorded for a PD test period of 30 min at constant DC test level. **b** Accumulated pulse charges recorded for the 30 min PD test period

be accumulated, as obvious from the green traces (CH_2) in Fig. 6.27. Another benefit of such a display mode is that the slope of the accumulated charge is proportional to the mean PD current, which can be regarded also as a valuable quantity to assess the PD activity. For extremely long recording times as well at higher PD activity, however, saturation effects might occur. Thus, it seems convenient to trigger a reset unit just before the saturation would occur, as shown in Fig. (6.27b).

As the PD pulses are scattering over a wide range in magnitude and repetition rate, a *statistical analysis* should be performed. For this purpose, the PD measuring

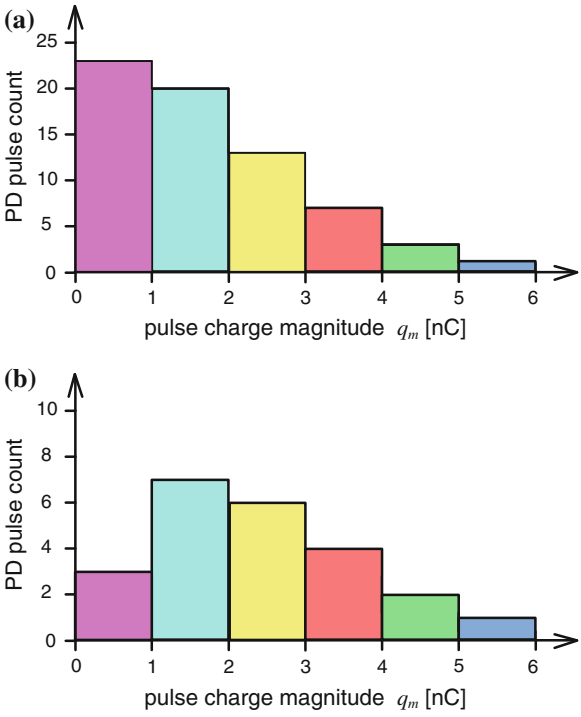

Fig. 6.29 Graphs recommended in the Amendment to IEC 60270 for statistical analysis of PD data. **a** Exceeding frequencies of PD pulses, which exceed the charges 0 nC, 1 nC, 2 nC, 3 nC, 4 nC and 5 nC. **b** Class frequencies of PD pulses, occurring within the following classes: (0–1) nC, (1–2) nC, (2–3) nC, (3–4) nC and (4–5) nC

system should also be equipped with a unit for counting the number of PD pulses exceeding preselected threshold levels (Fig. 6.29). In principle, this technique is conform to the classical pulse-height analysing originally introduced for PD measurements of HV apparatus under power frequency AC voltages (Bartnikas and Levi 1969) at a time when computerized PD measuring systems where not available. Even if the pulse repetition under DC stress is comparatively low, it has to be taken care that repetition rates down to approx. 5 Hz are resolved without superposition errors. According to practical experience, PD measurements of HVDC apparatus should cover a minimum time span of 30 min. In this context, it seems noticeable that with reference to PD measurements under DC test voltages, the following definitions have been added in the Amendment to IEC 60270 (Ed. 3): 2000, which is currently under revision (CD stage):

- *Accumulated apparent charge* q_a

sum of the apparent charge q of all individual pulses exceeding a specified threshold level, and occurring during a specified time interval Δt_i.

- *PD pulse count m*

total number of PD pulses which exceed a specified threshold level within a specified time interval Δt_i.

To evaluate the PD data gained under DC test voltage, the presentation of the graphs shown in the Figs. 6.28 and 6.29 is recommended.

Chapter 7
Tests with High Lightning and Switching Impulse Voltages

Abstract *Lightning impulse* (*LI*) *over-voltages* and *switching impulse* (*SI*) *over-voltages* are caused by direct or indirect lightning strokes or by switching operations in electric power systems, respectively. They cause transient stresses to the insulations, much higher than the stresses due to the operational voltages. Therefore, insulations must be designed to withstand LI and SI over-voltages, and the correct design has to be verified by withstand testing using *LI test voltages*, respectively, *SI test voltages*. This chapter deals with the generation of aperiodic and oscillating LI and SI impulse voltages and the requirements for their application in HV tests. Special attention is given to the interactions between the LI/SI generator and the test object. The deviations from the standardized impulse shape, e.g. by an over-shoot on the LI peak, are analysed, and the evaluation of recorded pulses according to IEC 60060-1:2010 and IEEE St. 4 (Draft 2013) is described. This is completed by the description of components and of the procedures for the correct measurement of LI/SI test voltages. Also the measurement of the test currents in LI voltage tests and the PD measurement at SI test voltages are included.

This chapter deals with the generation of aperiodic and oscillating LI and SI impulse voltages and the requirements for their application in HV tests. Special attention is given to the interactions between the LI/SI generator and the test object. The deviations from the standardized impulse shape, e.g. by an over-shoot on the LI peak, are analysed, and the evaluation of recorded pulses according to IEC 60060-1:2010 and IEEE St. 4 (Draft 2013) is described. This is completed by the description of components and of the procedures for the correct measurement of LI/SI test voltages. Also the measurement of the test currents in LI voltage tests and the PD measurement at SI test voltages are included.

W. Hauschild and E. Lemke, *High-Voltage Test and Measuring Techniques*,
DOI: 10.1007/978-3-642-45352-6_7,

7.1 Generation of Impulse Test Voltages

7.1.1 Classification of Impulse Test Voltages

A *lightning stroke* may cause—e.g. on a transmission line—a travelling wave of a current pulse with a peak value ranging from few kiloamperes up to about 200 kA (in very rare cases, even up to 300 kA). Investigations of Okabe and Takami on UHV transmission systems (Takami 2007; Okabe and Takami 2009, 2011) considered peak currents up to 300 kA and a front duration in the range between 0.1 and 5 μs for the calculation of LI over-voltages ("external over-voltage") based on the surge impedance of the overhead transmission line, the grounding resistance of a tower and the impedances of the involved components. Figure 7.1 shows the resulting over-voltages for a GIS and a power transformer. Whereas at the GIS, the shape and the peak of the over-voltage change with the front time of the current pulse, the over-voltage at the transformer is not influenced by the front time of the current impulse. In both cases, the front time of the over-voltage is in the order of 1 μs, but the over-voltage shows oscillations. IEC 60060:2010 defines all impulse voltages with *LI front times* $T_1 < 20$ μs being LI voltages. Standard LI test voltages are aperiodic impulses. They are characterized by $T_1 = 1.2$ μs and an *LI time-to-half-value* of $T_2 = 50$ μs, abbreviation 1.2/50. In the case of Fig. 7.1 (Okabe and Takami 2011), the LI over-voltages are quite well represented by *standard LI test voltages* 1.2/50.

A switching process "on" or "off" in a power system causes an "internal over-voltage" due to the excitation of internal oscillation circuit(s) formed by the inductances and capacitances of the involved components of the system. The SI over-voltages are also oscillating with one or several frequencies which are remarkably lower than those of LI over-voltages (Fig. 7.2). All impulse voltages with front time $T_1 > 20$ μs are defined in IEC 60060-1:2010 being SI voltages. Shape and parameters of SI test voltages shall not only represent SI over-voltages, but should also be generated with the same test generator as LI test voltages (see Sect. 7.1.2). Their *SI time-to-peak* of about $T_p = 250$ μs should meet a minimum breakdown voltage of non-uniform air gaps with distances of about 5 m (Fig. 7.3, averaged characteristics according to Thione 1983). Therefore, *standard SI test voltages* are aperiodic impulses and characterized by $T_p = 250$ μs and a time to half-value of 2,500 μs, abbreviation 250/2,500. They shall represent all kinds of SI over-voltages.

For on-site testing, also *oscillating impulse voltages* (*OLI*; *OSI*) are applied (IEC 60060-3:2006). OLI and OSI test voltages can be generated with a generator of efficiency factors about twice of those for LI and SI voltages (see Sect. 7.1.3). Even if this is made for easier transportation and handling of the test system, it should be mentioned that the used OLI and OSI test voltages represent quite well the related over-voltages (compare with Figs. 7.1 and 7.2). Also the so-called "damped alternating voltage" (IEC 60060-3:2006; DAC) used for PD testing of cable systems in the field—is an OSI voltage. OSI voltages can also be generated by test transformers (see Sect. 7.1.4).

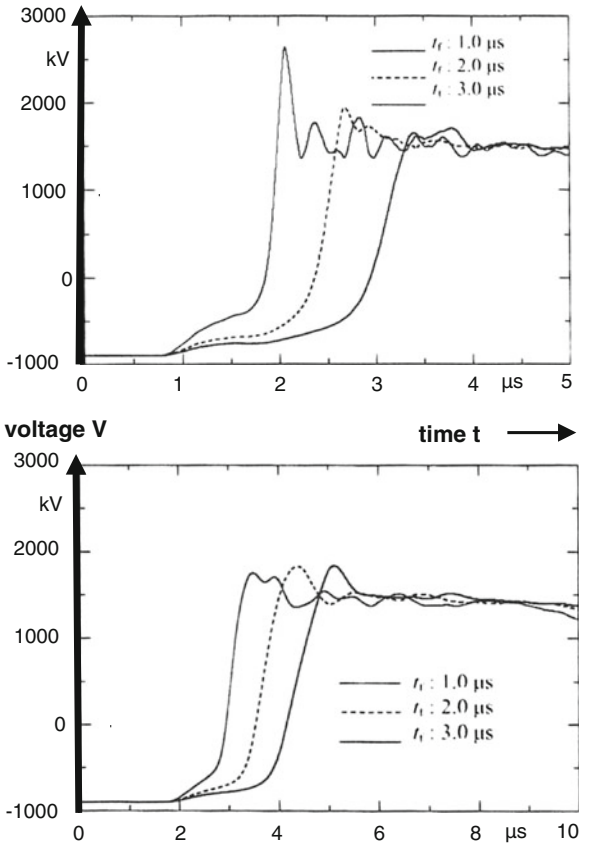

Fig. 7.1 LI over-voltage caused by 200 kA LI current pulse of different front times superimposed on the negative AC voltage peak at a GIS (*above*) and at a power transformer (*below*)

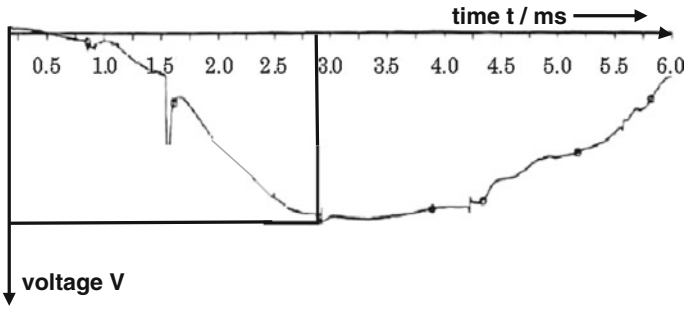

Fig. 7.2 Example for an SI over-voltage

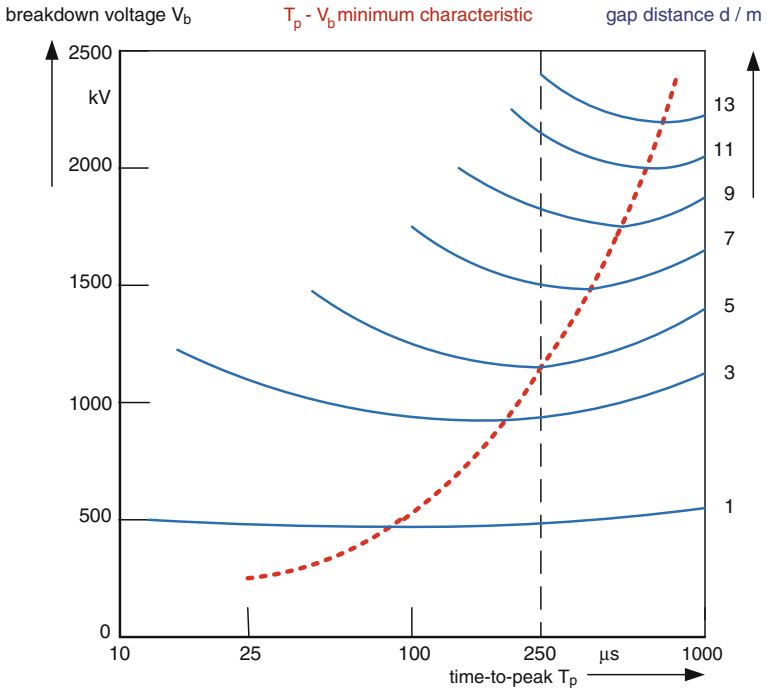

Fig. 7.3 SI breakdown voltage of long air gaps depending on the time-to-peak

Last but not least, it should be mentioned that in case of disconnector switching in SF_6-insulated systems (GIS), over-voltages faster than LI over-voltages are generated. They are represented by *fast front test voltages* (*FFV*) and generated by switching the disconnector in the GIS under test (see Sect. 7.1.5).

7.1.2 Basic and Multiplier Circuits for Standard LI/SI Test Voltages

7.1.2.1 Basic RC Circuit

The operation of the basic circuit for impulse voltages shall be explained by its equivalent circuit (Fig. 7.4a): When an *impulse capacitor*C_i is charged via a charging resistor R_c up to the DC breakdown voltage V_0 of the switching gap SG, the impulse voltage V_i is generated by the connected elements (Fig. 7.4b): Then, the load capacitor C_1 is charged via the front resistor R_f which forms the front of the impulse voltage. At the same time, the impulse capacitor C_i is discharged via the tail resistor R_t and forms the tail of the impulse voltage. The superposition of both processes delivers a peak voltage V_{ip} which is lower than the breakdown

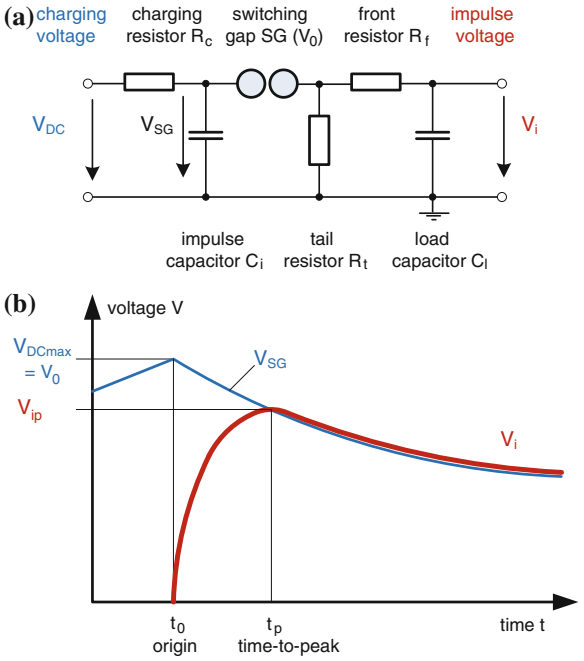

Fig. 7.4 Basic equivalent circuit for impulse voltage generation. **a** Equivalent circuit diagram. **b** Potential diagram

voltage V_0 of the switching gap. The relation between the two voltages delivers the *efficiency factor* (also: *utilization factor*) of the "one-stage" (basic) impulse generator:

$$\eta = \frac{V_{\text{ip}}}{V_0} < 1; \quad \eta = \eta_s \cdot \eta_c. \tag{7.1}$$

The efficiency factor η can be understood as a product of the efficiency η_s depending on the impulse shape and the efficiency η_c depending on the circuit parameters (Hylten-Cavallius 1988).The shape efficiency η_s increases with the relation between tail and front time of the impulse to be generated. When an LI impulse voltage (1.2/50) shall be generated, the relation is, e.g. about 40, when an SI voltage (250/2,500) is generated the relation is, e.g. 10 only. The circuit efficiency η_c depends mainly on the relation between impulse and load capacitor. The larger the impulse capacitance C_i in relation to the load capacitance C_l, the higher is the circuit efficiency η_c. The overall LI efficiency factor is relatively high ($\eta \approx 0.85 \ldots 0.95$) and the SI efficiency factor remarkably lower, $\eta \approx 0.70 \ldots 0.80$ only.

Note In addition of the circuit of Fig. 7.4a, a second basic circuit which has the tail resistor not before, but after the front resistor, is sometimes discussed in textbooks. This circuit has a lower efficiency factor. Therefore, it is not used practically and not discussed here.

The front of the impulse voltage is mainly determined by the time constant τ_f and its tail by τ_t

$$\tau_f = R_f \cdot C_l; \quad \tau_t = R_t \cdot C_i. \tag{7.2}$$

Usually, an impulse voltage generator is equipped with an impulse capacitor C_i and a basic load capacitor C_l of fixed values. The *front time* can be adjusted by a correctly selected front resistor R_f and the *timetohalf-value* by an appropriate tail resistor R_t. With the fixed values of C_i and C_l, the maximum SI peak voltage is only about 80 % of the maximum LI peak voltage.

Note The analytical calculation of the time parameters of impulse voltages and their efficiencies is given in older textbooks. Today, the analytical calculation is replaced by well-adaptable and commercially available software programs. This enables also the more detailed consideration of the characteristics of the test object and the stray capacitances in the test room and delivers more precise results.

The selection of the impulse capacitor C_i determines—together with the maximum charging voltage $V_{0\max}$ also the *impulse energy* of the generator:

$$W_i = \frac{1}{2} C_i \cdot V_{0\max}^2. \tag{7.3}$$

Whereas the maximum charging voltage of a generator depends on the required test voltages, the impulse capacitance must be selected according to the expected total load (basic generator load plus test object load), to guaranty $C_i \gg C_l$.

7.1.2.2 Multiplier RC Circuit

The basic circuit (Fig. 7.4a) is usually applied for students training and demonstrations with voltages below 200 kV. For higher voltages, multiplier circuits proposed by E. Marx in 1923 are applied (Fig. 7.5a, without the red short-circuit bars):

The impulse capacitors C_i of all n stages are charged via the charging resistors R_c which are connected in series to one column. When the charging resistors are dimensioned correctly, it does not play any role that the charging resistance of the highest stage is n-times larger than that of the lowest one, because the charging time is selected long enough that all impulse capacitors are equally charged. Today, a thyristor-controlled charging with a constant current up to a pre-selected voltage V_0 is used, at which the switching gap is triggered for breakdown. Now, the impulse capacitors start to discharge via the tail resistors on each stage (Fig. 7.5a: blue path). At the same time, the external load capacitance C_l (basic load of a capacitive divider plus stray capacitances of the generator to ground plus test object) is charged from the series connection of all impulse capacitors and front resistors (green path). An impulse voltage generator of n stages (Fig. 7.5b) charged with a DC voltage V_0 delivers with the efficiency factor η the output impulse voltage

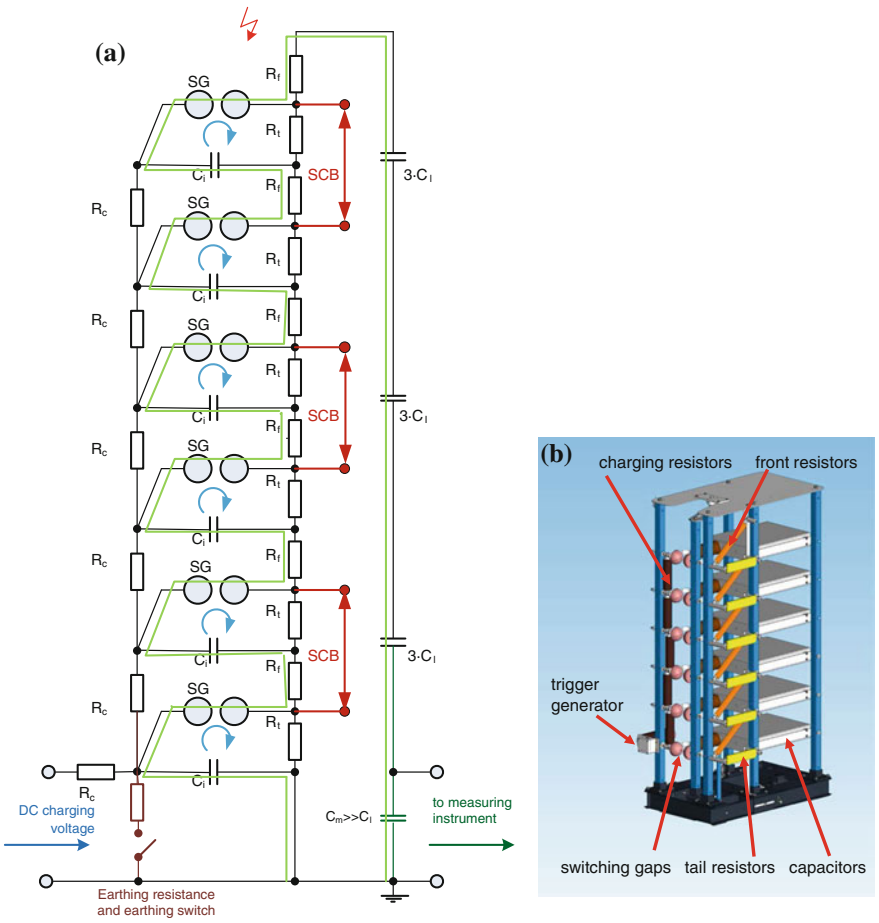

Fig. 7.5 Multi-stage impulse generator of n = 6 stages. **a** Multiplier circuit (explanations in the text). **b** Impulse generator

$$V_{in} = n \cdot \eta \cdot V_0 \tag{7.4}$$

The term $V_{0n\ max} = n \cdot V_{0\ max}$ is called the *cumulative charging voltage* of the generator and usually used as the rated voltage of the impulse test system because $V_{0n\ max} > V_{in\ max}$ one has to be careful with the valuation of rated voltages for impulse test systems. It is always necessary to know the efficiency factor for all impulse voltage shapes of interest for the calculation of the related output voltages additionally.

For calculation of its circuit elements, a multi-stage generator (*n* stages, elements R_f; R_t, C_i; C_l) is usually transferred into an equivalent basic circuit with the elements

$$\begin{aligned} R_f^* &= n \cdot R_f \\ R_t^* &= n \cdot R_t \\ C_i^* &= C_i/n \\ C_l^* &= C_l. \end{aligned} \tag{7.5}$$

After the calculation of the circuit elements of the basic circuits, the Eq. (7.5) is used for the determination of the multi-stage generator by re-transformation. The thermal design of the resistors—especially of the front resistors—determines the allowable impulse voltage repetition rate. The resistors are heated by the impulse current, which is flowing in case of the impulse voltage generation and should sufficiently cool down until the next impulse appears. A defined maximum temperature of the resistors must not be exceeded.

The controlled safe *triggering* characterizes a generator of high quality. Usually, only the lowest stage is equipped with a so-called "trigatron", a three-electrode arrangement (Fig. 7.6a). A small, battery-operated trigger device generates a voltage pulse of several kilovolts which causes a small trigger discharge at a pilot gap. This discharge triggers the breakdown of the main gap of the lowest stage. The trigger discharge delivers charge carriers and photons for the immediate, fast breakdown process, if the field strength in the main gap is high enough. This requires a certain minimum voltage, the so-called lower trigger limit (Fig. 7.6b). If the voltage at the trigger gap is too high, a breakdown is caused without triggering. This self-ignition delivers the upper trigger limit of the charging voltage. The *trigger range* between the two limits (Fig. 7.6b) should be as wide as possible. Usually, its width is between 5 and 20 % of the withstand voltage of the non-triggered gap (upper curve). It depends on the design of the trigatron, the energy of the trigger discharge and the height of the DC voltage at the main gap.

The charging voltage and the trigger instant must be well controlled to guarantee safe triggering of the whole generator and to avoid "no-triggering" or self-ignition without triggering. As soon as the lowest switching gap breaks down, an over-voltage appears at the second stage, runs as a travelling wave through the generator and shall cause the breakdowns of all further gaps. The over-voltages must remain high enough to cause all necessary breakdowns. This depends on the impulse shape to be generated (e.g. damping front resistors) and on stray capacitances to ground which increase the over-voltages, whereas longitudinal stray capacitances reduce them (Rodewald 1969a, b). Based on such investigations, additional trigger measures (e.g. supporting gaps and ignition capacitors) have been introduced to maintain the height of over-voltages also for huge generators (Rodewald 1971; Feser 1973, 1974). Generators with symmetric charging (Sect. 7.1.2.4, Fig. 7.7) allow a save triggering without these additional measures (Schrader 1971).

The modular design of multi-stage generators is helpful for later extension to higher voltages by additional stages. It enables also the parallel connection of stages for higher impulse energy at lower voltages (Fig. 7.5.a, red short-circuit

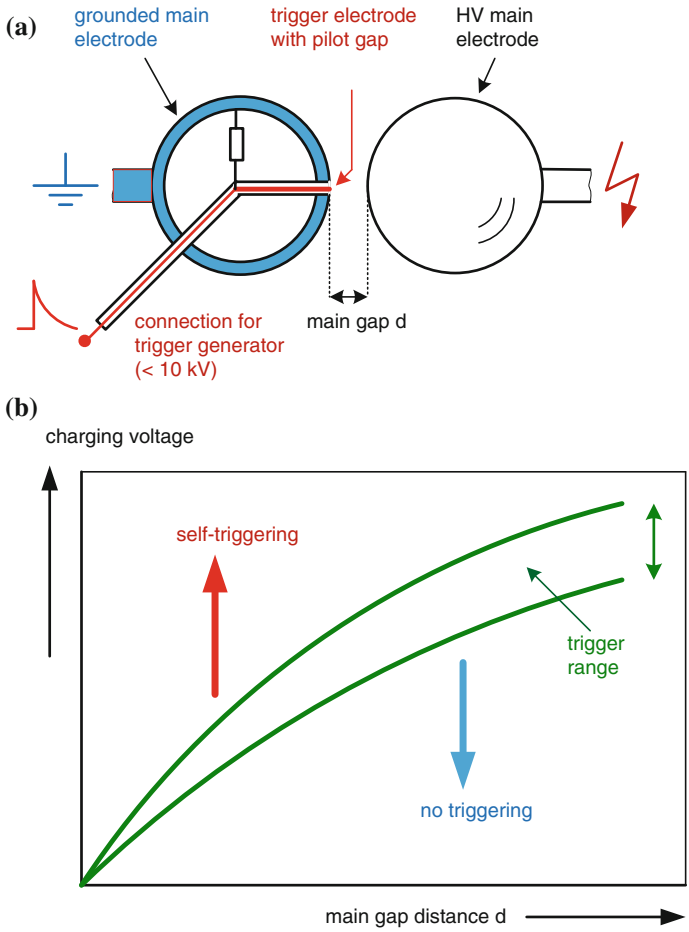

Fig. 7.6 Triggering of impulse voltage generators. **a** Trigatron spark gap. **b** Principle of the trigger range

bars (SCB)) as they are, e.g. required for testing the low-voltage winding of power transformers or medium-voltage capacitors. Also impulse test currents can be generated by impulse voltage generators with parallel stages.

7.1.2.3 Consideration of the Inductances in the Circuit

Till now, all explanations have not considered the inductances in the impulse test circuit which cannot be avoided. Inductances form oscillating circuits with the capacitances and cause damped oscillations superimposed on the aperiodic pulses. The damping depends on the front resistor. This is several 100 Ω for SI voltages and suppresses the oscillations completely. The more or less damped oscillations

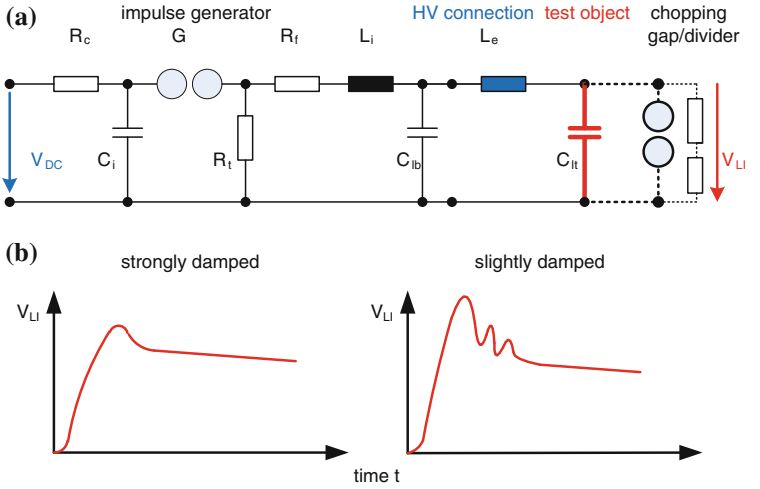

Fig. 7.7 Inductances in the impulse voltage generation circuit. **a** Equivalent circuit diagram with inductances. **b** Over-shoot superimposed on LI voltages (schematically)

and the "*over-shoot*" (only less than one period of the oscillation) are found at LI voltages only, because the LI generator is equipped with front resistances of few 10 Ω (Fig. 7.7). There are internal inductances of the generator and external of the test object and its connections.

Internal inductances L_i are those of the capacitors, the resistors and the connections between them. For estimations, the inductance for 1 m of the loop (e.g. green path in Fig. 7.5a) is about 1 μH. The reduction in the internal inductance of a generator requires its compact design with a loop as short as possible. A good generator should have an internal inductance of $L_i < 4$ μH per stage. Usually, the user cannot influence the internal inductance of the generator easily. When only a part of the stages is sufficient to generate the necessary voltage (so-called "part operation"), the loop should be short and should exclude the not-used part of the generator and of the basic load (voltage divider). For very old generators, one should check the inductance of the front resistors: The front resistors must be designed with low inductance, which can be reached by a bifilar winding. This means that two isolated, close together arranged wires are wound on a fibreglass tube in opposite directions. The magnetic fields of the wires have opposite directions and compensate each other to a remaining inductance which corresponds to the length of the resistor tube. A second possibility is a resistor band where the insulated resistance wires are woven into a fabric as a meander. Resistor bands are commercially available. The inductance of resistors can also be reduced when, instead of a single resistor, two or more parallel resistors are applied resulting in the same resistance.

External inductancesL_e are those of the test object (even if this mainly a capacitance), the HV lead to the test object and the voltage divider as well as those of the earth return. HV lead and earth return shall be especially very short and can

often be influenced. With increasing LI test voltage, the distances between generator and test object become longer and oscillations and over-shoot cannot be controlled in testing UHV equipment (see Sect. 7.3). Up to a certain degree, also the inductance of the lead can be reduced by its selection. Table 7.1 gives some indications of the inductances which depend also on the length of the connection. Never a thin wire should be used for the HV lead or the ground return, because its inductance is higher than those of copper foil of a width $w \geq 10$ cm or metallic tube of a diameter $d \geq 10$ cm. A further reduction can be reached with a wider foil or two parallel foils and spacers with a distance d in between. Also quite useful is the application of the mentioned resistor bands as HV lead and external damping resistor to the test object. To maintain the impulse shape, the internal front resistor must be reduced, but the external resistor increases the damping efficiency including the efficiency factor.

Over-shoot compensations can be designed as low-pass filters of L/C/R combinations (serial or parallel compensation unit) arranged inside the generator or outside as separate components: Figure 7.8 shows the principles of the two compensation units:

The series compensation unit (Fig. 7.8b; Wolf and Voigt 1997) prevents the penetration of higher-frequency contributions to the load capacitance which includes the test object. The series connection of compensation resistance R_c and compensation inductance L_c must be adjusted to that of the front resistor R_f and internal inductance L_i. Also the compensation capacitor C_c has to be related to the load capacitance C_l. The necessary adjustment covers a certain range of load cases, but if fine tuning is required, the compensation unit must be adapted. For larger impulse generators, the series compensation unit can be distributed to the different stages of the generator (with elements of the stage voltage, e.g. 200 kV) and without components of high-rated voltage (e.g. 3,000 kV).

The *parallel compensation unit* (Fig. 7.8a; Hinow and Steiner 2009; Hinow 2011) is always a separate unit which might be combined with a chopping gap and a voltage divider to one compact unit (Fig. 7.9). Its adjustment has to consider the natural frequency range caused by internal and external inductances. The efficiency of the two principles is about the same. It seems that especially for LI testing of UHV equipment the handling of compensation units becomes too time-consuming and does not fit to the operation of an industrial test field. The problem can be easily solved by increased damping due to larger front resistors, but this requires larger tolerances for the front time of LI impulses (for details see Sect. 7.2.1)

7.1.2.4 Some Details of the Design of Impulse Voltage Test Systems

The *LI/SI voltage test system* (Fig. 7.10) includes the HV circuit consisting of the HV generator which is optionally completed by an over-shoot compensation unit, an HV *chopping gap* and a measuring system including an HV LI/SI divider (see Sect. 7.5). The test object is also a part of the HV circuit, but later considered under Sect. 7.3. Furthermore, it includes *the* control and measuring system, *the*

Table 7.1 Inductances to be assumed for HV leads

Connection by length of connector (m)	Single wire, $d = 2$ mm (μH)	Metal foil, $w = 10$ cm (μH)	Metal tube, $d = 10$ cm (μH)	Metal foil, $w = 50$ cm or 2 foils with spacer in between (μH)
1	1.37	0.70	0.59	0.40
10	1.83	1.26	0.96	0.84

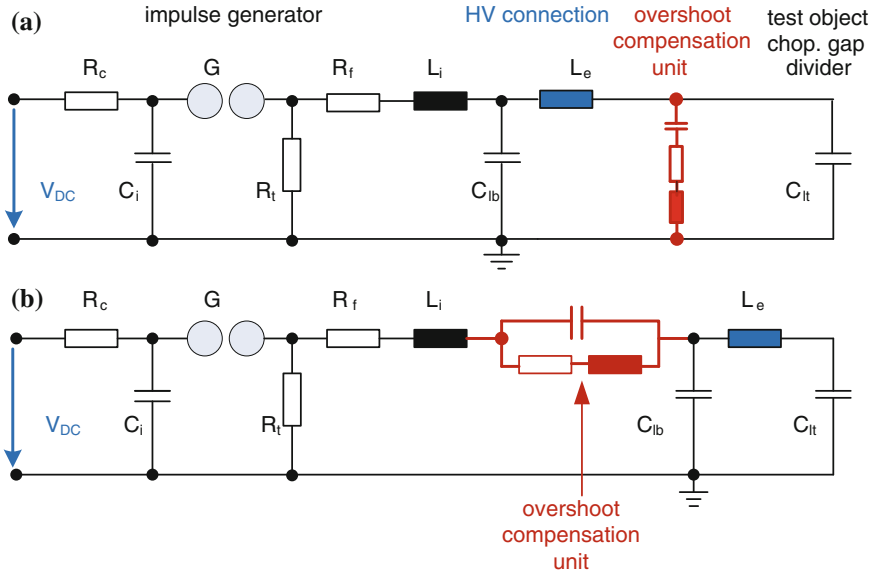

Fig. 7.8 Equivalent circuit diagrams of over-shoot compensation units. **a** Parallel compensation unit. **b** Series compensation unit

switching cubicle with the thyristor controller and the DC voltage generator. In the following, some characteristics of the main elements are given. For the generator, see the above explanations.

Generator with symmetric charging: For larger impulse voltage generators, the charging voltage per stage is usually 200 kV. Because of the limited rated voltage of capacitors, usually two 100-kV capacitors are connected in series for 200 kV. To guarantee identical charging of both capacitors of a stage, potential resistors R_p must be arranged at the connection point of both capacitors (Figs. 7.11a and 7.12a). With a special circuit patented by Schrader (1971), a symmetric charging with ± 100 kV is applicable (Figs. 7.11b and 7.12b). This requires a charging unit with symmetric output ± 100 kV.

For each polarity, a separate column of charging resistors R_c, but no potential resistors R_p are required. There are some advantages of the symmetric charging for larger impulse test systems with two capacitors in series per stage: In the first line, a stage with a short HV loop of low inductance can be designed (Fig. 7.12d).

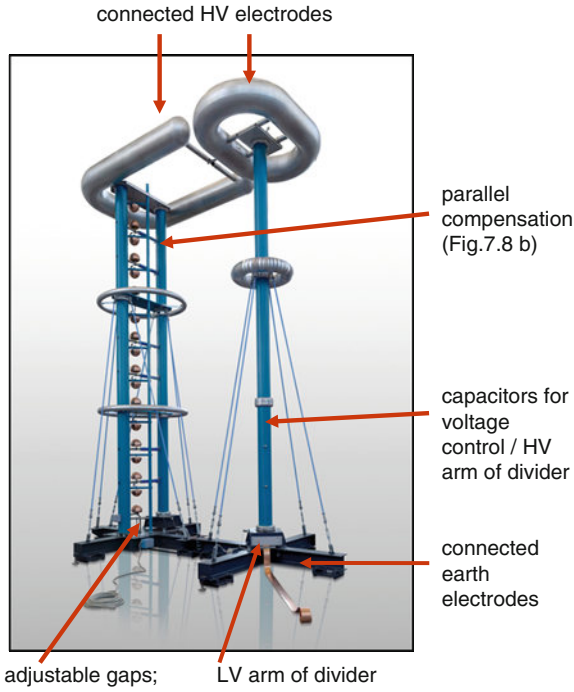

Fig. 7.9 Parallel compensation unit in combination with voltage divider and chopping gap

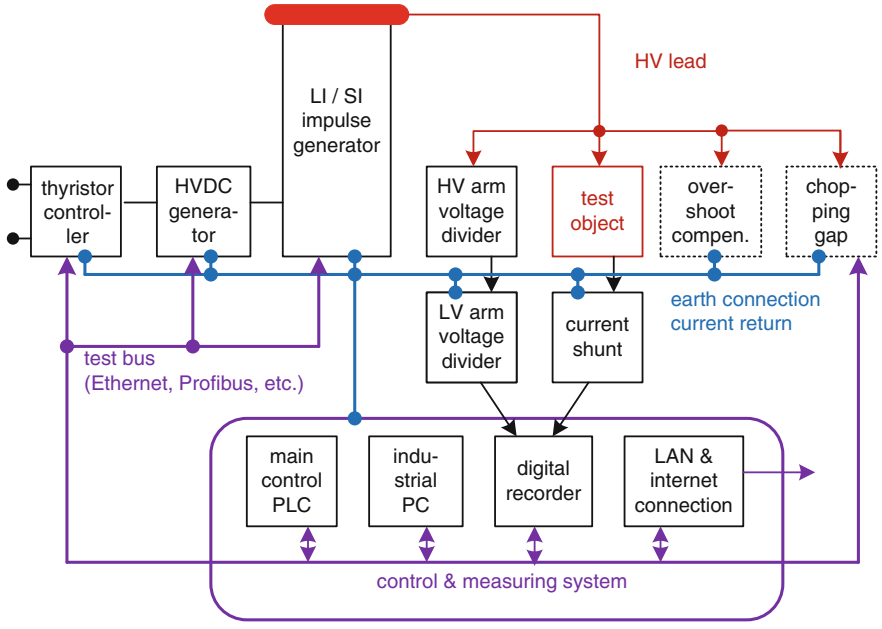

Fig. 7.10 Components of an LI/SI test voltage system

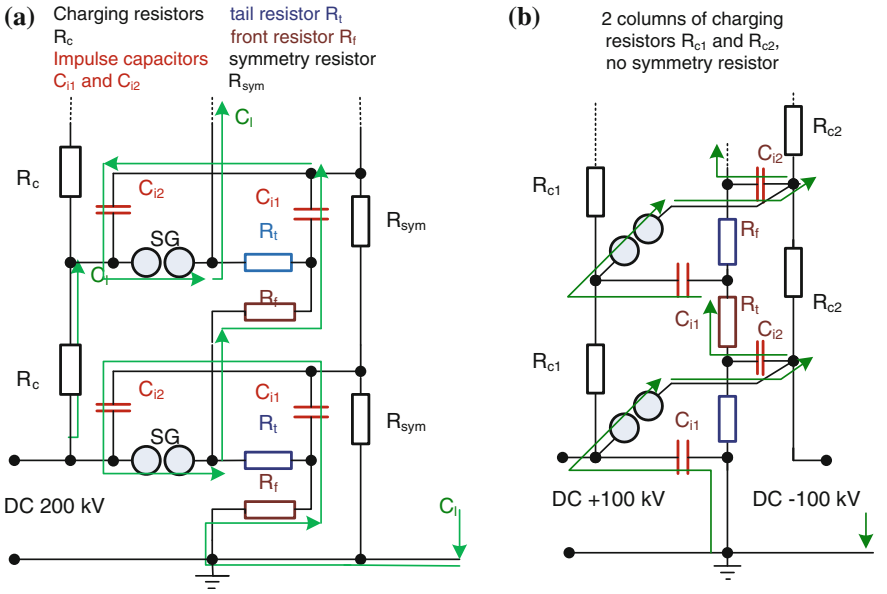

Fig. 7.11 Typical circuits for impulse voltage generators. **a** Unipolar charging (e.g. 200 kV). **b** Symmetric charging (e.g. ±100 kV)

The safe triggering of large generators with symmetric charging does not require the additional measures mentioned above. As there are no voltage-dependent circuit elements, the impulse shape (described by the time parameters) is independent from the peak voltage (Fig. 7.13). Also the parallel connection of stages for the generation of impulses with a higher energy is very simple.

Chopped lightning impulse (*LIC*) *voltagesand chopping gap*: An external over-voltage in the power system is limited to the protection level by a lightning arrester. This means the over-voltage is chopped and collapses to this protection level. The duration of the voltage collapse is very short, its steepness very high. Such steepness causes very non-linear stresses in equipment with windings (power, distribution and instrument transformers, reactors, rotating machines). The mainly stressed insulation at the HV terminals of the equipment must be designed accordingly and verified by a test with chopped lightning impulse (LIC; Fig. 7.14a) voltages.

An LIC test voltage is generated as an LI test voltage described above and then chopped by a separate chopping gap. For LIC voltages up to about 600 kV, a usual sphere-to-sphere gap can be used; for higher voltages, *multiple chopping gaps* become technically mandatory (Fig. 7.14b and c). The voltage collapse of a multiple spark gap is much faster than that of a single large sphere gap. The chopping gap consists of in-series-connected sphere-to-sphere gaps, usually one gap for one stage of the generator. One sphere of each gap is fixed and arranged at a fixed insulating column. The other one—on suitable insulating support—is

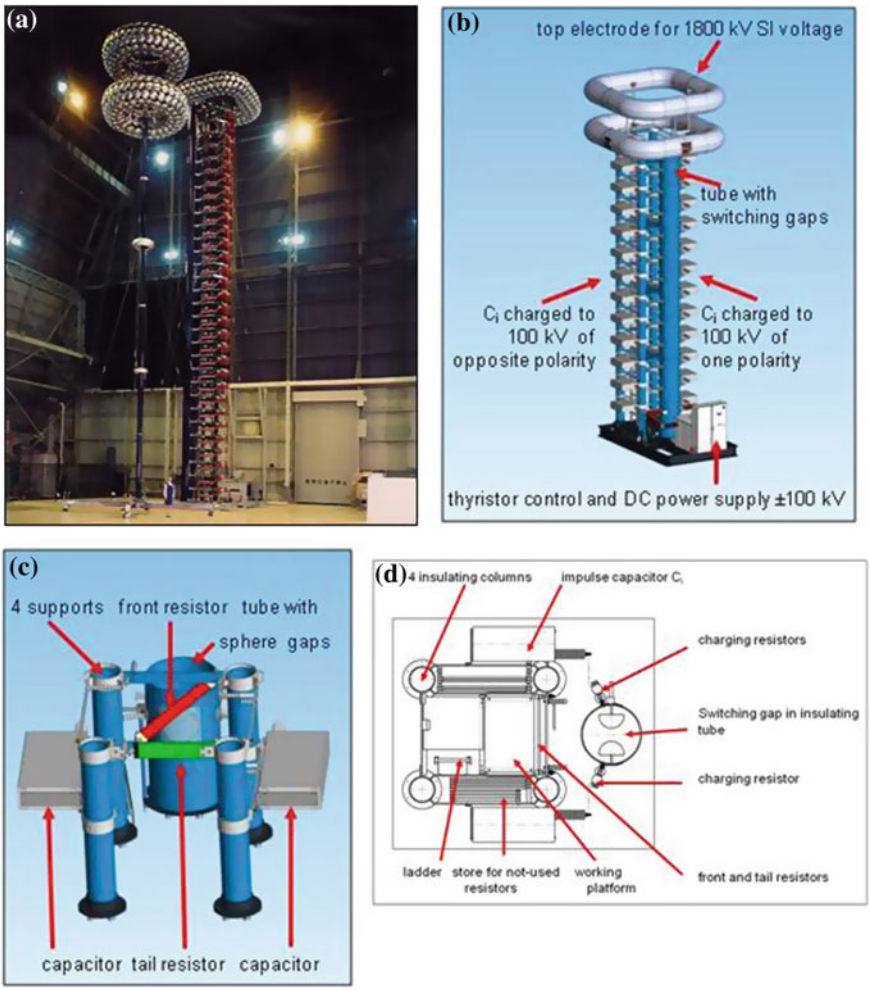

Fig. 7.12 Impulse voltage generators for unipolar and symmetric charging. **a** Generator with unipolar charging (Courtesy of Haefely, Basel). **b** Generator with symmetric charging. **c** One-stage of a multi-stage generator (inside view). **d** Cross section of a generator with symmetric charging

moveable by a motor drive and can be adjusted for the relevant voltage value. The parallel capacitor column controls the voltage distribution linearly. This column might also be used as a damped capacitive voltage divider, which is usually a separate component (see Sect. 7.5). The instant of the chopping can be triggered as described above for the generator (Fig. 7.6). Also the combination with an overshoot compensation unit is applied (Fig. 7.9).

Electrodes for the HV components: An impulse voltage generator and the other HV components require a sufficient clearance D from grounded or energized

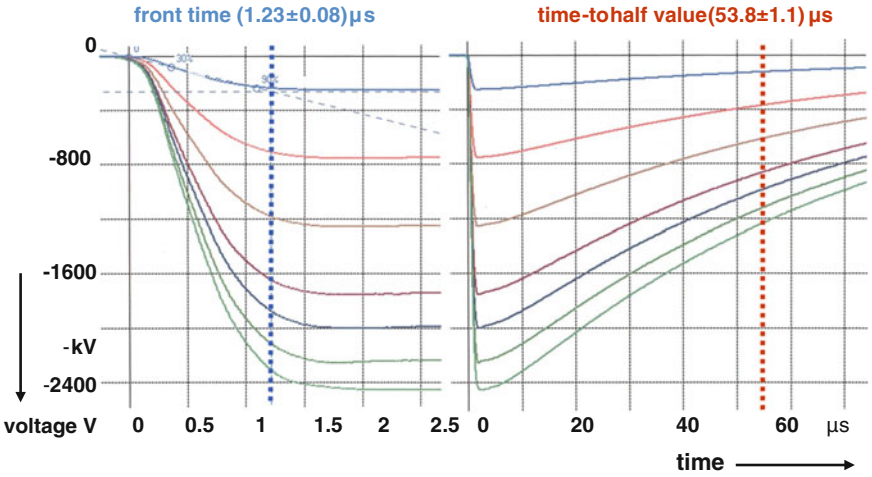

Fig. 7.13 Reproducibility of LI voltage shapes independent on peak voltage value

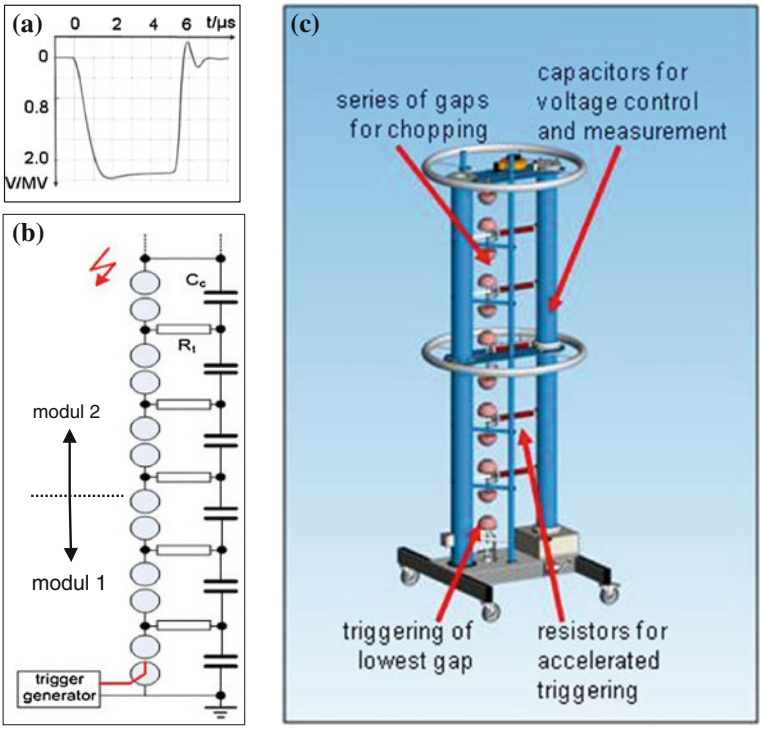

Fig. 7.14 Chopped lightning impulse generation. **a** Chopped lightning impulse (LIC) voltage. **b** Circuit of two modules of a multiple chopping gap. **c** Multiple chopping gap for 1200 kV (six single gaps)

objects in an HV test laboratory (Fig. 7.15a) to avoid breakdowns of the air gap between the HV circuit and the surroundings. The necessary clearance depends on the kind of pre-discharges which determine the breakdown process. The optimum design of the electrodes of the HV components enables not only the correct operation of an LI/SI test system but ensures also their minimum space in the test laboratory.

Note This clearance should not be mixed up with the clearances for the test object according to Fig. 2.1. The clearances there consider that the voltage distribution at the test object is not influenced by the surroundings. Here, the operation of the generator shall not be disturbed by undesirable discharges or even breakdowns.

At LI test voltages, the *streamer discharge* determines the breakdown voltage of a non-uniform electric field in air. The electric field of an LI generator in an HV test room is such a non-uniform electric field. Consequently, the specific breakdown voltage is equal to the voltage demand of streamers of about 5 kV/cm for positive and about 10 kV/cm for negative polarity of the electrode with the larger curvature. This means that for a 3 MV LI generator, the minimum clearance should be 6 m (plus a certain safety margin of—say—20 %). The curvature of the electrodes can be relatively small (Fig. 7.15b), because there is no need to avoid the streamer discharges.

Note The strong polarity effect is typical for streamer discharges in air. There is no remarkable polarity effect for internal insulation. If internal insulation, e.g. of a power transformer, shall be tested with LI voltage, a flashover of the air-part of the bushing is avoided when the test is performed at negative LI voltage.

At SI voltages, a combination of streamer and *leader discharges* determines the breakdown voltage between the generator and the surroundings. The electrodes of the HV components of the test system shall be designed in such a way that no leader discharge appears, this means with larger radii (Fig. 7.15c). The effect of enlargement of the distance to the surrounding is very week because of the low leader gradient (about 1 kV/cm). Therefore, it is recommended to optimize the electrodes of the HV components by a field calculation with the realistic conditions of the test room. As a rough hint, the distance must be in minimum 20 % larger than for LI voltage, and the surface field strength of the electrodes at SI voltage should be about 20 kV/cm.

When a generator and related HV components are used for LI and SI generation, the electrodes are determined by the maximum SI test voltages, even when they are about 25 % lower than the maximum LI test voltages. An optimum utilization of a test area can be reached when a generator is moveable in the laboratory, e.g. by air cushions. The design principles for outdoor generators (Fig. 7.15d) are identical. They require also large electrodes for SI voltage generation, but under rainy conditions, the maximum output voltages must be remarkably reduced.

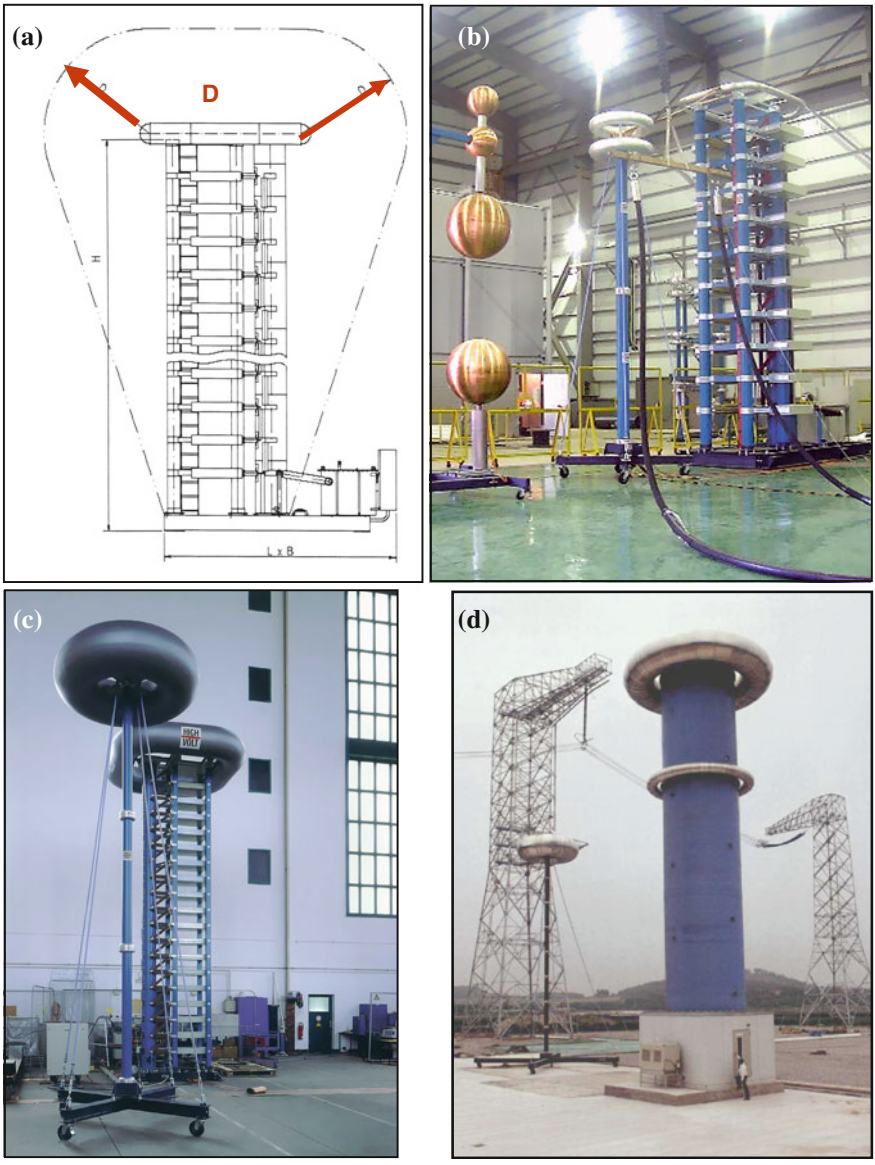

Fig. 7.15 Electrodes for the HV components of LI/SI voltage test systems. **a** Necessary clearance D around a LI/SI generator. **b** Test system only for LI voltage generation (2,000 kV), **c** Test system 1,800 kV for LI/SI voltage generation at limited clearance to the ceiling. **d** Outdoor test system 4,200 kV for SI and LI voltage generation (Courtesy of KEPRI, Korea)

Control and measuring system: This—today usually computer-aided—subsystem of an LI/SI test system (Fig. 7.10; see also Sect. 2.2) of an LI/SI voltage test system enables the adjustment of the generator for the test voltage value and a certain test procedure (see Sect. 7.4), the measurement of LI/SI voltages and of related impulse currents (see Sects. 7.5 and 7.6). It is available for one, two or all three following modes:

1. *Manual operation* with measurement and evaluation of LI/SI parameters: The operator has to control the test system including adjustment of the voltages and duration of the breaks between impulses, and the evaluation and presentation of the test result (test record). The charging and triggering process must be controlled. Control and measuring components are not connected to one system, and this gap is filled by the operator. This traditional mode is very seldom applied for industrial testing and research work, but applied for e.g. student's training.
2. *Computer-supported operation* and test result presentation: The test is performed manually, but the precise adjustment of test voltages—this means that of the distance of the switching gap as well as that of the charging DC voltage— and the test data presentation are overtaken by the system. Control and measuring components are connected. This mode is applied for larger and expensive test objects in industrial testing and for research work.
3. *Automatic testing* according to a pre-given test procedure by a computer control: The PC software for the test procedure is configured by the operator before, the HV test itself is performed, evaluated and presented automatically. Intervention of the operator is not necessary, but the test can be interrupted or terminated at any time by the operator. This mode is applicable for testing of very similar or even identical test objects in a larger scale or for statistical investigations in research work.

The control system delivers the commands for switching the breakers on and off, for adjusting the switching gaps of the generator for the pre-selected voltage and for the appropriate charging voltage adjusted by a thyristor controller. Based on the voltage measurement, the computer control checks that the voltage values are within the pre-given sequence and tolerances. Based on the evaluation of the voltage shape, breakdowns are recorded for the evaluation of the test. Also the evaluation of the related currents might indicate whether a test has been successful or has failed. The style of the *test record* depends fully from the intention of the user.

Switching cubicle *and DC rectifier unit*: An LI/SI test system has a relatively low power demand of some 10 kW. The switching cubicle contains the power switch and the operation switch, the instrument transformers for supply voltage and current measurement and protective equipment. The built-in thyristor controller enables a constant-charging current output of the connected rectifier unit. This DC rectifier unit is usually a doubler circuit (see Sect. 6.1.2 and Fig. 6.3) or for symmetric charging, a half-wave rectifier with symmetric output (Fig. 6.2). Depending on the rated power and energy of the impulse generator, the charging

voltage corresponds to the stage voltages (100–200 kV) and the charging currents are between few 10 mA and some 100 mA. The duration of the charging which determines the impulse voltage repetition rate depends on the total energy of the generator and is usually between 10 and 60 s. For special application, also faster charging processes and higher repetition rates can be realized.

7.1.3 Circuits for Oscillating Impulse Voltages

For factory testing with aperiodic LI voltages according to IEC 60060-1:2010 or IEEE St.4:1995, the inductances in the circuit are disturbing elements, but a defined inductance L_s in the circuit establishes an oscillating circuit of this series inductance and the load capacitances C_l. This circuit is excited by the triggered discharging of the impulse capacitors of the generator (Fig. 7.16a). The output voltage is a damped oscillation around the discharge curve of the impulse capacitances of the generator. The oscillating frequency is the natural frequency

$$f_0 = \frac{1}{2\pi \cdot \sqrt{L_s \cdot \frac{C_l \cdot C_i^*}{C_l + C_i^*}}}. \tag{7.6}$$

For a generator with n stages, one has to apply $C_i^* = C_i/n$ and $R_t^* = n \cdot R_t$ (Eq. 7.5). The total load $C_l = C_{lb} + C_{lt}$ is the sum of the basic load and the test object load. The fixed series inductance L_s replaces the front (damping) resistors. According to IEC 60060-3:2006, impulse voltages with oscillations $f_0 > 15$ kHz are considered as "*oscillating lightning impulse* (*OLI*) *voltages*" (Fig. 7.16a), such with $f_0 < 15$ kHz as "*oscillating switching impulse (OSI)* voltages" (Fig. 7.17a). The damping is determined by the losses in the circuit, for pure capacitive test objects mainly by the tail resistors R_t of the aperiodic impulse. As these are higher for OSI than for OLI voltages, OSI voltages show not only a lower frequency, but also a larger damping (Fig. 7.17a).

Theoretically, the oscillating impulse voltage (OLI or OSI) can reach a peak value which is twice the peak value of the relevant aperiodic impulse (LI or SI) voltage. In practice, it reaches about 90 % of that value. The efficiency factors are

$$\eta_{\mathrm{OLI}} = \frac{V_{\mathrm{OLI}}}{V_{0\Sigma}} \approx 1.7\ldots1.8 \quad \text{and} \quad \eta_{\mathrm{OSI}} = \frac{V_{\mathrm{OSI}}}{V_{0\Sigma}} \approx 1.3\ldots1.4. \tag{7.7}$$

As an example, Fig. 7.18 shows the remarkable influence of the test object (load) capacitance on the efficiency factor and the time-to-peak. The high-efficiency factors compared with those of the aperiodic impulse voltages are especially important when mobile impulse test systems are required for the testing in the field. Therefore, OLI and OSI voltages have been proposed for on-site testing (Kind 1974; Feser 1981), and meanwhile, they are standardized in IEC 60060-3:2006. For more details, see Sect. 10.2.1.

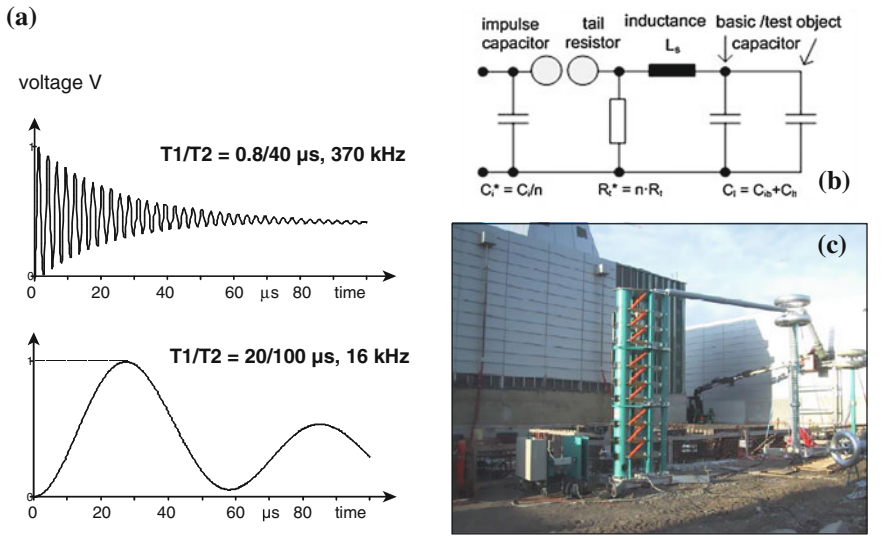

Fig. 7.16 Oscillating lightning impulse voltages (OLI). **a** OLI test voltages. **b** Equivalent circuit for oscillating impulse voltage generation. **c** 900 kV impulse test system for 850 kV LI and 1,600 kV OLI voltages (Courtesy of Siemens Berlin)

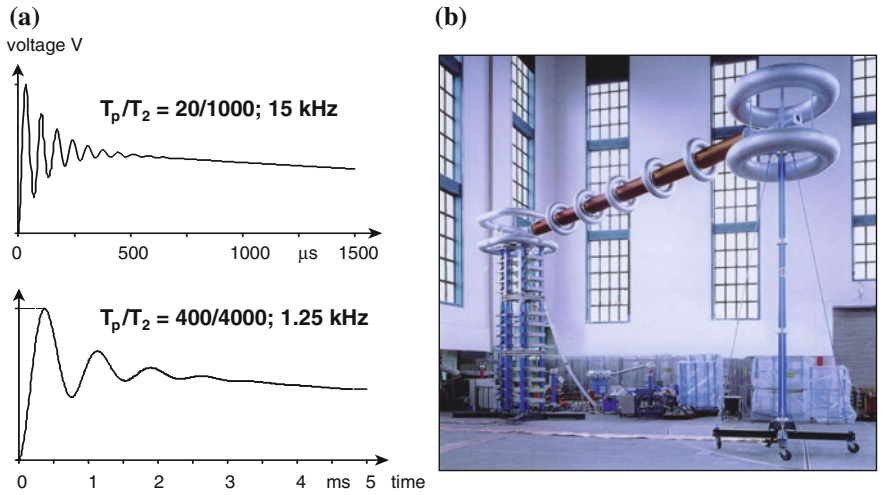

Fig. 7.17 Oscillating switching impulse voltages (OSI). **a** OSI test voltages. **b** 1,200 kV impulse test for 900 kV SI and 1,600 kV OSI voltages

When the generator has to be designed for a maximum cumulative charging voltage $V_{0\Sigma max}$, the basic load capacitance and also the series inductance must be able to withstand the maximum oscillating impulse voltage which is much higher

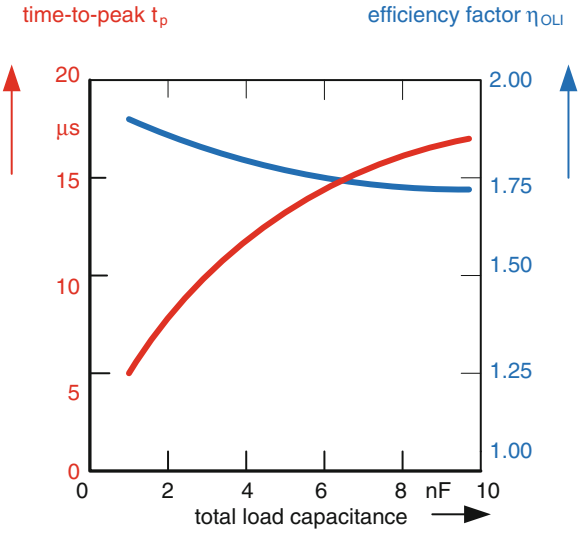

Fig. 7.18 OLI characteristic of an impulse voltage test system (250 kV/5 kJ)

than the $V_{0\Sigma max}$ (Eq. 7.7). The insulation design of the basic load capacitance for OLI and OSI voltages is practically identical, whereas that of the series inductance is very different (compare Figs. 7.16c with 7.17b). For OLI voltages, a low inductance is required which can be made easily. Contrary to that the OSI generation requires a much higher inductance. Now, stray capacitances must be taken into consideration which would cause a non-linear voltage distribution along the coil. To avoid that, a longitudinal voltage control by toroid electrodes is necessary. The coil for OSI voltage is much longer, thicker and heavier than the one for OLI voltage. Furthermore, it has been found that the benefit of OSI testing is low; therefore, mainly OLI testing is applied (see Sect. 10.3.1).

It should be mentioned that also bipolar oscillating impulse voltages can be generated based on impulse voltage circuits (Schuler and Liptak 1980). They arranged the inductance in parallel to the load capacitance and applied the bipolar OLI voltage for testing of rotating machines.

A special case of a bipolar OSI testing is applied for medium-voltage cables: The cable is charged with a DC voltage and then discharged via a suited switch (trigatron or semiconductor HV switch) in series with an inductance L_s and possibly a resistor R_d. The discharge causes a damped oscillation (Fig. 7.19). Under the term "*damped alternating voltage*" (*DAC*) (IEC 60060-3:2006), this bipolarly oscillating voltage is successfully used for *diagnostic PD measurements* on medium-voltage cable systems, but the whole test stress for the cable is a long DC ramp (duration in the order between 1 and 100 s) followed by the much shorter DAC voltage (duration in the order of few 100 ms). The duration of charging and the test frequency depends on the capacitance (length) of the cable, whereas the damping of the oscillation depends on the losses in the circuit. Therefore, the whole stress cannot be reproduced from cable test to cable tests. Occasionally, the

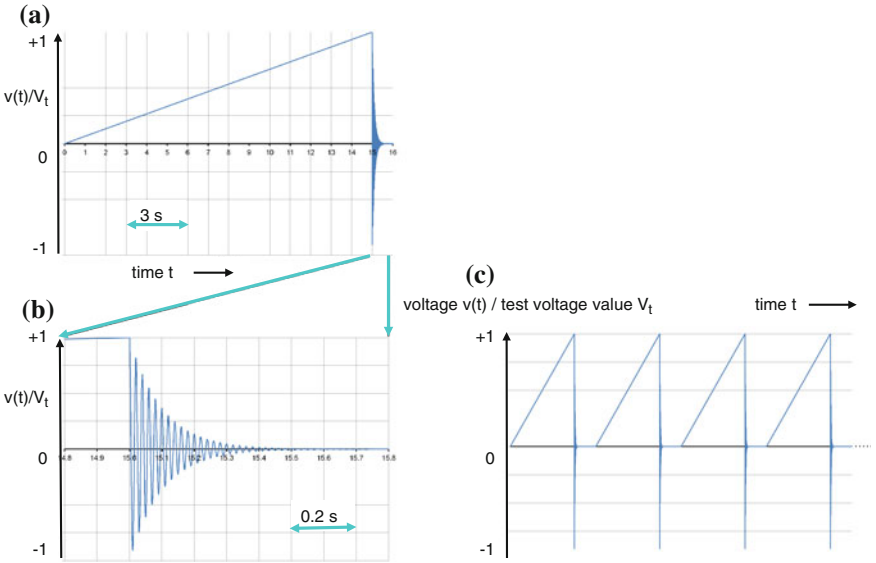

Fig. 7.19 Damped alternating (DAC) voltage. **a** A full DAC impulse (including the DC ramp for charging). **b** The short oscillating part of the DAC impulse. **c** A sequence of DAC impulses as occasionally used for withstand tests

voltage is used for withstand tests (Fig. 7.19c), but this cannot be recommended. (for more details, see Sect. 10.3.2).

7.1.4 OSI Test Voltage Generation by Transformers

When an *HV test transformer* is excited by controlled discharging a capacitor *bank* into its low-voltage (LV) side, this impulse causes an oscillation, which is transformed to the HV side according to the transformer ratio (Kind and Salge 1965; Mosch 1969). The schematic circuit diagram (Fig. 7.20a) is transferred with the transformer ratio into an equivalent circuit (Fig. 7.20b), which is used for calculations of the shape and frequency of the OSI voltage (Schrader et al. 1989).

Shape and frequency are determined by the stray inductance of the transformer (L_s) and the series connection of the bank capacitance (C_B) with the transferred load capacitance (C_l^*)

$$C = \frac{C_B \cdot C_l^*}{C_B + C_l^*}. \tag{7.8}$$

The impulse parameters can be influenced by adjustable elements, an inductance L_r and a damping resistor R_p. With the total capacitance C and the total inductance $L = L_s + L_r$, one gets the frequency and the time-to-peak:

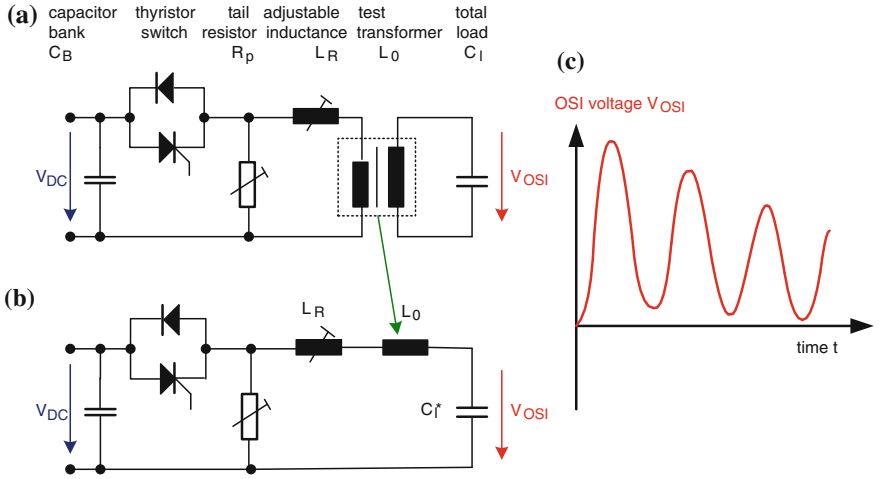

Fig. 7.20 Generation of unipolar OSI voltages by transformers (Schrader et al. 1989). **a** Schematic circuit diagram. **b** Equivalent circuit. **c** Unipolar OSI voltage

$$f = \frac{1}{2\pi\sqrt{L \cdot C}} \quad \text{and} \quad T_p = \frac{1}{2f} = \pi\sqrt{L \cdot C}. \tag{7.9}$$

The output (Fig. 7.20c) is a unipolar OSI voltage with frequencies of 100 up to 1,000 Hz; this means with time-to-peak $Tp > 500$ μs.

Bipolar OSI voltages can be generated with a modified circuit (Fig. 5.21a and b) (Schrader et al. 1989). The load capacitance is charged in the same way as for unipolar OSI voltages, but when the first peak is reached, a short-circuit switching by a thyristor causes the bipolar OSI voltage at the HV output (Fig. 7.21c). The capacitor bank is not any longer involved in the oscillation.

Even under optimum conditions, shorter time-to-peak than mentioned above cannot be generated because of the value of stray inductances of test transformers. In many cases, these times are remarkably longer. When a transformer cascade of three stages shall be used for OSI generation, the stray capacitance depends on the kind of feeding (Fig. 7.22) (Schrader et al. 1989). Feeding into the primary side of the lowest transformer means highest stray inductance and lowest frequency, say 100 Hz. When feeding is applied to the middle of the cascade (tertiary winding of the second transformer), the frequency increases by a factor of two (200 Hz). When feeding is realized into the tertiary windings of all three transformers, the stray inductance decreases to 1/40 compared with case a), and consequently, the frequency increases to more than 600 Hz. This principle has been applied to the mentioned 3-MV cascade transformer (Frank et al. 1991), (Figs. 3.15 and 7.23). On each stage, there is a capacitor bank with a rectifier unit. The DC voltage is generated on the stages from a low-frequency AC voltage supplied via the

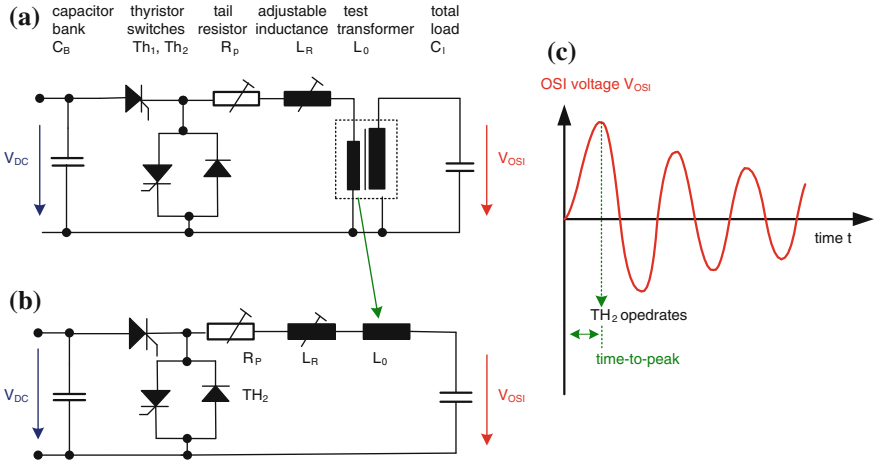

Fig. 7.21 Generation of bipolar OSI voltages by transformers (Schrader et al. 1989). **a** Schematic circuit diagram. **b** Equivalent circuit. **c** Bipolar OSI voltage

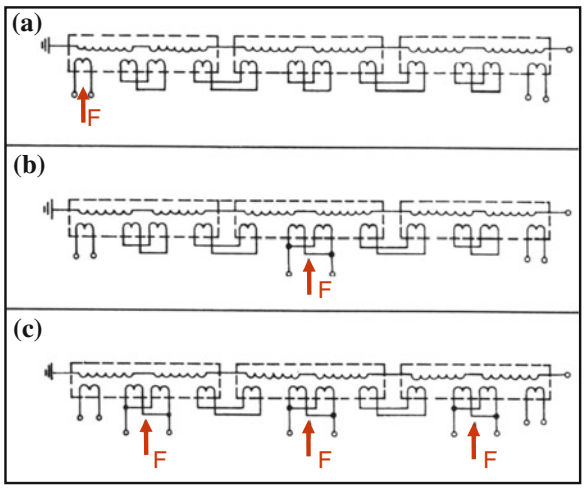

Fig. 7.22 Feeding modes of a three-stage cascade transformer for OSI voltage generation. **a** Single feeding into the primary winding of the lowest transformer. **b** Single feeding into the tertiary winding of the middle transformer. **c** Triple feeding into the tertiary winding of each transformer

windings of the transformer in a special mode. The three capacitor banks are discharged each into the tertiary winding of one transformer at the same time. This enables the generation of OSI voltages up to 4.2 MV. The leader discharges in air generated by this extremely high OSI voltage are very similar to natural lightning (Hauschild et al. 1991).

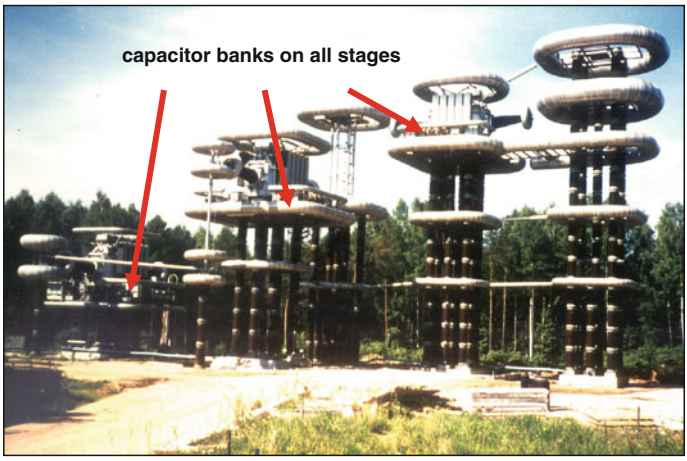

Fig. 7.23 3-MV transformer cascade with OSI attachment and triple feeding mode

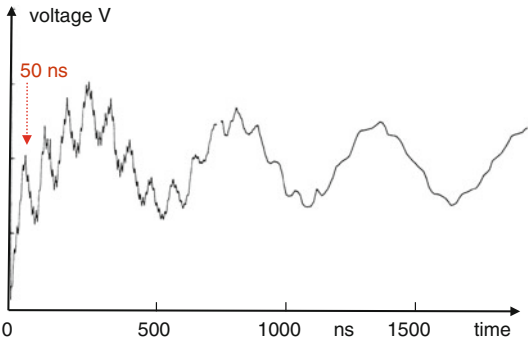

Fig. 7.24 Time characteristic of a VFF voltage

7.1.5 Circuits for Very Fast Front Impulse Voltages

VFF over-voltages are generated by switching GIS disconnectors and consecutive reflections in the GIS busbars, by steep LI voltage breakdowns of the insulation of overhead lines or by the operation of a lightning arrester. Similar voltages are expected in case of a nuclear explosion (EXO-EMP). They might be characterized by an oscillating impulse with a first front of some 10 ns up to few 100 ns and superimposed contributions of higher frequencies (Feser 1997). Figure 7.24 shows a typical example of a VFF voltage (CIGRE WG 33.03 1998)

VFF voltage testing of GIS is performed by defined switching of the disconnectors (IEC 61259:1994). There is no horizontal standard for VFF test voltages. For research and development of components which might be stressed by VFF over-voltages in service, VFF impulse voltages are usually generated by a Marx

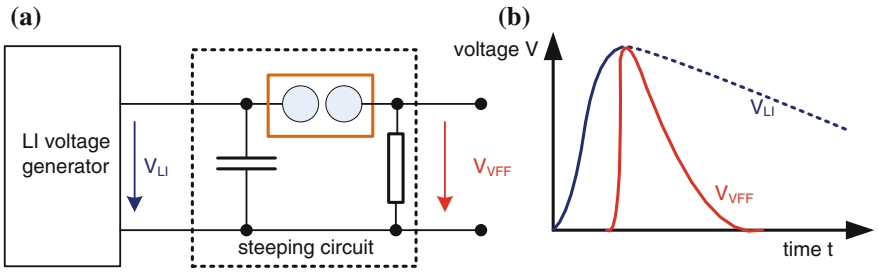

Fig. 7.25 Generation of VFF test voltages. **a** Equivalent circuit. **b** Potential diagram

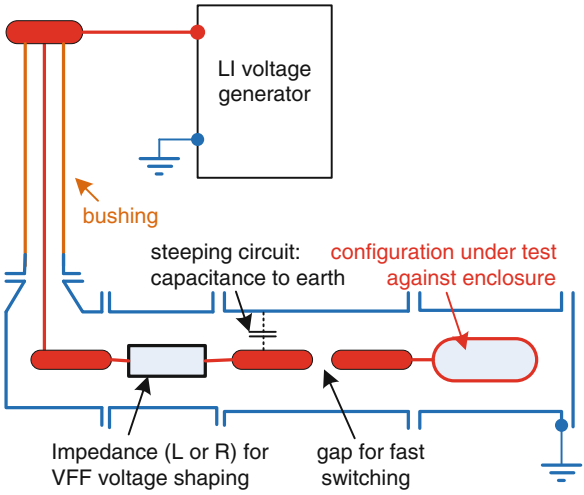

Fig. 7.26 Principle circuit for VFF investigation of gas insulation

impulse voltage generator with a connected steeping circuit (Kind and Feser 1999) (Fig. 7.25), consisting mainly of a capacitor and a fast sphere gap with compressed-gas insulation and high breakdown field strength. This gap is connected in series with the test object and enables front times in the order of few 10 ns. An impulse voltage generator without steeping circuit, operating without front resistors, can generate impulse voltages with front times down to about 100 ns.

The latest development of UHV equipment has directed the attention to the behaviour of compressed-gas insulation under VFF stress (Ueta et al. 2011; Wada et al. 2011). For VFF voltage generation, a metal enclosed, compressed-gas-insulated steeping circuit is applied (Fig. 7.26). In the field compartment before the series gap, an impedance (resistor or inductor) is arranged to generate different superimposed oscillations. When its position is changed related to the gap different superimposed oscillations appear (few MHz to 20 MHz). The test object is inside of the same metal enclosure.

7.2 Requirements to LI/SI Test Systems and Selection of Impulse Voltage Test Systems

The preceding subsections have shown that a wide variety of impulse voltage shapes can be generated. For research work, development and even diagnostic testing, this variety can be used. But for quality testing, impulse voltages shall be applied which represent external (lightning) and internal (switching) over-voltages being reproducible within certain tolerances. Requirements for these test voltages are given in standards like IEC 60060-1:2010 or IEEE Std. 4 (Draft 2013) and will be explained in the following.

7.2.1 LI Test Voltage and the Phenomenon of Over-shoot

7.2.1.1 Requirements of IEC 60060-1 and IEEE Std. 4 to Standard LI Voltages 1.2/50

The parameters of a LI test voltage shall be evaluated from the so-called "*test voltage curve*" which is based on an equivalent processing of the *recorded impulse voltage* with a possible over-shoot of different magnitudes and frequencies f (in MHz) using the *test voltage function*

$$k(f) = \frac{1}{1 + 2.2 \cdot f^2/\mathrm{MHz}^2}. \tag{7.10}$$

This empirically determined function (Fig. 7.27) shall represent that an over-shoot of long duration (low frequency) has a stronger influence on the breakdown voltage of insulation than one of short duration (high frequency). This is the well-known breakdown voltage—breakdown time characteristic of insulations. As a first step of introduction of this new type of evaluation, IEC 60060-1:2010 recommends the application of Eq. 7.10 to all types of insulation, for the necessary improvement of the method see Sect. 7.2.1.2. The determination of the test voltage curve $V_t(t)$ from the recorded curve $V_r(t)$ shall be made in the following steps (Fig. 7.28, for more details, see Annex B of IEC 60060-1: 2010):

1. Determine the *base curve*$V_b(t)$ as an estimate of the exponential function with the parameters V_0, τ_1 and τ_2:

$$V_b(t) = V_0 \cdot \left(e^{(t/\tau_1)} - e^{-(t/\tau_2)}\right). \tag{7.11}$$

The base curve (Eq. 7.11) represents the recorded curve without over-shoot and shall be characterized by its peak value V_B, whereas the full recorded curve is characterized by its extreme value V_E (Fig. 7.28a).

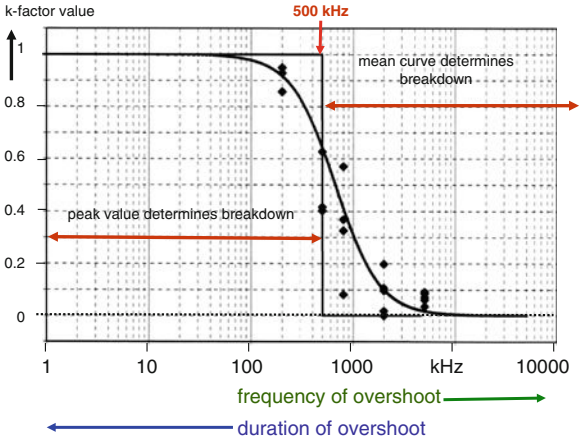

Fig. 7.27 Test voltage function (IEC 60060-1:2010) with empirical data and limit value of IEC 60060-1:1989

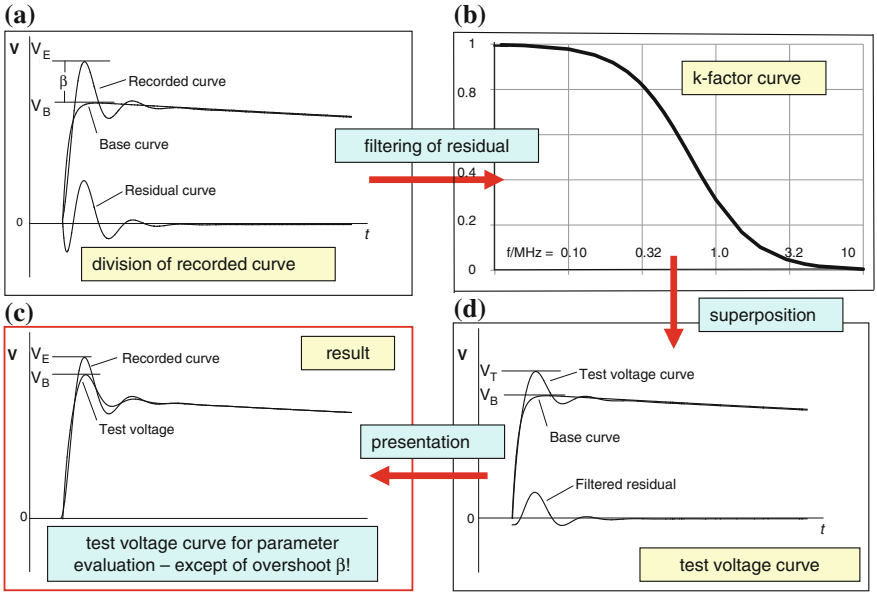

Fig. 7.28 Determination and presentation of the test voltage curve. **a** Recorded curve, base curve and residual curve. **b** Test voltage function. **c** Base curve, filtered residual curve and test voltage curve. **d** Presentation of test voltage curve and recorded curve

2. Find the *residual curve* as the difference between the recorded curve and the base curve (Fig. 7.28a):

$$V_R(t) = V_r(t) - V_b(t). \tag{7.12}$$

3. Use a digital filter with a transfer function (amplitude–frequency response) equal to the test voltage function $H(f) = k(f)$ (Eq. 7.10, as described in detail in IEC 60060-1:2010, Annexes B and C) and use it for filtering the frequency spectrum $V_R(F)$ of the residual curve. The result is the filtered residual curve in the frequency domain

$$V_{\mathrm{RF}}(f) = k(f) \cdot V_R(f), \tag{7.13}$$

and—after re-transformation to the time domain—the *filtered residual curve* V_{RF} (t) (Fig. 7.28b).

4. Superimpose the filtered residual curve on the base curve to get the *test voltage curve* (Fig. 7.28d):

$$V_t(t) = V_b(t) + V_{\mathrm{RF}}(t). \tag{7.14}$$

5. In a presentation of the result, both—the recorded curve and the test voltage curve—shall be shown (Fig. 7.78c).

Note It should be mentioned that the handling of the zero-level problem is not considered here. For the zero level and the details of the implementing, the evaluation software, see IEC 60060-1:2010, Annexes B and C and IEC 61083-2:2013, see for the filter curve also Lewin et al. (2008).

It should be mentioned that in addition to the computer-aided evaluation, also a manual calculation of the test voltage value V_T is described in IEC 60060-1:2010 (Annex B.4) and by Berlijn et al. 2007. This procedure considers not the whole frequency spectrum of the residual curve, rather its corresponding value $k(f_{\mathrm{os}})$ at the single main frequency f_{os} of the over-shoot which is simply multiplied with the maximum of the residual voltage $V_{\mathrm{Rmax}}(t)$. The result is superimposed on the estimated base curve to get the test voltage value V_T. In contrast, the filtering (Eq. 7.13) works also when the over-shoot is the result of a mixture of frequencies and when noise signals of higher frequencies are superimposed on the recorded curve.

In case of a smooth recorded curve (Eq. 7.11) with $V_E = V_B$, one gets $V_R(t) = V_{\mathrm{RF}}(t) = 0$ because of $k(f) = 1$. IEC 60060-1: 2010 requires that all parameters of the LI test voltage are evaluated from the test voltage curve. When an LI test voltage fulfils the following requirements, it is a standard LI test voltage 1.2/50:

The *test voltage value*V_T is the maximum value of the test voltage curve (Figs. 5.78c and 7.29). In an LI voltage test, the required test voltage value must be adjusted with a tolerance of ±3 %.

The *front time*T_1 is a virtual parameter defined as 1.67 times the interval between the instants when the impulse voltage is 30 and 90 % of the test voltage value (A and B in Fig. 7.29). The front time $T_1 = 1.2$ μs has a tolerance of ±30 %, this means the real front time has to be within (0.84–1.56) μs.

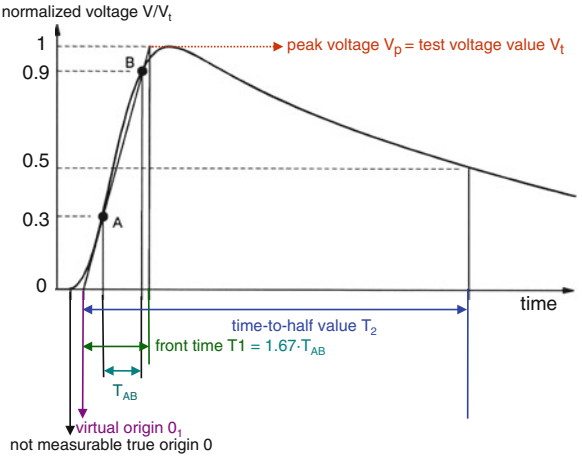

Fig. 7.29 Parameter definition for full LI test voltages

Note For test objects of high capacitance as cables or capacitors, the upper tolerance limit might be significantly enlarged to 5 μs or even more. Also for UHV equipment, an upper tolerance limit in the order of 2.5 μs is under discussion.

The *time to half-value*T_2 is a virtual parameter as the time interval between the virtual origin which is the intersection between the time axis and the straight line drawn through the points A and B in Fig. 7.29, and the instant when the voltage crosses the half of the test voltage value (Fig. 7.29): It is required $T_2 = 50$ μs with a tolerance of ± 20 %, this means the real value has to be within (40–60) μs.
The *relative over-shoot magnitude*β is the difference between the extreme value of the recorded curve and the maximum of the base curve related to the extreme value.

$$\beta = \frac{V_E - V_B}{V_E} \leq 10\,\% \tag{7.15}$$

The latest draft of IEEE Std. 4 recommends an over-shoot of 5 %, but allows an increase to 10 % for reasons "to allow waveforms accepted by the historical" smooth curve "over-shoot method" (IEEE Std. 4—1995 and IEC 60060-1:1989).

Quality tests require in addition to full LI test voltages also *chopped LI test voltages* (LIC) which represent the stress of the insulation after a protecting device (e.g. an arrester or a protection gap) has operated. An LIC voltage is also caused by any breakdown in the HV circuit, but in the following, only controlled breakdowns with a *chopping gap* will be considered (see Sect. 7.1.2.4).

The LI voltage can be chopped in the front (Fig. 7.30a) or on the tail (Fig. 7.30b). The instant of chopping is defined as the intersection of the line through the points C (0.7 V_{CH}) and D (0.1 V_{CH}) with the voltage level immediately

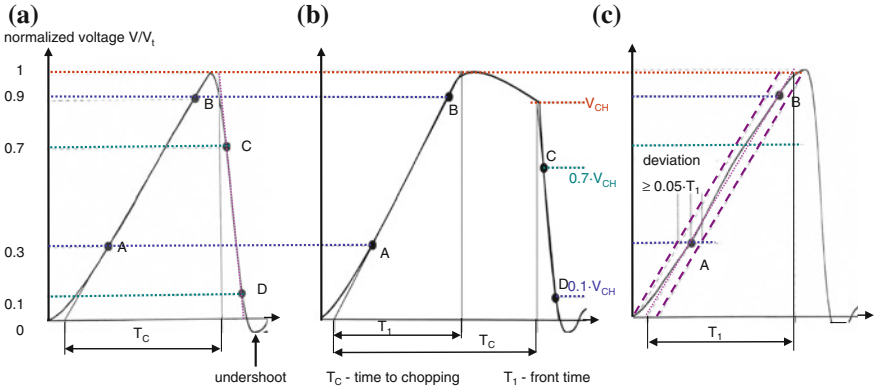

Fig. 7.30 Chopped lightning impulse voltages. **a** Front-chopped LIC voltage. **b** Tail-chopped LIC voltage. **c** Linearly rising front-chopped impulse

before the collapse. The time to chopping T_C is the interval between the virtual origin O_1 and the instant of chopping. The duration of the voltage collapse T_{CO} is defined as 1.67 times the time interval between the points C and D. The virtual steepness S_C of the chopping is calculated with the voltage V_{CH} at the instant of chopping and the duration of the voltage collapse T_{CO}:

$$S_C = \frac{V_{CH}}{T_{CO}}. \tag{7.16}$$

Whereas IEC 60060-1:2010 specifies only a tail-chopped LIC voltage of $T_C = 2$–5 μs (Fig. 7.30b), the IEEE Std. 4 specifies also a standard front-chopped LIC voltage of $T_C = 0.5$–1.0 μs (Fig. 7.30a).

Note According to the IEC opinion, a front-chopped LIC voltage is not required for testing objects with windings, because the tail-chopped LIC voltage causes a higher steepness and consequently a more non-uniform voltage distribution in the test object. The traditional IEEE opinion considers more the representation of high over-voltages limited by protection devices. It seems that in a future version of IEEE Std. 4, the IEC practice will be applied, too.

A linearly rising front-chopped LIC voltage is a voltage rising with an approximately constant steepness until it is chopped at a voltage V_E. The linearly rising front-chopped LIC voltage is mainly applied in the test practice according to the IEEE standards. It is defined by the extreme value V_E, the front time T_1 and the *steepness*

$$S_F = \frac{V_E}{T_1} \tag{7.17}$$

The voltage increase is considered to be approximately linear from 30 % up to the instant of chopping. The tolerance of the steepness is characterized by a band of $\pm 0.05 \cdot T_1$ from the mean line through AB (Fig. 7.30c). The parameters of linearly rising LIC voltages are not specified in the horizontal standards, but in the relevant apparatus standards.

The evaluation of tail-chopped LIC voltages can be made with a method adapted to the k-factor calculation. For this, two records are needed, one of the tail-chopped LIC voltage from the performed test and one full reference LI voltage on lower voltage without changing the set-up of the HV test circuit (except of the switching gaps and the charging voltage of the generator) and the measuring system. The reference LI curve is used for the determination of the base curve. The recorded LIC curve is treated with that base curve similar as described above. For more details, see IEC 60060-1:2010 (Annex B.5).

The problem of over-shoot does not appear for front-chopped impulses, they can be evaluated as shown in Fig. 7.30a.

7.2.1.2 Situation and Future of the Treatment of Over-shoot

The evaluation method according to the IEC and IEEE standards as described above is an important first step into the direction of a physically correct evaluation of LI test voltages with over-shoot, but it is also a compromise between new ideas and traditional thinking. Therefore, it shall be tried to explain in the following the possible directions of the further improvement of the k-factor method. Let us consider the new evaluation method in comparison with that of IEC 60-1:1989 (Fig. 7.27):

As considered in Sect. 7.1.2.3, the inductance and capacitances in the circuit may cause oscillations which are damped by the resistive losses in the circuit. The oscillations have remarkable influence on the breakdown behaviour when they appear in the region of the peak and increase the peak value of the LI test voltage. In case of a strong damping, the oscillation is reduced to a single half-wave, which is called "over-shoot". In the following, the term "over-shoot" shall also include oscillations of lower damping.

The previous version of IEC 60-1:1989 tolerated oscillations and over-shoot up to 5 % of the smooth peak. If their frequency "is not less than 0.5 MHz or the duration of the over-shoot not more than 1 μs, a mean curve should be drawn …for the purpose of measurement". The test voltage value was the peak of the recorded curve for over-shoot frequencies $f < 0.5$ MHz; for $f > 0.5$ MHz, it is the maximum of the drawn mean curve. There was no rule how to estimate the mean curve. This abrupt change of the evaluation at 0.5 MHz (Fig. 7.27) is physically wrong, causes an error of up to 5 % at that frequency, a certain arbitrariness for the operator or for provider of evaluation software. Therefore, a change had been urgent. On the mid of the 1990s, the CIGRE-Working Group 33.03 and a related European research project started experiments on the influence of the over-shoot (e.g. Garnacho et al. 1997, 2002; Berlijn 2000; Simon 2004). A combined voltage

(see Sect. 8.1.1) of a smooth LI voltage and an oscillating short impulse were applied to insulation samples of air, SF_6, oil-impregnated paper and polyethylene. The test voltage values of test series were usually limited up to 200 kV. The experiments delivered 50 % LI breakdown voltages for the breakdown of the impulse with over-shoot (extreme value V_E), for the smooth standard impulse (peak value V_{LI}) and enabled the determination of a well-defined base curve (Eq. 7.11; maximum V_B). For each sample, the results at different over-shoot frequencies have been combined as the frequency-depending test voltage factor (test voltage function)

$$k(f) = \frac{V_{LI}(f) - V_B(f)}{V_E(f) - V_B(f)}. \tag{7.18}$$

A clear decrease in the test voltage factor with increasing frequency has been found (Fig. 7.27, measuring points), but the dispersion of the results was so large, that no clear influence of the different types of insulations has been identified. Therefore, a common k-factor curve has been evaluated (Fig. 7.27 and Eq. 7.10), which is overtaken into the standards (see Sect. 7.1.2.1).

The results of the LI parameter evaluation according to the valid IEC 60060-1:2010 differ from those according to IEC 60-1:1989. Even if the new evaluation delivers physically better results, the differences may have certain consequences for design and testing of equipment. The results of the evaluation of numerous LI voltages (e.g. of IEC 61083-2: 2013) according to the old and the new procedure (Table 7.2) show the consequences. If there is an over-shoot with $f < 0.5$ MHz, an up to 3 % higher LI test voltage would be necessary now. The front time would become shorter and the time to half-value longer. For $f > 0.5$ MHz, an up to 6 % lower LI test voltage can be applied now, the front time increases and the time to half-value decreases. These results show the tendency, but they include not only the differences in the procedures, but also the uncertainties caused by the software. Further comparisons of the old and the new method are published by Pfeffer and Tenbohlen (2009).

An unexpected result was found for the values of the over-shoot which became usually higher according to IEC 60060-1:2010 than according to the old version. The reason is the missing rule for the old "*mean curves*" which got higher maxima by the old "user-friendly" software than the well-defined "*base curves*" (Eq. 7.11) by the new software. Also the definition of the over-shoot (Eq. 7.15) is physically not correct. It does not consider the duration of the over-shoot (Hinow et al. 2010), because the extreme value V_E of the recorded curve is the reference value. An over-shoot definition which considers the duration could follow a German proposal to TC 42 when the over-shoot magnitude would be defined from the test voltage curve—as the other parameters of LI voltage, too (Hinow et al. 2010):

$$\beta^* = \frac{V_T - V_B}{V_T} \tag{7.19}$$

The comparison of the two definitions (Fig. 7.31) shows that β^* delivers always lower values than β. For an over-shoot frequency of $f < 0.5$ MHz, β^* is typically

Table 7.2 Differences of LI parameter evaluation according to IEC 60060-1:2010 and IEC 60-1:1989

Parameter	Over-shoot frequency $f < 0.5$ MHz	Over-shoot frequency $f > 0.5$ MHz
Test voltage value $(V_{2010} - V_{1989})/V_{1989}$	0…−3 %	+2 %…+6 %
Front time $(T_{1\ 2010} - T_{1\ 1989})/T_{1\ 1989}$	0…−6 %	0…+15 %
Time to half-value $(T_{2\ 2010} - T_{2\ 1989})/T_{2\ 1989}$	0…+5 %	−4 %…7 %
Over-shoot $(ß_{2010} - ß_{1989})/ß_{1989}$	Independent on the frequency −10 %…+40 %	

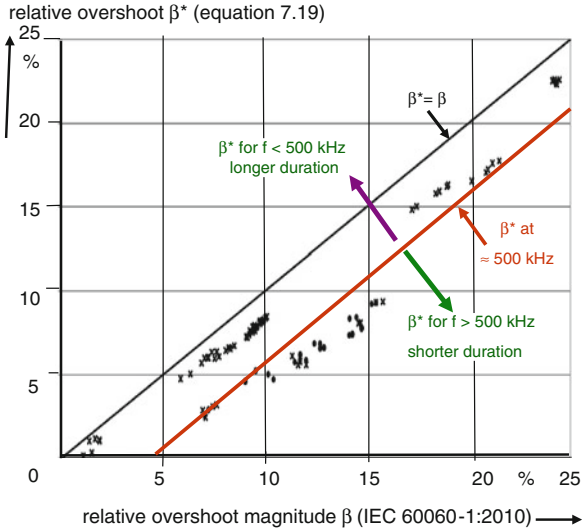

Fig. 7.31 Comparison of the over-shoot magnitudes of β (IEC definition Eq. 7.15) and ß* (Eq. 7.19)

higher than for the case $f > 0.5$ MHz. With respect to the duration of the over-shoot, this is a plausible characteristic.

A further point is the dependence on the frequency. The frequency is estimated from the duration of the over-shoot (Garnacho et al. 1997), but the breakdown process is influenced by the available time according to the well-known breakdown voltage—breakdown time characteristic (see Sect. 7.3). This characteristic can be described by a statistical time-lag followed by the formative time-lag. The latter can be described by the *formative voltage–time area* (Kind 1957) which might be also applied to the over-shoot treatment (Hauschild and Steiner 2009; Garnacho 2010; Ueta et al. 2011c). Then, the over-shoot will be characterized by

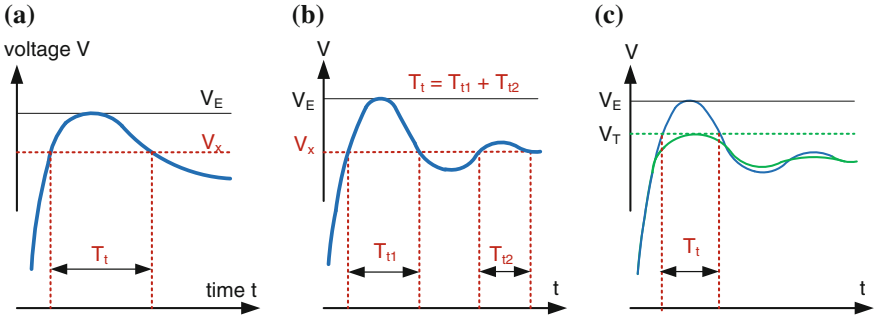

Fig. 7.32 Definition of over-shoot in conjunction with the formative time model. **a** Example for an aperiodic over-shoot using a percentage of extreme value V_E. **b** Example for oscillating over-shoot using $0.9 \cdot V_E$. **c** Example for oscillating over-shoot using the test voltage value V_T

the voltage–time area above a certain voltage value V_X (Fig. 7.32). This might be a certain percentage of the extreme value (Fig. 7.32 a, b) or the test voltage value V_T (Fig. 7.32c). Then, for example, the relative over-shoot magnitude would be calculated by:

$$\beta^{\circ} = \frac{1}{V_T \cdot T_t} \cdot \int^{T} (V_t(t) - V_T)\mathrm{d}t, \tag{7.20}$$

with the over-shoot duration: $T_t = \sum_{i=1}^{n} t_i(V_i \geq V_T)$.

A limitation of β° would mean a limitation of the formative voltage–time area which considers the really acting stress combination of voltage and time.

When an *over-shoot* definition related to the duration of the over-shoot is applied, it seems to be appropriate to apply also the test voltage function depending on the duration. The duration of an aperiodic over-shoot is related to the frequency by $T_t \approx 0.5/f$, and one can derive from Eq. (7.10), the new *test voltage function*

$$k^*(T_t) = \frac{4T_t^2/\mu s^2}{4T_t^2/\mu s^2 + 2.2}. \tag{7.21}$$

This function (Fig. 7.33) would not only improve the physical understanding. It has a linear scale with a direct relation to the time parameters of the LI voltage. The case $T_t = 0$ means no over-shoot. The determination of the duration is even simpler than that of the frequency. It would also consider the case that the oscillations are only slightly damped (Fig. 7.32b), and the second peak contributes to the formative voltage–time area. Instead of using the test voltage function of IEC 60060-1:2010 (Eq. 7.10), a different definition of the relative over-shoot magnitude can be used—e.g. as that of Eq. 7.20.

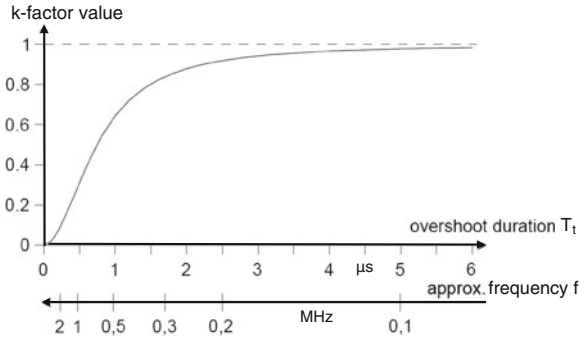

Fig. 7.33 Test voltage function depending on over-shoot duration (Eq. 7.21)

The *test voltage function* for higher voltages and different insulation samples is under investigation till now, e.g. by Garnacho (2010), Hinow with TU Cottbus (2011), Ueta et al. (2011b). The present function (Eq. 7.10) is based on experiments of small samples and voltages mainly $V_T < 200$ kV. Therefore, the breakdown is quite fast and the assumption to have a certain average characteristic seems to be not correct. It must be shifted (Fig. 7.34)—to the left (lower frequencies) for large insulation and/or relatively slow breakdown processes as for long air gaps or larger transformer insulation used for UHV transmission (Tsuboi et al. 2011, 2013; Ueta et al. 2012b) and only a bit to the right (higher frequencies) for small and compact insulation of very fast breakdown processes (SF_6; solids, vacuum, etc.), but till now, no final result of that international research work is available. It can be assumed that different characteristics will be found for different electric fields, different insulation materials and possibly even for different over-shoot magnitudes. Also the remarkable uncertainty of the determination of the test voltage function must be taken into consideration. Possibly, all available experimental results should be used to find one test voltage function for all parameter evaluation according to a future standard IEC 60060-1.

The *fitting method* for extracting the base curve as described above (Eq. 7.11) is also subject of ongoing investigation, e.g. (Satish and Gururaj 2001; Kuan and Chen 2006; Ueta et al. 2011a, b, c, d, 2012a, b; Garnacho et al. 2013). The introduction of a new evaluation method for the base curve could cause differences in the LI parameter evaluation. Contrary to the test voltage function, there seems to be no urgent need for the introduction of a new method for the determination of the mean curve. First, it must be shown that the present method is insufficient for practical cases.

Last but not least, there are many discussions to reduce the over-shoot in LI testing by the over-shoot compensation (see Sect. 7.1.2.3). A more effective (and cheaper!) way is the increase in the upper tolerance limit of the front time which is taken into account for testing UHV equipment (Gockenbach 2011; Okabe et al. 2013). It is expected that the upper tolerance limit for testing UHV equipment ($V_m > 800$ kV) will be in the order of 2.5–3.5 μs.

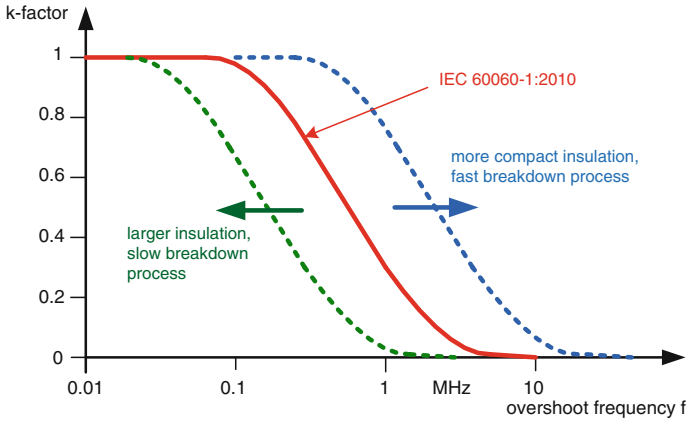

Fig. 7.34 Expected modifications of the test voltage function

7.2.1.3 Interaction Between HVLI Test System and Test Object

Most test objects—like insulators, bushings, GIS, power transformers or cable samples—provide a capacitive load for the test system. In few cases, test objects have an inductive characteristic, like the low-voltage winding of power transformers. Resistive test objects do not play any role, because outdoor insulations are not tested under wet or polluted conditions with LI voltages. The influence of the test object shall be explained by the equivalent single-stage circuit (Fig. 7.4).

Capacitive test objects: The load capacitance $C_l = C_b + C_i$ (usually consisting of the basic load C_b of the generator plus the test object capacitance C_{to}) determines the front time constant τ_f (together with the front resistor R_f, Eq. 7.2), the time constant for the tail τ_t (together with the impulse capacitor C_i and the tail resistor R_t) and the circuit efficiency factor η_c [together with the impulse capacitor C_i of the generator, Eq. (7.1)]:

$$\tau_f = R_f \left(\frac{C_i \cdot (C_b + C_{to})}{C_b + C_{to} + C_i} \right), \tag{7.22}$$

$$\tau_t \approx R_t (C_i + C_b + C_{to}), \tag{7.23}$$

$$\eta_c \approx \frac{C_i}{C_i + C_b + C_{to}}. \tag{7.24}$$

The *front time*T_1 (characterized by τ_f, Eq. 7.22) depends strongly from the test object capacitance because usually $C_i \gg C_b + C_{to}$ and consequently $\tau_f \approx R_f \cdot (C_b + C_{to})$ with often $C_{to} > C_b$. In many cases, the front time is nearly doubled when the test object capacitance is doubled. Considering that the width of the front time tolerance (0.84–1.56 μs) is less than doubling its lower limit, the front resistors R_f of a generator must be adapted accordingly. For a fixed value of

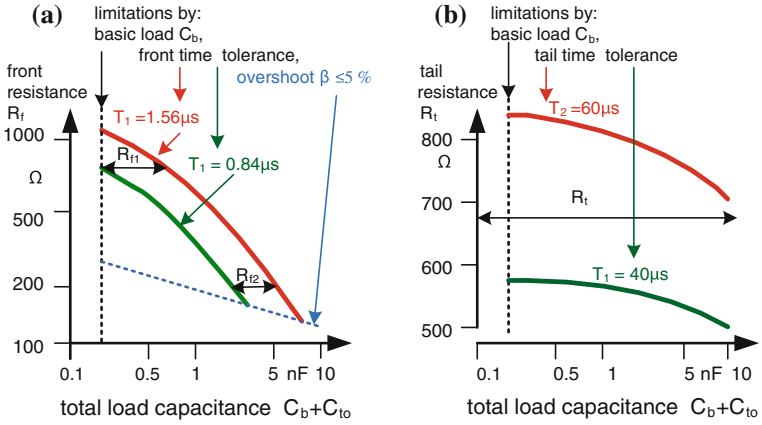

Fig. 7.35 Influence of the load capacitance on selection of front and tail resistors of a generator 2,000 kV/400 kJ of ten stages. **a** Principle of the selection of front resistance. **b** Situation of the tail resistance

τ_f—respectively, of the front time T_1—the necessary value of R_f for the upper, respectively, the lower tolerance limit of the front time can be calculated (Kind and Feser 1999) (Fig. 7.35a). A horizontal line through the resulting band corresponding to a certain range of load capacitance gives the range of load, for which one resistance R_{f1} can be applied to deliver standard LI voltages. For higher load capacitance, a lower resistance R_{f2} has to be applied and so on. If the front resistance becomes too low, an unacceptable over-shoot is generated which limits the generation of standard LI impulses. This is reached when the front resistance approaches about 100 Ω (This means 10 Ω per stage).

For the adaptation of the front resistance, each LI generator has several sets of resistors. Usually, these sets are designed in such a way that resistors can also be switched in parallel or even in series to vary the available values of front resistance by combinations for a wide range of capacitive load. For each single-resistance value, a certain load range is covered. Usually, a LI test system is equipped with three sets of front resistors enabling seven different resistance values by different parallel connections. For efficient handling of a larger LI test generator, the not-used resistors should be stored on the stages which should be easily reached by internal fixed ladders (Fig. 7.12c). Each impulse test system should be equipped with an instruction which resistors should be applied for which test object capacitance to cover a certain range of load capacitances (Fig. 7.36).

The *time to half-value*T_2 (characterized by τ_t, Eq. 7.23) is not strongly influenced by the test object capacitance because it is dominated by the impulse capacitance C_i (Fig. 5.35b). One tail resistance is sufficient to cover the whole tolerance band of the time to half-value between 40 and 60 μs.

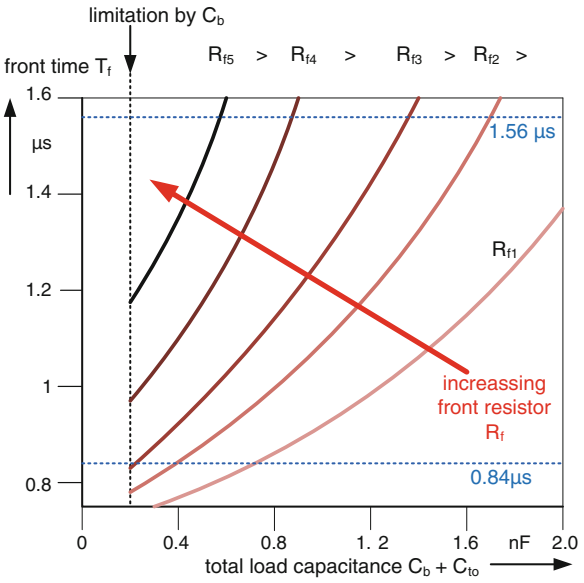

Fig. 7.36 Selection of front resistance depending on test object capacitance

The circuit *efficiency factor* can easily be estimated by Eq. 7.24. The generator with its basic load reaches usually a total efficiency factor $\eta \approx 0.95$ for $C_i \gg C_{to}$. It decreases slightly with increasing test object capacitance and values $C_{to} > 0.2\ C_i$ cannot be recommended.

An *inductive test object* combined with a capacitance is, e.g. found when the low-voltage side of a power transformer is tested (Fig. 7.37a). The inductance L_{to} forms an oscillating circuit especially with the impulse capacitance C_i and causes an impulse tail which is characterized by an oscillation instead by an exponential function. The oscillation shortens the time to half-value T_2, often outside the tolerance ($T_2 < 40\ \mu s$), an undershoot to the opposite polarity as well as a reduction of the efficiency factor (Fig. 7.37c). The influence on T_2 is especially serious and increases with decreasing impulse capacitance C_i of the generator (Fig. 7.37c). As the LI test voltages of the low-voltage side of the transformer under test are relatively low, several stages of a multi-stage generator are connected in parallel to increase C_i. If this is not sufficient, the problem can be solved by a so-called "Glanninger attachment": An inductance L_g is switched in parallel to the front resistor R_f and a resistor R_g in parallel to the test object inductance L_{to} (Fig. 7.37b). The Glanninger inductance $L_g < L_{to}$ is correctly selected when it bridges the front resistor only for lower frequency (tail of the impulse) and when the time to half-value is sufficiently extended, but the voltage is divided between $L_g//R_f$ and the test object ($L_{to}//R_g$) causing a further reduction of the efficiency factor. The "Glanninger" inductance shall be in the order of $L_g = (0.01–0.1)\ L_{to}$, and the "Glanninger" resistor is selected as $R_g \approx R_f \cdot L_{to}/L_g$. The Glanninger attachment is a separate unit switched to the parallel connected stages of the generator.

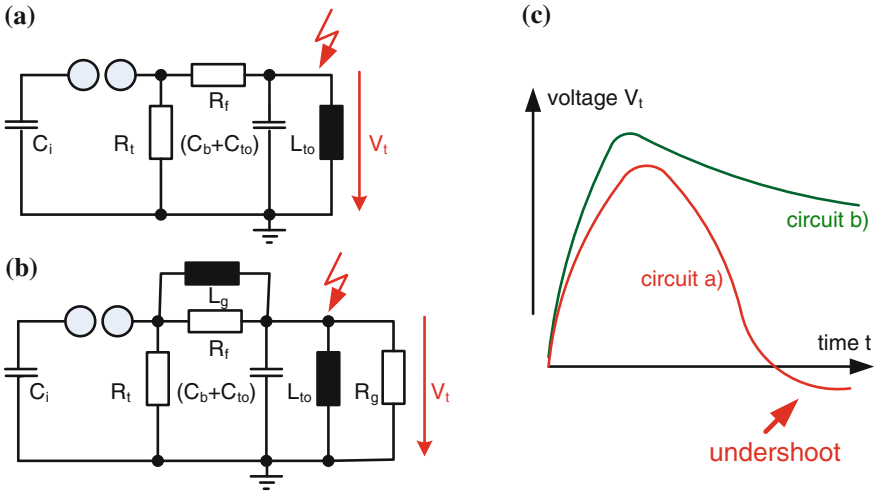

Fig. 7.37 Testing of objects with inductances. **a** Equivalent circuit. **b** Equivalent circuit with "Glanninger" attachment. **c** Comparison of the impulse shape

7.2.2 SI Test Voltages

7.2.2.1 Requirements of IEC 60060-1 and IEEE Std. 4

Over-shoot is not a problem for SI test voltages because a front resistor of quite high resistance is necessary to meet the front time parameter. The recorded curve has also a sharp beginning, the so-called "true origin", and does not require a virtual origin (Fig. 7.38). Therefore, the parameters are evaluated from the recorded curve directly. When an SI voltage fulfils the following requirements, it is a standard SI test voltage:

The *test voltage value*V_t is the maximum value of the recorded voltage curve (Fig. 5.39). In a SI voltage test, the required test voltage value must be adjusted with a tolerance of ±3 %.

The *time-to-peak*T_p is the time interval between the true origin and the maximum value of an SI voltage. It replaces the front time T_1 at LI voltages. The time-to-peak is determined also from the time of the intersection $T_{AB} = t_{90} - t_{30}$ (Fig. 7.39a) according to

$$\begin{aligned} &T_P = K \cdot T_{AB} \\ &\text{with } K = 2.42 - 3.08 \cdot 10^{-3} T_{AB} + 1.51 \cdot T_2 \\ &\text{and } T_p, T_{AB} \text{ and } T_2 \text{ are in microseconds } (\mu s). \end{aligned} \tag{7.25}$$

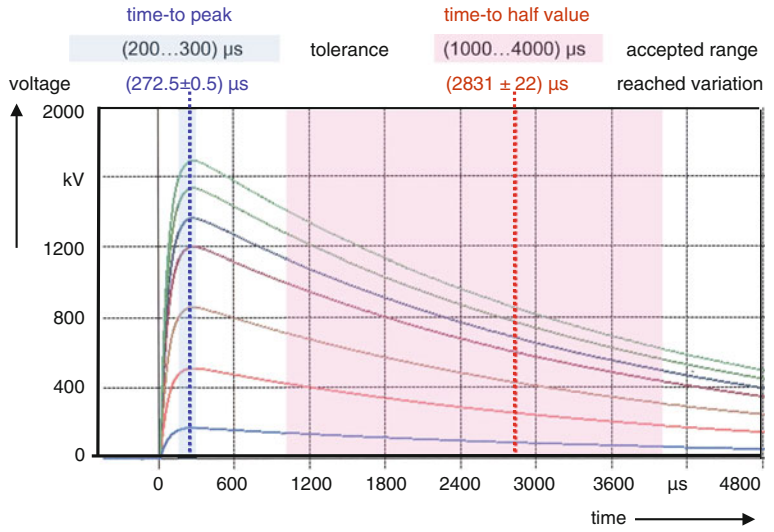

Fig. 7.38 Recorded curves of SI test voltages 250/2,500 and their reproducibility for different peak values

A standard SI test voltage requires $T_p = 250$ μs with a tolerance of ±20 %. This means the real front time has to be within (200–300) μs.

Note When SI testing was introduced in the late 1960s, the evaluation of the time-to-peak has been made according to all appearances. This principle has not been suitable for computer evaluation, and therefore, the evaluation based on the intersection has been introduced with IEC 60060-1:2010.
The definition front time—which would be in the order of $T_1 \approx 170$ μs—has not been introduced because the equivalent time-to-peak of $T_p = 250$ μs is used for decades, and for traditional reasons it should not be changed.

The *time to half-value* T_2 is a virtual parameter as the time interval between the true origin, and the instant when the voltage crosses the half of the test voltage value (Fig. 5.39a): It is required $T_2 = 2{,}500$ μs with a tolerance of ±60 %, this means the real value has to be within (1,000–4,000 μs).

Note The tremendous tolerance of T_2 is related to tests on equipment with saturation phenomena, e.g. caused by the iron cores of transformers and reactors. There the SI voltages cause a saturation of the magnetic core which leads to the immediate collapse of the voltage (Fig. 5.39b). For such tests additional parameters, the time above 90 % and the time to zero have been introduced (see below). The wide tolerance interval is acceptable because the breakdown process in air—development of leader discharges (see Fig. 7.3)—is determined by the steepness of the front of the SI voltage and very few by development of its tail.

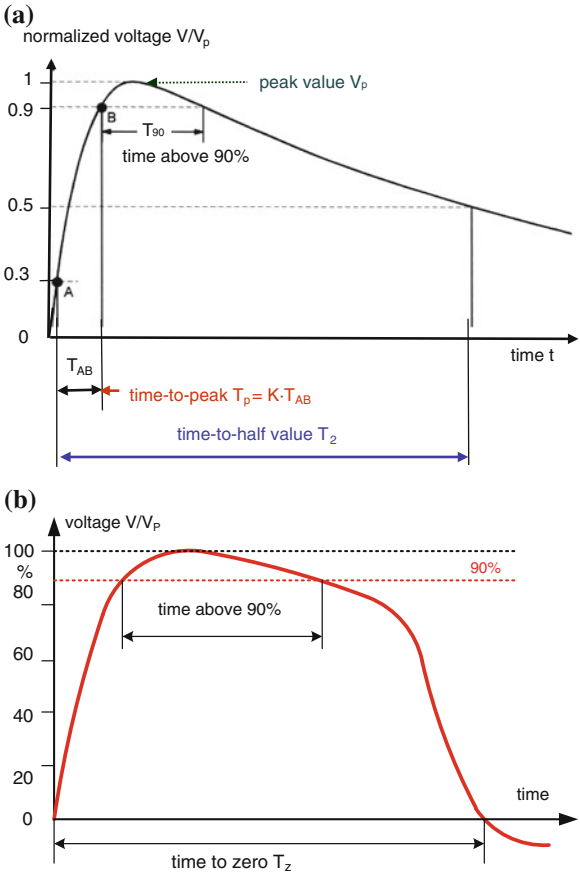

Fig. 7.39 Definitions of SI test voltages. **a** Standard impulse 250/2,500. **b** SI testing of equipment with saturation effects

The *time above* 90 %T_{90} is the interval during which the SI voltage exceeds 90 % of its maximum value (Fig. 7.39b).
The *time to* zeroT_Z is the interval between the true origin and the instant when the SI voltage has its passage through zero (Fig. 7.39b).

The parameters shall not been mixed up, because a standard SI test voltage 250/2,500 has to be characterized by the set (V_t; T_p; T_2) and for testing equipment with saturation effects the different SI set (V_t; T_p; T_{90}; T_Z) may be used.

7.2.2.2 Interaction Between HVSI Test System and Test Object

Consideration of polarity effects: Both, LI and SI voltage tests on internal insulation shall be performed at negative polarity to avoid flashovers at bushings or terminations in air. Whereas non-uniform air insulations have much lower breakdown voltages at positive polarity, there is approximately no, sometimes even a slight

opposite polarity effect for internal insulation. Also the design of the control electrodes and of the insulation structures of the HV components of an LI/SI test system is determined by the maximum positive SI voltage to be generated. Positive specific SI breakdown voltages of non-uniform fields in air can go down to the order of 1 kV/cm, whereas at LI voltage one can assume a value of 5 kV/cm.

Capacitive test objects: It has been shown in Sect. 7.1.2 that the efficiency factor can be understood as the product of the shape efficiency and the circuit efficiency (Eq. 7.1). The shape efficiency factor η_s of SI voltage is much lower than of LI voltage. The circuit efficiency factor η_c can be estimated according to Eq. 7.24 as for LI voltages. For a load capacitance $C_l = C_b + C_{to} = 0.2 \cdot C_i$, the circuit efficiency becomes $\eta c = 0.83$. With a shape efficiency of $\eta_s = 0.75$ one gets a total efficiency factor of only $\eta = 0.62$ (Eq. 7.3). The time-to-peak is less sensitive to changes of the load capacitance than the front time of LI voltage. The tolerance of the time to half-value is so large that changes of the test object do not play any role for the selection of the tail resistors. When an LI/SI test system is ordered the maximum expected test object capacitance must taken into consideration for the selection of the impulse energy per stage (Eq. 7.3).

Resistive test objects: Wet and pollution tests of external insulation are also performed at SI test voltages, especially for EHV and UHV equipment. The influence of the resistance of a polluted test object to the total front resistance of an SI generator (up to some 10 kΩ) remains negligible. But during testing heavy discharges with currents of some Amperes may cause remarkable voltage drops. This is not only a problem for wet and pollution tests, but also when long air gaps with leader discharges are investigated. As described above for AC and DC voltage, the voltage drop can be calculated when the height and duration of the current pulse are known or assumed. Impulse currents of peak values above 10 A and duration of some 10 μs have been observed (Les Renardieres Group 1977). There is not yet any standard on the acceptable voltage drop at a pre-given current impulse. In any case for the mentioned tests, an impulse generator of high impulse energy should be applied.

Inductive test objects with saturation effects: For testing power transformers, the IEC 60076-3: 2013 requires $T_p > 100$ μs; $T_{90} > 200$ μs and $T_Z > 1000$ μs. For the prolongation of the time to zero, a pre-magnetization of the core with SI voltage of opposite polarity and lower maximum value ($V_e > 0.7 \cdot V_t$) can be performed if necessary. Also after a SI voltage test, the core should be demagnetized by applying lower SI voltages of opposite polarity.

7.3 Procedures and Evaluation of LI/SI Voltage Tests

Breakdown and standardized withstand voltage tests as well as the statistical background are already described in Sect. 2.4. The following explanations are related to special LI/SI test procedures and refer to that section.

7.3.1 Breakdown Voltage Tests for Research and Development

The multiple-level method (MLM) is the most important and mainly used test method for the determination of the performance function of insulation samples (see Sect. 2.4.3 and Fig. 2.31). The performance function describes the relationship between stressing LI/SI voltages and breakdown probabilities completely. The MLM test can be easily performed on self-restoring insulation in air. The *independence* might be checked by independence tests. A procedure for that test is explained in Table 2.8. Usually the test results for air gaps are independent when the break between two LI/SI voltages is not shorter than several seconds.

For air or SF_6 insulation with surfaces to solid insulation (e.g. insulators), the check of independence is more important than for gases alone before the further evaluation of the test. If dependence is indicated, the test procedure should be modified, e.g. by longer breaks between two impulses following each other. Also the short application of a lower impulse voltage of opposite polarity or of a low AC voltage during the break may help to get independent results.

For liquid impregnated and solid insulation the MLM application requires for each LI/SI voltage stress a new test sample. This is a remarkable effort and the limited reproducibility of the test samples causes an additional contribution to the dispersion of the measured performance function. For such test objects it can be checked to apply the *progressive stress method* (PSM; Fig. 2.26c). where one sample is applied to a series of impulses until breakdown. A single test sample delivers more information in a PSM test than in a MLM test.

The statistical evaluation should be made with a powerful software package based on the maximum-likelihood method (Speck et al. 2009). This delivers (Fig. 7.40) estimations of the breakdown probabilities including confidence regions for the used seven voltage levels, point estimations of the performance function (red line in the middle), its confidence limits (blue limits) and also confidence limits of the quantiles (pink lines). Figure 7.40 shows the evaluation based on the normal (Gauss) distribution. It can be repeated for a different distribution function to find the optimum adaptation. All possible conclusions can be drawn from a diagram like Fig. 7.40.

When instead of the whole performance function, the estimation of a certain quantile (e.g. V_{50} or V_{10}) is sufficient, the *up-and-down method* can be applied (Sect. 2.4.4 and Figs. 2.38 and 2.39). Also for that test procedure a maximum-likelihood evaluation is possible and can be recommended.

7.3.2 LI/SI Quality Acceptance Tests

A passed quality acceptance LI/SI test verifies the insulation coordination (Sect. 1.2) by performing the test according to a standardized procedure, see Sect. 2.4.6 and IEC 60060-1:2010.

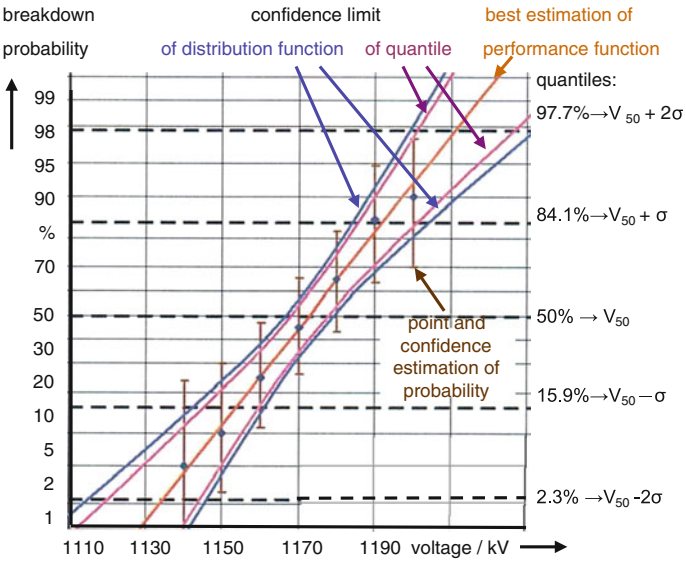

Fig. 7.40 Performance function of an air gap evaluated by the maximum-likelihood method based on a normal (Gauss) distribution

For external, self-restoring insulation (mainly of atmospheric air), two procedures are acceptable (see also 2.4.6):

A1. The LI/SI test voltage is lower than the 10 %—breakdown voltage: $V_t < V_{10}$.
A2. The LI/SI test voltage is 15-times applied and the number of breakdowns is $k \leq 2$.

For internal, non-self-restoring insulation (all solid or liquid impregnated insulation) no breakdown may occur during the quality acceptance test; therefore, the following procedure is applied:

B. The LI/SI test voltage is three times applied and no breakdown may occur ($k = 0$).

For insulation as that of a GIS consisting of a self-restoring (SF_6 gas) and a non-self-restoring (solid insulators) part, it has to be shown that the breakdown had happened in the self-restoring part. This can be indicated by a certain number of withstands at the LI/SI test voltage after the breakdown. A further indication can be a PD measurement which shows no increased PD level. The valid procedure is specified by the relevant apparatus committee of IEC or IEEE. In the following some examples for LI/SI acceptance test procedures are given:

Testing of external insulation (*IEC 60071-1*): The procedure A1 ($V_t < V_{10}$) requires the estimation of V_{10} from a performance function measured down to this low breakdown probability or for known V_{50} and standard deviation σ from

$V_{10} = V_{50} - 1.7\ \sigma$ or from an up-and-down test with seven impulses per voltage level (see Sect. 2.4.4). The procedure A2 ($n = 15/k = 2$) is applicable for all other cases when the above necessary parameters are not available and the effort for their determination is assumed to be too high. It is necessary to mention that the LI voltage tests are applied to dry insulation (see Sect. 2.1.2), whereas the SI voltage tests are applied to wet insulation (see Sect. 2.1.3).

Testing of gas-insulated substation (GIS) (IEC 62271-203:2003): The GIS insulation is characterized by a self-restoring part, the SF_6 gas, and a non-self-restoring part, the surface and the epoxy resin of the spacer insulators. The LI/SI voltage tests are combined with numerous dielectric, thermal, power and mechanical measurements and tests. The standard waveforms are applied and the procedure A2 (15/2) shall be applied. It has to be guaranteed that no breakdown or flashover occurs in the non-self-restoring part. This is considered as verified, if the last five impulses are without such a disruptive discharge. If the first breakdown appears after the impulse no. 10, the number of total impulses has to be extended accordingly. In the worst case of a breakdown at no. 15, the total number of test impulses becomes 20.

Note It is important to state that the "horizontal" IEC 60071-1:1993 requires only three impulse voltages and in case of one breakdown nine additional voltage impulses during which no disruptive discharge is tolerated. This procedure is of higher uncertainty, and therefore, it had not been considered as sufficient when the "vertical" GIS standard was established in 2003.

Testing of power transformers (IEC 60076-3/FDIS:2013): The used impulse generator shall exceed a minimum impulse energy. The standard recommends an energy $W_{i\ \min}$ (in joules) according to the empiric formula:

$$W_{i\min} > \frac{100 \cdot 2\pi f \cdot T_2^2\left(V_t^2\right) \cdot S_r}{Z \cdot V_m^2 \cdot \eta^2}, \tag{7.26}$$

with the parameters of the transformer under test:

V_m rated phase-to-phase voltage in volts;
f rated frequency in Hertz;
Z short-circuit impedance in % related to the test terminals;
S_r three-phase power rating in Volt-Amperes;

and with the test parameters:

V_t LI test voltage value in volts;
T_2 time to half-value of he LI voltage in μs;
η efficiency factor in per unit.

The LI voltage test is a routine test for power transformers $V_m > 72.5$ kV, for lower rated voltages a type test. For transformers $V_m > 170$ kV, the test includes also chopped LI voltages (LIC). An SI voltage test is a routine test for transformers $V_m > 170$ kV and for lower rated voltage a special test. The impulse shall be of

standard shape 1.2/50 within the usual tolerances. The evaluation according to the *k*-factor method is allowed, but alternatively IEC 60076-3: 2013 defines some strange differences to IEC 60060-1:2010:

As long as the over-shoot does not exceed 5 % ($\beta \leq 5$ %), the extreme value may be taken as the test voltage value. If the over-shoot exceeds 5 %, the front time might be extended up to $T_1 = 2.5$ μs and a test with chopped lightning impulses must be performed. Remains $\beta \leq 5$ % also now, the test voltage value is the extreme value. Only for rare cases, when the over-shoot $\beta > 5$ % cannot be avoided, the evaluation according to IEC 60060-1:2010 shall be applied for transformers of rated voltage ≤800 kV. For UHV transformers, even longer front times can be agreed between the parties of an acceptance test. Also the lower tolerance limit of the time to half-value can be reduced up to $T_2 = 20$ μs by agreement. The test shall be performed in the following sequence:

- one full LI reference voltage of (0.5–0.6)·V_t,
- one full LI test voltage V_t,
- two chopped (LIC) test voltages of 1.1 V_t,
- two full LI test voltages V_t .

If an SI voltage test is performed, it follows after the LI/LIC test and before the tests with AC voltages (see Sect. 3.2.5). It consists of

- one SI reference voltage (0.5–0.7) V_t and
- three SI test voltages V_t.

Both tests are successful if no internal breakdown collapses the voltage. For the LI test, additionally, the normalized voltage shapes of the reference LI voltage and of the LI test voltage, as well as the normalized shapes of the measured impulse currents (see Sect. 7.5) at the two voltage levels should be identical.

LI/SI testing of cables (IEC 62067:201): The routine test of cables does not include an LI/SI test voltage. The AC withstand test and a sensitive PD measurement are considered to be sufficient for verifying a correct production, but in defined intervals, more detailed *cable sample tests* are performed to confirm the correct production. A type test includes a long set of single tests including LI/SI tests which are performed at warm cable samples after a heating cycle voltage test, which includes 20 single cycles of one day each, and a PD measurement. First, the SI test is performed with 10 positive and 10 negative SI voltages. If no breakdown occurs, the sample has passed and can be stressed with LI voltages according to the same procedure. The PD test is repeated after the LI/SI test.

Additionally, there are *pre-qualification tests* on complete cable systems of about 100 m length with joints and terminations. The total test duration is about one year with in minimum 180 heating cycles. The LI test voltage shall be applied to the whole test assembly or to samples with a length of in minimum 30 m. The test temperature shall be in an interval between maximum conductor temperature and 5 K above. The test consists of 10 positive and 10 negative LI voltage applications again. It is passed if no breakdown occurs.

As the capacitances of the cable samples are between 0.15 and 0.3 nF/m, the test object capacitance for 30 m samples may reach 9 nF and for 100 m up to 30 nF. These are quite high capacitances, and therefore, the standard allows front times $T_1 = 1\ldots5$ μs, T_2 is within the standard values $T_2 = 40\ldots60$ μs. For SI test voltages, the usual tolerances shall be applied.

7.4 Measurement of LI and SI Test Voltages

For measuring the peak value of high impulse voltages originally, sphere gaps have been used, as already presented in Sect. 2.3.5. This direct measurement method, however, is nowadays only recommended for performance checks as well as linearity tests. Occasionally, also field probes described in Sect. 2.3.6 are applicable, particularly for measurement of fast transient voltages characterized by front times substantially below the μs range (Feser and Pfaff 1984). This subsection deals only with indirect measuring methods using a converting device and a measuring instrument both connected via a transmission system. As the design of the converting device is the most challenging task, particularly if intended for LI voltage measurements, the following treatment focuses mainly on this topic. In this context, it should be noted that more details on the fundamentals, instrumentation and procedures for LI voltage measurements can be found in a textbook of Schon published in 2010.

7.4.1 Dynamic Behaviour of Voltage Dividers

Lightning impulse voltages, particularly if chopped in the front, cover a frequency spectrum up to more than 10 MHz. To prove whether the scale factor remains constant within such a wide frequency band, the dynamic behaviour of the measuring systems applied must be known. As the transfer function is mainly governed by the voltage divider providing the converting device, only this component shall be investigated in the following. Basically, the transfer function can be determined in both the frequency and the time domain. A set-up used for the second method is sketched in Fig. 7.41.

Usually, a step voltage of several 100 V having a rise time in the order of one nanosecond is applied. The short rise time is accomplished by means of a mercury-wetted relay, often referred to as Reed relay. If switched at repetition rate around 100 Hz, disturbing background noises can effectively be rejected if the recording device is equipped with a feature for signal averaging. Due to the proximity effect, it has to be taken care that the voltage divider is arranged in agreement with real HV test conditions where neither the HV connection lead nor the measuring cable should be replaced after the performance test has been finished.

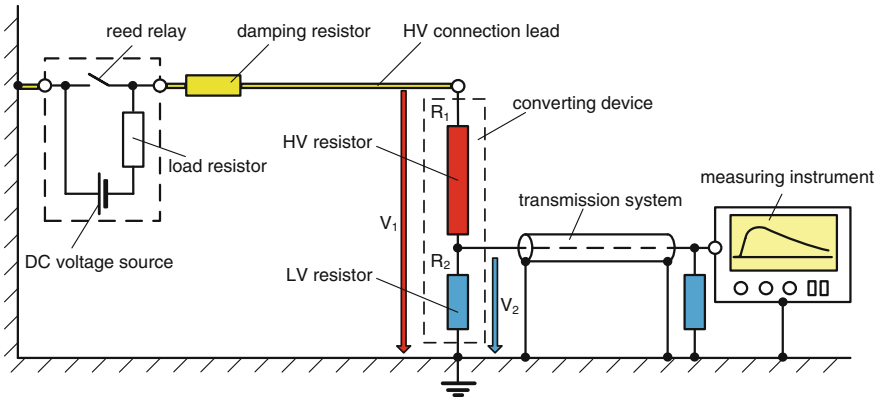

Fig. 7.41 Set-up for measuring the step voltage response of LI voltage dividers

Among others, the dynamic behaviour is mainly affected by the stray capacitances between divider column and earth as well as other grounded structures. For a better understanding, consider the equivalent circuit of a resistive voltage divider, as shown in Fig. 7.42a. Here, the HV arm is subdivided in n equal elements where the partial resistors and earth capacitance are linearly distributed:

$$R_{11} = R_{12} = \cdots = R_{1n} = R_1/n, \qquad C_{e1} = C_{e2} = \cdots = C_{\mathrm{en}} = C_e/n.$$

For such a network, the potential distribution along the HV divider column is given by a hyperbolical function equivalent to that of long transmission lines (Raske 1937; Elsner 1939; Asner 1960). In the following, it shall be assumed that the resistance R_1 providing the HV arm is much greater than the resistance R_2 providing the LV arm, which is always satisfied for HV dividers. Under this condition, the voltage v_2 (t) appearing across R_2 can be deduced from the voltage v_1 (t) applied to the top electrode using the Laplace transformation. For the network with distributed elements according to Fig. 7.42a, one gets

$$F(j\omega) = \frac{V_2(j\omega)}{V_1(j\omega)} \approx \frac{R_2}{R_1} \cdot \frac{\sin h(\gamma)}{\sin h(n \cdot \gamma)}, \tag{7.27}$$

with

$$(n \cdot \gamma)^2 = j\omega \cdot R_1 \cdot C_e. \tag{7.28}$$

To keep the measuring uncertainty as low as possible the condition, $(n \cdot \gamma)^2 \ll 1$ must be satisfied. Under this condition, Eq. 7.27 can be simplified as follows:

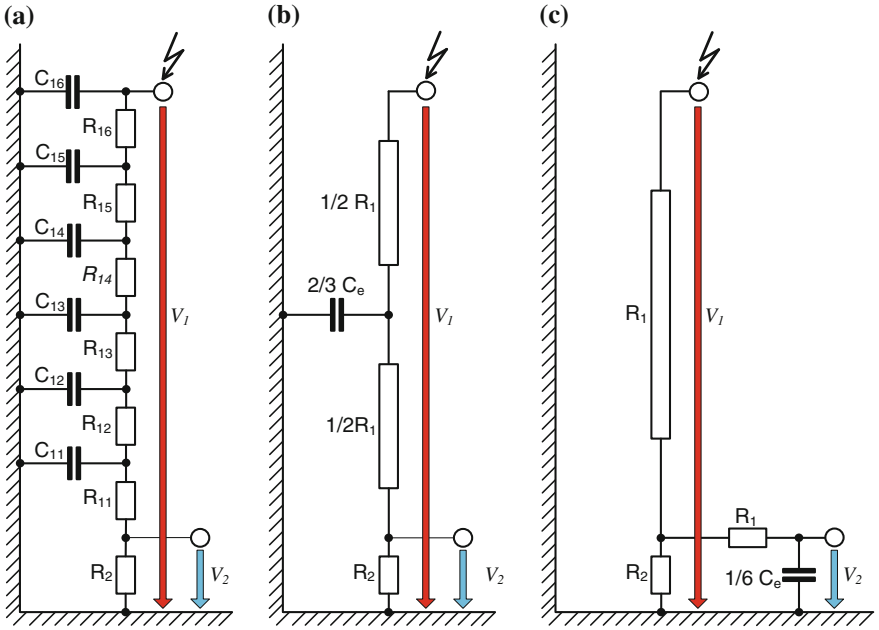

Fig. 7.42 Equivalent circuits of unshielded resistive voltage dividers. **a** Distributed capacitances (transmission line). **b** Lumped capacitance connected to the HV arm. **c** Lumped capacitance integrated in the LV arm (low-pass filter)

$$F(j\omega) \approx \frac{R_2}{R_1} \cdot \frac{1}{1 + \left[(n \cdot \gamma)^2\right]/6} = \frac{R_2}{R_1} \cdot \frac{1}{1 + [j\omega \cdot R_1 \cdot C_e]/6} = \frac{R_2}{R_1} \cdot \frac{1}{1 + j\omega \cdot \tau_f}. \tag{7.29}$$

As only the relative density of the amplitude spectrum is of interest, it can be written:

$$F_r(\omega) = \left|\frac{F(j\omega)}{F(0)}\right| = \left|\frac{F(j\omega)}{R_2/R_1}\right| = \frac{1}{\sqrt{1 + (\omega \cdot \tau_f)^2}}. \tag{7.30}$$

$$F_r(f) = \frac{1}{\sqrt{1 + (2\pi f \cdot \tau_f)^2}} = \frac{1}{\sqrt{1 + (f/f_2)^2}}. \tag{7.31}$$

This is equivalent to the transfer function of a low-pass filter of first order having an upper limit frequency of

$$f_2 = \frac{1}{2\pi \cdot \tau_f} = \frac{1}{2\pi \cdot R_1 \cdot C_e/6}. \tag{7.32}$$

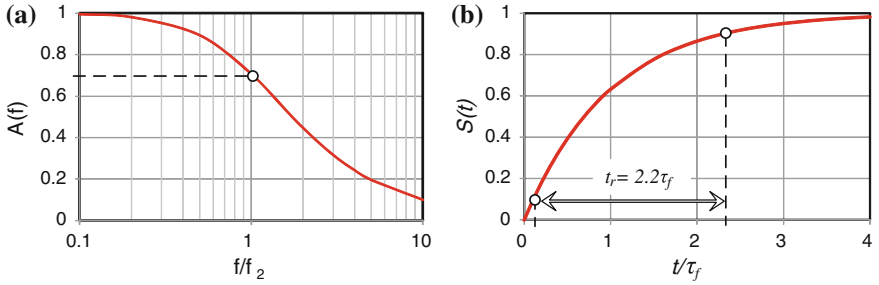

Fig. 7.43 Dynamic behaviour of a low-pass filter of first order. **a** Amplitude–frequency response. **b** Unit-step response

The network with distributed elements according to Fig. 7.42a can be replaced by a simplified equivalent circuit which contains only a single lumped capacitance, as illustrated in Fig. 7.42b. Even if this approach is commonly used in the relevant literature, it can also be substituted by the network shown in Fig. 7.42c which is more convenient to handle. Here, the series resistance R_s of the low-pass filter equals the resistance R_1 of the HV arm, and the parallel capacitance C_p amounts 1/6 of the total earth capacitance C_e of the HV divider column which can be estimated by means of the so-called antenna formula, as will be discussed more in detail below.

The relative *amplitude–frequency response* of the low-pass filter of first order according to (7.31) is plotted in Fig. 7.43a. For comparison purpose, additionally the *unit-step–impulse response* in the time domain is drawn in Fig. 7.43b, which reads

$$g(t) = 1 - \exp\left(-t/\tau_f\right). \tag{7.33}$$

Example For an LI divider with resistance $R_1 = 10$ kΩ of the HV arm and stray capacitance $C_e = 30$ pF between HV arm and ground one gets for an equivalent low-pass filter according to Fig. 7.42c, the values $R_s = R_1 = 10$ kΩ and $C_p = C_e/6 = 5$ pF, respectively. Based on this the following, values of the circuit elements can be estimated:

- Characteristic time constant $\tau_f = R_1 \cdot C_e/6 = 50$ ns
- Rise time $t_r = 2.2 \cdot \tau_f = 110$ ns
- Upper limit frequency $f_2 = 1/(2 \cdot \pi \cdot \tau_f) = 3.2$ MHz

To estimate the measuring deviation of a front-chopped LI voltage, this can be approximated by a linearly rising ramp, as illustrated in Fig. 7.44. Under this condition, the recorded voltage follows nearly the applied voltage but delayed by the time constant τ_f. Thus, at chopping time T_c, the following peak value has to be expected:

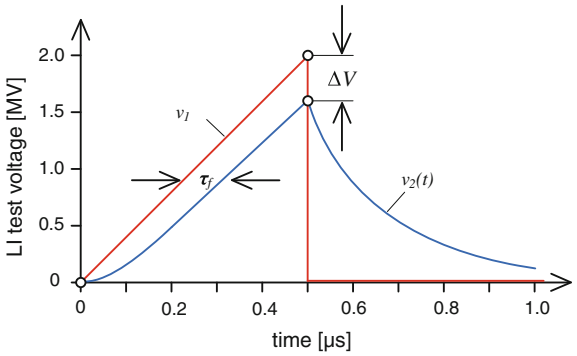

Fig. 7.44 Voltage ramp $v_1(t)$ chopped at time $T_c = 500$ ns and output signal $v_2(t)$ after passing a low-pass filter of first order characterized by the time constant τ_f

$$V_p = V_c\left(1 - \tau_f / T_c\right).$$

If the LI voltage is chopped after $T_c = 500$ ns, one gets for the above given time constant $\tau_f = 50$ ns the following relative deviation of the output voltage from the true value of applied LI test voltage:

$$\frac{V_c - V_p}{V_c} = \frac{\Delta V}{V_c} = \frac{\tau_f}{T_c} = \frac{50\,\text{ns}}{500\,\text{ns}} = 0.1 = 10\,\%.$$

In this context, it must be emphasized that under realistic condition instead of an exponential response, often an oscillating step-pulse response is encountered, as shown in Fig. 7.45. This is mainly due to the interaction between the inductance of the divider column with the earth capacitance. Thus, for comparison purposes, the area time constant τ_a has been introduced. This approach is based on the fact that the area between a unit-step and the related response function $g(t)$ of a low-pass filter according to Eq. 7.33 is direct proportional to the characteristic time constant τ_f of the low-pass filter:

$$\tau_a = \int_0^\infty \{1 - [g(t)]\}\mathrm{d}t = \tau_f. \tag{7.34}$$

The most important *unit-step response parameters* recommended in IEC 60060-2 are shown in Fig. 7.46, which are defined as:

- Experimental response time $T_N = T_\alpha - T_\beta + T_\gamma - T_\delta + T_\varepsilon$
- Partial response time T_α
- Residual response time $T_R = T_\beta - T_\gamma + T_\delta - T_\varepsilon \ldots$
- Over-shoot β_{rs}

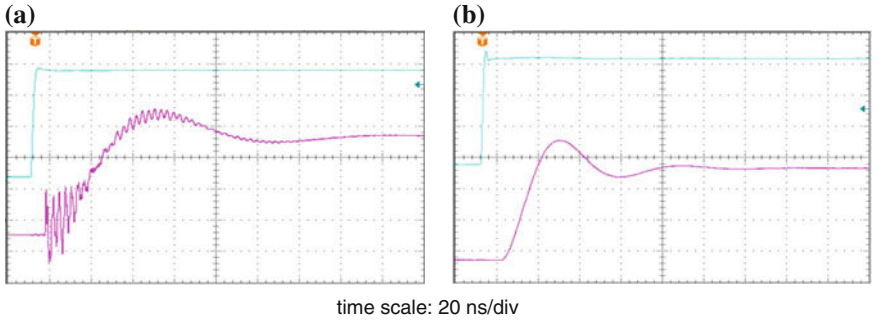

Fig. 7.45 Experimentally determined response (*red curves*) of a capacitive (**a**) and a resistive (**b**) divider subjected to a step voltage (*blue trace*)

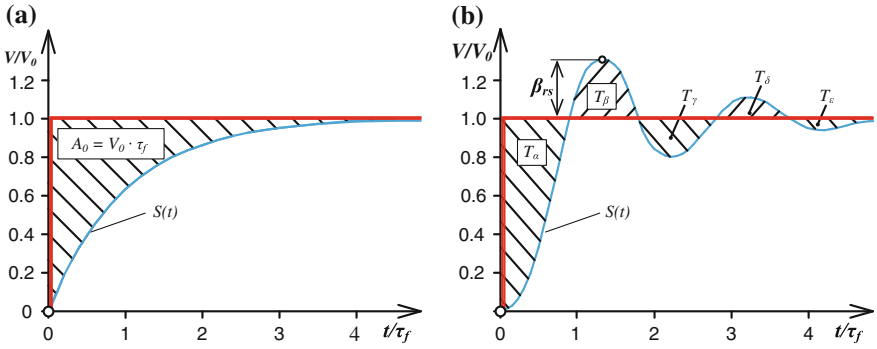

Fig. 7.46 Unit-step response parameters of voltage dividers. **a** RC circuit (low-pass filter of first order). **b** RLC circuit

In the past, it was a common practice to estimate the measuring uncertainty of voltage dividers by the convolution method, based on the characteristic unit-step response parameters. International comparative measurements revealed, however, that this method is not capable to determine the measuring uncertainty within limits specified in the relevant IEC standards. Among others, this is due to the fact that the origin of the recorded curve, denoted as O_1 in IEC 60060-2: 2000, appears more or less delayed if compared with the instant $t = 0$ when the step voltage is applied, see Fig. 7.45. This delay is governed by the travelling wave velocity which equals approx. 30 cm/ns for both the HV connection lead and the divider column, and almost 20 cm/ns for the measuring cable. Moreover, disturbing pulse distortions might appear, due to reflections at ends of the HV connection lead on one hand and, on the other hand, caused by a poor ground current return of the measuring system, as obvious from Fig. 7.45b. Consequently, the origin O_1 of the

recorded response function cannot exactly be determined and causes, thus, an erroneous determination of the response time parameters.

Despite the above-presented problems, the determination of the unit-step response parameters is widely used for the optimization of the dynamic behaviour of voltage dividers. Moreover, this method is recommended as a "finger print" for performance checks (see Sect. 2.3.2). To calibrate the *scale factor* as well as to prove the dynamic behaviour, the standard IEC 60060-2: 2000 recommends the comparision with *reference measurement systems* (*RMS*, see Sect. 2.3.3), which shall be capable to determine of the expanded measuring uncertainty within the following limits:

≤1 % for the peak values of full LI and SI voltages as well as tail-chopped LI voltages,
≤3 % for the peak value of front-chopped LI voltages,
≤5 % for the time parameters of LI and SI voltages in its range of use.

To prove the appropriate performance of a measuring system, the calibration shall be based on comparison against such a RMS. Its calibration shall be traceable to the standards of a National Metrological Institute. For this purpose, LI voltages of various front times shall be applied covering the nominal epoch range. Alternatively, the *scale factor* of the reference measuring system shall be established for one impulse voltage shape by means of a higher-class reference measuring system at the relevant test voltage level. Additionally, the measured *unit-step response parameters* of a RMS shall satisfy the recommendations summarized in the Table 7.3:

Due to the fact that the measuring uncertainty of a HV measuring system is mainly governed by the voltage divider, the above recommendations can in principle also be adopted for reference voltage dividers alone to be approved by a National Metrology Institute or by a Calibration Laboratory accredited by the National Institute of Metrology.

7.4.2 Design of Voltage Dividers

For measuring high voltages, resistive, capacitive or often mixed voltage dividers are applicable, see Fig. 2.10. The design of LI voltage dividers is the most challenging task. Thus, the following treatment deals mainly with this topic. Generally, it has to be taken into account that the divider should always be arranged "after" the test object, as illustrated in Fig. 7.47 and never "between" test voltage generator and test object. The current through the test object causes a voltage drop across the impedance of the HV connection lead, so that the measured voltage could become higher than the voltage applied to the test object.

Table 7.3 Response parameters recommended for LI and SI voltage reference measuring systems

Parameter	Full and tail-chopped LI voltages (ns)	Front-chopped LI voltages (ns)	SI voltages (μs)
Experimental response time T_N	≤15	≤10	
Partial response time T_α	≤30	≤20	
Settling time t_s	≤200	≤150	≤10

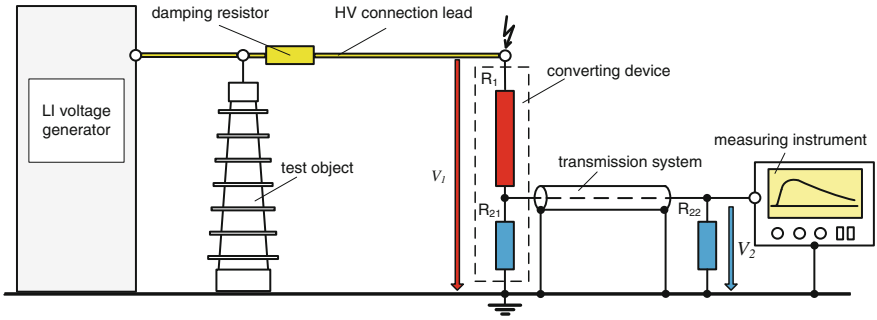

Fig. 7.47 Arrangement of a measuring system for LI test voltages

7.4.2.1 Resistive Voltage Dividers

For measuring high transient voltages in the μs range and below, resistive dividers are in use since the beginning of the last century (Binder 1914; Peek 1915; Grünewald 1921; Marx 1926; Bellaschi 1933; Burawoy 1936; Finkelmann 1936; Hagenguth 1937; Raske 1937; Elsner 1939). As discussed in the previous section, the dynamic behaviour and thus the measuring uncertainty of such dividers are mainly governed by the stray capacitance C_e between the divider column and the earth. This can roughly be assessed using the so-called antenna formula (Küpfmüller 1990). Replacing the divider column by a vertical metallic cylinder rod of high h and diameter d with $d \ll h$, the following approach is applicable:

$$C_e \approx \frac{2\pi \cdot \varepsilon_0 \cdot h}{\ln(h/d)} \approx 24(pF/m)\frac{h}{\ln(h/d)}. \tag{7.35}$$

Example Consider a 2 MV divider where the resistance providing the HV arm is $R_1 = 10$ kΩ. For a divider column of high $h = 5$ m and diameter of $d = 0.1$ m, one gets from Eq. 7.35 for the earth capacitance $C_e \approx 30$ pF. Applying the equivalent circuit according to Fig. 7.42c, the time constant of the low-pass filter would be $\tau_f = R_1 \cdot C_e/6 \approx 50$ ns. Measuring a front-chopped LI voltage with $T_c = 0.5$ μs, the voltage appearing across the LV arm of the here-considered divider at chopping time T_c would be 10 % lower if compared with that voltage magnitude measured with an "ideal" divider, as

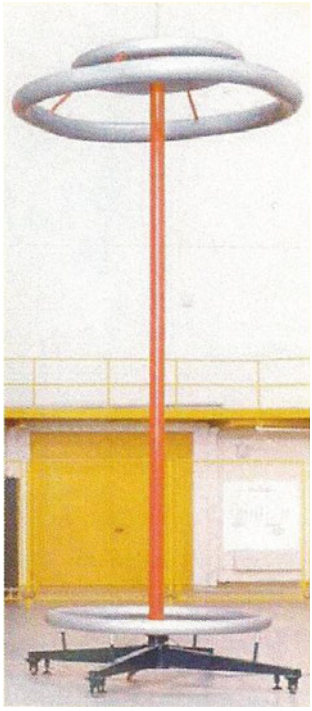

Fig. 7.48 Photograph of a shielded resistive 2.2-MV LI voltage divider (Courtesy of TU Dresden)

already discussed in the previous section. In conclusion: The here-considered voltage divider is not capable to measure chopped and full LI voltages at the measuring uncertainty specified in IEC 60060-2.

A photograph of a resistive divider having almost the equal parameters investigated in the above example is shown in Fig. 7.48. Despite of the comparatively high resistance of the high-voltage arm of 10 kΩ, an experimental response time close to 15 ns was determined, which is only 30 % of the value calculated above. Among others, this is achieved by reducing the impact of the earth capacitance using a "shielding" electrode as originally introduced by Davis in 1928 and Bellaschi in 1933. Under this condition, the partial currents I_{e1}, I_{e2} … and I_{e6} between divider column and earth are more or less compensated by the partial currents I_{h1}, I_{h2} … and I_{h6} between HV electrode and divider column, as illustrated in Fig. 7.49.

Additionally, the field grading along the divider column was optimized, as qualitatively shown in Fig. 7.50. This is obtained by varying the pitch of the wire wounded around an insulating core such that the field distribution approaches the electrostatic field between the electrodes in absence of the divider column,

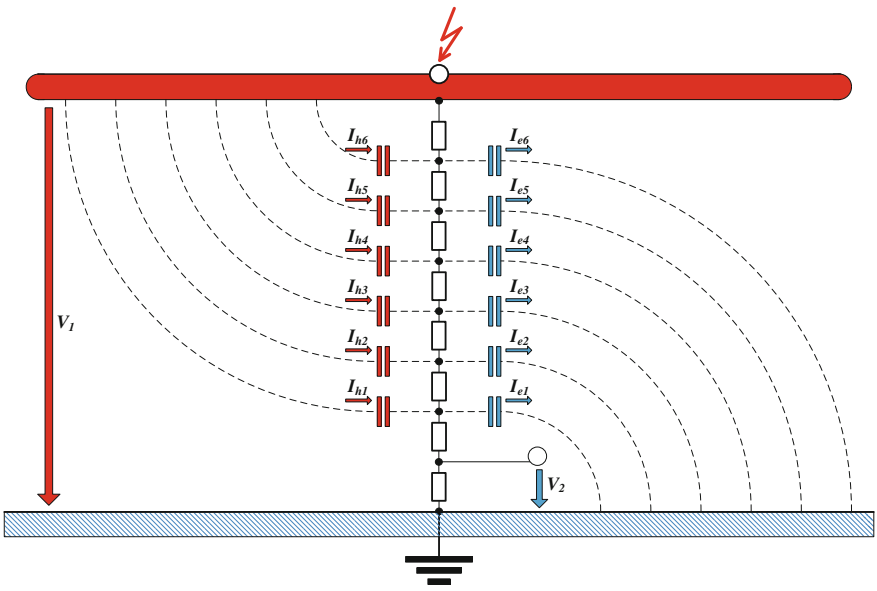

Fig. 7.49 Principle of the compensation of the partial currents between divider column and earth by the currents between HV electrode and divider column

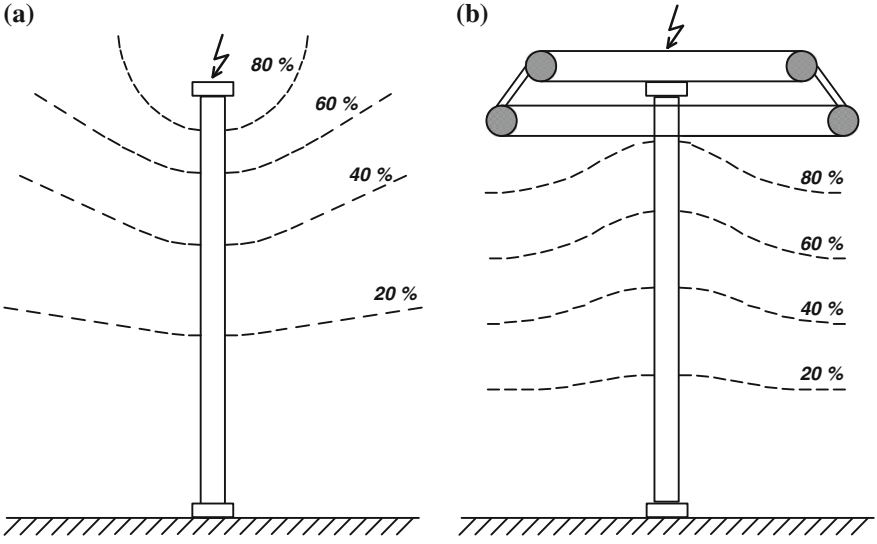

Fig. 7.50 Distribution of equipotential lines along the HV column of resistive LI voltage dividers. **a** Without field grading. **b** With field grading using a large shielding electrode

originally proposed by Goosens and Provoost in (1946). Moreover, the inductance of the resistor providing the HV arm was minimized using bifilar windings where each is wounded in opposite direction around a cylindrical core and insulated by a thin dielectric layer (Spiegelberg 1966). Another option for minimizing the inductance of the HV arm is the application of a meander-like designed HV resistor (Mahdjuri-Sabet 1977), commonly referred to as Schniewind-Band.

Basically, it can be stated that shielded resistive dividers having a resistance in the order of 10 kΩ are applicable only for measuring full LI voltages up to approx. 2 MV to accomplish the requirements according to IEC 60060-2: 2010. For higher voltages, excessively large shielding electrodes are required, which are expensive and reduce the mechanical stability of the tall divider column. The decrease in the earth capacitance by very carefully adapted shielding and potential grading is also limited because the clearance to grounded and energized structures must be as large as possible to avoid any disturbances of the optimized field grading. In principle, the dynamic behaviour could be improved by reducing the resistance of the HV arm substantially below 10 kΩ. However, this would decrease the output voltage as well as the tail time of the LI generator. Moreover, it has to be taken into account that the power dissipation and thus the temperature of the divider column increase with the square of the applied voltage. This is the main reason that pure resistive voltage dividers of experimental response time less than 10 ns, which require a resistance of the HV arm of only few kΩ, are not capable of measuring LI voltages above 500 kV.

7.4.2.2 Damped Capacitive Dividers

To overcome the above-mentioned drawbacks of pure resistive voltage dividers, it seems reasonable to use capacitive dividers as an alternative. This is because neither the output voltage of the LI generator nor the pulse duration is reduced at capacitive load. Moreover, the divider column will never be heated up even if voltages up to several MV are applied. The main disadvantage of capacitive dividers is, however, that fast transient voltages might excite heavy oscillations, as obvious from Fig. 7.51a.

This is due to the fact that the capacitive divider acts in the high-frequency range similar to a short circuit. Thus, the resulting impedance is governed by the inductance of a metallic cylinder having the length of the HV divider column, which interacts with the earth capacitances. To overcome this drawback, the HV arm should be composed of stacked capacitors connected via serial resistors, as proposed by Zaengl in 1964 and Spiegelberg in 1964. The main advantage of this approach is not only that the disturbing oscillations are effectively damped but also that the response time constant is not increased, as obvious from Fig. 7.51b, which is in contrast to the transfer characteristics of a classical RC low-pass filter where the time constant is proportional to the resistance.

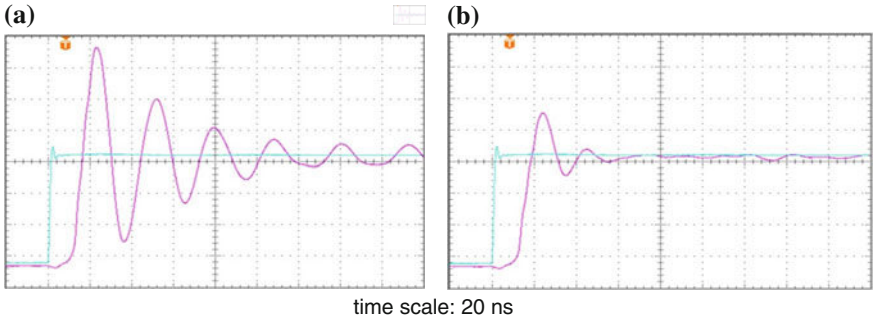

Fig. 7.51 Step-pulse response of a capacitive divider without and with a damping resistor

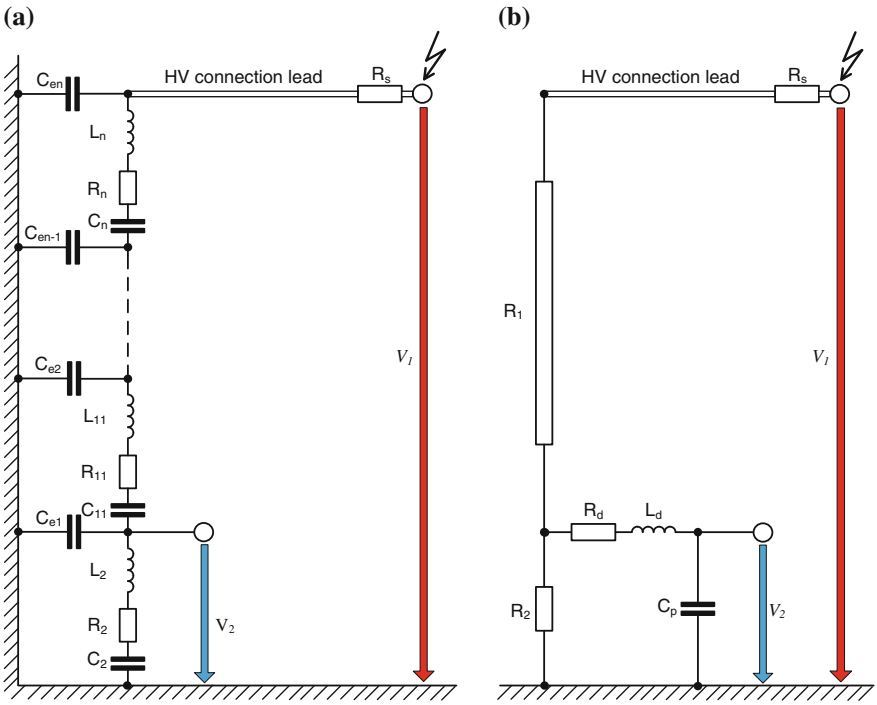

Fig. 7.52 Equivalent circuit of a damped capacitive divider. **a** Damped C-divider with distributed elements. **b** Ideal R-divider connected to a RLC network

To estimate the optimum value required for the damping resistor, the equivalent circuit shown in Fig. 7.52b shall be analysed. This network can be deduced from the circuit with distributed elements shown in Fig. 7.52a, introducing the simplifications which have been adopted for the resistive divider, as presented in the

foregoing subsection. As the series capacitances can be considered short-circuited in the higher-frequency range, only the following circuit elements have to be considered:

$$R_d = R_{11} + R_{12} + \cdots + R_{1n} = n \cdot R_{11},$$
$$L_d = L_{11} + L_{12} + \cdots + L_{1n} = n \cdot L_{11},$$
$$C_p = C_e/6.$$

To estimate the effective inductance $L_d = n \cdot L_{11}$ of the HV arm, the HV divider column shall be replaced by a metallic cylinder of high h and diameter d, so that the following simplified approximation can be adopted (Küpfmüller 1990):

$$L_d \approx \frac{\mu_0 \cdot [\ln(h/d)] \cdot h}{2\pi}. \tag{7.36}$$

Multiplying this term with the earth capacitance C_e given by Eq. (7.35), one gets the following expression which applies for rod antennas in the higher-frequency range (Küpfmüller 1990):

$$C_e \cdot L_d = \frac{2\pi \cdot \varepsilon_0 \cdot h}{\ln(h/d)} \cdot \frac{\mu_0 \cdot [\ln(h/d)] \cdot h}{2\pi} = h^2 \cdot \varepsilon_0 \cdot \mu_0 \tag{7.37}$$

From the classical network theory, it is known that the condition for the transition from an oscillating response to a monotonic one is accomplished if the damping resistor of the RLC circuit according to Fig. 7.52b becomes

$$R_d > 2\sqrt{\frac{L_d}{C_p}}. \tag{7.38}$$

Inserting $C_p = C_e/6$, where C_e is given by Eq. (7.35), one gets:

$$R_d > \frac{\sqrt{24 \cdot L_d \cdot C_e}}{C_e} = \frac{h \cdot \sqrt{24 \cdot \mu_0}}{C_e} = [\ln(h/d)] \cdot \frac{\sqrt{24}}{2\pi} \cdot \sqrt{\frac{\mu_0}{\varepsilon_0}} \approx [\ln(h/d)] \cdot 0.8 \cdot Z_0. \tag{7.39}$$

Inserting the wave impedance $Z_0 = \sqrt{\mu_0/\varepsilon_0} \approx 377\Omega$, it can also be written:

$$R_d > [\ln(h/d)] \cdot (290\Omega). \tag{7.40}$$

This simple approach is well confirmed by practical experiences although it is based on a rough approximation. In this context, it has to be taken into consideration that additionally to the "internal" damping resistor given by Eq. (7.40), also an "external" resistor in the order of 300 Ω is required at the input of the HV connection lead to avoid disturbing travelling wave phenomena.

Example Consider a 2-MV divider which is composed of five stacked capacitors, where the total divider column shall be 5 m in high and 0.25 m in diameter. Under this condition, one gets $R_d > [\ln(20)] \cdot (290\Omega) \approx 870\Omega$, so that a HV resistor in the order of 220 Ω

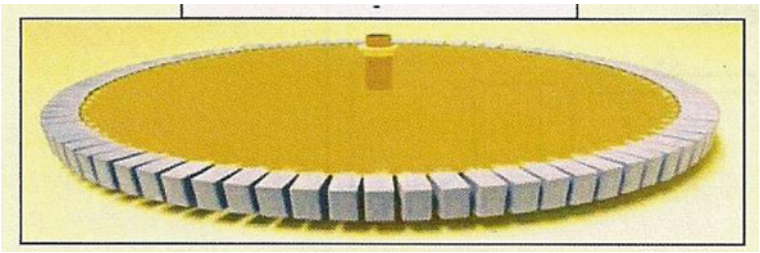

Fig. 7.53 LV arm of a damped capacitive divider comprising 60 parallel elements each composed of a resistor connected in series with a capacitor

should be connected between each HV capacitor. Using an additional external HV resistor of 300 Ω, the total resistance of the HV arm becomes 1,170 Ω which has to be taken into account for choosing the resistance of the LV arm.

In this context, it should be emphasized that the design of the LV arm of a damped capacitive divider is also a challenge. This is because the ratio between the inductances of the HV and LV arm must be equal to the divider ratio which is equal to the resistor ratio and inversely proportional to the capacitance ratio:

$$L_2/L_1 = R_2/R_1 = C_1/C_2.$$

Example Applying Eq. (7.36) the effective inductance of the HV arm of the above-considered divider having a height of $h = 5$ m and a diameter $d = 0.25$ m, one gets $L_1 = (1.257 \cdot 5/2\ \pi) \cdot \ln(5/0.25)\ \mu\text{H} \approx 3\ \mu\text{H}$. Assuming a divider ratio of, for instance, $R_2/R_1 = C_1/C_2 = 1/1000$, the inductance L_2 of the LV arm should be as low as 3 nH, which can only be achieved by disc-shaped elements.

The most effective way to minimize the inductance of the LV arm is the parallel connection of a great number of elements forming a disc as obvious from Fig. 7.53, where each element is composed of a capacitor connected in series with a resistor.

Comparing the different divider types, it can be stated that damped capacitive dividers provide a very good dynamic behaviour. Another benefit is that power dissipating in the resistors inserted between the stacked capacitors is quite low as only transient currents of short duration appear, so that the rated voltage is not limited. Moreover, the effective capacitance of the HV arm provides a basic load for the LI generator. As the charging current is inversely proportional to the frequency, damped capacitive dividers are also well capable for measuring SI and AC voltages as well as for composite voltages. If equipped with a high-ohmic resistor connected in parallel to the HV arm, such a "universal" divider shown in Fig. 2.10 is also capable of measuring DC voltages including superimposed voltage ripples covering a frequency spectrum of several kHz. Due to the wide

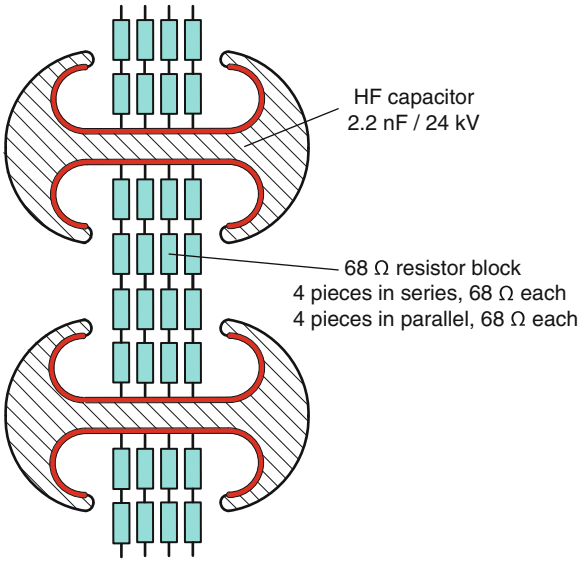

Fig. 7.54 Section of a damped capacitive divider, rated voltage 200 kV

field of application, the damped capacitive divider is often referred to as "*multi-purpose divider*".

Due to the above-presented benefits, most reference measuring systems (RMS) are equipped with damped capacitive dividers. To keep the inductance and temperature coefficient of the HV arm as low as possible, also disc-shaped ceramic HF capacitors are employed. Such elements are available for rated voltages up to approx. 25 kV and a nominal capacitance in the order of 2 nF. As an example for a RMS of LIC voltages, Fig. 7.54 shows a section of the HV arm of a damped capacitive divider, designed for a maximum LI voltage of 200 kV using a series connection of ten ceramic HF capacitors (each 2.2 nF and 24 kV rated voltage). Response time measurements revealed that an optimum dynamic behaviour is achieved for a series resistance of 680 Ω. Thus, in total, nine resistor blocks were inserted between the stacked capacitors, and one resistor block served as damping resistor at the HV side. Each resistor block was composed of 16 low-inductive metal-oxide resistors, four of them connected in series and four of them connected in parallel, see Fig. 7.54. For the complete 200 kV LI divider, the following response parameters were determined experimentally (compare Table 7.3):

Experimental response time: $T_N \approx 2$ ns
Partial response time: $T_\alpha \approx 5$ ns
Settling time: $t_s \approx 120$ ns

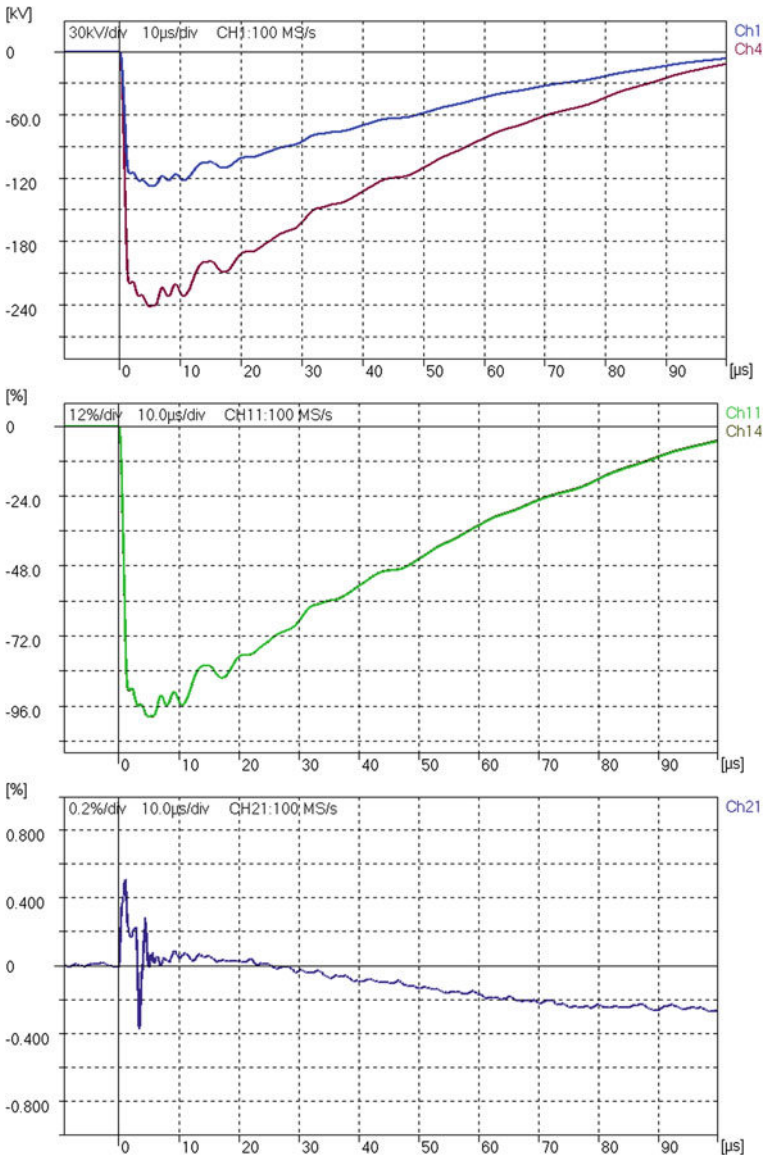

Fig. 7.55 Recording and processing of LI test voltages (From the top: records of 50 and 100 % test voltages; comparison of the normalized voltages; difference of the normalized voltages)

7.4.3 Digital Recorders

To measure fast transient signals in high-voltage technology, such as travelling wave phenomena on transmission lines due to lightning surges as well as LI test voltages

Fig. 7.56 Photograph of a stand-alone digital recorder

originally *cathode-ray oscilloscopes* (*CRO*) have been employed (Binder1914; Gabor 1927; Krug 1927). At that time, the electromagnetic capability (EMC) was not a problem because the available CRO were designed for HV measurements and thus not equipped with sensitive amplifiers for vertical and horizontal deflection. In the 1940s, additionally, peak voltmeters have been employed, commonly designed by the HV laboratory personnel itself using vacuum tubes for rectifying the fast LI signal. Digital recorders, originally referred to as "digitizers", entered in HV measuring technique in the early 1980s (Malewski et al. 1982). After the initial EMC problems have successfully been solved (Strauss 1983 and 2003; Steiner 2011); digital recorders are nowadays exclusively used for recording and processing LI and SI test voltages (Fig. 7.55). Due to the recent achievements in digital signal processing (DSP), computerized digital recorders are also increasingly employed not only for LI and SI test voltage measurements but also for AC and DC voltage measurements as well as for measuring composite and combined test voltages.

A photograph of a stand-alone device operating in connection with an IPC is shown in Fig. 7.56, and a simplified block diagram of a digital recorder is shown in Fig. 7.57. The main units are the voltage attenuator at the input followed by a low-noise amplifier, an analogue–digital converter, a memory unit and an industrial computer. A micro-controller serves for the adjustment of the input sensitivity as well as for controlling the various units for signal processing, acquisition and data storage. The industrial computer runs with a specific software package capable for both the acquisition of the stored raw data and the visualization of the time-dependent input signal. Simultaneously, the relevant impulse parameters are

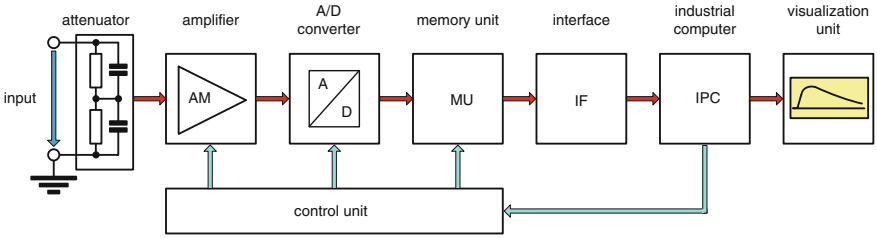

Fig. 7.57 Simplified block diagram of a digital recorder for HV measurements

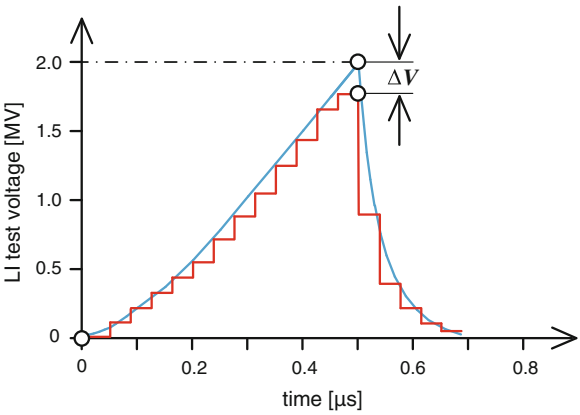

Fig. 7.58 Quantization error of a front-chopped LI test voltage due to the analogue–digital conversion

indicated, such as the peak value of the measured LI/SI test voltage, the front and tail time and occasionally the chopping time.

Basically, the measuring uncertainty is affected by both the hardware and the software. Due to the comparatively high quantization rate of nowadays available digital recorders, which is usually 14 bits and even more, as well as the high sampling rate of 100 MS/s and above, the contribution of the hardware to the measuring uncertainty is much lower than that of voltage dividers. As the quantization error is given by 50 % of the *least significant bit* (LSB), this is approx. 0.012 % for a slow-rising signal for a quantization rate of 14 bit. However, the deviation from the true value becomes much higher if a front-chopped LI voltage according to Fig. 7.58 is measured using a sample rate of 100 MS/s. This is because the voltage difference ΔV_s between each sample is inversely proportional to the sampling rate f_s. For an assumed chopping time $T_c = 0.5$ μs and crest voltage V_c, the voltage difference between each sample can be approximated by $V_s = V_c/(T_c \cdot f_s) = V_c/50 = 0.02 \cdot V_c$. Thus, the maximum deviation of the measured value from the true value, which is given by 0.5 LSB, becomes 1 % of the crest value V_c. Generally, it has to be taken care that the classical *Shannon theorem* is accomplished, i.e. the sampling rate should exceed twice the maximum frequency content of the signal to be measured where the analogue bandwidth

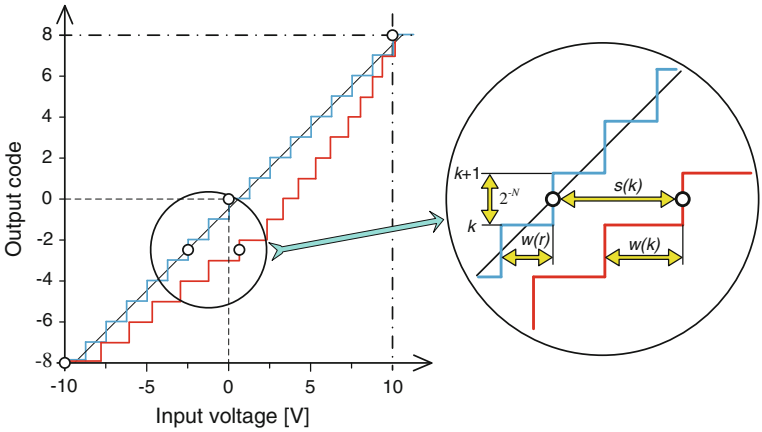

Fig. 7.59 Estimation of the differential non-linearity given by $w(k) - w(r)$ and integral non-linearity $s(k)$ given by the deviation of the actual input voltage from the reference voltage of an "ideal" ADC

must always be greater than the sampling rate (Shannon 1949; Stanley 1975; Robinson and Silvia 1978).

To validate the measuring uncertainty, various calibration procedures are recommended in IEC 61083-1: 2001 which refer to both the hardware and the software. To validate the uncertainty caused by the hardware, the *differential non-linearity* (*DNL*) as well as the *integral non-linearity* (*INL*) have to be determined using an "ideal" ADC as reference. The transfer function of such a reference ADC is characterized by a stepwise-increasing output code $k = 1, 2 \ldots 2^N$, if the input voltage is increased stepwise by $w(r) = V_{\text{fsd}}/2^N$. That means, for an output code, $k = 2^N \cdot V_{in}/V_{\text{fsd}}$, one gets for the next step $k + 1 = 2^N \cdot (V_{in} + w(r))/V_{\text{fsd}}$. Here are V_{in}—the input voltage, V_{fsd}—the full-scale deflection voltage and N—the resolution in terms of bit.

According to Fig. 7.59, the DNL is given by the difference $w(k) - w(r)$ for each possible value of the output code k, and the IDL presents the difference $s(k)$ between the input voltage of both the investigated ADC and the reference ADC. As the determination of the DNL and IDL at stepwise increasing DC voltage is extremely time-consuming, particularly for ADCs of more than 8 bit resolution, the experimental results might strongly be affected by the long-term stability of the DC voltage source.

As an alternative, thus the following method has been proposed by Steiner in 2011, see Fig. 7.60:

1. Apply a precise sine wave of low frequency (e.g. 50 Hz) and adjust the amplitude close to the full-scale deflection (e.g. between −10 V and +10 V).
2. Record in total ten periods of the applied AC voltage.
3. Compare the count of occurrences of each code (code rate) with the ideal number of occurrences.

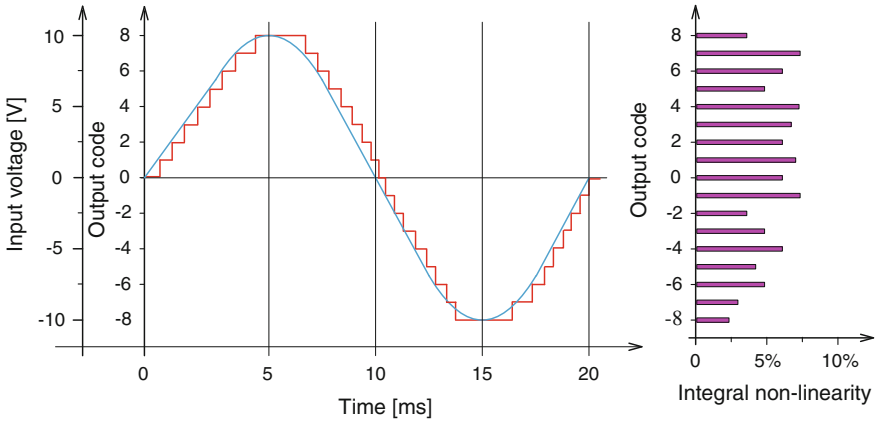

Fig. 7.60 Comparison of a sin-shape input voltage with the output code of a non-linear 4-bit ADC

4. Divide each code rate by the number of recorded periods, i.e. $n = 10$ for the here-considered case.
5. Calculate the differential non-linearity (DNL) for each code:

$$d(k) = \frac{h(k)_{\text{nonlin}}}{h(k)_{\text{lin}}} - 1.$$

6. Calculate the integral non-linearity (INL) for each code:

$$s(k) = \sum_{i=0}^{k} d(i).$$

The test is passed if $d(k) = 10.81\%$ code bin width $s(k) = 10.51\%$ of full-scale deflection is satisfied.

The software package is tested according to IEC 61083-2: 2013. It recommends new rules for the calibration including the calculation of the k-factor relevant for LI test voltages of substantial over-shoot. To verify the performance of digital recorders intended for LI voltage measurements, in total 52 reference curves are recommended to be created by a computerized test data generator (TDG). These artificial curve shapes are available from either a compact disc (CD) or even an USB stick. Basically, the reference impulse wave-shapes applied should be representative for the test voltage shapes specified in IEC 60060-1: 2010 and IEC 60060-3: 2006, such as:

- Full lightning impulse voltage (LI)
- Front-chopped lightning impulse voltage (LIC)
- Tail-chopped lightning impulse voltage (LIC)
- Oscillating lightning impulse voltage (OLI)
- Switching impulse voltage (SI)
- Oscillating switching impulse voltages (OSI).

After digital signal processing of the data received from the TDG, the significant impulse parameters are determined by means of the implemented software. The procedures shall follow the evaluation principles given in IEC 60060-1:2010. These refer to the measurement of the peak value and the over-shoot as well as to the characteristic time parameters, such as the front and tail time and the chopping time for CLI, as well. The software is assumed as properly working if the results obtained are within a tolerance band specified in IEC 61083-2: 2013, where any manipulation of the test data should be prevented.

Example Table 7.4 shows the comparison between the evaluated parameters of two reference LI waveshapes (waveshapes no. LI-A4 and LI-M7 of the test data generator (TDG)) and those required according to IEC 61083-2:2013. Whereas the evaluation of no. LI-A4 delivers results within the tolerances required by the standard, not all parameters of no. LI-M7 are correctly determined. This means the software has to be improved before it can be applied for practical tests.

Generally, it can be stated that the measurement of the peak voltage of full LI test voltages at measuring uncertainty of 2 % is accomplished if the amplitude resolution amounts 10 bits and the sampling rate is 100 MS/s, where the analogue bandwidth should not be lower than 100 MHz. Moreover, the integral non-linearity should be below 0.5 %, and the internal background noise level should not exceed ±0.4 % of the full-scale deflection. For more information in this respect, see Hällström (2002); Hällström et al. (2003), Wakimoto et al. (2007) and Schon (2010).

7.5 Measurement of High Currents in LI Voltage Tests

Performing LI voltage tests, high *impulse currents* may appear not only as consequence of a breakdown of the test object but also in case of withstand. This is because the current is correlated with the frequency content of LI voltages and the capacitance of the test object. Thus, the magnitude and shape of LI currents might be used as an indication of the insulation condition of the test object. For this reason, the *impulse current measurement* is mandatory for LI withstand tests of power transformers where first a reference voltage level of 50–70 % is applied, followed by the 100 % value of the specified LI test voltage, see Fig. 7.61. To compare the voltage and current shapes, the records are normalized to their

Table 7.4 Test of software with the test data generator (TDG) according to IEC 61083-2:2013

Reference in IEC 61083-2	Parameter	Reference value	Acceptance limits	Example: evaluated values	Remarks
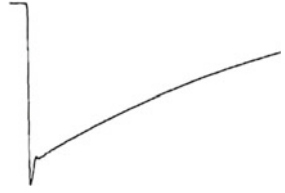 LI – A4	Test voltage value V_t	−856.01 kV	−(855.15…856.87) kV	−856.4 kV	Evaluation accepted
	Front time T_1	0.841 µs	(0.824…0.858) µs	0.851 µs	Evaluation accepted
	Time to half-value T_2	47. 80 µs	(47.32…48.28) µs	47.88 µs	Evaluation accepted
	Relative over-shoot β	7.9 %	(6.9…8.9) %	7.2 %	Evaluation accepted
 LI – M7	Test voltage value V_t	1272.3 kV	(1271.0…1273.5) kV	1272 kV	Evaluation accepted
	Front time T_1	1.482 µs	(1.452…1.512) µs	1.390 µs	Evaluation rejected*
	Time to half-value T_2	50.03 µs	(49.53…50.53) µs	5 0.10 µs	Evaluation accepted
	Relative over-shoot β	11.2 %	(10.2…12.2) %	9.9 %	Evaluation rejected*

*The tested software must be improved with respect to the evaluation of reference LI—M7
Compared with IEC 61083-2, the polarity of the reference impulses is opposite

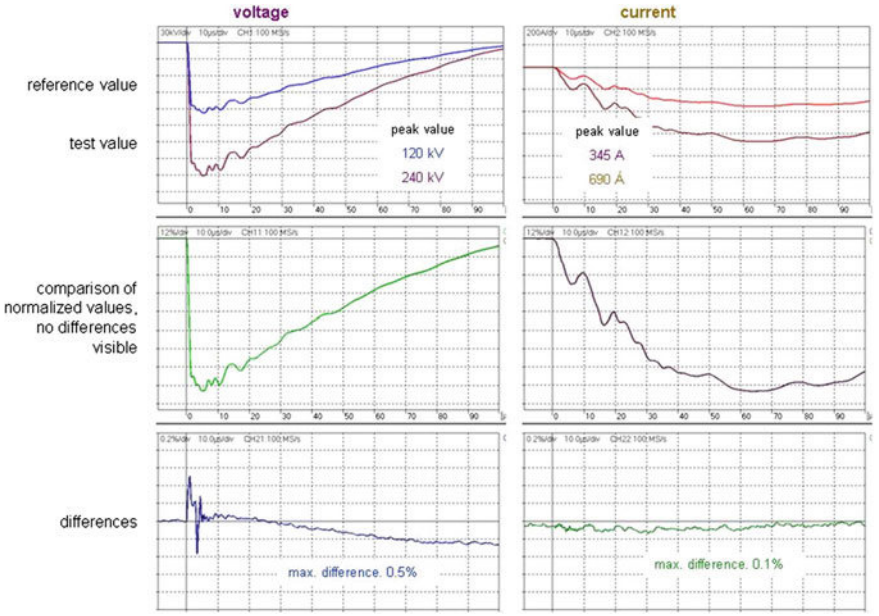

Fig. 7.61 Recorded voltage and current during a LI voltage test of a distribution transformer

respective extreme values. The test is passed if there are no significant differences between the normalized reference values and the normalized test values (IEC 60076-3:2013). A practical example is shown in Fig. 7.61 which reveals that the remaining differences are within the accepted tolerances. Thus, the test object has passed the LI test.

Comparable to LI voltage measuring systems, circuits for measuring high currents are also composed of the following components (see Fig. 7.62):

- *Converting device*, usually a shunt to convert the high current into a convenient measurable voltage,
- Transmission system, usually a fibre optic link or a measuring cable,
- Measuring instrument, usually a digital recorder.

The requirements for digital recorders are comparable to those already presented for LI voltage measurement (see Sect. 7.4.3 and IEC 61083-1: 2006). Thus, in the following, only the converting devices required for impulse current measurements between some 100 A's and some 10 kA will be presented. For more details in this respect, see Schon (2010).

Note The classic application of impulse currents is testing of *lightning arresters* and other protecting devices, where peak values up to 200 kA must be measured. However, high-current testing is not a subject in this book. For more details, see IEC 62475:2012 or the series of the IEC 60099 standards as well as the above-mentioned book of Schon (2010).

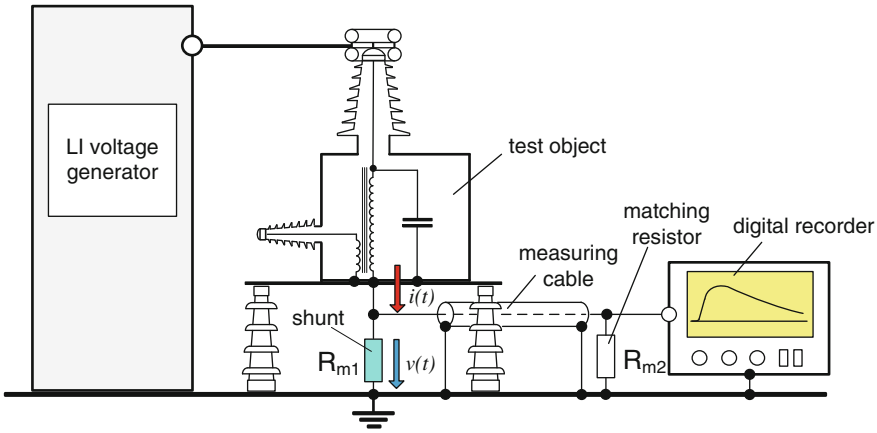

Fig. 7.62 Components of an LI current measuring system

To reduce the magnitude of high-current pulses down to a convenient measurable level, various types of converting devices are in use, such as resistive shunts, Rogowski coils, current transformers, hall-sensors and magneto-optic sensors which are described in a great detail in the textbook of Schon (2010). Thus, in the following, only a brief summary will be given which focuses on the converting device providing resistive shunts and Rogowski coils.

7.5.1 Resistive Converting Device (Shunt)

Even if the physical background of current measurements based on Ohm's law is easily understandable, it has to be taken into account that for measuring high impulse currents, the resistance of the converting must be extremely low, usually in the mΩ range. However, under this condition, the resulting impedance can substantially be determined by the inductance of the measuring circuit, as illustrated in Fig. 7.63. Here, the left record is obtained for a resistive shunt grounded via wire, whereas the right record is obtained for grounding the transducer via a Cu-foil of extremely low inductance. Consequently, the signal enhancement in the front region obvious from the left record in Fig. 7.63 is due to the superposition of the inductive component $v_L(t)$on the resistive voltage signal $v_R(t)$ as qualitatively illustrated in Fig. 7.64. Thus, the measured voltage signal $v_m(t)$ caused by a time-dependent current $i_m(t)$ can be expressed by:

$$v_m(t) = v_R(t) + v_L(t) = R_m \cdot i_m(t) + L_m \cdot \frac{\mathrm{d}i_m(t)}{\mathrm{d}t}. \tag{7.41}$$

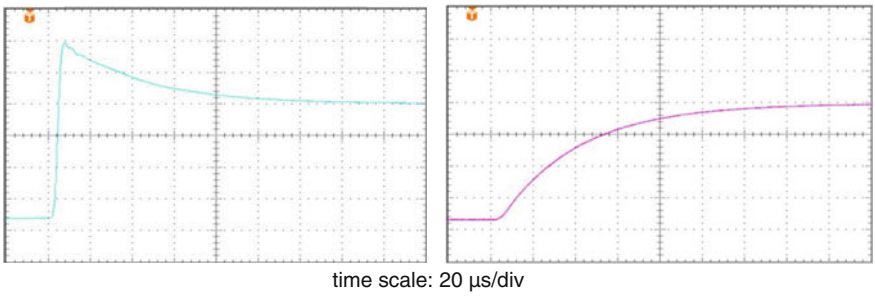

Fig. 7.63 Response of a current measuring system against an exponential rising current signal where the transducer is grounded via a wire (*left*) and a Cu-foil (*right*)

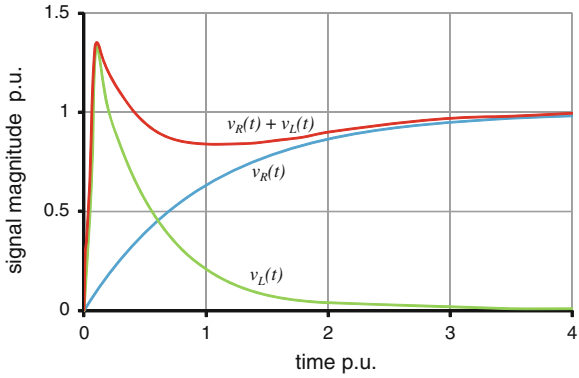

Fig. 7.64 Total voltage $v_m(t) = v_R(t) + v_L(t)$ appearing across a resistive shunt at fast rising impulse current due to the superposition of the resistive and inductive voltage components

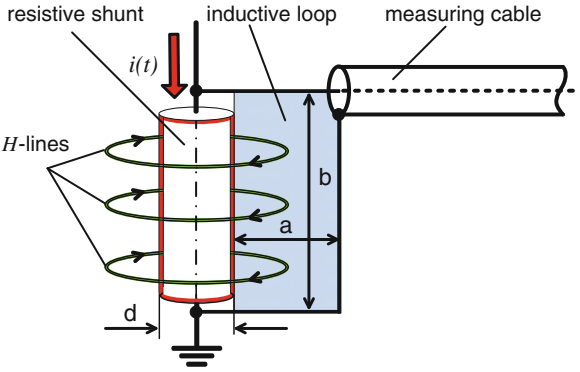

Fig. 7.65 Equivalent circuit for the estimation the induced voltage $v_L(t)$ due to the inductive loop formed by the connection leads between measuring cable and resistive shunt

Basically, the inductance L_c due to the connection leads between the transducers, and the measuring cable is governed by the shaded area shown in Fig. 7.65 which can be approximated as follows (Küpfmüller 1990):

$$L_c = \frac{\mu_0 \cdot b}{2\pi} \ln\left(\frac{2a}{d} + 1\right). \tag{7.42}$$

Additionally, the self-inductance of the resistive transducer has also to be taken into consideration. For a resistor of diameter d and length b, the following approach can be adopted (Küpfmüller 1990):

$$L_s = \frac{\mu_0 \cdot b}{2\pi} \ln\left(\frac{b}{d} - \frac{3}{4}\right). \tag{7.43}$$

Combining the Eqs. (7.42) and (7.44) and introducing the simplification $d \ll a$; $d \ll b$, one gets the following approach:

$$L_m \approx \frac{\mu_0}{2\pi} b \cdot \ln\left(\frac{2a \cdot b}{d^2}\right) = \frac{0.4\pi\,\mathrm{nH/mm}}{2\pi} b \cdot \ln\left(\frac{2a \cdot b}{d^2}\right). \tag{7.44}$$

To estimate the disturbing inductive voltage component, the following approximation can be used:

$$v_l(t) = (0.2\mathrm{nH/mm}) \cdot b \cdot \ln\left(\frac{2a \cdot b}{d^2}\right) \cdot \frac{\mathrm{d}i(t)}{\mathrm{dt}}. \tag{7.42}$$

Example Consider a resistive shunt characterized by the following parameters:

Shunt resistance	$R_s = 10\ \mathrm{m\Omega}$
Shunt diameter	$d = 10\ \mathrm{mm}$
Measuring loop	$a = b = 50\ \mathrm{mm}$

Assuming an exponential rising current pulse characterized by the time constant $\tau_c = 2\,\mu\mathrm{s}$ and a crest value of 1 kA, the voltage appearing across an "ideal" shunt would follow the function

$$v_r(t) = (100\,\mathrm{V}) \cdot [1 - \exp(-t/\tau_c)]$$

The inductance can be estimated as

$$L_m \approx (0.2\,\mathrm{nH/mm}) \cdot b \cdot \ln\left(\frac{2a \cdot b}{d^2}\right) \approx 40\,\mathrm{nH}.$$

Due to this, an additional voltage is induced which appears superimposed to the resistive voltage. At time instant $t = 0$, where the current steepness is 1 kA/2 μs = 0.5 kA/μs, the peak voltage of the inductive component becomes (40 nH) · (0.5 kA/μs) = 20 V. This is approx. 200 % of the peak voltage measurable across an "ideal" shunt after the instant $t \approx 3\tau_c = 6\,\mu\mathrm{s}$ given by (1 kA) · (10 mΩ) = 10 V.

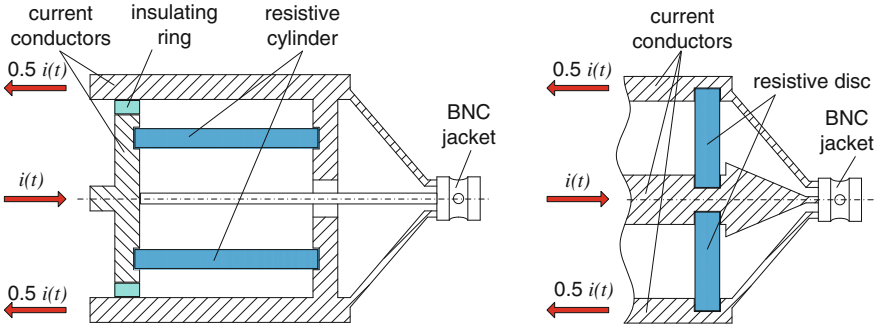

Fig. 7.66 Design principles of low-inductive shunts

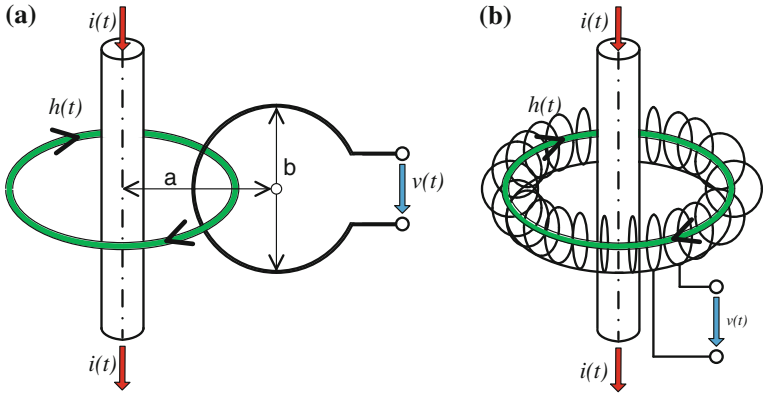

Fig. 7.67 Principle of inductive current sensors. **a** Single-turn current probe. **b** Rogowski coil

To minimize the measuring error due to the induced voltage, the area of the measuring loop must be as small as possible. This is usually realized using either coaxial shunts or even disc-shaped shunts as illustrated in Fig. 7.66.

7.5.2 Inductive Converting Device (Rogowski Coil)

The simplest way to eliminate the voltage induced in the measuring loop is to apply a pure inductive converting device. As illustrated in Fig. 7.67, this may consist either of only a single turn or even numerous turns known as Rogowski coil (Rogowski 1913). Based on the inductance law, the voltage detectable at the output of the coil without load (i.e. open loop) can be approximated by:

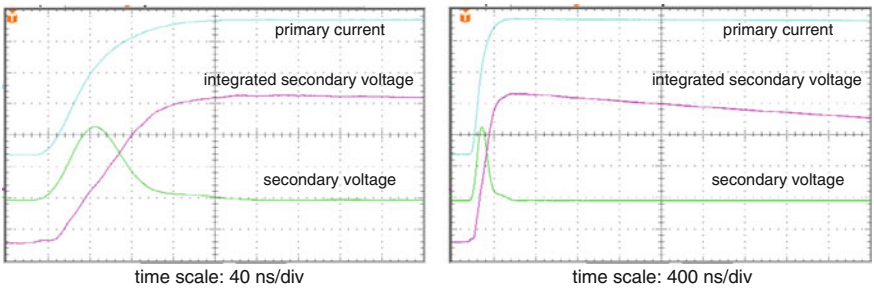

Fig. 7.68 Transfer characteristics of an LI current measuring system using a Rogowski coil

$$v_l(t) = M \cdot \frac{\mathrm{d}i}{\mathrm{d}t} = \left[\frac{\mu_0 \cdot n \cdot b}{8} \cdot \ln\left(\frac{2a+b}{2a-b}\right)\right] \cdot \frac{\mathrm{d}i}{\mathrm{d}t}, \tag{7.43}$$

with

M mutual inductance
μ_0 permeability of air
n number of turns
a distance between conductor and Rogowski coil
b diameter of turns

As the voltage $v(t)$ induced in the Rogowski coil is proportional to the derivate of the current, i.e. $\mathrm{d}i(t)/\mathrm{d}t$, an output signal appears only at changing current. Thus, this voltage has to be integrated to get a signal which is directly proportional to the pulse current to be measured, see Fig. 7.68.

In this context, it should be remembered that the behaviour of an inductive converting device is equivalent to that of a high-pass filter, i.e. a DC current component is not measurable. That means, the inherent measuring error increases with the duration of the current pulse and thus at lower-frequency content, see Fig. 7.68. To reduce the lower-limit frequency, the mutual inductance must thus be enhanced accordingly. This can effectively achieved if the classical Rogowski coil is substituted by a transducer comprising a fast current transformer where the coil windings are wounded around a high-permeable core. Generally, it can be stated that Rogowski coils are utilized only for measuring extremely high and fast current pulses characterized by a steepness of several 100 kA/μs, whereas fast current transformers are commonly employed for measuring impulse currents of a steepness which is significantly below 100 kA/μs where the duration may exceed several 100 μs and more.

As already discussed above, the output voltage of inductive converting devices without load is proportional to the derivate of the primary current. Thus, the measurement of the step-pulse response seems not feasible to analyse the dynamic behaviour of inductive current transducers. This is because the connected electronic devices such as the required integrator might be overloaded. Additionally,

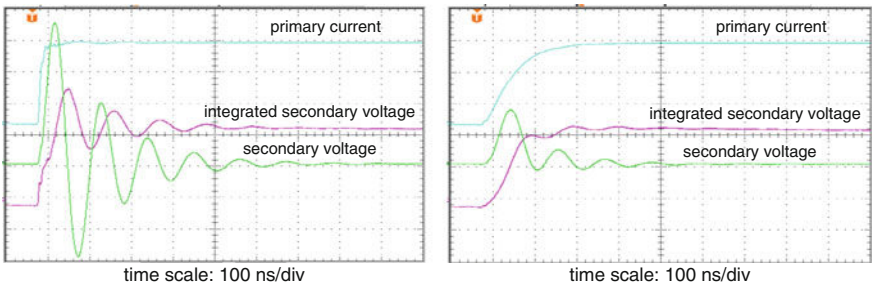

Fig. 7.69 Dynamic behaviour of a fast current transformer subjected to primary current pulses having a rise time of 10 ns (*left*) and 50 ns (*right*)

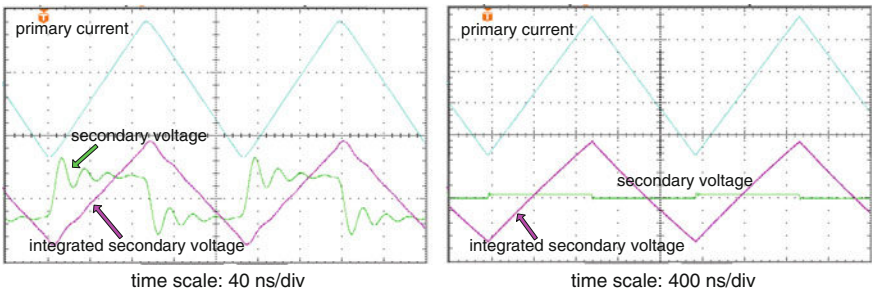

Fig. 7.70 Dynamic behaviour of a fast current transformer subjected to linearly rising and falling current ramps at repetition rate of 5.4 MHz (*left*) and 0.54 MHz (*right*)

disturbing oscillations could be excited causing inherent measuring errors, as obvious from Fig. 7.69. Consequently, for measuring the response parameters, the rise time should be selected in the order of the shortest time parameters to be expected under real measuring conditions. Another option is the application of linearly rising and falling current signals where the pulse repetition rate should be changed according to the time parameters of interest, as recorded in Fig. 7.70.

7.6 PD Measurement at Impulse Voltages

From a physical point of view, PD measurements of HV apparatus should be executed at voltages representative for service conditions. Therefore, the standard IEC 60270: 2000 is mainly addressed to PD measurements under power frequency AC voltages (see Chap. 4) and only a brief part deals with the particularities of PD tests under DC stress. As direct current is nowadays increasingly used also for power supply, currently an amendment to IEC 60270 (Ed. 3) is under preparation

which covers the related details (see Sect. 6.4). Under service condition, however, the insulation of HV apparatus is stressed not only by the continuously applied operation voltage but also different kinds of over-voltages, such as switching impulses (SI) and—especially caused by power electronic components—faster impulses similar to lightning impulses (LI) or very fast front (VFF) voltages (see Sect. 7.1). In the following, thus the PD occurrence encountered under impulse voltage stresses as well as the consequences for PD measurements will briefly be highlighted.

7.6.1 SI Test Voltages

The application of SI test voltages became of interest particularly for diagnostic on-site PD tests of medium-voltage power cables in the late 1980s, when XLPE distribution cables—which had replaced paper-insulated, lead-covered cables (PILC)—showed the phenomenon of "water trees"(Auclair et al. 1988). As mentioned previously, high-polymeric dielectrics are very sensitive to partial discharges because irreversible degradation processes might already occur if synthetic insulations are exposed to PDs having magnitudes as low as few pC. Performing diagnostic on-site tests combined with PD measurements would help identifying the degree of distortion and the condition assessment. The expenditure of power frequency AC tests became high due to the remarkable power demand for energizing the cable capacitance, because only test transformers and ACRL test systems had been available. To reduce the power demand, the cost of mobile test systems and to improve their handling, alternative voltages for diagnostic tests—mainly VLF and also SI test voltages—have been investigated. SI voltages have been found as a promising voltage source for PD measurement based on fundamental studies of surface, interfacial and cavity discharges, representative for PD failures in the polymeric insulation of power cables (Lemke et al. 1987).

The benefit of PD tests under SI voltages is not only the substantial reduction of the power demand of the voltage source, but also a similar voltage distribution in the test object as at power frequency voltages. This causes a certain comparability of the PD charge magnitudes, even if one considers PD pulse trains at single-impulse voltages quite different from those at continuous AC voltage. Single-stage SI generators for diagnositic PD tests of medium-voltage cables according to Fig. 7.71 do not cause transportation problems due to the comparatively low weight and small size. The energy is stored in the impulse capacitor. The spark gap traditionally used for triggering impulse generators is the only critical component because it causes heavy electromagnetic interferences. Therefore, it has been modified using low-noise solid state HV switches. As the capacitance of the power cables to be tested (around 0.25 μF/km) determines the front of the SI impulse, the SI generator must be equipped with an appropriate large impulse capacitor, preferably not below 1 μF for testing cable lengths up to some km.

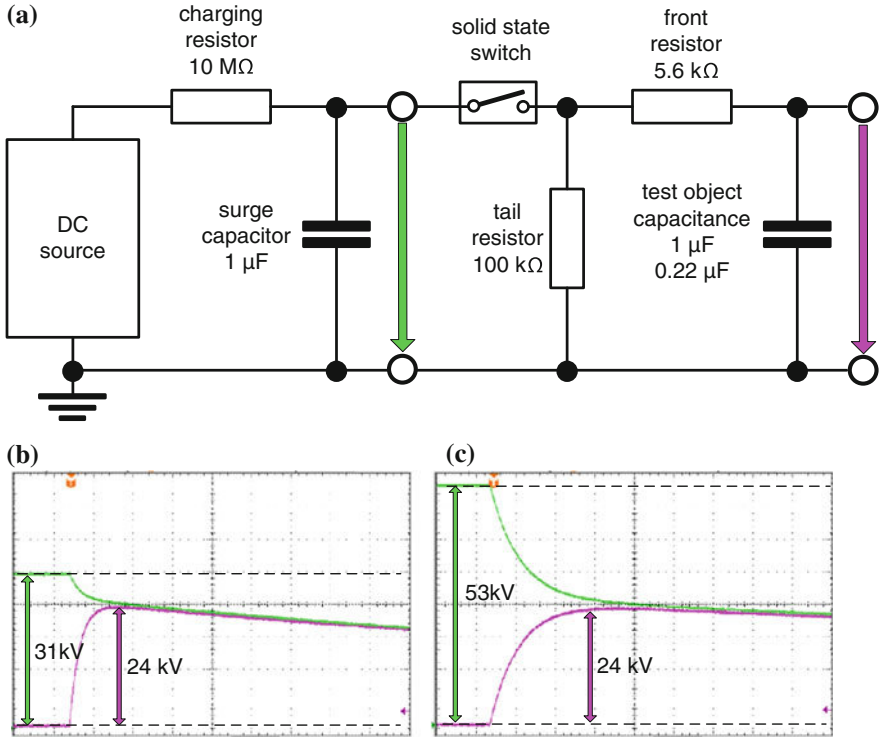

Fig. 7.71 SI voltage circuit for PD measurement. **a** Simplified block diagram of a single-stage SI generator. **b** Record of characteristic voltages with a 1 μF surge capacitor and a 0.22 μF cable capacitance. **c** Record gained for 1-μF cable capacitance

Example Performing on-site PD diagnostic tests of installed XLPE power cables rated 12/20 kV being subjected to SI voltages. Practical experiences revealed that severe PD defects can be recognized at high probability if the peak value of the applied SI voltage is approximately twice the phase-to-ground voltage expressed in terms of rms. Thus, for the considered medium voltage, a maximum test level of 24 kV is required. For the PD tests, a single-stage SI generator according to Fig. 7.71a shall be applied, which is equipped with a 1 μF surge capacitor and a 5.6 kΩ front resistor, as well. Testing a cable of 1 km length, the cable capacitance is close to 0.22 μF. Under this condition, the utilization factor determined from the oscilloscopic record according to Fig. 7.71b being almost 0.8. To get an SI test voltage level of 24 kV, thus the 1 μF surge capacitor must be charged up to a DC voltage of 31 kV just before triggering the SI generator (Fig. 7.71b). Testing a cable length of 5 km length, however, where the capacitance is close to 1 μF, the utilization factor becomes slightly below 0.5 so that the impulse capacitor must be charged up to a DC voltage level of 53 kV (Fig. 7.71c).

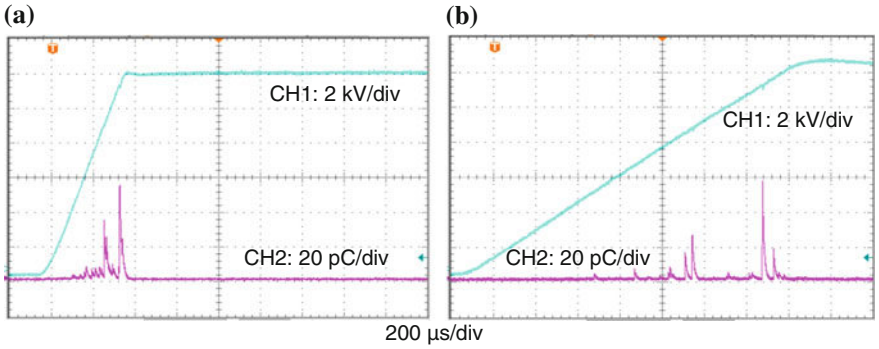

Fig. 7.72 PD signatures caused by an artificial cavity implemented in a cable sample at SI voltages of different steepness and almost identical peak values. **a** Rise times 400 μs, test voltage level 12 kV. **b** Rise time 1.6 ms, test voltage level 12.4 kV

Increasing the cable length is not only associated with a reduction of the utilization factor but also with a prolongation of the front time, see Fig. 7.71b and c. Experimental studies revealed, however, that the discharge behaviour of PD defects representative for extruded power cables is only slightly affected by the front time when ranging between approx. 100 μs and some milliseconds. An example for this is shown in Fig. 7.72 where the SI front times were close to 0.5 and 1.5 ms, respectively. The obtained screenshots yield that the magnitudes of the PD charge are well comparable for different front times even if scattering in a wide range. As expected, the pulse repetition decreases accordingly as longer the front time is. Thus, it seems not necessary to change the front resistor if power cables of lengths varying between some 100 m and few km are PD tested.

The above-mentioned independence of the PD activity on the front time is also confirmed if the charge magnitudes of the individual PD pulses are added. So, the oscilloscopic records displayed in Fig. 7.73 yield that the mean value of the accumulated charge is quite well reproducible and correlated with the instantaneous test voltage value, even if the single-PD charges are scattering over a wide range. Therefore, it can be recommended to measure at SI voltages not only the maximum pulse charge, but also—as for DC test voltages (Sect. 6.4)—the accumulated PD charge.

7.6.2 DAC Test Voltages

As discussed above, the main drawback of SI voltages used for PD tests of long cable lines is the substantial reduction of the utilization factor, see Fig. 7.71. To overcome this crucial problem, the cable capacitance could in principle also be charged directly from the DC voltage supply and not via a surge capacitor, so that the utilization factor becomes 100 %. This simple approach has been

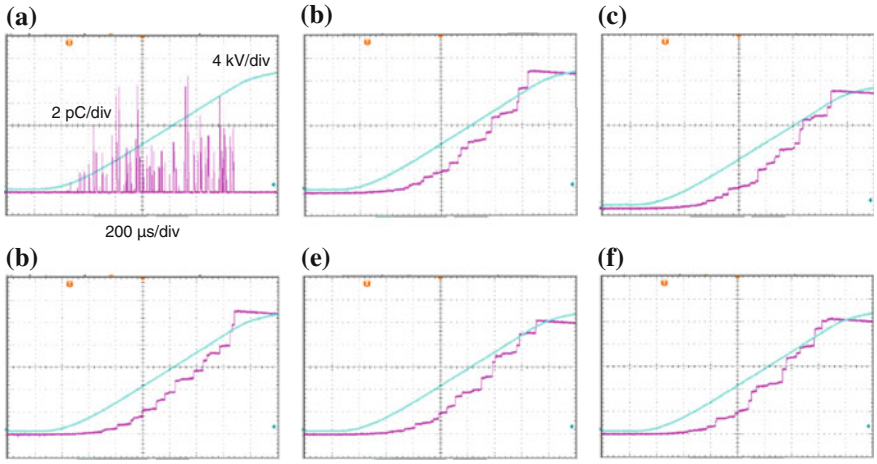

Fig. 7.73 Reproducibility of accumulated PD charges. **a** PD pulse train during the front of an SI voltage. **b–f** Accumulated pulse charges recorded at identical front time and test voltage level (time scale: 200 μs/div, voltage scale: 4 kV/div, pulse charge scale: 2 pC/div, accumulated charge scale: 20 pC/div)

recommended for after installation tests of extruded HV/EHV cables in the 1980s (Dorison and Aucort 1984; Auclair et al. 1988; Lefèvre et al. 1989). To generate an oscillating voltage and to reduce the local field enhancements due to the accumulation of space charges during the DC stress period, the cable is discharged via an inductor triggering a sphere spark gap (Fig. 7.74a). As mentioned in Sect. 7.1.3, the cable insulation is first stressed by a DC voltage ramp and just thereafter by a damped AC (DAC) voltage (Fig. 7.74b). The attenuation of the oscillating voltage is governed not only by the dielectric losses dissipating in the cable insulation but also by the resistance of the discharge inductor.

Initially attempts to combine DAC withstand tests of power cables with PD measurements were not successful because of the strong electromagnetic interferences radiated in case of the breakdown of the sphere spark gap shown in Fig. 7.74a. Moreover, the PD behaviour during the oscillating voltage stress was very different from that occurring under continuous power frequency AC test voltage. Without going into further details, it can be stated that this is mainly due to the statistical time-lag required for the availability of an initiatory electron. As already discussed above, this impact can be neglected if the oscillation frequency of the DAC test circuit approaches the power frequency (Lemke and Schmiegel 1995a, b). To examine the validity of this assumption, fundamental PD studies have been executed using the DAC circuit shown in Fig. 7.75 which is equipped with a 1 μF extension capacitor and 4 H discharge inductor, providing an oscillation frequency close to 80 Hz. Replacing the originally used sphere spark gap by a vacuum switch, the electromagnetic noises originally disturbing the PD measurements could effectively be suppressed.

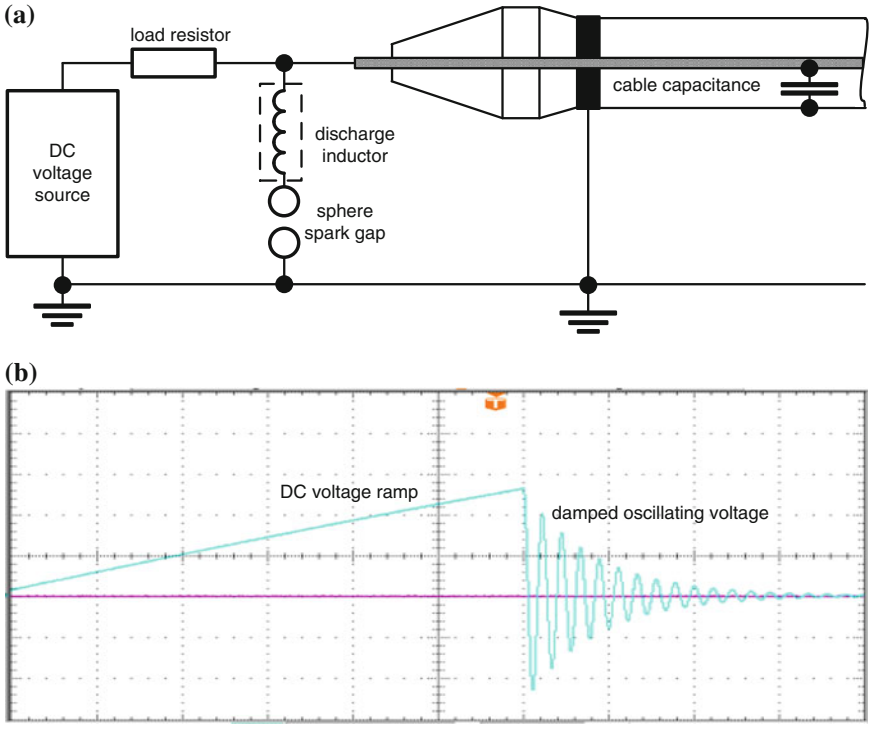

Fig. 7.74 Block diagram of a DAC test generator (**a**) and characteristic oscilloscopic record (**b**) showing the continuous rising DC stress and the damped AC voltage occurring just after the sphere spark gap has been triggered

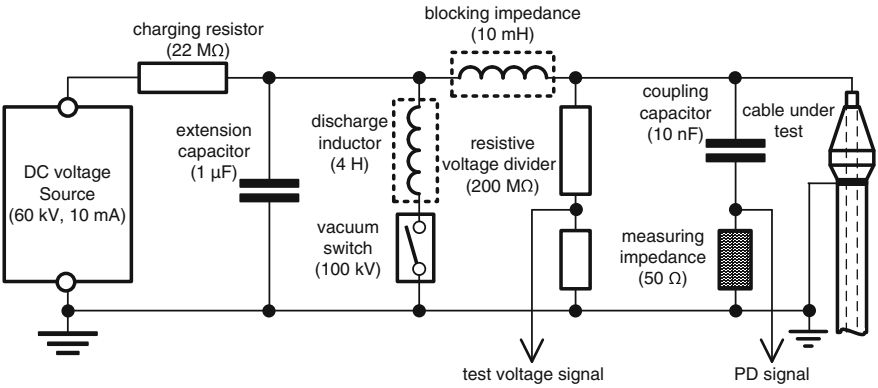

Fig. 7.75 Block diagram of a DAC test facility used for fundamental PD studies

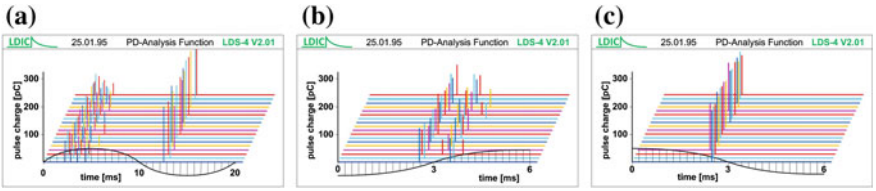

Fig. 7.76 Phase-resolved PD patterns of a void discharge in a cable sample. **a** Continuous 50-Hz AC voltage. **b** 80-Hz DAC voltage stress displayed for the first positive voltage sweep. **c** 80-Hz DAC voltage stress displayed for the first negative voltage sweep

Despite the DC pre-stress, which occurs during the initial stage when the cable capacitance is charged, it has been found that the PD mechanism occurring during the second stage, i.e. when the cable insulation is stressed by a damped alternating voltage, becomes very similar to that occurring under continuous power frequency AC voltage (Lemke et al. 2003b). A typical measuring example is shown in Fig. 7.76 which refers to a cavity discharge in a cable sample. Here, first a 50 Hz AC voltage slightly above the inception voltage has been applied, where subsequent 18 AC voltage cycles have been selected to display the phase-resolved PD pulses like a waterfall diagram (Fig. 7.76a). Thereafter, the test sample has been pre-stressed by a negative DC voltage to display the PD pulses occurring during the first positive DAC voltage sweep, which occurs just after closing the vacuum switch shown in Fig. 7.75.

This test procedure has been repeated also 18 times to create a waterfall diagram comparable to that gained for the power frequency (50 Hz) test voltage. Finally, the test sample was pre-stressed by a positive DC voltage to record the PD pulses occurring during the negative DAC voltage sweep (Fig. 7.76 b and c).

The equivalence of the PD mechanisms under both damped and continuous AC voltage follows also from the presentations shown in Fig. 7.77. These have been obtained for a defective MV cable termination. Here, the PD measurement was first performed at DAC voltage using a test level slightly above the inception voltage. For comparison purpose, only the PD events occurring during the first positive DAC sweep have been evaluated, see Fig. 7.76c. The computer screenshot shown in Fig. 7.77a has been created from 180 DAC voltage applications. Thereafter, the test sample was subjected to a continuous 50-Hz voltage choosing the test level also slightly above the inception voltage. For comparison purpose, the maximum charge of the PD pulse trains occurring during each AC cycle is displayed in Fig. 7.77b. Even if the PD measurement was extended over 30 min, only 180 from the total 90,000 AC cycles were selected using a windowing unit. This was triggered synchronously with the applied 50 Hz AC test voltage but at repetition rate of only 0.1 Hz, where the duration of each measuring windows was 20 ms. Despite the large scattering of the pulse charge magnitudes, it can be concluded from Fig. 7.77 that PD events measurable under continuous AC stress would also be detectable if damped AC voltage is applied provided the natural frequency is close to the power frequency.

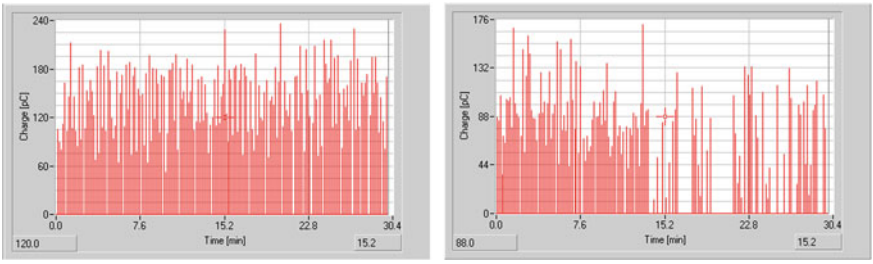

Fig. 7.77 Pulse charge magnitudes measured for a MV cable termination. **a** Damped AC voltage of 80 Hz. **b** Continuous AC voltage of 50 Hz

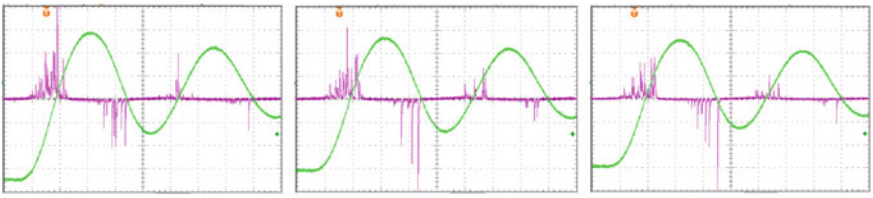

Fig. 7.78 PD signatures of a defective 20-kV cable termination at DAC test voltage using DC voltage ramps of 10, 50 and 250 s (from *left* to *right*; test voltage: 2 kV/div; pulse charge: 5 pC/div; time scale: 4 ms/div)

As already discussed above, to generate damped AC voltages for PD diagnostic tests of power cables, the cable insulation is pre-stressed by a DC voltage ramp (Fig. 7.74b). A measuring example is shown in Fig. 7.78 which refers to a surface discharge in a defective cable termination where DC voltage ramps of various durations have been applied. For this defect, the recorded PD signatures are not significantly affected by the duration of the DC pre-stressing.

7.6.3 Short Impulse Voltages (LI and VFF Test Voltages)

Short impulse voltages can permanently appear in power systems mainly caused by power electronic devices, such as frequency converters applied for adjustable speed drives and AC–DC converter stations as well as for photo-voltaic plants and wind farms. The insulation of rotating machines is especially influenced by these stresses which cause partial discharges. Therefore, PD measurement at short impulses covering the range of LI and VFF impulse voltages is of practical interest.

Increasing the steepness of the applied impulse voltage more and more, the PD occurrence is changing finally drastically. The records of interfacial discharges in a

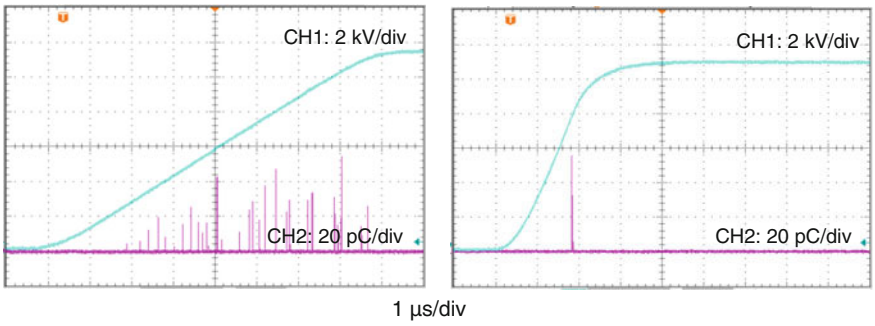

Fig. 7.79 Impact of the front time of SI voltages on the PD signature of a cavity discharge. **a** 80 µs front time, 11 kV test voltage. **b** 30 µs front time, 11.6 kV test voltage

cable termination caused by a defective field grading (Fig. 7.79) show the changed characteristic for front times below about 30 μs. Instead of a PD pulse train (Fig. 7.79a), a single-PD pulse of large magnitude (Fig. 7.79b) is observed. This is due to the impact of the statistical time-lag, the time period which elapses between the instant when the static inception voltage is achieved and the instant when an initiatory electron is available to ignite a self-sustaining avalanche discharge (Grey Morgan 1965). Thus, for steep front voltages, the first discharge is initiated at an inception voltage substantially above the static inception voltage. As a consequence, the pulse charge magnitude becomes very high which indicates a severe PD activity. Investigations of point-to-plane air gaps (Lemke 1967a, b) help to illustrate the phenomenon: Figure 7.80 refers to a point-to-plane gap of 20 cm gap spacing stressed by an SI voltage (Fig. 7.80a) and by a very steep impulse voltage (Fig. 7.80b, the long tail after the—not visible—short front can be neglected). Analysing the charge created by the single pulse at steep rising voltage shown in Fig. 7.80b, it has been found that this is well correlated with the accumulated pulse charge (as it would follow from Fig. 7.80a), providing that equal instantaneous values of the both test voltages are compared. This enables the practical conclusion to assess the maximum pulse charge depending on the peak value of short impulse voltages due to the fact that only a single-PD pulse is ignited which appears commonly at the instant when the peak value is achieved (Park and Cones 1956) (Fig. 7.80).

Under practical condition, pulse charge magnitudes exceeding often several tens or even some hundred nC which might become extremely harmful for the insulation because these can significantly reduce the life time. Thus, PD measurements have also been requested in the past for quality assurance test of components stressed by repetitive voltage impulses of very fast rise times.

Measuring partial discharges under short impulse voltages, however, is a challenge because LI and VFF voltages cover often the time parameters and thus the frequency spectrum of the PD pulses to be measured. Thus, the capacitive load current might significantly exceed the PD current magnitude, as exemplarily

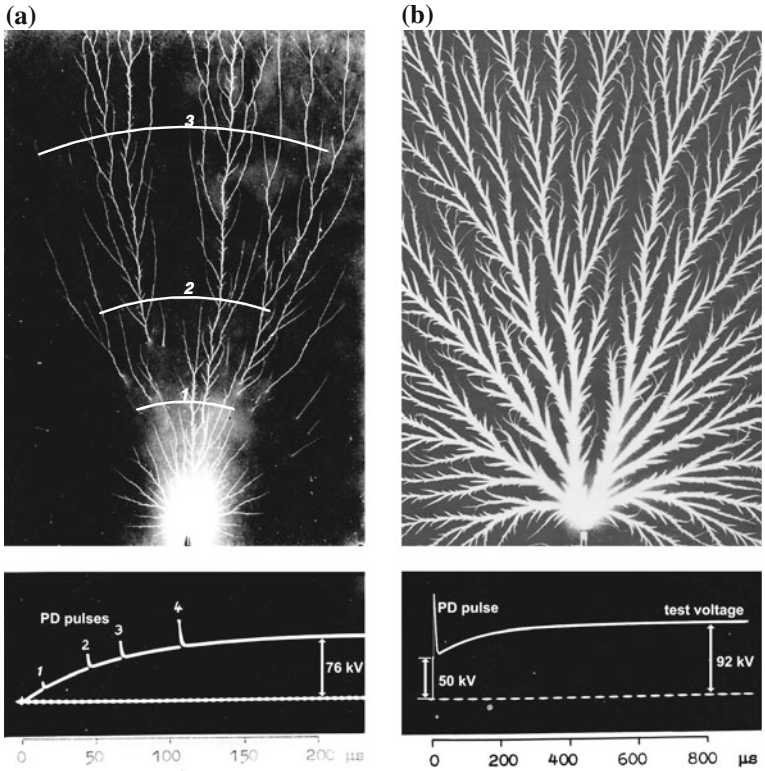

Fig. 7.80 PD occurrence at slowly rising SI voltage (**a**) and steep front voltage (*right*), explanation in the text

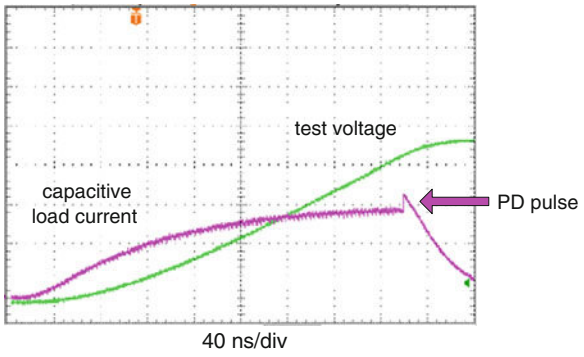

Fig. 7.81 PD signal recorded for a very fast transient voltage caused by a switching IGBT

shown in Fig. 7.81. Consequently, new approaches are required to detect potential PD defects under VFT stress which are still under development (IEC 61934: 2006) (Fig. 7.81).

Chapter 8
Tests with Combined and Composite Voltages

Abstract In power systems, the over-voltage stresses of insulations are often combinations of the operational voltage with over voltages. This can be neglected as long as the over-voltage value includes the contribution of the operational voltage. It cannot be neglected when the insulation between phases or of switching devices is considered. In that case, the resulting voltage is the combination of two voltage stresses on three-terminal test objects. In other cases, the stressing voltage is composed of two different voltage components, e.g. in certain HVDC insulations, as a composite voltage of AC and DC components. This chapter is related to the definition, generation and measurement of combined and composite test voltages on the basis of IEC 60060-1:2010 and IEEE Std. 4. Also some examples for tests with combined and composite voltages are given.

8.1 Combined Test Voltage

The definitions of combined and composite test voltages are related to the position of the test object to the test voltage sources. When the test object is arranged between the two test systems, a combined voltage stresses the test object via two different HV terminals. When the two test systems are directly connected, one composite voltage is generated stressing the test object from one HV terminal to ground. In both cases, each test system must be protected against the voltage generated by the other system by means of an element that lets pass its own voltage and blocks the voltage of the other one (coupling/protecting element).

8.1.1 Generation of Combined Test Voltages

The combined voltage appears between the two HV terminals of a *three-terminal test object* with the third terminal grounded (Fig. 8.1a). Typical three-terminal test objects are disconnectors and circuit breakers. Also the insulation between phases

W. Hauschild and E. Lemke, *High-Voltage Test and Measuring Techniques*,
DOI: 10.1007/978-3-642-45352-6_8,

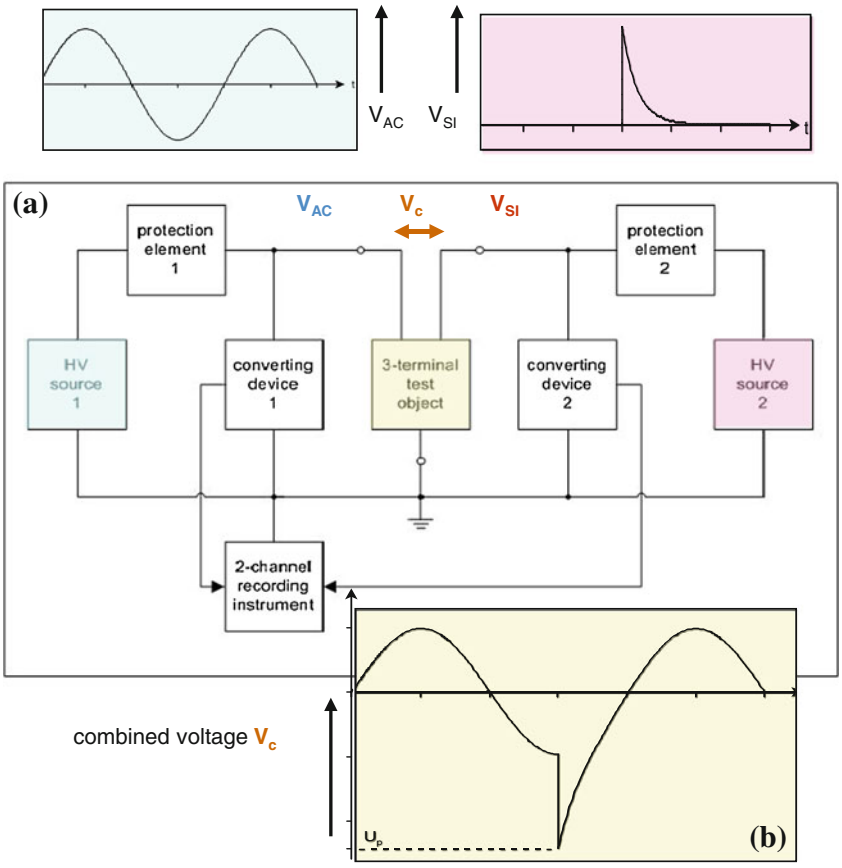

Fig. 8.1 Generation and measurement of combined voltages. **a** Schematic circuit diagram. **b** Combined test voltage as a difference of two voltages

in three-phase systems, e.g. metal-enclosed busbars of GIS and three conductor cables, form a three-terminal test object. For a HV test of a GIS, two phases are connected each to one HV source, the third phase and the enclosure are grounded.

The test object is stressed by the difference of the two single voltages (Fig. 8.1a: $V_c = V_{AC} - V_{SI}$). Figure 8.1b shows as an example the combined test voltage of an AC and a SI voltage. As long as the test object withstands the combined voltage stress V_c, it separates the two HV sources from each other. But when it breaks down, each test system is also stressed by the voltage of the opposite HV source. Then, it must be protected by a suited protection element that blocks the other voltage, at least down to an acceptable voltage stress. But this element must also couple—and not block—the voltage of the protected HV source. This means that elements must be applied that have different impedances for different voltages. For instance, an inductor has no impedance for DC voltage,

Table 8.1 Coupling/protecting elements for combined/composite test voltage circuits

Test voltage elements	DC voltage	AC voltage	SI voltage	LI voltage
Inductors (L)	Coupling	Coupling (L↓) (Protecting, L↑)	Protecting (L↑) (Coupling, L↓)	Protecting
Resistors (R)	Coupling (R↓) (Protecting, R↑)	Coupling (R↓) (Protecting, R↑)	Protecting (R↑) (Coupling, R↓)	Coupling (R↓)
Capacitors	Protecting	Coupling (C↑) (Protecting, C↓)	Coupling (C↑) (Protecting, C↓)	Coupling
Switches as triggered gaps, semiconductors	Coupling or protecting	Coupling or protecting	Coupling or protecting	Coupling or protecting

but an high impedance when stressed with LI voltages. Therefore, it may be used for protecting a DC voltage generator. It must be considered that the coupling/blocking elements influence the two components of the combined voltage. Therefore, the measurement of the two voltages has to be made after the coupling/protecting elements in parallel to the ground insulation of the test object (Fig. 8.1a). Compared with the impedance of the test object, the impedances of the coupling/protecting elements should be low.

Table 8.1 summarizes the characteristics of *coupling/protecting elements*. The preferred application of an element is shown in the first row, a second application with different parameters of the element is given in brackets. The arrows in brackets indicate a low (↓) or high (↑) value of the parameter (L, R, C). For instance, a capacitor of large capacitance (low impedance for power frequency) couples AC voltage of power frequency but one of low capacitance (high impedance) may block it. Triggered switches can be switched to positions "closed = coupling" or "open = protecting" and can consequently widely be applied.

Example When a DC/LI combined voltage shall be applied, the right element between DC voltage test system and test object is an inductor, because it couples the DC voltage and protects against LI voltage. Between the LI test system and the test object, a capacitor is the right element, it couples the LI voltage and protects the impulse generator against a DC voltage stress.

As mentioned before, the coupling/protecting elements influence the voltage generation of both voltage sources, and also the two sources show interactions. As a result, the combined voltage has not the shape as expected. The test of a disconnector shall be considered: The AC/SI combined test voltage shall be generated by a test transformer and an impulse generator (Fig. 8.2a). The AC voltage is dropped down if the AC source is not stiff enough (Fig. 8.2b: 20 %). If no powerful AC test system is available, a *supporting capacitor* $C_a \gg C_t$, larger than the test object capacitance C_t in parallel to AC source and test object, reduces the *voltage drop* remarkably (Fig. 8.2c: <5 %) (Cui et al. 2009). When a combined

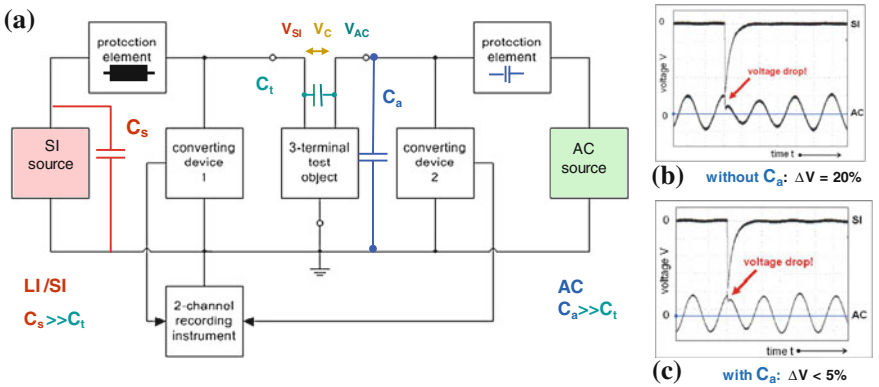

Fig. 8.2 Interaction between the two voltage sources. **a** Schematic circuit diagram. **b** Drop of the AC voltage without supporting capacitor. **c** Drop of the AC voltage with supporting capacitor C_a

(or composite) voltage test is planned, it is strongly recommended to analyse the test circuit by a suitable equivalent circuit.

8.1.2 Requirements to Combined Test Voltages

The test voltage value of the combined voltage is the maximum potential difference between the two HV terminals of the test object. Its tolerance, this means the difference between the specified value and the recorded value shall be within ±5 % of the specified value. This includes that also a voltage drop does not exceed 5 %. For each voltage component, the requirements mentioned above in the relevant Chaps. 3, 6 and 7 have to be applied. Furthermore, the *time delay*, this is the time difference between the two maxima of the voltage components, must be considered (Fig. 8.3). The tolerance of the time delay is 0.05 T_p, with T_p as the longer front parameter of the two voltages involved (where T_p is the LI front time or the SI time to peak or a quarter of an AC period).

8.1.3 Measurement of Combined Test Voltages

The two HV test systems require a HV measuring system each for the adjustment of their output voltages that contribute to the combined or composite voltage. These measuring systems must be able to record also the interactions between the two HV test systems.

The stressing combined voltage acts between the HV terminals of the test object (Fig. 8.1). A usual measurement of this voltage is difficult because there is no earth

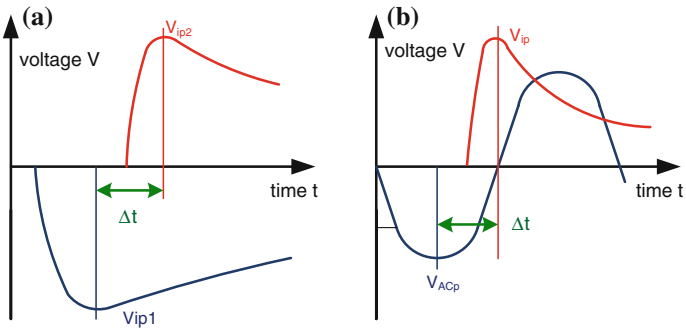

Fig. 8.3 Time delay of combined and composite voltages. **a** For two impulse voltages. **b** For an impulse voltage and an AC voltage

potential involved. IEC 60060-1:2010 allows therefore the calculation of the combined test voltage from the measurement of its two voltage components: Each of the two voltage dividers shall be arranged near to its relevant HV terminal of the test object. The two voltages are recorded, and the combined voltage is calculated as its difference. All three voltages should be monitored using an identical time scale (Fig. 8.1b).

8.1.4 Examples for Combined Voltage Tests

Disconnector testing: The testing of EHVAC disconnectors and phase-to-phase air insulation with a combined voltage of AC and SI components is the classical example of a combined voltage test. The interaction between the test voltage sources may cause a voltage drop as considered above in Sect. 8.1.1 (Fig. 8.2). Garbagnati et al. (1991) found that the atmospheric corrections of IEC 60060-1 (see Sect. 2.1.2) deliver sufficient results when they refer to that component of the test voltage value between the HV terminals that causes the maximum of the combined voltage.

Combined voltage tests with DC voltage component: The broader application of HVDC transmission systems will require test voltages that can be understood as combined voltages (Gockenbach 2010). There have been early investigations about the combination of DC voltage and oscillating SI voltage (Fig. 8.4) in preparation of test systems for the Russian HVDC transmission (Lämmel 1973). Meanwhile LI/DC voltage investigations are extended to compressed gas insulations of N_2 and SF_6 (Wada et al. 2011). They show that a DC voltage component below 50 % of the test voltage value has little influence on the breakdown voltage.

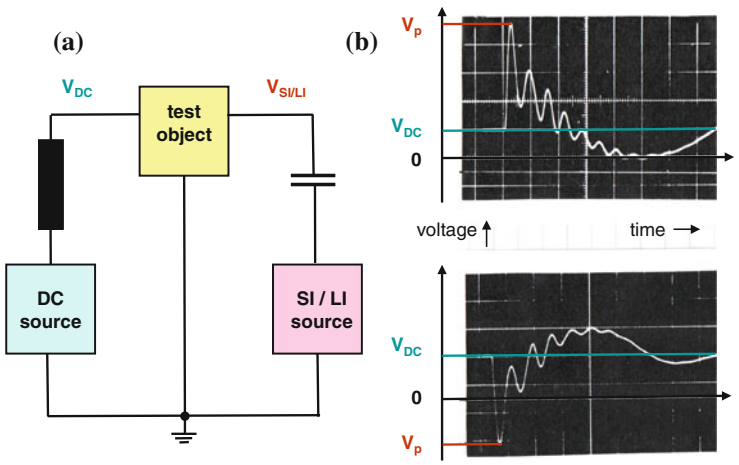

Fig. 8.4 DC/SI combined voltage. **a** Circuit with coupling/connecting elements. **b** OLI voltage superimposed on DC voltage

8.2 Composite Voltages

8.2.1 Generation and Requirements

The connection of two different test voltages to one terminal generates a composite test voltage because of their superposition at that point (Fig. 8.5a). The connection is realized with suitable coupling/protecting elements (Table 8.1). In opposite to combined voltages, the composite voltage is the sum of the two components (Fig. 8.5b: $V_{co} = V_1 + V_2$). If the two voltage sources are connected together, the interaction between the two HV sources including their coupling/protecting elements may play a role and should be analysed.

The test voltage value of the composite voltage is the maximum absolute value at the test object and shall meet the specified value within ±5 %. Also any voltage drop shall not exceed 5 %. The time delay is defined as for combined voltages (Fig. 8.3) and should be again within ±0.05 T_p (T_p as defined in Sect. 8.1.1). For the single-voltage components, the requirements in the relevant chapters of this textbook shall be applied.

8.2.2 Measurement of Composite Test Voltages

The stressing composite voltage acts between the HV terminal of the test object and the earth (Fig. 8.5). Therefore, it can be measured directly. The used

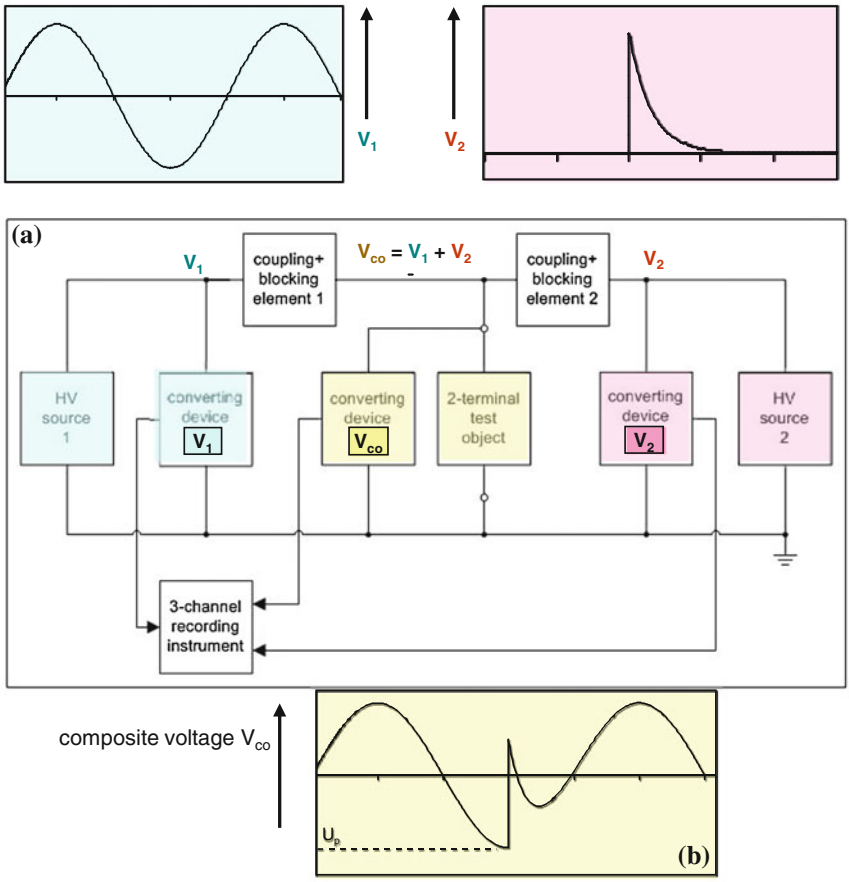

Fig. 8.5 Generation and measurement of composite voltages. **a** Schematic circuit diagram. **b** Composite voltage as the sum of the two voltages

measuring system shall fulfil the requirements of IEC 60060-2:2010 for both components. The direct measurement of the two voltage components is recommended. All three voltages shall be recorded synchronously and displayed with an identical time scale (Fig. 8.5).

8.2.3 Example for a DC/AC Composite Voltage Test

A composite DC/AC test voltage can be generated when the smoothing capacitor of the DC generator is grounded via the HV winding of a test transformer (Fig. 8.6). The DC generator must be fed via an insulating transformer (Fig. 6.8). If the test

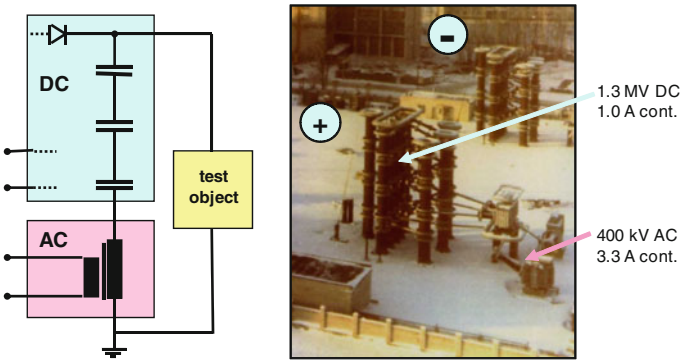

Fig. 8.6 Test system for DC/AC composite voltage up to ±1,300 kV DC and 400 kV AC (The principle is shown for one polarity only)

transformer is designed to withstand the DC stress in case of a breakdown of the test object, no additional coupling/protecting elements are required. The photograph in Fig. 8.6 shows such a DC/AC test system at NIIPT, St. Petersburg, Russia, used for the operation of a HVDC test line, corona investigations and other basic research work. Both voltage components can be adjusted separately.

Chapter 9
High-Voltage Test Laboratories

Abstract Efficient HV testing, research work or students training requires well-designed HV laboratories. This chapter is related to the planning of HV laboratories. The basis is a clear analysis of the requirements to the laboratory and corresponding selection of the HV test systems. This includes a general principle of the control and measuring systems, the internal data evaluation and communication structures. The planning of test buildings or test rooms depends strongly on the objective of the laboratory and of the available funds. The general principles for the grounding and shielding, for power supply, transportation and auxiliary equipment are explained. An important part of the planning is a safety system which guarantees both safety for the operators and reliable, quick testing. Some specialities to outdoor test laboratories and updating of existing test fields are submitted.

9.1 Requirements and Selection of HV Test Systems

9.1.1 Objective of a Test Field

The term "*HV test laboratory*" may range from a small single room with test equipment of few kilovolts rated voltage up to huge UHV laboratory complexes with several test fields of different test areas. An optimum planning of a HV laboratory well adapted to the objective of a company or institution is the basis for its later smooth operation. The users of HV test fields can be subdivided into the following groups:

- manufacturer and repair shops of equipment for power systems ("*equipment provider*"),
- companies of electric power generation, transmission and distribution ("*utilities*"),
- research institutes and HV test service provider ("*service provider*"),

W. Hauschild and E. Lemke, *High-Voltage Test and Measuring Techniques*,
DOI: 10.1007/978-3-642-45352-6_9,

Table 9.1 Objectives of HV tests (explanations in the test)

	Routine tests	Type tests	Tests for R & D	Calibrations	Educational tests
Equipment provider	X	X	X	–	–
Utilities	X	X	X	–	–
Test service provider	X	X	X	X	–
Calibration provider	–	–	X	X	–
Institutions	–	X	X	X	X

- measurement and calibration service institutions, national labs ("*calibration provider*"),
- universities and technical schools, education and training ("institutions").

The performed HV tests can be subdivided as follows:

- routine tests on new or repaired HV equipment ("*routine tests*"),
- type tests on newly developed equipment ("*type tests*");
- tests for research and development (R&D) of new HV equipment ("*development tests*"),
- tests for development of HV measurements and calibrations ("*calibration*"),
- tests for practical training and demonstrations ("*educational tests*").

The different kinds of HV tests are related to the different users of HV tests in Table 9.1. The darkness of a field shall indicate its importance for the user, dark blue means most important, light blue means useful, but not necessary, and white usually not necessary. It should also be mentioned that some users should be able to perform combinations of tests. Many universities with well-equipped HV laboratories perform HV research or even type testing. Last but not least, HV laboratories are very attractive and may support the image of an institution remarkably.

The combination of education and research fits well together, whereas *routine testing* and research work would disturb each other. A routine test is a part of the production and has to follow the technological flux in the company. Short and smooth transportation from the previous workshop to the routine test field and from there to the next station is as important as a simple and quick test process. For an equipment provider, it might be useful to have different routine test fields related to its significantly different products, but in minimum separated between routine tests and type/development tests.

Utilities have to investigate very different, service-aged equipment and only in special cases new equipment. Therefore, a laboratory for multi-purpose application

Table 9.2 Test systems for the different types of HV tests

	AC test systems	DC test systems	LI/LIC/SI test systems	HV systems for combined and composite tests
Routine tests	< 1200 kV	–	< 2000 kV	–
Type tests	< 1500 kV	< 1500 kV	< 4000 kV	
Development tests	< 1500 kV	< 1500 kV	< 4000 kV	
Calibrations	< 400 kV	< 400 kV	< 800 kV	–
Educational tests	< 200 kV	< 300 kV	< 800 kV	–

might be optimum. Service provider must also be very flexible and specialized in type tests and research/development tests.

9.1.2 Selection of Test Equipment

For the different kinds of tests, different test systems and different *special accessories* are necessary. Tables 9.2 and 9.3 give an overview on the required test systems and accessories.

As in Table 9.1, the dark blue colour indicates necessary equipment, the light blue useful equipment. The mentioned voltage values in Table 9.2 indicate the highest rated voltages of test equipment, selected according to the procedure described in the example of Sect. 1.2 (Figs. 1.5, 1.6). They are only necessary for UHV power equipment. In most other cases, the rated voltages of test equipment depend on the test objects of highest rated voltage (Tables 1.2, 1.3) or the targets of the HV research.

For *routine tests* (Table 9.2), the HV test systems must be sufficient for the products to be tested now and within the coming 10 years. It is recommended to avoid any over-dimensioning. AC voltage of power frequency is by far the most important voltage for routine tests. It is more and more connected with PD measurement. Therefore, the test rooms should be shielded or a shielded test chamber should be applied (Table 9.3; see also Fig. 9.32). Also a metal-enclosed test system (Fig. 3.47) is useful for metal-enclosed power equipment (GIS). If the AC voltage test system is metal-enclosed, the whole circuit is well shielded and does not require a shielded test room. It can be arranged in the workshop itself. Impulse voltage testing is required for routine tests of only few equipment, e.g. for power transformers. Then, related LI/SI test systems belong to the scope of supply. Routine tests with DC voltages are very seldom at the moment, but will become more and more necessary with the broader HVDC application.

Table 9.3 Special accessories for the different types of HV tests

	Shielding for PD/dielectric. measurement	Artificial rain equipment	Pollution chamber	Climatic chamber	Oil tank	Compress. gas tank	Corona cage
Routine tests	X	X	–	–	X	X	–
Type tests	X	X	X	X	X	X	X
Development tests	X	X	X	X	X	X	X
Calibrations	X	–	–	–	–	–	–
Educational tests	X	–	–	–	X	–	–

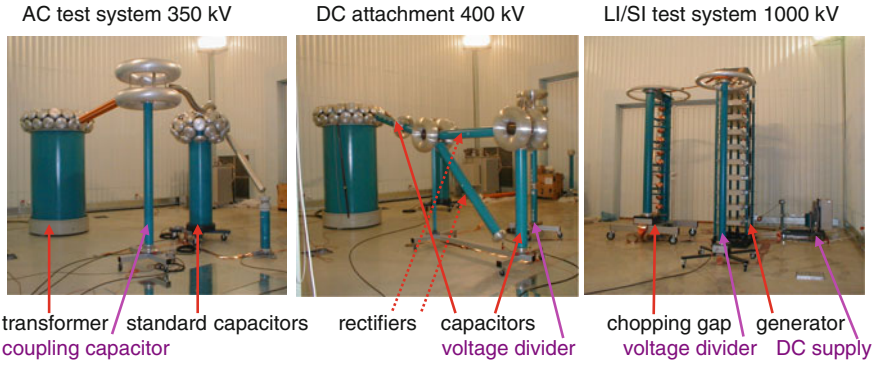

Fig. 9.1 Small HV test systems in a calibration laboratory

For *type and development tests* and for HV research work, all types of test voltages and most of the special accessories are required (Tables 9.1, 9.2, 9.3). Their rated values must be carefully selected considering the possible development within the next 2 decades.

Voltage calibrations (Table 9.2) can be performed at reduced voltages of >20 % of the rated voltage of the measuring systems to be calibrated. Therefore, the rated voltages for calibration are about 20 % of the rated voltages for type testing (Table 9.2) and small test systems are sufficient (Fig. 9.1, courtesy of TÜBITAK, Gebze, Turkey). Calibration requires always low electromagnetic noise; therefore, test rooms for calibration should be shielded.

Educational tests (Table 9.2) can be performed at high voltages up to some hundred Kilovolts (Fig. 9.2, courtesy FH Mittweida, Germany). Separate small rooms or areas for each HV test are recommended to enable several training groups to work in parallel without disturbing each other (Prinz 1965; Mosch et al. 1974; Hauschild and Fahd 1978; Kind and Feser 1999; Schwarz et al. 1999).

Fig. 9.2 Test areas for students training

Note For the selection of the rated data of test systems, special accessories and test areas, it is recommended to establish a list of power equipment to be tested with their rated electrical parameters, their test voltage values, test conditions, dimensions and weight. Also the standards which shall be applied should be summarized for the design of the laboratory as described in the following.

9.1.3 Clearances and Test Area

The size of a test room can be defined after the necessary HV test systems have been selected and the size of the largest test objects has been estimated. The necessary clearances between test objects and any grounded or energized structure have been discussed in Sect. 2.1.2 and are given in Fig. 2.1. This clearance is necessary to avoid any influence on the voltage distribution at the test object. In opposite, the distance in air between a HV test system and its surroundings must be selected in such a way that it withstands not less than about 120 % of the rated voltage V_r of the test system.

In the test voltage range up to 600 kV (peak), the simple calculation of the air distance d can be performed based on the voltage demand 5 kV/cm of the positive streamer discharge in air:

Example A 400-kV AC test circuit shall be arranged. Which distance d is required to guarantee withstand between its components and the grounded metallic fences and walls? The rated voltage is a rms value; therefore, the stressing peak value is given by $V_{peak} = \sqrt{2} \cdot 400\ \text{kV} = 566\ \text{kV}$ and the distance follows to $d > (1.2 \cdot 566\ \text{kV})/5\ \text{kV/cm} = 136\ \text{cm}$. It is decided that the distance to the metallic fence shall be 140 cm.

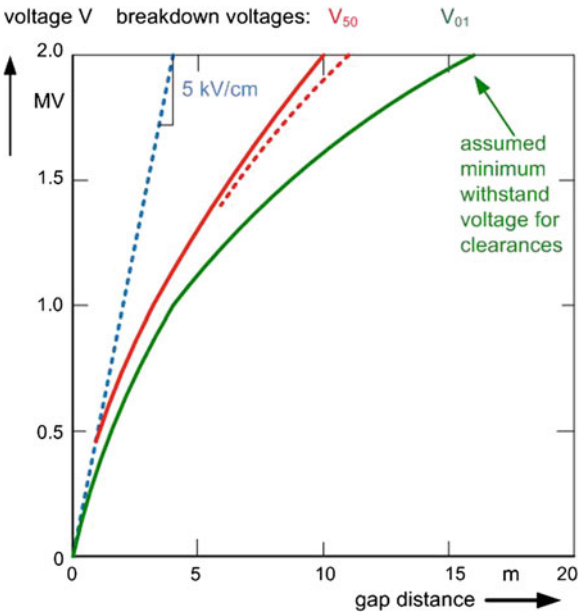

Fig. 9.3 Withstand voltage of a positive rod–plane gap in air

For higher voltages, the voltage demand decreases remarkably due to the leader discharge. According to the withstand voltage of the positive rod-to-plane arrangement (Fig. 9.3; Carrara and Zafanella 1968), a clearance of about 16 m to other objects would be required for a 2 MV SI or AC (peak) test voltage. Because of the high cost of the space in a HV laboratory, a much shorter distance must be reached by the application of suited *shielding and control electrodes*. Therefore, the impression of a UHV laboratory is determined by huge electrodes (Fig. 9.4).

There are many publications related to the design of HV electrodes, e.g. Moeller et al. (1972), Feser (1975), Mosch et al. (1979), Lemke et al. (1983) and Hauschild (1995), and electric fields can precisely be calculated now. The big problem remains to select the acceptable critical field strength. For PD-free electrodes, the concept of the streamer inception (Bürger 1976; Engelmann 1981; Dietrich 1982) can be used; otherwise, also the streamer–leader transition is applicable. For large electrodes, the streamer inception leads to a heavy streamer discharge which is immediately transferred into a leader discharge. The size of the electrode influences—in addition to the field strength distribution—also the probability of surface defects. This causes a distribution function of the inception field strength with a low increase for low probabilities and a steep one for high probabilities (Fig. 9.5). The dimensioning of electrodes is based on the low probabilities under consideration of the enlargement rule (Hauschild and Mosch 1992; Hauschild 1995). Usually, the dimensions of the electrodes are determined in an iterative process of field calculation and application of the streamer or leader inception criteria as described in the literature. Considering the enlargement of the electrode area and the prolongation of stressing time, the acceptable maximum

Fig. 9.4 Toroid electrodes in the UHV test laboratory of HSP Cologne (Germany)

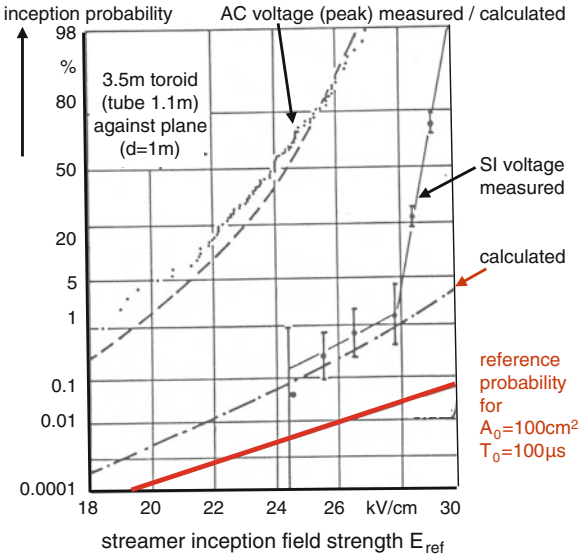

Fig. 9.5 Performance function of the streamer inception field strength in air (area element of 100 cm^2)

field strength for a large electrode can be assumed to be in a range of 10–15 kV/cm for AC and DC peak voltage and of 15–20 kV/cm for SI voltage.

For test voltages below 2,000 kV (peak), smooth electrodes like spheres and especially *toroids* are available. The *double toroid* (Fig. 9.4) is an ideal shielding element, because the necessary connections can be performed in the field shadow of the two rings.

For higher test voltage, composite electrodes are applied. Huge toroids can be realized by *cylinder segment electrodes* (Fig. 3.15). These are cylinder elements welded together to a toroid (Fig. 9.6). If the electrode is correctly designed, the

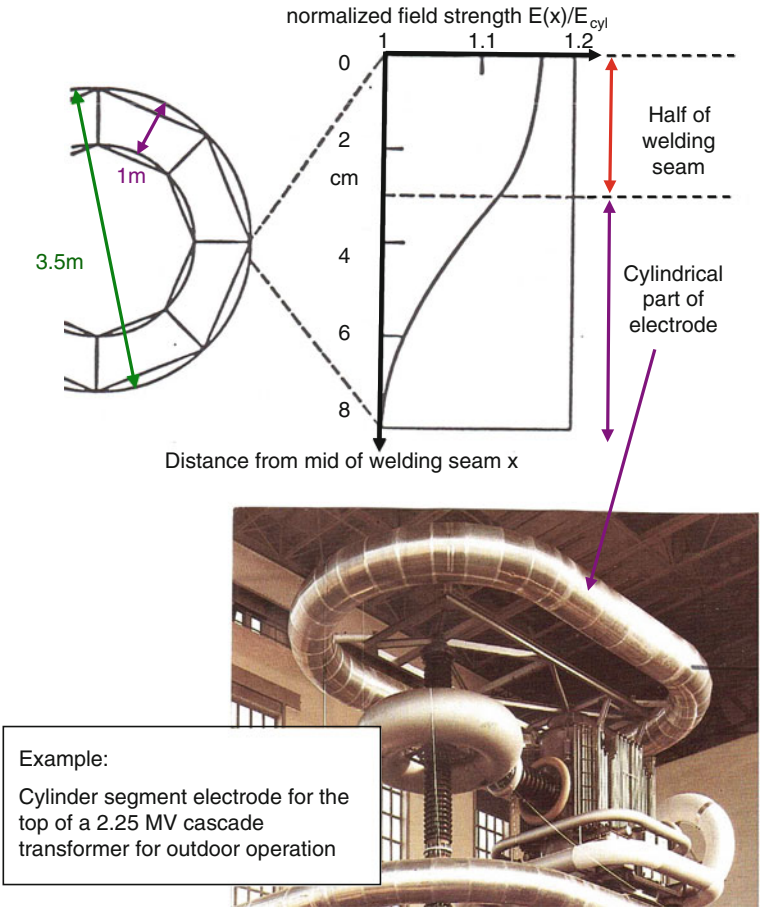

Fig. 9.6 Cylinder segment electrode for a 2.25-MV AC voltage cascade transformer

higher field strength at the welded joint is related to a small area and the danger of a discharge would be not higher than at the larger area of the cylinders of lower field strength.

So-called *polycon electrodes* are sometimes huge spheres consisting of many metal plates fixed on a spherical scaffold (Fig. 9.7). The design of the polycon electrodes is well developed (Singer 1972; Hauschild et al. 1987; Schufft 1991).

9.1.4 Control, Measurement and Communication

The controls in a HV laboratory should not only be related each to a single HV test system (Fig. 2.8), but also to their interaction among each other and with auxiliary

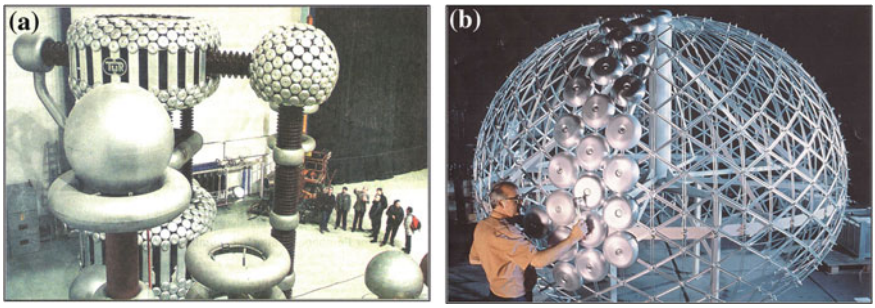

Fig. 9.7 Electrodes for UHV AC voltage components. **a** Different polycon electrodes and full-sheet sphere, respectively, toroid electrodes (EHV Laboratory of Dresden Technical University). **b** Framework of a polycon electrode (diameter 3 m)

equipment. It is recommended that all control and measuring devices are equipped with industrial personal computers (IPC) which are connected to a common bus system. This can even be made in such a way that a certain HV circuit can be controlled from any of the IPCs in the control room (Fig. 9.8). Also external test data, e.g. the atmospheric conditions, data of wet or pollution tests, etc., and the correct function of the safety system shall be recorded. The test engineer should use the computer-aided evaluation of the test and the preparation of the test record.

The *IPC control and measuring system* enables automatic operation of the HV test system, which guarantees a better reproducibility of the test parameters, the direct recording and the evaluation of the measured data. Therefore, it may shorten the test duration and safe manpower. This is especially important for the testing of mass products (possibly in combination with other non-high-voltage tests), for lifetime testing and for large-scale tests for research and development. A fully automatic test procedure cannot be recommended for HV tests on valuable, single equipment as power transformers or GIS bays. In this case, a computer-aided procedure with decisions from the operator is optimum.

The computer system of the laboratory can be connected with the local area network (LAN) of the company or institution. Most important is the connection between the HV test field and test fields for other tests and measurements. This enables a common test record for the product. Furthermore, the status of the actual test can also be observed from any other place, e.g. a customer room during an acceptance test or a student's gallery in a university during HV demonstrations. A connection to the Internet enables remote service from the supplier (see Sect. 2.2).

9.2 HV Test Building Design

There are many publications on the design of HV test laboratories, and their study is always useful for HV laboratory planning. It is impossible to mention here all of them, but the following section considers—in addition to the experience of the

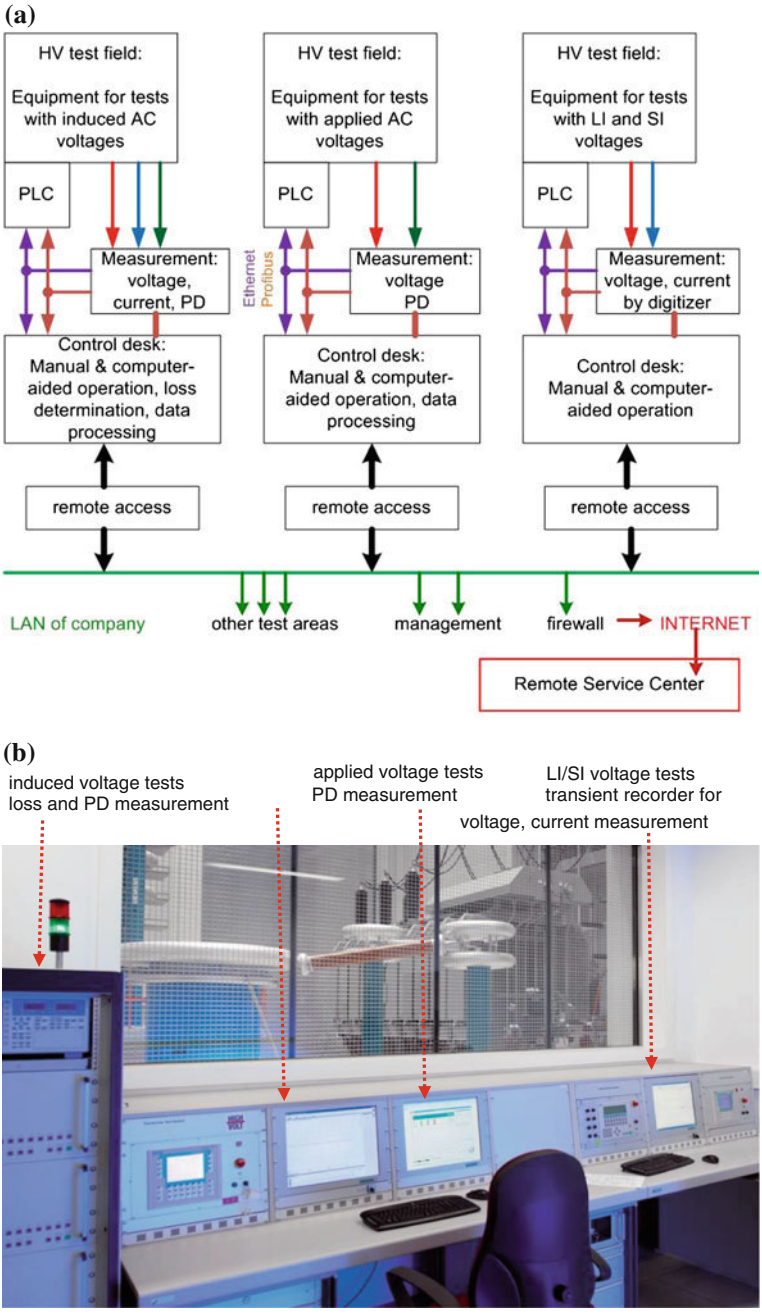

Fig. 9.8 Control room of a transformer test field (courtesy Siemens AG, TBD Dresden). **a** Principle circuit diagram. **b** Control desk and rack

Fig. 9.9 Test field for routine and type tests on power transformers (courtesy Siemens AG, TBD Dresden)

authors—especially the books of Prinz et al. (1965), Hylten-Cavallius (1988) and Schwarz et al. (1999) as well as publications by Läpple (1966), Mosch et al. (1974), Hauschild and Fahd (1978), Krump and Haumann (2011) and Hopke and Schmidt (2011). Each HV laboratory must be designed according to the special demand of the later user. This section will give suggestion for details to be considered during the planning of new or the refurbishment of existing HV laboratories.

9.2.1 Required Rooms and Principle Design

Minor details in a HV laboratory make the work of the test engineers efficient and easy. Good planning is therefore the necessary precondition for later smooth operation of the laboratory. Therefore, the application determines the basic design of the HV laboratory.

For *routine testing*, the HV test field may be a single test room or only a test area at the end of the production area. Then, the selected HV test systems and the dimensions of the test objects determine the size of the room. As an example, Fig. 9.9 shows such a quite compact, well-shielded test field for routine and type tests on power transformers up to 245 kV. It includes the facilities for induced and applied AC voltage tests and for LI/LIC/SI voltage tests in a room of only $L \times W \times H = 18.3\ \text{m} \times 13.3\ \text{m} \times 12.3\ \text{m}$ (Hopke and Schmidt 2011). Such a

test field must be well adapted not only to the requirements of the HV tests, but also to the demand of the production and the flow of products. This includes the kind of transportation of the test objects (e.g. air cushion, rails, crane), the necessary space and clearances for the HV tests as well as the necessary conditions of measurement (e.g. of PD) in an industrial environment. The test room must be completed by a shielded control room and a power supply room.

A *universal HV laboratory* for research, development and training requires many test and auxiliary rooms. The size of the largest laboratory room is determined by the highest required test voltages. It is useful to have a second universal test room for equipment of clearly lower rated voltage. For training, smaller test rooms are recommended with one or two test areas each. Furthermore, special laboratories for cable testing, pollution testing, calibrations as well as for oil and solid insulation are often required. The selection of rooms shall be explained based on the following example:

Example (Fig. 9.10) A universal EHV laboratory shall be erected as the National HV Laboratory of a country. It has been decided to erect the laboratory near the campus of an university and to use it also for student's training. The largest equipment to be tested is for a rated voltage of 550 kV. Therefore, the highest test voltages are 1,550 kV LI, 1,705 kV LIC, 1,175 kV SI (Table 1.2) and 680 kV AC (IEC 60076-3:2012). According to the principles described in Sect. 1.3, the following rated values of the largest HV test systems are selected: 3,000 kV impulse voltage (LI; LIC: SI) with a highest SI output voltage of 1,800 kV and 1,000 kV (AC). Additionally, it is decided to have a DC voltage test system of 1,000 kV (extendable up to 2,000 kV) to meet future requirements on DC testing. After consideration of the necessary clearances and the necessary space for the test objects, an EHV laboratory of a length of 40 m, a width of 30 m and a height of 25 m was selected (Fig. 9.10). The test systems are arranged in three corners of the EHV hall. The control room (yellow) is in the fourth corner.

The HV laboratory shall be used for testing power equipment of rated voltage up to 145 kV. It is therefore equipped with an 800-kV impulse test system and a 400-kV AC test system. The related control room (Fig. 9.10) is in a corner. The three MV labs are planned for students training. Each of them shall be equipped with two HV test bays for voltages in the range up to 100 kV.

The laboratory is completed by a number of special test rooms. There is a special HV ***laboratory for cable testing*** with a big door to outside for the cable drums. As the other two laboratories, this laboratory including its control room is well shielded. The cable test laboratory is completed by an open-air field for pre-qualification tests of cables. The related control room with a window to outside is in the mezzanine. The area in front of the EHV hall is kept empty for a later outdoor EHV or UHV test field. Also a related control room in the mezzanine is planned for the future. A ***pollution test laboratory*** can be connected via a bushing to the AC test system of the big hall (Alternatively, the room is big enough for its own powerful test transformer. Also an air-conditioned ***calibration laboratory*** is part of the planning (left).

There are many auxiliary rooms required, such as the *power supply room*(s), stores, workshops, seminar and meeting rooms, offices for the director and his staff. Additional functional rooms as IT server room, kitchens, washrooms, etc., should be planned. The arrangement of these rooms shall be explained with the continuation of the above example:

Usually, a HV laboratory cannot have too many store rooms. Possibly, the one between the EHV and the HV laboratory is not sufficient. In opposite to that, there is a mechanical

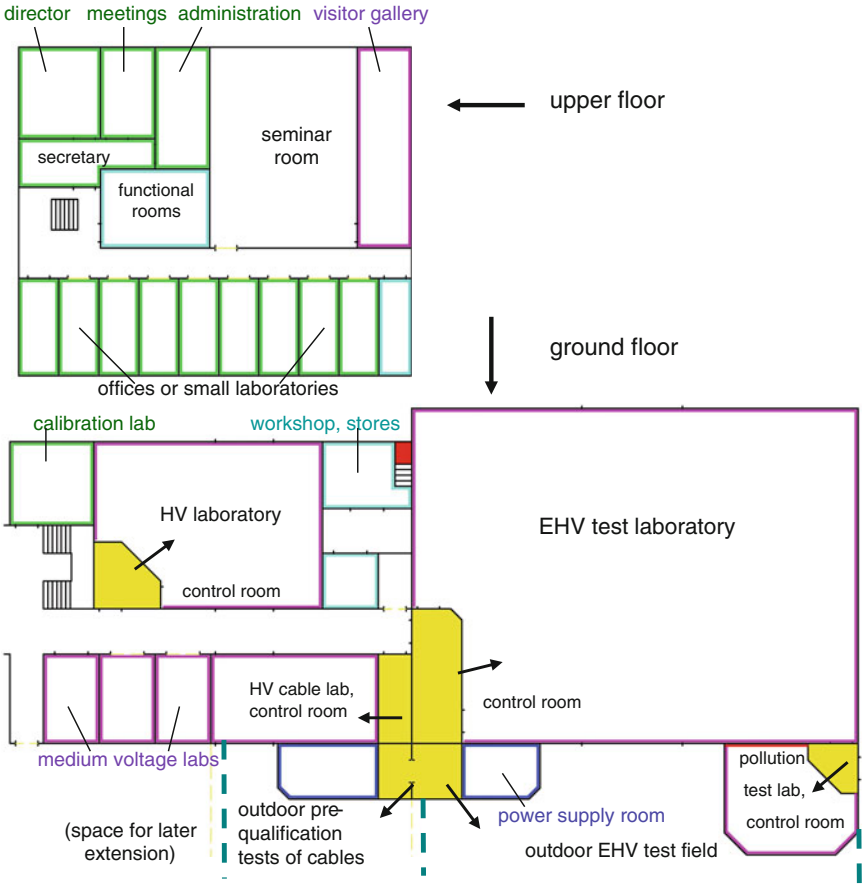

Fig. 9.10 Planning of the arrangement of rooms of an universal HV laboratory

workshop in the ground floor and an electronic workshop in the mezzanine. The area under the calibration laboratory can be used as a meeting room. In the upper floor (Fig. 9.10b), a seminar room enables the teaching of up to 60 students. The teaching room is connected with a visitors' gallery which enables the observation of experiments in the EHV hall (similar to Fig. 9.11). Additionally, the upper floor is used for all offices, for functional rooms and for small laboratories, for example for mechanical or chemical investigation of solid insulating materials and insulating oil.

Rectangular test rooms can be considered as optimum (Figs. 9.11, 9.12, 9.13). They can be well subdivided into two separate test areas by *safety fences* for parallel testing. The relation between width W and length L depends on the necessary test voltages. If only AC and impulse voltages are required, the relation $W/L \approx 0.5\ldots0.6$ seems to be optimum. In case of the three voltage sources (AC; DC and impulse), the relation $W/L \approx 0.7\ldots0.8$ is better adapted. Large test objects are arranged in between the test systems. Today, the HV generators can be placed on *air cushions*

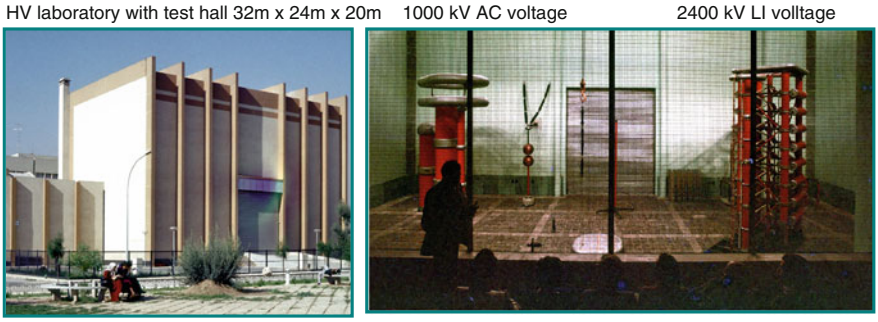

Fig. 9.11 Building and students gallery at the HV laboratory of Damascus University

(see Sect. 9.2.5.3) and moved to the optimum place for testing or to a corner when not used. Smaller components of the HV test circuit can be equipped with wheels and also be placed at optimum positions for testing or stored on an empty area.

Usually, the largest *clearances* to walls and ceiling are required at the top of the test systems. Therefore, a limitation of the clearance which is sometimes applied by a parabolic cross section (Fig. 9.14a) cannot be recommended, but a rectangular one (Fig. 9.14b). The lower demand of clearance near its floor can be used for additional small built-in test areas of lower test voltages or for stores within a rectangular structure.

HV laboratories are impressive technical rooms. Therefore, an advanced planning should not only consider the technical aspects, but also a certain aesthetic planning. The three-dimensional design offers best opportunities for the aesthetic planning (Fig. 9.15, which is related to Fig. 9.4). The balanced planning of the colours between HV test systems, wall, ceiling and floor is highly recommended. The control room is often the place where also visitors appear who conclude from their impression to the quality of the HV testing. Therefore, the control desk (or table or rack) should be clearly arranged, of uniform design (even for test systems of different suppliers) and well placed in the room. The height of a desk should correspond to the lower frame of the window (Fig. 9.8). There should be additional space in the desk for later extensions by different instruments, to avoid the poor impression of additional stand-alone device on a desk with built-in instruments.

9.2.2 Grounding and Shielding

Building grounding, test field grounding, electromagnetic shielding and earth return of a test circuit are often mixed up, not only theoretically, even worse in real test field operation. First, the different terms shall be defined by their descriptions:

Building grounding: Each HV laboratory building must be grounded, mainly for its lightning protection. The building grounding consists of the building's steel reinforcements, the foundation earth electrodes and possibly additional earthing

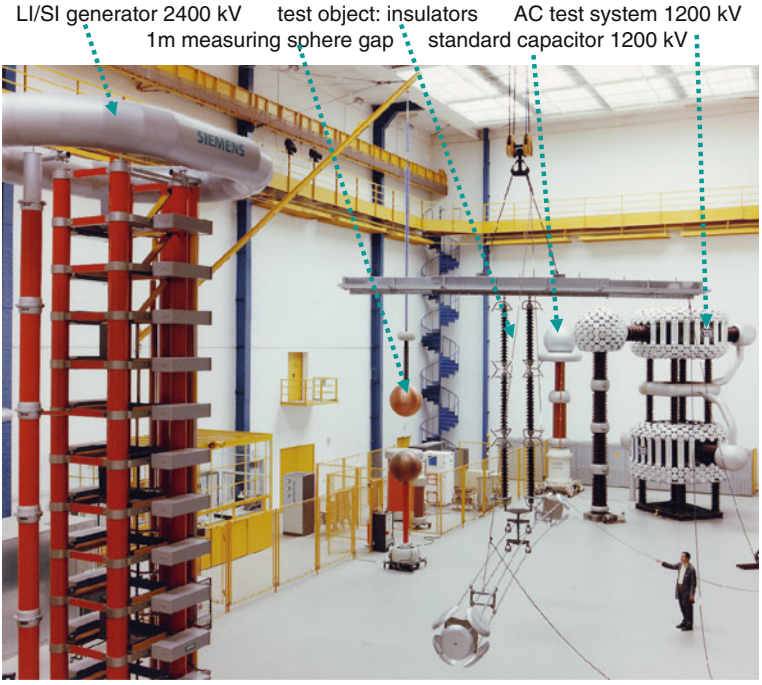

Fig. 9.12 EHV laboratory of Dresden Technical University (building erected in 1930)

rods. In a complex of buildings, the different building groundings are connected. The building grounding takes no care for external noise reduction.

Test field grounding: The upper layers of the ground are influenced by the earth return of power-electronic-driven machines and equipment in a factory. In brief, they are not free from noise signals. Therefore, a conductive contact of the test field grounding with the upper layers of soil and with the building grounding should be avoided. The test field grounding shall be realized by earthing rods which dip some metres into the ground water and which are electrically insulated along their first metres. The effective ground resistance of the parallel connection of all earthing rods should not exceed 2 Ω.

Electromagnetic shielding: An electromagnetic field caused by noise signals may disturb measurements in a HV circuit (Chap. 4). According to the famous observation of Faraday, no electric field exists inside a closed metallic container. Therefore, HV laboratories are shielded against the penetration of electromagnetic fields by a closed metallic structure which is separated from both the soil and the building grounding and only at one point connected to the test field grounding.

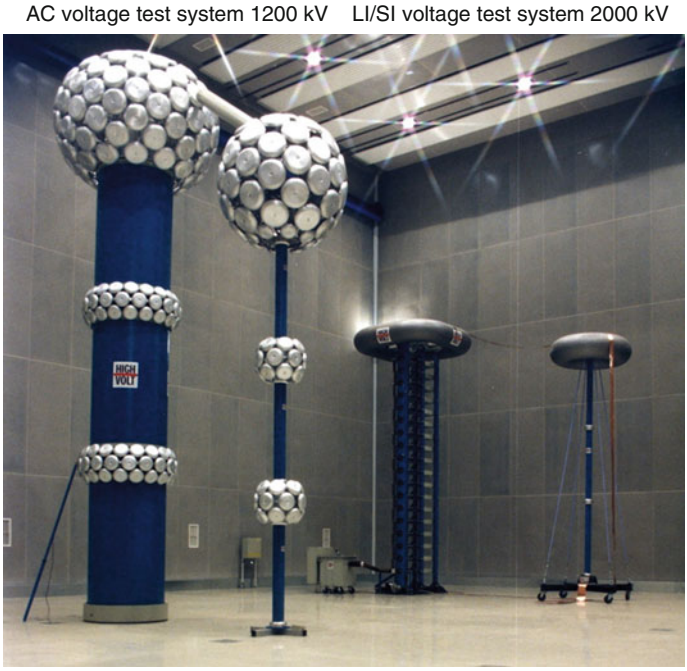

Fig. 9.13 EHV laboratory of Cottbus Technical University (established in 1998)

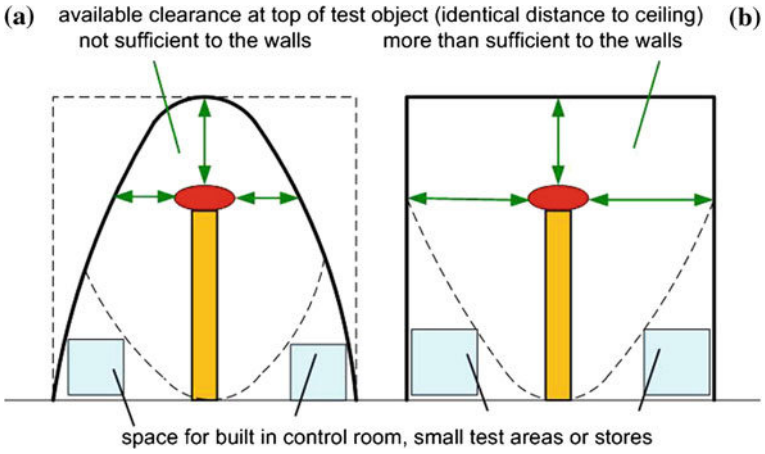

Fig. 9.14 Cross sections of HV laboratories

Earth return: Each HV test circuit must be connected to the test field grounding at one point near to the voltage divider or the test voltage generator. It should have its own earth return of lowest possible inductance (see Sect. 7.1.2.3). Only in

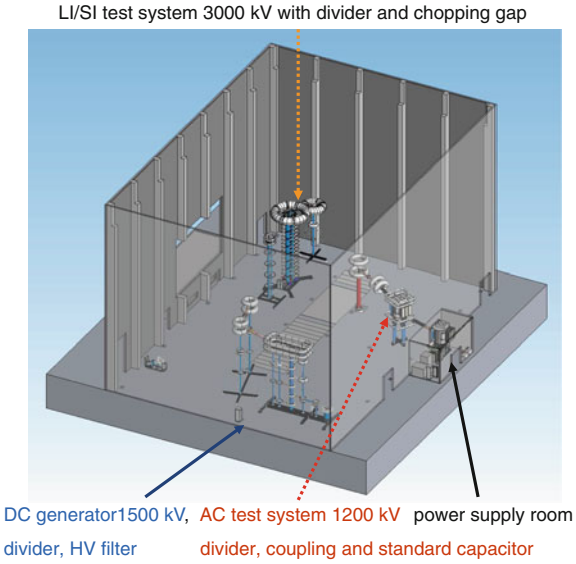

Fig. 9.15 Three-dimensional planning of a HV laboratory

special cases, it can be recommended to use the test field grounding as the earth return.

Building grounding, test field grounding, electromagnetic shielding and the earth return(s) of the single test systems must be connected **only at one point** to guarantee a common stationary ground potential and to avoid any grounding loop which may act as an antenna for noise signals. For power cables from the regulators to the test room, a cable trench along the walls with metallic frames and covers is necessary. Frames and covers must be connected to the shielding of the floor. The connection of the floor shielding to that of the walls has to be made via the cable trench.

When a HV laboratory is erected, the mechanical *design of the floor* is related to the required maximum load by test generators and test objects. Also the kind of transportation, e.g. by air cushions, must be taken into consideration. The steel reinforcement of the concrete forms one part of the shielding of the floor. It must be isolated from the soil by a suited plastic foil, the single steel rods must be welded together, and a wide mesh of metal band, also welded to the reinforcement steel, completes the shielding of the floor (Fig. 9.16a). The surface of the floor is interrupted by *earthing boxes* and *connection boxes* (Fig. 9.16b). The metallic earthing boxes are connected to the floor shielding. The internal part is isolated from that and connected to the earthing rods and/or their connections by isolated copper bars. Furthermore, inside the steel reinforcement of the floor, metallic tubes between the HV test systems and the control room are provided for control and measuring cables. They are accessible via the connection boxes. Even measuring instruments can be arranged in a connection box, for example the PD measuring

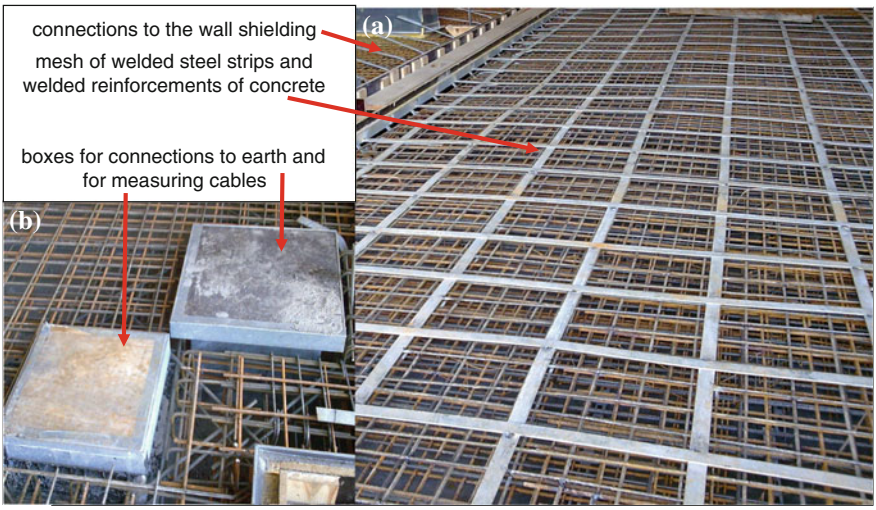

Fig. 9.16 Shielding of the floor of a HV laboratory. **a** Preparation of the shielding of the floor. **b** Earthing and connection boxes

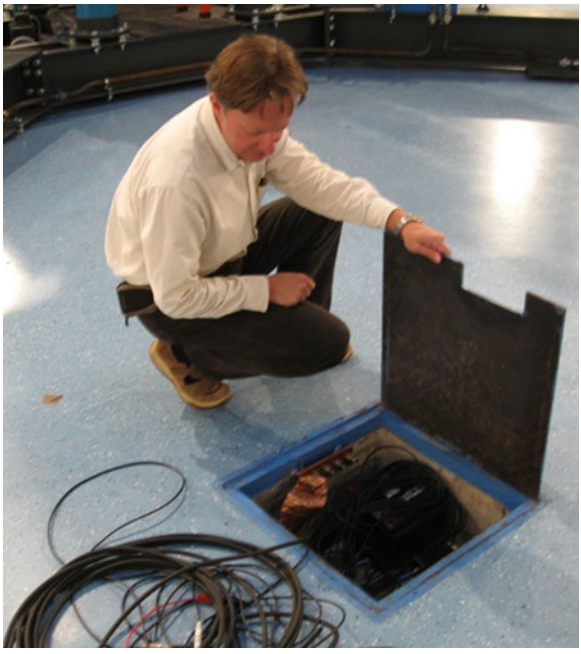

Fig. 9.17 Connection box with a measuring instrument (courtesy of HSP Cologne)

impedance and the PD measuring instrument in a box near to the coupling capacitor (Fig. 9.17).

The *shielding of the walls* shall enable multi-functions: In addition to the electromagnetic shielding, it shall be a heat isolation and a sound absorber. A perfect shielding of ≥100 dB up to 100 MHz—as usual for EMC shielding of computer centres and EMC test areas—is not necessary for a HV test room. The PD measurement according to IEC 60270 is usually performed at frequencies up to 1 MHz, and therefore, a damping ≤100 dB up to 5 MHz is sufficient for most laboratories. This can be reached with standard steel panels of two layers of galvanized steel (Fig. 9.18). The lower layer (Fig. 9.18a) carries the heat isolation (black, e.g. rock wool) which is at the same time the sound absorber. The upper layer is made of perforated steel panels and fixed to the lower panels (Fig. 9.18b, c). The panels of each layer among one another as well as of the two layers with each other should overlap and carefully screwed together for a reliable electric contact. Instead of screwing, welding of points every 50–100 cm is even more reliable.

The *shielding of the ceiling* (Fig. 9.19) may follow the same principle as that of the walls. But the ceiling usually contains panels of the heating system, the lighting system and the air conditioning (ventilation and aeration). The heating panels are also of steel and can be used as a part of the shielding. The shielding panels may be screwed or welded to the heating panels. For the lamps and the air conditioning, openings in the ceiling are necessary which must be covered by a wire netting of steel wires with welded crossing points (width of meshes <30 mm). Such a wire netting is also recommended for windows, for example of the control room or a visitor's gallery.

It can be recommended to design a shielding also for the *control room* (Fig. 9.8b). In that case, the shielding can be made of expanded steel under the plaster of walls and ceiling. The single sheets of expanded steel must overlap and be welded together. For windows and doors, the sheets should be welded to their metallic frames. The openings of the windows should be covered with glass and the mentioned wire netting which has to be welded to its frame. It is useful when also the power supply room is shielded (for details see 9.2.3).

The most sensitive and expensive parts of a shielding are the *shielded doors*. For very sensitive PD measurements, for example of extruded cables down to very few picocoulombs, special doors with metallic feeder contacts which are pressed to the frame of the door are available. In many cases, such doors are not required. Then, sliding doors of steel or roller shutter doors with metallic lamellae—both moving in overlapping frames—are economic alternatives.

It should not be forgotten that all supplies (water, compressed air, oil, etc.) entering into the test field and carrying the building ground must be isolated and inside connected to the shielding of the test room. Otherwise, they may carry noise signals into the shielded test area. Electric supplies must be filtered.

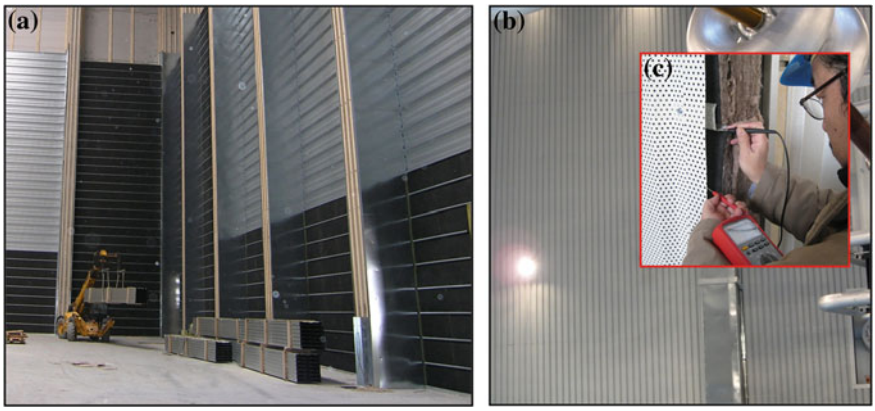

Fig. 9.18 Shielding of the walls (courtesy of HSP Cologne). **a** Lower layer carrying the heat isolation (*black*). **b** Upper layer of perforated steel panels. **c** Check of electrical contact

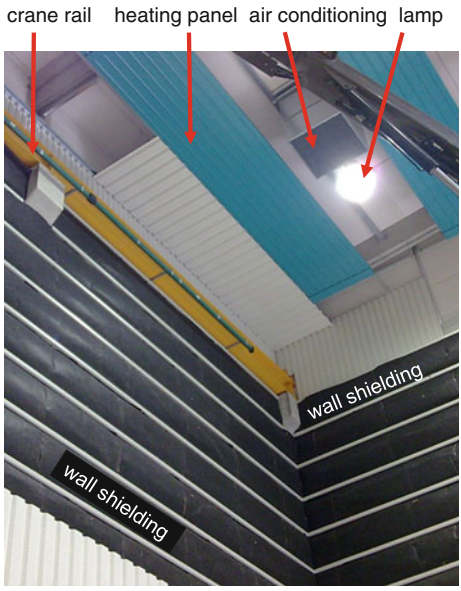

Fig. 9.19 Shielding of the ceiling including heating panels, lighting and air conditioning (courtesy of Siemens AG, TBD Dresden)

9.2.3 Power Supply and High-Frequency Filtering

The power for a complete HV laboratory is usually supplied from a medium-voltage network (Fig. 9.20). One or several three-phase distribution transformers in a nearby substation should be used for that purpose. Their ratings depend on the equipment to be supplied. One has to take into consideration the maximum required test power (active and reactive components), the supply power for control

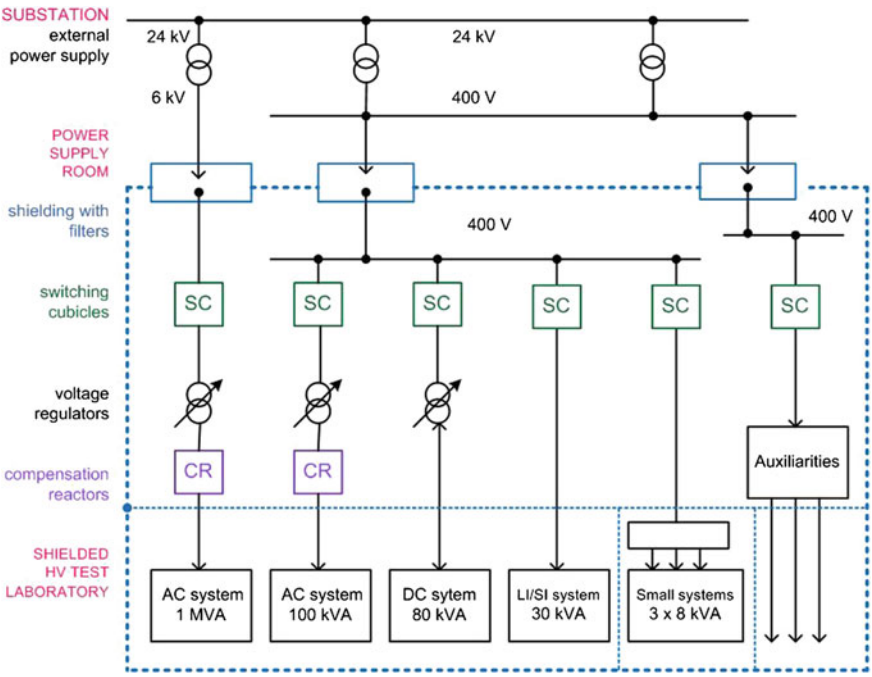

Fig. 9.20 Schematic power supply of a HV test laboratory

and measuring systems, the power for all auxiliary equipment (see Sect. 9.2.4) and an extra charge for later extensions.

Power cables connect this external power supply with the *power supply room*. This room should be arranged close to the HV test hall (e.g. Fig. 9.10) and should also be shielded in connection with the shielding of the related test room (Figs. 9.20, 9.21). The connection of the external power cables to the equipment for distribution and regulation in the power supply room is realized via high-frequency (HF) power filters attached to the shielding of this room (Fig. 9.22). The power control room contains the equipment explained in Sect. 2.2 (Fig. 2.5) for the "power supply":

- switching cubicles with main and operation switches, measuring equipment for primary voltages and currents, protection devices and control components (Fig. 2.8) like programmable logic controllers (PLC);
- regulators, one for each HV test system and
- compensation reactors and/or capacitor banks, to reduce the demand of external supply power.

  The size of this power supply room depends on the mentioned single components and their arrangement. The *HF-filter* consists mainly of a L-C network (Fig. 9.22a). Conducted noise signals of frequencies remarkably higher than the power frequency 50/60 Hz are blocked by the inductances and conducted to

Fig. 9.21 Shielded power supply room (courtesy HSP Cologne)

ground via the capacitances. The frequency characteristic of the HF filters shall be adapted to that of the shielding.

Note If the power supply room is not shielded, the HF filters must be attached between the regulators and the test generator at the shielding of the test room. Then, a separate filter is required for each test system and each of the auxiliary equipment. For the AC test system, even a larger filter is necessary because the compensation reactors are in the—unshielded—power supply room. The shielding of the power supply room simplifies the filtering and the wiring.

Communication lines—as long as they are not realized by fibre optic links—must also be filtered. As HF filters for power connection, also such for communication lines are available on the market.

9.2.4 Auxiliary Equipment for HV Testing

If accessories—as mentioned in Table 7.3—are used, consequences for the building design must be drawn. It might be necessary to have supply tubes for water, compressed air, etc. into the shielded area (test room(s), control room(s), power supply room(s)) from a machinery room or the unshielded outer areas; these connections must be isolated. This means that all metallic tubes must be interrupted by suited insulating tubes where they enter the shielding.

The size of the *artificial rain equipment* (see Sect. 2.1.3) must be adapted to the size of the largest HV equipment to be tested. This determines also the demand of water of the required conductivity, the water processing tank and the water

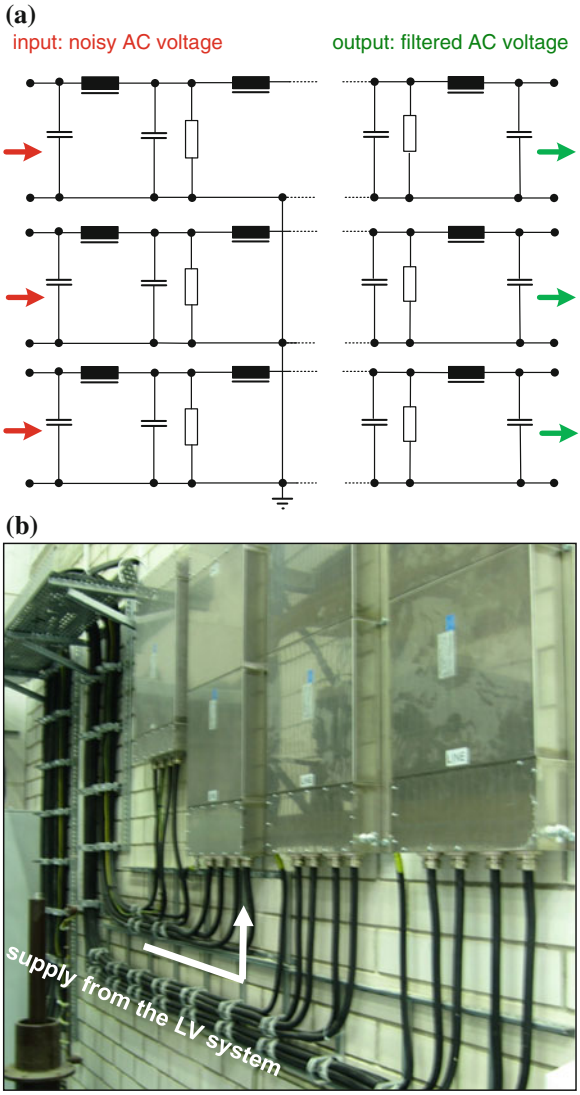

Fig. 9.22 HF filter for the power supply. **a** Principle circuit of low- and medium-voltage filters. **b** Arrangement of HF filters at the wall of an inside shielded power supply room (courtesy HSP Cologne)

connection from there to the rain equipment. Furthermore, the floor in the area of wet tests must be equipped with water drainage. This means it should have a certain slope which may come in conflict with the air cushion transportation system. At a too high slope, the air cushions with their load may run away by themselves. Therefore, no air cushion transportation in that area should be allowed or the slope must be very low. A slope below 1 cm/m might be necessary, but it must follow the instructions of the supplier of the air cushions.

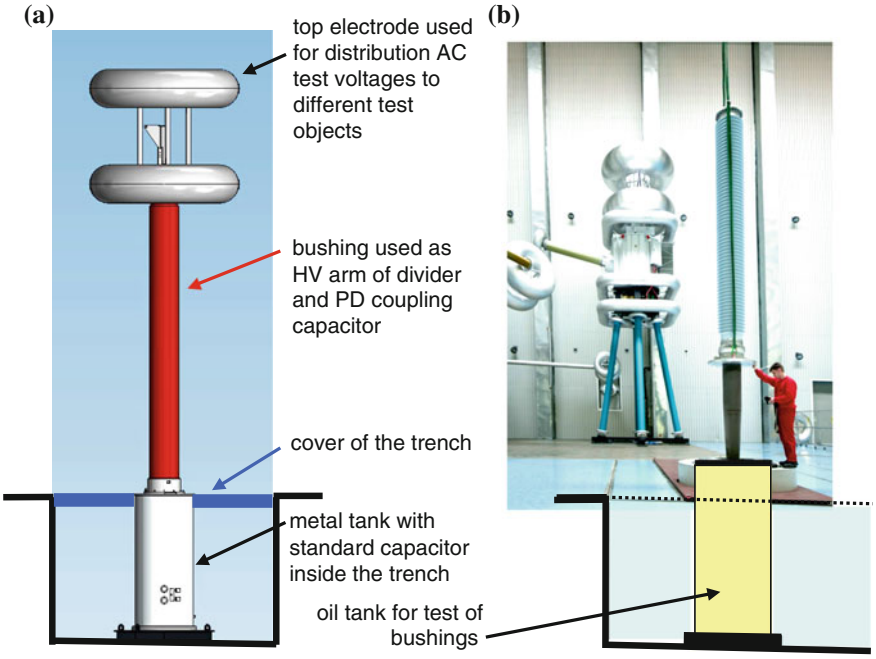

Fig. 9.23 Use of a trench in a HV laboratory. **a** Arrangement of a multifunctional capacitor. **b** Tank for testing bushings (courtesy HSP Cologne)

The pollution chamber must be equipped with a spray system, connections to water and compressed air, as well as drainage in the floor. The bushing for the pollution chamber must withstand the worst pollution conditions inside the chamber and therefore be well selected. Because the conductivity of the pollutant is controlled by salt and water, all materials used in the pollution chamber must be resistant to corrosion.

Using of a trench in a HV laboratory: *Tanks for insulating liquids*, usually for mineral oils, are necessary for testing transformer bushings and for R&D experiments on liquid-impregnated insulation structures. They are connected to oil (or liquid) processing units with related reservoirs outside the shielded area. It can be recommended to arrange the test tanks under the floor in a trench. Also other HV components can be arranged in a trench, especially when they include grounded tanks. This may even include test transformers or standard capacitors (Fig. 9.23). Figure 9.23a shows such an arrangement of a multifunctional capacitor which may even act as a central electrode for the HV laboratory. The trench must be carefully planned together with the floor shielding and the grounding system (see Sect. 9.2.2). All walls and the floor of the trench should be shielded. The tank should be isolated from the shielding of the floor. During a test, the tank is part of the test circuit and must be included into the ground return of the test circuit. If it is not used, it should be directly connected to the earthing system, but never to the

shielding system. The trench must be equipped with well-fitted covers which close the trench not only mechanically, but also close the shielding.

Tanks for compressed gases are used for testing bushings from air to SF_6 and for R&D experiments with gas-insulated structures. They are connected to gas processing units for conditioning the used gases. The arrangement of gas-filled test tanks is identical to those of liquids (Fig. 9.23).

Climatic chambers should be adapted to the principles described here for HV test circuits, grounding and shielding. The design of a commercially available chamber determines the necessary measures.

9.2.5 Auxiliary Equipment and Transportation Facilities

9.2.5.1 Lighting

Usually, HV test laboratories are designed without windows for natural light. Natural light might be useful in very special cases, e.g. when the room is also used for production or larger assembling work. Then, the windows must be supplied with a metallic frame connected to the shielding and covered by the above mentioned wire nettings with welded crossing points, also welded to the frames. Darkening of the windows should be possible.

Artificial *lighting*—the standard case—should be realized with incandescent lamps in all shielded rooms—and not with fluorescent lamps which may cause noise signals during sensitive PD measurement. For many observations and photographs, it would be helpful if the light can be dimmed. Because this is realized with a power electronic adjustment, another source of noise signals, the lamps should be outside the shielding behind wire nettings (Fig. 9.19). Preferably, the lamps can be arranged at the ceiling. A separate emergency lighting is necessary. The local requirements and safety rules have to be considered.

9.2.5.2 Heating, Ventilation and Air Conditioning

HV test equipment should be specified for a temperature range not smaller than between 10 and 35 °C; for the control and measuring systems, a minimum range between 15 and 30 °C is required. The installation of a comfortable *heating system* in a large HV test hall seems to be only necessary when the minimum temperature of 10 °C cannot be guaranteed for a longer period than few days per year. In opposite to that, it is recommended to have an air-conditioned control room with a temperature in the range of 20 °C. The power supply room requires no heating as long as the temperature remains above 5 °C. Small HV test rooms where HV test equipment and the control and measuring system are in one common room should be heated for an acceptable room temperature.

The experience of the last years has shown that an optimum heating system for a big HV test room is a radiant ceiling heating system which is used as a part of the shielding as described above (Sect. 9.2.2 and Fig. 9.19). Such radiant heating systems of quite large panels are usual for industrial buildings today.

For countries with tropic conditions or very high summer temperatures, a ventilation system for the test hall which uses low night temperatures for cooling the HV test hall may be sufficient. Smaller test rooms should be air-conditioned. When during a test, a larger amount of heat is generated, for example during heat run tests of transformers, a well-designed ventilation system has to transfer the heat to the environment (Fig. 9.19). This avoids an unacceptable temperature rise in the test room. The necessary ventilators are arranged behind openings (covered with wire nettings) of the shielding of the ceiling.

9.2.5.3 Transportation Facilities

One or two *portal cranes* covering the whole area of a large HV test hall guarantee its efficient use (Fig. 9.24a). This may come into conflict with HV components which could be fixed at the ceiling, for example voltage dividers, central electrodes or rectifiers. In some laboratories, this had been done; consequently a single-rail crane had to be applied (Fig. 9.24b; Prinz et al. 1965, courtesy of TU Munich). The comparison of the two solutions shows clearly that in minimum for industrial HV test laboratories, the portal crane is by far superior to the one-rail crane. With two or three portal cranes in one HV test hall, a compromise between the two solutions is reached. Fig. 9.25 (Krump and Haumann 2011) shows a test room with three cranes; the crane in the middle carries the large, PD-free connection electrode (1,200 kV rms.), between the central connection point and the test object, whereas the cranes of both sides are available for transportation and fixing of test objects. In addition to the portal crane, lifts with a single rope from a hole in the ceiling can be taken into consideration. They are for fixing a test object only during a test. Such lifts and hand-operated cranes are also useful in small test rooms.

The maximum load of a crane depends on the maximum load of a test object, in some cases also of the weight of the heaviest HV test component, whatever is heavier. For the small hand-operated cranes and lifts, a load up to 1,000 kg should be sufficient. It should be mentioned that transportation by air cushions can influence the maximum necessary load of a crane.

Air cushions are a very helpful tool for the ground transportation in a HV laboratory. On the one hand, they can be used for the generators and HV components (see Sect. 9.2.1), on the other hand for the transportation of heavy test objects as, e.g. power transformers or GIS. The air cushions replace the transportation on rails as it has been applied for generators or test objects in the past quite often. The rails interrupt the smooth floor and may even influence the optimum erection of test circuits. The ground transportation of smaller HV components can be made on wheels. Also transportation by the crane is often applied.

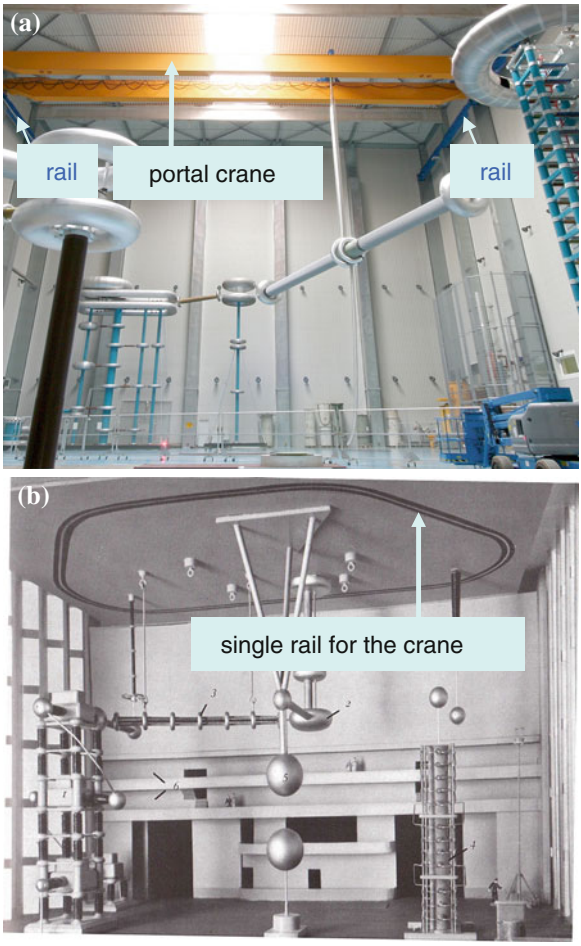

Fig. 9.24 Cranes in HV laboratories. **a** Portal crane (courtesy HSP Cologne). **b** Single-rail crane

Well-selected air cushions, usually arranged under the base frame of the generator, can carry up to the highest loads required for HV test systems. Number and size of the single-air-cushion modules depend on the load and the load distribution. But they require a well-levelled, smooth and stable floor. The surface can be a fine concrete, in most cases covered with a special epoxy resin. Air cushions can damage the floor if it shows gaps and cracks or is not smooth enough. Usually, the air pressure is 0.2 MPa, in special cases up to 0.4 MPa. It is recommended to order HV test equipment with frames and with the necessary stability suitable for air cushion transportation (Fig. 9.26). When the movement of air cushions suddenly stops due to an obstacle, the mechanic stress to the insulating supports, for example of an impulse voltage generator, is considerable.

Fig. 9.25 UHV laboratory with three cranes (courtesy of HSP Cologne)

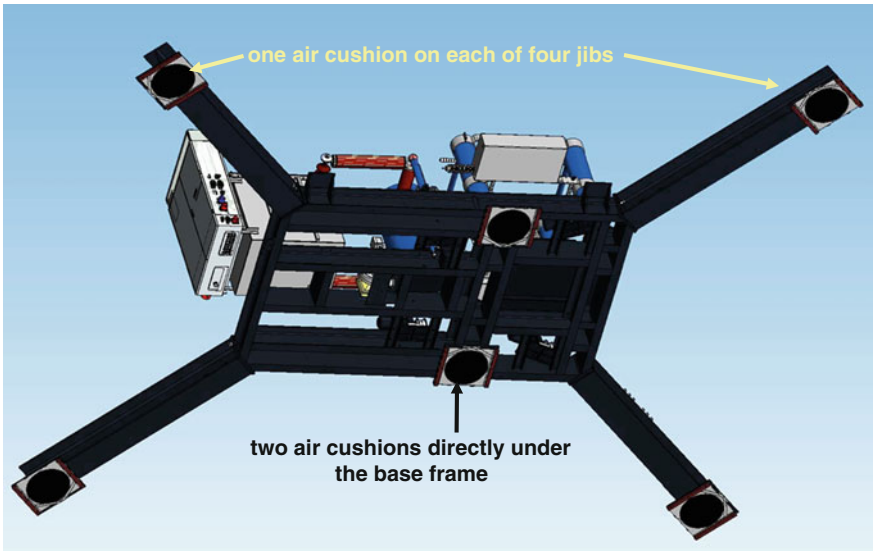

Fig. 9.26 Frame of a test generator with air cushions

9.2.5.4 Technical Media

The *electric power supply* is described in Sect. 9.2.3. In the single test and control rooms, a sufficient number of LV sockets should be arranged. This includes the sockets in the control desk or rack for instruments. Everywhere, sockets are necessary for electric tools, spot lights or additional instruments. Again, all electric power lines which enter shielded rooms must be filtered.

Data communication and *telephone* lines should be as far as possible realized by fibre optic links. They do not require filtering. All wire lines for communication must be filtered.

Compressed air is necessary for the air cushions (see Sect. 9.2.5.3), but also certain tools as well as pollution tests require compressed air. The necessary pressure depends on the local demand. The metallic tubes for compressed air must be isolated when they enter the shielded rooms.

A *water supply* is necessary for artificial rain and pollution equipment (see Sect. 7.2.4), for other special tests and for cleaning. Therefore, few water taps might be arranged in a big and only one in smaller test rooms.

Other technical media as oil and other liquids, SF_6 and other gases should be supplied via installed facilities if there is a permanent demand (see Sect. 9.2.4).

9.2.6 Safety Measures

High electric fields, generated by high voltages between energized electrodes and all earthed objects in the HV test rooms, are very dangerous: When the electric field exceeds the dielectric strength of the surrounding air, electrical discharges appear with currents up to kiloamperes. But the rate of accidents in HV laboratories is low, because the operators are conscious of the high risk when the "safety concept" is not carefully considered. The *safety concept* includes all technical matters related to the test laboratory as a whole and related to the single HV test systems as well as the instructions for the personnel. The latter includes the general behaviour in HV testing and the instructions for the operation of test equipment.

There is no special IEC Document on safety in HV test laboratories; the IEC Publication 62061:2005 is partly applicable to the control- and power-feeding equipment. IEEE Guide 510 recommends a practice for safety in high-voltage and high-power testing. There is also the European Standard EN 50191 (2005) on the erection and operation of electrical test systems. The hints in this subsection cannot release the users from applying these internationally accepted documents, standards and special national rules. Also the instructions and hints of the suppliers of HV test systems shall be considered.

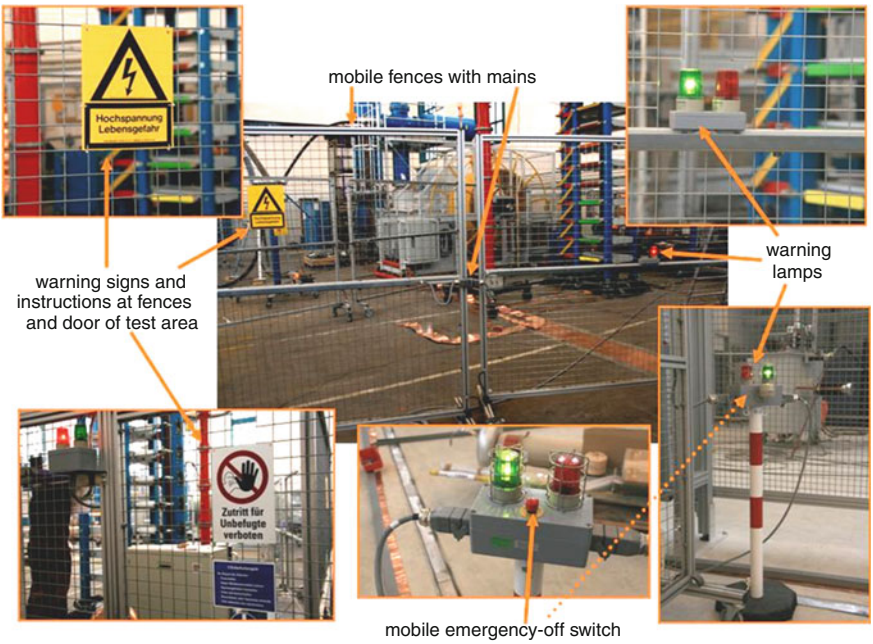

Fig. 9.27 Safety fences with warning signs and lamps, safety loop and emergency-off switch

9.2.6.1 Safety in HV Test Fields and Areas

A *HV test field* is a room with one or several fenced-in *HV test areas* and related control areas, completed by a power supply area. A *HV test laboratory* may contain several HV test fields (Fig. 9.10). The basis for the safety of a whole test field is its correct grounding and shielding as described in Sect. 9.2.2. The recommended *current return* of a test circuit is only connected at one point to the grounding system. In special cases, the grounding system may be used as the current return. The shielding shall never be used as a current return.

In a HV test area, the safe *clearances* (see Sect. 9.1.3) of HV components to the walls, the fences or the ceiling as well as to earthed or energized objects in neighbouring fenced-in test areas shall be selected according to the maximum test voltages which can be generated there. If several fenced-in test areas are in one test field, metallic *safety fences* with a minimum height of 2 m and a maximum mesh size of 4 cm shall be applied. The single elements of the fence shall be electrically connected to each other and connected to the earthing system only at one point. A complete loop of fences shall be avoided. If the HV components in a test area are rearranged, interactions to neighbouring fenced-in areas must be considered (Fig. 9.27).

The HV test area must be marked from outside by a *warning sign* and by *warning lamps* indicating the condition within the area: The "red" light indicates

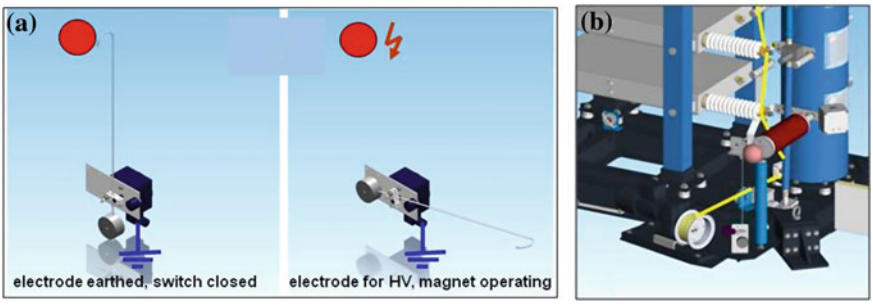

Fig. 9.28 Earthing equipment. **a** Earthing switch (earthing by gravity). **b** Earthing rope with motor drive

the HV test circuit is degrounded and possibly energized. The "green" light means the HV test circuit is grounded, the area is safe for entering (see Sect. 7.2.6.3). Warning signs must be arranged at all doors into the test area. In addition to the signs and lamps, the test area must be equipped with a safety loop and emergency-off switches.

A *safety loop* is a ring main integrated into the walls, fences and doors of a test area. The loop must be closed, before the test system is degrounded and energized. Contacts at the door shall ensure that the loop is closed. As soon as the loop is opened anywhere, the emergency-off switch has to operate (see Sect. 9.2.6.2). *Emergency-off switches* shall be large, red pushbuttons mounted preferably on a yellow background at the related control desk or rack, near the doors of the test areas and in observation areas. The actuation of an emergency-off switch results in the operation of the power (main) switch and operation switch of the relevant HV test system. It has to be checked whether also all HV sources of the whole test field shall be switched off. It should not deenergize the lighting system (in minimum an emergency lighting must remain).

Control and observation areas are outside the test area and its safety loop. Both shall be equipped with warning signs and lamps and emergency-off switches. For the power supply room, the relevant national regulations for the erection of electrical substations shall be applied.

9.2.6.2 Safety of HV Test Systems

There is a close connection between the safety system of a HV test area and that of the related HV test system. Both work together, and if the first fails, the second cannot operate. Therefore, a safety check of the related safety equipment should precede each test.

A HV test generator is energized in two steps: first, the power (main) switch supplying the energy from the grid up to the power supply unit, and then, the operation switch connects the generator (see Sect. 2.2). The two switches are part of the safety concept of a HV test system (Fig. 3.1).

Table 9.4 Survey of inspections of the safety equipment

Inspected equipment	Inspected component	Reference	Interval of inspections
Earthing system of the test area	Grounding resistance; earth connection boxes	9.2.2 Measurement of the ground resistance	<5 years
Test systems	earthing bars, switches and ropes	9.2.6.1 Safe connections	<1 year Observations before each test
Safety equipment including controls	Safety loop, signal lamps, emergency-off switch	9.2.6.1	Check before each test

The earthing of the HV test circuit shall guarantee a safe stationary operation, whereas the earth return has to minimize transient phenomena, e.g. after a breakdown of the test object (see Sect. 7.2.2). If not in use, the HV components must be discharged and permanently grounded. For that, they are equipped with *discharging switches* and *earthing switches*. The switches (Fig. 7.28a) can be realized by earthed rods with an electric or hydraulic drive. They open the grounding when the main switch is switched on. They close the earthing, e.g. by gravity or by a spring, when the power switch opens and the voltage is off after a test or an emergency off.

Earthing ropes (Fig. 7.28b) consist half of a flexible metallic cord and half of an insulating rope. In case of grounding the HV component, the metal rope connects the HV electrode and all intermediate electrodes with the earthing system. In case of HV potential at the component, the metallic rope is replaced by an insulting rope. Both ropes are moving by a motor drive. One should look for reliable earthing ropes; otherwise, they might become the weak point of the equipment.

Earthing bars for manual operation (Fig. 6.14) are often applied for smaller HV test systems. They are from insulating material with a handle at one side and a hook at the opposite site. The hook is connected to the earthing system by a flexible cord. It is recommended to arrange earthing and discharging bars at the door to the test area not to forget their application after a HV test.

Capacitors are charged during operation, keep the charge—at least partially—after switching off the test system and must be discharged, shorted and earthed, also when they are not in service. The discharging is performed by resistors in series with earthing bars, earthing switches and earthing ropes.

The *control* of a HV test system realizes not only the HV test procedures, but activates also the *safety functions*. This includes the interactions between position of the power switch and the operation switch with the status of the safety loop, the signal lamps and the earthing equipment. Furthermore, the control system shall react in case of breakdown of the test object, opening of the safety loop or emergency-off application. All these functions must be periodically checked according to the relevant instructions of the supplier of the test systems. Table 9.4 shows a timetable for such instructions as a brief example.

9.2.6.3 Operation of HV Test Systems

A HV laboratory should have a "*safety concept*" which describes the mentioned safety measures for test fields, test areas and test systems. Furthermore, it should include the following *safety instructions* for operating HV test systems and also the list of necessary inspections of safety-relevant equipment (Table 9.4). On the basis of the safety concept, the personnel should be instructed about the danger at HV tests according to national rules, but at least annually.

Before a HV test starts, the test engineer should take the following actions:

1. Final check of earth connections and clearances of the test set-up!
2. Check that no other personnel is in the test area, take off all manually operated earthing devices!
3. Close the safety loop!
4. Switch on the control power for the control and measuring system (green lamps "on")!
5. Switch on the power (main) switch (red lamps "on")!
6. Warn by horn and loudspeaker "Attention, high voltage is switched "on" (automatic earthing "off")!
7. Switch on the operation switch and start the test.When a test is terminated the following should be done:

1. Reduce the voltage to a level <50 % or to zero!
2. Switch off the operation switch (automatic discharging and earthing moves to "on", also red lamp still "on".)!
3. Switch off the power (main) switch (red lamp "off", green lamp "on")!
4. Open the safety loop and perform the manual discharging and earthing, if necessary!
5. Switch off the control power, the test system is out of operation (green lamp "off")!

The described steps of operation shall also be part of the instructions for the personnel working in the HV laboratory. The instructions shall include all international and national rules on safety in electrical testing, the information of the supplier of the test systems and the own experience. The instructions may include demonstrations in the laboratory. They should be performed in minimum once a year and shall be recorded.

9.3 Outdoor HV Test Fields

When an *outdoor test field* completes a traditional "indoor" laboratory (compare Fig. 9.10), the test voltages might be transferred to outside via bushings or big doors. Even complete HV test systems can move on air cushions to the open-air test area. Outdoor test fields are usually equipped for research and development of

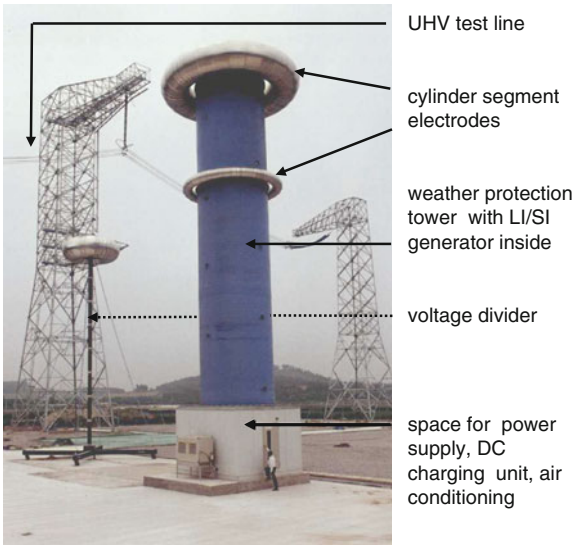

Fig. 9.29 Outdoor impulse voltage generator 4,000 kV/ 400 kJ (courtesy KEPRI Korea)

EHV and UHV overhead transmission lines including the related open-air substations. In most cases, they are connected to test lines of some hundred metres length to test the design of towers, the arrangement of the conductors or to measure corona losses.

The HV test systems are placed on a concrete area which gives also space for tests on substation equipment. This area may be applicable for air cushions (see Sect. 9.2.5.3) and should be well connected to roads for the transportation of test objects. Transportation and assembling work must be done by mobile cranes. The HV test systems placed outdoor have a special design for the local climatic situation. Sometimes, the local conditions are the reason to have an outdoor test field, e.g. on high altitude to perform tests under low air density. Pollution of the test systems is a challenge which needs both good design and permanent maintenance.

For LI and SI voltage testing, impulse generators of more or less indoor design are arranged in an insulating tower for weather protection (Fig. 9.29). The air inside such a tower is conditioned to avoid dew on inner surfaces due to too low outer temperatures. Also too high inner temperatures shall be avoided. The rated voltage of outdoor impulse generators exceeds usually 3 MV.

For AC voltage testing, metal-tank transformers (see Sect. 3.1.1) are well suited for both single-transformer application and transformer cascades (Fig. 9.30). They have proven high reliability for that application, because the design uses the experience with power transformers. The rated voltages of AC test systems are usually above 1 MV.

For DC voltage testing on test lines, quite powerful generators (of rated voltages up to 2 MV and currents of several 100 mA) are required (Fig. 9.31). It is very difficult to design the outdoor DC insulation of such HV test components.

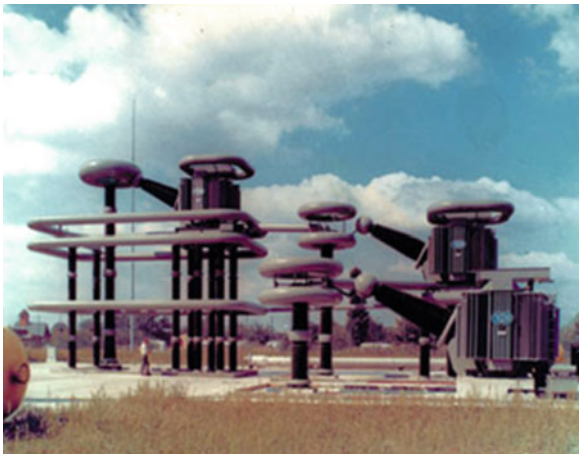

Fig. 9.30 Outdoor transformer cascade 1,800 kV/1.25 A (courtesy of Siemens AG, Berlin)

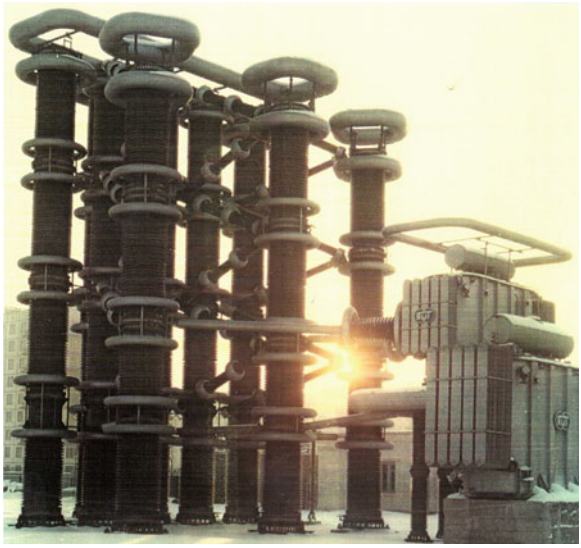

Fig. 9.31 Outdoor DC generator 1,300 kV/1 A

The safety measures in outdoor laboratories may follow the principles described in 9.2.6, but have to consider the broad range of atmospheric influences as temperature, humidity, rain, snow, ice, sandstorm, etc. This requires larger clearances. The earthing system of an outdoor laboratory can be made as for indoor laboratories (see 9.2.2), but the steel reinforcement of the concrete should be welded and used—in addition to earthing rods—as an area earthing, no isolation from the soil should be made. It has to be connected to the earthing system of the indoor laboratory only at one point.

9.4 Updating of Existing HV Test Fields

The erection of a new HV laboratory is a big investment. The updating (sometimes also called upgrading or refurbishment) of an existing test field is often an economically and technically acceptable alternative to a new test laboratory. In the simplest case, it is related to the replacement of complete HV test systems, the addition of new or the exchange of old components. The updating of existing HV test rooms is often more difficult. Viewpoints for updating existing HV test fields are given in the following. Generally, the updating of existing HV test fields shall follow the principles described in this chapter for new test fields as far as possible (see Sects. 9.1–9.3).

9.4.1 Updating of HV Test Systems

The lifetimes of HV and power components are usually higher than those of the components of control and measuring systems. Sometimes, also regulating transformers or thyristor controllers have a shorter lifetime than generators for high AC, DC or impulse voltages. Therefore, updating is often related to the control and measuring units. It cannot be recommended to replace only some of these components and to operate with a mixture of new and old control and measuring instruments. The control and measuring system should enable easy and reliable control, safe data recording and evaluation, communication within local data networks and remote service as shown in Fig. 2.8 and described in Sect. 9.1.4. The necessary interfaces between digital control and measurement systems and the components of the power circuit should be individually established depending on the design and age of the equipment to be refurbished.

If a new HV test system—possibly of higher rated voltage—shall be arranged in an existing laboratory, necessary clearances must be taken into consideration (see Sect. 9.1.3). In case of limited clearance between HV components (generator, divider, connections, etc.) and neighbouring grounded or energized objects, the application of larger control electrodes can be taken into consideration. This requires the calculation of the conditions of the electric field between the HV components and their surroundings. Additionally, the necessary clearance for test objects must be guaranteed (Fig. 2.1). To save space in the test area, tank-type test transformers and reactors can be arranged outside with their HV bushing into the test room (Fig. 9.21). For the safety requirements, see Sect. 9.2.6.2.

9.4.2 Improvement of HV Test Rooms

The safety system has to follow the principles explained in Sect. 9.2.6.1 completely. Any reduction in the safety requirements is not acceptable. When auxiliary

Fig. 9.32 Shielded cabin in a routine test field

equipment (Sect. 9.2.5) is modified or improved, the reliable operation of the test systems including the necessary sensitivity of PD and dielectric measurement must not be influenced: Clearances should sufficiently be maintained, and shielding effects should not be reduced.

Most expenditure is necessary to improve the grounding and shielding of a HV test field. This is often necessary because withstand tests are more and more completed by sensitive PD and/or dielectric measurement. Often, an unshielded test room is not longer sufficient for these monitored withstand tests. Then, consequences for filtering the supply power, for shielding and improved grounding become unavoidable.

Usually, old grounding rods are corroded and must be replaced to reach an effective ground resistance of the order of 1 Ω. The grounding should be independent from the shielding (Sect. 9.2.2), but in older test fields, the grounding is realized by a combination of earthing rods and an area grounder covering the whole test field area. This means grounding and its shielding are combined in the floor. It should be investigated whether it is necessary to separate grounding and shielding in the floor (Sect. 9.2.2) or not. The shielding of the floor is not as important as that of the walls and the ceiling, which shall be performed as described above (Figs. 9.18, 9.19). If the floor grounding is considered to be necessary, one had to put an insulation foil over the area grounder, followed by a suited metal mesh or metal panels forming the floor shielding and a protection layer, usually of concrete with an upper layer of epoxy resin for air cushion transportation.

In some cases, it should be considered whether the shielding of the whole test field is necessary or the application of a shielded cabin (Fig. 9.32) is sufficient. Inside such a self-carrying cabin the lowest PD noise levels can be reached. If the

space of such a commercially available cabin is sufficient, no expensive shielding of the whole test area is required. A similar effect can be reached with a metal-enclosed test system (Fig. 3.41). A perfect shielding must be completed with a perfect filtering of all voltages penetrating into the shielded area (Sect. 9.2.3).

Chapter 10
High-Voltage Testing on Site

Abstract High-voltage (HV) tests and measurements are applied for two different reasons on site: When new equipment or systems are finally assembled on site, a quality acceptance test, usually a HV withstand test (more and more completed by PD or dielectric measurements), is required to demonstrate the necessary quality and reliability for commissioning. This test completes the quality tests in the factory and should follow their philosophy based on insulation coordination. The aim of the second group of tests on service-aged equipment, the so-called diagnostic tests, is related to the condition assessment of insulation for the estimation of the remaining lifetime. For diagnostic purposes, usually a set of tests and measurements is performed. HV tests after repair are in between the two, because the repaired part is new, but the other insulation of the equipment or system is service-aged. After a consideration of the general requirements to HV test systems used on site, the applied test voltages according to IEC 60060-3: 2006 are introduced. The chapter is closed with examples for both, quality acceptance withstand tests and diagnostic tests on site, for compressed-gas-insulated equipment (GIS), cable systems, power transformers and rotating HV machines.

10.1 General Requirements to HV Test Systems Used on Site

10.1.1 Quality Acceptance Tests

High-voltage (HV) testing is not only related to tests in a factory. The whole life cycle of insulation is accompanied by HV tests (Fig. 10.1). The quality of equipment and systems which are finally assembled on site is carefully verified by quality acceptance tests of their components in the factory. These HV withstand tests are completed by quality acceptance tests on site, which verify the sufficient quality of both, transportation and on-site assembling, for reliable operation. All

W. Hauschild and E. Lemke, *High-Voltage Test and Measuring Techniques*,
DOI: 10.1007/978-3-642-45352-6_10,

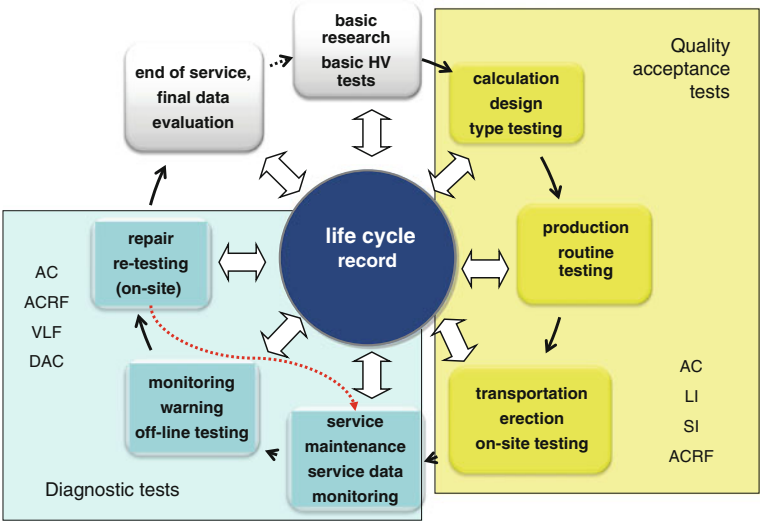

Fig. 10.1 HV tests and measurements in the life cycle of equipment

quality acceptance tests shall follow the same principles that the test voltages shall represent stresses in service and shall be well reproducible. After successful tests (Fig. 10.1, yellow area), the equipment can be commissioned and handed over from the supplier to the user.

The user of the equipment may arrange the *in-service monitoring* of the insulation (Cigre TF D1.02.08 (2005)), e.g. by online, non-conventional PD measurement using built-in sensors. The *monitoring* applies to the trend of suited parameters (possibly the combination of different PD measurands) for the condition assessment. If an indicator value (combination of parameters) reaches a magnitude for warning, an off-line *diagnostic test* might be useful for the identification and location of the defect. The diagnostic test should repeat some principles of the quality test, but this is not absolutely necessary. It should include a set of measurements at different test voltage levels and should be able to deliver information about the endangering of the insulation by a detected defect. The off-line diagnostic test with an external voltage source enables measurements at different voltage levels including the determination of inception and extinction voltages. Therefore, it delivers more information than the in-service (online) monitoring. Nevertheless, both monitoring and diagnostic tests complete each other and play a common role for *condition assessment* (Fig. 10.1, blue area).

It is very useful to compile all tests and checks on a cable system in a HV grid and its components in a "*life cycle record*" (Fig. 10.1). This record supplies information on trends of diagnostic indicator values. Quality acceptance tests and diagnostic tests have developed during the last 20 years quite independent on each other. It seems to be necessary to overcome this difference and to consider all HV

tests with one general view based on the physical phenomena and the requirements of the practice.

The *insulation co-ordination* (see Sect. 1.2) of the insulation of the components of a power system shall guarantee its reliable operation as well as the protection of the operating personnel and important equipment. This is realized by protection levels of protecting devices (arresters) and test voltage levels for the equipment. The diversity of defects in insulations prevents to establish general equivalence between different test voltages. ***Therefore, the used test voltages shall represent typical stresses in service*** (Hauschild 2013). This principle is the basis for the verification of insulation coordination by test voltages. Consequently, it is also mandatory for quality testing on new equipment including quality acceptance test in the field (Fig. 10.1, yellow area). The typical stresses in service, and the related test voltage according to horizontal standards, are explained in Sects. 1.1 and 1.2. Test voltages for field tests have wider tolerances than those for laboratory tests.

The following general requirements to test voltages for quality acceptance tests are well considered for many years:

(a) Test voltages shall represent stresses in service.
(b) Test voltages shall be reproducible within defined tolerance limits for their parameters. The tolerances reflect both the feasibility of the test voltage generation and the dispersion of real stresses in service.
(c) All quality acceptance tests shall be comparable to each other, because the different tests are related to the common system of quality control.
(d) Quality acceptance tests require a clear pass/fail criterion and a comparable test procedure. The results of "direct" withstand tests do not require explanations, and an "indirect" test based on a measurement requires a limit which has to be agreed in a standard or a contract.

Withstand tests on non-self-restoring insulation require a detailed consideration:

The test voltage value and the test duration should be selected in such a way that a healthy insulation (Fig. 10.2a, green line) is not influenced, whereas one with a serious defect breaks down (orange line). It seems to be wrong to slander a withstand test as "destructive". If there is a defect which is dangerous for operation, then the test object should break down. For example, a failure of a cable system with an internal defect is even welcome during a withstand test and much better than one during service. A withstand test of service-aged cable systems may take potential lifetime. To indicate that a withstand test has not harmed the insulation, it should be combined with the measurement of a suited measurand, e.g. PD's or tanδ. The principle of such a *PD-monitored withstand tes*t procedure is shown in Fig. 10.2b (Cigre TF D1.33.05 2012).

The "upwards procedure" of a PD-monitored withstand test should start on a voltage step which shall be PD-free (operational voltage or slightly above) and goes up with another two steps to the withstand voltage level. Also, at that level, a PD measurement is recommended. Then, the "downwards procedure" repeats the same voltage steps in opposite sequence. In addition to the withstand test and PD pass/fail criteria, the comparison of the PD characteristics at identical voltage steps

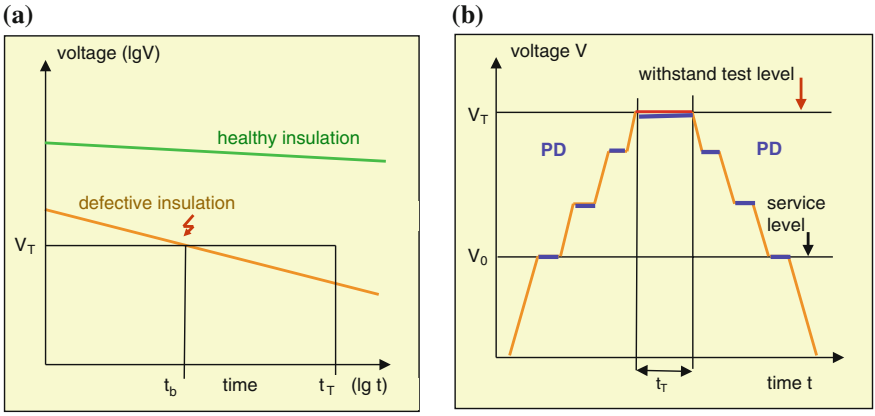

Fig. 10.2 Background and procedure of a PD-monitored withstand test. **a** Lifetime characteristic (schematically). **b** Example of the procedure for a monitored withstand test

before and after the withstand level completes the information on the condition of the test object. It is an indication that the withstand test has not damaged the equipment or system under test, when the PD characteristic of the "downwards procedure" is very similar to that in the "upwards procedure".

A quality acceptance test is always connected with important decisions. For example, a successful type test is the technical condition for starting the production of a HV component. A new equipment or system must pass the quality acceptance test on site before it can be handed over to the user. This means that also the quality acceptance test justifies the fulfilment of a contract.

10.1.2 Diagnostic Tests

Diagnostic tests are performed for condition assessment with the aim to estimate the remaining lifetime of the tested equipment or system. The result of such a test is the classification of the test object according to their performance, for example to the classes

"safe and reliable",
"keep under observation",
"insufficient, repair or replace".

This cannot be done by a single withstand test, and it usually requires a set of tests and measurements and the consideration of the trend of the related data according to the *life cycle record*. These may be PD measurements of different characteristics at different voltage levels, e.g. inception and extinction voltages, apparent charge or repetition rate (IEEE Guide P400^{TM}-2012). PD measurements

deliver information about weak points in the insulation. When methods of dielectric response are applied, one gets an overall—or integral—condition assessment of the cable system. Such methods are measurements of the dissipation factor, of polarization/depolarization current, of leakage current or of recovery voltage (IEEE Guide P400™-2012). Also, monitored withstand tests as described above (Fig. 10.2b) may deliver valuable information. The service-aged insulation should be stressed with test voltages higher than the operational voltage, but lower than the test voltages before commissioning.

In opposite to the mentioned quality acceptance tests, there are no general rules or standards when diagnostic tests and measurements must be performed. The related decisions are a matter of the users of the equipment or systems. Decisions for diagnostic tests may be made

- according to fixed time schedules,
- after a certain increase in defects,
- after certain overload of the cable system,
- after a warning from the monitoring.

If a system has been repaired or sections or components are exchanged, the quality of the repair or extension work should be tested. The problem for the test is the service-aged part of the system which cannot simply be stressed as a new one. In such cases, also principles of diagnostic tests might be applied to avoid an overstress of the service-aged part. Only if the considered equipment is relatively new, a quality acceptance test as described above can be recommended.

10.1.3 Overall Design of Mobile HV Test Systems

The overall design of a mobile HV test system has to consider the set of criteria listed in the following:

The selection of appropriate test voltages has the highest priority. The selected test voltage influences the mechanical design and the power demand remarkably. For quality acceptance tests, they should be related to the test voltages required by insulation coordination. For diagnostic tests, they should be selected in conjunction with measurements which are efficient for condition assessment.

Weight and compactness of the HV test system are important for the optimum *weight-to-test power relation* of the system, for the acceptable size for transportation and for arrangement at the site of the test.

Bothtransportability and *assembly* influence the handling of the test system. It shall be equipped with accessories for transportation, robust against mechanical shocks and well protected against environmental conditions which may endanger the function of the test system (rain, snow, ice, very low and very high temperatures, sand storms, etc.). There should be few assembling work on site until the test system is ready for tests. Smaller test systems—ready for the connection of the test object via a shielded cable—can be arranged inside a van, trailer or container

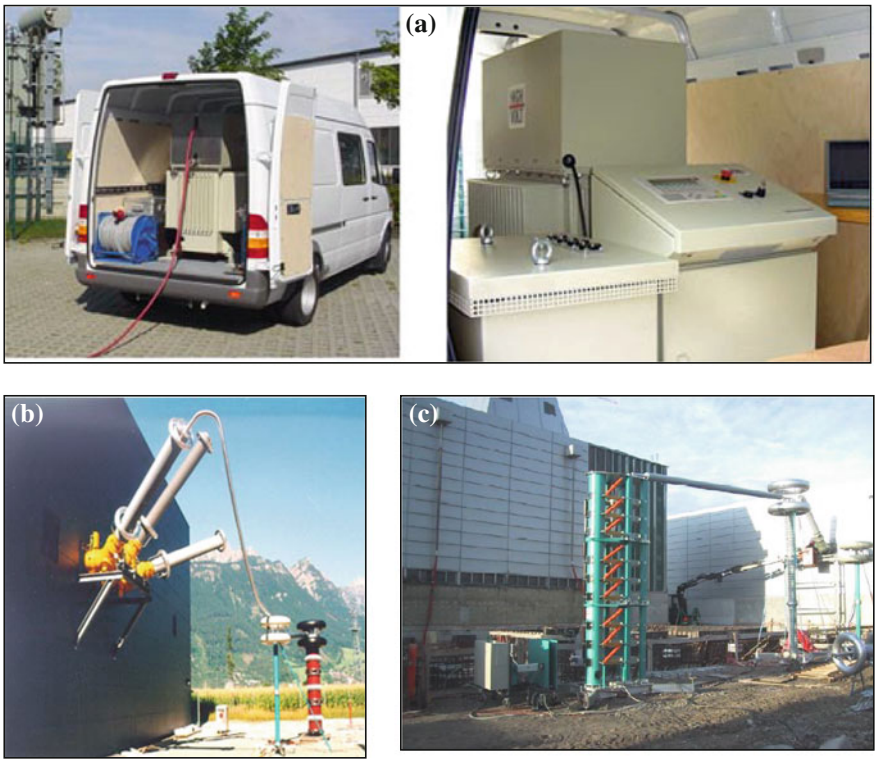

Fig. 10.3 Principle design of HV on-site test systems. **a** Outside and inside view of a van with an ACRF test system for distribution cables. **b** Assembled ACRF test system with three modular reactors. **c** Assembled impulse test system for 900 kV cumulative charging voltage and 1,600 kV OLI output voltage (Courtesy of Siemens AG, Berlin)

completely (Fig. 10.3a; see Sect. 10.2.1.1). The HV components (exciter transformer, reactor, voltage divider) of the shown ACRF test system are metal-enclosed to fulfil the safety requirements. Heavy and large systems—as, e.g. for testing HV and UHV cable systems—are arranged on a trailer (Fig. 10.4). The total weight of HV test system, trailer and truck must not exceed the permitted value for roads (e.g. in Europe 42 t) to avoid special transportation. A second possibility is the use of components which can easily assembled on site. Figure 10.3b shows an ACRF test system with three modular reactors and a separate voltage divider. Figure 10.3c shows a test circuit for OLI voltages (see Sect. 10.2.1.3), consisting of a DC charging unit, three generator modules for 300 kV each, the HV inductance connecting the generator to the last component and the voltage divider/basic load capacitor.

The power demand for testing shall be an optimum relation between the reactive test power and the active power demand from a voltage source. Considering the capacitive load of the test objects, this can be established by the

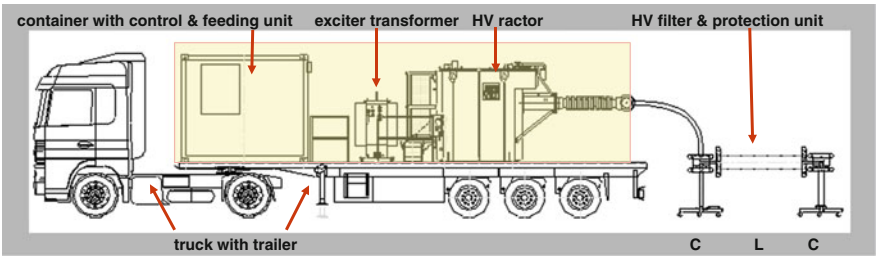

Fig. 10.4 Mobile ACRF test system for HV and EHV cable systems

application of oscillating circuits and the principle of resonance. When the power supply on site is a *Dieselgenerator set*, it must be considered that it is not a "stiff" source. Its rated power should exceed the necessary active power remarkably.

The control and measuring system of the HV test system should be easy to be handled. A computer system is recommended. In case of unexpected events, e.g. breakdown of the test object, failure of the test system and interruption of feeding power, this would save all data of the test and all measuring results.

Between the mentioned technical requirements, a compromise must be found for the selection of a suited HV test system. It cannot be expected that one system is optimum for all rated voltages and all kinds of off-line tests, especially when the cost is taken into consideration, too.

10.2 Test Voltages Applied on Site

Whereas the test voltages for quality acceptance tests shall be related to the other quality tests, test voltages for diagnostic tests do not require such a stringent selection. The priority is the interpretation of the set of results based on knowledge rules for the applied voltage. Therefore, additional special voltages can be applied. The following chapter considers test voltages for field testing as described in the relevant IEC Standard 60060-3: 2006 or in the IEEE guide P400^{TM}-2012.

10.2.1 Voltages for Withstand Tests

10.2.1.1 Alternating Voltage of the Power Frequency Range (HVAC)

AC voltage of power frequency (see Chap. 3) is considered as the most important test voltage, especially if the withstand test is PD-monitored. Therefore, it serves as reference for many test voltages applied in the field. Power frequency test

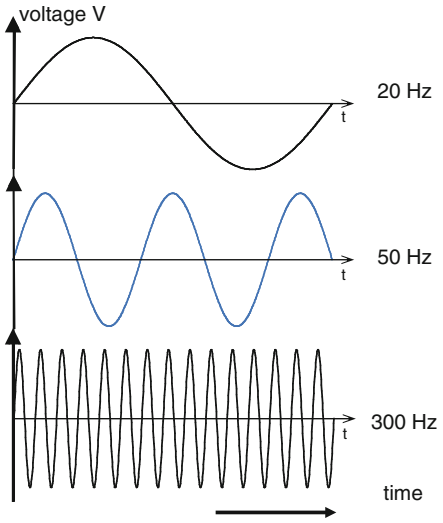

Fig. 10.5 AC voltages for on-site tests of extruded cable systems

voltage for laboratory testing is defined with a frequency range from 45 to 65 Hz (IEC 60060-1:2010). For field testing, AC voltages are often generated by mobile, *frequency-tuned resonant* (*ACRF*) *test* systems because of their much better weight-to-test power relation (see Sect. 3.1.2.4). That is why for on-site testing, a much wider frequency range and wider tolerances are accepted by the relevant IEC 60060-3:2006:

Test voltage value	Peak/$\sqrt{2}$
Test voltage frequency	10–500 Hz
Tolerance of test voltage value	±3 % up to 1 min ±5 % for >1 min
Relation of peak to rms value	Within $\sqrt{2} \pm 15$ %
Uncertainty ($k = 2$) of	
Peak value measurement	5 %
Frequency measurement	10 %

The single apparatus committees apply reduced frequency ranges; for example, the range 20–300 Hz (Fig. 10.5) is recommended for field tests on cable systems (IEC 62067: 2011; IEC 60840: 2011). Numerous practical field tests show that the test frequency remains in the quite narrow range between 30 and 100 Hz very often. It shall be demonstrated that the application of AC test voltages of the power frequency range is very important.

As an example, Fig. 10.6 (Schiller 1996), (Gockenbach and Hauschild 2000) shows withstand voltages of models of *extruded cable insulation* depending on the frequency. The red line represents the withstand voltage of a technical perfect insulation, whereas the blue line characterizes heavy artificial defects. Real defects in extruded cable insulation cause withstand voltages between the two lines. Each

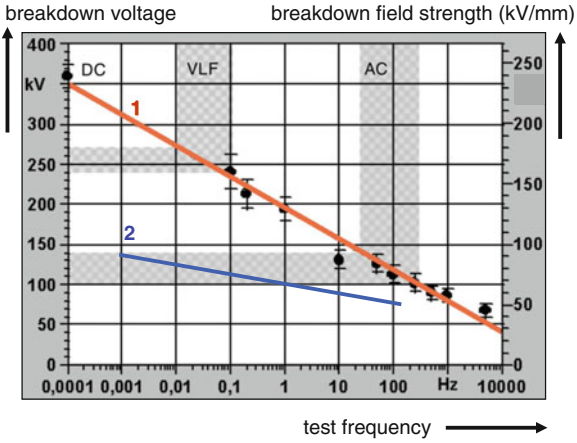

Fig. 10.6 Withstand voltage of XLPE cable models and test frequency (*1*) without artificial defects and (*2*) with artificial defects

type of defect influences the breakdown process in a different way. This prevents the application of a general equivalence factor between two different test frequencies. The deviations between the breakdown voltages at 20–300 Hz and at 50/60 Hz remain in an acceptable small range <10 % (Fig. 10.6, hatched area: "AC"). Also, PD patterns are very little influenced by the frequency in the usual frequency range (Fig. 10.7; Schreiter et al. 2003). This is the reason for the wide and successful application of AC voltages of variable frequency for quality acceptance tests of HV and EHV cables in the field for more than 15 years.

As a second example, the on-site testing of *SF_6-insulated switchgear (GIS)* shall be considered. Their most dangerous defects are *free-moving particles*. Figure 10.8 (Mosch et al. 1979) shows the motion of such particles in a horizontal coaxial model at different voltages: At DC voltage, the particle lifts off and reaches immediately the inner electrode. Then, a nearly regular motion between the electrodes is observed, which causes the breakdown when the position of particle is near to the inner electrode at a sufficiently high voltage. The LI voltage is too fast for causing any motion of the particle. Even at SI voltage, the mechanical motion of the particle is so slow that it reaches the inner electrode only when the voltage has been reduced to zero. A realistic motion of particles is only caused by AC voltage of the power frequency range. Because of changing the directions of the electric field, the particle changes also the direction of its motion. The particle is hovering and may cause the breakdown only if it touches the inner electrode. Whereas particles cannot be detected with LI and SI test voltages, a DC test would detect particles which are never dangerous in service. This confirms the principle that the only efficient tests can be made with AC voltages representing the power frequency voltage.

For the generation of AC voltages on site, the principles explained in Sect. 3.1 can be applied (Fig. 10.9). When testing capacitive objects <0.5 μF by test voltages <20 kV, a test system based on a test transformer should be the most economic solution. For higher test parameters, a resonant test system has to be applied

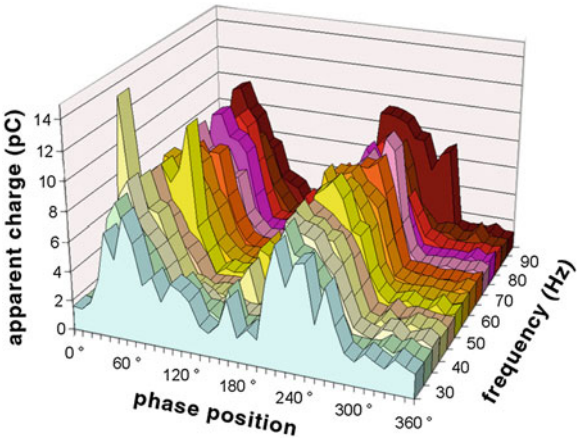

Fig. 10.7 PD pattern of XLPE models at different test frequencies

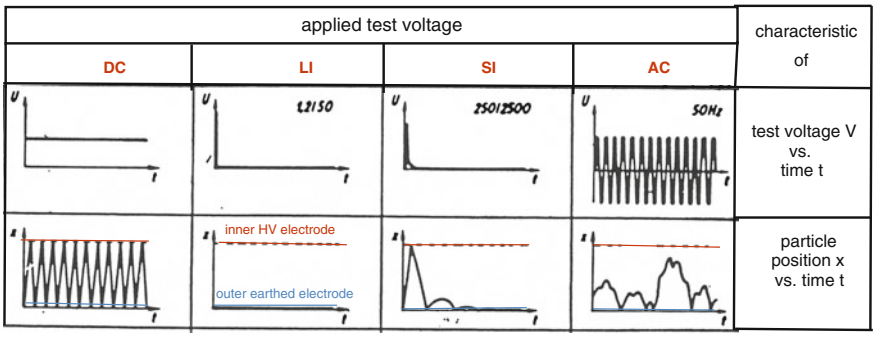

Fig. 10.8 Position–time characteristics of spherical particles between coaxial electrodes at different voltage waveforms

where the *frequency-tuned circuits* have a much better weight-to-test power ratio than the inductance-tuned systems (Table 3.2; Fig. 10.9). The design of the transformers and reactors depends strongly on the test objects and will be discussed in Sect. 10.3.

10.2.1.2 High Direct Voltage

DC voltage (see Chap. 6) can be applied for on-site testing of HVDC components. For historic reasons and based on long experience (Fig. 10.10), it is also still applied for field tests on oil-paper-insulated AC cable systems and for the insulation of some rotating machines as well. A DC generator can charge such a capacitive test object even with a very low current if sufficient time is available. The DC testing of other AC equipment cannot be recommended. IEC 60060-3: 2006 requires the following parameters of DC voltages for on-site tests:

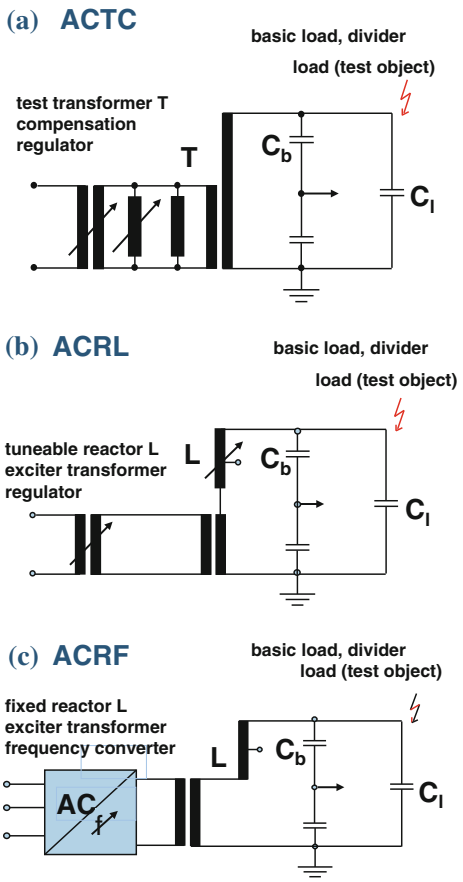

Fig. 10.9 AC test voltage generation and approximate weight-to-test power ratio. **a** Based on transformers (about 15 kg/kVA). **b** Based on inductance-tuned resonant circuits (about 5 kg/kVA). **c** Based on frequency-tuned resonant circuits (about 1.5 kg/kVA)

Test voltage value	Arithmetic mean value
Tolerance of test voltage value	±3 % up to 1 min
	±5 % for > 1 min
Ripple factor	≤3 %
Uncertainty of voltage measurement	≤5 %
Uncertainty of ripple measurement	≤10 %

For the generation of DC voltages, usually modular HVDC test systems are applied. They can be air-insulated or—for higher current—oil-insulated, see Figs. 6.1c, 6.9 and 6.10). For testing internal or clean external insulation, a HVDC test system of very low current is sufficient, but for diagnostic tests on service-aged or polluted insulation, test systems of higher current must be taken into consideration.

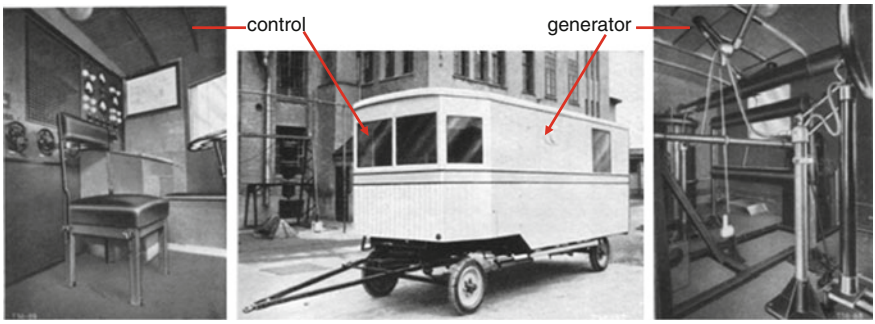

Fig. 10.10 Historical HVDC test system 250 kV for oil-paper-insulated cable systems made by Koch and Sterzel 1936

10.2.1.3 Impulse Voltage (LI, OLI, SI, OSI)

Impulse voltages (see Chap. 7) cannot replace tests with continuous voltages on site. They complete tests with AC or DC voltages. IEC 60060-3:2006 allows on site not only aperiodic impulse voltages of wider tolerances of the time parameters, but also oscillating impulse voltages (Sect. 7.1.3, Figs. 7.16 and 7.17). Parameters within the following ranges shall be generated:

	LI/OLI	SI/OSI
Test voltage value	Peak	Peak
Tolerance of test voltage value	±5 %	±5 %
Front time/time to peak	0.8–20 μs	20–400 μs
Time to half-value	40–100 μs	1,000–4,000 μs
Frequency	15–500 kHz	1–15 kHz
Uncertainty (voltage measurement)	±5 %	±5 %
Uncertainty (time/frequency measurement)	±10 %	±10 %

Oscillating lightning impulse (OLI) and oscillating switching impulse (OSI) voltages are applied for their much higher utilization factor (see Sect. 7.1.3). For the oscillating impulses (OLI, OSI), the time parameters are determined from the enveloping curve.

LI and OLI test voltages are useful for the detection of fixed defects in GIS. For GIS, a related OLI acceptance test is recommended on site if the PD measurement at AC voltage is not sensitive enough. Till now, power transformers are tested with aperiodic LI voltages after repair on site, oscillating impulse voltages are not yet applied for these tests.

10.2.2 Voltages for Special Tests and Measurements

IEC 60060-3:2006 distinguishes between the test voltages in relation to IEC 60060, and this means voltages for withstand tests (Sect. 10.2.1) and those for special (=diagnostic) tests. The latter are *verylowfrequency* (*VLF*) voltages and damped AC (DAC) voltages considered in the following. Additional voltages for special tests can be specified by relevant IEC Technical Committees.

10.2.2.1 Very Low Frequency Voltage

To avoid the high power demand when cables are tested with 50/60 Hz voltages, a test voltage of a very low frequency (VLF), preferably of 0.1 Hz, had been introduced in the early 1980s (Nelin et al. 1983; Boone et al. 1987). This reduces the power demand to 0.2 % compared with 50 Hz (Fig. 10.11a). The frequency range of VLF test voltages is fixed to 0.01–1 Hz by IEC 60060-3: 2006, respectively, by the IEEE Guide 400.2. The standards accept very different wave shapes between sinusoidal and rectangular for on-site testing (Fig. 10.11b) if the following additional requirements of a test are fulfilled:

Test voltage value	Peak (for some application rms value)
Tolerance of test voltage value	±5 %
Frequency range	0.01–1 Hz
Uncertainty of voltage measurement	≤5 %
Uncertainty of frequency measurement	≤10 %

VLF test voltages are far from stresses in service, but VLF test systems (Fig. 10.12) are well introduced for medium-voltage cables. They are compact and of low power demand.

The comparison between 0.1 and 50 Hz (Fig. 10.11a) delivers an impression what it means for the discharge process when the power frequency in service is 500 times higher. The much lower repetition rate of stresses with polarity reversals causes a different discharge mechanism, which leads to higher breakdown voltages. Figure 10.6 shows that the breakdown voltage of a healthy insulation at 0.1 Hz is about twice of that at 50 Hz (red line)! Consequently, the applied VLF test voltages must be 50 % higher than those at power frequency.

Because of their compactness and low power demand, VLF voltages are well introduced for diagnostic tests and even for quality acceptance tests on medium-voltage cables (Fig. 10.12a). According to the European Standard EN HD 620 S (1996), the test voltage value is the rms value, with the consequence that the peak value of a sinusoidal VLF test voltage shall be by a factor $\sqrt{2}$ higher than that of a rectangular VLF voltage. Their application to quality acceptance tests of extruded HV and EHV AC cables cannot be recommended. VLF voltage is not a stress,

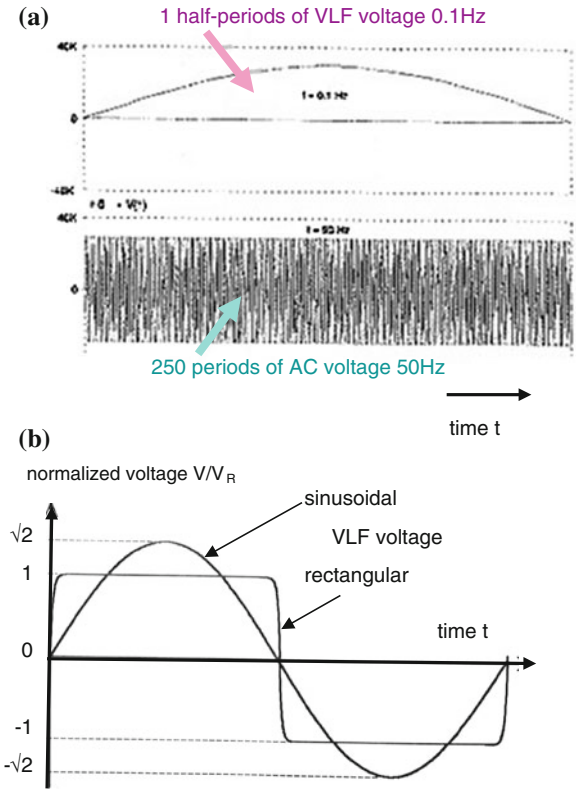

Fig. 10.11 VLF test voltages and power frequency AC voltage. **a** Comparison 0.1 and 50 Hz. **b** Sinusoidal and rectangular VLF voltages of identical rms value

which appears under operation of a cable. In combination with the higher stress in HV and EHV cables, the test result may not correspond to test results with power frequency voltages.

10.2.2.2 Damped Alternating Voltage

In the late 1980s and 1990s, SI and OSI voltages have been used for PD diagnosis on cable systems (Dorison and Aucourt 1984; Lemke et al. 1987; Plath 1994; Lemke and Schmiegel 1995; Gulski et al. 2000). At the beginning, the energy has been stored in the impulse capacitor of the impulse generator; now, the capacitive test object itself is charged and stores the energy (see Sect. 7.1.3 and Fig. 7.19). The DAC voltage is generated when the charged test object is discharged via a suited switch (trigatron or semiconductor switch), an inductance and possibly a resistor. IEC 60060-3: 2006 considers only the oscillating (OSI) part as a voltage for PD measurement, but not the DC ramp for charging the cable (Fig. 10.13) and defines the following requirements:

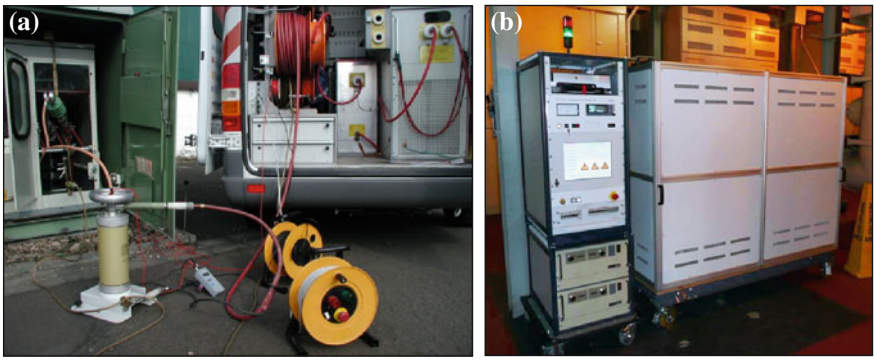

Fig. 10.12 VLF test system for 60 kV. **a** Mobile test system for land cables up to few μF. **b** Test system for submarine cables up to 25 μF (courtesy of SEBA KMT, Germany)

Test voltage value	Peak
Tolerance of test voltage value	±5 %
Frequency	20–1,000 Hz
Damping of subsequent peaks	≤40 %
Uncertainty (voltage measurement)	±5 %
Uncertainty (time/frequency measurement)	±10 %

If the test object is used as the energy storage for the oscillation, it is stressed by the unipolar ramp and then with a fast polarity reversal to nearly the same, but opposite peak value by the oscillation. (At 1,000 Hz, the polarity changes within 500 μs, at 20 Hz within 25 ms.) The frequency of the DAC voltage depends on the test object capacitance and the inductance of the test circuit [see Eq. (7.6)] and the damping on the losses in the circuit. The DAC voltage causes for a low number of cycles a voltage stress in the cable similar to that at power frequency suited for PD measurement. The highest peak value of the oscillation is identical with that of the DC ramp. The duration of the DC ramp depends on the capacitance of the test object, for example the length of a cable system (Fig. 10.14), and may change from less of one second to more than one minute.

The generation of DAC voltage even for large test object capacitances requires few components (Fig. 10.15): a DC generator, a HV reactor (inductance) and a voltage divider/basic load (which can also be used as coupling capacitor for PD measurement). The system is compact, and transportation and assembling are easy. With respect to their overall design, DAC systems would be well suited for on-site application, but the DAC voltage with its pre-stressing DC ramp does not fulfil the requirement of a test voltage for quality acceptance tests (Sect. 10.1.1):

- The DAC voltage with its DC charging ramp does not represent any stress in service.
- The duration of the ramp depends on the test object capacitance and is not reproducible.

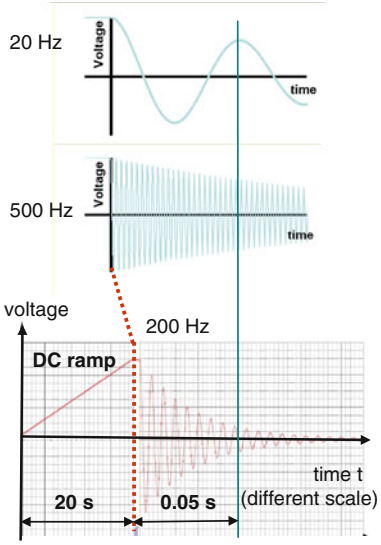

Fig. 10.13 DAC voltages after charging the test object

- The frequency of the DAC voltage depends on the test object capacitance and is not reproducible.
- The damping rate of the DAC voltage depends on the losses in the test circuit and is also not reproducible.
- The sequence of DAC pulses with DC ramps (Fig. 7.19c)—proposed for replacing AC withstand tests—cannot represent AC voltage of power frequency and may cause cumulative space charge effects.

Nevertheless, IEC 60060-3:2006 considers it as a voltage for diagnostic tests. In combination with PD measurement, it is an interesting tool for condition assessment, especially for medium-voltage cables (Gulski et al. 2007; Cigre TF D.1.33.05). A PD-monitored withstand test might be applicable for quality acceptance of some medium-voltage equipment. For HV and EHV equipment and systems of higher operational stress, the pre-stress of the DC ramp followed by the fast polarity reversal of the DAC voltage causes test results which are hardly comparable to those at AC voltage of power frequency. As DAC is an impulse voltage, DAC testing should never be applied to GIS (compare Fig. 10.8).

10.3 PD Measurement and Diagnostics on Site

As mentioned already, the insulation of HV apparatus suffers from ageing due to the permanently applied service voltage and transient over-voltages as well as thermal and mechanical stresses. Partial discharges are the first indication of a weak spots (defects) in the insulation caused by the degradation process. To avoid

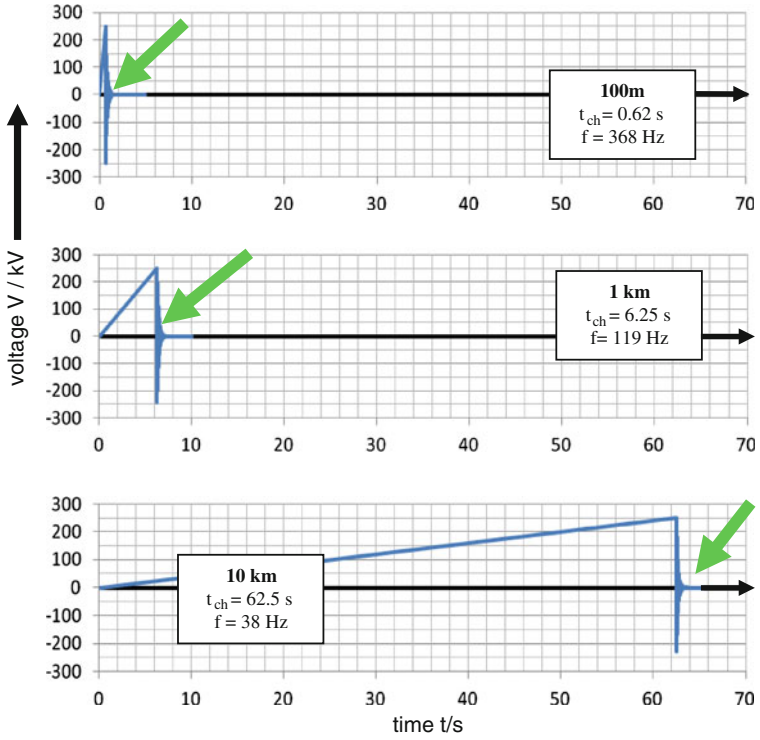

Fig. 10.14 DC ramp and DAC voltage for different lengths of cable systems

an unexpected outage associated with serious consequences not only for the supplier and customer but also for the environment, the asset management based on *diagnostic PD measurement* is becoming increasingly important. So the traditional *time-based maintenance* is nowadays replaced by the scheduled *condition-based maintenance*. The necessary *condition assessment* is focused on HV equipment and components indicating progressive insulation deterioration. As a consequence, advanced diagnostic tools are increasingly used to judge both the global (integral) deterioration and local (selective) deterioration of the insulation (Fig. 10.16). As the global insulation, ageing causes also weak spots in the insulation, which might become the source for PD events to be considered as a precursor for a breakdown. Thus, on-site PD diagnosis tests have become an indispensable tool for the maintenance and replacement policy of power equipment. PD measurement on site is also important for *PD-monitored, quality acceptance withstand tests* after the assembling of the apparatus on site.

With reference to electrical PD measurements, the PD signals radiated from the PD source are captured by *PD couplers* (also referred to as *PD sensors* or PD antennas) and acquired by the PD monitoring system to provide the asset manager with reliable information on the insulation condition to decide further actions

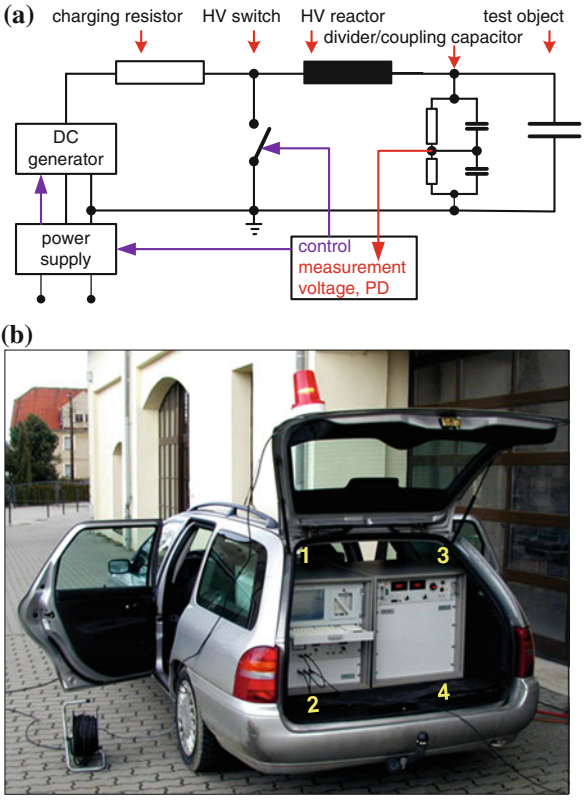

Fig. 10.15 Generation of DAC voltage. **a** Principle circuit diagram. **b** DAC test system for 30 kV (*1* PC for PD mapping, *2* test voltage control, *3* measuring control and *4* 30-kV DAC generator)

(Fig. 10.17). Without doubt, the key components for reproducible measurements are the PD couplers as well as the PD monitoring and data acquiring system (Fig. 10.18). In this context, it must be underlined that besides technical aspects, also economic consequences have to be taken into consideration. So a holistic approach for continuous PD monitoring is desired only for strategic important and expensive EHV/UHV apparatus. When the apparatus is provided with a monitoring system, the related sensors are used for PD-monitored acceptance tests, too. Medium-voltage equipment, however, must not be PD-monitored permanently but only inspected from time to time.

Generally, it must be emphasized that sensitive electrical PD measurements under on-site condition are a challenge due to the always-present electromagnetic interferences. Thus, besides the traditional measurement of the charge of PD pulses specified in IEC 60270: 2000 (see Sect. 4.3), alternative principles are proposed in the relevant paragraphs of the draft of IEC 62478, such as the *UHV/VHF PD measurement* and the *acoustic PD measurement* (see Sects. 4.7 and 4.8). The following Sect. 10.4 is mainly focused on the *decoupling* of electrical PD signals and the acquisition of the PD data (Fig. 10.18) considering typical examples (see Sects. 10.4.1–10.4.4) which refer to both periodical and continuous PD monitoring.

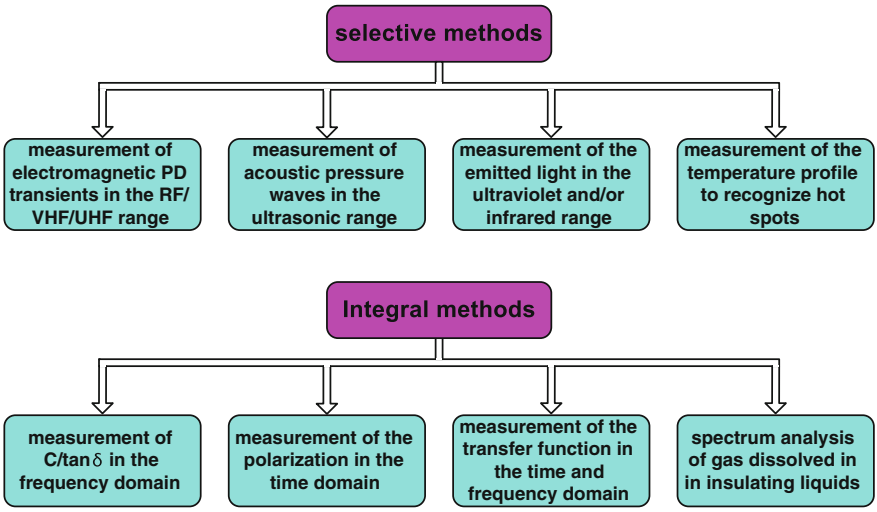

Fig. 10.16 Survey on diagnostic measurements used for insulation condition assessment of HV apparatus under on-site condition

10.4 Examples for On-Site Tests

Before a HV equipment or system is put into service, numerous electrical, mechanical, thermal and functional tests and checks shall be performed. The *quality acceptance test* of the insulation is an important one of these and—together with *diagnostic insulation tests*—considered in the following. Cigre, IEC and IEEE have published guides and standards which give an overview on the required tests, test procedures and test systems (Cigre WG 33 TF 04 2000; Cigre WG D1.33 TF 05 2012; IEEE Draft P1861TH/D1 2011).

10.4.1 Testing of Gas-Insulated Systems (GIS, GIL)

10.4.1.1 Some Basics

GIS has been introduced in the 1960s and is characterized by the final assembling of transportation units to a complete substation on site. The return of experience (Cigre JW 33/23.12 1998) shows a low dielectric failure rate in the order of 1 per 100 bay-years operation. The reason is the early introduction of HV withstand tests and PD measurements for quality acceptance on site. Nevertheless, about 35 % of the dielectric failures in service are caused by insufficient site work. From a physical point of view (Mosch and Hauschild 1979; Mosch et al. 2 1979; Cigre TF D1.33.05 (2012)), the defects can be classified into

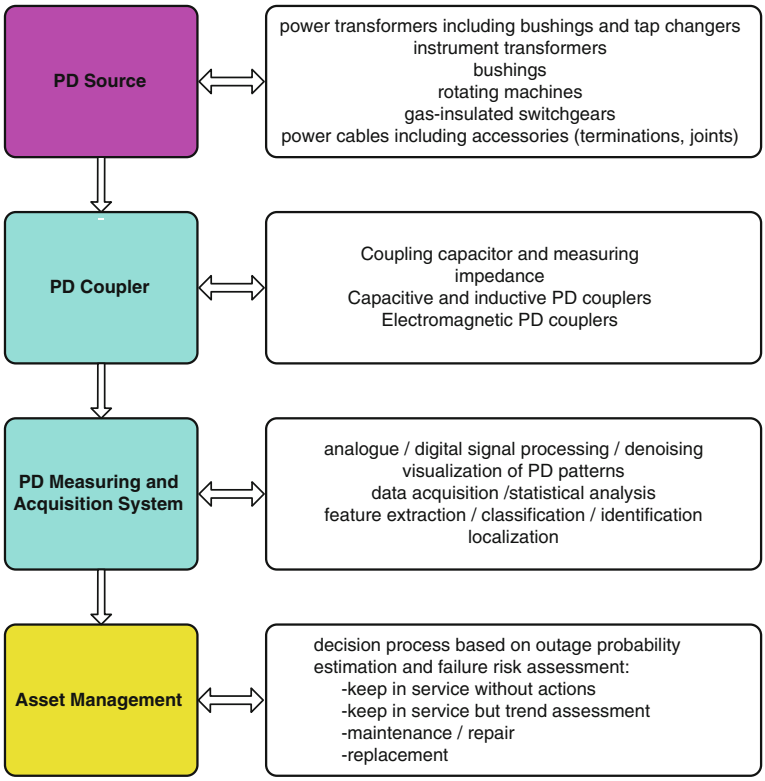

Fig. 10.17 General structure of on-site PD diagnostics of HV equipment

- free-moving particles,
- sharp protrusions and fixed particles on HV electrodes,
- particles sticking on spacers,
- floating parts (shields, also left tools),
- defects in spacers (voids, cracks).

Different test voltages are differently efficient in the detection of the mentioned defects. Table 10.1 gives a survey on the efficiency of acceptance test methods.

10.4.1.2 Acceptance Tests

The relevant standard IEC 62271-203:2010 (see also IEEE C 37.122) recommends either a PD-monitored AC withstand test (procedure B) or—if the sensitivity of the PD measurement is not sufficient because of the noise level ($q_N > 5$ pC)—the combination of an AC withstand test and an LI/OLI withstand test (procedure C)

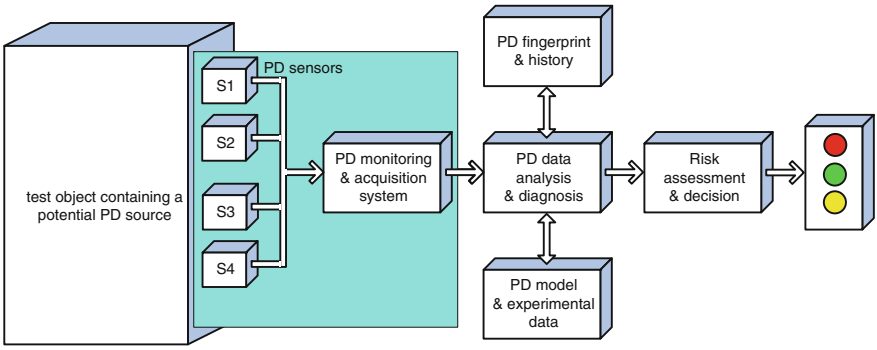

Fig. 10.18 Major components of a PD monitoring system for periodical and continuous measurements

Table 10.1 Efficiency of test methods for on-site quality acceptance tests of GIS

Test procedure Kind of defect	AC withstand	PD-monitored AC withstand	LI/OLI withstand	SI/OSI withstand
Free-moving particle	X	X	o	o
Sharp protrusions and fixed particle	o	X	X	x
Particle on spacer	o	X	X	x
Floating parts (left tools)	x	X	x	o
Defects in spacers	x	X	x	x

X very efficient, *x* less efficient, *o* not efficient)

for GIS of 245 kV and above. For voltages <245 kV, an AC withstand test is considered as sufficient (procedure A). This standard defines the test voltages (slightly different from IEC 60060-3:2006) and the test procedures as follows:

AC voltage	Frequency 10–300 Hz; withstand for 1 min (followed by a PD measurement at 1.2 U_r with requirements $q \leq$ 10pC)
LI/OLI voltage	Front time $T_1 = 0.8$–8 μs, for OLI voltage ≤15 μs, withstand to three impulses of each polarity;
SI/OSI voltage	Time to peak $T_p = 0.15$–10 ms, only applicable if no AC source is available

An on-site test with DC voltage is under no circumstances recommended. It would not represent any stress in service and would cause very different PD and space charge phenomena.

The recommended test voltage values are given in Table 10.2.

Whereas medium-voltage GIS can be tested by transformers, all GIS for higher-rated voltages are tested by resonant test systems. With respect to the lower weight, resonant test systems of variable frequency (ACRF test systems) are preferred. A frequency higher than about twice the power frequency enables the inductive

Table 10.2 Preferred test voltage values for GIS on-site tests (IEC 62271-203)

Rated voltage of GIS kV (rms)	AC withstand voltage kV (peak/$\sqrt{2}$)	LI/OLI Withstand voltage kV (peak)	SI/OSI Withstand voltage kV (peak)
72.5	120	260	–
123	200	440	–
170	270	600	–
245	380	840	–
362	425	940	760
420	515	1,140	840
550	560	1,240	940
800	760	1,680	1,140
1,200	960*	2,040*	1,440*

The star values (*) are calculated by 0.8 times the rated insulation levels

voltage transformers that may remain at the GIS during the on-site test. There are two principle designs:

Modular ACRF systems consist of cylinder-type reactors (Fig. 10.19, each 230 kV, 3A, 200H) which can be switched in series for higher voltages and in parallel for higher current. Then consequently, also the inductance and the natural frequencies are changed. Figure 10.20 shows the resulting load–frequency characteristics of the three reactors (Hauschild et al. 1997). The parallel (p) or series (s) connections are not only useful for the adaptation of voltage and current, but also for that of the test frequency.

The air-insulated test system requires a bushing of the GIS for the connection of the ACRF test system. The capacitor provides both the voltage divider and the coupling capacitor for PD measurement (IEC 60270:2000). If the GIS is not equipped with a bushing, a test bushing or a cable adapter must be added. The connection between the reactors and the capacitor is realized by a blocking impedance. But the PD measuring circuit is exposed to the environment. Therefore, electromagnetic noise signals may penetrate and reduce the sensitivity of the PD measurement.

A *metal-enclosed ACRF test system* of lightweight SF_6-insulated reactors avoids the penetration of radiated noise: It can be flanged directly to the GIS under test (Figure 10.21), causing a shielded HV circuit. When the electromagnetic UHF PD measurement is applied, no further components must be connected to the GIS. For PD measurement, according to IEC 60270:2000, the system includes a coupling capacitor (Fig. 10.21). The operation characteristic of such a system is shown in Fig. 3.25 and explained in Sect. 3.1.2.3. Two SF_6-insulated reactors can also be connected in series or in parallel (Fig. 10.22) when suited adapters of the enclosure are available (Pietsch et al. 2005).

Example A 245-kV GIS with a capacitance of $C_{GIS} = 2.2$ nF shall be tested after assembling with a metal-enclosed ACRF test system $U_r = 460$ kV, $I_r = 1.5$ A and $L = 720$ H. For the test circuit, a quality factor $Q = 50$ can be assumed. According to Table 8.2, the test voltage is 380 kV. Determine the test frequency, the necessary test current, the reactive test power and the necessary feeding power! Is the test system suited

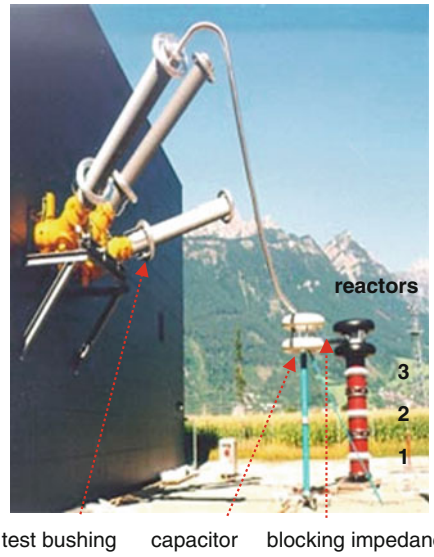

Fig. 10.19 GIS test with a modular 680-kV ACRF test system (courtesy of Siemens AG, Berlin)

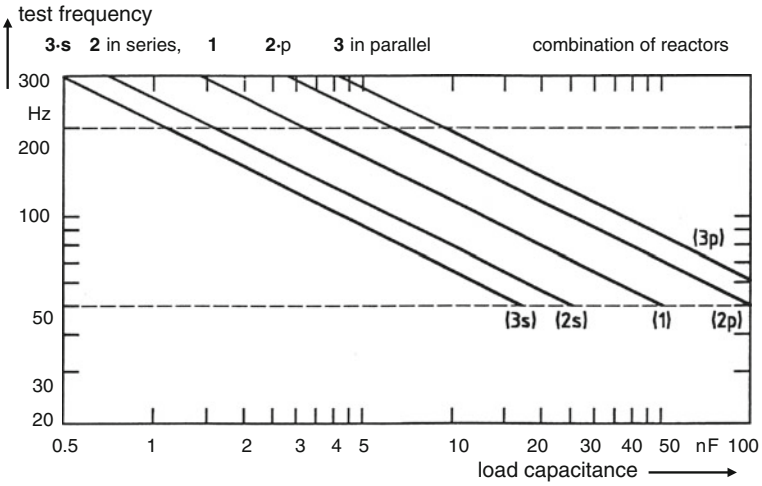

Fig. 10.20 Frequency–load characteristics of the combinations of three modular reactors

for the test? Can a coupling capacitor $C_k = 1.2$ nF be added for PD measurement? Can the inductive voltage transformers remain on the GIS during the test?

Test frequency	$f_t = \frac{1}{2\pi\sqrt{L \cdot C_{\text{GIS}}}} = 126.5$ Hz
Test current	$I_t = 2\pi f_t \cdot C_{\text{GIS}} \cdot U_t = 0.66$ A
Reactive test power	$S_t = I_t \cdot U_t = 250$ kVA
Active feeding power	$P_t = S_t/Q = 5$ kW

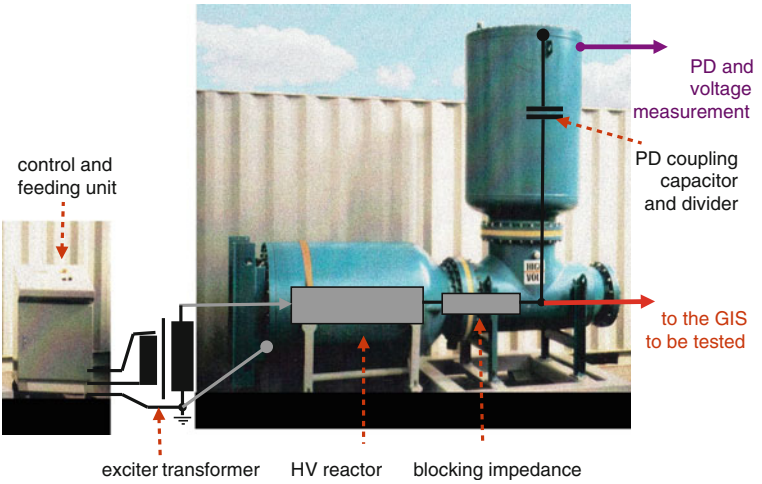

Fig. 10.21 Metal-enclosed ACRF test system of SF_6-insulated components

The additional coupling capacitor increases the capacitance to $C = C_t + C_k = 3.4$ nF, which reduces the frequency to $f_t = 101.8$ Hz and increases the test current to $I_t = 0.83$ A. In both cases, the test current is lower than the rated current of the ACRF test system and the test frequency is in the accepted range. Because the test frequency is more than the doubled power frequency, the inductive voltage transformers may remain at the GIS during the test.

Acceptance tests with *impulse voltage* are usually performed with oscillating voltages (see Sect. 7.1.3 and Figs. 7.16, 7.17 and 7.18). As shown in Table 10.2, the testing with OLI voltages is of practical importance, when no sensitive PD measurement can be applied. The OLI application enables generators with lower-rated cumulative charging voltage, lower size and lower weight. The connection between the test voltage generator and the GIS under test requires always a bushing at the GIS as also mentioned above for the modular ACRF test system.

For acceptance testing of *gas-insulated lines* (*GIL*) (IEC 61640: 1998; Cigre JWG 23/21/33-2003; Cigre JWG B3/1.09-2008) of considerable capacitance, AC test voltages as shown in Table 10.2 should be applied. The higher capacitances of GIL in comparison with GIS require ACRF test systems of higher power. This can be generated by using the series connection of ACRF test systems as described in Sect. 10.4.2 for testing HV/EHV cable systems. In addition to a withstand test, the acceptance depends on the results of sensitive PD measurement (Okubo et al. 1998).

10.4.1.3 PD Measurement for Acceptance and Diagnostics

PD measurement is important for both acceptance testing and diagnostic testing and also for *monitoring of GIS* and GIL. The general requirement is a "PD-free" insulation which has to be demonstrated with high sensitivity. One has to consider that

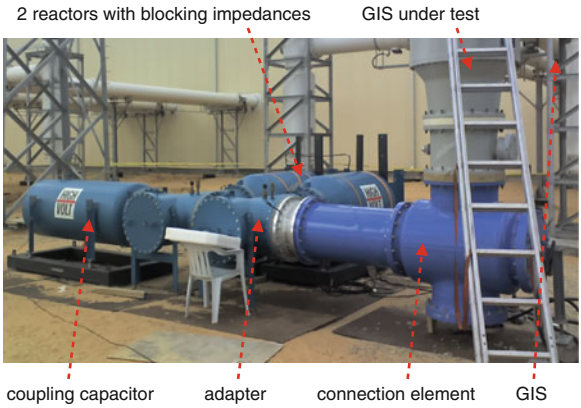

Fig. 10.22 ACRF testing of a large GIS using two reactors in parallel

there is practically no ageing of the SF6 insulation. Therefore, any diagnostic testing of GIS insulation is replaced by periodic PD measurement or PD monitoring.

To discover defects in GIS or GIL including cavity discharges in spacers, a measuring sensitivity in the pC range is desired. This is only achievable under on-site condition if the non-conventional PD detection is performed in the UHF range, as already presented in Sect. 4.7. To capture the PD pulses from the test object, different kinds of *UHF sensors* have been developed, such as mobile window sensors and fixed disc/cone sensors (Fig. 4.63), which might be arranged in a separate assembling flange, as well as field grading sensors (Boggs et al. 1981). As also treated in Sect. 4.7, from a physical point of view, the UHF method cannot be calibrated in terms of pC. Therefore, the "pass/fail" criterion is based on a sensitivity check (comparisons in the laboratory with the IEC 60270 method) intended for the determination of the PD threshold level achievable by the UHF technique applied. In this context, it seems noticeable that the phase-resolved PD patterns are often very similar for both the IEC 60270 and the UHF method. Therefore, the classical PD pattern recognition is also applicable for the non-conventional PD measuring method to identify and classify typical PD defects, such as free-moving particles, protrusions fixed on the electrodes, floating metallic parts as well as cavities due to voids and cracks in spacers (Mosch and Hauschild 1979; Kranz 2000).

After a potential PD defect has been detected, the site of origin must be known to assess the risk for an unexpected breakdown. A common procedure is the time-of-flight measurement. As the PD signal is travelling in all directions close to the light velocity (30 cm/ns), the oscilloscope applied should have a rise time below the ns range to get an appropriate resolution in time and space.

Using the test arrangement illustrated in Fig. 10.23, where the PD signal is caused by a fixed metallic particle designed P, the time difference between the PD signals arriving at the sensors S_1 and S_2, is given by

$$\Delta t_{12} = \frac{x_{1P} - x_{2P}}{v_g}.$$

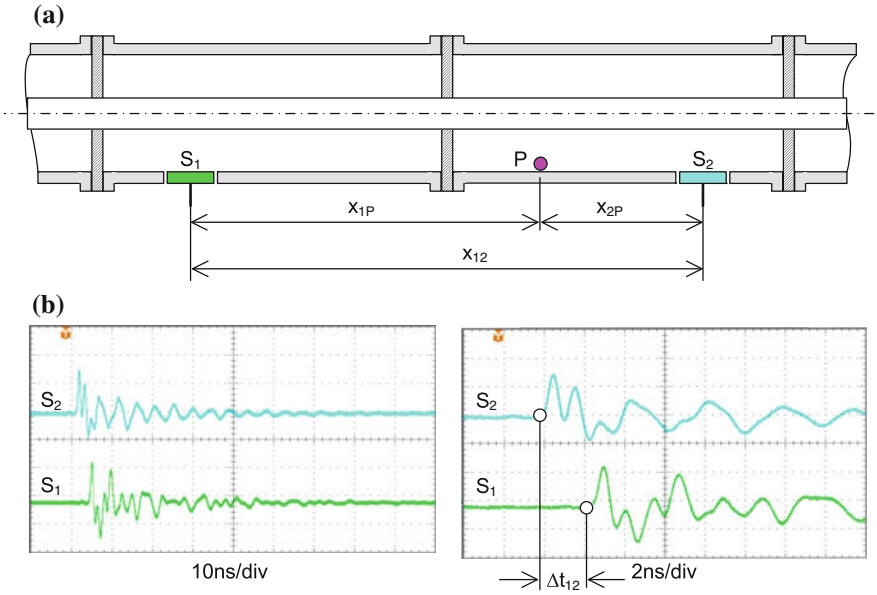

Fig. 10.23 Principle of PD fault localization based on the time-of-flight measurement. **a** Significant geometric parameters. **b** Oscilloscopic records gained from a GIS dummy

The distance of the PD site P from the right sensor S_2 can be simply calculated:

$$x_{2p} = \frac{1}{2}\left(x_{12} - v_g \cdot \Delta t_{12}\right).$$

The measurement shown in Fig. 10.23 delivers with $\Delta t_{12} \approx 2$ ns and $v_g \approx 30$ cm/ns for an assumed distance $x_{12} = 100$ cm between the both sensors the following distance between the right sensor S_2 and the PD source $x_{P2} = 20$ cm.

Propagating along the GIS/GIL, the PD signal is strongly attenuated by the spacers separating the different sections. This effect can also be used to localize the PD site, sometimes referred to as *PD sectionalizing* method.

Another promising tool is the *acoustic PD detection*, particularly if the measuring system is triggered by the electric signal, see Sect. 4.8. A practical example is shown in Fig. 10.24, which refers to a free-moving metallic particle at 68 Hz test voltage frequency. Typical for such kinds of PD defects is that the repetition rate of the detectable pulses is comparatively low, often below the test frequency, where the pulses are not correlated with the test frequency (Fig. 10.24). The use of an array of *acoustic transducers* could also be helpful for the localization of PD defects because the acoustical signal is also subjected to strong attenuation if travelling along the GIS/GIL compartment.

On-site PD tests of GIS/GIL are commonly only performed after assembling or repair. The sensors pre-installed for commissioning can be used for periodic diagnostic measurement, too. A continuous monitoring is applied for important

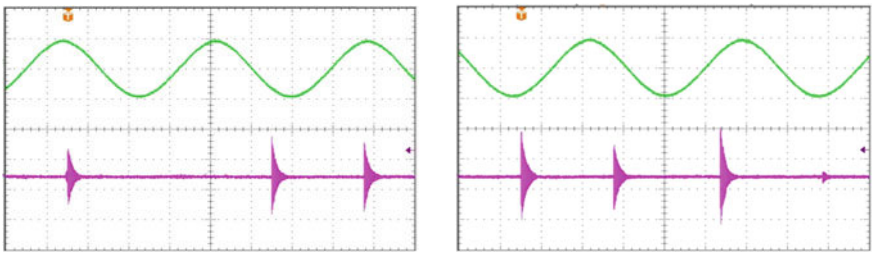

Fig. 10.24 Acoustic PD signal caused by a free-moving particle in a GIS subjected to AC test voltage of variable test frequency (68 Hz)

GIS and recommended after a "low-risk" PD failure has been identified in the course of a periodic PD diagnosis test.

10.4.2 Testing of Cable Systems

The application of power cable systems has a long tradition. It starts with liquid-impregnated-paper (LIP)-insulated cables more than 100 years ago and continues more and more with extruded cables since the 1960s. Meanwhile, both types of cables are available up to rated voltages of 550 kV. For economic and environmental reasons, extruded cables are dominant for application at AC and DC voltages (Fig. 1.2). The following explanations are mainly focussed on AC cable systems with extruded insulation.

The cable system can only be assembled on site, and therefore, on-site testing of cables has also a long history. Table 10.3 delivers an overview on the available voltages for on-site testing, before some examples are explained more in detail.

10.4.2.1 Historical DC Voltage Testing of AC Cable Systems with LIP Insulation

The insulation resistance of an *oil-paperinsulation* is much lower than that of an extruded insulation. Therefore, the voltage distribution inside such a cable for AC and DC has similarities, even in the vicinity of defects. Furthermore, LIP insulation is quite resistant against partial discharges. Additionally, decades ago, only mobile *DC voltage test systems* were available (see Fig. 10.10). Therefore, if AC cable systems had to be tested, DC test voltages were applied. The high DC

Table 10.3 Characteristics or different test voltages for on-site testing of cable systems

Test voltage IEC 60060-3; IEEE 400 Characteristic	DC	AC 50/60 Hz	ACRF 20…300 Hz	VLF 0.01…1 Hz	DAC DC ramp; 20…500 Hz; damping <40 %
Representation of stresses in service	Identical for DC cables, very different for AC cables	Identical for AC cables	Close to AC voltage	Much different from the AC 50/60 Hz stress	Impulse voltage, much different from AC 50/60 Hz stress
Description of voltage	Unipolar and continuous voltage (reference for all DC cables)	Alternating voltage (reference for all AC cables)	Alternating; in the range of the reference frequency	Very slowly alternating; far from reference frequency	Direct voltage ramp followed by damped oscillation
Discharge and breakdown process	Slow and determined by space charges	Typical for AC of power frequency	Very similar to AC of power frequency	Different, higher test voltage values necessary	Different, charge accumulation during ramp, then polarity reversal
Reproducibility at different cable systems	Perfect	Perfect	Acceptable, frequency mainly within 30…100 Hz	Good	Poor, change in • ramp duration, • frequency, • damping
Generation in the field	Easy	For HV/EHV: impossible, MV: few seconds	Good for MV cables, acceptable for HV/EHV cables	Good for MV cables, questionable for HV cables	Good for MV cables
Recommended for acceptance testing	All DC cables; (AC cables with LIP insulation traditionally)	Only for AC medium-voltage cables	All AC cables from MV to EHV	Partly applied for MV cables, not for HV cables	Partly applied for MV cables, not for HV cables
Recommended for diagnostic testing	All DC cables	MV AC cables	All AC cables from MV to EHV	MV cables	MV AC cables

withstand voltage test levels up to $4U_0$ are related to the limited sensitivity of defects at DC voltage. For details, see IEEE Std 400.1™-2007.

Today, for condition assessment, LIP-insulated AC cable systems are mainly tested with AC, VLF or DAC voltages as mentioned in the following sections for extruded cable systems, especially the general ageing of the LIP insulation can be indicated by dissipation factor and/or dielectric response measurements. Defects in joints are indicated and located by PD measurements.

10.4.2.2 Testing of Medium-Voltage AC Cable Systems with Extruded Insulation

The relevant IEC Standard 60502:1997 mentions that *acceptance test* of cable systems up to $U_r = 30$ kV must only be performed if "required" in the contract and considers three alternatives:

1. a DC voltage test by 4 U_0 for 15 min (which cannot be recommended because of different voltage distributions at DC compared with AC and additional space charge effects in the cable);
2. an AC voltage withstand test with 1.7 U_0 for 5 min;
3. the application of the normal operating voltage for 24 h on the no-loaded cable.Very often no test or method 3 is applied, because it does not require a separate HV test system as no. 2. The IEEE Guide 400™-2012 considers PD-monitored AC/ACRF and VLF withstand tests as "useful", but the application of any acceptance test is left to the contract between user and supplier. Quality acceptance testing does not play an important role for *medium-voltage cable systems*. This is related to their relatively high reliability due to the design of cable and accessory insulation of low dielectric stress compared with HV/EHV cables. Unlike that, the first generation of cross-linked polyethylene (XLPE) MV cables was not protected against the penetration of water causing the phenomenon of "*water trees*" and this means the enhanced development of partial discharges in the electric field under the influence of water. This endangered many thousands of kilometres of cable systems worldwide and stimulated the development of diagnostic tests.

Diagnostic tests remain very important with respect to the long-time utilization of cable systems and the mentioned water tree problems. When the research work had shown that DC test voltage creates dangerous space charges (Montanari 2011; Choo et al. 2011) and is not an acceptable tool for the identification of water trees, *VLF testing* has been developed as an alternative of low power demand and lightweight equipment (Boone et al. 1987), see Sect. 10.2.2.1 and Fig. 10.12. The voltage application has been completed by dissipation factor measurement and also by PD measurement. The measurements of Schiller (1996) (Fig. 10.6) are sometimes taken as an indication for the high sensitivity of VLF withstand voltages against defects. This might be correct for the investigated large defects, but not for the full scale of possible defects from small to large, see Sect. 10.2.1.1. The

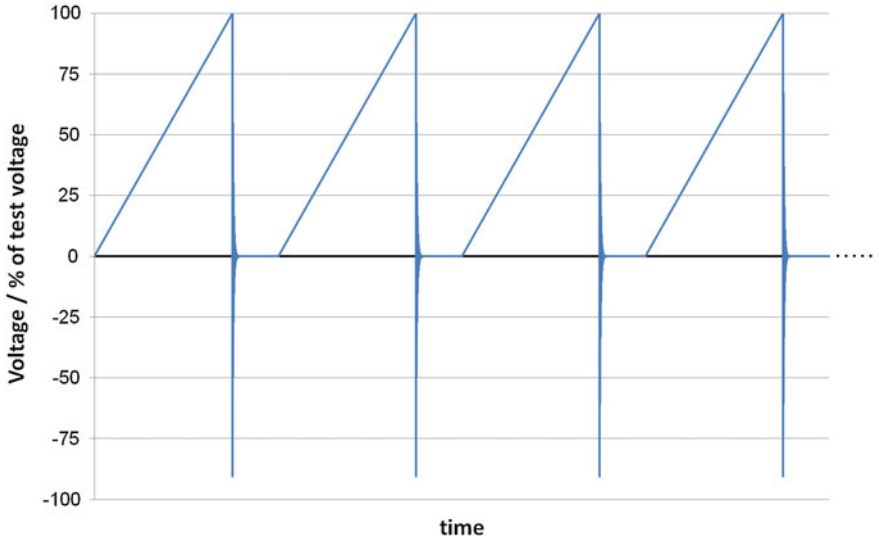

Fig. 10.25 Sequence of DAC voltages including the DAC ramps

large number of diagnostic VLF tests and related measurements, performed in the last 25 years, delivered experience for the condition assessment. The latest experiences of VLF tests on cable systems up to 69 kV are summarized in the IEEE Guide 400.2-2012.

The great difference between the VLF test frequency and the power frequency led to the development of damped alternating voltages (see Sect. 10.2.2.2) and its combination with PD measurement (Fig. 10.15). The damping of the oscillations is even used for the estimation of the dissipation factor (Houtepen et al. 2011).

DAC withstand testing with a sequence of DC ramps followed by AC oscillations (Fig. 10.25 see also 10.14)—as taken into consideration by a draft of IEEE 400.4 (2013)—cannot be recommended as mentioned in Sect. 10.2.2.2. DAC voltage is an introduced tool for diagnostic testing of medium-voltage cable systems. In opposite, there are good reasons for applying ACRF voltages also for diagnostic tests (Weck 2003).

10.4.2.3 Testing of HV and EHV AC Cable Systems with Extruded Insulation

In *XLPE insulation* with defects, the breakdown process is determined by space charges depending on the frequency (Cavallini and Montanari 2006; Nyamupangedengu and Jendrell 2012). Consequently, for testing, the higher-stressed insulations of extruded HV and EHV cables require a more stringent selection of the test voltages and their frequency (Table 10.3).

Table 10.4 AC withstand voltages for acceptance tests on extruded cable systems (IEC 60840:2011 and IEC 62067:2011)

Highest voltage for equipment V_m/kV	Range of nominal voltages V_n/kV	Reference voltage line to ground V_0/kV	Test voltage value according to IEC Standard $V_{t\min}$/kV	Test voltage value according to $V_t = 1.7\ V_0$/kV
52	45–47	26	52	–
72.5	60–69	36	72	–
123	110–115	64	128	–
145	132–138	76	132	–
170	150–161	87	150	–
245	220–230	127	180	216
300	275–287	160	210	272
362	330–345	190	250	323
420	380–400	220	260	374
550	500	290	320	493

For *quality acceptance test* on site, IEC 60840:2011 for HV cables (rated voltage 50–150 kV) and IEC 62067:2011 for EHV cables (rated voltage 150–500 kV) accept AC voltages in the frequency range 20–300 Hz, according to Table 10.4.

All test voltages shall be applied for 1 h. As an alternative, instead of a test by separate test equipment, a 24-h check with the nominal voltage can be applied. This is related to the practice in some countries, but in most countries, a test according to Table 10.4 is performed. For EHV cable systems ($Um \geq 245$ kV), a range of test voltage values is proposed $V_{t\min} \leq V_t \leq 1.7\ V_0$. The test voltage value to be applied is always a matter of agreement between supplier and user of the cable system.

The HVAC acceptance test of an extruded cable system can only be performed with an ACRF test system (Hauschild et al. 2002, 2005), and alternatives cannot supply the necessary test power on site or their test voltage shape does not fulfil the requirements of an acceptance test (Table 10.3). If long or super-long cable systems shall be tested, several ACRF test systems can be combined as shown in the following example.

Example A 400-kV cable system of a length of 22 km and a capacitance of $C_t = 4.9$ μF shall be tested in a Middle East country. The test voltage has been agreed between supplier and user to $V_t = 260$ kV/20, to 300 Hz for 1 h. The environmental temperature at the place of the test can be remarkably above 30 °C. The super-long cable system requires the combination of some single ACRF test systems.

There are several test systems available in that region: three systems for 260 kV with in total four reactors of $L = 16.2$H/83A and one system for 160 kV with two reactors of 23H/55A each. A suitable combination of the reactors must be found, to meet the requirements to the test voltages, the test frequency and the test power. Because of their

limited voltage, the two 155-kV reactors must be connected in series. Then, the test current should be—also for thermal reason—as low as possible, which means that the test frequency should be only slightly above 20 Hz. The series connection of the 155-kV reactors suggests that also the other reactors should be arranged accordingly (Fig. 10.26a). Then, the total inductance of the test system and the frequency are

$$L_t = \frac{(16.2 + 16.2)\text{H} \cdot (23 + 23)\text{H}}{2 \cdot (16.2 + 46)\text{H}} = 12\text{H},$$
$$f_t = 1/(2\pi\sqrt{L_t \cdot C_t}) = 21 \text{ Hz}.$$

With the known frequency and the test voltage, the test current and the test power can be calculated:

$$I_t = 2\pi \cdot f_t \cdot C_t \cdot U_t = 168 \text{ A},$$
$$\text{S}_t = I_t \cdot U_t = 43.7 \text{ MVA}.$$

If the test would be performed at 60 Hz, an equivalent test power $S_{60} = (60 \text{ Hz}/21 \text{ Hz}) \cdot 43.7 \text{ MVA} = 125 \text{ MVA}$ would be required. Even if the current can be supplied by two frequency converters, all four frequency converters are used to keep the load for each of them low. The three reactor branches are grounded via their frequency converters and connected in parallel (Fig. 10.26a). All converters are connected in parallel to the power supply. The control of one converter operates as the master and the other three controls as slaves. A quality factor of $Q = 80$ is usually assumed to calculate the feeding power $P_t = S_t/Q = 550$ kW, which is necessary for the compensation of the losses in the test arrangement. The real test (Fig. 10.26b) has confirmed the pre-calculated data except for the assumed quality factor, and the real one was $Q = 141$, which means the required feeding power has been only $P_t = 310$ kW. The real test has been a PD-monitored withstand test. The monitoring was realized by a non-conventional PD measurement with sensors in the cable joints and terminations as described in Sect. 10.4.2.5.

When *diagnostic tests* on HV/EHV cable systems are performed, usually the procedure of the PD-monitored acceptance test cycle is repeated with a reduced withstand voltage level, but identical PD reference voltage levels before and after the withstand level shall be applied (compare Fig. 10.2b). Especially the joints and terminations may be aged. Therefore, the trend of the PD measurements by means of sensors is an indication of the condition of joints and terminations.

10.4.2.4 Testing of AC and DC Submarine Cable Systems with Extruded Insulation

Submarine cable systems are characterized by their length of several 10 km or even more. The required very long cables are manufactured in factories at the coast and—after routine test—directly reeled to the laying ship (Figs. 3.45 and 10.27). The Cigre Working Group B1.27 has investigated conditions, voltages and procedures for testing *HVAC submarine c*ables (Cigre WG B1.27 2012). Even for the AC routine tests in the factory, AC test voltages of variable frequency 10–500 Hz are accepted with respect to the high capacitances of the test objects (Karlstrand

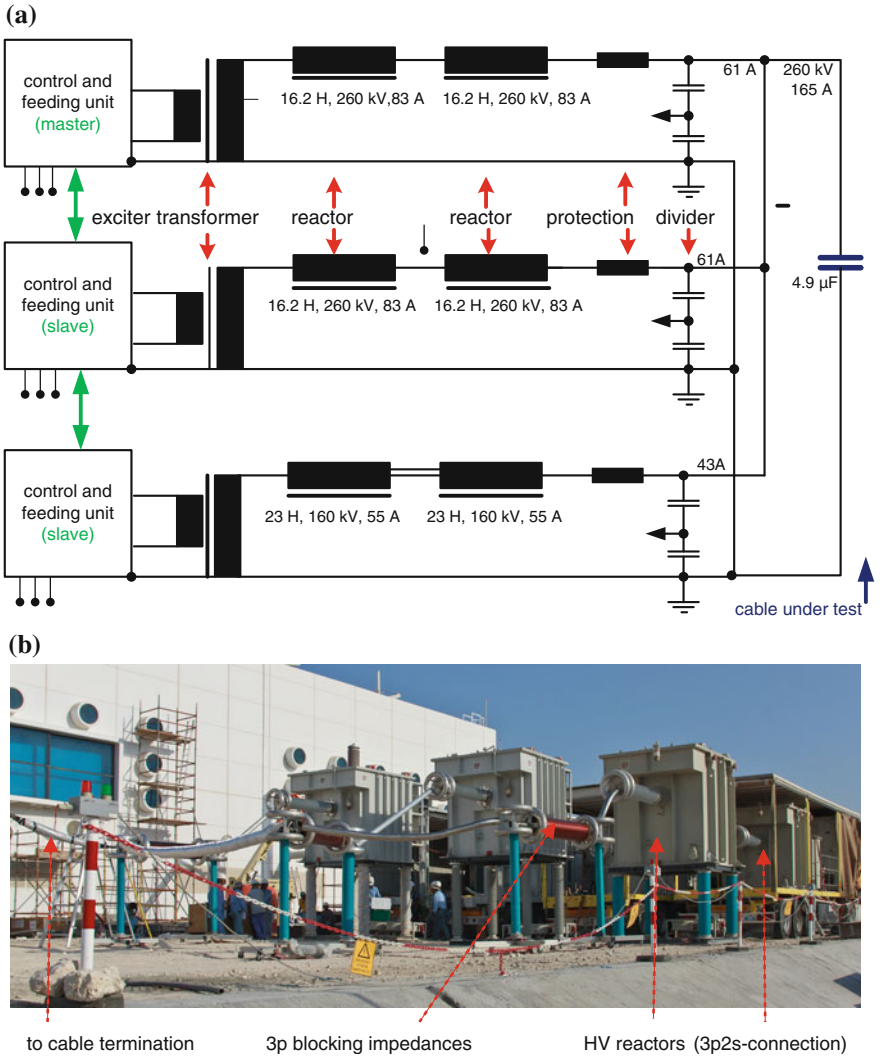

Fig. 10.26 Quality acceptance test of a 400-kV/22-km cable system of 4.9 µF. **a** Simplified circuit diagram. **b** Test arrangement (courtesy of CEPCO, Saudi Arabia)

et al. 2005). The extended frequency range down to 10 Hz enables the reduction in the test power compared with 20 Hz to its half, but the breakdown mechanism remains similar as for power frequency.

After installation, an *AC quality acceptance test* identical to that of land cables, but with the wider frequency range, shall be performed. The test voltages with the duration are selected according to Table 10.4.2-2. If the cable system is too long for testing with the specified values, a reduced test voltage with a longer duration

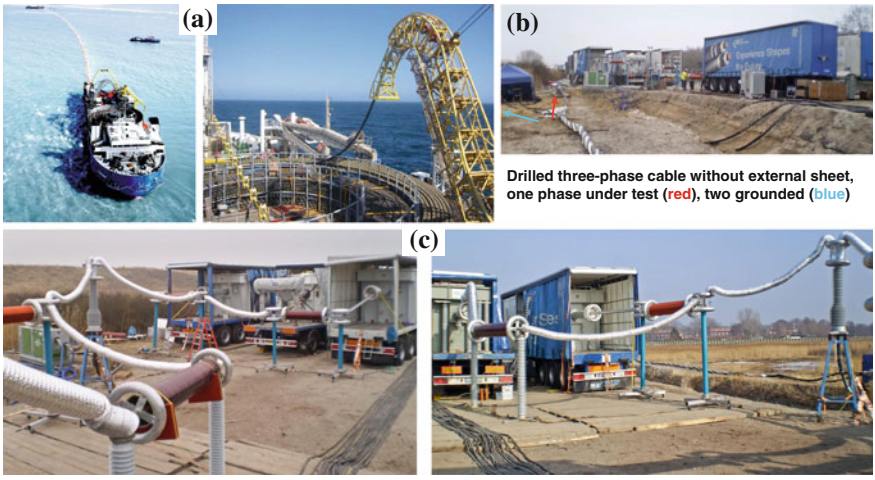

Fig. 10.27 After-laying test at 174 kv of a submarina cable (150 kv, 62 km, 13.8 μP). **a** Laying ship (Courtesy of ABB Karlskrona) **b** Cable end prepared for the single-phase test, **c** Test voltage generation by five test systems (260 kv, 83A each) in parallel

can be agreed between supplier and user. If a suitable test voltage source is not available, a check with the nominal voltage for 24 h can also be agreed. Special voltages as VLF and DAC cannot be recommended for tests after installation (Cigre WG B1.27 2012).

HVDC cable systems can transmit a much higher power than AC cables. Therefore, they might become very important for future power systems including submarine applications. The latest developments of extruded DC insulations offer economic perspectives. The testing of super-long DC cables is a challenge for the test techniques (Pietsch et al. 2010). The realistic test with DC voltage completed with *polarity reversals* (changeover time in the order of 1 min) is easy to perform, but it is not very efficient. The DC breakdown is a long-time process and—for time reasons—it cannot be simulated in a DC withstand test of some hours. Furthermore, a PD measurement of the required sensitivity cannot be reached because of the damping of PD signals when travelling along the long cable (see Sects. 3.6 and 10.4.2.5 or Cigre TF D1.33.05 2012). It is proposed by the Cigre Working Group 21.01 2003 to perform an HVAC test in addition to the HVDC test, because a serious defect causes the breakdown much faster at HVAC than at HVDC. This test should be performed by an ACRF test system operating in the extended frequency range 10–500 Hz. The sheet resistance of an HVDC cable is significantly higher than the conductor resistance and contributes to the losses in the test circuit remarkably. Therefore, in case of testing a HVDC cable, the quality factor of the test circuit is lower than that for HVAC cable of identical length. For the latter, only the ACRF test system itself determines the losses (Hauschild et al. 2005).

When the routine tests in factory are not yet clear, recommendations for the quality test after installation of HVDC cable systems are even more difficult. In

addition to tests with HVDC, HVAC tests as used for AC submarine cable systems are applied. Also tests with VLF and DAC voltages are discussed. But the applicability and feasibility of VLF and DAC tests in the EHV range is still very questionable (Pietsch et al. 2010; Cigre WG B1.27 2012). Further research work is needed for both quality testing and diagnostic testing.

10.4.2.5 PD Testing on Cable Systems

On-site PD measurements became of interest in the late 1980s, when paper-insulated, lead-covered cables (PILC) were increasingly replaced by extruded power cables due to the fact that the high-polymeric insulation is very sensitive to partial discharges even if the PD activity is comparatively low. In this context, it seems noticeable that PD magnitudes in the picocoulomb range might cause an immediate breakdown of extruded *HV/EHV cables* due to the high operational field strength which is significantly above 10 kV/mm. In contrast to this, *medium-voltage cables* (field strength <10 kV/mm) are not so sensitive against such low PD magnitudes, and an immediate breakdown is usually not indicated. Consequently, the philosophy for diagnostic on-site PD tests of extruded power cables shall be very different for both MV and HV/EHV cables.

Medium-voltage cable systems: The length of a MV cable system very seldom exceeds 5 km, corresponding to a capacitive load in the order of 1 μF. The circuit applied for periodical PD tests under on-site condition is well comparable with that applied under laboratory condition (IEC 60270: 2000; IEC 60885-3: 1988). That means after the operation, voltage has been switched off and the three phases of the cable line have been disconnected from the power network, and each phase is individually PD-tested. For this purpose, a coupling capacitor in series with a measuring impedance is connected to one cable end to capture the PD signal, which is transmitted to the PD measuring system, see Fig. 4.17a. After calibrating the complete measuring circuit in terms of pC, the cable is energized up to the desired test voltage to record the phase-resolved PD pulses. In case of potential PD failures, a localization of the site where the PD's originate and a PD mapping described in Sect. 4.4 is required for further decisions.

The application of *diagnostic tests* of MV cables was first required in the 1980s, when XLPE distribution cables—installed about a decade before—showed the PD phenomenon of "*water trees*" (Auclair et al. 1988). At that time, no ACRF test systems have been available and AC test systems based on transformers (ACT) or tuneable reactors (ACRL) have been too heavy and too expensive for on-site diagnostic tests. Therefore, alternative test voltages are applied, such as very low frequency (VLF) and damped AC (DAC) voltages specified in IEC 60060-3: 2006. VLF voltage is not so well suited for PD measurement because of the long duration of a period (see Sect. 10.2.2.1; Fig. 10.11), and it is more applied for diagnostic

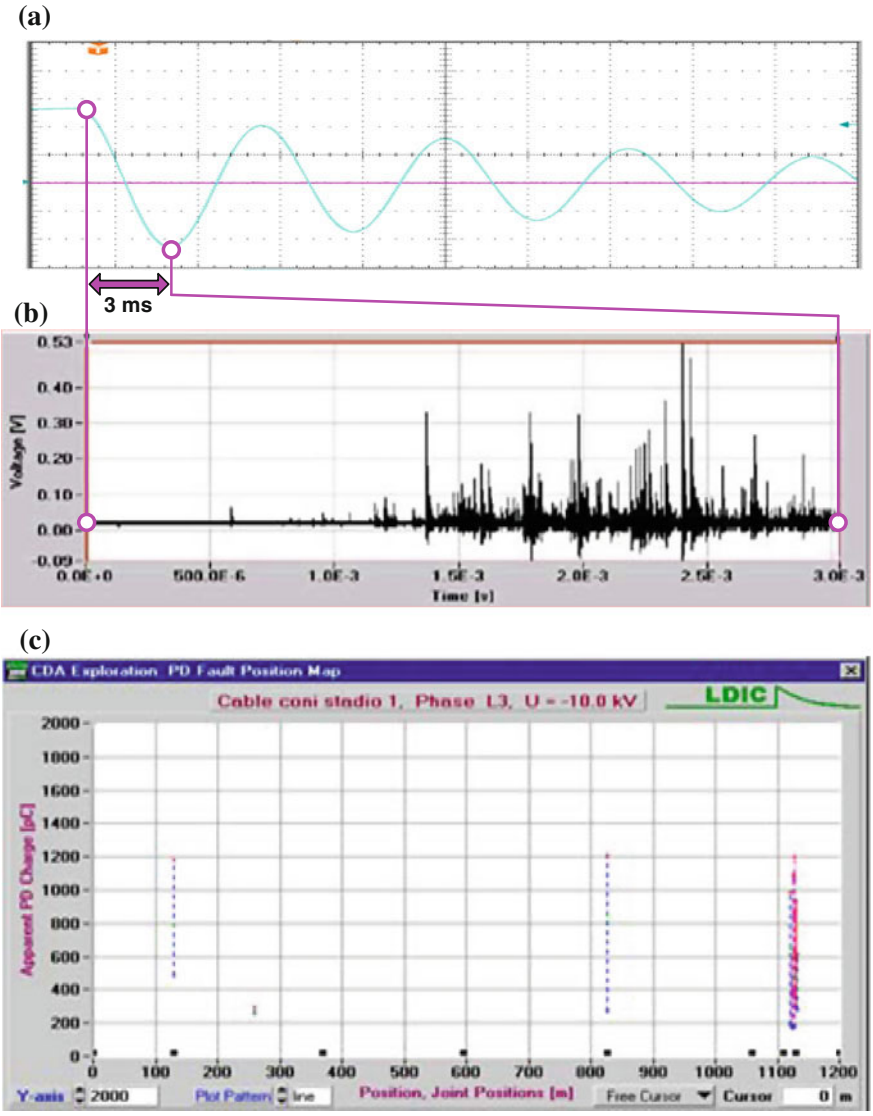

Fig. 10.28 PD mapping of a 30-kV XLPE cable (length 1,200 m) at DAC test voltage. **a** DAC test voltage, 24 kV peak-to-peak value. **b** PD pulse train during the first negative voltage sweep. **c** PD fault position map showing the position of the three identified joints

withstand tests and loss factor measurement. The main benefit of the *DAC voltage* (see Sect. 10.2.2.2, Fig. 10.13 as well as Sect. 7.6) is that significant PD quantities, such as the inception/extinction voltage and the pulse charge magnitude, are in a certain relation to values measurable at power frequency stress. Further benefits

Table 10.5 Parameters recommended for on-site PD diagnosis tests of MV cables at DAC test voltages

Cable insulation	Test voltage level (V_0)	Voltage applications	Accepted PD level (pC)
XLPE, aged	0.7	5	<50
	1.0	5	<50
	1.5	5	<50
	2.0	5	<50
XLPE, new	3.0	20	<20
Oil-paper, aged	1.0	10	<2,000
	1.5	10	<2,000
	2.0	10	<2,000
Oil-paper, new	3.0	20	<500

are the low power demand and thus the low weight and easy mobility of the DAC test facility (Fig. 10.15). Therefore, DAC voltages are considered in the following.

Commonly, it seems sufficient to acquire only the PD pulses occurring during the first positive and/or negative DAC voltage sweep resulting from a negative and/or positive DC charging voltage. A practical example of *PD mapping* is shown in Fig. 10.28, which refers to a 1,200-m-long extruded MV power cable (20 kV rated voltage) subjected to a damped AC voltage where the time interval between the peak-to-peak values representing the duration of the first negative voltage sweep being 3 ms.

Using only a single DAC voltage application of 24 kV peak to peak, the PD pulses occurring during the first negative voltage sweep have been extracted to create the PD map, as described in Sect. 4.4. Figure 10.28c shows three typical clusters indicating the position of three defective joints showing PD magnitudes between some 100 pC and more than 1,000 pC. Therefore, it was decided to replace the identified joints. Thereafter, the PD test has been repeated and no any PD signals were detected.

To specify the PD test parameters, it is a common practice to express the pre-stressing DC voltage in terms of the conductor-to-ground voltage of the cable network, in Table 10.5 designed as V_0. Practical experiences revealed that the scattering of the inception voltage is comparatively low if compared with continuous power frequency voltage. This is likely due to the DC pre-stress causing a minimizing of the statistical time lag required for the availability of an initiatory electron. Thus, usually only few DAC voltage applications at each test level are required. A survey on the test parameters initially recommended for on-site PD diagnosis tests of MV cables is given in Table 10.5.

HV/EHV cable systems: As mentioned already above, for on-site PD testing of extruded HV/EHV cables, a very high *detection sensitivity* is required due to the fact that PD events in the pC range might already cause an immediate breakdown of high-polymeric dielectrics. This is forced by the very high operational field strength much above the design field strength of MV cables. The PD test for both

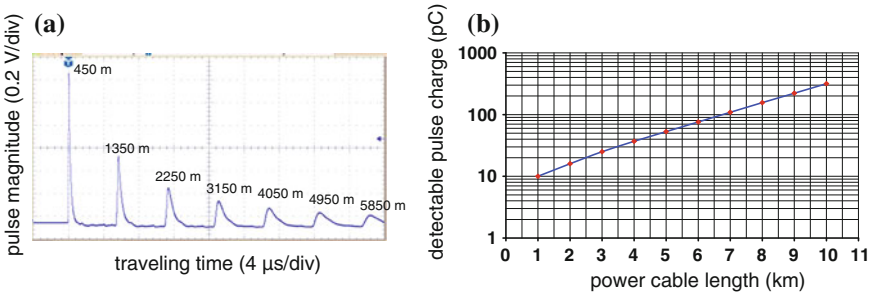

Fig. 10.29 Attenuation of PD pulses when travelling along an extruded HV cable. **a** Attenuated PD pulses. **b** Detection sensitivity versus the cable length

acceptance after laying and diagnostics shall be performed with an AC voltage usually generated by an ACRF test system.

Using the classical PD measuring circuit according to IEC 60270: 2000, the PD detection sensitivity desired for HV/EHV cables is not achievable, which is not only due to the always-present ambient electromagnetic noises but also as a consequence of the strong PD pulse attenuation if travelling from the PD source to the cable ends. A typical measuring example for this is shown in Fig. 10.29a where a 2,000 pC calibrating pulse has been injected in the remote end of a 450-m-long cable and the direct and reflected pulses have been recorded. Based on such measurements, the PD detection sensitivity versus the cable length can be estimated, as shown in Fig. 10.29b (Lemke 2003).

Assuming, for instance, that for a cable of 1 km length, a minimum PD level of 10 pC would be detectable using the IEC method under noisy on-site condition, the threshold level for detectable PD events would increase up to approx. 50 and 150 pC for cable lengths of 5 and 10 km, respectively, which is not acceptable for extruded HV/EHV cables, as mentioned above. Thus, on-site PD diagnosis tests are focused only on the cable accessories, where the PD signal is captured in the VHF/UHF range using inductive, capacitive or electromagnetic PD couplers, as treated in Sect. 4.7. The test philosophy is based on the fact that HV/EHV cables are carefully PD-tested in the factory after manufacturing, so that critical PD failures have to be expected only due to a pure assembling of the cable terminations and joints (Fig. 10.30). The concept applied is very similar to that applied for PD monitoring of power transformers, as described below. That means the PD couplers first used for the commissioning test remain installed to perform periodic as well as continuous PD monitoring.

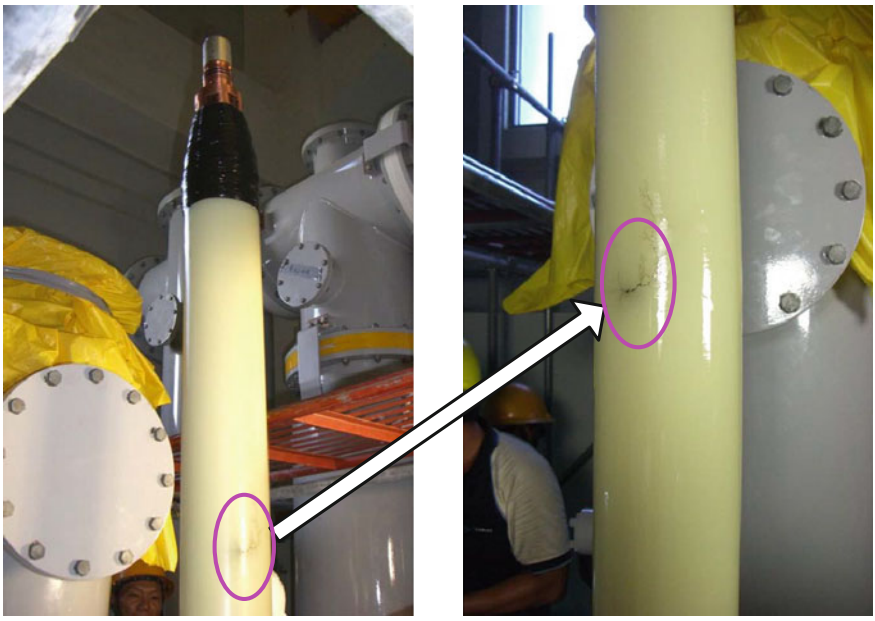

Fig. 10.30 Severe PD failure discovered in a 380-kV power cable termination during the commissioning test

10.4.3 Testing of Power Transformers

Whereas GIS and cable systems are finally assembled on site, complete power transformers are carefully tested in factory. Up to a certain size of the transformers, only bushings, conservator and similar parts exceeding the transport profile are dismounted for transportation. On-site assembly was quite limited. Therefore, no need for on-site acceptance tests on power transformers was seen (Kachler et al. 1998). Meanwhile, the situation has been changed and large units are assembled on site, especially in areas of insufficient transportation possibilities (Yamagata and Okabe 2009; Ohki 2010). Because of increasing transportation costs for power transformers, the available technology for on-site assembly is used for repair and refurbishment. Transformer manufacturers provide also the related service including HV testing (Siemens 2007; ABB 2006). On-site testing for quality acceptance and diagnostics of power transformers is well introduced now.

10.4.3.1 Quality Acceptance Testing

IEC 60076-3:2012 states for tests on transformers having been in service: “Any transformer that is to be regarded as complying with this standard in the same way

as a new transformer (for example following a warranty repair or complete rewind and refurbishment intended to restore the transformer to 'as new' condition) shall be subject to all routine tests required by this standard at 100 % of the required test voltages (Table 10.6) after the repair or refurbishment is complete". This statement which does not distinguish between repair in a factory and *on-site repair* would also be applicable to power transformers assembled on site. In case of a repair, repaired parts should be tested at a level between 80 and 100 % of the original test voltage (Table 10.6). New parts should be tested at 100 %. The induced voltage acceptance test with PD measurement (AC-IVPD test, see Sect. 3.2.5, Table 3.6 and Fig. 3.51) shall be performed on the same voltage level as required for the routine test. As a consequence of these requirements of IEC 60076-3, HV on-site test systems have to generate test voltages with parameters as for routine tests in factory.

A detailed consideration shows that AC test systems of variable frequency based on *static frequency converters* are applicable (Table 10.6, last line) (Hauschild et al. 2006; Martin and Leibfried 2006; Werle 2007; Thiede et al. 2010). As shown before, these test systems have remarkable advantages for mobile application (e.g. see Tables 3.2 and 3.3 and Sect. 10.1.3). They are also in the scope of IEC 60060-3:2006 and enable optimum conditions for HV tests on site (Fig. 10.31). Besides the applied and induced voltage withstand tests, the systems shall also be applicable for no-load and load-loss (short-circuit impedance) measurements. The HVAC test system must be selected according to the requirements of the test and the characteristic of the test object, especially its necessary test power demand:

Applied voltage withstand test	The transformer under test is a capacitive load (<50 nF), and the test ($f > 40$ Hz) can be performed by an ACRF test circuit with rated current of some Amps
Induced voltage withstandtest	In most cases, the transformer is a linear, mixed resistive–capacitive load, and the test can be performed with a frequency converter-based test system ($f > 100$ Hz) and requires relatively low test power
No-load loss measurement	The transformer is a nonlinear, mixed resistive–capacitive load in most cases, and the test can be performed with a frequency converter test system ($f = 50/60$ Hz) of relatively low power but sufficient stability against harmonics
Load-loss measurement	The transformer is a linear resistive–inductive load, and the test can be performed with a powerful frequency converter test system ($f = 50/60$ Hz) generating a fine, sinusoidal wave shape

The load–loss test (determination of short-circuit impedance) determines the power selection of the test system. (A heat run test has a similar test power demand.) The frequency converter of a mobile system can supply an active power in the order of 600 kW or even more and a reactive power in the order of 1,200 kVA (Fig. 10.32). For higher output parameters, several systems can be connected in parallel. If a higher reactive power is required, a capacitor bank must be added. Three-phase test systems can also operate in a single-phase mode.

Table 10.6 Selected routine test voltages of power transformers (IEC 60076-3:2012)

Test voltage Highest voltage for equipment V_m/kV	Applied voltage AC withstand test V_a/kV for 1 min	Induced voltage AC withstand and PD test V_{in} and V_{PD}/Kv (Figure 10.4.3-1)	LI and LIC voltage withstand test V_{LI} and V_{LIC}/kV (3 impulses each)	SI voltage withstand test V_{SI}/kV (3 impulses each)
123	230	128 and 112	550 and 605	460
145	360	151 and 132	650 and 715	540
245	460	255 and 224	1,050 and 1,150	850
420	630	437 and 382	1,425 and 1,570	1,175
550	680	572 and 501	1,675 and 1,845	1,390
800	–	832 and 728	2,100 and 2,310	1,675
1,200	–	1,248 and 1,092	2,250 and 2,475	1,800
Recommended HV test system	ACRF test system of $f > 40$ Hz (see 3.1.2.3 and 3.2.5)	Frequency converter system $f > 100$ Hz (see 3.1.3 and 3.2.5)	Impulse test systems for aperiodic LI and SI voltages according to IEC 60060-1	

U_m is a phase-to-phase value; all test voltages are phase-to-ground values

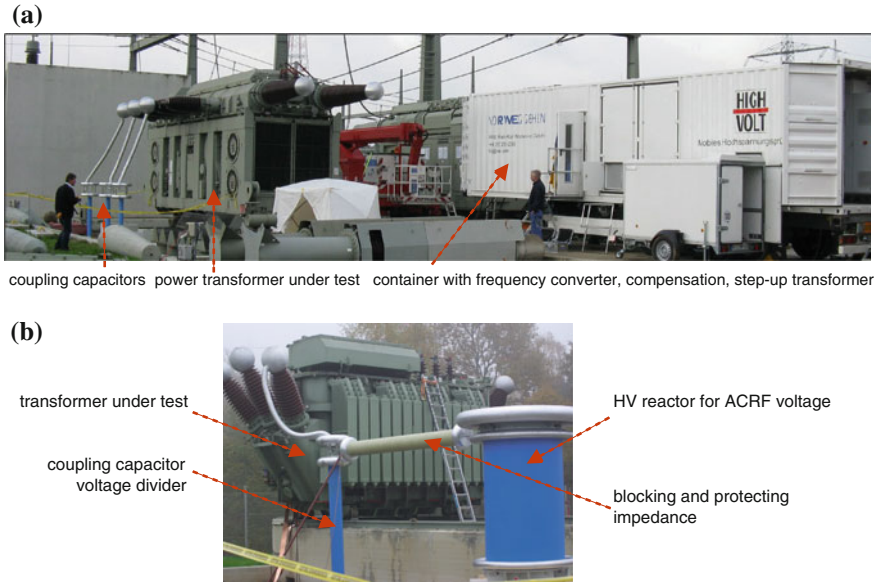

Fig. 10.31 On-site transformer tests. **a** Mobile system with frequency converter for induced voltage tests. **b** Mobile ACRF test system for applied voltage test

The applied voltage test is a single-phase test between the short-circuited HV side and the grounded short-circuited low-voltage side. The excitation voltage of the resonant circuit can be generated by the frequency converter for the tests with induced voltages. But a small separate converter completes an independent ACRF test system, which might be even more practicable for separate application.

The components of a stationary frequency converter system are well arranged in a 40-feet container which fits to the dimensions for standard road transportation (Fig. 10.33). It includes the frequency converter, the step-up transformer, the control room, the space for HVHF filters and measuring equipment for voltage and current.

Additionally, to the AC voltage tests, IEC 60076-3:2012 requires aperiodic impulse voltages for LI and SI on-site application. The oscillating impulse (OLI; OSI) voltages which are generated with a much higher utilization factor are not accepted for transformer testing on site. This means that an impulse generator for on-site testing of UHV power transformers would be a quite huge and a not-easy-to-handle unit (see Sects. 7.1.2.4 and 7.2.1.3). It seems to be questionable whether LI test voltages above 2 MV can be generated on site. It can be assumed that reduced test voltage levels or OLI voltages will be applied.

In all the applications of the very stringent requirements of IEC 60076-3: 2013 for on-site acceptance tests of power transformers, we could find their limits of practicability. Therefore, the real necessary tests should be considered, and the required parameters of the test system defined and agreed between supplier and

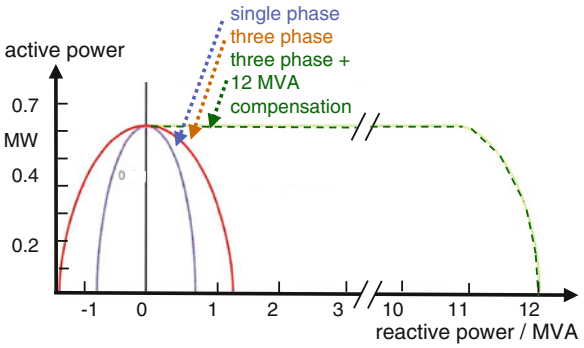

Fig. 10.32 Active and reactive test power of a frequency converter without and with a capacitor bank (schematically)

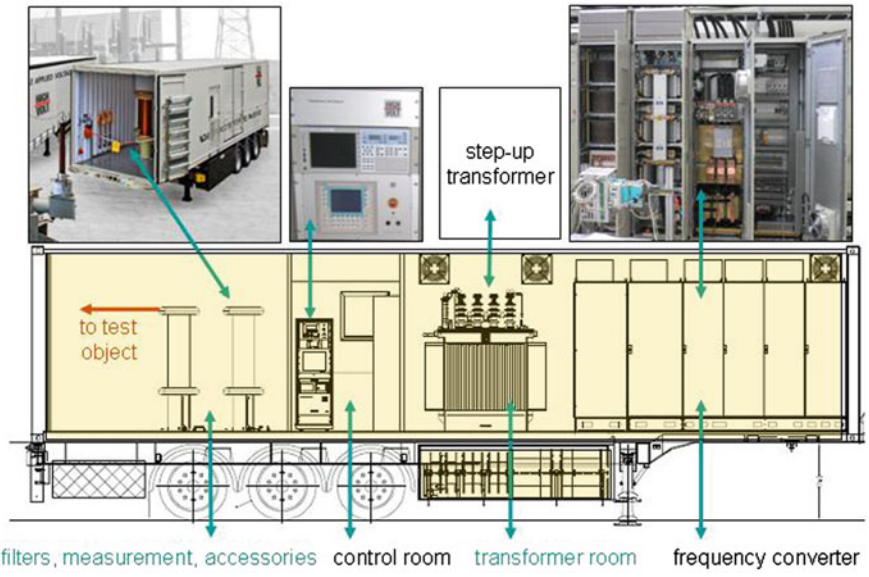

Fig. 10.33 Design of a mobile transformer test system

user. The most important insulation test seems to be the PD-monitored, induced voltage withstand test which is also important for diagnostics. When a utility plans to operate a system for induced voltage tests, it seems to be not optimum to order the frequency converter for testing their largest power transformer. Rather the later extension by combination of two or more test systems should be taken into consideration for rare tests. The new IEEE Guide on diagnostic field testing on power transformers (IEEE 62-PC 57.152-2012) recommends also test systems based on frequency converters, which might also be helpful when acceptance and diagnostic tests have to be agreed.

10.4.3.2 PD Measurement in HV Tests and PD Monitoring

The very complex insulation system of a power transformer and its components is an object of numerous electrical, chemical, physical and thermal tests and checks for condition assessment. A survey is found in the "ABB Service Handbook for Transformers" 2006 and in many publications (e.g. Leibfried et al. 1998; Singh et al. 2008; Zhang and Gockenbach 2008).

In the following, only HV off-line tests and PD measurements/monitoring are considered. Induced voltage tests might be well related to online PD monitoring. The PD monitoring can only deliver measuring results at operational voltage, and their trend over time is evaluated. The *off-line induced voltage test* enables the change in the stressing voltage and the measurement of PD characteristics important for condition assessment.

Before the HV test on a service-aged power transformer is started, several low-voltage and chemical tests and checks—insulation resistance, power factor, turns ratio, dielectric strength, moisture and dissolved *gas-in-oil analysis*—should be performed. The HV test is recommended when the measured parameters are within their acceptable tolerances. The HV test procedure should follow similar procedures as for PD-monitored acceptance tests (Fig. 3.51), but can be modified as useful for the diagnostic purpose.

For condition assessment, power transformers have commonly been inspected periodically and only continuously from time to time when a severe PD activity was supposed, e.g. indicated by spectral gas-in-oil analysis. For periodic PD monitoring, the transformer is commonly disconnected from the power network and excited by a separate power supply (today usually a frequency converter, as already presented in Sect. 3.1.3). Under this condition, the *bushing tap PD coupling mode* in compliance with IEC 60270: 2000 can be considered as the most convenient method (Fig. 10.34), where the ambient noise level is usually not higher than few hundreds of picocoulombs, which is usually tolerated for liquid-immersed power transformers.

The main benefit of the traditional IEC method is that the PD measuring circuit can be calibrated in terms of pC, which ensures not only well-reproducible test results but also a comparison with fingerprints established in quality acceptance tests in the factory and during commissioning on site. Another benefit of the bushing tap coupling mode is the capability for multi-terminal, phase synchronous measurements to create *PD star diagrams*. As already treated in Sect. 4.6, such graphs are a promising tool for the identification of typical insulation failures as well as for the recognition and thus the elimination of disturbing noises.

The philosophy of periodical on-site PD measurements is based on the assumption that the insulation of liquid-immersed power transformers ages over a comparatively long time. Nevertheless, the development of weak spots cannot always be excluded within the time span between two periodic inspections. Thus, it could happen that an abnormal PD activity remains undiscovered and could thus initiate a potential insulation failure or even an unexpected outage (breakdown of insulation). Therefore, strategic important EHV/UHV transformers are nowadays

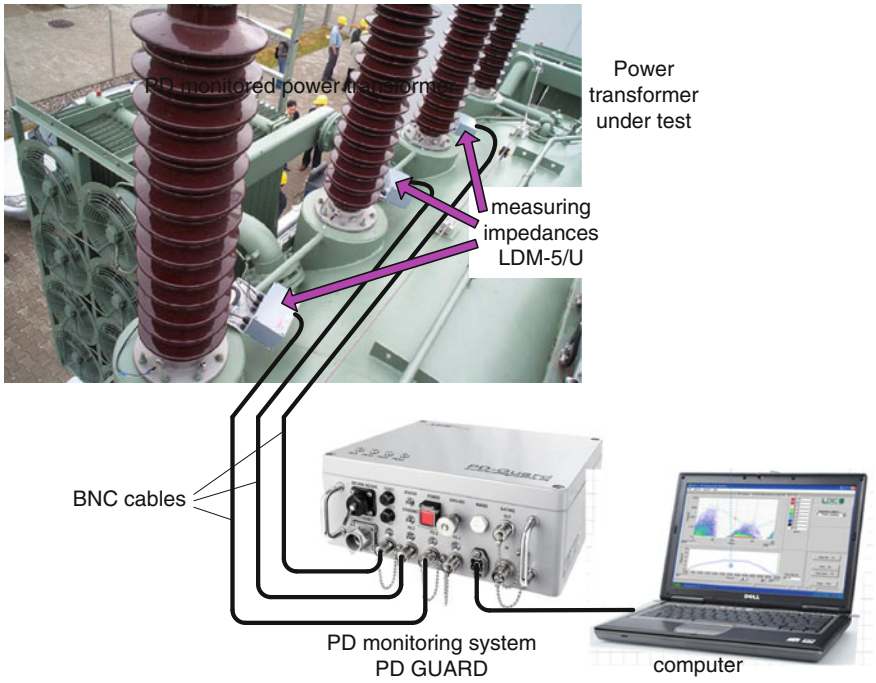

Fig. 10.34 Set-up for periodical on-site PD monitoring of power transformers using the bushing tap coupling mode in compliance with IEC 60270: 2000 (Courtesy of Doble Lemke)

continuously PD-monitored. As this occurs under service condition, the measurement under field conditions is commonly strongly interfered by ambient noises which may exceed tens of nano-coulombs. A promising tool to eliminate such disturbances is the application of the UHF/VHF technology, see Sect. 4.7. For this purpose, different kinds of UHF PD couplers have been developed in the past, such as the *drain-valve sensor* and the *plate-hatch sensor*, as shown in Fig. 10.35 (Markalous 2006; Coenen et al. 2007).

Due to the strong attenuation of UHV signals if propagating from the PD source to the sensor, the use of several UHF PD couplers is highly recommended even if single-phase transformers are monitored. The installation of a multiple sensor array offers also the possibility for a so-called *dual-port performance check* (Coenen et al. 2007). For this purpose, an UHF signal of known parameters is injected in one of the installed sensors, and the amplitude–frequency spectrum obtained from all other sensors is recorded. Additionally, the measuring sensitivity should be verified, preferably performed under factory condition. This can be executed by comparative PD studies applying both the traditional IEC 60270 method and the UHF method, where the signal radiated from an artificial PD source implemented in the transformer tank is measured simultaneously by both methods. Recording the pulse charge in terms of pC and the UHF signal in terms

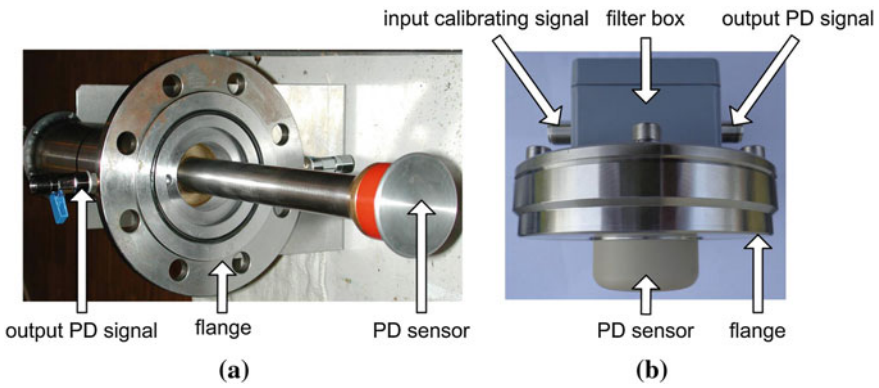

Fig. 10.35 Drain-valve sensor (**a**) and plate-hatch sensor (**b**) developed for continuous PD monitoring of power transformers in the UHF range (Courtesy of Doble Lemke)

of mV, the threshold PD level can roughly be estimated, and in some cases, it can be investigated whether there exists a sufficient correlation between the measurands in pC, respectively, in mV even if the magnitudes of both signals are scattering over an extremely wide range.

Performing continuos PD monitoring, it has to be taken into account that the complete *PD data stream* cannot be stored for a long period of time due to the limited memory capacity of the PD monitoring and acquisition system. This PD system is installed in the vicinity of each power transformer to be monitored, as illustrated in Fig. 10.36. Thus, the raw PD data stream is commonly not stored permanently but rather from time to time due to the fact that the transformer insulation ages comparatively slowly, as mentioned above. Therefore, the mean PD level is recorded permanently—to recognize any trends immediately—whereas the phase-resolved and time-dependent PD pulse trains are stored and acquired only for preselected time intervals, for instance, during 5-min periods repeated on an hourly basis.

If desired, the characteristic PD patterns can be observed in the control room of the substation, as usual also in case of factory tests. Recognizing drastically rising trends, however, the data can be transmitted via Internet permitting an investigation by experts for further decisions. Today's PD monitoring systems are also equipped with tools to generate a warning or even an alarm (compare Fig. 10.18). Based on practical experience, an appropriate set of parameters should be chosen to avoid an alarm release due to sporadic PD events or stochastically appearing interferences. Appropriate parameters for triggering an alarm relay are, for instance

- threshold level for critical PD pulse magnitudes, for instance 10 mV,
- mean number of PD pulses exceeding the critical threshold level, for instance 10 per minute,

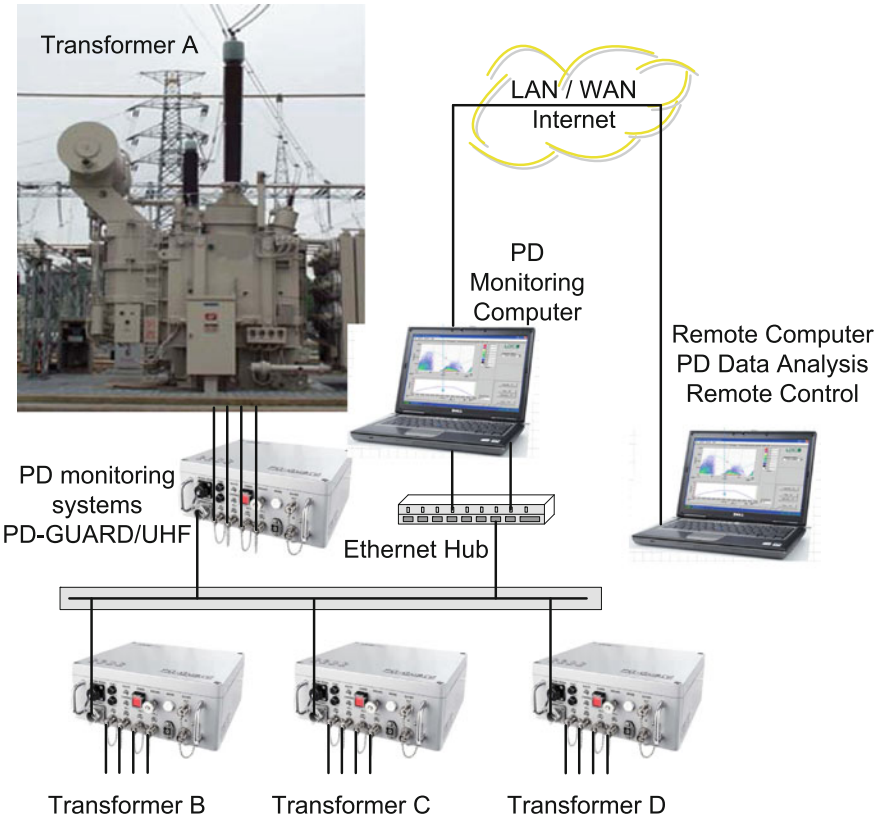

Fig. 10.36 Layout of a continuous PD monitoring system (Courtesy of Doble Lemke)

- time interval accepted for exceeding the critical threshold level, for instance 10 min.

If an alarm was released, further actions—preferably in an off-line induced voltage test—are required for the identification and localization of potential PD sources. The acoustic emission (AE) technique described in Sect. 4.8 (Figs. 4.70, 4.71 and 4.72) is well suited for this task.

10.4.4 Testing of Rotating Machines

Usually, rotating machines are assembled and tested in factory (IEC 60034-1:2010), and on-site acceptance tests are applied in rare cases after agreement between manufacturer and user. The test should be performed with AC voltage, but a test with DC voltage is not excluded.

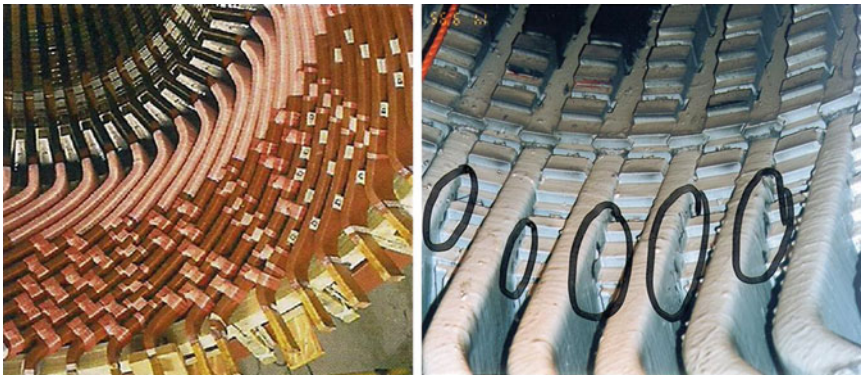

Fig. 10.37 Overhang section of a rotating machine after manufacturing (*left*) and failures identified by periodical PD monitoring (*right*) (courtesy of Doble Lemke GmbH)

The degradation of insulating materials used for rotating machines, such as hydro- and turbogenerators as well as HV motors, is not only caused by high local electrical field strengths but also due to thermal and mechanical stresses caused by numerous repetitive starts and stops as well as by strong load fluctuations during long-term operation. Thus, besides *lossfactor* and *recovery voltage*, also *PD tests* have become an important diagnosis tool for rotating machines (IEC 60034-27:2006; Cigre TF D1.33.05 2012). The philosophy and thus the layout for on-site tests as well as for periodic and continuous monitoring of rotating machines are very similar to those already presented above for power transformers. The only difference is, however, that the UHF/VHF technique is not applicable. This is not only due to the winding inductance but also due to the close electromagnetic coupling between the stator bars providing the three phases of an electrical machine, as can be imagined from Fig. 10.37.

For on-site tests, different HVAC sources are applied. When the test voltage remains below 20 kV and the required test power below 150 kVA, the AC test system can be based on a transformer. For higher voltage and test power, resonant circuits should be applied. The dissipation factor depends on frequency by definition; therefore, the inductance-tuned ACRL test system (Fig. 10.38) is well suited for both *dissipation factor* and *PD measurement*.

The dissipation factor itself does not characterize the insulation condition, but it increases with the voltage ($\Delta\tan\delta/\Delta u$). Measurement at different test frequencies indicated that this parameter is not depending on frequency (Fig. 10.39a). Therefore, also *ACRF test systems* (Fig. 10.3a) can be used for off-line, on-site testing with $\tan\delta$ and PD measurements which are considered to be most important for condition assessment (IEC 60034-27:2006; IEEE 1434-2000), (Fig. 10.39b). The measured characteristic PD charge versus test voltage (Fig. 10.39c) shows the

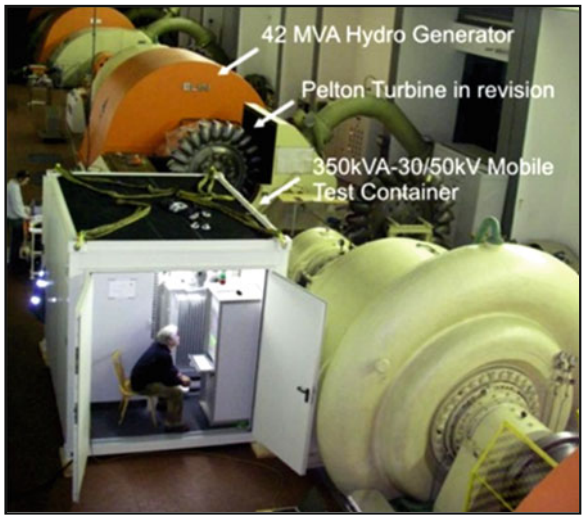

Fig. 10.38 Mobile ACRL test system (30–50 kV, 350 kVA) during a generator test (courtesy of TU Graz, Austria)

typical "ionization bend" and different PD charges for increasing, respectively, decreasing test voltage.

The *PD monitoring* of turbo- and hydrogenerators became an indispensable tool for insulation condition assessment in the 1980s when—besides the PD-resistant epoxy–mica insulation—vacuum-pressure-impregnated (VPI) epoxy insulation was introduced (Henriksen et al. 1986; Kemp 1987; Fruth et al. 1989; Grünewald and Weidner 1994). At that time, the PD signal has been decoupled either via so-called slot couplers or even via capacitive couplers of comparatively low capacitance, commonly below 100 pF. Such PD couplers, however, are characterized by a lower limit frequency usually significantly above 10 MHz. Thus, only slightly attenuated PD signals originating in the vicinity of the PD couplers could be detected. As a consequence, several PD-monitored rotating machines failed, mainly due to slot and end-winding discharges as well as discharges in cavities due to delamination.

The capability of *PD couplers* for PD signal transmission can simply be proven by injecting calibrating signals in the neutral points of rotating machines and measuring the pulse response at the terminals providing the phases $L1$, $L2$ and $L3$ where the power network is connected. The measuring example shown in Fig. 10.40 refers to a 300 MVA motor/generator where calibrating pulses of 10 nC have been injected in the neutral point. Using a 100 pF PD coupler, not any signal exceeding the mV range could be detected. Increasing the coupling capacitance from originally 100 pF up to 2 nF, however, signal magnitudes around 20 mV were obtained, as obvious from Fig. 10.40. Such a signal magnitude is well measurable by means of conventional PD monitoring systems.

In this context, it seems noticeable that the PD level of rotating machines under operation condition cannot be kept below the nC range, which means that a PD detection level below the nC is not necessary. Performing periodical PD

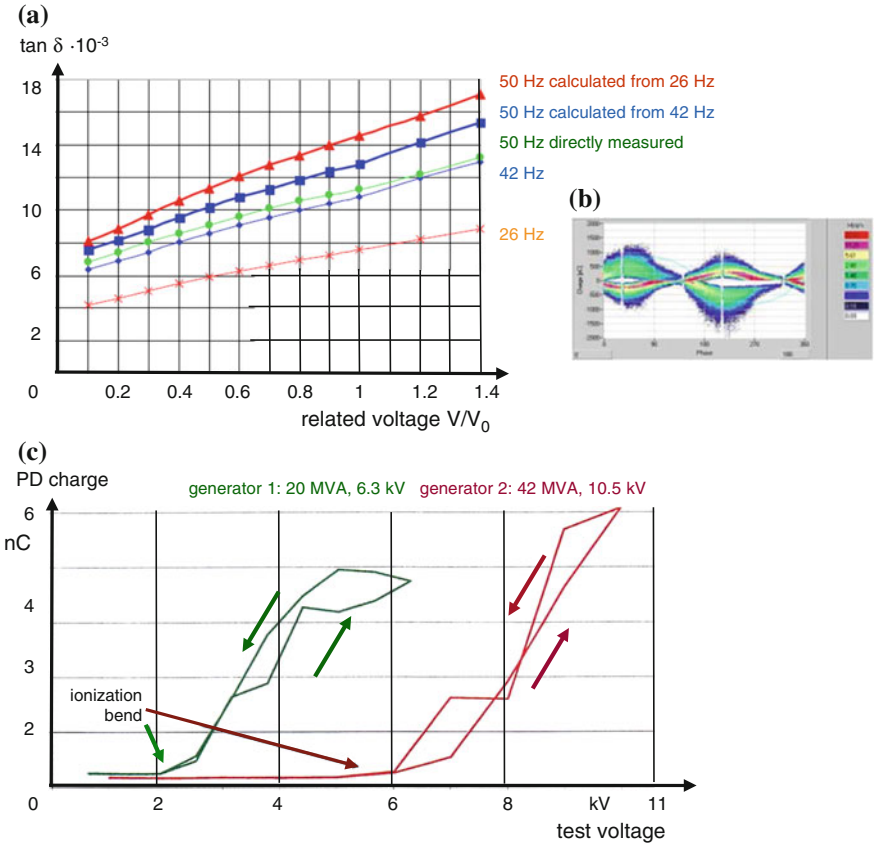

Fig. 10.39 Measured characteristics of two generators (Cigre TF D1.33.05 2012). **a** Dissipation factor depending on test voltage. **b** PD pattern (at 42 Hz, comparable to 50 Hz). **c** PD charge of two different generators depending on test voltage

diagnostics, the machine is usually excited by a mobile test voltage source (Fig. 10.38), where the individual phases are tested in turn, while the other phases not tested are connected to the grounded stator. Another option is illustrated in Fig. 10.41, which refers to a PD test under online condition. That means the three phases are subjected simultaneously to the operational voltage and therefore subjected to the actual service stress.

Under this condition, however, the measurement is extremely disturbed by high commutation pulses originating in the six-pulse converters of the auxiliary power supply for static excitation of the rotor. A typical example for this is shown in Fig. 10.42a, which is recorded for 300 MVA motor/generator in a pumped storage plant under service condition (rated voltage 21 kV). The noise pulses (with magnitudes up to 10 nC and above) can clearly be distinguished from real PD events which are scattering around 5 nC. Thus, a suppression of the noise by gating seems not necessary while observing the PD patterns on the computer

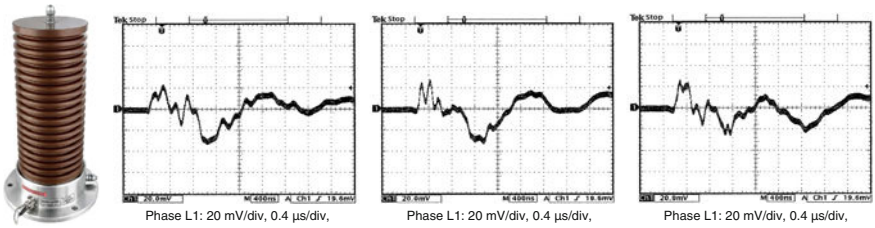

Fig. 10.40 PD coupler equipped with a 2 nF/24 kV capacitor used for measuring the pulse response of a 300 MVA motor/generator due to 10 nC calibrating pulses injected in the neutral point (courtesy of Doble Lemke

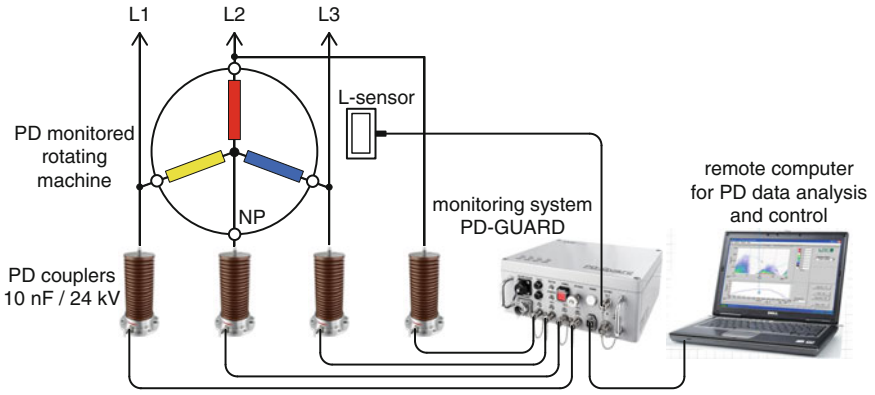

Fig. 10.41 Set-up for diagnostic online PD tests of rotating machines under service voltage

monitor. Following the PD trend, however, is only possible after suppressing the noise pulses. Thus, for continuous PD monitoring, an automatic *noise gating* is recommended, as described in Sect. 4.5. For picking up the disturbing commutation pulses, an *inductive sensor* (frame antenna type) can be installed adjacent to the slip rings of the motor/generator and connected via a BNC measuring cable to the monitoring system, as has been proven under real test conditions in numerous power plants. An example for this is shown in Fig. 10.42. Here, the phase shift between the consecutive PD clusters is surprisingly not 90° and 180°, respectively, typical for phase-to-ground discharges, but 120° or 240°. Due to this, it is supposed that phase-to-phase discharges appear, as can readily be shown based on the potential diagram of a three-phase network, which will not be discussed here more in detail.

Performing PD monitoring of large hydro- or turbogenerators, the rotor is commonly removed from the stator. This offers the possibility for a convenient localization of PD defects. For this purpose, the measurement of the light emission in the UV range or the acoustic emission (AE) technique is often used. Another option is the PD probing which has successfully been proven for the inspection of

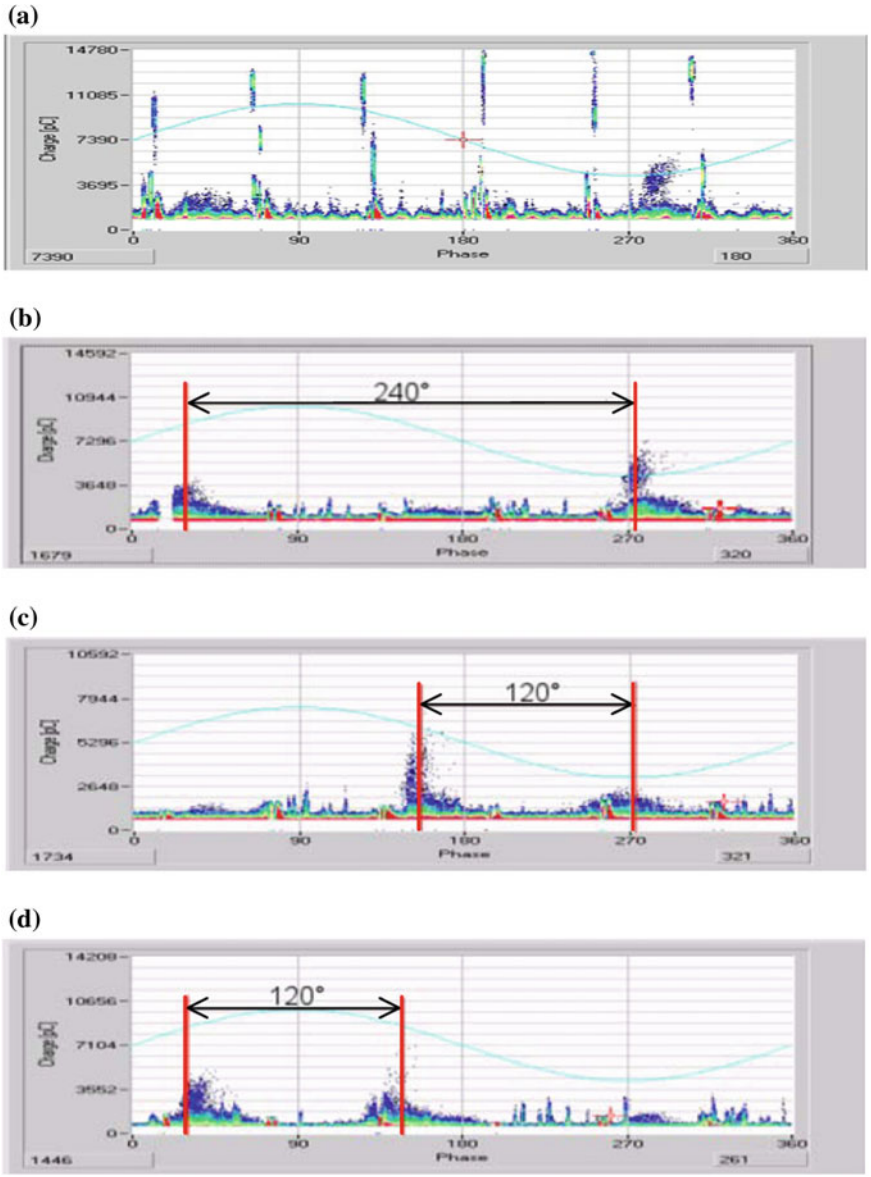

Fig. 10.42 PD signatures recorded for of a 300 MVA motor/generator operating at service condition. **a** Phase *L*1 showing PD clusters and superimposed noises from 6-pulse AC/DC converter of auxiliary power supply. **b** Phase *L*1, noise gating activated. **c** Phase *L*2, noise gating activated. **d** Phase *L*3, noise gating activated

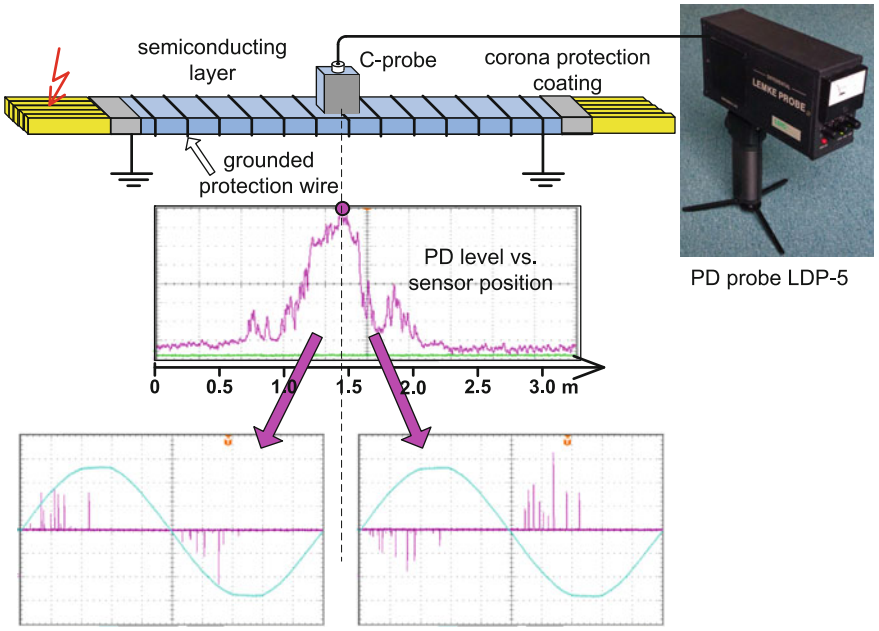

Fig. 10.43 Arrangement for pinpointing the PD source in a stator bar by a differential PD probe

numerous hydrogenerators (Lemke 1991). In some cases, stator bars—showing a high PD activity but not visible damage—have been removed to perform a deeper investigation by pinpointing to localize the PD defect *inside* the stator insulation. The set-up applied for this purpose is illustrated in Fig. 10.43. First, a capacitive sensor connected to the PD probe has been moved along the stator bar to localize the critical region indicated by the highest PD level. Thereafter, two capacitive sensors have been adapted to the inverting and non-inverting input of the potential-free operating differential PD probe, which has been moved along the stator bar within the region where the PD source was supposed. Under this condition, the PD site could exactly be located, where the tolerances were below the cm range. This could be achieved because the polarity of the recorded PD pulses is inverted suddenly after crossing the PD source, as obvious from Fig. 10.43.

Biography of W. Hauschild

Wolfgang Hauschild

Wolfgang Hauschild received the diploma degree in 1965, the Ph.D. in 1970 and the *habilitation* (university lecturing qualification) in 1976 from the Technical University (TU) of Dresden, Germany. In 2007, he became *doctor honoris causa* of the Technical University of Graz, Austria. From 1966 to 1979, he was a researcher of TU Dresden managing a research group on SF_6 insulation. In 1976/1977, Dr. Hauschild was a guest professor at Damascus University, Syria, and responsible for the erection of a large HV laboratory there. In 1980, he moved to industry and has been in leading positions of HV test equipment production in Dresden, from 1990 to 2007 as the Technical Director of HIGHVOLT Prüftechnik Dresden GmbH. After retirement, he is still active as a consultant. Dr. Hauschild was German speaker to IEC TC 42 (HV test technique) from 1995 to 2009 and is a member of IEEE, VDE and CIGRE. He published two books and numerous papers on HV engineering, especially HV testing.

Dr. Wolfgang Hauschild
DRESDEN
Germany
E-Mail: hauschild@highvolt.de

W. Hauschild and E. Lemke, *High-Voltage Test and Measuring Techniques*,
DOI: 10.1007/978-3-642-45352-6, © Springer-Verlag Berlin Heidelberg 2014

Biography of E. Lemke

Eberhard Lemke

Eberhard Lemke graduated from the Technical University (TU) Dresden, in 1962, where he was involved in research and education in the field of high-voltage engineering for more than three decades and received the Ph.D. degree and Dr.sc. techn. degree in 1967 and 1975, respectively. In 2010, he was awarded an honorary doctorate (Dr.h.c) from the Technical University Graz, Austria. From 1978 until 1981, he joined a power cable factory in Germany. During this time, he developed the so-called Lemke Probe using the non-conventional field coupling mode for PD diagnostics of HV apparatus in service. In 1987, he was appointed Professor at TU Dresden and founded the company Lemke Diagnostics GmbH in 1990, which manufactures among others instruments for PD diagnostics of HV equipment. Eberhard Lemke is author and coauthor of several textbooks. He published numerous technical papers, holds various patents and is active in several national and international organizations, such as VDE, CIGRE, IEC and IEEE.

Prof. Dr. Eberhard Lemke
RADEBURG
Germany
E-Mail: lemke@doble-lemke.eu

W. Hauschild and E. Lemke, *High-Voltage Test and Measuring Techniques*,
DOI: 10.1007/978-3-642-45352-6,

References

ABB (2006). Service handbook for transformers. ABB Management Services LTD/Transformers.

Achillides, Z., Georghiou, G. T., & Kyriakides, E. (2008). Partial discharges and associated transients: The induced charge concept versus capacitive modeling. *IEEE Transaction on Dielectrics and Electrical Insulation,15*(6), 1507–1516.

Achillides, Z., Kyriakides, E., & Georghiou, G.E. (2013). Partial discharge modeling: An improved capacitive model and associated transients along medium voltage distribution cables. *IEEE Transaction on Dielectrics and Electrical Insulation*, *20* (3), 770–781.

Albiez, M., & Leijon, M. (1991). PD measurements in GIS with electric field sensor and acoustic sensor. 7th ISH, Dresden, paper No. 75.08.

Allibone, T. E., & Dring, D. (1972). Influence of humidity on the breakdown of sphere and rod gaps under impulse voltages of short and long wave fronts. In *Proceedings IEE* (Vol. 119, pp. 1417–1422).

Allibone, T. Z., Achillides, Z., Kyriakides, E., & Georghiou, G. T. (2013). Partial discharge modeling: An improved capacitive model and associated transients along medium voltage distribution cables. *IEEE Transaction on Dielectrics and Electrical Insulation,20*(3), 770–781.

Anderson, J. G. (1956). Ultrasonic detection and location of electric discharges in insulating structures. *AIEE Transactions,75*, 1193–1198.

Anderson, J. M. (1971). Wide frequency range current transformers. *Review of Scientific Instruments,42*, 915–926.

Arman, A. N., & Starr, A. T. (1936). The measurement of discharges in dielectrics. *Journal of the Institution of Electrical Engineers,79*, 67–81, 88–94.

Arora, R., & Mosch, W. (2011). *High voltage and electrical insulation engineering*. Hoboken: Wiley.

Asner, A. (1969). Progress in the field of measuring very high fast transient surge-voltages. BBC-Mitteilungen, 47, 239–267.

Asner, A. M. (1974). *High-voltage measuring techniques (in German)*. New York: Springer.

Auclair, H., Boone, W., & Papadopulos, M. S. (1988). Development of a new after laying test method for high voltage power cables. CIGRE Session Paris, France, paper 21-06.

Bach, R. (1993). Investigation to the on-site testing of medium voltage cables using different voltage shapes (in German). PhD Thesis TU Berlin.

Bachmann, H., et al. (1991). Hardware and software for computer-aided impulse voltage tests. 7th ISH Dresden, Paper 5.14.

Bailey, C. A. (1966). A study of internal discharges in cable insulation. *IEEE Transactions on Electrical Insulation,31*(2), 360–366.

Balzer, G., et al. (2004). Evaluation of failure data of HV circuit-breakers for condition-based maintenance. CIGRE Session Paris Report A3–305.

Bärsch, R., Jahn, H., & Lambrecht, (1999). Test methods for polymeric insulation materials for outdoor HV insulation. *IEEE Transaction on Dielectrics and Electrical Insulation,9*, 668–675.

W. Hauschild and E. Lemke, *High-Voltage Test and Measuring Techniques*,
DOI: 10.1007/978-3-642-45352-6, © Springer-Verlag Berlin Heidelberg 2014

Bartnikas, R. (2002). Partial discharges–their mechanism, detection and measurement. *IEEE Transaction on Dielectrics and Electrical Insulation,9*(5), 763–808.

Bartnikas, R., & Levi, H. R. (1969). A simple pulse-height analyzer for partial discharge rate measurements. *IEEE Transactions on Instrumentation and Measurement,IM-18*, 341–345.

Beigert, M., Henke, D., & Kranz, H-G. (1991). Isothermal relaxation current measurement, a destruction free tracing of pre-damage at synthetic compounds. 7th ISH, Dresden Paper 72.05.

Beinert, J., Kadry, E. A., & Schuppe, W. (1977). The role of PD measurement for the detection of defects in extruded medium-voltage cables (in German). *Elektrizitätswirtschaft,76*(26), 925–928.

Bellaschi, P. L. (1933). The measurement of high surge voltages. *Transactions of the American Institute of Electrical Engineers,52*(2), 544–552.

Bellaschi, P. L. (1934). Heavy surge currents generation and measurement. *Transactions of the American Institute of Electrical Engineers,53*(1), 86–94.

Bellaschi, P. L., & Teague, W. L. (1935). Sphere-gap characteristics of very short impulses. *The Electric Journal*, *32*(3).

Bellm, H., Küchler, A., Herold, J., & Schwab, A. J. (1985). Rogowski coils and sensors for the magnetic field for the measurement of transient currents in the nanoseconds range. *Archiv für Elektrotechnik*, *68*(part I), 63–74, (part II), 69–74.

Bengtsson, T., Kols, H., & Jönsson, B. (1997). Transformer PD diagnosis using acoustic emission technique. In *10th ISH Conference Proceeding* (Vol. 4, pp. 115–119). Montreal, Canada.

Bergman, A., et al. (2001). Demonstration of traceability in high-voltage tests by means of a record of performance. *Electra,199*, 35–43.

Berlijn, S. (2000). Influence of lightning impulses to insulating systems (Dissertation, Graz Technical University).

Berlijn, S., et al. (2007). Manual evaluation of lightning impulses according to the new IEC 60060-1. 15th ISH, Ljubljana.

Bernard, G. (1989). Application of Weibull distribution to the study of power cable insulation. *Electra,127*, 75–83.

Bernasconi, F., Zaengl, W., & Vonwiller, K. (1979). A new HV-series resonant circuit for dielectric tests. 3rd ISH Milan, Report 43.02.

Beyer, J. (2002). Space charge and partial discharge phenomena in HVDC devices. Ph.D. Thesis, TU Delft, The Netherlands.

Beyer, M. (1978). Possibilities and limits of PD measurement and localization—basics and measuring systems (in German). *ETZ-A*, *99*(2), 96–99, (3), 128–132.

Beyer, M., & Borsi, H. (1977). PD measurement on HV cables—reasons for failures and possibilities for improvement (in German). *Elektrizitätswirtschaft,76*(26), 931–936.

Beyer, M., Boeck, W., Moeller, K., & Zaengl, W. (1986). *High-voltage technology: theoretical and practical basics (in German: Hochspannungstechnik)*. Berlin: Springer.

Beyer, M., Borsi, H., & Hartje, M. (1987). Some aspects about possibilities and limitations of acoustic PD measurements in insulating fluids. 5th ISH (pp. 1–4). Braunschweig, Germany.

Binder, L. (1914). About switching processes and electrical travelling waves (in German). *ETZ*, 35, 177–203.

Black, I. A. (1975). A pulse discrimination system for discharge detection in electrically noisy environments. 2nd ISH Zürich, paper 3.2-02.

Blake, W. (1870). On a method of producing, by electric spark, figures similar to those of Lichtenberg. *American Journal of Sciences and Arts,II-49*, 289.

Boggs, S. A., Ford, G. L., & Madge, R. C. (1981). Coupling devices for the detection of partial discharges in gas-insulated switchgear. *IEEE Transactions on Power Apparatus and Systems,10*, 3969–3973.

Boggs, S. A., & Stone, G. C. (1982). Fundamental limitations in the measurement of corona and partial discharge. *IEEE Transactions on Electrical Insulation,17*(2), 143–145.

Boggs, S. A., Pecena, D. D., Rizzett, S., & Stone, G. C. (1987). Limits to partial discharge detection-effect of sample and defect geometry. In L. G. Cristophorou (Ed.), *Gaseous Dielectrics*. Pergamon Press: Oxford.

Boggs, S. A., & Stone, (1982). Fundamental limitations in the measurement of corona and partial discharges. *IEEE Transactions on Electrical Insulation,17*(2), 143–150.

Bolza, A., et al. (2002). Prequalification test experience on EHV XLPE cable system. CIGRE Session Paris, Report 21-104.

Böning, P. (1938). Remarkable relations of anomalous currents, loss factor, apparent capacitance and the return voltage of insulating materials (in German). *Zeitschrift für technische Physik*, *109*, 241–247.

Boone, W., Damstra, G. C., Jansen, W. J., & de Ligt, G. (1987). VLF HV generators for testing cables after laying. 5th ISH Braunschweig, Paper 62-04.

Bürger, W. (1976). Beitrag zum Entladungsverhalten großflächiger,schwach gekrümmter Elektroden in Luft bei großen Schlagweiten [Contribution to the discharge mechanism of large, slowly bended electrodes in air of lang gap distances]. (Dissertation, Dresden Technical University).

Burawoy, (1936). The delay of sparks at very short impulse voltages (in German). *Archiv für Elektrotechnik,16*, 186–219.

Burstyn, W. (1928). Losses in layer insulation (in German). *ETZ,49*, 1289–1291.

Carrara, G., & Dellera, L. (1972). Accuracy of an extended up-and-down method in statistical testing of insulation. *Electra,23*, 159–175.

Carrara, G., & Hauschild, W. (1990). Statistical evaluation of dielectric test results. *Electra,133*, 109–131.

Carrara, G., & Zafanella, L. (1968). UHV Laboratories: Switching impulse clearance tests. IEEE Power Summer Meeting, project no. 68 CP 692–PWR.

Cavallini, A., Contin, A., Montanari, G. C., Psini, G., & Puletti, F. (2002). Digital detection and fuzzy classification of partial discharge signals. *IEEE Transaction on Dielectrics and Electrical Insulation,5*(3), 335–348.

Cavellini, A., Contin, A., Montanari, G. C., & Puletti, F. (2003). Advanced PD interference in on-field measurements. Part I: Noise rejection. *IEEE Transaction on Dielectrics and Electrical Insulation,10*(2), 23–30.

Cavellini, A., Contin, A., Montanari, G. C., & Puletti, F. (2003). Advanced PD interference in on-field measurements. Part II: Identification of defects in solid insulation systems. *IEEE Transaction on Dielectrics and Electrical Insulation,10*(3), 528–538.

Cavallini, A., & Montanari, G. C. (2006). Effect of supply voltage frequency on testing of insulation systems. *IEEE Transaction on Dielectrics and Electrical Insulation,*, *13*, 111–121.

CENELEC Study Group. (2010). Technical guidelines for HVDC grids. Minutes of meeting 2010-11-29.

Charlton, E. E., et al. (1939). *Journal of Applied Physics*, 10, 374 (cited after Kuffel, Zaengl, Kuffel 2006).

Chen, S., & Czaszejko, T. (2011). Partial discharge test circuit as a spark gap transmitter. *IEEE Electrical Insulation Magazine,27*(31), 36–43.

Choo, W., Chen, G., & Swingler, S. G. (2011). Electric field in polymeric cable due to space charge accumulation under DC and temperature gradient. *IEEE Transaction on Dielectrics and Electrical Insulation,18*(2), 596–606.

Chubb, L. W., & Fortescue, C. (1913). Calibration of the sphere gap voltmeter Trans. *AIEE,32*, 739–748.

Cigre JWG 33/23.12 (1998). Insulation co-ordination of GIS: Return of experience, on-site tests and diagnostic techniques. *Electra*, *176*, 67–97.

Cigre JWG 23/21/33 (2003). Gas-insulated transmission lines (GIL). Technical Brochure No. 218.

Cigre JWG B3/B1 (2008). Application of long, high-capacity gas-insulated lines in structures. Technical Brochure No. 351.

Cigre TF 33.03.04 (2000). Proposed requirements for HV withstand tests on-site. *Electra*, *195*, 13–21.

Cigre TF 33.04.01 (2000). Polluted insulators: A review of current knowledge. CIGRE Technical Brochure No. 158.

Cigre TF D1.02.08 (2005). Instrumentation and measurement for in-service monitoring of high-voltage insulation Technical Brochure No. 286.

Cigre TF D1.33.05 (2012). HV on-site testing with PD measurement. Technical Brochure No. 502.

Cigre WG 21.03 (1969). Recognition of discharges. *Electra*, *11*, 61–98.

Cigre WG 33.03 (1998). Measurement of very fast front transients. *Electra*, *181*, 71–91.

Cigre WG D1.33 (2010). Guidelines for unconventional partial discharge measurements. Technical Brochure No. 444.

Cigre WG B1.23 (2012). Recommendations for testing of long AC submarine cables with extruded insulation for system voltage above 30 to 500 kV. Technical Brochure 490.

C.I.S.P.R. (1977). Specification for radio interference measuring apparatus and measurement methods (International. Special Committee on Radio Interference, edited by IEC), Document no. 16.

Cockcroft, J. D., & Walton, E. T. S. (1932). Experiments with high velocity ions. *Proceedings Royal Society, London, Series A,136*, 619–630.

Coenen, S., Tenbohlen, S., Markalous, S., & Strehl, T. (2007). *Performance check and sensitivity verification for UHF PD measurements on power transformers* (pp. 157–264). CIGRE SC A1 & D1 Joint Colloquium, Gyeongju, Korea.

Cousineau, D. (2009). Fitting the three-parameter Weibull distribution: Review and evaluation of existing and new methods. *IEEE Transaction on Dielectrics and Electrical Insulation,10*(1), 281–288.

Creed, F., Kamamura, T., & Newi, G. (1967). Step response of measuring systems for high impulse voltages. *IEEE Transactions on Power Apparatus and Systems,86*(11), 1408–1420.

Crichton, G. C., Karlsson, P. W., & Pedersen, A. (1988). A theoretical derivation of the transients related to partial discharges in ellipsoidal voids. In *Conference Record IEEE, International Symposium on Electrical Insulation (ISEI)* (p. 238). IEEE Publication 88CH2594-0-DEI.

Crichton, G. C., Karlsson, P. W., & Pedersen, A. (1989). Partial discharges in ellipsoidal and spherical voids. *IEEE Transaction on Dielectrics and Electrical Insulation,24*, 335–342.

Csepes, G., Hamos, I., Schmidt, J., & Bognar, A. (1994). A DC expert system (RVM) for checking the refurbishment efficiency of high voltage oil-paper insulating system using polarization spectrum analysis in range of long-time constants. CIGRE Session Paris, Paper 12-206.

Cui, D., et al. (2009). Discussion on insulation levels and dielectric test technology requirements of AC UHV transmission and transformation equipment in China. 16th ISH Johannesburg, paper A-23.

Dakin, T. W., & Malinaric, P. J. (1960). A capacitive bridge method for measuring integrated corona-charge transfer and power loss per cycle. *Power Apparatus and Systems, Part III. Transactions of the American Institute of Electrical Engineers,79*(3), 648–653.

Davis, R., Bowdler, G. W., & Standring, W. G. (1930). The measurement of high voltages with special reference to the measurement of peak voltages. *Journal IEE, London,68*, 1222.

Dawson, G. A., & Winn, W. P. (1965). A model of streamer propagation. *Zeitschrift für Physik,183*, 159–171.

Dennhardt, A. (1935). Reason and measurement of the high-frequency noise caused by insulators (in German). *Elektrizitätswirtschaft,34*, 15.

Densley, R. J. (1979). Partial discharges under direct-voltage conditions. *Engineering Dielectrics*, *1*. In R. Bartnikas, E. J. McMahon (Eds.), *Corona measurement and interpretation* (Vol. STP669). Philadelphia: ASTM.

Devins, J. C. (1984). The physics of partial discharges in solid dielectrics. *IEEE Transaction on Electrical Insulation,19*, 475–495.

Dietrich, M. (1982). Dimensioning of large electrodes for HV test equipment of the UHV range (in German). (Dissertation, Dresden Technical University, 1982).

Dong, B., Jiang, X., Hu, J., Shu, L., & Sun, C. (2012). Effects of artificial polluting methods on AC flashover of composite insulators. *IEEE Transactions on Dielectrics and Electrical Insulation,19*(2), 714–722.

Dorison, E., & Aucourt, C. (1984). After laying tests of HV and EHV cables. Jicable Versailles. Paper BV-5.

Eager, G. S., & Bader, G. (1967). Discharge detection in extruded polyethylene insulated power cables. *IEEE Transactions on Power Apparatus and Systems,86*(1), 10–34.

Eager, G. S., Bader, G., & Silver, D. A. (1969). Corona detection experience in commercial production of power cables with extruded insulation. *IEEE Transactions on Power Apparatus and Systems,86*(4), 342–346.

Edwards, F. S., & Smee, J. F. (1938). The calibration of the sphere spark gap for voltage measurement up to one million volts (effective) at 50 cycles. *Journal of the Institution of Electrical Engineers,82*(1938), 655–669.

Eleftherion, P. M. (1995). Partial Discharge. Part XXI: Acoustic emission-based PD source location in transformers. *IEEE Electrical Insulation Magazine,11*(6), 22–26.

Elmore, W. C. (1948). The transient response of damped linear networks with particular regard to wideband amplifiers. *Journal of Applied Physics,19*(1), 55–63.

Elsner, R. (1939). Measurement of steep HV impulses by voltage dividers (in German). *Archiv für Elektrotechnik,33*(1), 23–40.

Elstner, G., et al. (1983). Powerful DC and mixed voltage testing equipment up to 2.25 MV for outdoor installation. 4th ISH Athens (1983) paper 51.04.

Emanuel, H., Kalkner, W., Plath, K. D., & Plath, R. (2002). Synchronous three-phase PD measurement on power transformers on site and in the laboratory (in German). In *ETG Conference on Diagnostik elektrischer Betriebsmittel*.

Engelmann, E. (1981). Contribution to the discharges on large electrodes with defects in air (in German). Thesis Dresden Technical University 1981.

EN, C. S. (2000) 0.50191 Erection and operation of electrical test equipment (German version DIN EN 50191-VDE0104).

EN HD 620 S (1996/A3: 2007). Power cables—Part 620: Distribution cables with extruded insulation for voltages rated 3.6/6 kV to 20.8/36 kV.

Fan, J., & Li, P. (2008). Effect of sandstorm on external insulation. Presentation at the TC 42 Meeting, Sao Paulo.

Farneti, F., Ombello, F., Bertani, E., & Mosca, W. (1990). Generation of oscillating waves for after-laying test of HV extruded cable links. CIGRE Session Paris, France, paper 21-10.

Feser, K. (1973). Extension of the trigger range of multi-stage impulse generators for the generation of SI voltages (in German). *ETZ,94*(3), 171–174.

Feser, K. (1974). Problems of the generation of SI voltages in the test field (in German). *Bulletin SEV,65*(6), 496–506.

Feser, K. (1975). Dimensioning of electrodes in the UHV range illustrated with the example of toroid electrodes for voltage dividers (in German). *HAEFELY Publication E-130 !975 and ETZ-A,96*, 206–210.

Feser, K. (1981). HV tests of metal-enclosed, gas-insulated substations (in German). *Bulletin SEV,72*(1), 19–26.

Feser, K. (1997). Thoughts to the test and measuring techniques at steep impulse voltages (in German). HIGHVOLT Kolloquium, Dresden, Paper 1.4 (pp.37–40).

Feser, K., & Pfaff, W. R. (1984). A potential free spherical sensor for the measurement of transient electric fields. *IEEE Transactions on Power Apparatus and Systems,PAS-103*, 2904–2911.

Feser, K., & Hughes, R. C. (1988). Measurement of direct voltage by rod-rod gap. *Electra,117*, 23–34.

Finkelmann, J. (1936). Electrical breakdown of different gases under high pressure (in German). Ph.D. Thesis Technische Hochschule Hannover.

Frank, H., Hauschild, W., et al. (1983). HVDC testing generator for short-time polarity reversal on load. 4th ISH Athens, paper 51.05.

Frank, H., Schrader, W., & Spiegelberg, J. (1991). 3 MV AC voltage testing equipment with switching voltage extension—Technical concept, first operation, results. 7th ISH Dresden, paper 52.04.

Fromm, U. (1995). Interpretation of partial discharges at DC voltage. *IEEE Transactions on Dielectrics and Electrical Insulation,2*(5), 761–770.

Fromm, U. (1995). Partial discharge and breakdown testing at high DC Voltage. Ph.D. Thesis TU Delft, The Netherlands.

Frommhold, L. (1956). The potential of the charge of electron avalanches within parallel plates and side effects (in German). *145*(3), 324–340.

Fruth, B., Liptak, L., Ullrich, L., Dunz, T., & Niemeyer, L. (1989). Ageing of rotating machine insulation – Mechanisms, measurement technique. In *Proceedings of the 3rd International Conference on Conduction and Breakdown in Solid Dielectrics* (pp. 597–601).

Fruth, B., & Gross, D. (1994). Phase resolving partial discharge pattern acquisition and spectrum analysis. In *Proceedings of the ICPDAM* (pp. 578–581). Brisbane NSW, Australia, 94CH3311-8.

Fuhr, J., Haessig, M., Boss, P., Tschudi, D., & King, R. A. (1993). Detection and location of internal defects in the insulation of power transformers. *IEEE Transactions on Electrical Insulation,28*(6), 1057–1067.

Fujimoto, N., Boggs, S. A., & Madge, R. C. (1981). Electrical transients in gas-insulated switchgear. Transactions on the March 1981 Meeting of the Canadian Electric Association.

Fujimoto, N., Boggs, S. A., & Madge, R. C. (1981). Coupling devices for the detection of partial discharges in gas-insulated switchgear. *IEEE Transactions on Power Apparatus and Systems,100*(8), 3369–3973.

Gabor, D. (1926). Oscillographic records of travelling waves. *Archiv für Elektrotechnik*, *16*, 296–298.

Garbagnati, E., et al. (1991). *The influence of atmospheric conditions on the dielectric strengths of phase-to-phase insulation when subjected to switching impulse*. CESI Publication.

Garnacho, F. (2010, February). K-factor results for air dielectric medium. Presentation to CIGRE Working Group D1.36.

Garnacho, F., et al. (1997). Evaluation procedure for lightning impulse parameters in case of waveforms with oscillations and/or an overshoot. *IEEE Transactions on Power Delivery,12*(2), 640–649.

Garnacho, F., et al. (2002). Evaluation of lightning impulse voltages based on experimental results—proposal for the revision of IEC 60060-1 and IEC 61083-2. *Electra*, *204*, 31–37.

Gemant, A., & v. Philippoff, W. (1932). Spark gap with pre-capacitor (in German). *Zeitschrift für Technische Physik,13*(9), 425–430.

Gockenbach, E. (2010). Voltage shapes in HVDC systems—static and dynamic loads (in German). ETG Fachtagung: Isoliersysteme bei Gleich- und Mischfeldbeanspruchung, Cologne paper 1.2.

Gockenbach, E., & Hauschild, W. (2000). The selection of the frequency range for HV on-site testing of extruded cable systems. *IEEE Insulation Magazine,16*(6), 11–16.

Gockenbach, E., et al. (2007). Challenges on the measuring and testing techniques for UHV AC and DC equipment. IEC/CIGRE UHV Symposium Beijing, Paper 4–2.

Goosens, R. F., & Provoost, P. G. (1946). The registration of high impulse voltages by a cathode oscilloscope (in German). *Bulletin SEV*, (37), 175–184.

Graybill, H. Q., Cronin, J. C., & Field, E. J. (1974). Testing of gas insulated substations and transmission systems. *IEEE Transactions of Power Apparatus and Systems,PAS-93*(1), 404–413.

Grey Morgan, C. (1965). Fundamentals of electric discharges in Gases, Vol. II: Physical electronics. In A. H. Beck (Ed.), *Handbook of vacuum physics*. Oxford: Pergamon Press.

Greinacher, H. (1920). Generation of direct voltage of multiple amount of an AC voltage (in German). *Bulletin SEV*, 66.

Gross, D. (2011). Locating partial discharge using acoustic sensors. In *HIGHVOLT KOLLOQUIUM '11 Conference Proceedings* (pp. 99–106).

Grönefeld, P. (1983). A very low frequency 200 kV generator as precondition for testing insulating materials with 0.1 Hz alternating voltage. 4th International Symposium on High Voltage Engineering (ISH), Athens, Greece, paper 21.02.

Grünewald, F. (1921). Characteristics of open-air insulators under high-frequency voltages (in German). *ETZ,42*, 1377.

Grünewald, P., & Weidner, J. (1994). Possibilities and experience with off- and on-line diagnosis of turbine generator stator winding insulations. CIGRE-Session, Paris, France, paper 11-206.

Gubanski, S. M., Boss, P., & Csepes, G., et al. (2002). *Dielectric response methods for diagnostics of power transformers*. *Electra*, *202*, 25–3 (Report of CIGRE TF 15.01.09).

Gulski, E. (1991). Computer-aided recognition of partial discharges using statistical tools. PhD Thesis, Delft University Press.

Gulski, E., Smit, J. J., Seitz, P. N., & Tuner, M. (1999). On-site diagnostics of power cables using oscillating wave test system. 11th ISH London, UK, paper 5.112.

Gulski, E., Smit, J. J., van Breen, H., de Vries, F., Seitz P. P., & Petzold, F. (2000). Advanced PD diagnostics of medium-voltage power cables using oscillating wave test system. *IEEE Electrical Insulation Magazine*, *16*(2).

Gulski, E., et al. (2007). Dedicated on-site condition monitoring of HV power cables up to 150 kV. In *8th International Power Engineering Conference*, Singapore.

Gutman, I., & Derfalk, A. (2010). Pollution tests for polymeric insulators made of hydrophobicity material. *IEEE Transaction on Dielectrics and Electrical Insulation,17*, 384–393.

Hagenguth, J. H. (1937). Short time spark-over of gaps. *Transactions of the American Institute of Electrical Engineers,56*, 67–76.

Hagenguth, J. H., et al. (1952). Sixty cycle and impulse sparkover of large gap spacings. *Transactions AIEE Part III,71*, 455–460.

Hague, B. (1959). *Alternating-current bridge methods* (5th ed.). London: Pitman & Sons.

Hällström, J. (2002). A calculable impulse voltage calibrator. Acta polytechnica scandinavia, Electrical Engineering, Series No. 109.

Hällström, J., Li, Y. & Lucas, W. (2003). High accuracy comparison measurement of impulse parameters at low voltage levels. 13th ISH Delft, paper 432.

Harrold, R. T. (1975). Ultrasonic spectrum signatures of under-oil corona sources. *IEEE Transactions on Electrical Insulation,EI-10*(4), 109–112.

Harrold, R. T. (1976). The relationship between ultrasonic and electrical measurement of under oil corona sources. *IEEE Transactions on Electrical Insulation,EI-11*(1), 8–11.

Harrold, R. T. (1996). Acoustic theory applied to the physics of electrical breakdown in dielectrics. *IEEE Transactions on Electrical Insulation,EI-21*(5), 781–792.

Hauschild, W. (1970). About the breakdown of insulating oil in a non-uniform field at SI voltages (in German). Ph.D. Thesis, Dresden Technical University.

Hauschild, W. (1995). Engineering the electrodes of HV test systems on the basis of the physics of discharges in air. 9th ISH Graz, invited paper.

Hauschild, W. (2007). A common view on high-voltage testing and insulation diagnostics Proceedings of HIGHVOLT Kolloquium '07,0.7-13 (also: CIGRE D1.33 Colloquium Gyeongju, 2007).

Hauschild, W. (2013). Critical review of voltages applied for quality acceptance and diagnostic field tests on HV and EHV cable systems. *IEEE Electrical Insulation Magazine*, *29*(2), 16–25.

Hauschild, W.,& Fahd, I. (1980). Installation of a HV laboratory at the faculty of mechanical and electrical engineering of Damascus University. *Elektrie*, *32*(3), pp. 124–127(in German). *Monthly Technical Review*, *24*(1), 4–11 (in English).

Hauschild, W., Küttner, H., & Thümmler, K. (1981). Systems for the wideband PD measurement in HV insulations (in German). *Elektrie,35*(7), 353–357.

Hauschild, W., & Mosch, W. (1992). *Statistical techniques for high-voltage engineering*, (Statistik für Elektrotechniker, Berlin: Verlag Technik Berlin, 1984). IEE Power Series 13. London: Peter Peregrinus Ltd.

Hauschild, W., & Steiner, T. (2009). The design of HVLI tests fort he improvement of the k-factor function. CIGRE D1.33 Meeting Budapest.

Hauschild, W., Rausendorf, S., & Schufft, W. (1987). Calculation of field strength and streamer inception voltage for multi-segment electrodes of UHV test equipment. 5th ISH Braunschweig, paper 33.10.

Hauschild, W., Wolf, J., & Spiegelberg, J. (1987). Calculation of the pollution test characteristic of a powerful DC voltage generator. 5th ISH Braunschweig, paper 62.03.

Hauschild, W., Spiegelberg, J., & Lemke, E. (1997). Frequency tuned resonant test systems for HV on site testing of SF_6 insulated apparatus. 10th ISH Montreal, (Vol. 4, pp. 457–460).

Hauschild, W., Schufft, W., & Spiegelberg, J. (1997). Alternating voltage on-site testing and diagnostics of XLPE cables: The parameter selection of frequency-tuned resonant test systems. 10th ISH Montreal, (Vol. 4, pp. 75–78).

Hauschild, W., Schierig, S., & Coors, P. (2005). Resonant test systems for HV testing of super-long cables and gas-insulated transmission lines. 14th ISH Beijing paper J-02.

Hauschild, W., Thiede, A., Leibfried, T., & Martin, F. (2006). Static frequency converters for HV tests on power transformers (in German), High Voltage Symposium Stuttgart.

Hauschild, W., et al. (1982). The influence of stochastic processes on the breakdown of slightly non-uniform fields in SF_6 (in German). *Z. elektr. Informations- und Energietechnik*, *12*(4 &5), 289–318, 385–403.

Hauschild, W., et al. (1991). Breakdown voltage characteristic of long rod-to-plane air gaps at bipolar oscillating switching voltages. 7th ISH Dresden paper 42.25.

Hauschild, W., et al. (1993). Computer-aided performance tests and checks for LI voltage measuring systems. 8th ISH Yokohama, paper 53.01.

Hauschild, W., et al. (2002). The technique of AC on-site testing of HV cables by frequency-tuned resonant test systems. CIGRE Session, Report 33-304.

Henriksen, M., Stone, G. C., & Kurtz, M. (1986). Propagation of partial discharge and noise pulses in turbine generators. *IEEE Transactions on Energy Conversation*. *EC-1*(3).

Herb, R. G., Parkinson, D. B., & Kerst, D. W. (1937). The development and performance of an electrostatic generator operating under high air pressure. *PhysicalReview, 51*(75).

Hinow, M. (2011). *Optimized test field for power transformer testing.* HIGHVOLT Kolloquium (Dresden) (pp. 123–126).

Hinow, M., Hauschild, W., & Gockenbach, E. (2010). Lightning impulse and overshoot evaluation proposed in drafts of IEC 60060-1 and future UHV testing. *IEEE Transaction on Dielectrics and Electrical Insulation*, *17*(5), 1628–1634.

Hinow, M., & Steiner, T. (2009). Influence of the new k-factor method of IEC 60060-1 on the evaluation of LI parameters in relation to UHV testing. 16th ISH Cape Town, paper G-14.

Hoof, M., & Patsch, R. (1994). *Analyzing partial discharge pulse sequences: A new approach to investigate degradation phenomena*. In IEEE Symposium on Electrical Insulation (ISEI), (pp. 327–331). Pittsburgh, USA.

van Hoove, C., & Lippert, A. (1973). Measurements related to the electric strength of polyethylene and HV cables (in German). *Elektrizitätswirtschaft,71*, 630–635.

van Hoove, C. (1993). Partial discharges in cable accessories. In D. König & Y. N. Rao (Eds.), *Partial discharges in electrical power apparatus* (pp. 173–181). Berlin: VDE-Verlag.

Hopke, F., & Schmidt, M. (2011). Factory test field for power transformers based on a static frequency converter. *HIGHVOLT Kolloquium Dresden*, 127–132.

House, H., Waterton, F. W., & Chew, J. (1979). 1000 kV standard voltmeter. 3rd ISH Milan, Italy, paper 43.05.

Houtepen, R., et al. (2011). Estimation of dielectric loss using damped AC voltage. *IEEE Insulation Magazine,27*(3), 14–19.
Howels, E., & Norton, E. T. (1978). Detection of partial discharges in transformers using acoustic emission techniques. *IEEE Transactions on Power apparatus and Systems,PAS-97*(5), 1538–1546.
Hughes, R. C., et al. (1994). Traceability of measurement in HV tests. *Electra,155*, 91–101.
Hylten-Cavallius, N. (1957). Impulse tests and measuring errors. *ASEA-Journal,5*, 75–84.
Hylten-Cavallius, N. (1988). *High-voltage laboratory planning*. Switzerland: Haefely.
ICEA T-24-380 (2006). Standard for partial discharge test procedure.
IEC 60034-1 (2010). Rotating electrical machines—Part 1: Rating and performance.
IEC 60034-27 (2006). Rotating machines—Part 27: Off-line partial discharge measurements on the stator winding insulation of rotating electrical machines.
IEC 60038 (2009) IEC standard voltages.
IEC 60052 (1960). Recommendations for voltage measurement by means of sphere gaps.
IEC 60052 Ed. 3 (2002). Voltage measurement by means of standard air gaps.
IEC 60060-1 (1989). High-voltage test techniques, Part 1: General definitions and test requirements.
IEC 60060-1 (2010). High-voltage test techniques, Part 1: General definitions and test requirements.
IEC 60060-2 (2010). High-voltage test techniques, Part 2: Measuring systems.
IEC 60060-3 (2006). High-voltage test techniques, Part 3: Definitions and requirements for on-site testing.
IEC 60071-1 (2006). Insulation co-ordination—Part 1: Definitions, principles and rules.
IEC 60071-2 (1996). Insulation co-ordination—Part 2: Application guide.
IEC 60071-2 (2010) Amendment to Part 2.
IEC 60071-5 (2002). Insulation co-ordination—Part 5: Procedures for high-voltage direct current (HVDC) converter stations.
IEC 60076-3 (2013). Power transformers—Part 3: Insulation levels, dielectric tests and external clearances in air.
IEC 60099-4 (2009). Surge arresters—Part 4: Metal-oxide surge arrestors without gaps for AC systems.
IEC 60143-1 (2004). Series capacitors for power systems—Part 1: General.
IEC 60250 (1969). Recommended methods for the determination of the permittivity and dielectric dissipation factor of eletrical insulating materials.
IEC 60270 (2000). HV test techniques—Partial discharge measurement.
IEC 60502 (1997). Power cables with extruded insulation for rated voltages from 1 to 30 kV.
IEC 60505 (2011). Evaluation and qualification of electrical insulation systems.
IEC 60507 (1991). Artificial pollution tests on high-voltage insulators to be used in AC systems.
IEC 60840 (2011). Power cables with extruded insulation for rated voltages from 30 to 150 kV.
IEC 60885-3 (2003). Electrical test methods for electric cables—Part 3: Test methods for partial discharge measurements on lengths of extruded power cable.
IEC 61083-1 (2001). Instruments and software used for measurement in high-voltage impulse tests - Part1: Requirements for instruments.
IEC 61083-2 (2013). Instruments and software used for measurement in high-voltage impulse tests – Part2: Requirements for software for tests with impulse voltages and currents.
IEC 61083-3 (2012). Draft—Instruments and software used for measurements in high-voltage and high-current tests—Part 3: Requirements for instruments for tests with alternating and direct voltages and currents.
IEC 61245 (2013). Artificial pollution tests on HV insulators to be used on DC systems. Draft 36/329/CD.
IEC 61259 (1994). Gas-insulated metal-enclosed switchgear for rated voltages 72.5 kV and above—Requirements for switching of bus charging currents by disconnectors.

IEC 61640 (1998). Rigid high-voltage gas-insulated transmission lines for rated voltage of 75 kV and above.
IEC 61934 (2006). Electrical measurement of partial discharges during short rise time repetitive voltage impulses.
IEC 62061 (2005) Safety of machinery—functional safety-related electrical, electronic and programmable electronic control systems.
IEC 62067 (2006). Power cables with extruded insulation and their accessories for rated voltages above 150 kV up to 500 kV—test methods and requirements.
IEC 62271-203 (2010). HV switchgear and control gear,-Part 203: Gas-insulated, metal-enclosed switchgear for voltages above 52 kV.
IEC 62475 (2010). High-current test techniques: Definitions and requirements for test currents and measuring systems.
IEC 62478 (2013). High voltage test techniques—Measurement of partial discharges by electromagnetic and acoustic methods (CDV).
IEC TC 115: HVDC (2010). Transmission for DC voltages above 100 kV. Strategic Business Plan, IEC 115/35/INF.
IEEE Std.4 (1995). IEEE standard techniques for high-voltage testing.
IEEE P5™/D006 (2013). Draft trial-use standard for high-voltage testing techniques. 200 9(new edition harmonized with IEC 60060-1:2010 is expected for 2014).
IEEE 62-PC57.152 (2012). Guide for diagnostic field testing of fluid filled power transformers, regulators and reactors.
IEEE Std.400™ (2012). IEEE Guide for field testing and evaluation of the insulation of shielded power cable systems rated 5 kV and above.
IEEE Std.400.1 (2007). Guide for field testing of laminated dielectric, shielded power cable systems rated 5 kV and above with high direct current voltage.
IEEE P400.2 ™ (2012). Draft Guide VLF for field testing of shielded power cable systems using very low frequency (VLF).
IEEE Standard 400.4 (Draft 2012). Guide for field testing of shielded power cable systems rated 5 kV and above with damped alternating current (DAC) voltage.
IEEE Std. C37.122 (2010). Standard for HV gas-insulated substations rated 52 kV and above.
IEEE Std C57.113 (2010). IEEE Recommended practice for partial discharge measurement in liquid-filled power transformers and shunt reactors.
IEEE 510 (1983). Recommended practice for safety in high-voltage and high-power testing.
IEEE Std.1313.1 (1996). Standard for insulation coordination—Definitions, principles and requirements.
IEEE 1434 (2000). Trial-use guide to the measurement of partial discharges in rotating machinery.
IEEE P1861™/D1 (2012). Draft Guide for on-site acceptance tests of electric equipment and commissioning of 1000 kV AC and above system.
ISO/IEC Guide 98-3 (2008). Uncertainty of measurement—Part 3: Guide to the expression of uncertainty in measurement (= GUM:1995).
Illias, H., Chen, G., & Lewin, P. L. (2011). Modeling of partial discharge activity in spherical cavities within a dielectric material. *IEEE Electrical Insulation Magazine,27*(1), 38–45.
Illias, H., Chen, G., & Lewin, P. L. (2011). Partial discharge behavior within a spherical cavity in a solid dielectric material as a function of frequency and amplitude of the applied voltage. *IEEE Transaction on Dielectrics and Electrical Insulation,18*(2), 432–443.
Jiang, X., Shu, L., et al. (2008). Positive switching impulse performance and voltage correction of rod-plane air gaps based on tests at high-altitude site. *IEEE Transaction on Power Delivery*, *24*(1).
Jiang, X., et al. (2008). Switching impulse flashover performance of different types of insulators at high altitude sites of above 2800 m. *IEEE Transaction on Dielectrics and Electrical Insulation,15*(5), 1340–1345.

Jiang, X., et al. (2009). Study on AC pollution flashover performance of composite insulators at high altitude sites of 2800–4500 m. *IEEE Transaction on Dielectrics and Electrical Insulation,16*(1), 123–132.

Jiang, X., et al. (2010). Equivalence of influence of pollution simulating methods on DC flashover stress of ice-covered insulators. *IEEE Transactions on Power Delivery,25*(4), 2113–2120.

Jiang, X., et al. (2011). DC flashover performance and effect of sheds configuration on polluted and ice-covered insulators at low pressure. *IEEE Transaction on Dielectrics and Electrical Insulation,18*, 97–105.

Jouaire, J., & Sabot, A., et al. (1978). HV measurements—present state and future development. Revue General de l'Electricite, Special Number.

Judd, M. D., Farish, O., & Hampton, B. F. (1996). The excitation of UHF signals by partial discharges in GIS. *IEEE Transaction on Dielectrics and Electrical Insulation,3*, 213–228.

Judd, M. D., Cleary, G. P., & Bennoch, G. J. (2002). Applying UHF partial discharge detection to power transformers. *IEE Power Engineering Review*, 57–59.

Kachler, A. J. (1975). Contribution to the problem of impulse voltage measurement by means of sphere gaps. 2nd ISH Zurich (pp. 217–221).

Kachler, A. J., Kroon, C., & Machado, T. (1998). Pro and contras of on-site testing on power transformers and reactors. Cigre Session Paris paper 12-201 (see also: the discussion to that paper by W. Hauschild: A necessary clarification to the activities of Cigre WG 33.03 related to HV on-site tests. Cigre 1998).

Kapcov, N. A. (1955). *Electrical phenomena in gases and vacuum (in German)*. Berlin: Deutscher Verlag der Wissenschaften.

Karlstrand, J., Henning, G., Schierig, S., & Coors, P. (2005). Factory testing of long submarine cables using frequency-tuned resonant systems. CIRED Turin.

Kaufhold, M., Kalkner, W., Obralic, R., & Plath, R. (2006). Synchronous 3-phase partial discharge detection on rotating machines. CIGRE Session Paris, paper D1-105.

Kaul, G., Plath, R., & Kalkner, W. (1993). Development of a computerized loss factor measurement system, including 0.1 Hz and 50/60 Hz. 8th International Symposium on High Voltage Engineering, Yokohama, Japan, paper 56.04.

Kawamura, T., Nagai, K., Seta, T., & Naito, K. (1984). DC pollution performance of insulators. CIGRE Session Paris, Report 33-10.

Keller, A. (1959). Constancy of capacitance of compressed gas capacitors (in German). *ETZ-A*, *80*, 757–761.

Kemp, I. J. (1987). Calibration difficulties associated with PD detectors in rotating machines. In *Proceedings of IEEE Electrical Insulation Conference*, Chicago, USA.

Kind, D. (1957). The formative area at impulse voltage stress of electrode arrangements in air (in German). (Dissertation, Technical University Munich, 1957).

Kind, D. (1961). Basics of measuring equipment for corona – insulation tests (in German). *ETZ-A,84*, 781–787.

Kind, D. (1974). Recommendations for the performance of HV tests on GIS and GIL (in German). *ETZ-A,95*(11), 588–589.

Kind, D., & Salge, J. (1965). On the generation of switching impulse voltages using HV test transformers (in German). *ETZ-A,86*(11), 588–589.

Kind, D., & Shihab, S. (1969). Partial discharges in solid insulating material subjected to high direct voltages (in German). *ETZ-A,90*, 476–468.

Kind, D., & Feser, K. (1999). *High-voltage test technique* (2nd English Edn). Vieweg and SBA Publishers (First German Edn. 1972).

Kindersberger, J. (1997). Why plastic compound insulators require test procedures different from ceramic insulators? (in German). 2nd HIGHVOLT Kolloquium, Dresden 1997, Paper 1.5 (pp. 41–51).

King, R. W. P. (1983). The conical antenna as a sensor or probe. *IEEE Transactions on Electromagnetic Compatibility,25*, 8–13.

Kleinwächter, H. (1970). The influence-E-meter used as an electrostatic amplifier of extremely high amplification and its application as a sensitive measuring instrument (in German). *Archiv technisches Messen*, (413), R62–R64.

Köhler, W. (1988). Voltage sources for pollution testing (in German). (Dissertation, University of Stuttgart, 1988).

Köhler, W., & Feser, K. (1987). Test sources for DC pollution tests. 5th ISH Braunschweig, paper 62.08.

König, D., & Rao, Y. N. (1991). *Partial discharges in electrical power apparatus*. Berlin: VDE-Verlag.

Koske, B. (1938). Tests of insulations of HV overhead lines under operation (in German). *Elektrizitätswirtschaft,36*(11), 291.

Kranz, H. G. (2000). Fundamentals in computer aided PD processing, PD pattern recognition and automated diagnosis in GIS. *IEEE Transactions on Dielectrics and Electrical Insulation,7*(1), 12–20.

Kranz, H. G., & Krump, R. (1988). Computer aided partial discharge evaluation about the surface material of the PD source in gas-insulated substations. In *IEEE International Symposium on Electrical Insulation (ISEI),* Boston, USA.

Krefter, K. H. (1991). *Tests for condition assessment of medium cable systems (in German)*. Frankfurt a.M: VWEW-Verlag.

Krug, W. (1929). Investigation of the behaviour of impulse circuits using records by means of a cathode-ray oscilloscope (in German). ETZ 19, Ch. 4.2.

Krueger, M. (1989). Field test of the insulation of cable systems of rated voltages 10 to 30 kV using VLF voltage 0.1 Hz (in German). PhD Thesis TU Graz.

Krump, R., & Haumann, T. (2011). *Possibilities and limits of a modern HV test laboratory* (pp. 115–122). Dresden: HIGHVOLT Kolloquium.

Kreuger, F. H. (1989). *Partial discharge detection in high-voltage equipment*. London: Butterworths.

Kübler, B., & Hauschild, W. (2004). New ways of HV testing of electric power apparatus including power transformers. In *Proceedings of TRANSFORM*.

Küchler, A. (2009). *Hochspannungstechnik, Grundlagen-Technologie-Anwendungen* (3rd Edn in German). Berlin: Springer (1st Edn.1997).

Küchler, A., Dunz, T., Hinderer, A., & Schwab, A. (1987). Transient field-distribution measurements with "electrical long" sensors. 5th ISH Braunschweig Paper 32.08.

Kuan, J. T., & Chen, M. K. (2006). Parameter evaluation for lightning impulse with oscillation and overshoot using the eigensystem realization algorithm. *IEEE Transactions on Dielectrics and Electrical Insulation,13*(6), 1303–1316.

Kuffel, E. (1956). The effect of irradiation on the breakdown of sphere gaps in air under direct and alternating voltages. In *Proceedings IEE* (Vol. 108, pp. 133–139).

Kuffel, E. (1961). The influence of nearby earthed objects and of the polarity of the voltage on the direct breakdown of horizontal sphere gaps. *Proceedings of the IEE-Part A: Power Engineering*,*108*, 302–307.

Kuffel, E., Zaengl, W., & Kuffel, J. (2006). *High-voltage engineering: fundamentals* (2nd Edn). Elsevier/ Newness (First edition 1984 by Pergamon Press).

Kuhlmann, K., & Mecklenburg, W. (1935). Ohmic measuring resistor (in German). *Bulletin SEV,26*, 737.

Küpfmüller, K. (1990). Introduction into theoretical electrical technique (in German). Ed. 13, Springer Berlin, Heidelberg, New York.

Kurrat, M. (1992). Energy considerations for partial discharges in voids. *ETEP, 2*(1), 39–44.

Kuschel, M., Plath, R., & Kalkner, W. (1995). Dissipation factor measurement at 0.1 Hz as a diagnostic tool for service-aged XLPE-insulated medium voltage cables. 9th ISH Graz, Paper 5156.

Kutschinski, G. S. (1968). Determination of the life time of oil-impregnated paper of capacitors based on the PD quantities (in German). *ELEKTRIE, 22*, 183–186.

Lämmel, J. (1973). Design of HV test systems for the superimposition of DC voltages with impulse voltages (in German). (Dissertation, Technical University of Dresden, 1973)
Läpple, H. (1966). The HV test field of the Schaltwerk of Siemens-Schuckert Werke (in German). *Siemens-Zeitschrift*, (40), 428–435.
Lalot, J. (1983). Statistical processing of dielectric testing methods. *EDF Bulletin de la Direction des Etudes et Recherches–Series B*, (1/2), 5–30.
Lazarides, L. A. (2010). Negative impulse flashover along cylindrical insulating surfaces bridging a short rod-plane gap under variable humidity. *IEEE Transactions Dielectrics and Electrical Insulation, 17*, 1585–1591.
Lazarides, L. A., & Mikropoulos, P. N. (2011). Positive impulse flashover along smooth cylindrical surfaces under variable humidity. *IEEE Transactions Dielectrics and Electrical Insulation,18*, 745–754.
Leibfried, T., et al. (1998). On-line monitoring of power transformers—trends, new developments and first experiences. CIGRE Paris Report 12-211.
Lemke, E. (1967). Breakdown mechanism and breakdown vs. gap-distance characteristics of non-uniform air gaps at SI voltages (in German) Ph.D. Thesis, Technische Universität Dresden.
Lemke, E. (1967). The breakdown in in-homogenous fields in air at switching voltages. *Periodica Polytechnica, Electrical Engineering (Budapest), 11*(3), 229–239.
Lemke, E. (1968). A principle for the measurement of impulse charges (in German). *Periodica Polytechnica, Electrical Engineering, Budapest, 12*(1), 31–37.
Lemke, E. (1968). Development of streamer discharges in ai rat positive SI voltages (in German). *ELEKTRIE, 22*(4), 166–168.
Lemke, E. (1966). Electrical breakdown in air at switching voltages (in German). *ELEKTRIE, 20*(5), 195–198.
Lemke, E. (1969). A new principle fort he wide-band PD measurement (in German). *ELEKTRIE, 23*(11), 468–469.
Lemke, E. (1974). System for the PD measurement (in German). *ELEKTRIE, 26*, 165–167.
Lemke, E. (1975). Contribution to electrical measurement of partial discharges highlighting a wide-band procedure for evaluating the accumulated charge (in German). Habilitation Thesis, TU Dresden.
Lemke, E. (1979). A new method for PD measurements on polyethylene insulated power cables. 3rd ISH Milano, paper 43.13.
Lemke, E. (1981). A new procedure for PD measurement on long HV cables (in German). *ELEKTRIE, 35*(7), 358–360.
Lemke, E. (1981). Problems of the localization of PD defects in extruded HV cables (in German). *ELEKTRIE, 35*(7), 360–362.
Lemke, E. (1987). A new procedure for partial discharge measurements on the basis of an electromagnetic sensor. 5th ISH Braunschweig, paper 41.02.
Lemke, E. (1989). PD probe measuring technique for on-site diagnosis tests of HV equipment. 6th ISH, New Orleans, paper 15.08
Lemke, E. (1991). Progress in PD probe measuring technique. 7th International Symposium on High Voltage Engineering (ISH) Dresden, paper 72.01.
Lemke, E. (2004). *Possibilities and limits of localization of PD failures in extruded power cables under on-site condition (in German)*. Cologne: VDE/ETG Fachtagung "Diagnostik elektrischer Betriebsmittel". pp. 209–213.
Lemke, E. (2012). A critical review of partial discharge models. *IEEE Electrical Insulation Magazine, 28*(6), 11–16.
Lemke, E. (2013). Analysis of the PD charge transfer in extruded power cables. *IEEE Electrical Insulation Magazine*, *30*(1), 24–28.
Lemke, E., et al. (1983). Dimensioning of electrodes for ultra high voltage. 4th ISH Athens paper 44.01.
Lemke, E., Röding, R., & Weissenberg, W. (1987). On-site testing of extruded cables by PD measurements at SI voltages. CIGRE Symposium Vienna paper 1020-02.

Lemke, L., & Schmiegel, P. (1991). Progress in PD probe measuring technique. 7th ISH Dresden, paper 72.02.

Lemke, E., & Schmiegel, P. (1995). Experience in PD diagnosis tests on site based on the PD probe technique. In *3rd Workshop & Conference on HV Technology*. IISc Bangalore/India, (pp. 199–203).

Lemke, E., & Schmiegel, P. (1995). Complex Discharge Analyzing (CDA)—an alternative procedure for diagnosis tests on HV power apparatus of extremely high capacitance. 8th ISH Graz, paper 56.17.

Lemke, E., Rußwurm, D., Schellenberger, L., & Zieschang, R. (1996). Computer-aided system for PD diagnostics (in German). 7. Tagung "Technische Diagnostik", Merseburg, Germany.

Lemke, E., Schmiegel, P., Elze, H., & Rußwurm, D. (1997). *Procedure for the evaluation of dielectric properties based on Complex Discharge Analyzing (CDA)* (pp. 385–388). Montreal, Canada: ISEI.

Lemke, E., & Strehl, T. (1999). Advanced measuring system for the analysis of dielectric parameters including PD events. In *Electrical Insulation Conference (EIC/EMCW),* Cincinnati, USA.

Lemke, E., & Strehl, T. (1999). Advanced measuring system for the analysis of dielectric parameters including PD events. In *5th International Conference on Insulated Power Cables (Jicable),* Versailles, France, paper A9.4.

Lemke, E., Strehl, T., & Rußwurm, D. (1999). New developments in the field of PD detection and location in power cables under on-site condition. 11th ISH London, UK.

Lemke, E., Strehl, T., & Boltze, M. (2001). Advanced diagnostic tool for PD fault location in power cables using the CDA technology. 12th ISH Bangalore, India, paper 6-46, (pp. 983–986).

Lemke, E., Gockenbach, E., & Kalkner, W. (2002). Measuring devices for the diagnostics of electrical equipment (in German). *ETG-Fachbericht Diagnostik elektrischer Betriebsmittel*, (87), 25–32.

Lemke, E., Elze, H., & Weissenberg, W. (2003). Experience in PD diagnosis tests of HV cable terminations in service using an ultra-wide-band PD probing in the real-time mode. 13th ISH, Delft, the Netherlands, paper 11.20, (p. 339).

Lemke, E., Strehl, T., Singer, M., Schneider, M., & Hinkle, J. L. (2003). Practical experience in on-site PD assessment of XLPE and PILC distribution power cables using damped AC exciting voltages. Nordic Insulation Symposium (NORD-IS) Tampere, Finland, pp. 47–54.

Lemke, E., Gulski, E., Hauschild, W., Malewski, R., Mohaupt, P., Muhr, M., Rickmann, J., Strehl, T., & Wester, W. F. (2006). Practical aspects of the detection and location of partial discharges in power cables. [CIGRE Technical Brochure no.297]. *Electra*, *226*, 63–70.

Lemke, E., Berlijn, S., Gulski, E., Muhr, M., Pultrum, E., Strehl, T., Hauschild, W., Rickmann, J., & Rizzi, G. (2008). *Guide for partial discharge measurements in compliance with IEC 60270*. [CIGRE Technical Brochure no.366].

Lemke, E., Strehl, T., & Markalous, S. (2008). Ultra-wide-band PD diagnostics of power cable terminations in service. *IEEE Transactions on Dielectrics and Electrical Insulation,15*(6), 1570–1575.

Les Renardieres Group (1974). Research on impulse measuring systems—Facing UHV measuring problems. *Electra*, *35*.

Les Renardieres Group (1977). Positive discharges in long air gaps at Les Renardieres. *Electra*, *53*, 31–153.

Lefèvre, A., Legros, W., & Salvador, W. (1989). *Dielectric test with oscillating discharge on synthetic insulation cables* (pp. 270–273). France: CIRED Paris.

Lewin, P. L., et al. (2008). Zero-phase filtering for LI evaluation: A k-factor filter for the revision of IEC 60060-1 and -2. *IEEE Transactions on Power Delivery,23*(1), 3–12.

Lewis, I. A. D., & Wells, F. H. (1959). *Millimicrosecond pulse techniques*. Oxford: Pergamon Press.

Lichtenberg, G. C. (1777). De nova method naturam ac motum fluidi electrici investigandi. Novi Commentarii SocietatisRegiae Scientiarum Gottingae Tom 8, p. 168 (Part 1) (For German text see Ostwald′s Klassiker der exakten Wissenschaften, No. 246, Akademische Verlagsgesellschaft, Leipzig 1956).

Lichtenberg, G. C. (1778). Commentationes SocietatisRegiae Scientiarum Gottingae Tom 1, p. 65 (Part 2) (For German text see Ostwald′s Klassiker der exakten Wissenschaften, No. 246, Akademische Verlagsgesellschaft, Leipzig 1956).

Lloyd, W. L., & Starr, E. C. (1928). Investigation of the AC corona using a cathode-ray oscilloscope (in German). *ETZ,49*, 1279.

Loeb, L. B. (1939). *Fundamental processes of electrical discharges in gases* (p. 429). New York: Wiley.

Loeb, L. B. (1939). *Basic processes of gaseous electronics*. London: Wiley.

Loeb, L. B., & Jaeger, G. (1906). Kinetic theory of gases.*Winkelmanns Handbuch der Physik*, *3*(2). (Barth-Verlag Leipzig).

Long W, Nilsson S (2007, March/April) HVDC Transmission: Yesterday and today. *IEEE Power and Energy Magazine*, 22–31.

Lukaschewitsch, A., & Puff, E. (1976). PD measurement on long cables (in German). *Zeitschrift für praktische Energietechnik,28*(2), 32–39.

Lundgard, L. E. (1992). Partial discharge. Part XII: Acoustic partial discharge detection-Fundamental considerations. *IEEE Electrical Insulation Magazine*, *8*(4).

Lundgard, L. E., Hansen, W., & Dursun, K. (1989). Location of power transformers using external acoustic sensors. 6th ISH, New Orleans, USA.

Lundgard, L. E., Runde, M. P., & Skyberg, B. (1990). Acoustic diagnoses of gas insulated substations: A theoretical experimental basis. *IEEE Transactions on Power Delivery,5*(4), 1751–1759.

Mahdjuri-Sabet, (1977). Transfer characteristic of textile resistor bands of low inductance in HV test circuits (in German). *Archiv für Elektrotechnik,59*, 69–73.

Malewski, R. (1968). New device for current measurement in exploding wire circuits. *Review of Scientific Instruments,39*, 90–94.

Malewski, R. (1977). Micro-Ohm shunts for precise recording of short-circuit currents. *Transactions PAS-96*, 579–585.

Malewski, R., Corcoran, R. P., Feser, K., McComb, T. R., Nellis, C., & Nourse, G. (1982). Measurements of the transient electric and magnetic field components in HV laboratories. *IEEE Transactions on Power Apparatus and Systems,PAS-101*, 4452–4459.

Mann, N. R., et al. (1974). *Methods for statistical analysis and life data*. New York: Wiley.

Markalous, S. M. (2006). Detection and location of partial discharges in power transformer using acoustic and electromagnetic signals. Ph.D. Thesis Technische Universität Stuttgart.

Markalous, S. M., Tenbohlen, S., & Feser, K. (2008). Detection and location of partial discharges in power transformers using electric and electromagnetic signals. *IEEE Transactions on Dielectrics and Electrical Insulation,15*(6), 1576–1583.

Martin, F., & Leibfried, T. (2006). An universal HV source based on a static frequency converter ISEI Toronto, 420–423.

Marx, E. (1952). HV test practicals/Hochspannungspraktikum (2nd Edn, in German). Berlin: Springer.

Marx, E. (1926). Breakdown voltage of insulators depending on the voltage waveshape (in German). *Hescho-Mitteilungen, Heft 21*(22), 657.

Matsumoto, T., Ishii, M., & Kawamura, T. (1983). The requirement of a DC source for tests on contaminated insulators. 4th ISH Athens paper 62.03.

Maucksch, S., et al. (1996). Calibration of HV measuring systems for the mutual recognition of HV test results in Eastern and Western Europe. In *ERA Conference Milan*.

Maxwell, J. C. (1873). *A treatise on electricity and magnetism* (Vol. 1, 3rd Edn). Oxford: Clarendon Press, (Reprint by Dover, 1981, pp. 450–461).

Meek, J. M. (1940). A theory of spark discharges. *Physical Review,57*, 722–728.

Meek, J. M., & Craggs, J. D. (1953). *Electrical breakdown of gases*. New York: Wiley (2nd Edn. 1978).

Meiling, W., & Stary, F. (1969). Nanosecond Pulse Techniques. Berlin: Akademie-Verlag.

Meinke, H., & Gundlach, F. W. (1968). *Handbook of high-frequency techniques (in German)*. New York: Springer.

Melville, D. R. G., Salvage, B., & Steinberg, N. R. (1965). Discharge detection and measurement under direct-voltage conditions: Significance of discharge magnitude. In *Proceedings IEEE* (Vol. 112, pp. 1815–1817).

Menke, P. (1996). Optical current sensor of high accuracy using the Faraday effect. Ph.D. Thesis, University Kiel.

Merkhalev, S. D., & Vladimirsky, L. L. (1985). Requirement to and design of HV rectifiers for polluted insulation tests. Meeting Cigre SC 33 (Budapest).

Mikropoulos, P. N., et al. (2008). Positive streamer propagation and breakdown in air: The influence of humidity. *IEEE Transaction on Dielectrics and Electrical Insulation,15*(2), 416–425.

Millmann, J., & Taub, H. (1956). *Pulse and digital circuits*. New York: McGraw-Hill Book Co.

Moeller, J. (1975). Metal-clad test transformer for SF_6–insulated switchgear.2nd ISH Zurich, Paper 21-09 (pp. 161–164).

Moeller, J., Steinbigler, H., & Weiß, P. (1972). Field strength distribution on shielding electrodes for UHV test systems (in German). 1st ISH Munich, (pp. 36–41).

Mole, G. (1954). The E.R.A. portable discharge detector. CIGRE Session, Paris, France, No. 105, App. I.

Mole, G. (1970). Measurement of the magnitude of internal corona in cables. *IEEE Transactions on Power Apparatus and Systems,89*(2), 204–212.

Montanari, G. C. (2006). Effect of supply voltage frequency on testing of insulation systems. *IEEE Transactions on Dielectrics and Electrical Insulation*, *13*(1), 111–121 (see also the discussion to this publication by Hauschild W in *IEEE Transactions on Dielectrics and Electrical Insulation*, 1189–1191).

Montanari, G. C. (2011). Bringing an insulation to failure: The role of space charges. *IEEE Transactions on Dielectrics and Electrical Insulation,18*(2), 339–364.

Montanari, G. C., & Cavallini, A. (2013). Partial discharge diagnostics: From apparatus monitoring to smart grid assessment. *IEEE Electrical Insulation Magazine,29*(3), 8–17.

Morshuis, P. H. F. (1993). Partial discharge mechanisms. Ph.D. Thesis, Delft University.

Morshuis, P. H. F. (1987). Degradation of solid dielectrics due to internal partial discharges: Some thoughts on progress made and where to go now. *IEEE Transactions on Dielectrics and Electrical Insulation,12*, 905–913.

Morshuis, P. H. F., & Smit, J. J. (2005). Partial detection at DC voltage: Their mechanism, detection and analysis. *IEEE Transactions on Dielectrics and Electrical Insulation,12*(2), 328–340.

Mosch, W. (1969). The simulation of switching over-voltages in EHV systems by HV test equipment (in German). *Wiss. Zeitschrift TU Dresden,18*(2), 513–517.

Mosch, W., & Hauschild, W. (1979). *HV insulation with sulphur hexafluoride (in German)*. Berlin: Verlag Technik, Heidelberg: Hüthig.

Mosch, W., et al. (1974). The HV laboratory of the section of electrical engineering of Dresden technical university in education and research (in German). *Wiss. Zeitschrift TU Dresden,23*(5), 1125–1135.

Mosch, W., et al. (1979). Dimensioning of screening electrodes for UHV test equipment based on a critical streamer intensity. 3rd ISH Milan, paper 52.04.

Mosch, W., et al. (1979). Phenomena in SF_6 insulations with particles and their technical valuation. 3rd ISH Milan paper 32.01.

Mosch, W., et al. (1988). Hochspannungsisoliertechnik. In E. Philippow (ed). *Taschenbuch Elektrotechnik* (Vol. 6, pp. 235–425). Berlin: VEB Verlag Technik Berlin (2nd Edn in German).

Mosch, W., et al. (1988). Model of the creeping flashover of polluted insulators and direct voltage generators for pollution tests. CIGRE Session Paris, Report 33-05.

Müller, K. (1934). About the measurement of characteristics of radio noise (in German). *Veröffentlichungen auf dem Gebiete der Nachrichtentechnik,2*, 159.

Müller, P. H. (1974). *Probability calculations and mathematical statistics—encyclopedia of stochastic (in German)*. Berlin: Akademie Verlag.

Müller, K. B. (1976). On the performance of extruded PE-cables under high direct voltage long-term stress (in German). Ph.D. Thesis TH Darmstadt, Germany.

Müller, U. (1927). Newer measurements by a Klydonograph (in German). *Hescho-Mitteilungen,37*, 1049.

Naderian, J. A., et al. (2011). Load-cycling test of HV cables and accessories. *IEEE Electrical Insulation Magazine,27*(5), 14–28.

Nelin, G., Ryzko, H., & Kvarngreen, M. (1983). Improved infra-frequency high-voltage test generator. 4th ISH Athens, paper 52.07.

NEMA 107 (1987). Methods of measurement of radio influence voltage (RIV) of high-voltage apparatus. NEMA Publication No. 107.

Nemeth, E. (1966). Non-destructive testing of insulations by discharging and recovery voltages (in German). 11th. Wiss. Konferenz Ilmenau (pp. 87–91).

Nemeth, E. (1972). Proposed fundamental characteristics describing dielectric processes in dielectrics. *Periodica Polytechnica, Budapest,15*(4), 305–322.

Nieschwitz, H. (1982). Localization of partial discharges (in German). 50th VDE-Seminar.

Nieschwitz, H., & Stein, W. (1976). PD measurement on HV power transformers—a tool of quality control (in German). *ETZ-A*, *Heft 11*.

Nyamupangedengu, C., & Jendrel, I. R. (2012). PD spectral response to variations in the supply frequency. *IEEE Transactions on Dielectrics and Electrical Insulation,19*(2), 521–532.

Obenaus, F. (1958). Pollution flashover and creeping path (in German: Fremdschichtüberschlag und Kriechweglänge). *Deutsche Elektrotechnik,4*, 135–136.

Ohki, Y. (2010). News from Japan: Advanced site assembly technologies for UHV transformers. *IEEE Electrical Insulation Magazine,26*(2), 55–57.

Okabe, S., & Takami, J. (2011). Occurrence probability of lightning failure rates at substations in consideration of lightning stroke current waveforms. *IEEE Transaction on Dielectrics and Electrical Insulation,18*(1), 221–231.

Okabe, S., & Takami, J. (2009). Evaluation of improved lightning stroke waveform using advanced statistical method. *IEEE Transactions on Power Delivery*, *4*, 2197–2205.

Okabe, et al. (2013). Discussion on standard waveform in the LI voltage test. *IEEE Transactions on Dielectrics and Electrical Insulation,20*(1), 147–156.

Okubo, H., et al. (1998). Insulation design and on-site testing method for a long distance, gas-insulated transmission line (GIL). *IEEE Electrical Insulation Magazine,14*(6), 13–22.

Olearczyk, M., Hampton, R. N., et al. (2010, November/December). Notes from underground—cable fleet management. *IEEE Power and Energy Magazine*, 75–84.

Ortega, P., Waters, R. T., et al. (2007). Impulse breakdown voltages of air gaps: A new approach to atmospheric correction factore applicable to international standards. *IEEE Transaction on Dielectrics and Electrical Insulation,14*(6), 1498–1507.

Palm, A. (1932). Schering measuring bridges (in German). *Archiv für Technisches Messen*, 921–923.

Park, E. H. (1947). Shunts and inductors for current measurements. *NBS Journal Research,39*, 191–212.

Park, J. H., & Cones, H. N. (1956). Surge voltage breakdown of air in a non-uniform field. *Journal on Research of the National Bureau of Standardization,56*(4), 201–224.

Pearson, J. S., Hampton, B. F., & Sellars, A. G. (1991). A continuous UHF monitor for gas-insulated substations. *IEEE Transactions on Electrical Insulation,26*(3), 469–472.

Pedersen, A. (1986). Current pulses generated by discharges in voids in solid dielectrics. A field theoretical approach. IEEE International Symposium on Electrical Insulation (IESI),IEEE Publication. 86CH2196-4-DEI, 112.

Pedersen, A. (1987). Partial discharges in voids in solid dielectrics, an alternative approach. In *Annual Report—Conference on Electrical Insulation and Dielectric Phenomena*, IEEE Publication 87CH2462-0, 58.

Pedersen, A., Crichton, G. C., & McAllister, I. W. (1991). The theory and measurement of partial discharge transients. *IEEE Transactions on Electrical Insulation,26*, 487.

Pedersen, A., Crichton, G. C., & McAllister, I. W. (1995). Partial discharge detection: theoretical and practical aspects. *IEE Proceedings—Science, Measurement and Technology*, *142*, 29.

Pedersen, A., Crichton, G. C., & McAllister, I. W. (1995). The functional relation between partial discharges and induced charge. *IEEE Transactions on Dielectrics and Electrical Insulation,2*, 535.

Peek, F. W. (1913). Law of corona and dielectric strength of air III. *Transaction of the AIEE II,32*, 1767–1785.

Peek, F. W. (1915). The effect of transient overvoltages on dielectrics. *Transaction of the AIEE,34*, 1915.

Peier, D., & Graetsch, V. (1979). A 300 kV DC measuring device with high accuracy. 3rd ISH Milan, Italy, paper 43.08.

Peschke, E. (1968). Breakdown and flashover at high direct voltages in air (in German). Ph.D. Thesis Munich Technical University.

Peschke, E. (1969). Influence of humidity on the breakdown and flashover behavior at high direct voltages in air (in German). *ETZ-A,90*, 7–13.

Petcharales, K. (1986). Numerical calculation of breakdown voltages of standard air gaps (IEC 52) based on streamer breakdown criteria. PhD thesis, ETH Zurich.

Pfeffer, A., & Tenbohlen, S. (2009). Analysis of full and chopped lightning impulse voltages from transformer tests using the new k-factor approach. 16th ISH Cape Town, paper A-10.

Pietsch, R., et al. (2005). SF_6-insulated, frequency-tuned resonant test system for spacer testing with AC voltage up to 1000 kV. 16th ISH Beijing paper J-56.

Pietsch, R., Hinow, M., & Steiner, T. (2010). Challenge to the HV test techniques for testing HVDC cables (in German). Kolloquium "Isoliersysteme" Cologne, ISBN 978-3-8007-3278-4.

Pietsch, R., & Hauschild, W., et al. (2012). High-voltage on-site testing with partial discharge measurement. CIGRE Technical Brochure No. 502, Working Group D1.33.

Pigini, A. (2010). Design of insulators under pollution. In *International Conference on development of a 1200 kV national test station* (pp. 265–280). New Delhi.

Pigini, A., et al. (1985, October). Influence of air density on the impulse strength of external insulation. *IEEE Transaction on PAS*, *104*(10).

Pilling, J. (1976). A contribution tot he interpretation of life-time characteristics of solid insulations (in German). Habilitation Thesis Technische Universität Dresden.

Plath, R. (1994). Oscillating test voltages for on-site testing and PD measurement of extruded cables (in German). (Dissertation, TU Berlin, 1994).

Plath, K., Plath, R., Emanuel, H., & Kalkner, W. (2002). Synchronous three-phase PD measurement on power on site and in the laboratory (in German). ETG-Fachtagung Diagnostik elektrischer Betriebsmittel, Berlin, paper 11 (pp. 69–72).

Plath, R. (2005). Multi-channel PD measurements. 14th ISH, Bejing, China.

Poleck, H. (1939). Measuring bridges for the measurement of capacitances and loss factors of grounded test objects (in German). *Archiv für Technisches Messen*, 921–951.

Pommerenke, D., Krage, I., Kalkner, W., Lemke, E., & Schmiegel, P. (1995). On-site PD measurement on high voltage cable accessories using integrated sensors. 9th ISH Graz/ Austria.

Praehauser, T. (1973). PD measurement on HV apparatus using the bridge method (in German). *Bulluetin SEV,64*, 1183–1189.

Prinz, H., et al. (1965). *Fire, lightning and spark,(in German: Feuer Blitz und Funke)*. Munich: Verlag F. Bruckmann KG.

Ramirez, M., et al. (1987) Air density influence on the strength of external insulation under positive impulses: Experimental investigations up to an altitude of 3000 m a.s.l. CIGRE WG 33.03. IWD.

Raske, W. (1937). Measuring dividers for high voltages—Part I: Resistive dividers (in German). *Archiv für Elektrotechnik,31*(10), 653–666.

Raske, W. (1939). Measuring dividers for high voltages—Part II: Capacitive dividers (in German). *Archiv für Elektrotechnik*, *1*(33).

Raske, W. (1939). Measuring dividers for high voltages—Part II: Mixed dividers (in German). *Archiv für technisches Messen*, Z 116-5.

Raether, H. (1939). The development of the electron avalanche to the spark channel (in German). *Zeitschrift für Physik,112*, 464–489.

Raether, H. (1940). On the development of channel discharges (in German: Zur Entwicklung von Kanalentladungen. *Archiv für Elektrotechnik,34*, 49–51.

Raether, H. (1941). On the formation of gas discharges (in German: Über den Aufbau von Gasentladungen). *Zeitschrift für Physik*, *117,* 375–524.

Raether, H. (1942). On the electrical breakdown of gases (in German: Über den elektrischen Durchschlag in Gasen). *ETZ,63*, 301–303.

Raether, H. (1964). *Electron avalanches and breakdown in gases*. London: Butterworths.

Reichel, R. (1977). Influence of a parallel capacitance on the pollution flashover and its role for the determination of the pollution flashover voltage (in German). (Dissertation, Dresden Technical University).

Reid, R. (1974). High-voltage resonant testing. IEEE PES Winter Meeting. Paper C74 038-6.

Renne, V. T., Stepanov, S. I., & Lavrov, D. S. (1963). Ionization processes in the dielectric of paper capacitors under direct voltage (in Russian). *Elektricestvo*, 269–278.

Rethmeier, K., Kraetge, A., et al. (2008). Separation of superimposed PD faults and noise by synchronous multi-channel data acquisition. International Symposium on Electrical Insulation (ISEI), Toronto, Canada, (pp. 611–615).

Rethmeier, K., Obralic, A., Kraetge, A., Krüger, M., Kalkner, W., & Plath, R. (2009). Improved noise suppression by real-time pulse-waveform analysis of PD pulses and pulse-shaped disturbances. 16th ISH, Cape Town, South Africa.

Rethmeier, K., Kraetge, A., & Hummel, R. (2012). About the influence oft the PD repetition rate on the apparent charge value in PD measurements according to IEC 60270 (in German). Kolloquium Diagnostik Elektrischer Betriebsmittel, Fulda (15–16.11.2012), VDE Verlag GmbH Berlin, Offenbach.

Reynolds, P. H. (1985). DC insulation analysis. A new and better method. *IEEE Transactions PAS,104*(7), 1746–1749.

Rizk, F. A. (1981). Mathematical models for pollution flashover. *Electra,78*, 71–103.

Rizk, F. A., & Bourdage, M. (1985). Influence of the AC source parameters on flashover characteristics of polluted insulators. *IEEE Transaction PAS,104*, 948–958.

Rizk, F. A., & Nguyen, D. H. (1987). Digital simulation of source-insulator interaction in HVDC pollution tests. IEEE PES WM 168-8, New Orleans.

Robinson, R. A., & Silvia, M. T. (1978). *Digital signal processing and time series analysis*. San Francisco: Holden-Day.

Rodewald, A. (1969). Transient processes in the Marx multiplier circuit after the ignition of the first switching gap (in German). *Bulletin SEV,60*, 37–44.

Rodewald, A. (1969). Probability of ignition of the switching gaps in the Marx multiplier circuit (in German). *Bulletin SEV,60*, 857–863.

Rodewald, A. (1971). Marx multiplier circuit with supporting switching gaps for the extension of the trigger range (in German). *ETZ-A,92*, 56–57.

Rogers, E. C., & Skipper, D. J. (1960). Gaseous discharge phenomena in high-voltage DC cable dielectrics. *Proceedings IEE, Part A*, *107*, 241–254.

Rogowski, W. (1913). About some applications of magnetic voltage measurement (in German). *Archiv für Elektrotechnik,1*, 511–527.

Salvage, B. (1962). Electrical discharges in gaseous cavities in solid dielectrics under direct voltage conditions. In *Proceedings of International Conference on Gas Discharges and the Electricity Supply Industry* (pp. 439–446). Butterworth, London.

Salvage, B., & Sam, W. (1967). Detection and measurement of discharges in solid insulation under direct-voltage conditions. *Proceedings IEE*, *114*, 1334–1336.

Satish, L., & Gururaj, B. I. (2001). Wavelet analysis for estimation of mean curve of impulse waveforms superimposed by noise oscillations and overshoot. *IEEE Transactions on Power Delivery,16*(1), 116–121.

Schenkel, M., v. Issendorf, I., & Schering, H. (1919). Bridge for loss measurement (in German). Tätigkeitsbericht der Physikalisch-Technischen Reichsanstalt, Berlin.

Schering, H. (1919). Bridge for loss measurement (in German). Tätigkeitsbericht der Physikalisch-Technischen Reichsanstalt, Braunschweig, Germany.

Schering, H. (1933). Determination of the high-voltage value during loss factor measurement by a bridge (in German). *ETZ,45*, 51.

Schering, H., & Vieweg, F. (1928). A measuring capacitor for highest voltages (in German). *Zeitschrift für Technische Physik,9*, 442.

Schiller, G. (1996). The breakdown behavior of cross-linked polyethylene at different test voltages and pre-stresses (in German). (Dissertation, University of Hanover).

Schmuck, F., Aitken, S., & Papailiou, K. O. (2010). Proposal for intensified inspection and acceptance tests of composite insulators as an addition to the Guidelines of IEC 61109 and IEC 61952. *IEEE Transactions on Dielectrics and Electrical Insulation,17*(2), 394–401.

Schon, K. (2010). *Impulse voltage and impulse current measuring techniques (in German)*. Heidelberg: Springer.

Schon, K. (1986). Concept of PD measurement at PD tests (in German). *ETZ Archiv,8*(9), 319–324.

Schon, K., & Schuppel, W. (2007). Precision Rogowski coil used with numerical integration. 13th ISH Ljubljana, paper T10-130.

Schrader, W. (1971). Multi-stage high-voltage test system fort he generation of electrical impulse voltages (in German). DDR-Patent No. 86049, issued on 20.11.1971.

Schrader W et al. (1989) The generation of switching impulse voltages up to 3.9 MV with a transformer cascade of 3 MV. 6th ISH New Orleans paper 47.39.

Schreiter, F., Jilek, U., & Schufft, W. (2003). Combined diagnostic and withstand test to upgrade the operational voltage of 10 kV cables. 13th ISH Delft, paper P 08.07.

Schufft, W. (1991). Considerations on the area effect at large electrodes for HV test equipment. 7th ISH Dresden paper 54.03.

Schufft, W., et al. (2007). Paperback of electrical power engineering (in German). Fachbuchverlag Leipzig im Carl Hanser Verlag Munich.

Schufft, W., & Gotanda, Y. (1997). A new DC voltage test system with fast polarity reversal. 10th ISH Montreal (Vol. 4, pp. 37–40).

Schufft, W., & Schrader, W. (1993). A new Marx generator for the simulation of lightning impulse voltages and currents. 8th ISH Yokohama, paper 79.03.

Schufft, W., et al. (1995). Powerful frequency-tuned resonant test system for after laying tests of 110 kV XLPE cables 9th ISH Graz Volume Paper 4486.

Schufft, W., et al. (1999). Frequency-tuned resonant test systems for on-site testing and diagnostics of extruded cables. 11th ISH London, paper 5.335.P5.

Schuler, R. H., & Liptak, G. A. (1980). A new method for HV testing of field windings on large rotating electrical machines. CIGRE Session Paris Report 11-04.

Schulz, W. (1979) Free-hovering particles causing low breakdown voltages in air (in German). *ETZ Archiv*, 123–126.

Schuman, W. O. (1923) *Electrical breakdown field strength of gases (in German)*. Berlin: Springer.

Schwab, A. J. (1971). Low-resistance shunts for impulse currents. *IEEE Transactions PAS-90*, 2251–2257.
Schwab, A. J. (1981). *High-voltage measuring technique* (2nd English Edn). Berlin: Springer (1st German Edn. 1969).
Schwarz, H., et al. (1999). *Megavolts in Cottbus—planning and erection of a HV laboratory* (book in English and German).
Schwaiger, A. (1923). *The theory of the electric strength (in German)*. Berlin: Springer.
Schwaiger, A. (1925). *About discharge processes on insulators (in German)*. Rosenthal-Mitteilungen, Heft 6, (pp. 1–23).
Seifert, J. M., Petrusch, W., & Janssen, H. (2007). A comparison of the pollution performance of long-road and disc type HVDC insulators. *IEEE Transactions Dielectrics and Electrical Insulation,14*(1), 125–129.
Shannon, C. E. (1949). Communication in the presence of noise. *Proceedings IRE*, *37*, 10–21.
Shockley, W. (1938). Current to conductors induced by a moving point charge. *Journal of Applied Physics,9*, 635.
Shu, Y. (2010, October). Current HVDC development and standardization demand. Presentation on the Plenary Meeting IEC TC 115 Seattle.
Seitz, P., & Osvath P. (1979). Microcomputer controlled transformer ratio-arm bridges. 3rd ISH, Milan, paper 43.11.
Siemens, A. G. (2007). "Final electrical testing of transformers and reactors" and "Transformer life management" Technical Brochures of Siemens AG, Power Transmission and Distribution, Nuremberg.
Simmons, J. G., & Tam, M. C. (1973). Theory of isothermal currents and the direct determination of trap parameters in semiconductors and insulators. *Physical Review B,7*(8), 3706.
Simon, P. (2004). Research of the characteristic parameters of the behaviour of dielectric media under non-standard impulses in high-voltage. Doctoral Thesis, Polytechnical University of Madrid.
Singer, H. (1972). The electric field of the polycon electrode (in German). 1st ISH Munich (pp. 59–66).
Singh, J., Sood, Y. R., Jarial, R. K., & Verma, P. (2008). Condition monitoring of transformers-bibliography survey. *IEEE Electrical Insulation Magazine,24*(3), 11.
Sklenicka, V., et al. (CIGRE TF 33.04.09) (1999). Influence of ice and snow on the flashover performance of outdoor insulators. *Electra*, 187, 91–111.
Slama, M. E. A., et al. (2010). Analytical computation of discharge characteristic constants and critical parameters of flashover of polluted insulators. *IEEE Transactions Dielectrics and Electrical Insulation,17*, 1764–1771.
Speck, J. (1987). Statistical evaluation of test data of the aging of electrical apparatus (in German). 11. Scientific Conference of the Section Electrical Engineering, TU Dresden.
Speck, J., et al. (2009). Statistical estimation of the life time of solid insulations in consideration of defects. 16th ISH Cape Town, Paper C-13.
Spiegelberg, J. (1966). Contribution to the design and calibration of resistive LI voltage dividers (in German). PhD Thesis Technical University Dresden, Institute of HV Engineering.
Spiegelberg, J. (1984). Powerful HVDC and composite voltage test systems for open air arrangement (in German). *Elektrie,38*(10), 368–371.
Spiegelberg, J. (2003). Highlights of HV test equipment manufactured in Dresden—Review of the last century (in German). In *Proceedings HIGHVOLT Kolloquium*, pp.7–20.
Spiegelberg, J., et al. (1993). A new series of resonant testing systems for cable testing. 8th ISH Yokohama, paper 55.05.
Stanley, W. D. (1975). Digital signal processing. Reston.
Starke, H. & Schröder, R. (1928). Electrometer for the measurement of very high DC and AC voltages (in German). *Archiv für Elektrotechnik 20,* 115–117.
Steenis, E. F., & van de Laar, A. M. (1989). Characterization test and classification procedure for water-tree aged medium voltage cables. *Electra*, 125, 88–101.

Steiner, T. (2011). Standardization of digital recorders, IEC 61083-1, -2, -3 and -4. HIGHVOLT Kolloquium Dresden, paper 1.5.

Storm, R. (1976). Probability calculations-mathematical statistics-statistical quality control (in German). Fachbuchverlag Leipzig.

Strauss, W. (1983). Automatization of impulse voltage tests using microcomputers operating in real-time domain and transient recorders (in German). Ph.D. Thesis, Technical University Berlin.

Strauss, W. (2003). Progress and calibration of digital recorders for HV impulse testing (in German). HIGHVOLT Kolloquium Dresden, paper 3.3.

Strehl, T., Lemke, E., & Elze, H. (2001). On-line PD measurement: Diagnostic tools on monitoring strategy for generators and power transformers. 12th ISH, Bangalore, India, paper 6-72.

Strehl, T., & Engelmann, A. (2003). Mobile Test system for insulation diagnostics of electrical equipment (in German). ETZ, Heft 18.

Su, Z., et al. (2005). The DC rain flashover of station insulators under contamination conditions. 14th ISH Beijing paper D-59.

Sun, Z. Y., Liao, W. M., Su, Z. Y., & Zhang, X. J. (2009). Test study on the altitude correction factors of air gaps of ±800 kV UHVDC projects. In *International Conference on UHV Power Transmission*, Beijing, Paper FP0557.

Swedish Power Circle (2010). Electricity for sustainable energy. Presentation for the Swedish Academy of Engineering.

Takami, J. (2007). Observation results of lightning currents on transmission towers. *IEEE Power Delivery,22*, 547–556.

Tanaka, T., & Okamoto, T. (1978). A minicomputer-based partial discharge measurement system. In IEEE International Symposium on Electrical Insulation (ISEI) Philadelphia, USA, Conference Records 86-89.

Tanaka, T., & Okamoto, T. (1985). Micro-computer application to in-site diagnosis of XLPE cables in service. In *International Conference on Properties and Application of Dielectric Materials*, *Xián* (pp. 499–502).

Thiede, A., & Martin, F. (2007). Power frequency inverters for HV tests. HIGHVOLT Colloquium Dresden, paper 1.7 (pp. 57–61).

Thiede, A., Steiner, T., & Pietsch, R. (2010). A new approach of testing power transformers by means of static frequency converters. CIGRE Session Paris, Report D1.202.

Thione, L. (1983). Evaluation of switching impulse strength of external insulation. Electra, No. 94.

Toepler, M. (1898). On sliding discharges along a clean glass surface (in German). *Wied. Annalen der Physik and Chemie,66*, 1061.

Townsend, J. S. (1915). *Electricity in gases*. Oxford: Oxford University Press.

Townsend, J. S. (1925). *Motion of electrons in gases*. Oxford: Clarendon Press.

Townsend, J. S. (1937). The equations of motion of electrons in gases. *Philosophical Magazine*, *VII*(23), 481.

Trichel, G. W. (1938). Mechanism of the negative point-to-plain corona near onset. *Physical Review,54*, 1078–1084.

Tretter, S. A. (1976). *Introduction to discrete-time signal processing*. New York: Wiley.

Tsuboi, T., et al. (2010a). Weibull parameter of oil-immersed transformer to evaluate insulation reliability on temporary overvoltages. *IEEE Transactions Dielectrics and Electrical Insulation,17*(6), 1863–1876.

Tsuboi, T., et al. (2010b). Experiment on multiple times voltage application to evaluate insulation reliability of oil immersed transformer. *IEEE Transaction Dielectrics and Electrical Insulation,17*(5), 1657–1664.

Tsuboi, T., et al. (2010c). Transformer insulation reliability for moving oil with Weibull analysis. *IEEE Transactions Dielectrics and Electrical Insulation,17*(3), 978–983.

Tsuboi, T., et al. (2011). Insulation breakdown characteristics of UHV class GIS for LI withstand voltage test waveform-k-factor value and front related characteristics. *IEEE Transactions on Dielectrics and Electrical Insulation,18*(5), 1734–1742.

Tsuboi, T., Ueta, G., & Okabe, S. (2013). K-factor value and front-time related characteristics in negative polarity LI test for UHV-class air insulation. *IEEE Transactions on power delivery*, *26*(2), 1148–1155.

Ueta, G., Tsuboi, T., & Okabe, S. (2011a). Evaluation of overshoot rate of LI withstand voltage test waveform based on new base fitting methods-study on overshoot waveform in an actual test. *IEEE Transactions on Dielectrics and Electrical Insulation,18*(3), 783–791.

Ueta, G., Tsuboi, T., & Okabe, S. (2011b). Evaluation of overshoot rate of LI withstand voltage test waveform based on new base fitting methods-study by assuming waveforms in an actual test. *IEEE Transactions on Dielectrics and Electrical Insulation,18*(6), 1912–1921.

Ueta, G., Wada, J., & Okabe, S. (2011c). Evaluation of breakdown characteristics of CO_2 gas for non-standard LI waveforms- breakdown characteristics under single-frequency oscillating waveforms of 5.3 to 20.0 MHz. *IEEE Transaction on Dielectrics and Electrical Insulation,18*(1), 238–245.

Ueta, G., Wada, J., & Okabe, S. (2011d). Evaluation of breakdown characteristics of CO_2 gas for non-standard impulse waveforms- method for converting non-standard LI waveforms into standard LI waveforms. *IEEE Transactions on Dielectrics and Electrical Insulation,18*(5), 1724–1733.

Ueta, G., et al. (2012a). k-factor value and front related characteristics of UHV-class air insulation for positive polarity LI test. *IEEE Transactions on Dielectrics and Electrical Insulation,19*(3), 877–885.

Ueta, G., et al. (2012b). Study on the k-factor function in the LI test for UHV power equipment. *IEEE Transactions on Dielectrics and Electrical Insulation,19*(4), 1383–1391.

Van Brunt, R. J. (1992). Stochastic properties of partial discharge phenomena. *IEEE Transactions on Electrical Insulation,26*(5), 902–948.

Vardeman, S. B. (1994). Statistics for engineering problem solving. Boston: IEEE Press-PWS Publishing Company.

Verma, M. P., & Petrusch, W. (1981). Results of pollution tests on insulators in the $\geq$1100 kV range and the necessity of testing in the future. *IEEE Transactions on Electrical Insulation*, *3*.

Vilbig, F. (1953). High-frequency measuring technique (in German). Carl Hanser Verlag, München.

Wada, J., Ueta, G., & Okabe, S. (2011). Evaluation of breakdown characteristics of N_2 gas for non-standard lightning impulse waveforms-Breakdown characteristics under single-frequency oscillation waveforms and bias voltage. *IEEE Transactions on Dielectrics and Electrical Insulation,18*(5), 1759–1766.

Wada, J., Ueta, G., & Okabe, S. (2011). Evaluation of breakdown characteristics of CO_2 gas for non-standard lightning impulse waveforms und non-uniform electric field—breakdown characteristics for single-frequency oscillation waveforms. *IEEE Transactions on Dielectrics and Electrical Insulation,18*(2), 640–648.

Wagner, K. W. (1912). On the measurement of dielectric losses using the alternating current bridge (in German). ETZ, *33*, 635–637.

Wagner, K. W. (1914). Explanation of dielectric relaxatuations by models of Maxwell (in German). *Archiv für Elektrotechnik, II*(9), 371–387.

Wagner, K. W. (1922). The physical nature of electrical breakdown in solid dielectrics. *Journal of American Institution of Electrical Engineering,61*, 1034.

Wakimoto, T., Hällström, J. Cherukov, Y., Ishii, M., Lucas, W., Piiroinen, J. & Shimizu, H. (2007). High-accuracy comparison of lightning and switching impulse calibrators. *IEEE Transactions on Instrumentation and Measurement. 56*, 619-623.

Ward, B. H. (1997). Digital techniques for partial discharge measurements. *IEEE Transactions on Power Delivery,7*(2), 469–479.

Ward, A. D., Exon, J., & La, T. (1993). Using Rogowski coils for transient current measurements. *IEE Engineering Science and Education Journal,2*, 105–113.

Weck, K. H. (2003). Condition assessment of LIP-insulated medium voltage cables—a contribution to the risk management of distribution cables (in German). HIGHVOLT Kolloquium '03, Paper 5.2 (pp. 159–166).

Weicker, W. (1927). Voltage measurements with the air gap (in German). Hescho-Mitteilungen, 31, 899–902.

Weicker, W., & Hoercher, W. (1938). Fundamentals for the establishment of calibration data for sphere spark gaps (in German). *ETZ,59*, 1029–1064.

Shu, E. W., & Boggs, S. A. (2008). Dispersion and PD detection in shielded power cable. *IEEE Electrical Insulation Magazine,21*(1), 25–29.

Werle, P., et al. (2006). Repair and HV testing of power transformers on site (in German). ETG Fachtagung "Diagnostic elektrischer Betriebsmittel" / ETG Fachbericht 104, Kassel.

Werle, P., (2007). On-site tests of power transformers. HIGHVOLT Kolloquium '07 paper 4.5, (pp. 143–149).

Whitehead, S. (1951). *Dielectric breakdown of solids*. Oxford: Clarendon Press.

Winter, A., et al. (2007). A mobile transformer test system based on a static frequency converter. HIGHVOLT Kolloquium '07, paper 4.4 (pp. 137–142).

Wolf, J., & Voigt, G. (1997). A new solution for the extension of the load range of impulse voltage generators. In *14th ISH Montreal* (Vol 4, pp. 363–366).

Wu, et al. (2009). Uncertainties in the application of atmospheric and altitude corrections as recommended in IEC standards. 16th ISH Cape Town, Paper A-15.

Witt, H. (1960). Response of low ohmic resistance shunts for impulse currents. *Elteknik,3*, 45–47.

Yakov, S. (1991). Statistical analysis of dielectric test results. Electra Brochure No. 66.

Yamagata, Y., & Okabe, S. (2009). Utility's experience on design and testing for UHV equipment in Japan. 2nd International Symposium on Standards for UHV Transmission.

Yu, Y-Q., et al. (2007). Standardization of HVDC transmission field. IEC/CIGRE UHV Symposium Beijing, Paper 5-3.

Zaengl, W. (1965). A new divider for steep impulse voltages (in German). *Bulletin*, *SEV57*, 1003–1017.

Zaengl, W., et al. (1982). Experience of AC voltage tests with variable frequency using a lightweight on-site series-resonant device. CIGRE Session (Paris) Report 23-07.

Zhang, G., Luo, C., & Pai, S.T. (1995). Magneto-optical sensors for pulsed current measurements. 9th ISH Graz, paper 7851.

Zhang, X., Gockenbach, E., et al. (2007). Estimation of the life time of electrical equipment in distribution networks. *IEEE Transactions on Power Delivery,22*(1), 515–522.

Zhang, X., & Gockenbach, E. (2008). Asset management of transformers based on condition monitoring and standard diagnosis. *IEEE Electrical Insulation Magazine,24*(4), 26–40.

Zhang, Z., et al. (2010). Study of the influence on DC pollution flashover voltage on insulator strings and its flashover process. *IEEE Transactions Dielectrics and Electrical Insulation,17*(6), 1787–1795.

Zhang, Z., et al. (2010). Study on DC flashover performance of various types of long string insulators under low atmospheric pressure conditions. *IEEE Transactions on Power Delivery,25*(4), 2132–2142.

Index

W. Hauschild and E. Lemke, *High-Voltage Test and Measuring Techniques*,
DOI: 10.1007/978-3-642-45352-6, © Springer-Verlag Berlin Heidelberg 2014